LIBRARY COPY

The Proceedings of the 79th AESF Annual Technical Conference SUR/FIN® '92

'92 AESF SUR/FIN

June 22-25, 1992
Atlanta, Georgia

The American Electroplaters and Surface Finishers Society, Inc. (AESF) is an international, individual-membership, professional, technical and educational society for the advancement of electroplating and surface finishing. AESF fosters this advancement through a broad research program and comprehensive educational programs, which benefit its members and all persons involved in this widely diversified industry, as well as government agencies and the general public. AESF disseminates technical and practical information through its monthly journal, *Plating and Surface Finishing,* and through reports and other publications, meetings, symposia and conferences. Membership in AESF is open to all surface finishing professionals as well as to those who provide services, supplies, equipment, and support to the industry.

According to the guidelines established by AESF's Meetings and Symposia Committee, all authors of papers to be presented at SUR/FIN® have been requested to avoid commercialism of any kind, which includes references to company names (except in the title page of the paper), proprietary processes or equipment.

Statements of fact or opinion in these papers are those of the contributors, and the AESF assumes no responsibility for them.

All acknowledgments and references in the papers are the responsibility of the authors.

Published by the
American Electroplaters and Surface Finishers Society, Inc.
12644 Research Parkway • Orlando, FL 32826-3298
Telephone: 407/281-6441 • Fax: 407/281-6446

Copyright 1992 by American Electroplaters and Surface Finishers Society, Inc. All rights reserved. Printed in the United States of America. This publication may not be reproduced, stored in a retrieval system, or transmitted in whole or part, in any form or by any means, electronic, mechanical, photocopying, recording, or otherwise without the prior written permission of AESF, 12644 Research Parkway, Orlando, FL 32826-3298.

Printed by AESF Press

SUR/FIN® is a registered trademark of the American Electroplaters and Surface Finishers Society, Inc.

Table of Contents
Volume I

SESSION A
Quality & Statistical Methods

Achieving Competitive Edge Through the Application of Total Quality Management 1
Dr. D. Paul Piplani, CEF, Acteron Corporation, Redwood City, CA
Paper Not Available in Time for Publication

Practical Guide for Measuring HD Undercoat Thickness 3
F. Matsui, T. Guiala, D. Liston, Uyemura International Corporation, Ontario, CA, Yasuyuki Yamamoto, C. Uyemura & Co., Ltd., Tokyo, Japan

Why Johnny Can't Do SPC 17
David J. Sugg, Eastman Kodak Company, Dayton, OH

Statistical Process Control for Reel-to-Reel Plating: Thickness Control on Short Runs 27
Dale Miller, P.E., C.Q.E., Consultant, Harrisburg, PA, and David J. Sugg, Eastman Kodak Company, Dayton, OH

TQM Implementation in a Plating Environment 37
Paul Horgan, Quality Golden West, Yorba Linda, CA

SESSION B
Research

A Microstructural Evaluation of Fe-Zn Couples by Cross-Section Transmission Electron Microscopy 43
Lucille A. Giannuzzi, CEF, Paul R. Howell, Dr. Howard Pickering and Dr. William R. Bitler, Department of Materials Science & Engineering, The Pennsylvania State University, University Park, PA

Plating of Iron-Nickel Alloys in the Presence of Organic Additives 53
Dr. B.N. Popov, Ken-Ming Yin, and Dr. R.E. White, Department of Chemical Engineering, Texas A&M University, College Station, TX

Electroformed, Single-Piece, Cassegrain Mirror 75
Darell Engelhaupt, Chen Feng and John Cernosek, University of Alabama, Huntsville, AL

Compositionally Modulated Alloys 81
Dr. D. S. Lashmore, Laboratory for Materials Science and Engineering, National Institute of Standards and Technology, Gaithersburg, MD
Paper Not Available in Time for Publication

Electrochemical Array Sensors for Plating Waste Stream Monitoring 83
Robert S. Glass and Keith C. Hong, John C. Estill, Robert A. Reibold, Wade M. Thompson, Dennis W. O'Brien, and Dino Ciarlo, Lawrence Livermore National Laboratory, Livermore, CA and Victoria E. Granstaff, Sandia National Laboratory, Albuquerque, NM

Electrodeposition Modeling of Nickel-Iron Alloys in the Presence of Organic Additives 103
Ken-Ming Yin, B.N. Popov, and R.E. White, Center for Electrochemical Engineering, Department of Chemical Engineering, Texas A&M University, College Station, TX

SESSION C
Light Metals

Micro Finish Hard-Anodized Coatings on Aluminum 123
Chris Steffani, CEF, Lawrence Livermore National Laboratories, Livermore, CA

The Hot-Cold Impregnation of Anodized Aluminum Influences the Impurities on the Porous-Layer Barrier of the Sealing Bath 133
Xavier Albert Ventura, Barcelona, Spain

Mechanical Properties of Anodized Aluminum Coatings 143
Robert S. Alwitt, Boundary Technologies, Inc., Buffalo Grove, IL and R. Craig McClung, Southwest Research Institute, San Antonio, TX

Recycling Chemicals on the Anodizing Line - Cost Savings and Quality Improvements 153
Kevin Munns, P. Eng., Eco-Tec Inc., Ontario, Canada

SESSION D
Physical Vapor Deposition
Organized by the Society of Vacuum Coaters

An Introduction to Physical Vapor Deposition (PVD) Process 177
D.M. Mattox, Society of Vacuum Coaters, Albuquerque, NM

An Electroplater's View of PVD Processing 185
J.W. Dini, Lawrence Livermore National Laboratories, Livermore, CA

Production Techniques for Large-Area PVD Coatings 207
D.L. Chambers, DC Industries, Columbus, OH
Paper Not Available in Time for Publication

High Volume Automotive-Type Aluminum Coating by Ion Vapor Deposition 209
Graham Legge, Abar Ipsen Industries, Bensalem, PA
Paper Not Available in Time for Publication

TiN Coatings for Wear Resistance and Gold-like Decorative Coatings 211
M.E. Graham and P. Chang, Basic Industry Research Laboratory, Northwestern University, Evanston, IL

Decorative and Wear-Resistant Coatings by PVD Processing 217
D. Butrymowicz and J.R. Snyder, Leybold Technologies, Enfield, CT
Paper Not Available in Time for Publication

Ion Vapor Deposition of Aluminum 219
Brian T. Nevill, Embee Incorporated, Santa Ana, CA

SESSION E
Surface Finishing— The Year 2000 & Beyond

Papers were not prepared for publication for this session.

Industrial Finishing—The Year 2000
Michael A. Pfaff, President, Metal Finishing Suppliers Association, USA (business affiliation: MacDermid, Inc., Waterbury, CT)

Surface Finishing in 2000: A European View
Dr. David R. Gabe, Honorable Secretary General of the International Union for Surface Finishing (business affiliation: Institute of Polymer Technology & Materials Engineering, Loughborough University of Technology, Loughborough, Leicestershire, UK)

Future Trends in the Electroplating Industry in the Asia/Pacific Region
Tadao Hayashi, University of Osaka Prefecture, Osaka, Japan

The Manufacturing Vision for the 21st Century
Charles Kimzey, Chief, Manufacturing Programs Div., Office of the Assistant Secretary of Defense, Washington, DC

Finishing for Space Applications
Mitch Mendrek, Materials & Structures, Marshall Space Flight Center, Alabama

Opportunities for Industry Collaboration with Governmental Laboratories
John Hnatio, Director, Technology Management Group, Department of Energy Defense Programs, Washington, DC

The Role of the AESF in the Year 2000 and Beyond
Richard O. Watson, CEF, AESF First Vice President, Benchmark Chemical Corp., Indianapolis, IN)

Surface Technology in the Service of Society
M. Schlesinger, Dept. of Physics, University of Windsor, Canada

SESSION F
Electronics I

Trends in Precious Metal Plating Within the Connector Industry 233
Ken Fleck, Fleck International, Huntington Beach, CA

Microhardness Testing of Plated Coatings: Defining Precision and Bias for ASTM B578 263
Jack Horner, Allied-Kelite Division, Witco, New Hudson, MI

The Relationship Between Vickers Hardness and Universal Hardness 277
Prof. Dr.-Ing. W. Weiler, Physikalisch-Technischen Bundesanstalt in Braunschweig, Germany

Solderability Characteristics of Palladium, Palladium-Nickel, Hard and Soft Gold Electrodeposits 285
I. Kadija, J.A. Abys, E.J. Kudrak, J.J. Maisano, AT&T Bell Laboratories, Murray Hill, NJ

Magnetic Properties and Structure of Cobalt-Hardened Gold 305
Dr. David Kahn, AMP, Inc., Harrisburg, PA

Scanning Tunneling Microscopy Studies of Electrochemical Deposition 343
Michael P. Green and Karrie J. Hanson, AT&T Bell Laboratories, Murray Hill, NJ

SESSION G
Environmental I

Insurance Coverage for Environmental Liability 355
John S. Vishneski III, Keck, Mahin & Cate, Chicago, IL

Environmental Issues Associated with Financing of an Electroplating Facility 363
Roger A. Dhonau and Sec Donohue, Pace Incorporated, Warrendale, PA

Pollution Prevention Planning for Electroplaters 371
Daniel P. Reinke, P.E., Capsule Environmental Engineering, Inc., St. Paul, MN

Assessment and Options for Waste Minimization in the Metal Finishing Industry 379
Dr. Clifford W. Walton, CEF, and Kevin J. Loos, University of Nebraska-Lincoln, Department of Chemical Engineering, Lincoln, NE

Application of Microcomputers as a Technical Resource for Identification of Pollution Prevention Opportunities in Metal Finishing/Electroplating Operations 393
Lisa Wilk, P.E. and Robert Capaccio, P.E., CChE, DEE, Mabbett, Capaccio & Associates, Inc., Bedford, MA

SESSION H
Aqueous Cleaning

What Are Our Cleaning Options? 399
L.M. Thompson, R.F. Simandl, H.L. Richards, A.L. Glover, Martin Marietta, Oak Ridge, TN

Impingement: The Key to Effective Aqueous Cleaning 413
Michael J. Rowney and Stephen D. Temple, Ransohoff Corporation, Hamilton, OH

Membrane Filtration 423
Tom Weaver, Prosys Corporation, Chelmsford, MA

Recycling and Recovery of Cleaning Solutions 431
Tom Weaver, Prosys Corporation, Chelmsford, MA

Cleaning—Emerging Technologies 439
Bob Srinivasan, EPI Electrochemical Products Inc., New Berlin, WI

SESSION I
Environmental II

Waste Minimization Via Source Reduction for the Plater Pt (III). Source Reduction Initiatives: The Prerequisite to Closed-Loop 443
Dr. D. Paul Piplani, CEF, Acteron Corporation, Redwood City, CA
Paper Not Available in Time for Publication

Electrochemical Processing for the Minimization of Waste in the Electroplating Industry— A Critical Review 445
Prof. Dr. Andreas Moebius, Langhein-Pfanhauser Werke AG, Neuss, Germany

Evaluating the Economics and Effectiveness of Source Reduction Options in Metal Finishing 451
Matthew L. McCullough, P.E., McLaren/Hart, Irvine, CA

Silver Recovery with Ion Exchange and Electrowinning 467
John Lindstedt, Artistic Plating Company, Inc., Milwaukee, WI and Mike Doyle, P.E., Triad Engineering, Inc., Milwaukee, WI

Pollution Prevention with Advanced Technologies: A Success Story With a Payback 483
Michael G. Green, Bio-Recovery Systems, Inc., Las Cruces, NM

SESSION J
Electronics II

Growth Morphology and Melting Characteristics of Electrodeposited AuSn Eutectic Alloys 491
G. Holmbom, M. Svensson, Centre of Industrial Microelectronics and Materials Technology, Linkoping University, Linkoping, Sweden and J.A. Abys, H.K. Straschil, AT&T Bell Laboratories, Murray Hill, NJ

New Autocatalytic Gold Bath and Diffusion Barrier Coatings 511
Charles D. Iacovangelo, Advanced Inorganic Materials Laboratory, GE Corporate Research and Development, Schenectady, NY

Bumping Process on Integrated Circuits by Electroless Plating 531
Charles W. Lin, Ian Yee, and Brad Nelson, Microelectronic Computer Technology Corporation (MCC), Austin, TX

Laser-Induced Gold Deposit on InP Substrates 541
Wang Xuhong, Yu Zuzhan and Zhao Guoqing, Fudan University, Shanghai, People's Republic of China

High Performance Gold Plating for Microdevices 553
Dr. A. Gemmler, Dr. W. Keller, Fraunhofer Institute of Manufacturing and Automation (IPA), Stuttgart, Germany, Dr. H. Richter, and K. Ruess, SEL-Alcatel Research Center, Stuttgart, Germany

SESSION K
Alloy Deposition

Electrochemical Deposition of Sn/Zn Alloys 575
Jean Rasmussen, Danfoss A/S, Nordborg, Denmark

Electrodeposition of Ni-Fe Alloys from Sulfate, Sulfate-Chloride and Chloride Baths 583
N. Furukawa, M. Hanabusa and T. Hayashi, Department of Applied Chemistry, University of Osaka Prefecture, Osaka, Japan

Optimization of the Alkaline Zinc-Iron Alloy Plating Bath Composition for Optimum Corrosion Results Using Taguchi D.O.E. Methodology 593
B. Dafonte, Jr. and Naomi Holmes, Quin-Tec, Inc., Warren, MI and Sally Escota, Rampart Industries, Detroit, MI
Paper Not Available in Time for Publication

Electrochemical Deposition of Zinc-Nickel Alloys in the Presence of Organic Additives 595
Dr. B.N. Popov, Ken-Ming Yin, O. Velev and Dr. R.E. White, Department of Chemical Engineering, Texas A&M University, College Station, TX

Internal Stress Control of Electroformed Nickel-Iron Alloys 629
Dr. H.M. Wu and H.J. Shy, Chung Shan Institute of Science & Technology, Taiwan, Republic of China, and Prof. Chein-Ho Huang, Chemistry Department, Soochow University, Taiwan, Republic of China

Development of High-Speed Black Electroplating Process 643
Katsushi Saito, Nippon Steel Corporation, Chiba Kimitsu, Japan

*** PAPER NOT AVAILABLE IN TIME FOR PUBLICATION ***

Achieving Competitive Edge Through the Application of Total Quality Management

Dr. D. Paul Piplani, CEF, Acteron Corporation, Redwood City, CA

The global marketplace, with a new economic order, is creating an educated consumer who is loyal only to product quality, competitive pricing, and on-time delivery with every shipment. A changed corporate culture is a must for the implementation of total quality management (T.Q.M.) to achieve first time right plating quality. This paper examines the plating specification criteria in the incoming purchase order, genuine participation by all personnel involved, and the use of quality aids, such as statistical process control (S.P.C.) to go beyond rather than just meeting minimum requirements.

*** For copies of this paper please contact the author directly:**

Dr. D. Paul Piplani, CEF
Chemist
Acteron Corporation
851 Shasta Street
Redwood City, CA 94063
415/369-5217
Fax 415/364-9748

PRACTICAL GUIDE FOR MEASURING HD UNDERCOAT THICKNESS

Fujio Matsui*, Teresita E.Guiala*, David J.Liston*
and Yasuyuki Yamamoto**
* Uyemura International Corporation, Ontario, California
** C. Uyemura & Co. Ltd., Tokyo, Japan

ABSTRACT

This paper will discuss and review various methods of thickness measurement of Ni-P undercoat on aluminum magnetic hard disk (HD). Accurate measurement of these films is of considerable importance due to the trend of the hard disk industry towards smaller size disks as well as thinner Ni-P undercoat.
Focus will be on the X-ray Fluorescence (XRF) method, pointing out the different variables effecting the accuracy of this method.

Introduction

The magnetic disk drive industry is still experiencing market growth evidenced by a smooth spiral in electroless nickel (EN) sales. There has been major shifts during recent years. Industry publications have expressed that the market has boomed for the 3.5-inch drives while the larger format 8-inch and 14-inch drives is *almost gone* . The personal notebook computers have moved to a 2.5-inch and 3.5-inch format disk drives.[1] Keeping up with technology advances, price competiveness and changing conditions remain as barriers for the magnetic disk industry's success.

Not only has the size of the disk decreased, the high phosphorous (12%) EN coating thickness has also decreased. We are seeing that where 30-40μm thicknesses were common, now 6-10μm has become common. Cost increases in proportion to the plating thickness, so we must be able to provide a sufficient film thickness, corrosion resistance, wear resistant and a durable non-magnetic surface.

The process of selecting a measurement method requires you to consider accuracy, the cost of the measuring device, repeatability and confidence levels. Accurately measuring the thickness of the undercoat poses a significant challenge as films become thinner.

Four basic thickness measurement techniques are gravimetric, microscopic cross sectioning, beta backscatter and, X-ray fluorescence (XRF). The trend over the past years has been away from

the first three stated above and toward XRF.[2] XRF is favored mainly because of the accuracy and repeatability that can be achieved with minimal measurement times. XRF is capable of better than ±5 % accuracy, especially where extra precautions are taken to eliminate errors. Acquiring significantly greater accuracy would be difficult because of the inherent roughness of the substrate and the coating surface themselves.

Comparison of the different thickness measurement methods for high phosphorous content electroless nickel (HPEN) hard disk undercoat.

Gravimetry (two-types, non-destructive [weight gain] and destructive.): Non-destructive: Accuracy using this method causes the result to be affected by the loss in weight during etching due to the dissolution of the Al substrate material.
Destructive method: Ni-P/Al plated parts are dissolved in 10% w/v NaOH allowing nickel to peel-off from the Al substrate. The dry Ni foil can then be weighed. Thickness is calculated as equal to weight of Ni divided by the product of the density and the area.[3] This destructive method is considered the most accurate and a good reference.

Microscopic cross section (destructive, optical): Good reference. The coating thickness is measured in a magnified image of a cross section of the coating. Normal metallographic procedures are used for mounting, polishing, and etching the specimens. A filar micrometer ocular or image-splitting eyepiece is used to measure the thickness. In some instances, the image is projected onto a ground glass plate, the measurement is made with a ruler at an appropriate magnification.[4] This is accurate for films of about10-100 μm ± 5%. Thickness capability is dependent on microscopic equipment used and skilled technician.

Beta backscatter (non-destructive, mass per unit area method): The principle of beta backscatter is that when beta particles impinge upon a material, a certain portion are backscattered. The intensity of the backscatter can be used for the measurement of mass per unit area of the coating, which is directly proportional to

the thickness. Measure thicknesses ranging from 0.5 - 40 µm. For best accuracy with the backscatter method, appropriate isotope for the target coating and to have standards established for each turnover to adjust for phosphorous increase. Two disadvantages of beta backscatter are that frequent calibration is necessary to compensate for decay of the isotope material.[5] Second is that parts to be tested come in contact with the isotope probe and this will leave surface marks that may affect the integrity of the HD undercoat deposit, especially after polishing.

X-Ray Fluorescence (non-destructive, mass per unit area method): A contactless measurement that indicates thickness by directing an X-ray beam through the coating . The beam is absorbed and the amount of absorption yields an instanteous readout of thicknesses between 0.5µm-30µm. Advantages are the ability to measure every part, with very high speed and without contacting and destroying the test piece. Areas as small as 2 mm in diameter can be measured.[6] Disadvantages are the one-time cost of the special equipment and the upper limitation to measuring thickness.

Table 1 Compares the different methods.

Gravimetric		Cross-section	Beta Backscatter	XRF
Non-destructive	Destructive	Destructive	Non-destructive	
Plating operator	Skilled technician		Plating operator	
Less than 60 sec.	More than 1 hour		Less than 60 seconds	
Common laboratory equipment			Speciality equipment	
0.4 µm-unlimited		10-100 µm	0.5-40 µm	0.5-30 µm

Based on the above data , we chose to explore to explore applications of XRF for measuring Hard-disk electroless nickel undercoating.

XRF Experimental Details

The following experiments were carried out using a Seiko SFT-157 Fluorescent X-ray Coating Thickness Gauge. The phosphorous content was set at 12% unless otherwise specified. X-ray intensity was 10 for collimator size 0.1 and 0.3 mm and X-ray intensity 4 was used for collimator 1.0 mm. The instrument was calibrated with 4.93µm and 21.1µm Ni standards on Al; and with Ni, Al and 10.6 wt.%P Ni-P infinite standards .

Effect of measurement time
The thickness of a Ni-P foil (5, 10, and 15μm) on aluminum was measured 30 times using different count times (2,5,10,20,30,60 and 100 sec.).

Effect of different collimator sizes
The thickness of Ni-P foils on Al of various thicknesses were measured using different collimator sizes (0.1, 0.3 and 1.0 mm). The count time for each measurement (10 trials) was 60 seconds.

Effect of Z-stage height
The thickness of Ni-P /Al magnetic disk (approx. 13 μm) was measured for 30 sec. (10 trials) using a collimator size of 1.0 mm with the sample stage at different heights, ranging from 5 mm below to 3 mm above the focal position*. This experiment was also performed using collimator sizes of 0.1 and 0.3 mm.
* The point where the sample parts appears clear with defined sharp image when viewed through the C.R.T. monitor .

Effect of thickness of the Al substrate
The thickness of Ni-P foil was measured with increasing number of Al foil pieces (0.02 mm per piece) using a measurement time of 20 sec. (10 trials). The procedure was repeated until the thickness of the Al was 0.3 mm.

Effect of Phosphorous content
The thickness of a 22.1μm Ni-P/Al disk with a phosphorous content of 12.3% was measured using a collimator size of 1.0 mm using different % P content in the calibration.

X-ray drift
The thickness of a Ni-P/Al standard disk was measured over time to check for any shift .[7]

Results and Discussion

We found these six factors which influence the measurement of thickness of Ni-P films on Al.

1. Measurement time
2. Collimator size
3. Position of stage
4. Thickness of substrate
5. Phosphorous content
6. Instrumental drift over time

1. Effect of Measurement Time

Measurement time is the length each measurement lasted. The results in figure 1 show that the accuracy and precision of the measured Ni-P thickness can be increased with an increase in the measurement time, until a maximum point where any time increase had no significant effect.

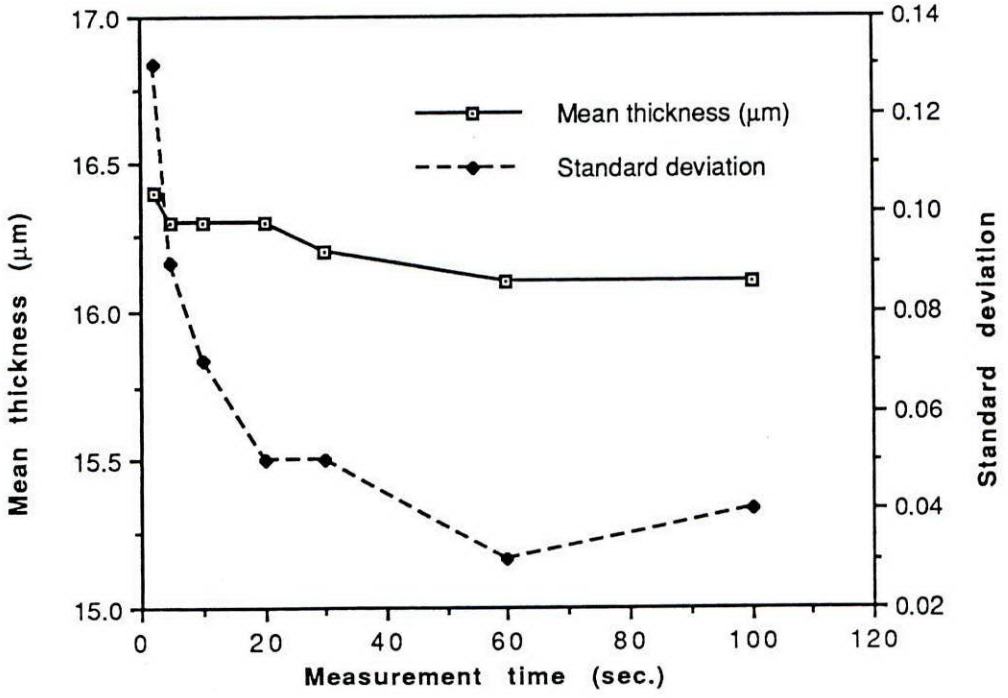

Figure 1 Effect of measurement time on the Thickness of Ni-P film on aluminum.

Similar trends were observed using a 5μm and a 10μm Ni-P foils on Al. The standard deviation decreased with measured thickness. These results suggest reliable thickness with 95% confidence level for both 0.3 mm and 1.0 mm collimator size can be obtained using a

measurement time of 10 seconds. However, even better results were obtained with slightly longer times. For example, using the 1.0 mm collimator most reproducible results to measure a Ni-P film of about 15μm in shortest time was when measurement time of 20 seconds was used .

However, your production situation will dictate whether the time required obtaining the extra precision is cost efficient.

2. Collimator size

XRF Coating Thickness Gauges are designed to measure film thickness on small areas by focusing the X-ray beams from the X-ray tube into a concentrated ray. A collimator is used for this purpose.

Cross section is a good reference to counter-check XRF results. One direct way of comparing accuracy is to graph the measurements from one method against the other. Thus, the results in figure 2 show that the best overall correlation of the thickness obtained using these two methods was found using a 1.0 mm collimator.

For Ni-P films with thicknesses below 20μm , the deviation of the thickness obtained using the 2 methods was less than 2.5%, using collimator sizes of either 0.3 mm or 1.0 mm; however, for the 0.1 mm collimator, the thickness difference was up to 8%.

The error in the measurement of Ni-P/Al thicknesses outside the range of calibration, that is in the present study below 5μm and above 21μm showed a tendency to increase with the thickness of the Ni-P coating. Thus, the small deviation of less than 0.5% for the 58.4μm Ni-P film using the 1.0 collimator is misleading as the XRF measurement above 40μm-50μm is generally less than that obtained by cross-sectioning. This is in contrast to the situation using the smaller collimators (0.1 mm or 0.3 mm) where the XRF measured thickness showed an increase, after 25μm compared to the cross-sectioned thickness measurement.

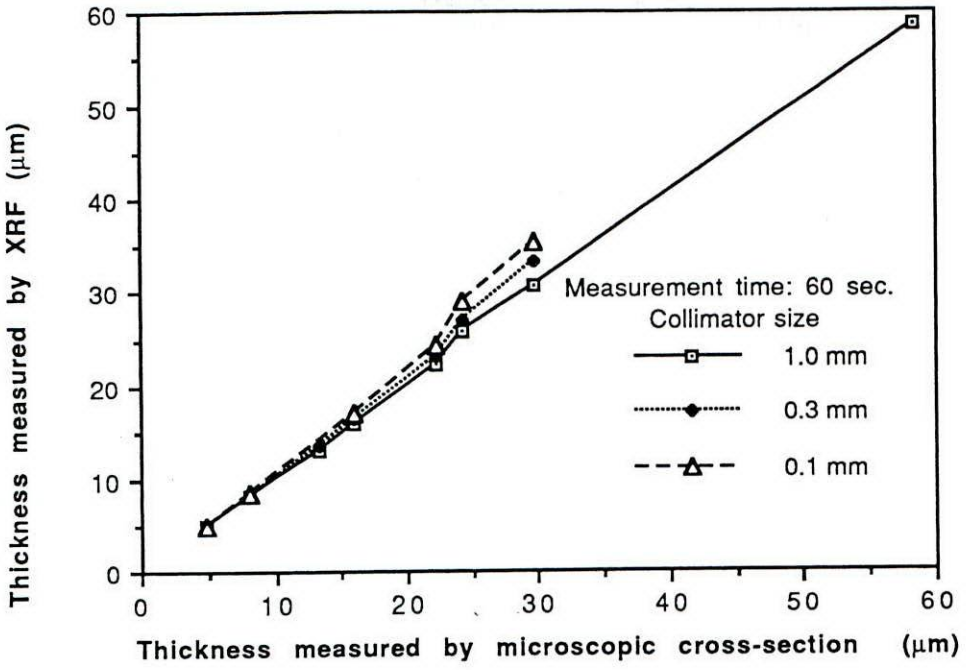

Figure 2 Effect of collimator size on the thickness measurement of Ni-P films on alluminum alloy.

The collimator size also has a large effect on the reproducibility of the measurement as the smaller the collimator the larger the measurement's standard deviation for a given measurement time and coating thickness.

3. Effect of the Position of the Sample

The sample is positioned on the stage and its height is adjusted so that the image of the sample on the C.R.T. monitor is in focus. The results in figure 2 show the effect of changing the position of the sample in the Z- direction on the thickness measurement.

In some of our experiments the position that corresponded to the highest thickness position was not the focus position ,in fact, the image was just out of focus at the highest thickness reading. This was also confirmed with a different collimator size and by testing on another XRF instrument.

The position of the Z-stage can be changed by about 3.5 mm and still obtain a measurement with a 95 % confidence level.

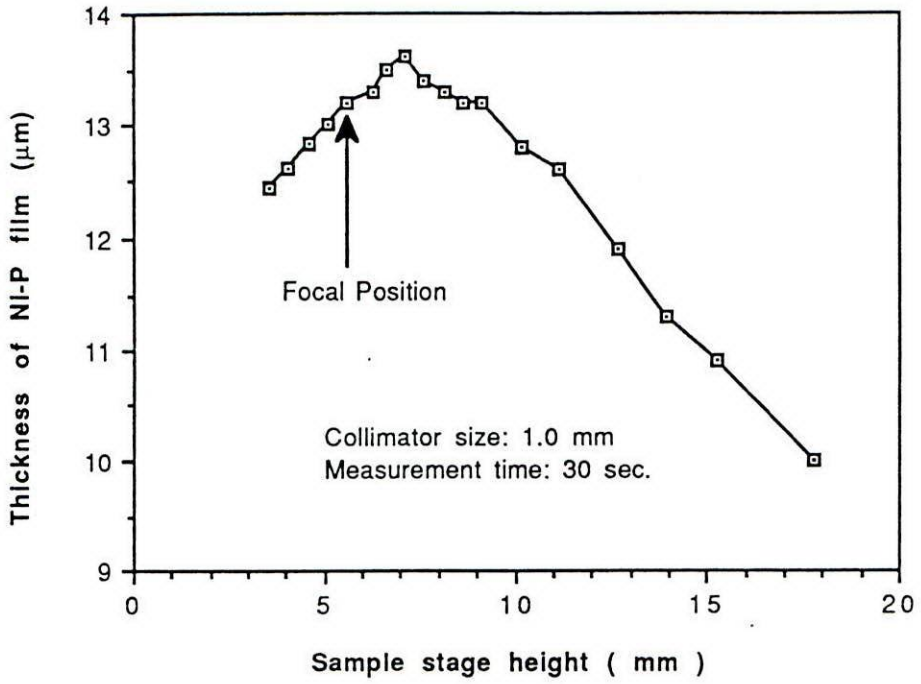

Figure 3 Effect of changing stage height on the thickness measurement.

4. Substrate Thickness

Below are data from current industry producers. As you can see, not only is the physical size of the disk being reduced, but the disk thickness itself is being forced down by the demand for compactness.

Table 2 Thicknesses of Al substrate currently being manufactured for HD.

Outer diameter (mm)		Thickness (mm)
210	8-inch	1.8
130	5.25-inch	1.8
95	3.5-inch	1.2
95		0.88
65	2.5-inch	0.86
50	2-inch	0.58*
36	1.5-inch	0.38*

* The thickness of the 36 mm and 50 mm disk is not yet a function of the market place as these are not in wide commercial use yet.

In regards to the substrate thickness, it is known that silver coatings[8] for example, are influenced by the thickness of the underside film, especially if the substrate is thin. This phenomena can be understood from the following diagrams - one where the substrate is regular and the other where the thin substrate allows for the secondary fluorescent X-ray is from the underside coating as well as the base material.

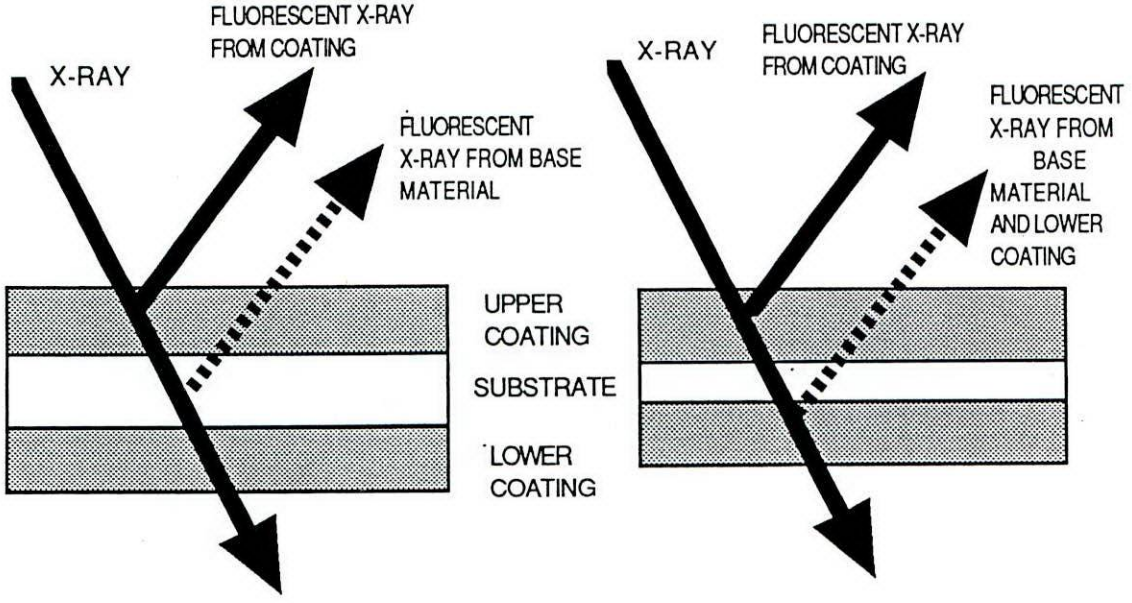

Figure 4 Theoretical effect of decreasing the substrate thickness.

The results in figure 5 (next page) show that a thickness of the Ni-P film can be obtained with 95% confidence if the substrate is over 0.12 mm. Thus, for the present, this effect is negligible, however, care should be exercised in the future to take this phenomena into account.

5. Phosphorous content

XRF measurements are based on conversion of mass per unit area to thickness, the coating density must be accounted for when using this method. The phosphorous content in a Ni-P film affects the density of the deposit and thus at least a close approximation of the deposit's phosphorous must be entered into the calibration. The results in figure 6 show that the phosphorous content entered at the time could only be changed by about ± 1% to obtain a thickness with a 95% confidence level.

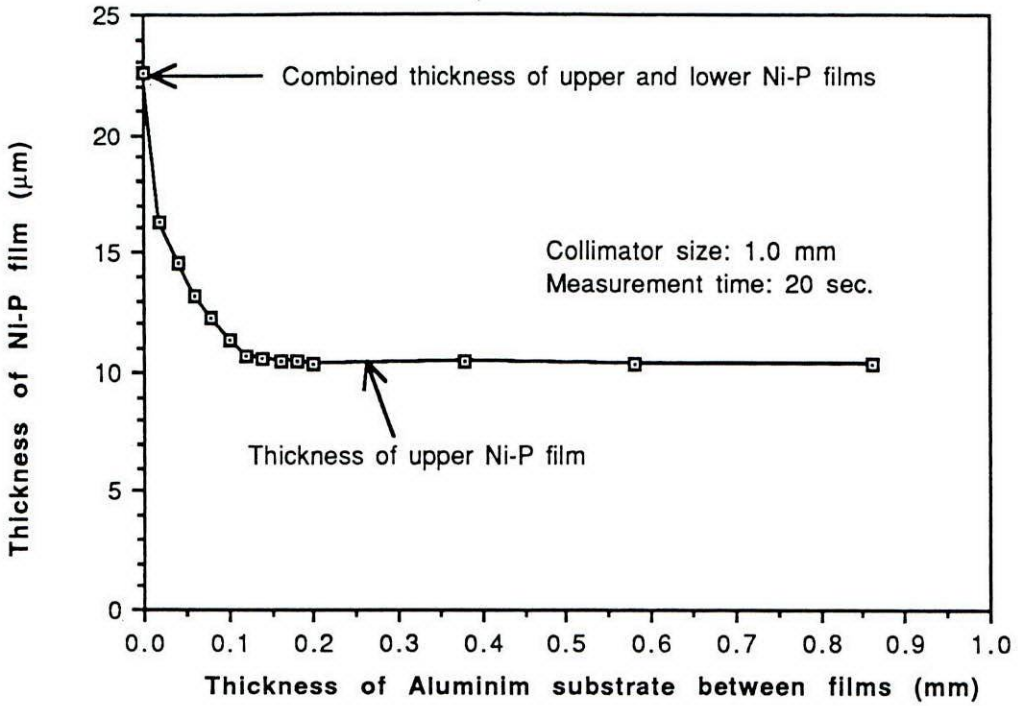

Figure 5 XRF measurements with Al substrate size changes.

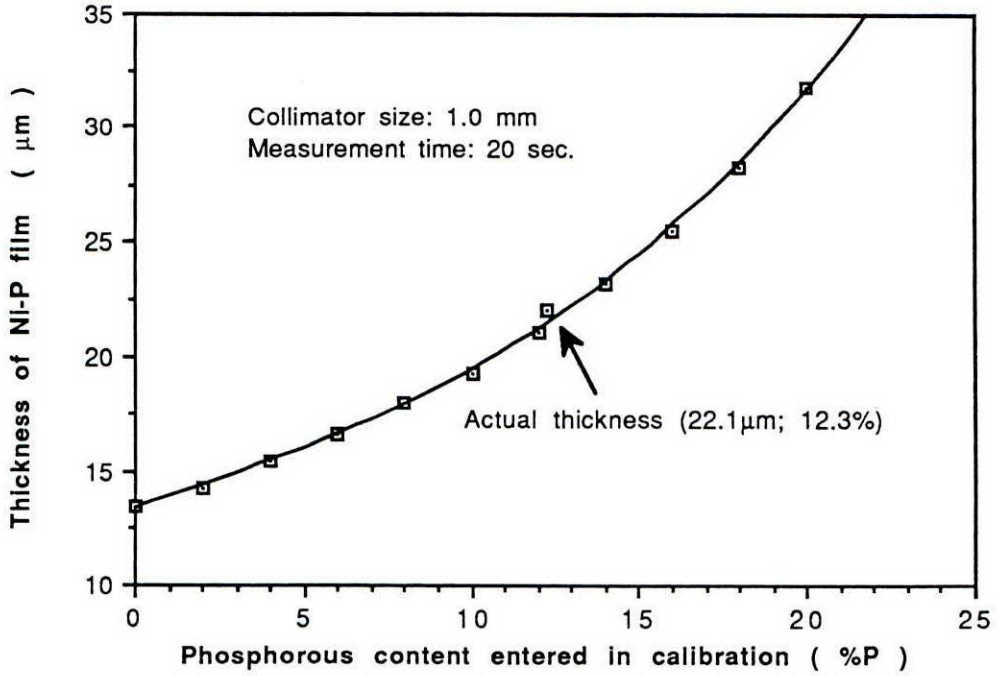

Figure 6 Effect of Phosphorous content on Ni-P film thickness.

6. Instrumental Drift with Time

Note that another source of inaccurate readings is the uncorrected drift of the X-ray detector and/or tube. You will need to determine for yourself, the correction interval that will work best for your operation. Drift was tracked by plotting the thickness of a Ni-P film (10.8μm) on Al over time when no corrections were made (Figure 7). Over a period of 8 hours, the thickness drifted downward by about 0.03μm. The coefficent of variation was 0.3 %, hence no correction factor was necessary in our case, to maintain a 95% confidence for 8 hours.

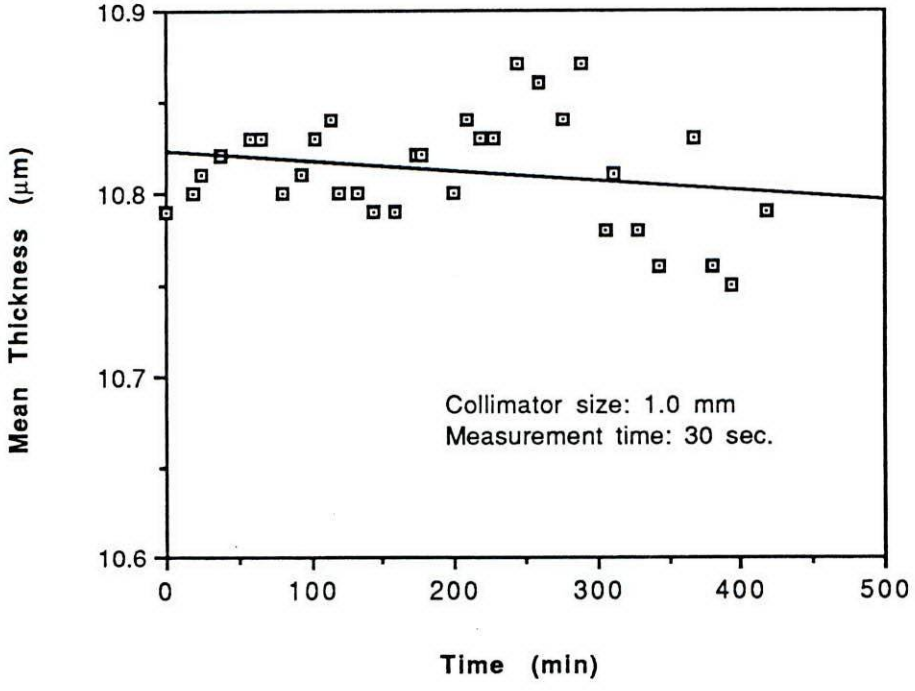

Figure 7 X-ray drift (average thickness vs. time)

Summary

Ensuring precision and accuracy of Hard disk Ni-P undercoat thickness measurement using X-ray fluorescence method requires:

1. Measurement time: The longer the measurement time, the more precise and accurate the result . Production application of 10 seconds produced relatively good results.

2. Position : Focus distance between the sample and the collimator determines the confidence level of the measurement. This varies from instrument to instrument, if absolute rather than relative data is desired , you will need to experiment with ideal positioning for your application.
3. Collimator size: Exposing the maximum area, especially for thicker deposits gave a more precise measurement. Larger measurement area lessens any localization effect. We would recommend 1.0 mm collimator for use in the hard disk industry.
4. Substrate thickness: As disks have become smaller they have also become thinner. As this trend progresses to even thinner aluminum alloy substrates, the thickness measurement techniques for the EN undercoating are sure to be effected.
5. %P: Take extra care to enter the proper phosphorous content in the calibration to maximize the accuracy of your measurement using XRF equipment.
6. Instrument drift: Protecting against natural drift in X-ray test equipment is the responsibility of you, the user. To maintain the XRF instrument at its ideal calibration before testing a sample , read the pages relating to calibration procedure in the USER GUIDE. The time spent doing this will prove worthwhile.

References

1. Arensman,R., Electronic Business Asia, Nov. 1990, p. 77.
2. Hoffman,P.L., "Thickness Measurement on Electronic Connectors: The Key to Plating Process Control", Plating and Surface Finishing, Sept. 1985, p. 20.
3. Sajdera,N., Thickness Testing, Metal Finishing, Vol. 88, No. 1A (1990) p. 552.
4. Ogburn,F. , Methods of Testing; F. Lowenheim, Ed.; In Modern Electroplating, 3rd ed. N. J.,1974 ; p. 686.
5. ASTM Designation B 567-91, Measurement of Coating Thickness by Beta Backscatter Method, American Society for Testing and Materials, 1991.

6. ANSI/ASTM A 754-79, Coating Thickness by X-Ray Fluorescence, American Society for Testing and Materials, 1979.
7. Seiko Instruments & Electronics Ltd., Fluorescent X-Ray Coating Thickness Gauge Operation Manual, Stability Check, p. 153.
8. Koga, T. and Tomoda, K. ; Kinzoku (Jap.), July ,1982, Special Ed., pp. 1-6.

WHY JOHNNY CAN'T DO SPC

By: David J. Sugg
Eastman Kodak Company
Dayton, Ohio

ABSTRACT

Increasingly American businesses must concern themselves with the problem of illiteracy. Vast percentages of the young workforce cannot even read well enough to understand a bus schedule, much less a complicated process specification. Related to this problem is innumeracy, the inability to deal with mathematical ideas, or even simple arithmetic.

This problem becomes particularly acute when a company seeks to start a Total Quality Management program. How can you teach someone to do SPC who can't read, or calculate an average? How can you talk about percent defective to someone who cannot understand the idea of 'percent'?

This paper provides some suggestions on how to deal with these problems in the modern workplace. Examples will be given of a new control chart that does not require any calculations. Emphasis will also be placed on the use of visual or graphical means of communication to supplement more traditional written communication.

THE PROBLEM DEFINED

For many years we have heard about the illiteracy problem in this country. A nation that once prided itself on having the highest literacy rate in the world, has seen a steady decline in the percentage of its citizens that can read at even modest levels.

Experts give many reasons for the decline. Some claim that television has taken away the motivation to read. At one time, a young person had to read a book to 'escape' into fantasy. Now, a push of the on-off button provides the same 'escape.' Instead of spending hours lost in books, young people (and old!) now spend those hours as 'couch potatoes' in front of the 'boob tube.'

Others cite the change away from the use of phonics in reading instruction as the source of the decline. With only a knowledge of words they could 'sight read,' students coming across a new word had little idea how to continue. With an understanding of phonics, the student could at least sound out the word, and perhaps recognize it from their spoken vocabulary.

More recently, the poor math skills of most high school graduates have also become a major concern. This concern ranges from the inability to add, subtract, multiply and divide; to the failure of most to understand the more complicated math behind risk assessment. How do we expect someone who cannot even calculate an average, to understand that simply being below average does not mean that something

is wrong? Author John Allen Paulos gave the name "Innumeracy" to this lack of math skills, corresponding to Illiteracy for a lack of reading skills.[1]

As with illiteracy, the experts cite many causes of innumeracy. Some claim that the arrival of electronic calculators totally destroyed student's ability to do even basic math without one. Others claim that the 'New Math' emphasis on set theory in the early sixties did not leave time for drilling on the basic skills.

Whatever the cause, business today must deal with the effects. In 1990, Motorola announced that 80 percent of job applicants could not pass a test involving seventh-grade English, and fifth grade Math. As shocking as this seems, I find it even more shocking that **only 20 percent could even read a bus schedule!** Sixty percent of the applicants could not make change for a three-dollar meal.[2]

WHY SHOULD BUSINESS CARE?

Some respond to such evidence in the typical U.S. business fashion. Once you discover a problem, look for WHO is responsible, and blame them. Business leaders across the country have blamed illiteracy and innumeracy on everyone from their local school board to the President of the country.

Still others have responded to these problems by saying it is not their problem. It is the schools' job, and the government's, to deliver an educated work force to the employer's front door. It is business's job to make product, not train employees in basic reading and writing skills.

We must concentrate on **HOW** we can **CORRECT** the situation that now exists, and **PREVENT** it in the future, if we want to survive in the world marketplace. Pointless debates about whom we can blame will not solve the problem. Business must become part of the solution to illiteracy and innumeracy.

Perhaps an example will show why business must take these problems seriously. I recently read of a case where an employee of a fast food restaurant accidentally entered $ 100 instead of $ 1.00 for the money given by a customer for a cup of coffee. The employee looked at the 'change' portion of the cash register display, and started counting out $ 99.50 in change, even though he knew the customer had given him only one dollar. If the machine said $ 99.50, then it must be right.[3]

More ominously, if someone cannot read, how can he understand a warning label? How can he tell the difference between a drum label that reads "Cyanide Salts," and one that reads "Acid Salts"? The ability to tell the difference could be the difference between life and death.

How can your business comply with the "Right To Know" regulations, if your employees cannot read or write? How can they pass a written test showing they have not only attended a training session on hazardous chemicals, but also that they understood what they were taught?

WHAT CAN BUSINESS DO?

Some businesses respond to the problems of illiteracy and innumeracy by refusing to hire anyone who does not have basic reading and writing skills. This prevents the situations described above from happening, at least with new employees.

What about those people already employed? Should you fire someone who cannot 'read, 'rite, or do 'rithmatic? Can you legally fire an existing employee you learn is illiterate? Even if you legally have the right to fire them, should you? Do you have any responsibility to help the employee learn the skills needed to keep their jobs?

If we define quality as "minimizing the total loss to Society," as Dr. Taguchi has, then I believe we understand that we must do more than simply weed out the illiterate and innumerate. We must be part of the solution to the problem.

I believe that business should look at the problem of illiteracy and innumeracy from the viewpoint of supply and demand. If any item of commerce has a demand more than supply, the price will rise. If business only weeds out the illiterate and the innumerate, and if the percentages given above accurately represent the population, then the business community will soon find itself short of an item of commerce, labor. When this shortage comes, labor rates for the literate and numerate will rise. Labor costs for surface finishers typically run from 30 to 50 percent of sales. Any increase in labor cost quickly multiplies the cost of the product produced. If for no other reason, business must solve the problems of illiteracy and innumeracy to preserve profitability.

THE SOLUTIONS DESCRIBED

We, as a country, did not fall to this low level of literacy and numeracy overnight. Nor will we recover overnight. The solution to these problems will require a massive effort sustained over time.

As with any business problem, our response to the problems of illiteracy and innumeracy must take three approaches. First, we must seek short term relief from the problem, so we can continue to ship product and make money. Second, we must develop corrective action procedures to deal with the affected "product." Third, we must seek long-term, fundamental solutions, which seek to eliminate the cause of the problems.

The short term solutions take the form of "band-aids." These allow us time to complete the longer term activities. They must not supplant the long term activities. We must view them as temporary aids, buying time to find and start using the longer term solutions.

The numbers given above make the need for corrective action steps self-evident. It will take time to turn our educational systems around. During that time, more illiterate and innumerate students will come out of our schools. Business must deal with the reality of illiteracy and innumeracy among present employees, and those they will hire in the future.

The long term activities seek to correct, and control, the fundamental causes underlying the problems. To deal with these causes we must first discover them. Once we uncover the root causes, we must then find ways to eliminate, control, or compensate for them.

To illustrate the three steps, let's assume that we discover a leak in the roof of our house. The leak is so severe, water is coming through our living room ceiling! Our short term tasks may include putting out pots to catch the water, and spreading a tarp over the area of the roof that is leaking. Our corrective action tasks may include wiping up the water, drying out the carpet, or patching the roof temporarily. Our long term tasks may call for replacing the roof.

THE SHORT TERM TASKS

1. THE VISUAL FACTORY

The visual factory offers a powerful tool to overcome the obstacle of illiteracy in the workplace. Simply stated, the visual factory replaces written forms of communication with graphical, or pictorial forms. Instead of issuing status reports in writing, with tables of data, you convert the information into graphs, and charts.

The visual factory makes use of pie charts, trend charts, histograms, and scatter diagrams to convey numerical information. These charts do not simply use lines and dots to get the message across. Dollar Signs ($), or dollar bills, replace bars in Pareto Diagrams, to remind everyone that each defect costs money. You can use other symbols, as needed, to make the chart meaningful.

Process specifications in the visual factory contain many diagrams, photographs, and flow charts; not just words. If the operator controls the color of the part, include color swatches showing the right color. A drawing, or photograph, showing the proper way to put the part on the plating rack will prevent many more racking problems than any verbal description.

Using the elements of the visual provides many side benefits to the literate. It takes much less time to review a trend chart for sales, than to review several columns of data in a sales report. Improved retention of the information in the chart comes from presenting the same data in different ways. Prevention of defects, through comparing colors with swatches for instance, can be made easier, reducing defects.

2. USE THE BUDDY SYSTEM

Another short term task to reduce the impact of present illiteracy and innumeracy involves the use of the buddy system. The buddy system teams two, or more, workers together. Ideally, this approach produces a 'synergy,' with the whole greater than the sum of the parts. An employee with good reading and writing skills teams up with one, or more, employees with weak reading and writing skills. The literate employee reviews the paperwork for all jobs before processing. They then explain written instructions verbally, or graphically, to the less literate employees.

I think that the typical management team offers an appropriate analogy for the buddy system. Not every member of Management is 'literate' in the language and techniques of finance. Instead of weeding out managers who do not understand finance, as well as their own discipline, we have a specialist as a member of the team who can explain the financial information about the company.

Many companies already use a form of the buddy system. They have employees who mask parts better than others, so on critical jobs they do the masking. Other employees are better at racking, and fixturing. On the same critical job, they take the masked part from the other employee, and rack it for plating. Perhaps another team member inspects the finished part for compliance to specifications.

I will freely admit that, in both examples, it would be preferable that everyone could do every job, interchangeably. This offers the company the greatest flexibility and safety. While this may be preferable, it is far from necessary.

Wise partnerships draw on the unique strengths and abilities of each partner. Where one partner lacks a needed skill or knowledge, the other partner supplies that skill or knowledge. It will take time until remedial education of the illiterate and innumerate among our employees can take place. Until then, carefully selected partnerships of employees, through the buddy system, offer a powerful tool to overcome the problems of illiteracy and innumeracy.

3. USE COMPUTERS

Computers offer a unique tool to overcome problems with innumeracy. Even if an employee cannot understand how to calculate the average and standard deviation of a data set, you can teach them how to enter the numbers into a computer, and let the computer do the work for them. In some cases the computer could be as simple as a sophisticated calculator, with statistical functions.

I have three objections to the use of computers to overcome innumeracy. First, many innumerate employees have a fear of computers, and resist using them. Many literate and numerate people fear computers, and I find that this fear usually increases with people uncomfortable with math.

I have two suggestions to overcome this fear of computers. I find that many people afraid of computers will nonetheless play computer games. Providing a computer, complete with games, for employees to play around with, will allow them to learn basic skills in a non-threatening way. Microsoft realized this when they released Windows! 3.0. To give people practice using the Windows! operating system, they included two games, Solitaire and Reversi. People with no experience using a mouse could learn how, and have some fun at the same time.

My second suggestion can be a part of the first; provide computers the employees can take home for a while. While someone may not want to sit down in public and struggle with learning how to use a game, they may do so in the privacy of their home. Perhaps their kids could even teach them how!

The second objection rests on the first law of computer science: Garbage In, Garbage Out. An employee that does not understand the idea of average, and how to calculate it, will likely not recognize a garbage number in the output. If you understand what an average is, and end up with a value for the average greater than any of your data points, you will suspect that something is wrong.

The use of automatic data checking can provide some relief from this objection. Software exists that allows specifing a range within which all input values must fall. If an employee forgets to enter a decimal point, 5567 instead of 55.67, the program signals an alarm, and asks the employee to verify the entry before proceeding. You could also use more elaborate statistical tests to check for internal consistency in the data.

Automatic data collection and analysis can provide the best solution to this objection, where feasible. Many test devices now come equipped with some type of computer interface, to allow automatic recording of the test results. Once recorded, the device can then perform the analysis required, down to outputting the control chart, with out-of-control points identified.

The use of computer based systems often leads to losing contact with the data. This underlies my third objection to computer based systems; the computer can become a large 'black-hole,' into which data enters, never to be seen again. If you fill out an SPC chart by hand, you become involved with the data. The mere act of recording the results on the chart, makes you at least think about the location of the value compared with the control limits. In a computer based system, the computer plots the charts, and it becomes very easy to file the charts away, without looking at, or taking action on them.

If you use a computer based SPC system, it must have built-in alarms that go off when an out-of-control point occurs. Ideally, this alarm should not only tell the operator that the process is out of control, but also should guide them through the process of detecting the cause of the problem, and the corrective action required. I have only seen a few computer systems with this sophistication.

4. USE SPECIAL SPC TOOLS

Statistical Process Control offers a powerful tool to reduce process variation, and to identify sources of errors in processes. As traditionally taught, however, SPC can make demands on employees to develop mathematical abilities. At the minimum, most charts require that the operator calculate the average and the range of the value charted. When a company first introduces SPC on their shop floor, the problem of innumeracy may become visible for the first time. The problem can be so severe, that companies give up on SPC, concluding it just won't work for them.

This is why I chose to name this paper "Why Johnny Can't Do SPC" rather than "Why Johnny Can't do TQM." While literacy and numeracy are important everywhere in a TQM program, they become vital in SPC. Special SPC tools are available, however, that minimize the need for good math skills.

To overcome the need to calculate the average, you can substitute the median in its place. The median is the value greater than one-half the data, and less than one- half the data. If you arrange the data from smallest to greatest, the value in the middle will be the median. To make the task simpler, all sample sizes should be an odd-number. Typically, the sample size will be 3,5 or 7.

You can construct a fully graphical, variables control chart for the median, and the range.[4] To prepare for using this control chart, you must calculate the control limits based on a group of about 20 samples of 5 values each. You then give the operators forms, with the control limits for the median already drawn. You also give the operator a piece of clear plastic film, containing the control limits for the range, drawn to the same scale as the medians limits.

The operator takes a sample from the work, performs the measurements needed, and then plots the chart, using a 6 step process. First, plot all the sample values on the control chart in a single, vertical line. Second, connect the dots with a vertical bar. Third, find the median, the middle value, and circle it. Fourth, lay the plastic film with the range control limits over the vertical line. As long as the vertical bar fits within the control limits, the process variation is under control, and you can go on to step five. If the vertical bar exceeds the control limit spacing, the process variation is out of control, and you must take corrective action. Since the median control limits are only valid when the range is in control, skip to step six. Fifth, if the range is in control, check to see that the circled median value falls within the control limits on the chart. If it does, the process is in control, take no corrective action. Six, if the median, or the range, falls out of control, you must start corrective action.

Notice that in this procedure, the operator made no calculations, once you determined the control limits. The operator simply plots the data, and compares the range to the see-through template control limits, and the median to the control limits on the chart. Given this great reduction in calculations, most people expect this control chart to be much less sensitive than an X-Bar-R chart. In fact, you only suffer a sensitivity loss of about 10 percent.[3] I highly recommend this graphical control chart for applications involving operators with weak math skills. Its simplicity also commends its use for applications involving operators with strong math skills.

Besides the graphical control chart, Pre-Control also offers a calculation free control chart.[4] Pre-Control is particularly suited for control charts based on individuals. See the references for more information on how to set up this control chart.

THE CORRECTIVE ACTION TASKS

1. CONDUCT TESTING COMPANY-WIDE TO IDENTIFY PEOPLE WHO NEED HELP

I believe company-wide testing should start any corrective action plan for illiteracy and innumeracy. I really mean company-wide, from the CEO on down. If everyone takes the test, it will not seem as though you have a single group picked out. It also shows the commitment of top management to facing the reality of these problems, and their seriousness about dealing with them.

I cannot understate the importance of eliminating any sense of fear related to this testing. Do not create an environment of "sink or swim," with those who fail the test being thrown out the door. You must carefully explain that you want to test everyone, solely to allow you to plan your training program.

That someone cannot read, write, or do simple math should not disqualify them for their job. One of the best hard chrome platers I have worked with could only write his name, address, and telephone number, and could read little beyond that. Yet he had an uncanny knack for fixturing and racking parts for chrome plating.

If we brought in a new plating process to our shops, would we think we needed to get rid of all our workers, since they don't know how to do this new type of plating? No! We would pick the ones that do the best job on their current lines, and train them with the skills needed to run the new line. In the same way, we need to train our workers to read, write, and do math at the level now required.

As we conduct this testing, we must be sensitive to the stigma attached to illiteracy in this country. Even though the numbers indicate widespread functional illiteracy, those with the problem feel ashamed that as adults they cannot read as well as a child. Take care not to label someone as 'stupid' simply because they cannot read. You must keep all test results strictly confidential.

You can obtain standard tests for reading, writing, and math skills from most schools. I think it better to develop a test that more closely relates to the materials involved in the job. I believe this based on the dictum of adult education that says adults learn best when they see how it relates to their job. Modifying this slightly, I think the testing will be most accurate if it is work related. I believe this, if for no other reason than the employees will take the test more seriously, and believe its results, if they see that it directly grows out of their work. If you do develop your own test, remember to try it out on several small groups before giving it to everyone. This will save you the embarrassment of having to test everyone a second time to get the information you want.

2. START REMEDIAL EDUCATION IN THE WORKPLACE

Once you have identified employees with learning deficiencies, you must now plan on how you will correct the situation. Most likely, you will find the need for some form of remedial education. You have several options for providing this education.

Most areas have some form of adult education program, sponsored in part by the local school system. These programs offer courses on a variety of levels, from basic reading and math skills, up to higher level literature and math courses. Some employees will prefer to attend this type of formal, structured, schooling.

Other employees feel too ashamed of their illiteracy to attend a formal class at an adult school. For these employees, private tutors may offer the best course of training. Many communities offer adult literacy programs, often in conjunction with the community library. These programs make use of volunteers to work one-on-one with adults who want to learn to read. This intimate arrangement will usually overcome the shame and embarrassment of the first awkward steps in reading. Later, after the employee has gained confidence, they may feel more inclined to continue in the adult education program.

A new alternative involves the use of cassette or videotape courses. These allow the employee to learn in the privacy of their home. Most have seen the adds on TV for programs, such as "Hooked on Phonics." Programs like these would be good investments for companies serious about dealing with these problems and educating their workers.

THE LONG TERM TASKS

1. SUPPORT LITERACY PROGRAMS IN YOUR COMMUNITY

If we are really serious about dealing with the problems of illiteracy and innumeracy, then we must become part of the solution. We must support whatever literacy programs we can. Where possible, we should try to support these programs by personal involvement as a tutor. If we cannot do this, then we should try to support in whatever way we can.

2. BECOME INVOLVED WITH LOCAL SCHOOLS

Most importantly, we must become proactive and seek to improve the quality of our educational systems. Part of this will require our involvement in communicating the needs of business today, both to the school administration and teachers, and as well to the students.

Somehow we must get the message out to students in school that the days of high paying jobs with low skills are gone. During the heyday of mass-production, many people could find well-paying jobs that required little or no skills. The time for that type of production has passed, and is not likely to return. The business community must convince the students that only those that have the skills required will find well-paying jobs.

I don't pretend to have all the answers to the educational crisis in this country. One thing I do believe strongly in, though, is that we must run schools like businesses, with a real sense of fiscal responsibility and accountability. For too long in this country, we have tried to throw money at problems, hoping they would go away. What we must do now is find the real problems that have created the illiteracy problem we now face, and deal with them head-on.

NOTES

1.Paulos, John Allen. ***Innumeracy***. New York: Hill and Wang. 1988.

2.Cited in **Products Finishing** magazine, "Job Shops in the 90's", December, 1991. p61.

3.PC Magazine, April, 1992.

4. The author first read of this type of control chart in:
Taylor, Wayne A.. ***Optimization & Variation Reduction in Quality***. McGraw-Hill Inc., New York,NY. 1991. p 218-219.

5. The exact values of plotting a point as out of control, when in fact it is in control, is 1 in 370 points for an X-bar chart, 1 in 340 points for a Medians chart.

6. For more information on Pre-Control Charts, see:

Sugg, David J. and Miller, Dale. "Statistical Process Control For Reel-To-Reel Plating: Thickness Control on Short Runs." *Procedings of the 79th AESF Annual Technical Conference- Session A, Quality and Statistical Methods*. Atlanta: American Electroplaters and Surface Finishers Society, Orlando,FL, 1991.

Bhote, Keki R.. ***World Class Quality: Using Design of Experiments to Make it Happen***. Amacom, New York, NY. 1991. pp 171-195.

STATISTICAL PROCESS CONTROL FOR REEL-TO-REEL PLATING: THICKNESS CONTROL ON SHORT RUNS

By: David J. Sugg
Eastman Kodak Co.
Dayton, Ohio

Dale Miller, P.E., C.Q.E.
Consultant
Harrisburg, PA

ABSTRACT

Operators of reel-to-reel plating lines must closely control plating thickness. Too much plating, and the plater loses money. Too little plating, the customer rejects the job.

While standard SPC techniques help control plating thickness in many applications, reel-to-reel plating brings special problems. For job-shop platers, this problem is particularly acute. With fast line speeds and routinely short coils, operators normally splice and replace reels every ten to thirty minutes.

How can platers use SPC to insure that they meet plating thickness specifications? How can they keep up with the constantly changing reels? What shortcuts would allow rapid charting, but yet maintain adequate control?

This paper will look at the use of Pre-Control, Narrow Limit Gauging, and entral target control of the plating thickness. The paper will also discuss using SPC to control the inputs to the process, not just the output. Standard SPC charts help control the inputs, while the modified techniques control the outputs.

DESCRIPTION OF THE PROBLEM

Reel-to-reel plating provides a convenient method for plating continuous strips of substrate. The substrates can range from steel strip, plated with zinc, to electronic lead frames, plated with gold. The substrate spools off one reel, is guided through the cleaning and plating solutions by rollers, then collected on a take up reel. This allows plating parts too small, or too long, for conventional rack plating.

Frequently the plater must closely control the plating thickness. Particularly with the precious metals, the plater needs to control the plating thickness closely. If he fails to plate the required thickness, the customer may reject the lot. If the plater plates an excess of the metal on the substrate, he loses money.

Statistical Process Control offers many advantages to control plating thickness. It acknowledges the reality of the inherent process variation, measurement variation, and unknown sources of variation. Given these variations, the operator must take care to not overcontrol the process, making corrections when not needed. By use of control limits, with or without added decision rules, you can separate a real change in the process average from the normal variation.

Reel-to-reel plating presents special challenges in the application of SPC for plating thickness control. For those in job shop plating, the challenges become particularly acute. With fast line speeds and routinely short coils, operators of reel-to-reel plating lines normally spice and replace reels every ten to thirty minutes. Added to this tight schedule, the operator may also have responsibility for monitoring line processes, maintaining the machinery, and maintaining the bath chemistry. Is it any wonder that these operators protest when on top of all this, we ask them to keep SPC charts?

Where can operators find the time to calculate control limits for each new coil? How can they even find the time to calculate the average and range for each sample? When will they fit in the time to chart all the data onto the control chart? More importantly, when will they find the time to look at the chart, and decide what they will do to the process?

THE SOLUTIONS DESCRIBED

This paper presents several suggested solutions to this real world problem. We do not present these solutions to determine the one 'best' solution. The solutions are not mutually exclusive, and you should not see any one of them as the best in all situations. Any one of these solutions may work in a given plant, or it may take a combination of several of the solutions to solve the problem.

The solutions presented in this paper are:

1. Central Target Control Charts
2. Pre - Control Charts
3. Graphical Medians -- Range Charts
4. Narrow Limit Gauging
5. Computer Based Control Charting
6. Fully Automated Data Collection and Analysis
7. Controlling the Inputs

1. CENTRAL TARGET CONTROL CHARTS

Central Target Control (CTC) charts offer a great reduction in the calculations needed for standard control charts. This reduction comes at the expense of sensitivity in detecting changes. If the chart meets the conditions and assumptions underlying it, then it remains more than sensitive for normal use.[1]

The name 'Central Target' derives from trying to keep the plating thickness centered within the specified tolerance. In use, you do not calculate control limits. Instead you use the plating thickness tolerance. This simplifies the task of the operator, as they do not calculate new control limits for each reel. As the operator places a new reel on the plating machine, the only information needed to start the control chart for that reel is the plating thickness tolerance.

You cannot control every process with such a simple control chart. In particular, processes controllable with this chart must have small amounts of process variation compared to the tolerance range. If the total process spread occupies 75 % of the tolerance, or less, you can control the process with a Central Target Control chart.

Do not take this requirement lightly. Rarely will a process not presently under SPC meet this requirement. This solution works best on existing lines, with a large amount of data available to determine the amount of process spread. Such a study will also allow a determination of any plating jobs that may not follow the 'normal' process spread. You can then treat these jobs separately from the other jobs.

To use the Central Target method, the operator takes the plating thickness tolerance for the reel and divides it into four or eight sections. The divisor depends on the estimated percentage of the tolerance occupied by the normal process variation. If the process variation fills 75 per cent of the tolerance, divide the tolerance into eight sections. If the process variation fills 50 per cent of the tolerance, divide the tolerance into four sections.

In either case, any point in the outermost zone, on either side of the average, shows the process drifting out of control. The operator must take corrective action to prevent production of defective plating. It is very important that the plating thickness average fall near the nominal of the tolerance. A shift from the nominal value weakens the detectability on the side away from the move. Figure 1 shows two examples of Central Target Control Charts.

It is interesting to point out that a plating shop has used this technique for many years, with great success. Only within the last ten to fifteen years has Dr. Taguchi demonstrated the importance, and great value, of producing all parts near the nominal, instead of at the extremes.

2. PRE - CONTROL CHARTS

Frank Satterthwaite developed Pre-Control charts while working for the consulting firm of Rath and Strong. Pre-Control offers an alternative to standard Shewhart type control charts. The consultant Dorian Shanin remains one of the leading proponents of Pre-Control[2], along with his disciple, Keki Bhote[3]. While similar in some ways to Central Target charts, Pre-Control offers several refinements, that improve the utility of the technique.

Pre-Control uses four basic rules for chart formation and operation.

Step one:

Divide the specification width by 4. The two innermost quarters form the "green zone." The boundary between this central area and the outer two quarters form the "PC Control" lines. These outer two quarters are the "yellow zone." The area outside the specification limits is the "red zone."

Step Two:

To determine a preliminary estimate of the present process capability, take five consecutive parts from the process output. If five consecutive parts fall within the green zone, before two consecutive parts fall within the yellow zone, consider the process in a state of control.

If even one part falls outside the green zone from the first five, the process is not in control. You must take corrective action to improve the process before starting production.

Step Three:

Once you start production, take two consecutive samples from the process output on some periodic basis.

1. If both fall within the green zone, continue production without change.

2. If one part falls in the green zone, with the other in the yellow zone, consider the process in control, and continue production.

3. If both parts fall within the yellow zones, two possible actions exist. If both parts fall in the same yellow zone, you must adjust the process. If the parts are in opposite yellow zones, the process is out of control, and production must stop. Do not resume production until you discover the cause of the excess variation, and correct it.

4. If even one part from the sample falls in the red zone, all production must stop. This means the part is defective. You must find the cause and take corrective action.

Anytime you stop production as a result of violating rules 3 or 4, return to Step Two above, and insure the process has returned to a state of control by producing five consecutive parts within the green zone.

Step Four:

Calculate the frequency for taking the two consecutive samples by dividing the average time between stopping production by six. If the process runs for six days without breaking rule 3 or 4, then take the two samples once a day. For example, a process that averages 60 minutes between stoppages would require samples every 10 minutes.

While you do not have to plot the data for Pre-Control to work, I always advise that you do not skip this step. Plotting the data will often reveal subtle patterns or clusters in the data, that reduce the sensitivity of the test. The plotting takes so little time, the potential benefits far outweigh the time spent.

3. GRAPHICAL MEDIANS -- RANGE CHARTS[1]

Control charts using the sample median, $\tilde{X}$, provide a reasonable alternative to $\bar{X}$ charts for measured (variables) data. Median charts tell us the process center location and they answer the same questions as a chart for averages.

Plotting medians offers several advantages to plotting averages.

1) Median charts are simple to use. After calculating the centerline and control limits, you do not need any other calculations to plot the sample results.

2) Operators need only plot individual readings on a graph so it is usually easier to get a SPC control chart program accepted in the shop.

3) When using charts for medians, you plot the individual measurements directly on the chart, so it may not need to write down the actual numbers.

4) Since this chart requires no calculations, once the control limits are set, the chart provides a fast, accurate tool for process control.

For a given sample size, medians charts lack the sensitivity to process changes as charts for averages. In most situations this is of minor consequence considering how easy the charts are to use.

The R chart for ranges is the same as that used in $\overline{X}$-R charts. You should not use the median chart without the R chart. A R chart is necessary to detect patterns caused by variations in the process spread.

Making the Chart for Medians and Ranges, $\tilde{X}$-R Charts

Set up the chart as if you were making an $\overline{X}$-R chart. Gather the measurements on 20 or more samples of size n in production order. During the initial performance study period write down the data, even if you do not plan to do so once the chart enters routine use.

Plot the individual readings on the upper graph. Find the median value and circle it. Small sample sizes consisting of an odd number of measurements (n=3, 5, and 7) are ideal for median charts. Connect the sample medians with straight lines to emphasize the pattern profile. Again, during the study period, write down the median values.

You can obtain range values by subtracting the lowest reading from the highest reading in the sample. You could also count the increments between the extreme values on the plot. A third method transfers the interval between extreme values to the edge of a piece of paper. You then transfer that distance onto the R chart.

A fourth alternative, and the one I prefer, involves the use of a clear piece of plastic. Calculate the control limits for the range and mark them on the clear piece of plastic. Once you have plotted the sample values on the medians chart, set the piece of plastic over them. If all the points lie within the limits, the range is in control.

1) Obtain the centerline and control limits for the R chart as before.

2) Calculate the centerline for the X chart by averaging the medians.

We symbolize the average of the medians with $\tilde{\bar{X}}$.

3) Use the average range, $\bar{R}$, to calculate distance between the centerline and the limit lines for the median chart. You must use special A5 factors to figure the limits for medians. These factors vary with the sample size n. Tables in books on SPC list these values.

Interpretation of Median and Range Charts, $\tilde{X}$-R

Interpret the $\tilde{X}$-R chart for out-of-control points, unusual patterns, etc., the same as for the $\bar{X}$-R charts.

Remember, if the R chart is out of control, you cannot accurately interpret the $\tilde{X}$ chart. Do not interpret the $\tilde{X}$ chart until the R chart has returned to a state of control.

4. NARROW LIMIT GAUGING

If you can measure the plating thickness with some type of a go/no-go gauge, Narrow Limit Gauging (NLG) may offer a time saving alternative to the traditional control charts. In practice the NLG chart bears many similarities to the Pre-Control chart discussed earlier. In essence, Narrow Limit gauging offers the advantages of small sample sizes, and good discrimination, with the speed and simplicity of go/no-go gauging.

As in Pre-Control, you base the NLG control limits on the tolerance range specified for the part. NLG differs from Pre-Control in that any subdivision of the tolerance into smaller zones depends on having go/no-go gauges within the tolerance band. These tighter gauges allow the use of cautionary lines, similar to the yellow zone in Pre-Control.

For more information on Narrow Limit Gauging, see reference 5.

5. COMPUTER BASED CONTROL CHARTING

One solution, used by many, turns all the calculation and charting over to a computer. The operator collects the data, and enters it into a computer. The computer calculates the average and range, and produces an updated graph. In some systems, points out of control generate an error message, with possible items to check listed on the screen, along with corrective actions 6.

6. FULLY AUTOMATED DATA COLLECTION AND ANALYSIS

To reach our goal of maintaining control of the plating thickness, while at the same time not overloading the operator, will likely require some automated data acquisition and control equipment. Operating under the control of a computer, a sensor measures one of the variables, and records the data in a database. To reach full potential, the system should also have the capability of closing the loop, by sending out a signal to turn on an addition pump, or make some other adjustment. The operator should only need to monitor the system occasionally, providing servicing as needed. Some alarm mechanism should be a

part of the system, to signal an out-of-control condition.

For many years, reel-to-reel precious metal platers have used continuous on-line X-ray fluorescence (XRF) spectrophotometers to measure the plating thickness on the reel, just as it comes out of the plating tank. The XRF unit can connect with a computer that controls the plating rectifier. If the plating thickness climbs out of control, the XRF can signal the rectifier to reduce the amperage. If the plating thickness falls out of control on the low side, the XRF signals the computer to increase the amperage from the rectifier.

Similar units have slowly made inroads into controlling other plating parameters in real time. Electronic stress gauges now available are capable of measuring internal deposit stress in real time. The unit can connect, through a computer, to the rectifier, adjusting the current density to maintain the desired stress level. Plating rate monitors can measure the real time plating rate of the solution, while the parts plate. If you locate the monitor plates at the same current density and agitation conditions as the parts, very tight plating ranges can result. Even if you cannot match the exact plating conditions at the probe, a correlation may be possible between the probe and the parts, allowing improved plating rate estimates.

7. CONTROLLING THE INPUTS

Controlling the inputs to the process offers the best overall solution to our problem. We can view processes as computer programs. For a given set of inputs, another set of outputs will result. We readily admit that real world processes seldom reach this ideal, but the basic strategy remains the same. We should strive to identify all the inputs to a given process, measure their effect on the process, and then control the inputs that affect the output.

Each electroplating solution has its own set of inputs, and differing set of functions relating the inputs to the outputs. While the exact set of important inputs varies with bath type, certain fundamental input variables will usually need tight control.

You should control the plating current density, in electroplating solutions closely. Faraday's law states that the amount of metal deposited depends on the amount of current applied, and the time of application. Since we want to control the plating thickness, we need to know the surface area, and the density of the metal. Then, if we control the current density, we can estimate the plating thickness by knowing the time we plated the part.

In controlling the current density, remember that current density contains two parts. The numerator contains the current applied from the rectifier. The denominator contains the area plated. You must control both for lasting success. Often platers forget the denominator, and start to think of long running jobs as so many amps for so many minutes. The problem comes when someone places fewer parts on a rack, thus less area, yet runs for the same amount of time. Only after overplating the parts does the operator remember that he must concern

himself with more than just the amps, he must remember the area as well.

An often overlooked control variable for electroplating, except for most chrome platers, is voltage. Electroplating baths form a simple direct current (DC) circuit. DC circuits obey Ohm's law, which states that the voltage drop (E) in the circuit equals the current flow (I) in the circuit times the resistance (R) of the circuit. Expressed mathematically:

$$E = I R$$

From this scientific principle we can gain more insight into the condition of a plating system. If the voltage needed to maintain a given amount of amps changes, then the resistance of the circuit must have changed. If the voltage drops, the resistance has dropped. If the voltage rises, the resistance has risen. The cause of the change in resistance could come from a change in bath chemistry, or from physical causes, such as a poor connection.

In reel-to-reel plating, the voltage can give an early indication of the need for preventive maintenance. A simple control chart on the voltage required to maintain a set amperage level can provide early warning of problems with passive anodes, poor connections, worn contact brushes, weak bath chemistry, or changing area of the surface plated.

Controlling the inputs ties in well with the sixth solution given above, use of automated data acquisition and control devices. You can easily automatically measure and control the solution temperatures, amperages, voltages, and substrate transfer rate. You can buy continuous, on-line solution chemistry analyzers for many plating solutions.

FIGURE 1

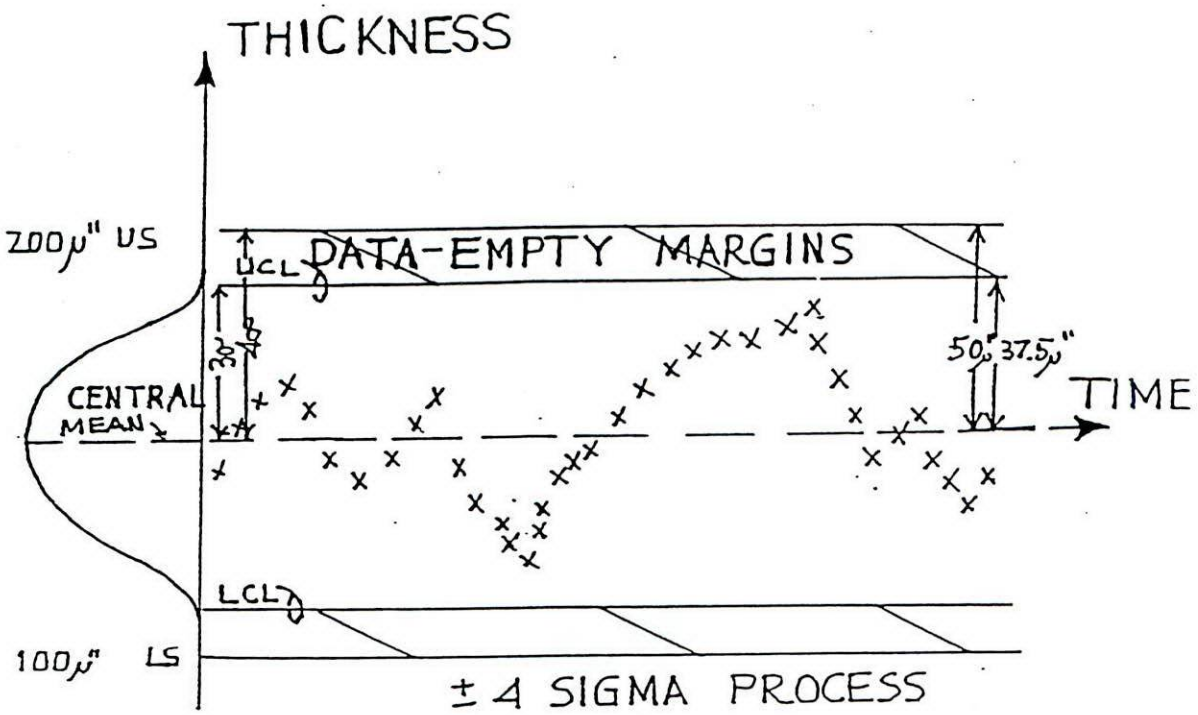
THICKNESS
200μ" US
UCL
DATA-EMPTY MARGINS
30μ"
37.5μ"
50μ"
CENTRAL MEAN
TIME
LCL
100μ" LS
± 4 SIGMA PROCESS

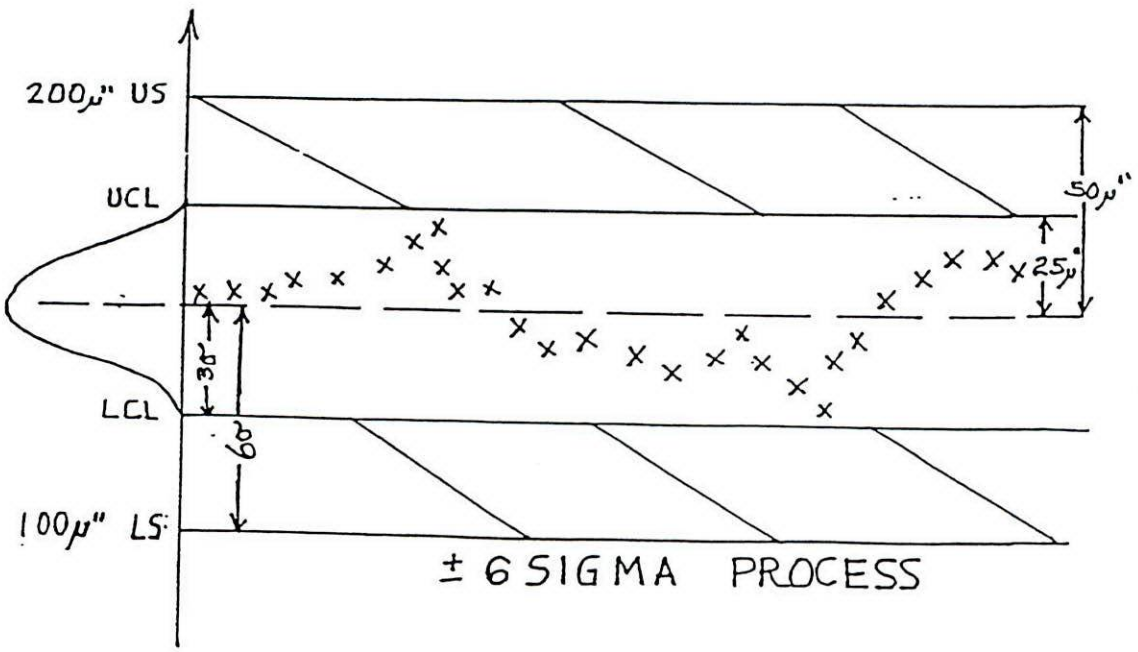
200μ" US
UCL
50μ"
25μ"
30μ"
60μ"
LCL
100μ" LS
± 6 SIGMA PROCESS

NOTES

1.The authors would like to give credit to an experienced electroplater, Mr. Charles Patterson at Charles D. Snyder & Son Inc.. He developed the method outlined here for plating to a central target, in order to cope with the time demands of his organization.

2.Shainin, Dorian. "Better Than Good Old X & R Charts asked by Vendees." ***Transactions of 38th Annual Quality Congress***. Chicago. ASQC Press, Milwaukee,WI. 1984. p 302-307.

3.Bhote, Keki. ***World Class Quality: Using Design of Experiments to Make it Happen***. AMACOM, New York, NY. 1991 p 171-195.

4.Material in this section first appeared as section 6.3 in ***Introduction to SPC for Surface Finishers***. American Electroplaters and Surface Finishers Society. Orlando,FL. 1992. p 89-92.

5.Yu, Shawn S., Case, Kenneth E.. "An Updated Look At NLG For Process Control." ***Transactions of the 38th Annual Quality Congress***. Chicago. ASQC Press, Milwaukee,WI. 1984. p308-314.

6.For a discussion of the potential problems with this approach, see: Sugg, David J. "Why Johnny Can't Do SPC." ***Proceedings of the 79th AESF Annual Technical Conference- Session A, Quality and Statistical Methods***. Atlanta: American Electroplaters and Surface Finishers Society, Orlando, FL. 1991.

TQM Implementation
In a Plating Environment

Paul Horgan
Quality Golden West
Yorba Linda, CA

Having implemented Total Quality Management (TQM) programs in several plating job shops, it has become clear that such an implementation can be broken down into several basic steps. These steps are the same no matter the company or type of finishing process. It is the purpose of this paper to define those steps in their proper order and to suggest how a Total Quality Management program can be implemented in a job shop.

TQM in a plating job shop can be broken down into a series of steps:

Planning Phase	The determination of what the TQM will be for this particular company.
Training Phase	The time necessary to get all personnel on board with essential principals of TQM and Statistical Process Control (SPC).
Implementation Phase	The implementation phase is where we begin to actually implement TQM on the shop floor. Prior to this point we are talking to managers of the enterprise. It is important to note this phase may only begin after training of top management is complete.
Results Phase	The Results Phase begins anywhere from six months to a year after the TQM process imple mentation has begun. Here we begin to see the results of all the work begun in the earlier steps. The Cost of Quality typically goes down by as much as 50% from the previous year. The normal result is that efficiencies improve, down time decreases, and morale improves.

Having defined the four steps to TQM implementation, we will now discuss, in depth, necessary activities needed to accomplish each step.

The Planning Phase of TQM is most often neglected. This is usually because we think that the need for TQM is too obvious and requires little or no explanation. After all, TQM means we are going to put in an SPC program and make quality better - right? Unfortunately, TQM implementation is nothing if not ambiguous. What works well for Motorola will not necessarily work for

the mom-and-pop shop down the street. The company implementing TQM must first have some vision of what TQM is - defined in company terms. This is not simply giving a speech to the workforce on this great adventure of TQM. It is a process of definition. What does TQM mean to "**No Mistakes Plating**" company (a fictional company created for our purposes)? Most often, companies will try to define TQM within the context of some other company's program. This approach seldom works. **Total Quality Management** begins with a definition of what **TQM** is within a **company context.** Does it mean we don't want to create any defective product? Does it mean we want to service our customers to the greatest possible degree? Does it mean we want to earn 3 times the industry standard profit? Do we define TQM in terms of our Ideals, our Profits, or our Customers?

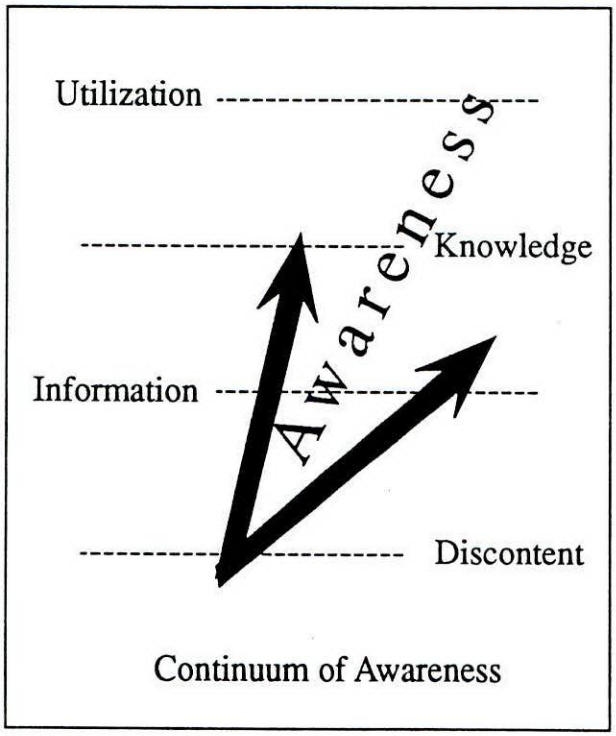

Most often this goal setting and TQM definition begins with an assessment of needs. We need to benchmark where we are now in the Continuum of Awareness. This benchmarking is not relevant to other companies. It is simply a statement of what now exists. In the benchmarking process we tend to say what we are doing now. This statement of current practice helps us to define our strengths and our weaknesses. When we are done, we should have a good idea of where we are in the **Continuum of Awareness,** which is the process needed to develop, define, and implement the Total Quality Management Program. The Continuum of Awareness begins with discontent. We are no longer happy with the current state of affairs. We are making too much scrap, too much rework, or are not productive enough. It is the rare CEO who experiences discontent before the company begins to lose money or is truly on the ropes. The now uneasy CEO begins to gather **information** about TQM. He asks help of his quality control manager, business friends who have experience with TQM, or he enlists the aid of a consultant to help define his program. He or she may write for information on the Malcolm Baldrige award, or a key customer may demand SPC or Design of Experiments. As a result of this seemingly endless torrent of information, along with discontent, our CEO becomes confused and despairs of fully understanding what TQM is. The president has now entered the **Information** phase. If he persists in his quest, the time will come when he has read the sage words of all of the gurus, analyzed the conflicts between approaches, and understands the program and its implications for "No Mistakes Plating" completely. The president now has **Knowledge** of TQM. The

last stage is **Utilization** of TQM. This begins when the president is finally ready to begin the process of implementation of TQM within his or her company. It is at this point where the Planning Stage begins.

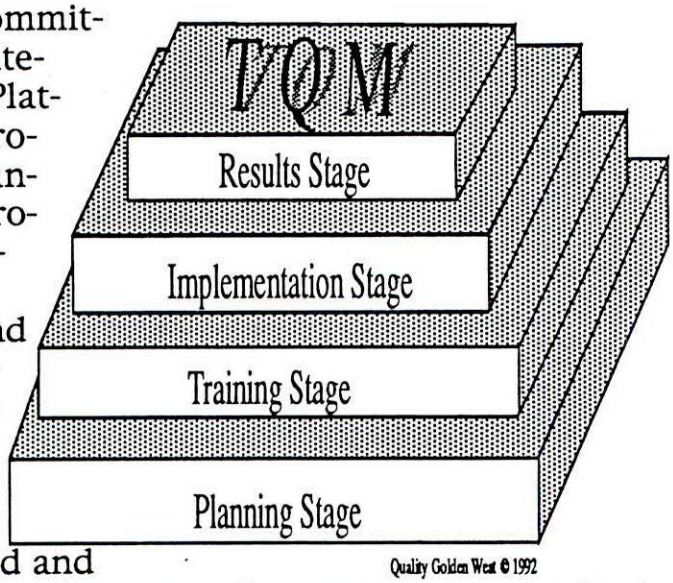

The **Planning Stage** begins with a commitment. The president must make a statement to all hands that "No Mistakes Plating" has begun a three-to five-year program to implement a Total Quality Management Program. The goals of the program must be clear, explicit, and written. It must be made clear that this program is a management program and will be the primary work of the management team. Since TQM is a way to manage a company, it must be made clear who is responsible for what aspects of the program. It is also clear that this task cannot be delegated and must be given priority as high or higher than any other management task. A question often asked just now is **"How much time do managers need to spend on TQM out of our already busy day"**. The answer is simply this - the more time spent on TQM, the faster the **Implementation Phase** and the sooner the **Results Phase** will be evident. I suggest that the manager spend **100%** of his or her time on TQM. With TQM's emphasis on management effectiveness and efficiency, the manager spending his or her time working from a TQM point of view will have better results due to improved problem solving, better focus on things that matter, and better and more cooperative production workers. Remember, TQM is a <u>management</u> philosophy, a way to run a business.

A **Steering Committee** is formed of top managers. This includes people from Quality, Production, Accounting, Engineering, Computer Services, as well as any others who have knowledge needed to assure success. Usually, the Steering Committee will consist of the 5-8 most influential people in the company who have the confidence of the president. Note that the Steering Committee need not be all management personnel. Often floor people who are opinion leaders make great team members and may be included in the Steering Committee. A coordinator is designated. It will be his or her continuing task to ensure the proper and effective implementation of the TQM program. The coordinator would report to the chairman of the Steering Committee (most often the president of the company). Other persons will be brought into the Steering Committee meetings as needed. Since the TQM program will be most effective if it is based on economic gain, the Cost of Quality programs will begin and the basic data assembled by the accounting department. Pareto analysis will identify those projects that are high in terms of COQ and show a substantial chance of being recovered. The Steering

Committee will make determinations of likely projects and hold them in reserve for the teams who have by now begun their training.

Training starts with the Steering Committee and proceeds to the shop floor only after all managers, supervisors, and lead people are trained. Training and implementation of the TQM program are from the top down. However, an important and often forgotten part of TQM planning is involvement of the hourly and production people in the planning process. Their information can be invaluable to both planning and implementation phases and must be elicited.

Basic training can usually be accomplished by three eight-hour classes (24 class hours per person). Program Module 1 is an indoctrination into the principals of TQM. This program emphasizes the reasons for the program's being adopted, and the company's goals, beliefs, and ideals. How the program is to be implemented, whether or not jobs will be protected, the responsibility of management to TQM and the responsibilities of the shop people make up the last half of the program. During Module 1 many problems will turn up. Some of these issues are structural (management policies, wage concerns, fairness issues, management style problems etc.). Other issues may relate to the allocation of resources to accomplish goals defined by the Steering Committee. These issues must be addressed before progress in implementing TQM can be made. Managers should use Deming's 14 points as a touchstone to determine if management attitudes are those necessary for the successful implementation of TQM. The second training program is on Statistical Process Control. The training is limited to basic coding of data, understanding the concept of control charts, control limits and entering data on the chart, calculating average and range, and interpreting the results. The Module 3 defines the relationship between the customer and the company. These programs often go by catchy names such as "Kiss 'em till they Bleed" or "Quality is Job 1". Whatever the name, the goal of the program is the better and continuing satisfaction and definition of the customer's needs.

Once training programs one through three are complete, the teams are now ready to begin the **Implementation Phase** of the TQM program. Projects, previously identified by the Steering Committee, are assigned to the Quality Improvement Teams who will solve the problems with the help of the facilitator. If the facilitator is unable to help with the problem, he or she will marshall such abilities as needed to effect a solution. Extensive use is made of control charts, cause-effect diagrams, scatter graphs and other problem-solving tools. Problem-solving and troubleshooting will often be taught either to the teams or to all employees.

The **Results Phase** is seen soon after implementation begins. The Cost of Quality will usually decrease from 30 to 50% during the first year of a TQM

program. The second year will yield a smaller reduction as the "easy targets" will have been hit during the first year. It is important for the Steering Committee to have defined the desired results in terms of measurable quantities. Whether we are looking at Cost per Direct Hour, COQ as a Percentage of Sales, or Inventory turns, in order to see any improvement we must have taken data prior to any change.

The Steering Committee continues the training process by either providing or taking courses in TQM Planning, Continuous Improvement, Cost of Quality Analysis, Management and Leadership, Just in Time production systems, and/or many others depending on the company, its markets, and the goals defined for the program by the Steering Committee. For instance, platers doing business with the auto industry will want training in Design of Experiments and JIT programs. Electronics plating companies may want to know more about reliability. Job shops may want to understand advanced techniques of Statistical Process Control for purposes of controlling tanks and results.

For those readers who felt this was going to be a tract on the implementation of SPC in the plating shop, the following suggestions. Basic to the question of process control in the job shop is the control of the plating baths. These are most often controlled by chemical analysis in the laboratory. Often, as many as ten different characteristics need to be controlled on any one bath. A Chrome bath, for instance, needs charts on tri and hexavalent Chrome, Sulfates, pH, and contaminants. Generally speaking, Quality Golden West has found that the Moving Average and Range chart gives the best results for control of the plating bath. Due to the fact that many baths are only checked on a weekly or bimonthly schedule, this chart is useful in that it allows for the construction of a control chart with a minimum amount of data. The plating process is based on a tank of known parameters, which will give the proper results if we plate with the correct current for the right time at a given current density. The optimum point for the tank chemistry is at the nominal concentration for which the process is designed. Increases or decreases in the tank concentration result in plating thicknesses that are incorrect with respect to our target thickness. We have found that it requires an integrated computer program utilizing SPC charts to maintain control of the plating process variables. In addition, we have found that it is necessary to institute a program of making regular replenishments to the baths which allow them to maintain their nominal levels.

For purposes of acceptance and control of product, we can use Average and Range charts, Fraction Defective Charts and Run Charts. We won't discuss such charts here as they are available from a variety of sources.

Total Quality Management is a continuing process of improvement that entails complete involvement of all persons within the company. The successful implementation of the program requires planning, training, and proper implementation to assure the desired results. It is hoped that this paper will illuminate what is for many a "dark and stormy" process.

A MICROSTRUCTURAL EVALUATION OF Fe-Zn COUPLES BY CROSS-SECTION TRANSMISSION ELECTRON MICROSCOPY

L.A. Giannuzzi, P.R. Howell, H.W. Pickering, and W.R. Bitler

Department of Materials Science and Engineering
The Pennsylvania State University
University Park, PA 16802 USA

Introduction

The Fe-Zn system has widespread technological applications because of the frequent use of zinc as a surface finish for iron. The role of the zinc is to inhibit corrosion of the iron by cathodic protection. Over the past 20 years or so the Fe-Zn phase diagram has undergone numerous changes. Differences in published phase diagrams have made it clear that uncertainties exist concerning the phase boundaries of the terminal solid solution phases as well as the number of intermediate compound phases and their properties. These discrepancies in the literature can be attributed to the difficulty in preparing homogeneous alloys of known composition and because of the high vapor pressure of Zn. Therefore, phase boundary determinations and thermodynamic measurements are difficult to perform accurately. Reproducible results have been obtained by producing alloys by isothermic diffusion [1] and by a technique known as liquidus-hot-pressing [2]. The Zn-rich portion of the Fe-Zn phase diagram was drastically changed in the 1970's as a result of several publications on the topic during this time [3]. Kubaschewski has compiled the most up-to-date Fe-Zn phase diagram which includes experimental observations of the Fe-Zn system through 1980 [3]. A recent thermodynamic evaluation of the Fe-Zn system supports the diagram by Kubaschewski [4].

The formation of intermediate phases in a binary alloy system can be deleterious because of the typically brittle nature of these phases and the resulting impact they have on the mechanical stability of the system. The Fe-Zn intermediate phases are primarily low temperature phases which are found in the Zn-rich portion of the phase diagram. The intermediate compounds found in order of increasing Zn composition are labeled Γ, Γ_1, δ, and ζ. Intermediate phases may form in Zn coated Fe during processing operations such as baking cycles used to cure paint for automobile parts. These phases may also be produced during heat treatments designed to stabilize the system prior to subsequent thermal excursions such as those encountered during welding operations. Formation of intermediate phases may also occur during the coating process itself. Such phases are evident in the process of hot dip galvanizing where the Fe-based material is coated by submersion in a molten Zn bath [5]. Therefore, it is important to understand the nucleation and growth behavior of the intermediate phases, to allow processes to be designed to avoid the formation of undesirable phases, or to control the amount of such phases to within acceptable limits. In this paper, a microstructural evaluation of the intermediate phases present within the interdiffusion region of an Fe-Zn binary couple, via the application of cross-section transmission electron microscopy (XTEM), is presented.

Experimental

Fe-Zn couples were diffusion annealed at either 450°C for 10 min., 406°C for 10 min., or 450°C for 10 min. and then 406°C for 7 hrs. The heat treatment scheme above the melting

point (Tmp) of Zn is analogous to a hot-dip galvanized steel operation, and similarly, that below Tmp of Zn corresponds to a heat-treated electrogalvanized steel specimen. The details of the couple fabrication, and the difficulty in producing a XTEM specimen from an Fe-Zn couple have been discussed in prior work [6-8]. A brief description of the XTEM specimen preparation technique is given below. The aspect of cross-sectional specimen preparation which presents the most difficulty is that Zn ion mills at a rate which is 3 to 4 times faster than Fe [9]. This difference in milling rates make it very challenging to produce a thin region across the Fe-Zn interface which is suitable for XTEM examination. To compensate for the faster eroding Zn region, the couple was dimpled to perforation on the Fe side of the couple. This created a gradient of increasing thickness from the Fe extending to the Zn region of the interface. The specimen was then ion milled using a liquid nitrogen cooling stage until the hole of the original perforation broke through to the Zn region. Further details are given in reference [8]. Specimens were examined in a Philips EM420T operating at 120kV.

Results and Discussion

The Zn side of the interdiffusion zone, from an Fe-Zn couple heat-treated at 450°C for 10 min., consisted of the single phase η (Zn solid solution) region followed by the two phase (ζ + η) zone, and then the single phase ζ intermetallic, as the distance into the diffusion zone increased toward the Fe side of the couple [6,7]. A concentration profile showing the composition of Zn starting from within a single ζ particle and proceeding into the η region is shown in fig. 1. In accordance with the equilibrium Fe-Zn phase diagram [3], the equilibrium η concentration at 450°C should contain < 0.1 w/o Fe. However, the profile in fig. 1 shows that the average concentration of the η is ~ 3.5 w/o Fe (96.5 w/o Zn) which indicates that the η phase is supersaturated with Fe. It is suggested that during the anneal above the melting point of Zn, Fe and Zn interdiffuse prior to any intermetallic phase formation and the liquid becomes supersaturated with Fe with respect to these as of yet unformed phases. Upon quenching, the ζ phase precipitates from the supersaturated liquid and reaches its equilibrium concentration of ~ 8 w/o Fe (92 w/o Zn), and the liquid transforms to η while retaining the supersaturation of Fe.

The difference in microstructure from the Zn side of the Fe-Zn interdiffusion zone between a couple annealed above the Tmp of Zn and below the Tmp of Zn is now addressed. Fig. 2 is a bright field (BF) micrograph of the η/ζ interface from a couple annealed at 406°C for 10 min. Note that a two phase (η + ζ) region does not exist, but rather, the η and ζ phases are positioned immediately adjacent to one another. In addition, there is a large amount of porosity in the vicinity of the interface. Furthermore, pores on the order of 25 to 50 nm are observed along the ζ grain boundaries in the vicinity of the η/ζ interface (fig. 3). This porosity is presumed to be an effect of Kirkendall diffusion. Since the porosity is largely found on the ζ side of the interface, it may be inferred that the atomic jump frequency of Fe atoms toward the Zn is faster than the atomic jump frequency of the Zn toward the Fe across the η/ζ interface.

The intermetallic formation and microstructural features on the Fe side of the interdiffusion region are similar for the 10 min. anneals, both above Tmp of Zn and below the Tmp of Zn. The primary difference in microstructure between the two annealing temperatures in the Fe-rich region is in scale. That is, the width of each intermetallic phase region, and the grain size within each phase, are smaller for the diffusion anneal performed below the Tmp of Zn. The $\delta/\Gamma/\alpha$Fe interfacial region is shown in the BF micrograph in fig. 4 and a closer view of the Γ/αFe interface is shown in the BF micrograph of fig. 5. Note that the Γ grain boundaries are perpendicular to the Γ/αFe interface and a columnar grain structure develops. The Γ/αFe interface appears to be relatively planar with little deviation on this microscopic scale. According to the equilibrium phase diagram [3], the Γ_1 phase should be located between the δ and Γ

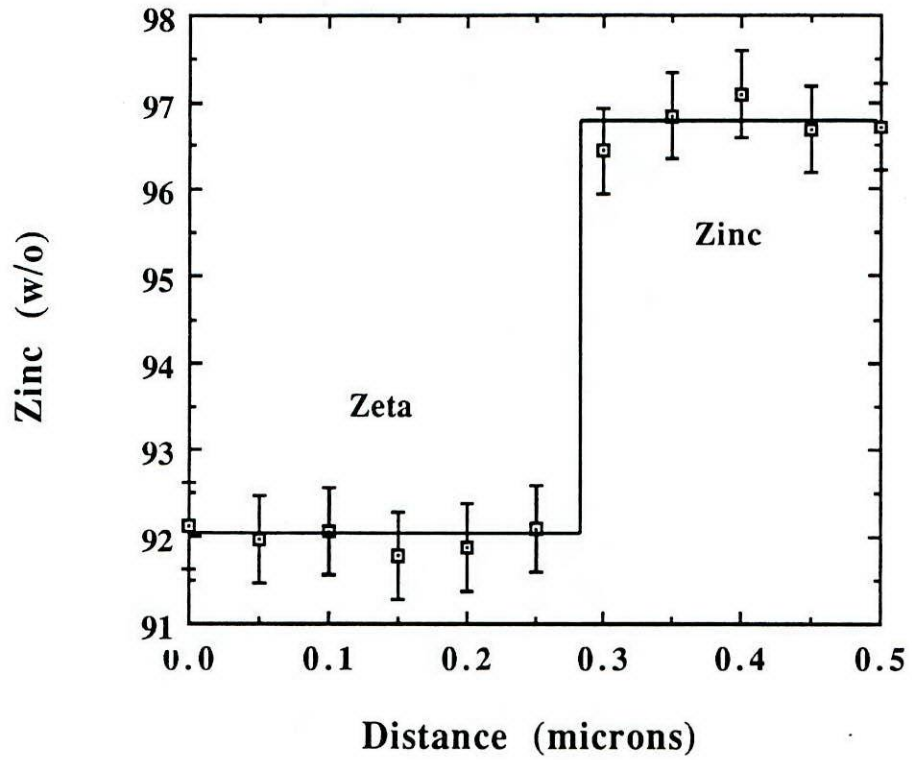

Fig. 1 Concentration profile of zinc from a single ζ particle into the η solid solution phase.

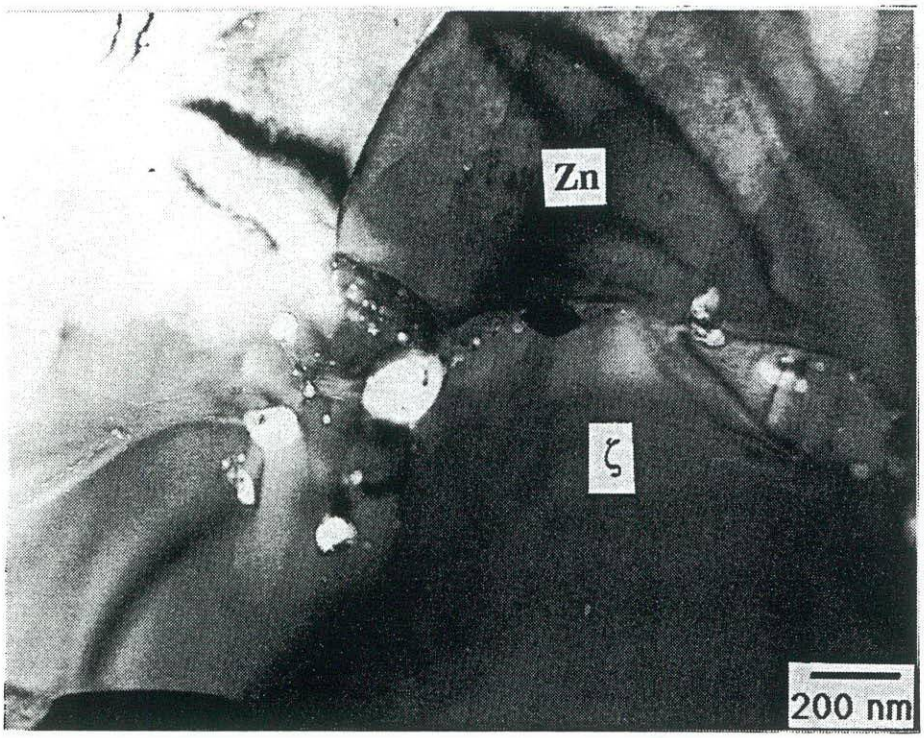

Fig. 2. A BF micrograph of the η/ζ interface from an Fe-Zn couple annealed at 406°C for 10 min.

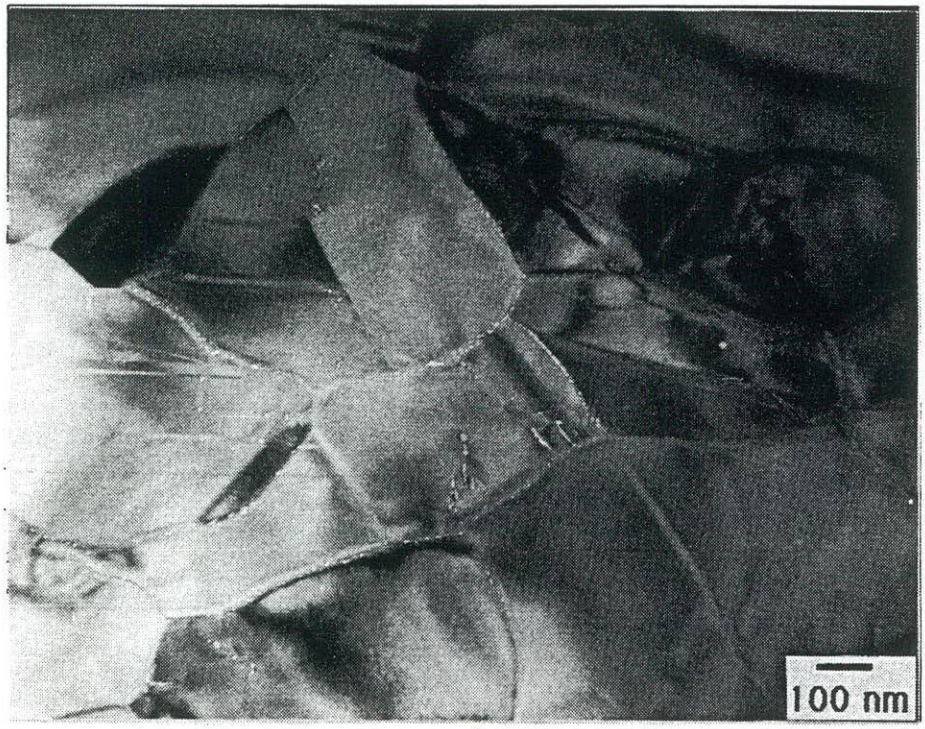

Fig. 3. A BF image showing porosity on the ζ grain boundaries from an Fe-Zn couple annealed at 406°C for 10 min.

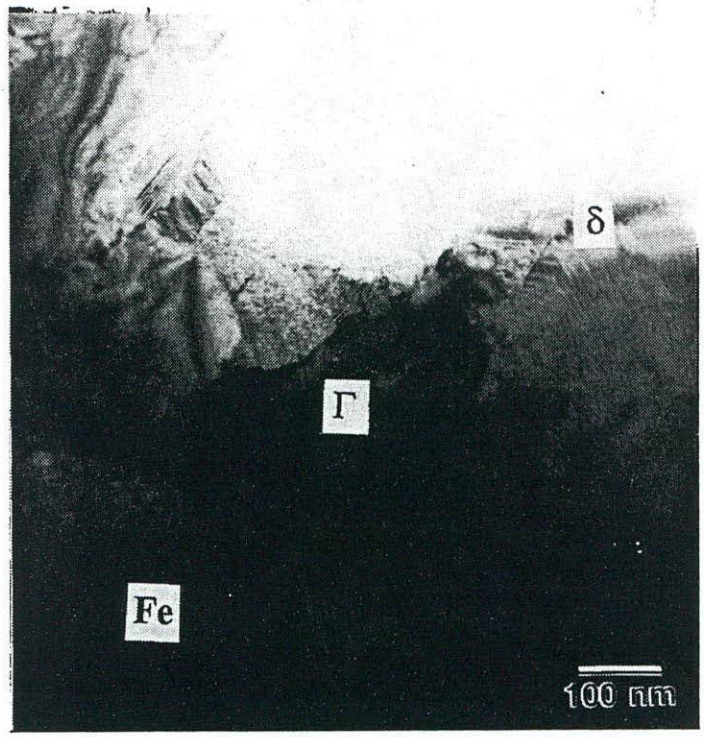

Fig. 4. A BF image of the δ/Γ/αFe interface.

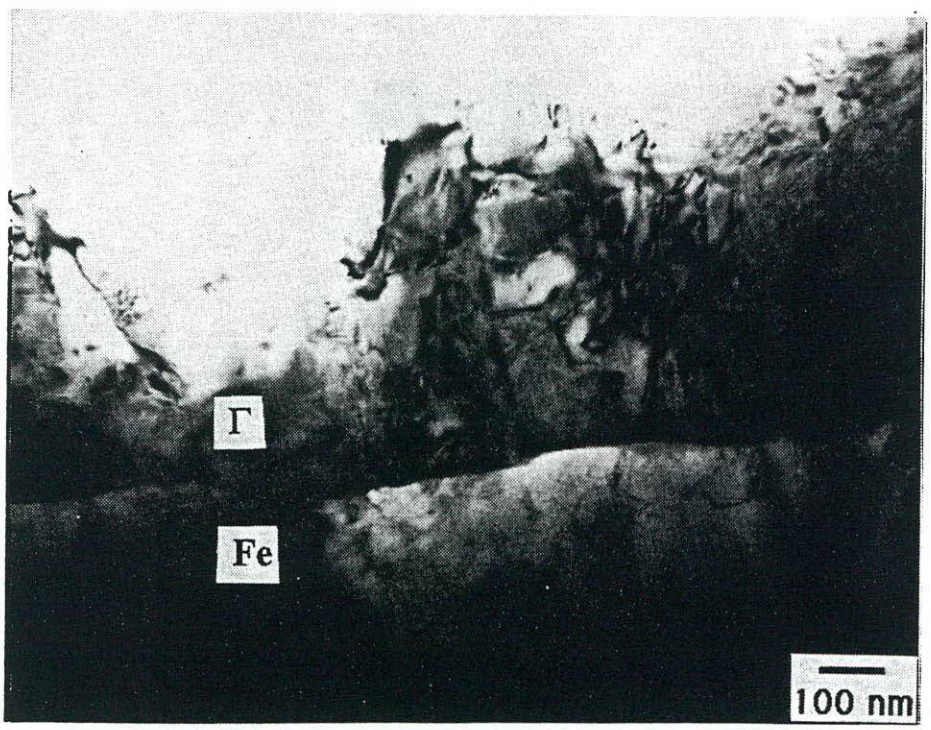

Fig. 5. A BF image of the Γ/αFe interface.

intermetallic phases. However, the Γ_1 phase does not form at either of these 10 min. annealing temperatures (fig. 4). The absence of the Γ_1 phase in this pure Fe-Zn couple is consistent with observations of commercial galvannealed samples [10].The formation (or lack thereof) of the Γ_1 phase will be referred to in a subsequent section of this paper.

Fig. 6 contains selected area diffraction patterns (SADPs) and indexed computer generated diffraction patterns of the αFe, Γ, and δ phases. The pseudo six-fold zone axes of the phases (i.e., αFe [111], Γ [111], and δ [0001]) are of the same camera length. This indicates their compactness in reciprocal space. Extra reflections are present in the Γ SADP, however, the [111] zone of a single grain is apparent. Also note that the positions of the strongest reflections in the Γ [111] and the δ [0001] SADPs match reasonably well with the positions of the $\{\bar{1}10\}$ αFe reflections. This suggests that the Γ and δ phases may be ordered versions of αFe. Additional work is needed to confirm these observations.

We were unable to locate the Γ_1 phase in the interdiffusion zone of the Fe-Zn couples annealed for 10 min. This is not surprising since the Γ_1 phase has only been found to form after long term anneals [1]. Therefore, an Fe-Zn couple was heat-treated for a long term anneal as described in the "Experimental" section. As expected, the Γ_1 phase did form during the long term anneal and a BF image of the δ/Γ_1 interface is shown in fig. 7. It is evident that there is a relatively long incubation time for the formation of the Γ_1 phase, and that the Γ_1 phase must have a larger barrier to nucleation than the other intermetallic phases. This implies that the Γ_1 phase is not likely to occur in commercially available Zn coated steel products since hot-dip galvanizing, paint baking of electrogalvanized pure Zn coatings, or the galvannealing of originally pure Zn coatings occur at times and temperatures which may not be sufficient for the nucleation of Γ_1 [11-13].

Conclusions

1. A method for the production of thin foils for XTEM examination of the interdiffusion zone of Fe-Zn couples has been developed.

2. The ζ, δ, Γ and Γ_1 intermetallic phases, as well as the solid solution αFe and ηZn phases, have been identified by XTEM in Fe-Zn binary couples annealed under different conditions.

3. Microstructural differences have been documented for Fe-Zn couples annealed above and below the Tmp of Zn. Above the Tmp of Zn, a two phase ($\eta + \zeta$) region separates the η and ζ single phase regions. The η phase is supersaturated with Fe. Below the Tmp of Zn, the η and ζ single phase regions are adjacent to each other. Porosity exists at the η/ζ interface and along the ζ grain boundaries in the vicinity of the η/ζ interface. This porosity is assumed to be caused by Kirkendall diffusion.

4. Evidence that the Γ and δ intermetallic phases may be ordered versions of αFe has been presented.

5. The Γ_1 intermetallic phase forms only under conditions of long term anneals, which suggests that there is a large energy barrier for nucleation of the Γ_1 phase. This implies that the Γ_1 phase is not likely to form in galvanized steels.

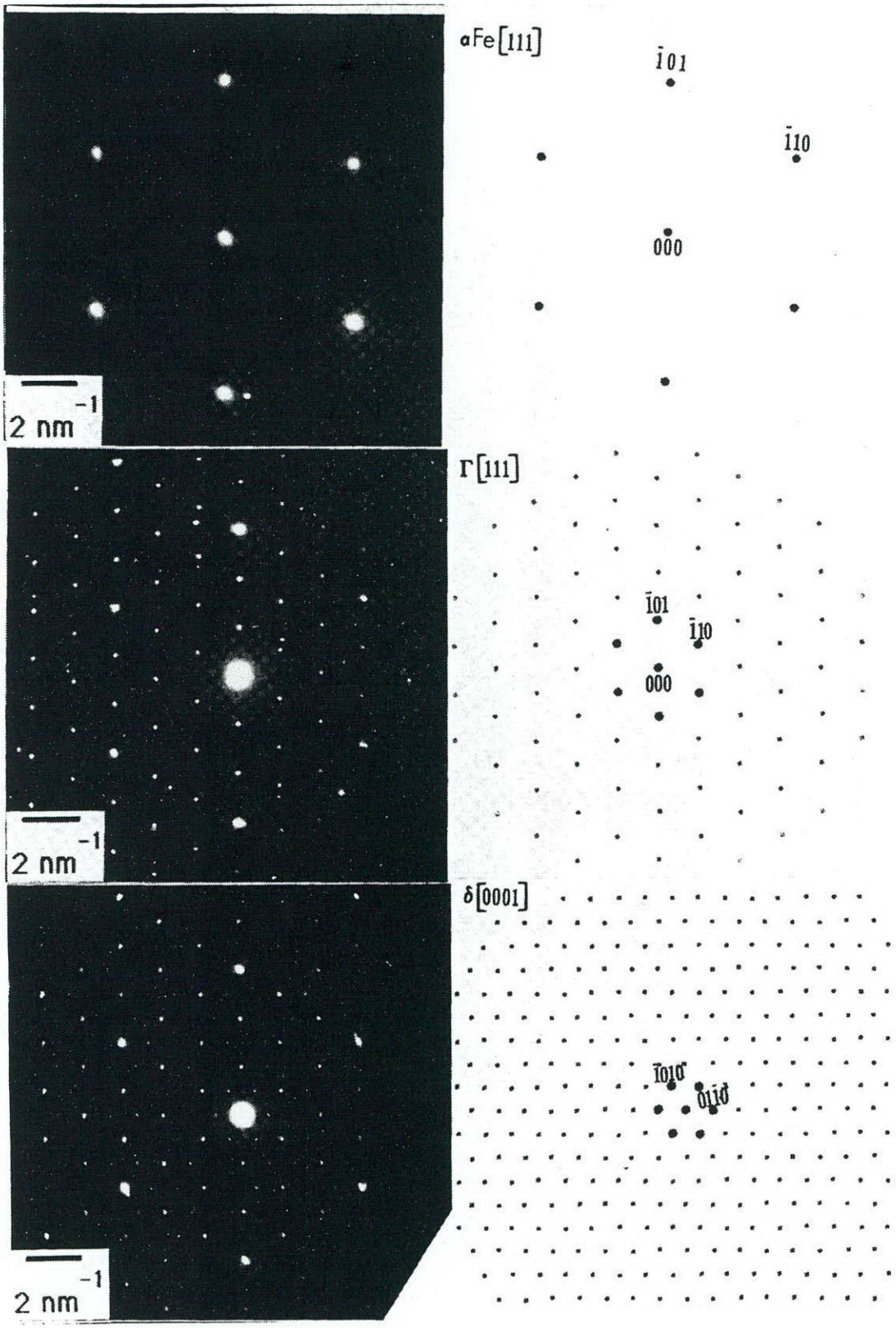

Fig. 6. SADPs and indexed computer generated diffraction patterns of αFe [111], Γ [111], and δ [0001].

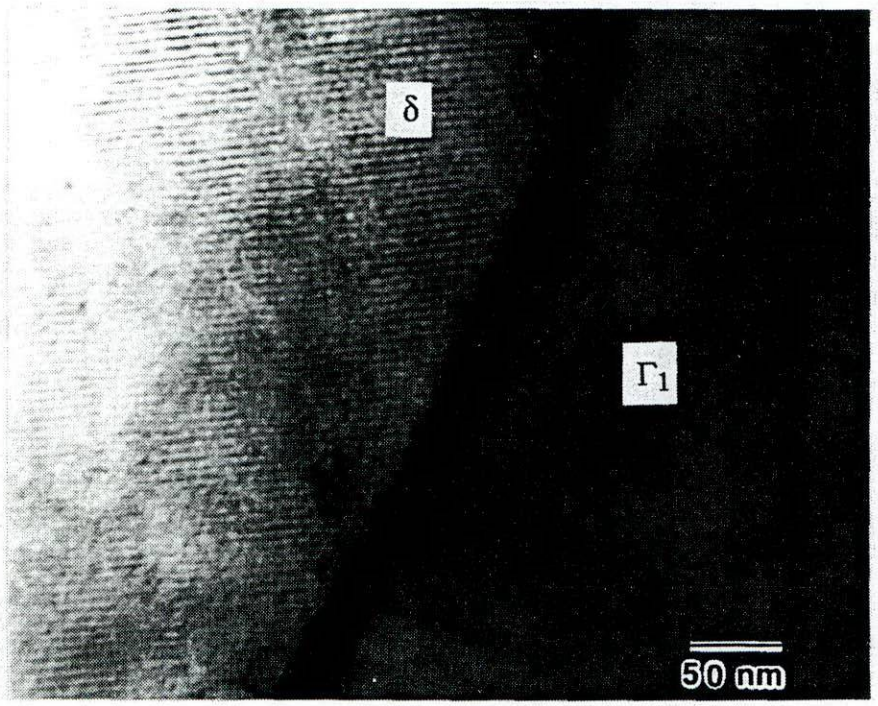

Fig. 7. A BF image of the δ/Γ_1 interface from an Fe-Zn couple annealed at 450°C for 10 min. then 406 °C for 7 hrs.

Acknowledgements

This research was supported by the American Electroplaters and Surface Finishers Society Research Project #76 and Inland Steel Corporation. The Fe-Zn couple was prepared courtesy of C. Cheng, Inland Steel. Analytical microscopy was performed with the help of the NCEM staff at The Lawrence Berkeley Laboratories.

References

[1] G.F. Bastin, F.J.J. van Loo, and G.D. Rieck, Z. Metallkde., **65**, 656, 1974.

[2] P.J. Gellings, E.W. de Bree, and G. Giermann, Z. Metallkde, **70**, 312, 1979.

[3] O. Kubaschewski, Iron-Binary Phase Diagrams, Springer Verlag, Berlin, 173, 1982.

[4] S. Petersen, P.J. Spencer, and K. Hack, Thermochim. Acta, **129**, 77, 1988.

[5] R.F. Lynch, Journal of Metals, **39**, 39, 1987.

[6] L. A. Giannuzzi, P. R. Howell, H. W. Pickering, and W. R. Bitler, Proceedings of the American Electroplaters and Surface Finishers Society, SUR/FIN '91, Toronto, June 1991.

[7] L. A. Giannuzzi, P. R. Howell, H. W. Pickering, and W. R. Bitler, to be published, Proceedings of the ASTM STP Symposium on Metallography: 75 Years Later, Atlantic City, May 1991.

[8] L. A. Giannuzzi, P. R. Howell, H. W. Pickering, and W. R. Bitler, to be published, MRS Fall 1991 meeting, Workshop on TEM Specimen Preparation III.

[9] P.J. Goodhew, "Thin Foil Preparation for Electron Microscopy", in Practical Methods in Electron Microscopy, **vol. 11**, ed. A.M. Glauert, Elsevier, Amsterdam, (1985), 110.

[10] L.D. L'Ecuyer, M. Gagne, C.C. Cheng, and G. L'Esperance, in Electron Microscopy 1990, Proceedings of the XIIth International Congress for Electron Microscopy, eds. L.D. Peachey and D.B. Williams, San Francisco Press, 4, (1990), 1036.

[11] E.V. Proskurkin and N.S. Gorbunov, Galvanizing, Sheradizing and Other Zinc Diffusion Coatings, Technicopy Limited, England, (1980), 75.

[12] Y.L Chen and D.D. Snyder in Zinc-Based Steel Coating Systems: Metallurgy and Performance, eds. G. Krauss and D.K. Matlock, TMS, (1990), 95.

[13] E.V. Proskurkin and N.S. Gorbunov, Galvanizing, Sheradizing and Other Zinc Diffusion Coatings, Technicopy Limited, England, (1980), 137-139.

PLATING OF IRON-NICKEL ALLOYS IN THE PRESENCE OF ORGANIC ADDITIVES

B. N. Popov, Ken-Ming Yin and R. E. White

Center for Electrochemical Engineering
Department of Chemical Engineering, Texas A&M University, TX, 77843–3122

ABSTRACT

Linear sweep voltammetry can be used as an ***in situ*** technique for characterization of electrodeposited thin layers of FeNi alloy. It is shown that organic additives are essential to enable depsition of the binary alloy from sulphate electrolytes. The optimum operating plating conditions have been determined and a new formulation of the plating bath is defined.

INTRODUCTION

Ni-Fe deposition is classified as anomalous deposition. At most operating conditions, the less noble species Fe has a much higher deposition rate than Ni. According to Dahms (1) and Dahms and Croll (2), anomalous codeposition appears to be closely related to the local pH rise at the surface. They assumed this surface pH increase causes the formation of a ferrous hydroxide which suppresses the discharge of Ni. Other mechanisms have also been proposed. Nikol and Philip (3), who also review other theories of anomalous codeposition, have invoked the anomalous deposition of Fe on Ni-Fe to account for the elevated Fe content of the deposit. However, this model is not supported by experimental evidence. Andricacos et al. (4–5) used a rotating ring-disk electrode and a rotating disc electrode to study Ni-Fe deposition. They found that Fe deposition is under mass transfer limitation, while Ni deposition is kinetically controlled. Furthermore the inhibition of Ni was found to be proportional to the Fe(II) flux. Several other researchers investigated the influence of anions, buffer agents and current density on the deposited alloys (6–10). Lieder (11) investigated the codeposition of Ni and Fe from chloride solutions with organic additives such as D-mannitol, citric or ascorbic acids. He suggested that Ni-Fe alloy codeposition might proceed through Ni discharge and formation of Ni monolayer on which water molecules are chemisorbed with a creation of $Ni(OH)^+$ species. According to Lieder, as a result of competition between Ni(II) and Fe(II) ions to occupy active sites, the preferential deposition of Fe and suppression of Ni(II) discharged are observed. Recently, a steady state Ni-Fe deposition model was proposed by Hessami and Tobias (12). According to Gangasingh and Talbot (17), boric acid was not found to affect alloy deposition current efficiency, to eliminate anomaleous codeposition.

In spite of the fact that anomalous deposition of Fe-Ni alloys has been studied by several investigators, this process is not yet fully explained and needs extensive experimental studies. In this work linear sweep voltammetry and a potentiostatic pulse method were used to characterize electrochemically formed Ni-Fe alloys. An objective of this work was also to evaluate the most promising inhibitors for hydrogen evolution in the electrolyte bath, for electrodeposition of Fe-Ni alloy. The structure and the morphology of the deposited alloy was studied using X-ray diffraction, SEM and EDAX.

EXPERIMENTAL

Measurements were carried out with two types of electrodes: (a) Platinum rotating disc electrode with a geometric area of 1 cm^2 and (b) rotating copper disc electrodes with a geometric area of 0.8 cm^2. A platinum gauze electrode was used as the counter electrode. The potential of the working electrode was measured against the standard calomel electrode (SCE). The cell was connected PAR Potentiostat/Galvanostat, Model 273. The potentiostat was connected to a personnel computer and was used in all electrochemical studies. Analytical grade $NiSO_4$, Na_2SO_4 and $FeSO_4$ and high purity water were used to prepare the solutions. All measurements in this study were carried out at room temperature. The pH of the solution was adjusted with addition of 30% NH_4OH or 20% H_2SO_4.

RESULTS AND DISCCUSSION

Linear sweep voltammetry (LSV) was used as an ***in situ*** technique to characterize the electrochemically formed thin layers of Fe-Ni alloys. LSV was applied to dissolve anodically an Fe-Ni alloy by using a fixed and rotating disc electrode. Two procedures were applied to all deposited alloys. In the first procedure, all Fe-Ni alloys were deposited from an electrolyte containing ions of both metals by a cathodic and anodic linear sweep of potential. In the second procedure thin layers of 1 to 2 μm of Fe-Ni alloys were deposited from a solution containing ions of both metals by a potentiostatic pulse technique, followed by dissolution of the deposited alloy by anodic linear sweep voltammetry.

According to Dahms (1) and Dahms and Croll (2), anomalous codeposition of Fe-Ni alloy appears to be closely related to the effect of hydrogen evolution and a local pH rise at the surface. The present study has included investigations of some aspects of hydrogen evolution. Specifically, the effectiveness of different concentrations of organic additives, such as thiourea and saccharin in suppressing the hydrogen evolution reaction was studied. Pt rotating disc electrodes were used as working electrodes. The hydrogen evolution reaction was investigated in 0.5 M Na_2SO_4 solutions, containing neither Ni(II) or Fe(II) ions. This study was conducted to determine the optimum concentration of the organic additives which could be used in the electrodeposition process.

In Figure (1), curve (1), the peak that is observed at –0.65 V (SCE) corresponds to the hydrogen evolution reaction. It was found that the peak height increases as the solution pH decreases. A linear dependence has been observed when peak current was plotted vs a_H^+. The slope gave a diffusion coefficient of $D=7.2 \times 10^{-5}$ cm^2/s, in agreement with the values tabulated by Riddiford (14). Thus, the entire cathodic current, as it will be shown later, corresponds to the combination of hydrogen evolution and reduction of Fe and Ni. It can be observed from Figure (1), curve (2) and curve (3) that the hydrogen evolution peak decreases with an increase in the concentration of thiourea till a concentration of 12 g/l is reached. The hydrogen evolution reaction is the lowest when the concentration of the additive is sufficient to exceed the minimum fractional coverage of the surface.

Boric acid is used extensively in Ni plating systems as a buffer to lessen the pH rise at the surface. Tilak et al. (15) attribute the greater buffer capacity in nickel containing solutions to a complexation of Ni(II) with boric acid. The effect of thiourea and boric acid on hydrogen evolution is shown in Figure (2). The curves were obtained using a scan rate of 30 mV/s and scanning from –0.1 V to –1.4 V vs SCE. The important futures of the results presented in Figure (2) are the decrease of the hydrogen evolution peak current at –0.65V vs SCE and a cathodic shift of 200 mV for the hydrogen overpotential from water reduction.

Figure (3) and Figure (4) show the limiting hydrogen current obtained for different rotation speeds of Pt disc rotating electrode in a 0.5 M Na_2SO_4 solution in the presence and absence of thiourea. Again a cathodic shift of the water reduction overpotential and a decrease of the hydrogen limiting current was observed. The limiting current has a linear dependence of the square root of the disc rotation speed "w", indicating a diffusion controlled process for hydrogen evolution in the presence of thiourea.

In Figure (5), the experiments were carried out in 0.5 M Na_2SO_4 in the presence of saccharin. The hydrogen peak current again decreases and the water reduction overpotential shifts for 150 mV in the cathodic direction. The maximum decrease in the hydrogen evolution peak occurs when the concentration of saccharin in the solution is 2 g/l, indicating that the minimum fractional coverage of the surface when saccharin was used is reached at a lower concentration of the additive than in the case when thiourea was used.

The cathodic peak due to iron is covered by the hydrogen evolution reaction peak and by water reduction at higher overpotentials. However, the anodic peak due to the stripping of the electrodeposited iron can be observed during the reverse scan. Thus, in order to determine the nature of the electrodeposition of iron in Na_2SO_4 solution, the effects of the concentration of $FeSO_4$ in the electrolyte, the scan rate, the extent of the cathodic overpotential applied and the rotation speed of the copper disc electrode on the anodic iron peak were investigated. From Figure (6) one can see that the iron anodic peak increases with an increase of the concentration of Fe(II) ions in the electrolyte. The charges calculated by integrating the surface under the peaks increase from 2.3 mC/cm^2 for 0.1 M Fe(II) to 6.9 mC/cm^2 for 0.5 M Fe(II).

If the electrodeposition of iron is a mass transfer controlled reaction, then more iron will be deposited and subsequently stripped at a lower scan rate. It can be seen from Figure (7) that the anodic peak of iron decreases with the decrease in scan rate and it can be concluded qualitatively that the electrodeposition of iron is not a diffusion controlled reaction.

Figure (8 A) shows the effect of the extent of the cathodic polarization on the anodic iron peak. When the cathodic polarization becomes more negative than – 0.95 V (SCE) a current peak with E_{pa}= –0.58 V (SCE) appears on the anodic branch. As it is shown in Figure (8A), the peak height increases by increasing the cathodic overpotentials indicating that the limiting current for iron deposition is not reached at applied potentials.

Potentiodynamic stripping voltammograms of an Fe film electrodeposited on a Cu rotating disc electrode at – 1.1 V (SCE) for different electrode rotation speeds are shown in Figure (9) for (w= 0 rpm; w=50 rpm; w=100 rpm and w=250 rpm) and in Figure (10) for (1000 rpm and 2000 rpm). According to the Levich equation, if the electrodeposition of iron is a mass transfer controlled reaction, then more iron will be deposited and subsequently stripped at a higher rotation speed "w" in the case of a constant sweep rate. Stripping voltammograms in Figure (9) and Figure (10) show opposite results than those expected. A decrease of the iron anodic peak area is observed indicating that iron deposition at –1.1 V (SCE) does not obey the Levich equation. Accordingly, at –1.1 V (SCE) the iron limiting current is not achieved. At this potential only hydrogen evolution is enhanced with increasing the sweep rate and increasing the rotation speed of the electrode. As it is shown in Figure (11), when the deposition potential was shifted to more cathodic values than –1.250 V (SCE) more iron was stripped at higher rotation speeds. However, from the data obtained it is not possible to conclude if the iron deposition is transport controlled.

An example of a voltametric curve recorded in the solution containing 0.5 M $NiSO_4$ + 0.5 M Na_2SO_4, pH=3.0 is shown in Figure (12). When cathodic polarization becomes more negative than

–0.85 V (SCE) a current peak with E_{pa}= –0.195 V (SCE) appears on the anodic branch. The deeper that the reverse potential is the higher is the peak current. The peak current levels off at –1.1 V (SCE). Potentiodynamic stripping voltammograms of Ni film electrodeposited on Cu rotating disc electrode at v=30 mV/s and different electrode rotation speeds are shown in Figure (13) and Figure (14).

The nickel anodic peak increases when the electrode rotates. A peak current of 2 mA/cm^2 was obtained for w=0 compared with a value of I_{pa}= 7.2 mA/cm^2 for w=50 rpm. However, the amount of the stripped nickel does not increase by increasing the rotation speed. On the contrary as the electrode rotation speed increases from w = 50 rpm to w = 1000 rpm in Figure (14), the nickel anodic peak decreases from I_{pa}=7.2 mA/cm^2 to I_{pa}=1 mA/cm^2, respectively, indicating that nickel deposition from sulfate electrolytes is not mass transfer controlled.

By comparing LSV voltammograms of pure metal deposition with those when both metals are present in solution one can obtain information about interaction between the deposition processes and deposited metals.

The linear sweep voltammograms recorded on fixed copper disc electrodes in electrolytes containing: (1) 0.5 M $NiSO_4$ + 0.5 M Na_2SO_4 (curve 1) and (2) 0.5 M $FeSO_4$+ 0.5 M Na_2SO_4 are given in Figure (15). In both cases one distinct current peak at E_{1pa}=–0.58 (SCE) for dissolution of iron and E_{2pa}=–0.19 V (SCE) appear on the anodic branch.

Voltametric curves recorded in the solutions containing both metals are shown in Figure (16) and Figure (17). The curves in Figure (16) were recorded in solutions containing 0.5 M Na_2SO_4 + 0.5 M $NiSO_4$ for different concentrations of $FeSO_4$ and at reverse potential of –1.0 V (SCE). The curves in Figure (17) were obtained in the same electrolyte as in Figure (16) but at higher cathodic polarization potential, E = –1.1 V (SCE). As it is shown in Figure (15), the LSV when both metals are present in solution is different to the one which would be obtained by superposition of the LSVs pertaining to electrolytes containing pure iron and nickel ions. This indicates that interaction between the two deposition processes and deposited metals does exist. As shown in Figure (16) and Figure (17), the shape of the voltammograms depends on the concentration of Fe(II) ions in the electrolyte and on the value of the cathodic potential applied in preparing the deposits.

LSV recorded in electrolyte containing 0.5 M Na_2SO_4+ 0.05 M $FeSO_4$ + 0.5 M $NiSO_4$ and the deposition carried out at –1.05 V (SCE), shows two distinct current peaks on the anodic branch with E_{1pa}= –0.4 V (SCE) and a broad peak at E_{2pa}= –0.195 V (SCE). At higher cathodic polarization both peaks are almost unchanged except for a small decrease of the more electronegative peak, Figure (17), curve (1). The peak at – 0.4 V (SCE) is more noble than the iron dissolution peak observed in Figure (15) and could be due to two causes: some kinetic factor (formation of intermetallic compounds) or a significant free energy change of mixing of Fe-Ni may cause the shift of the peak away from its reversible position.

Curve (2) in Figure (16) and Figure (17) was obtained in electrolyte containing 0.5 M Na_2SO_4 + 0.5 M $NiSO_4$ + 0.2 M $FeSO_4$. The deposition of Fe and Ni carried out at – 1.075 V, [Figure (16)] shows on the anodic branch three distinct current peaks with E_{1pa}= –0.58 V (SCE), E_{2pa}= –0.4 V (SCE) and a broad peak at –0.195 V (SCE). At higher cathodic polarization, [Figure (17)] all three peaks are also observed. The first peak corresponds to dissolution of iron deposited on the iron-nickel layer during the anodic scan in the cathodic region relative to the reversible potential of iron, while the second and third correspond to dissolution of Fe from the Fe-Ni intermetallic compound, followed by Ni dissolution peak.

Curve (3) in Figures (16) and (17) was obtained in electrolyte containing 0.5 M Na_2SO_4 +0.5 M $NiSO_4$ + 0.5 M $FeSO_4$. The LSV of the deposition carried out at lower cathodic overpotential,

Figure (16) corresponds reasonably well to the one which would be obtained by superposition of the LSV pertaining to the electrolytes containing pure nickel and iron ions. The only difference is the decrease of the nickel dissolution peak. At higher cathodic overpotentials, [Figure (17)], the peak at – 0.58 V (SCE) splits in two distinct peaks at E_{1pa}= –0.57 V (SCE), E_{2pa}= – 0.41 V (SCE) and E_{3pa}= – 0.195 V (SCE).

As shown in Figure (18), I_{pa} at –0.4 V (SCE) increases when higher cathodic overpotentials are applied for the deposition of the alloy indicating that the interaction between the two metals is more pronounced at more negative potentials. A small increase of Ni dissolution peak at E_{pa}= –0.19 V (SCE) is also observed.

Potentiodynamic stripping voltammograms of Fe-Ni film electrodeposited on the Cu rotating disc electrode at different rotation speeds in the electrolyte containing 0.5 M $NiSO_4$ + 0.5 M Na_2SO_4 + 0.2 M $FeSO_4$, pH=3, are shown in Figure (19). The peak at – 0.58 V (SCE) completely disappears and only two distinct peaks at E_{1pa}= –0.4 V (SCE) and E_{2pa}= –0.195 V appear, corresponding again to dissolution of iron from Fe-Ni intermetallic compound and dissolution of Ni at –0.195 V (SCE).

Thin layers 1 to 2 μm of Fe-Ni alloys were deposited in the solution containing ions of both metals by potentiostatic pulse technique. The deposited alloys were then analyzed by anodic linear sweep voltammetry. Potentiostatic I-t transients of deposition of thin layers of Fe-Ni alloy were recorded on copper rotating disc electrodes in electrolytes containing ions of both metals (0.5 M $NiSO_4$ + 0.5 M Na_2SO_4 + 0.5 M $FeSO_4$). The deposition was carried out for 25 s. The corresponding LSV dissolution of these alloys is shown in Figure (20) and in Figure (21). As it is seen in Figure (20), when the applied potential is more positive than – 0.85 V only Ni is deposited on the rotating copper disc electrode. Further increase of the deposition overpotential does not have any influence on the nickel anodic peak. As the deposition potential in Figure (20) increases from – 1.0 V (SCE) to –1.1 V (SCE), the transient current increases from 10 mA/cm^2 to 30 mA/cm^2. At –1.1 V (SCE) two distinct peaks appear at E_{1pa}=– 0.58 V (SCE) and at E_{2pa}= – 0.195 V (SCE), corresponding to dissolution of iron and Ni respectively.

According to Figure (21), at higher cathodic deposition potentials, the deposition current increases up to 100 mA/cm^2 and the peak at E_{1pa}= –0.58 V (SCE) splits in two well defined anodic peaks with E_{1pa}= – 0.58 V (SCE) and E_{2pa}= – 0.4 V SCE. The nickel peak appears at – 0.19 V (SCE).

In the case when the interaction between iron and nickel in the solid phase is negligible, the reversible potential and accordingly the free energy of each component in the Fe-Ni alloy should be the same as the reversible potential of the pure component. Thus the dissolution of such an alloy should result in only two separate peaks as is shown in Figure (16), curve 3 in the case when the deposition was carried out at lower cathodic overpotentials. When the applied potential is more positive than – 0.85 V (SCE) only nickel is deposited on the rotating disc electrode. At higher cathodic deposition potentials, codeposition with Fe occurs.

The dissolution peak potential being more noble than that of the pure metal ions may result from a significant free energy change in mixing in the solid phase or formation of intermetallic compounds. This may cause the shift of the peak away from its reversible position in the positive direction. According to the theory of dissolution of alloys (16), the LSV of dissolution of solid solution should possess two separate not sharp peaks, the first one corresponding to preferential dissolution of the less noble component at more negative potentials. Taking into account that iron and nickel make intermetallic compounds Fe_3Ni, FeNi and $FeNi_3$, see Fe-Ni phase diagram in Figure (21) According to the LSV data obtained in this study, the peak at – 0.4 V (SCE) corresponds to dissolution of Fe from Fe-Ni

intermetallic compound. As shown in all Figures analyzed, the dissolution peak at –0.4 V (SCE) is very well defined, its height depends on the amount of deposited nickel, concentration of the electroactive species in the electrolyte and upon the applied deposition potential.

ELECTRODEPOSITION STUDIES

The electrodeposition of Ni-Fe alloys was studied potentiostatically in the presence and absence of organic additives. Fe-Ni alloy was deposited using electrolyte containing (1) 0.5 M $NiSO_4$ + 0.05 M $FeSO_4$ + 0.5 M Na_2SO_4. A ratio of 10:1 for Ni(II):Fe(II) was kept in all deposition experiments because of the anomalous behavior of Fe-Ni deposition, The other solutions were modifications of bath (1) as follows: bath (2) is bath (1) + 4 g/l thiourea, bath (3) is bath (1) + 4 g/l sodium saccharin, bath (4) is bath (1) + 2 g/l sodium saccharin + 0.5 M H_3BO_3, bath (5) is bath (1) +0.5 M H_3BO_3 + 4 g/l sodium saccharin + 1 g/l 2–butyne-1,4 diol. All solution were adjusted to pH=3. The deposition was carried out using copper working electrode with exposed area 1.5 cm^2 and platinum gauze anode. SCE reference electrode was adjacent to the back of the working electrode. Three samples were prepared at different potentials. The first sample was dissolved in nitric acid in order to determine the alloy composition by atomic adsorption. The second deposited sample was used to determine the surface morphology using SEM and EDS. The third sample was used to determine the alloy structure by XRD.

Figures 22–25 show the total current density i_T, Fe partial current density i_{Fe}, Ni partial current density i_{Ni}, and H_2 partial current density i_{H2} obtained at different electrolytes. Ni and Fe partial current density were determined by AA, while the H_2 rate was obtained by the difference between i_T and $i_{Ni}+i_{Fe}$. As it is shown in Figure (22), the presence of the organic additives in the plating bath decreases the total current density, enhancing the uniformity of the alloy. According to Figure (23), and Figure (24), the iron partial current density and the nickel partial current density also decreased when the deposition was carried out in the presence of the additives. However, in Figure (26), the iron atomic percentage is observed to increase when the organic additives are present in the electrolyte, indicating that nickel deposition rate is more inhibited in the presence of the additives than the iron deposition rate. In the absence of the organic additives and at higher cathodic overpotentials, the Fe content in the alloy decreases, indicating that the iron deposition rate at these potentials levels off and is slower than nickel deposition rate. Similar behavior was observed by Lieder and Biallozor (11). One of the functions of the additives used in this study was to maintain lower pH at the interface. In the presence of the additives as it is shown in our studies, less nickel is deposited and accordingly the Fe content in the alloy increases, which doesn't agree with the predictions of Dams and Croll theory. According to this theory one can expect that decreasing the pH at the interface will favor an increase of nickel content . The theoretical explanation of these observations will be discussed in our next paper. Current efficiencies as a function of the applied poptential is given in Figure (27).

On the basis of these preliminary measurements we have formulated our own composition of iron-nickel bath. The best results concerning iron-nickel deposition were obtained with a bath, whose composition is given as bath (5) in the text. As it is shown in Figure (32), an alloy with the best appearance was observed when bath (5) was used to deposit Fe-Ni. Figure (28) represents EDS spectrum and SEM of deposits plated in the absence of additives in the electrolyte. Cracks and black deposits appear at the corners and at the edges of the electrode. When bath (2), Figure (29), bath (3), Figure (30) and bath (4), Figure (31) were used to deposit Fe-Ni alloy, black deposits were not observed until the polarization potential reached a value of $E_{app.}$=-1.2V (SCE). In the experiments when bath (5) was used, the black deposit was not observed even at –1.4V (SCE). Bath (2) plates matted color deposits

and as shown in Figure (29), a specific circular surface nucleation pattern is observed. The SEMs at the black edges in Figure (28) show a porous structure. Such structure results from the higher current density and consequently from a high hydrogen evolution rate. The higher H_2 rate causes higher rise of pH at the edges, which in turn induces a porous precipitation of $Ni(OH)_2$ or $Fe(OH)_2$. Figure (33) gives the composition of Ni from EDS at the central regions, and in certain cases, the composition of the alloy at the black edges. Higher Ni content at the edges and the presence of oxygen suggests that the precipitate is $Ni(OH)_2$. The inclusion of sulfur from additives is shown in Figure (29) and Figure (30). It seems that thiourea and small amounts of saccharin are included in the deposits. The sulfur content in the deposits was determined using EDS and is given in Figure (34) for bath (2) and bath (3).. The alloy deposited in bath (3) and at potential E=–1.2V (SCE) shows no evidence of cracks. Only porous structure is observed at the black edges.

The XRD pattern of Ni-Fe alloys is shown in Figure (35), indicating a gamma phase structure.

CONCLUSION

Two procedures of investigation were applied to all deposited alloys. In the first procedure, all Fe-Ni alloys were deposited from electrolyte containing ions of both metals by a cathodic and anodic linear sweep of potential. In the second procedure, thin layers of 1 to 2 μm of Fe-Ni alloys were deposited from a solution containing ions of both metals by a potentiostatic pulse technique, followed by dissolution of the deposited alloy by anodic sweep voltammetry.

LSV recorded in electrolyte containing: 0.5M Na_2SO_4 + 0.005 M + 0.5 M $NiSO_4$ and the deposition carried out at –1.05 V (SCE), shows on the anodic branch two distinct current peaks with E_{1pa}= – 0.4 V (SCE) and a Ni dissolution broad peak at E_{2pa} = – 0.195V (SCE). The peak at E_{1pa}= –0.4 V (SCE) is more noble than an iron dissolution peak observed in this study at E = – 0.6 V (SCE) and for nickel-iron alloy could be due to two causes: some kinetic factor (formation of intermetallic compounds) or a significant free energy change of mixing of Fe-Ni may cause the shift of the peak away from its reversible position. According to the LSV studies and taking into account that iron and nickel make intermetallic compounds (Fe_3Ni, FeNi and $FeNi_3$), the peak at – 0.4 V corresponds to dissolution of Fe from Fe-Ni intermetallic compound. This peak is very well defined with a peak current which depends upon the amount of deposited nickel, concentration of the electroactive species in the electrolyte and upon the applied deposition potential.

The bath formulation for the electrodeposition of Fe-Ni has been modified by incorporating saccharin, thiourea and butyne-1–4 diole, and noticing their effect on the electrodeposition process by using LSV. These additives suppress the hydrogen evolution reaction by absorbing on the surface of the substrate. Also, saccharin relieves the stress of the deposited alloy. The presence of the organic additives in the plating bath decreases the total current density, enhancing the uniformity of the alloy. The nickel partial current density and the iron partial current density also decreased when the deposition was carried out in the presence of the additives. The Ni deposition rate is more inhibited in the presence of the additives than the Fe deposition rate. In the absence of the organic additives and at higher cathodic overpotentials, the Fe content in the alloy decreases, indicating that the iron deposition rate at these potentials is slower than the nickel deposition rate.

Alloys with the best appearance were obtained from a bath containing: 0.5 M $NiSO_4$+ 0.05 M $FeSO_4$ + 0.5 M H_3BO_3 + 4g/l sodium saccharin + 1 g/l butyne-1,4 diole.

Acknowledgment

This work was supported by Sandia National Laboratories and AESF project RF-83.

REFERENCES

1. H. Dahms, ***J. Electronal. Chem. Interfacial Electrochem.,*** **8** 5, (1964).
2. H. Dahms and I.M. Croll, ***J. Electrochem. Soc.*** **112**, 771, (1965).
3. M. J. Nikol and H. I. Philip, ***J. Electroanal. Chem. Interfiacial Electrochem.*** **70**, 233 (1976).
4. P. C. Andriacos, C. Arana, J. Tabib, J. Dukovic and L.T. Romankiw, ***J. Electrochem. Soc.*** **136**, 1336, (1989).
5. P. C. Andriacos, J. Tabib, and L. T. Romankiw, ***J. Electrochem. Soc. 135*** 1172, (1988).
6. J. Horkans, ***ibid 126***, 1861, (1979).
7. J. Horkans, ***ibid 128***, 45, (1981).
8. E. Beltowska-Lehman and A. Riesenkampf, ***Surf. Tech. 12***, 163, (1981).
9. M. Lieder and S. Biallozor, ***ibid 21***, 1, (1984).
10. D. L. Grimmett, M. Schwartz and K. Nobe, ***J. Electrochem. Soc. 137***, 3414, (1990).
11. M. Lieder and S. Biallozor, ***Surf. Tech., 26***, 23 (1985).
12. S. Hesaami and C. W. Tobias, ***J. Electrochem. Soc., 136***, 3611, (1989).
13. R. Macdonald, L. D. Potter Jr., ***Solid State Ionics, 23***, 61, (1987).
14. A. C. Riddiford, in ***"Advances in Electrochemistry and Electrochemical Enginering" Vol. 4*** P. Delahay, Editor, p89, Interscience, New York, (1966).
15. B. V. Tilak, A. S. Gendron, and M. A. Mosoiu, ***J. Appl. Electrochem. 7,*** 495, (1977).
16. S. Swathirijan, ***J. Electrochem. Soc., 133*** 671, (1986)
17. D. Gangasingh and J.B. Talbot, ***J. Electrochem. Soc., 138,*** 12, 3605, (1991).

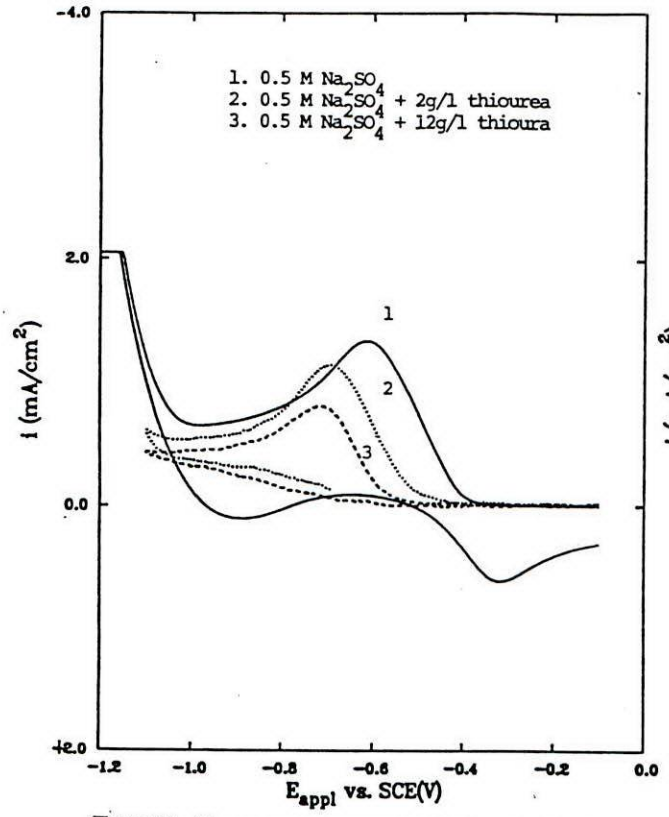

Figure (1) – Linear sweep voltammetry of a Pt rotating disc electrode in 0.5 M Na_2SO_4, pH=3, sweep rate v=30mV/s.
Effect of thiourea on hydrogen evolution.

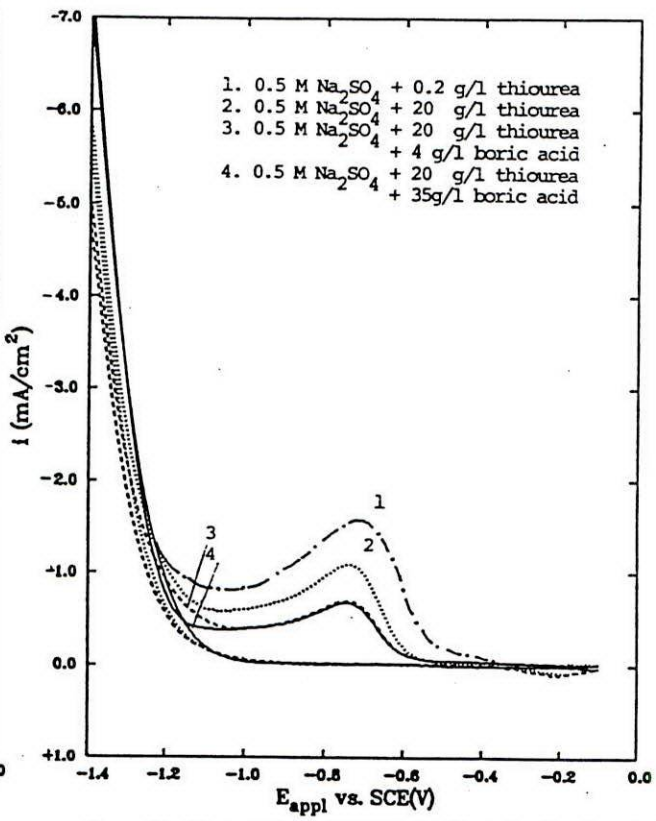

Figure (2) – Linear sweep voltammetry of a Pt rotating disc electrode in solution of 0.5 M Na_2SO_4. Sweep rate, v=30 mV/s
pH=3, w=0. Effect of thiourea and boric acid on hydrogen evolution.

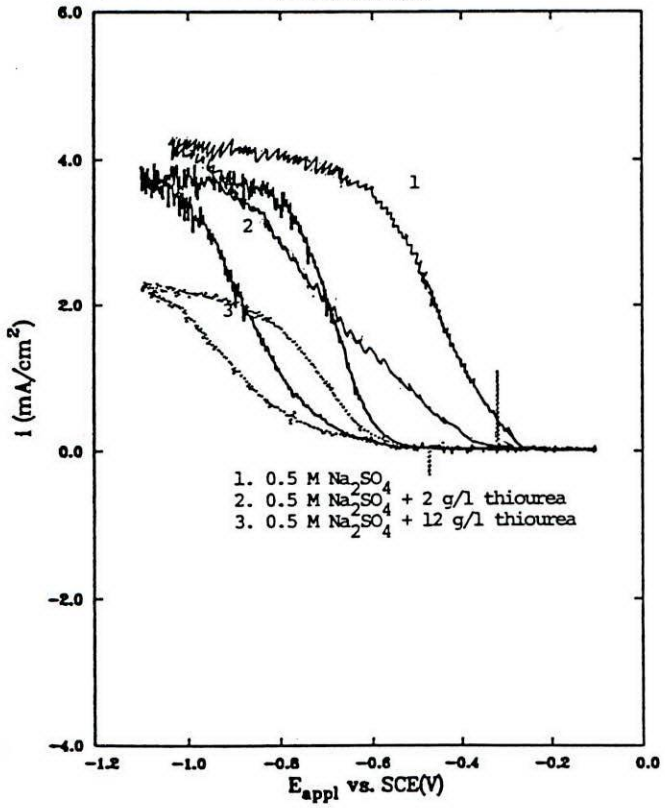

Figure (3) – Linear sweep voltammetry of Pt rotating disc electrode in 0.5 M Na_2SO_4. Sweep rate, v=30 mV/s,pH=3, w=250 rpm.
Effect of thiourea on hydrogen evolution.

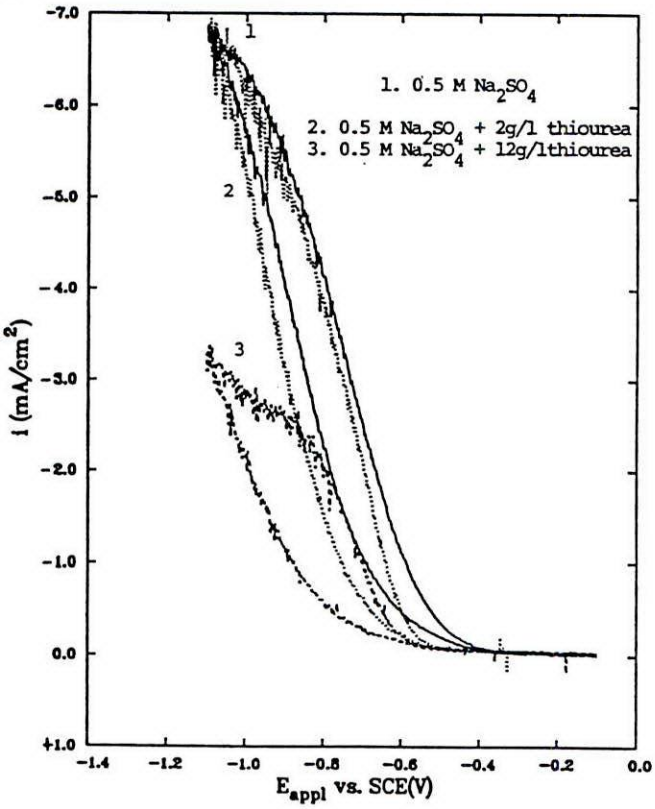

Figure (4) – Linear sweep voltammetry of a Pt rotating disc electrode in 0.5 M Na_2SO_4. Sweep rate v=30 mV/s, w=750 rpm.
pH=3.0. Effect of thiourea on hydrogen evolution.

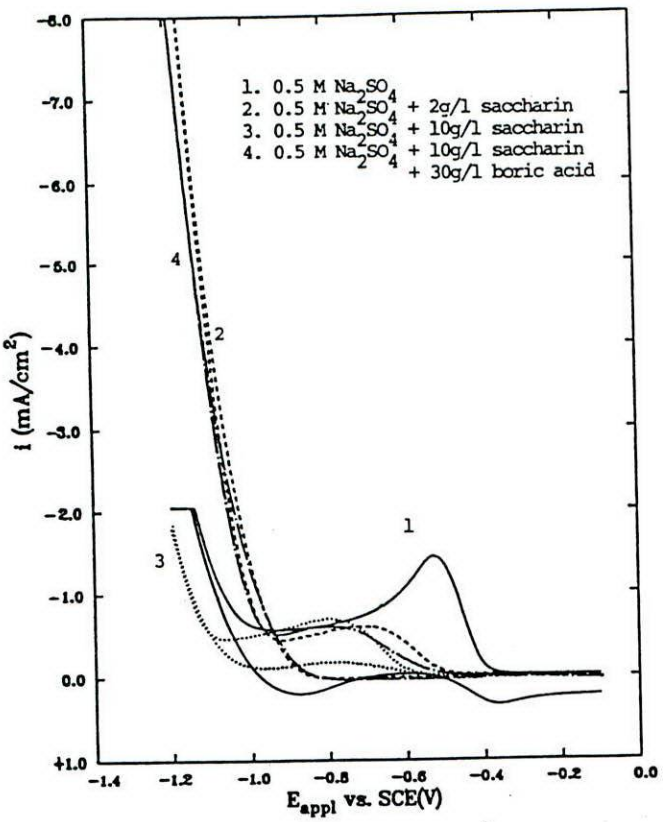

Figure (5) – Linear sweep voltammetry of a Pt rotating disc electrode in 0.5 M Na_2SO_4. Scan rate, v=30 mV/s, w=0, pH=3.0.
Effect of saccharin on hydrogen peak at – 0.6 V (SCE).

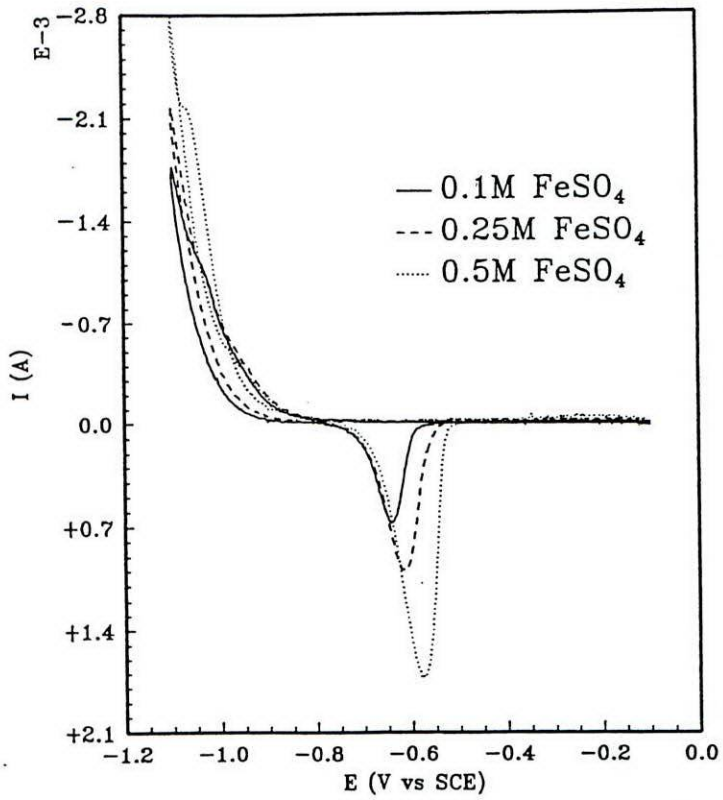

Figure (6) – Linear sweep voltammograms of a rotating Cu disc electrode in 0.5 M Na_2SO_4 solution, obtained for different $FeSO_4$concentrations. Reverse potential = – 1.1 V (SCE), v=30 mV/s, pH=3, w=0.

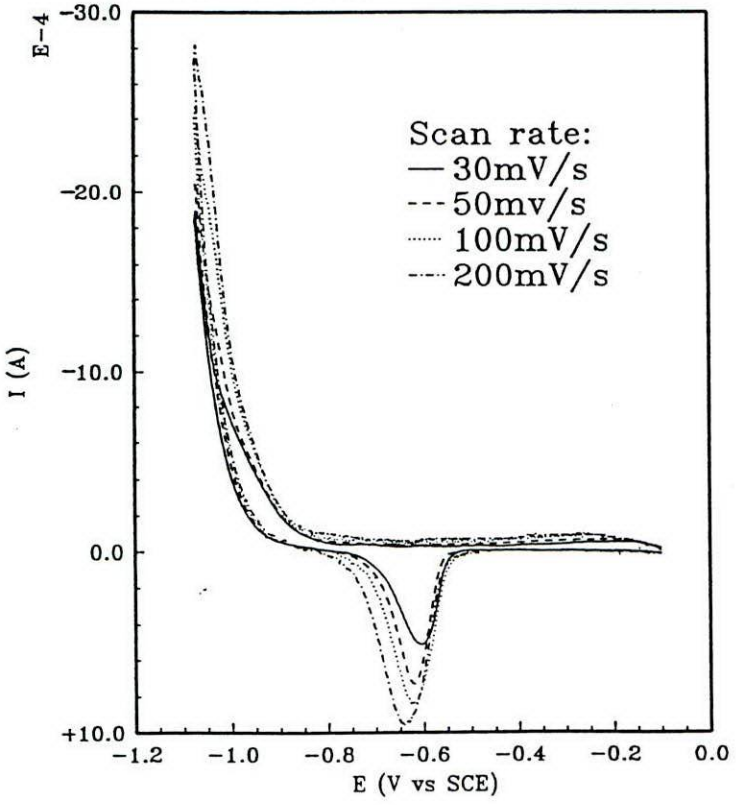

Figure (7) –Linear sweep voltammograms of a rotating Cu disc electrode in 0.5 M Na_2SO_4 + 0.5 M $FeSO_4$ solution, obtained for different scan rates. Reverse potential – 1.075 V (SCE). pH=3.0, w=0

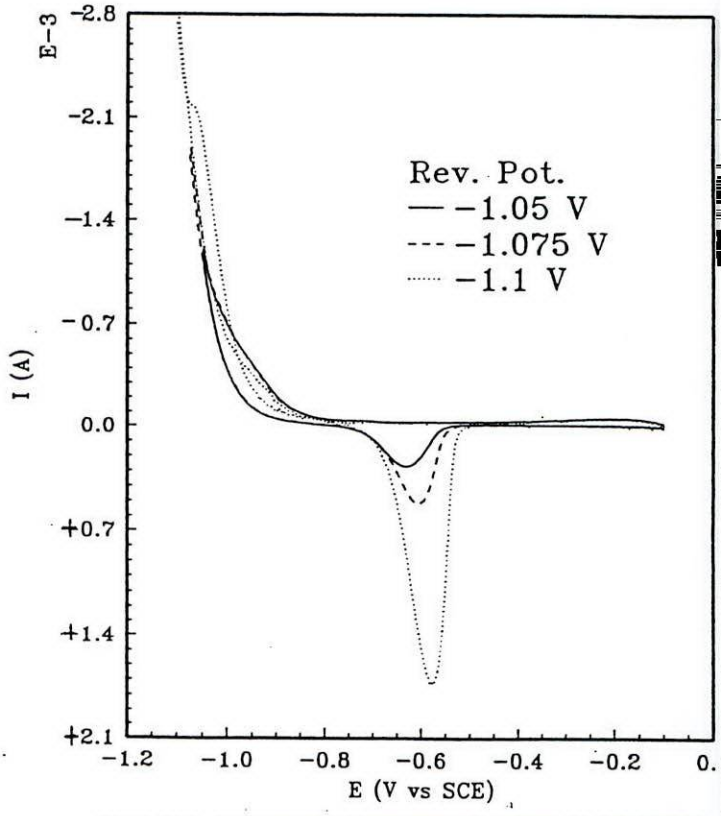

Figure (8A) – Linear sweep voltammograms of a rotating Cu disc electrode in 0.5 M Na_2SO_4+ 0.5 M $FeSO_4$ solution, pH=3, obtained at different reverse potentials. v=30 mV/s.

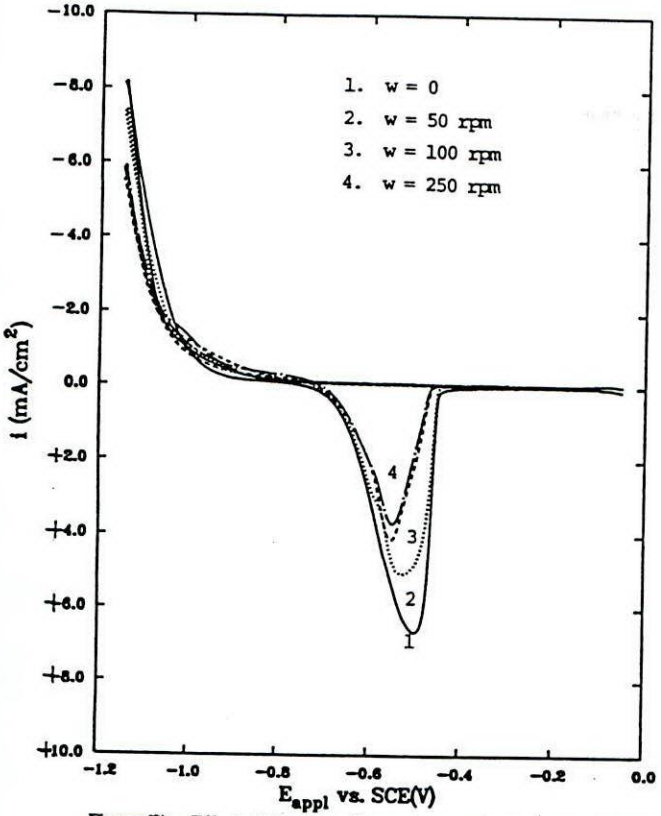

Figure (9) – Effect of the electrode rotation speed w on the anodic iron peak. Potentiodynamic stripping voltammogram of a Fe film electrodeposited on Cu rotating disc electrode from 0.5 M Na_2SO_4+0.2 M $FeSO_4$, pH=3.0.

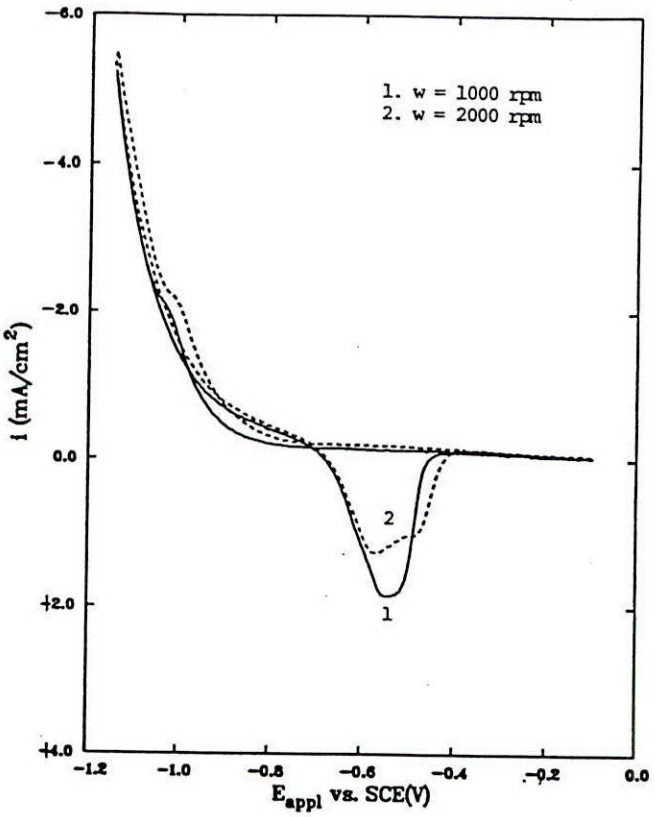

Figure (10) – The same conditions as in Figure (9), but at different electrode rotation speeds.

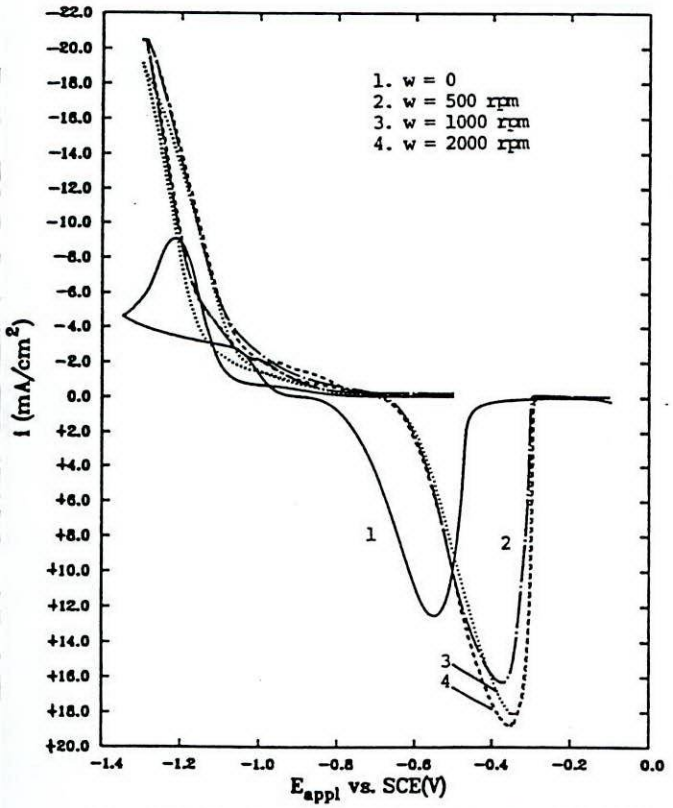

Figure (11) – Potentiodynamic stripping voltammograms of a Fe film electrodeposited on Cu rotating disc electrode from : 0.5 M Na_2SO_4+ 0.2 $FeSO_4$, pH=3.0, v=30 mV/s. Reverse potential= –1.350 V (SCE). Effect of the rotation speed on the anodic iron peak.

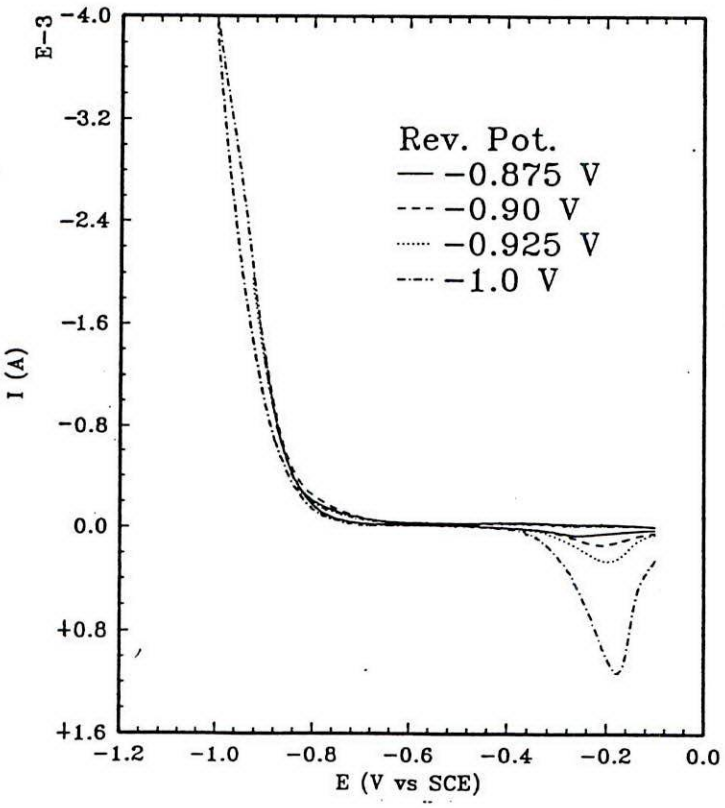

Figure (12) – Linear sweep voltammograms of a rotating Cu electrode in 0.5 M Na_2SO_4 + 0.5 M $NiSO_4$, obtained at different reverse potentials. Scan rate, v=30 mV/s, pH=3.0.

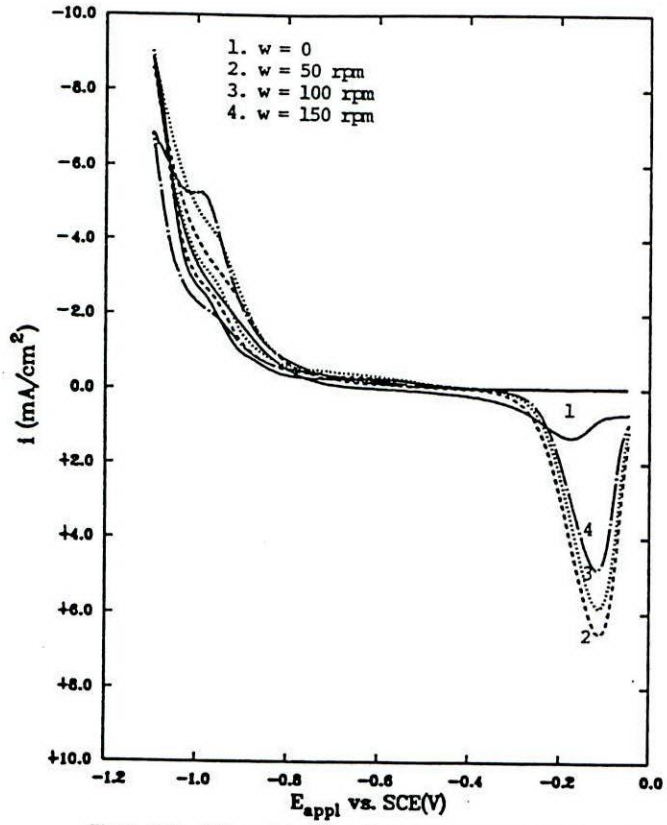

Figure (13) – Effect of the electrode rotation speed "w" on the anodic nickel peak. Potentiodynamic stripping voltammograms of Ni film electrodeposited on Cu rotating disc electrode from 0.5 M Na_2SO_4+ 0.5 M $NiSO_4$, pH=3. Sweep rate, v=30 mV/s.

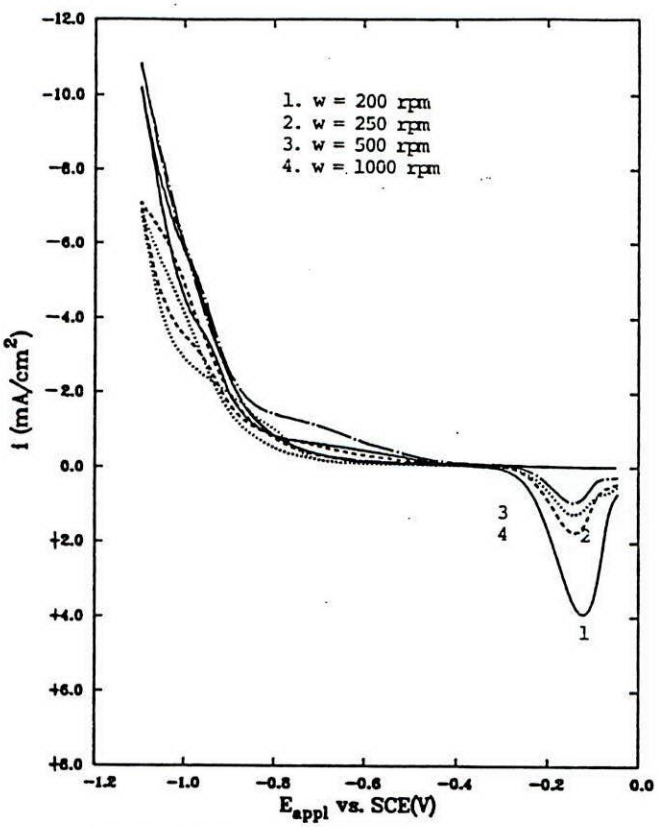

Figure (14) – Effect of the electrode rotation speed "w" on the anodic nickel peak. The same conditions as in Figure (13) but at different electrode rotation speeds.

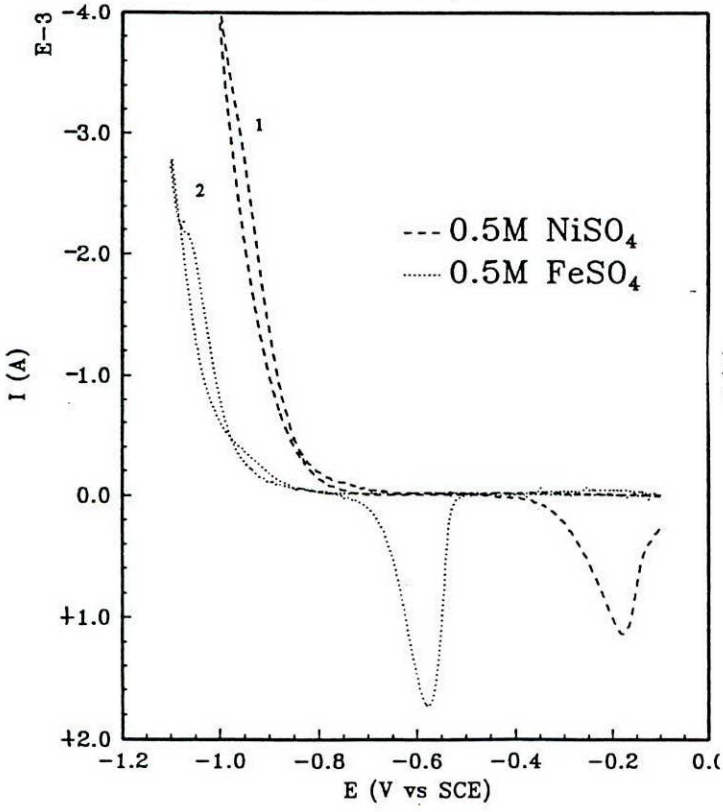

Figure (15) – Linear sweep voltammograms recorded on fixed copper disc electrodes in electrolyte containing: (1) 0.5 M $NiSO_4$+ 0.5 M $NaSO_4$ and (2) 0.5 M $FeSO_4$ + 0.5 M Na_2SO_4.

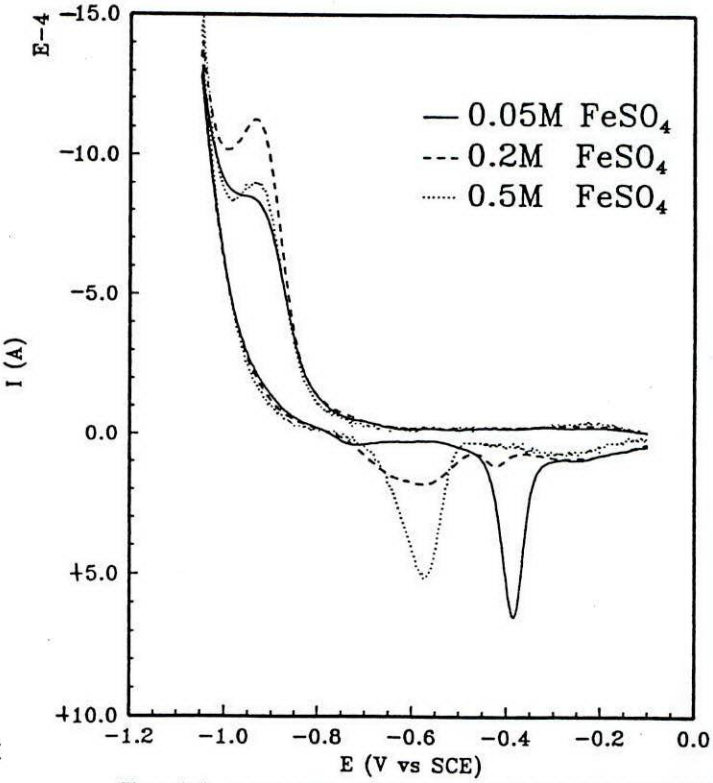

Figure (16) – Linear sweep voltammograms recorded on fixed copper disc electrode in 0.5 M Na_2SO_4 + 0.5M $NiSO_4$at different concentrations of $FeSO_4$. Reverse potential = – 1.05V (SCE), v=30 mV/s.

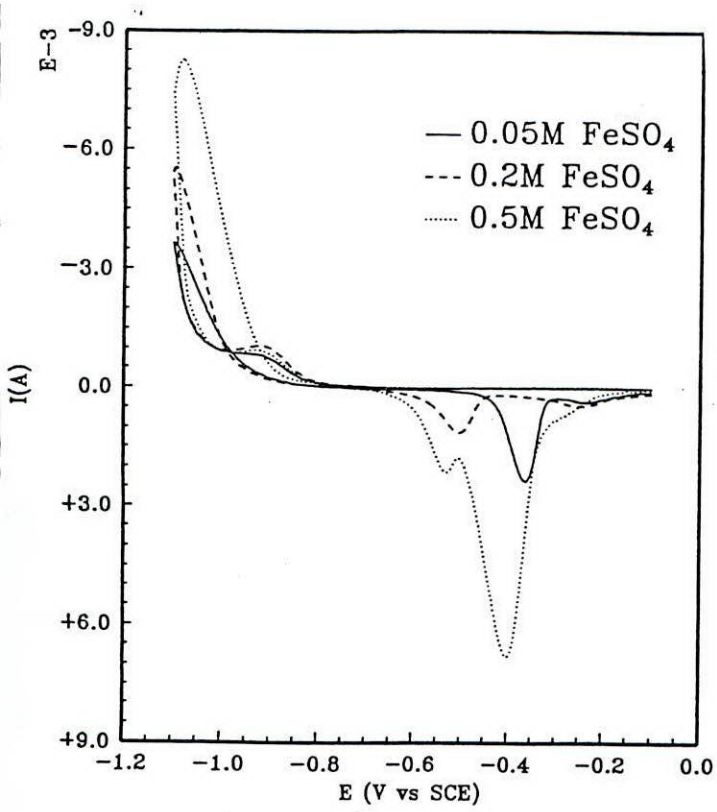

Figure (17) – Linear sweep voltammograms recorded on fixed copper disc electrode in 0.5 M Na_2SO_4 + 0.5 M $NiSO_4$at different concentrations of $FeSO_4$. Reverse potential = – 1.1V(SCE), v=30 mV/s.

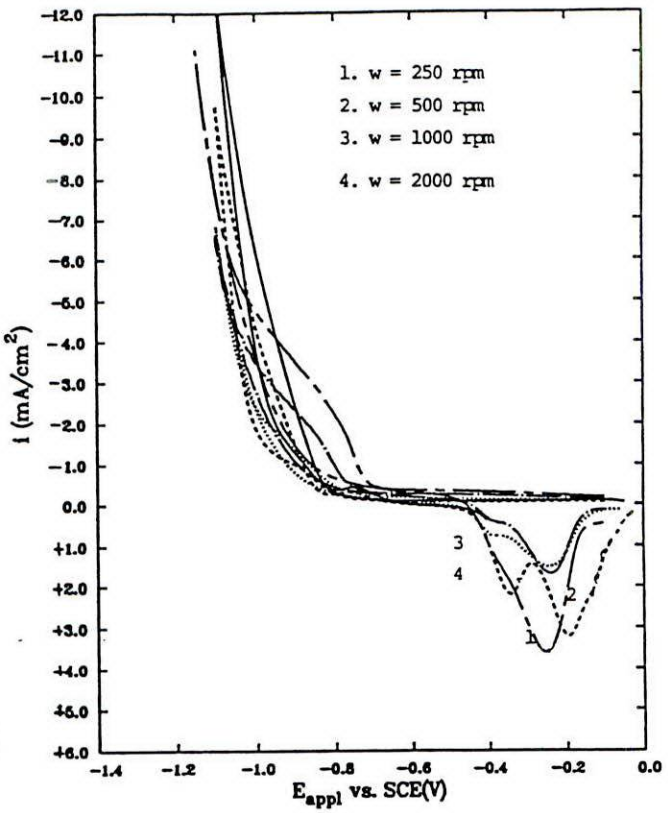

Figure (18) – Linear sweep voltammograms recorded on fixed copper disc electrode in 0.5 M Na_2SO_4 + 0.5 M $FeSO_4$ + 0.5 M $NiSO_4$ at different reverse potentials. v=30mV/s. pH=3.0

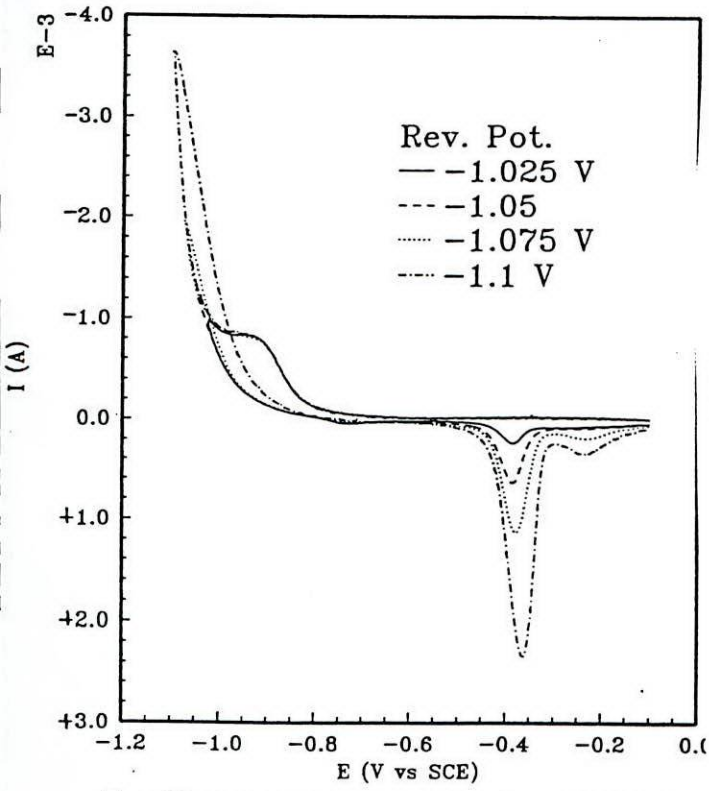

Figure (19) – Effect of the rotation speed "w" on the anodic Fe-Ni peaks. Potentiodynamic stripping voltammograms of Fe-Ni film deposited on copper rotating disc electrode at different rotation speeds in the electrolyte containing: 0.5 M $NiSO_4$ + 0.5 M Na_2SO_4 + 0.2 M $FeSO_4$.

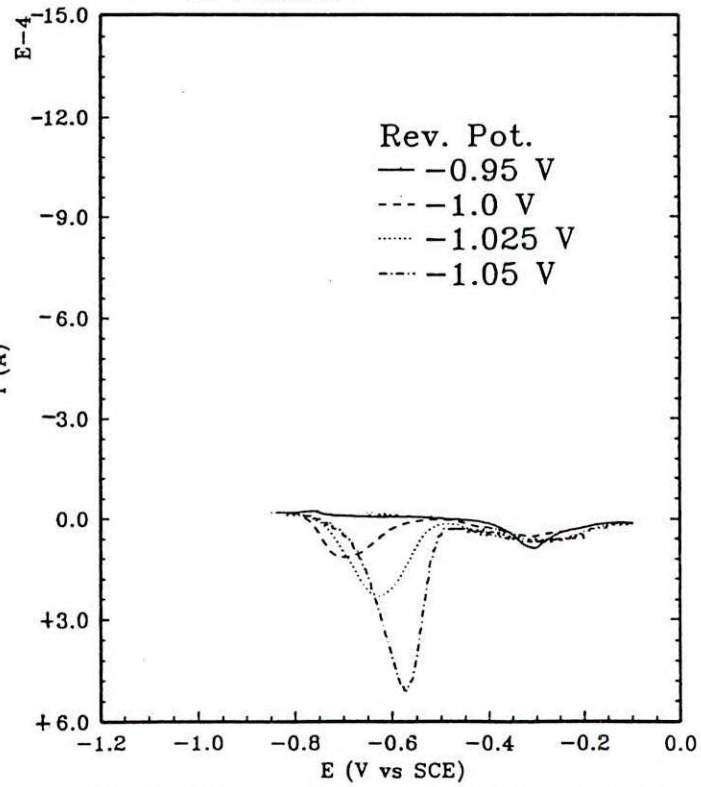

Figure (20) – Stripping voltammograms of Fe-Ni films recorded on fixed copper disc electrodes. Potentiostatic J-t transients of deposition of Fe-Ni alloy were carried out in electrolytes containing ions of both metals (0.5 M $NiSO_4$ + 0.5 M Na_2SO_4 + 0.2 M $FeSO_4$. pH=3.0, v=30 mV/s.

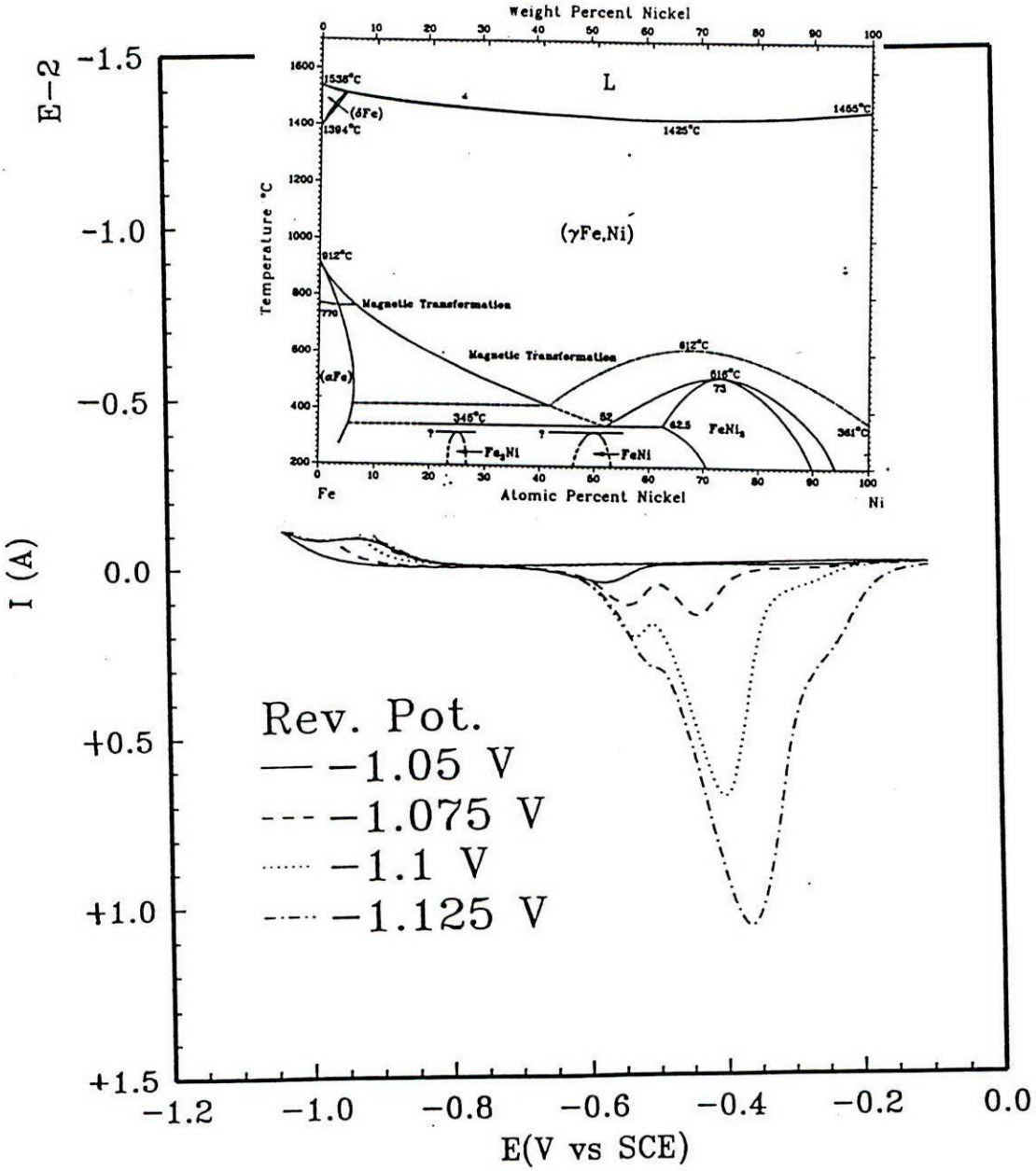

Figure (21) – Same as in Figure (20), but at higher cathodic deposition potentials.

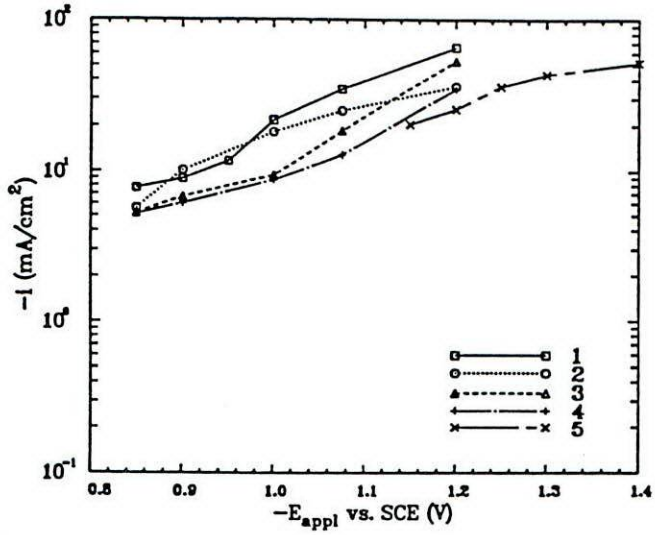

Figure (22) – Polarization curves for different baths.

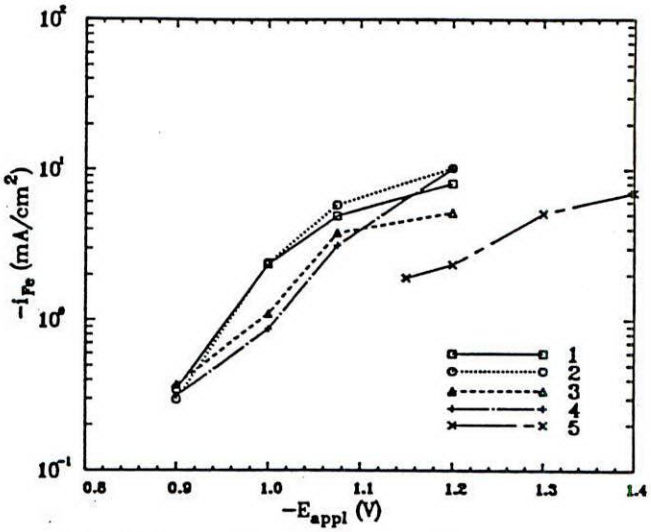

Figure (23)– Fe partial current density as a function of potential.

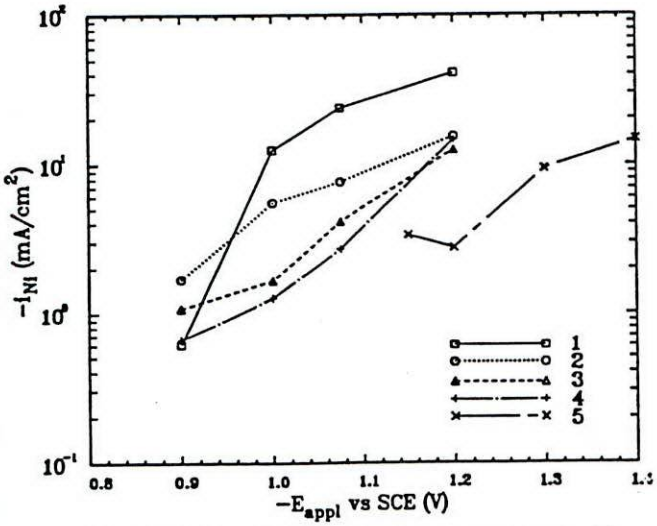

Figure (24) – Ni partial current density as a function of potential.

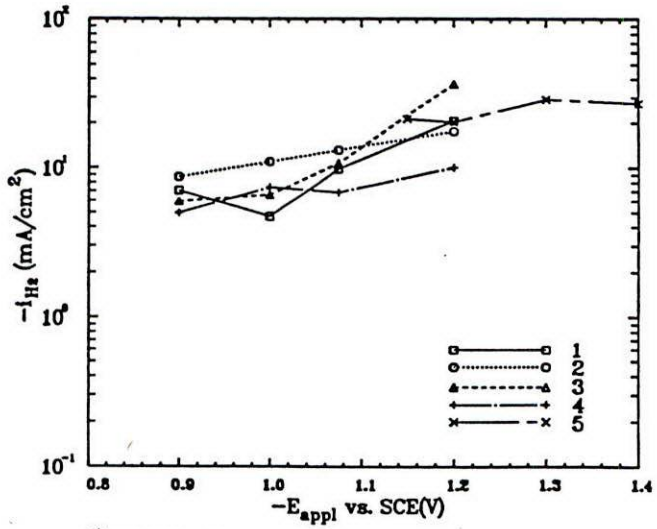

Figure (25) – Hydrogen partial current as a function of potential.

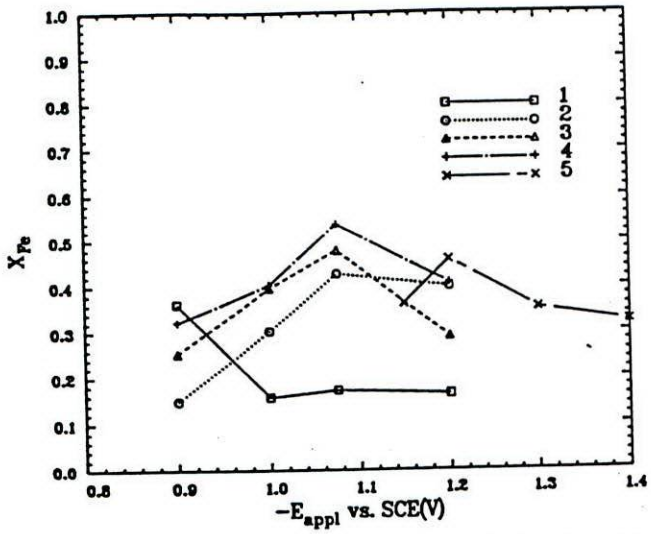

Figure (26) – Overall Fe atomic percentage as a function of potential

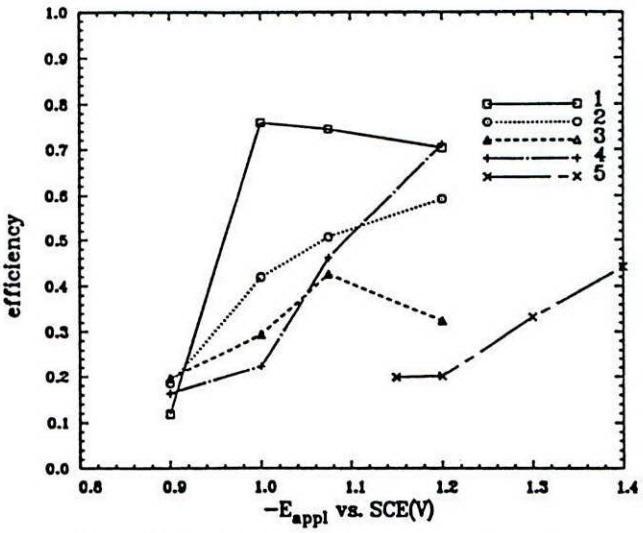

Fig.(27) Current efficiency as a function of the applied potential.

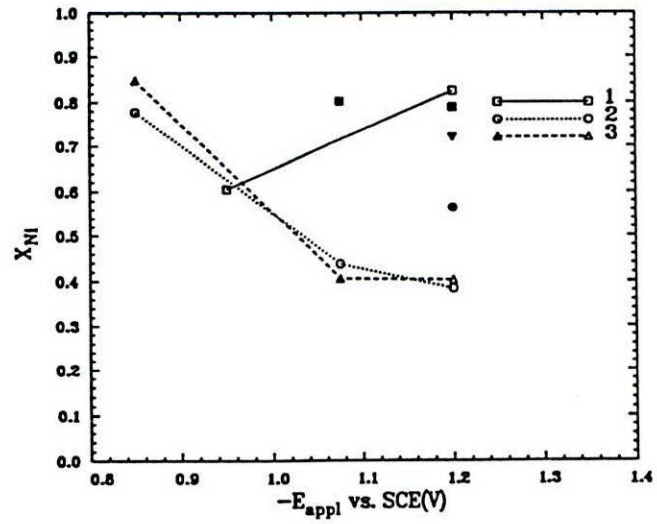

Figure (33). Ni atomic percentage at central regions and edges from EDS.

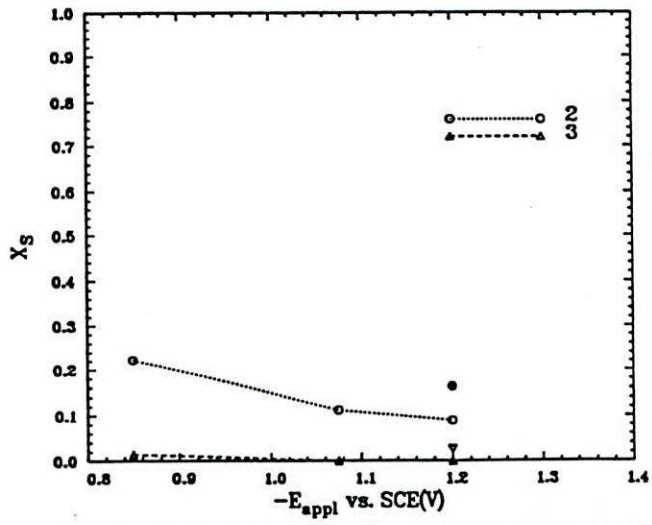

Figure (34). Sulfur atomic percentage at central regions and edges from EDS.

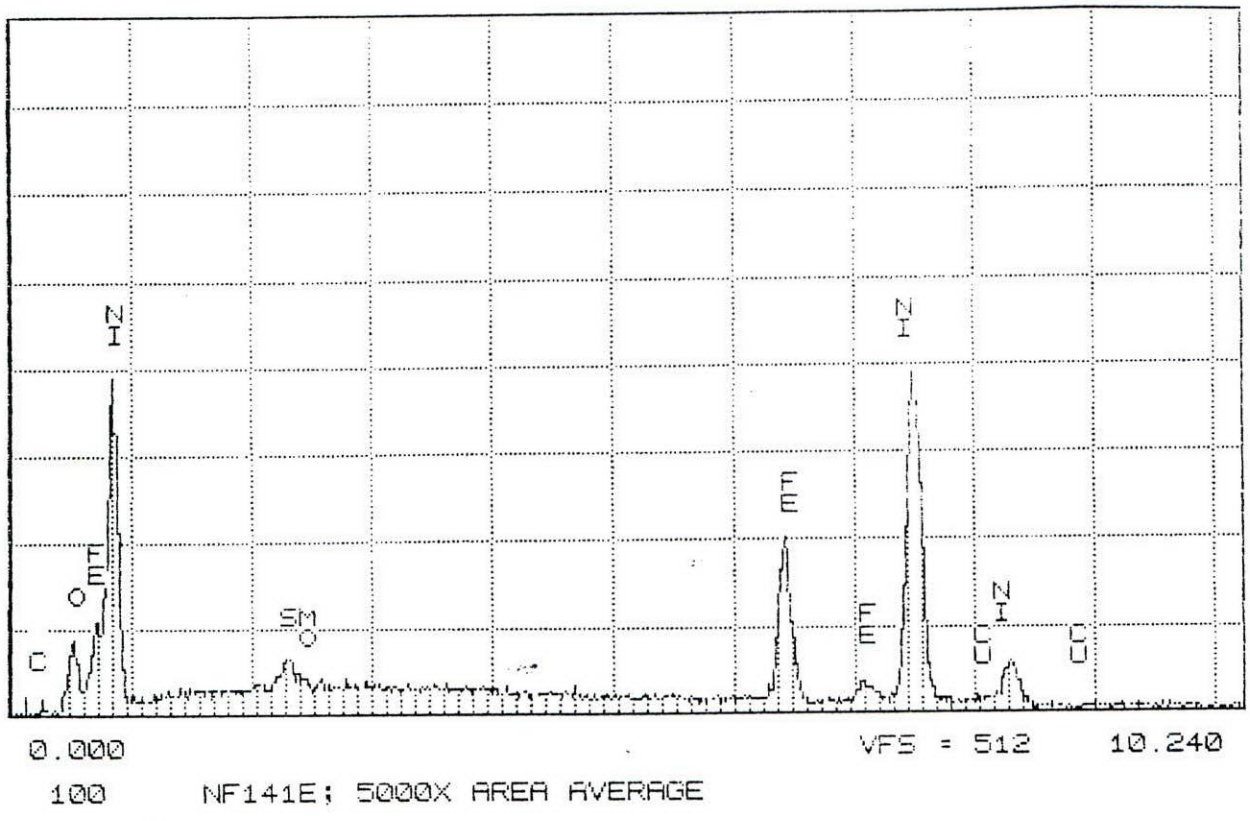

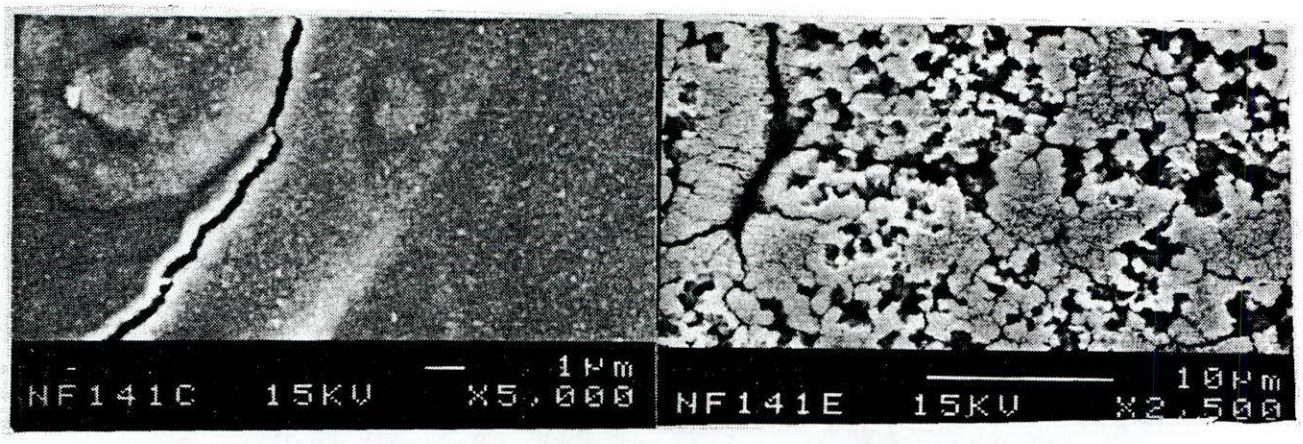

Figure (28) SEMs and EDS spectrum for alloys deposited from bath containing; 0.5M $NiSO_4$, +0.05M $FeSO_4$+0.5M Na_2SO_4.

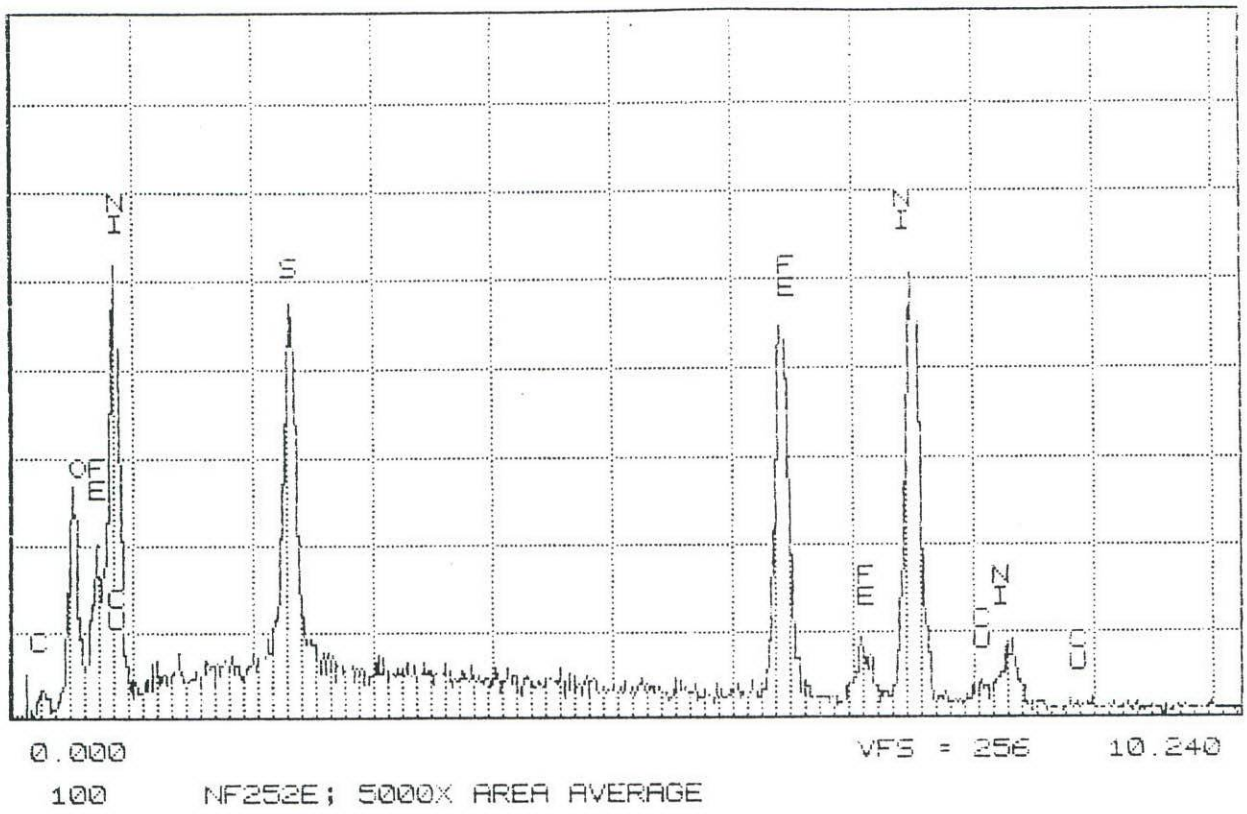

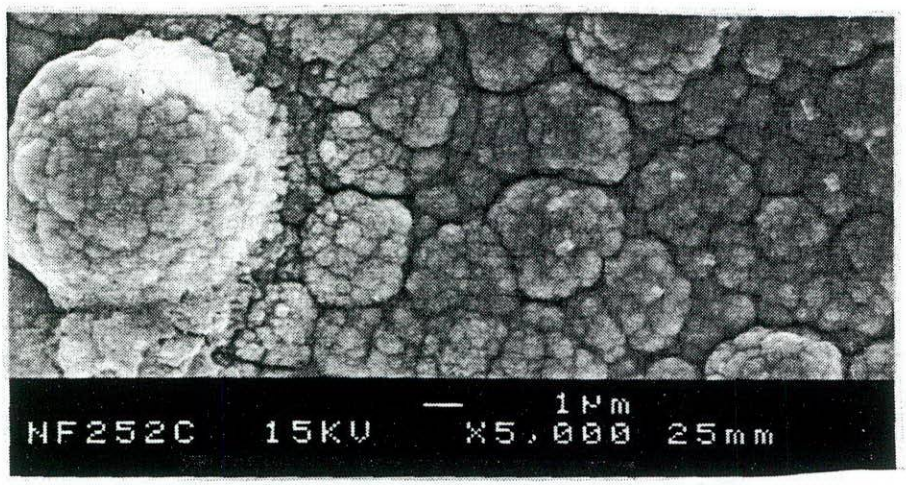

Figure (29) SEMs and EDS spectrum for alloy deposited from bath containing electrolyte in Figure 28 + 4 g/l thiourea, pH=3.

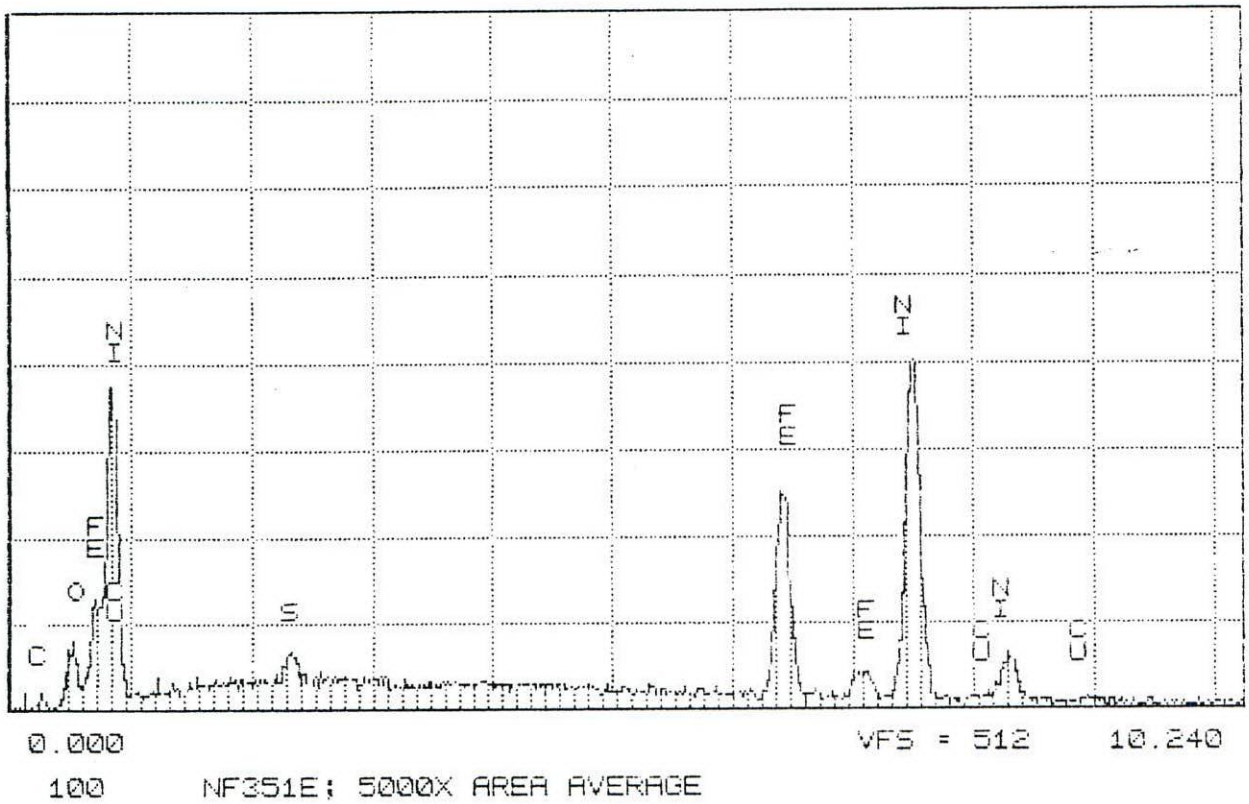

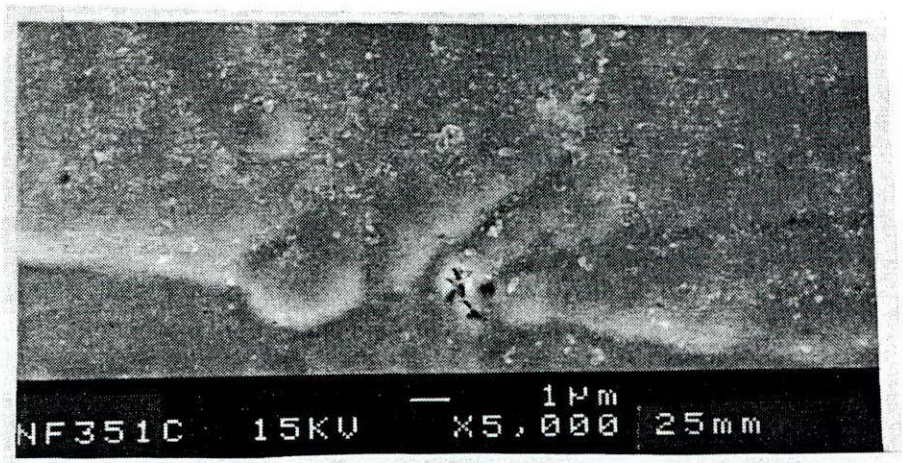

Figure (30) SEMs and EDS spectrum for alloy deposited from bath containing electrolyte in Figure (28) + 2g/l Na saccharin, pH=3.

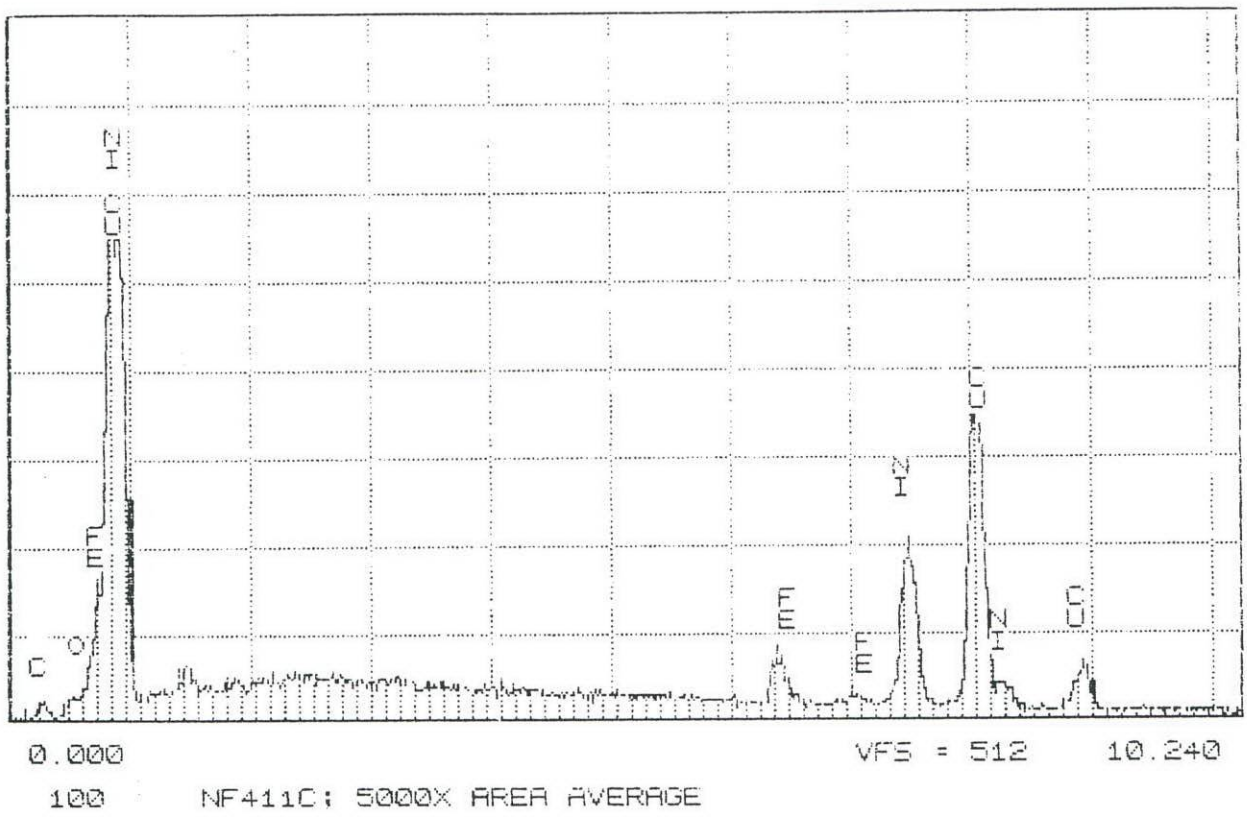

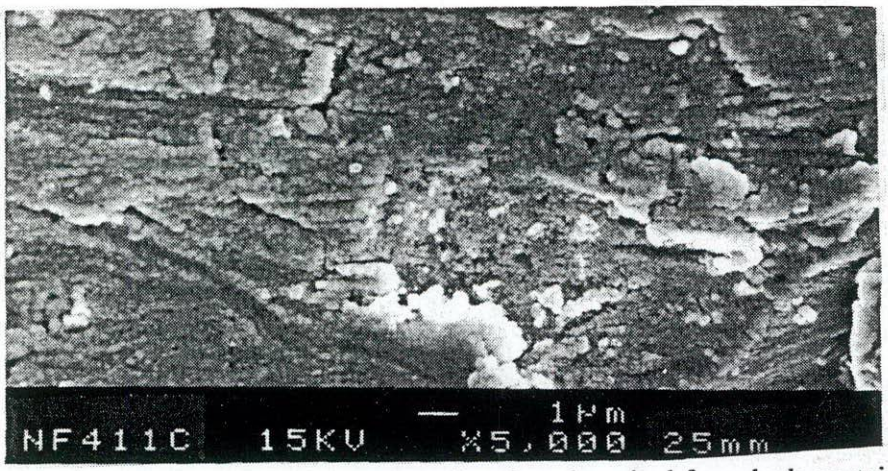

Figure (31) SEM and EDS spectrum for alloy deposited from bath containing electrolyte in Figure (28)+4g/l Na Saccharin + 0.5M boric acid, pH=3.

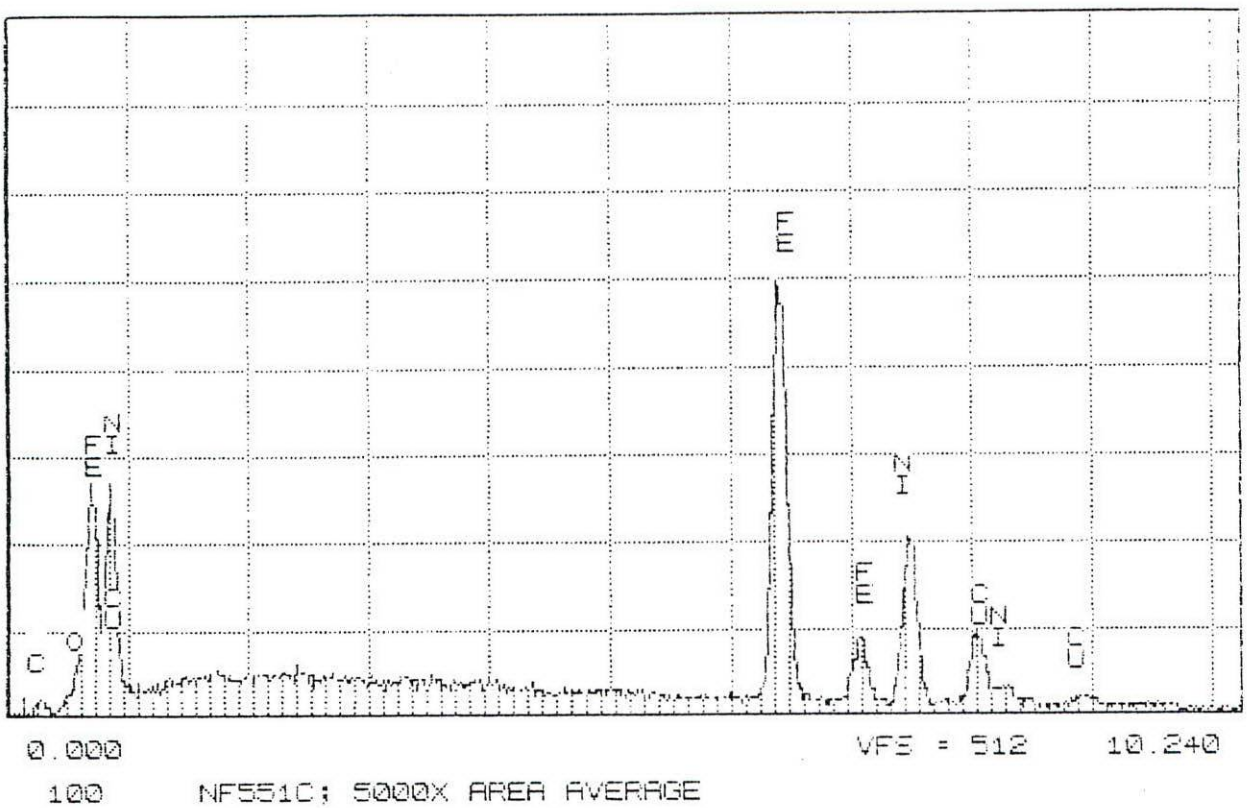

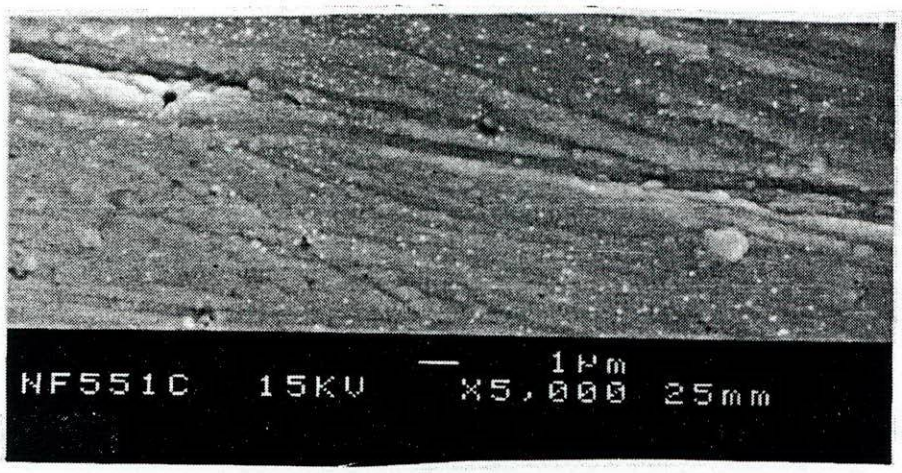

Figure(32) SEMs and EDS spectrum for alloy deposited from bath containing electrolyte in Figure (31) + 1 g/l 2–btyne-1–4 diol.

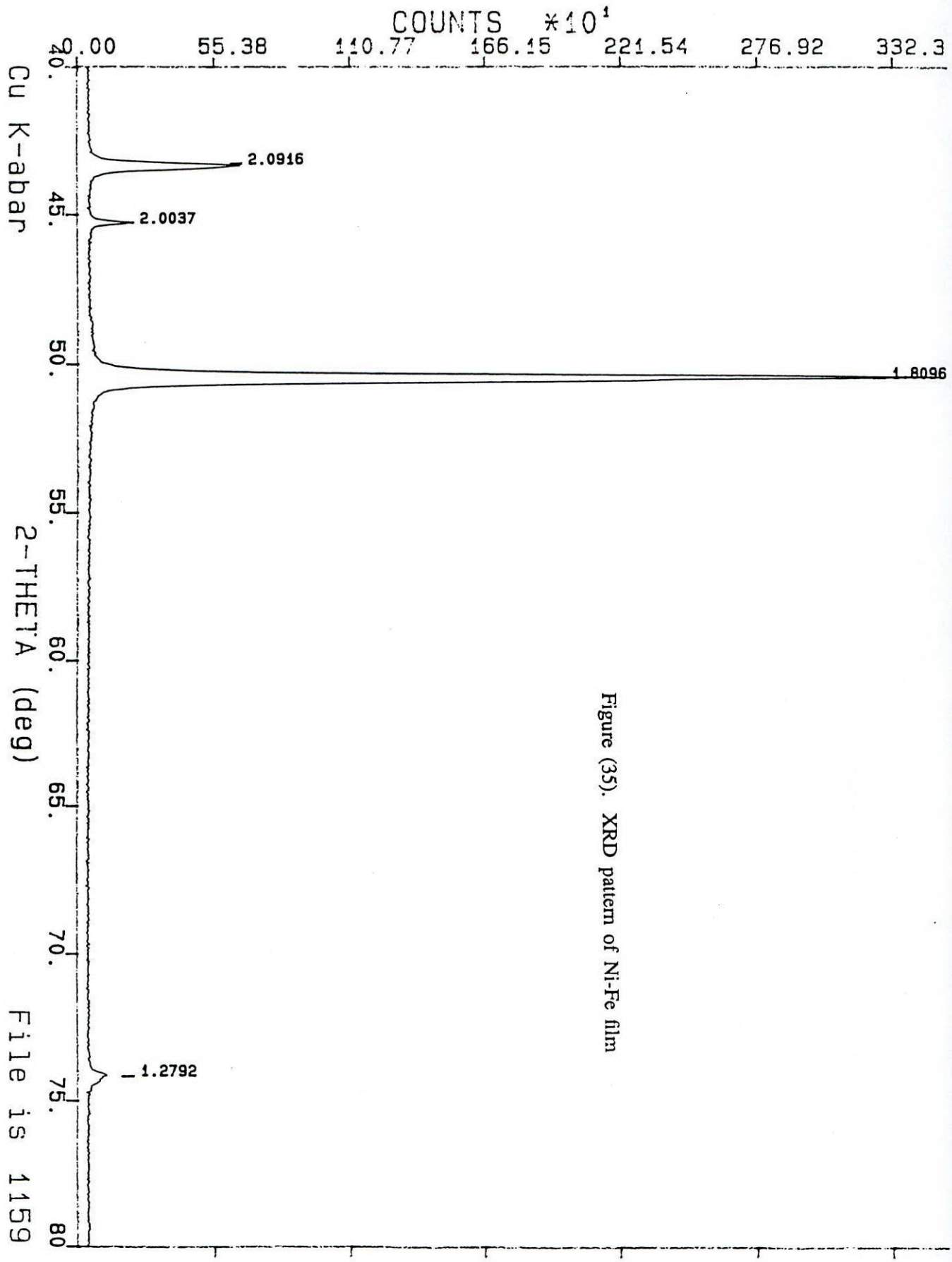

Figure (35). XRD pattern of Ni-Fe film

ELECTROFORMED SINGLE PIECE CASSEGRAIN MIRROR

Darell Engelhaupt, Chen Feng, John Cernosek
Center for Applied Optics
The University of Alabama in Huntsville

SUMMARY

Serious testing of imaging IR cooled detectors and focal plane arrays is expensive and difficult due to the lack of versatile coupling optics. Often the need is for broad band and very low level images to be coupled to an array detector which is planar. It is imperative that the signal-to-noise be optimized. The two approaches considered were modification of the dewar and fabrication of image couplers. The first approach requires suitable cooled baffles. This does not provide for control of the desired field of view other than to provide a stop or an iris. Beam diameter and focus are controlled only from outside the dewar. This approach also does not provide a versatile system which is easily modified for a number of applications.

The second approach is to design a modular image coupler and develop a low cost manufacturing process to produce a variety of similar components to simplify testing of cooled optics including focal plane arrays. In most cases the optical system must be small, light, free of stray light effects and yet cooled to liquid cryogenic fluid temperatures.

Mirrors offer nearly complete absence of chromatic aberration and attenuation with respect to broad wavelength requirements, unlike lenses. Aspheric mirrors which produce the image quality needed, have previously been notably expensive and difficult to machine and align. Manufacturing techniques for fabricating aspheric afocal and imaging systems by use of replication electroforming and single point diamond machining have demonstrated that custom designed aspherical mirror systems can be readily produced. Image couplers following principals of Cassegrain optical systems have been designed and fabricated.

A four mirror concept has been developed at UAH which enables an extremely compact folded image system to be contained within a small housing attached to a conventional low cost cryogenic dewar. The design of the system can be performed with conventional ray-tracing software and converted to actual hardware with minimal effort by single point diamond machining a standard aluminum blank into a mirror mandrel. This mandrel is then coated with appropriate layers of electroplated metal forming both mirrors and the supporting housing and ribs in one piece completing the telescope. The mandrel is removed with an alkaline etchant and the resulting single piece optical component is ready for mounting in the system without further alignment. A modular afocal beam expander was designed and built.

INTRODUCTION:

Focal plane array research is constrained by the fact that versatile, modular test stations are not available commercially. Typical imaging detector tests mandate fabrication of expensive unique image coupling devices simulating the actual systems under consideration. Stray light and field-of-view are often not well controlled during tests, leading to lowered signal-to-noise levels and ambiguity regarding performance of an actual system. The University of Alabama in Huntsville has developed an inexpensive process for producing image coupling devices suitable for testing and developing cooled focal plane array systems. Model image couplers for cryogenically cooled focal plane array detector research have been produced by this process. Electrodeposition procedures and precision single point diamond machining, combined with optical design procedures, permits fabrication of unique optical systems.

Applications include laboratory and field studies of beam expanders, broadband and thermal image couplers suitable for non-contact measurement, IR Spectroscopy and durable lightweight compact telescopes which image on focal plane arrays. Low cost, high strength, small and light weight deployable systems are also candidates for this technology.

This project has provided technology for producing electroformed replicate reflective optical systems which can be taken from concept through fabrication at low cost and minimal effort. Optical systems specifically designed to couple information to cooled detectors have been considered. The use of aspheric reflective optics is used to achieve broad bandpass, minimize chromatic effects and control stray light, coma and aberration. Additional control is achieved by selective non-reflective coatings applied to specific surfaces.

A four optical surface design has been employed using two small one piece interchangeable Cassegrain mirrors to achieve a wide range of optical properties. In this modular fashion, almost unlimited imaging or afocal collimating designs can be readily fabricated with excellent optical properties in very compact folded optical path configurations. Aspheric designs are used permitting excellent control of distortion.

DISCUSSION:

Testing of cooled optical systems and in particular focal plane arrays, has often not revealed the true behavior of the final system design. Overlooking problems involving field of view and stray light by using inexpensive dewars with no more than a window to allow imaging of a scene upon the detector can lead to serious design errors in the final product.

Notably an accurate model of the system using conventional practice may require an expensive mock-up approaching the value of the system under consideration. Field testing of true scenes has also been a formidable task. A low cost, modular image coupler approach was selected to provide an improvement over the present practice. Small reflective optical systems which can be used inside a commercial dewar are not available.

The use of replication processes to fabricate optical components has been reported. Commercial electroformed optics are available but do not include aspheric designs or compound mirror sets. The quality of these devices is usually less than required for imaging optical systems.

Two methods of improving the signal-to-noise of test systems are baffling of the optical path and closed path image coupling optics. The final device under consideration may consist of a complex optical system comprised of both.

An important aspect is the control of stray light in the form of radiant heat from the walls of a cryogenic dewar as well as the reflection of light from internal components. This is best achieved in an enclosed system with all optical paths defined, simulating the actual design under consideration. By cooling the entire enclosed image coupling assembly the apparent temperature of all other components is not radiant upon the detector.

By fabricating telescopes or other optical components using a single piece construction of only one material or materials with similar isotropic thermal expansion properties, it is in principal possible to completely eliminate the optical distortion effects of thermal contraction or expansion. The conic constants for aspheric mirrors remain constant while the physical dimensions change due to the contraction or expansion induced by thermal changes. The optical properties are essentially the same at any temperature so long as the assembly is of virtually the same thermal expansion material. The materials selected include either copper or nickel structures with or without thin gold reflecting surfaces which have closely matched thermal expansion properties. Blackened etched aluminum was selected for non-reflecting housing surfaces not attached to the mirrors. The designs may be easily repeated. The units developed can be coupled directly to the dewar cold finger for efficient cooling.

This task has defined low cost processes which expedite accurate design and fabrication of realistic broadband image coupling systems. The use of single point diamond machining and an enclosed one piece design using a soluble mandrel permit extremely rugged aspheric components to be designed and built with high accuracy. Controlled low-stress electrodeposition processes

reduce distortion. By using the UAH design, an entire four reflector cooled telescope can readily be as small as 30 mm diameter and 50 mm in length. The total weight of the optics can be 30 grams or less with an individual telescope weighing only a few grams. The design developed permits face to face pairs of Cassegrain or other two mirror systems to be developed for a wide variety of applications. Modular mounting components enable additional versatility.

Stray Light Control:

The imaged field of view for an imaging array must be controlled to avoid excessive noise levels. For the case of a single element detector such as those used for temperature measurements, spectral response and intensity sensitivity are the requirements. This type system may not require imaging if the spectral response can be demonstrated to be adequate. However it is still requisite that the signal observed at the detector is an accurate view of the scene of interest for accurate measurements, particularly when low temperature measurements are of concern. Most test setups have only a small window and do not account for stray light control. The field of view is often disregarded with no focusing or collimating optical components.

Signal to Noise Improvement:

1. The detector must be in direct contact with the cold finger or cooled chamber wall.

2. Only light from the selected FOV must reach the detector. Scattered and reflected light (or heat) must not subsequently be reflected back into the sensor.

3. Stray light (or heat) must not be reflected tangent to input baffles, or mounts reaching the sensor.

4. The FOV must usually be of infinite depth and rapidly convergent upon a flat detector array within the system. This in turn complicates the design of a system in terms of through focus distortion.

5. Obscuration should be less than 20% of the diameter of the imaging concentrator to avoid serious loss in signal intensity when low level signals are encountered. This is very difficult in compact two mirror Cassegrain or Ritchey-Cretien designs since the secondary mirror necessarily obscures the signal and proper coma correction is difficult without increasing the size of this mirror.

This task has identified that by using a unique four mirror system, folded ray paths can be made to rapidly converge an image accurately upon a flat sensor array element of 50X50 microns or

less over an area of 0.41 square centimeters. In the present face-to-face Cassegrain image coupler design the optical path can be corrected to minimize obscuration at the expense of imaging quality in the smaller mirror which in the first set of the pair is the primary. Subsequently the image may be re-corrected to provide good imaging in the smaller mirror of the second pair which is the secondary. This design yields a reduction in the obscuration observed.

Applications:

Thermal Imaging
Image Couplers
Focal Plane Arrays
Low Resolution Detectors
Non-Contact Temperature Measurement
Spectroscopy
Selective FOV
Remote IR Detection
Stray Light Control
Collimated Beam Expanders
Multiple Reflection Designs
Chromatic Aberration Free Designs
Broad Band Operation - IR to UV
Minimized Coma
Minimized Obscuration
Mass Production
Cooled Interchangeable Assemblies
Collimated Designs
Focused Designs

Deposition Processes Permit;

Aspheric Designs
Low Cost Accurate Optics
Light Weight
Elimination of Alignment
Rapid Replication or Design Change.

ACCOMPLISHMENTS:

The fabrication of a specific dewar design would only serve to satisfy the needs of an individual requirement. Proper shielding and coating of the cryogenic dewar and associated housing components for an experimental set-up would not likely satisfy a large number of individual tests. Therefor the approach pursued was to design a modular optical image coupler which could be modified easily to accomplish the task of coupling sensor elements such as focal plane arrays to the actual scene of interest while controlling the field of view and stray light. The use of compact face-to-face Cassegrain mirror pairs eliminates extraneous light from reaching the detector array.

Fabrication processes were developed to investigate low cost reflective optics of this type to circumvent the problems of baffling and coating the dewar walls as described. By using reflective optics many types of detectors and detector systems can be isolated when an environmental test is required. The use of a reasonably long standoff reflecting objective inside a system of shielding will enable focusing or defocusing a source to match the needs of a given detector system. Reflected light from a mirror has no chromatic aberration and as such mirrors can be focused in the visible and used from UV to IR with no change in focus and no variation in chromatic aberration correction. Thus the total aberration e.g. spherical, may be about one fourth that of comparable quality lens systems. The principal disadvantage is that imaging devices incorporating additional optics are inherently dimmer, i.e. the image formed is less intense than the object by the number of reflections times the reflectivity even in an off axis system. When central obscuration is also an issue, the intensity suffers as a function of the required obscuration.

Collimating afocal and imaging optical systems have been designed. Included is a very compact four mirror high order aspheric system designed to image to a 50X50 micrometer pixel in a plane array of 128x128. Optical design computer codes were used to develop the optical designs taking advantage of the aspheric options to minimize coma and distortion due to the planar focal requirements. An additional computer simplification was performed from this data to develop a table of values including all required machining information along with the optical surface data for input to the UAH, diamond machining center to fabricate the electroforming mandrel. Cooled mirror telescope designs can be ready for input to manufacturing in one day. Diamond machining can be implemented quickly since master programs and blanks exist at this point. Diamond machining has been used to fabricate aluminum mandrels with external optical surfaces enabling inspection of the surface quality. An optional gold optical surface is formed by depositing a layer of gold prior to copper or nickel. A copper mirror with nickel reflective surfaces is likewise produced by depositing a thin layer of nickel prior to the heavy copper deposit. These mandrels were then plated with a 0.040 inch coating of either copper or nickel to form the telescope with the optical surfaces inaccessible due to the re-entry shape obtained. The aluminum was dissolved away leaving a single piece mirror telescope including the secondary mirror support ribs. The one piece structure requires no alignment. Data analysis for modular pairs of mirrors has been completed and allows selection of pairs to produce afocal beam expanders with selective gain from 0.2 to 5.0. Diffraction limited optics are entirely possible including diffraction grating coatings and AR coatings. Engineering properties of materials may be selected. Copper may be used for high thermal conductivity and nickel for strength in light weight designs. Vacuum and electrodeposition combinations are possible.

*** PAPER NOT AVAILABLE IN TIME FOR PUBLICATION ***

Compositionally Modulated Alloys

Dr. D. S. Lashmore, Laboratory for Materials Science and Engineering, National Institute of Standards and Technology, Gaithersburg, MD

The electrodeposition and properties of compositionally modulated alloys (CMA) will be presented with emphasis on their magnetic and mechanical properties. A new technique for conducting tensile tests on thin foils has confirmed that the introduction of layers on the scale of several monolayers of atoms gives rise to extraordinarily strong materials. Magnetic properties of these materials has been shown to be an extremely sensitive probe of the degree of interdiffusion across the interface, and, indeed, electrochemically produced Cu/Ni. CMA have demonstrated the highest degree of saturation magnetization yet measured for Cu/Ni. A new and unexpected magnetic after-effect has been demonstrated.

*** For copies of this paper please contact the author directly:**

Dr. David S. Lashmore
Laboratory for Material Science and Engineering
National Institute of Standards & Technology
Building 224/B164
Gaithersburg, MD 20899
301/975-6405

ELECTROCHEMICAL ARRAY SENSORS FOR PLATING WASTE STREAM MONITORING

Robert S. Glass, Keith C. Hong, John C. Estill, Robert A. Reibold, Wade M. Thompson, Dennis W. O'Brien, and Dino R. Ciarlo, Lawrence Livermore National Laboratory, P. O. Box 808, Livermore, CA 94550 and Victoria E. Granstaff, Sandia National Laboratory, P. O. Box 5800, Albuquerque, NM 87185

Abstract

Electrochemical sensors are being developed to aid in waste reduction efforts for plating operations and in environmental remediation. An important feature of these sensor systems are solid-state multielement microelectrode arrays. The individual elements of these arrays will be selected so that a variety of chemical species can be detected using a single device. In addition, we are developing a compact electronics package, consisting of a potentiostat, signal generator, and microcomputer with user-friendly software to use in conjunction with the arrays. This report discusses the selection process for array elements, advantages of the use of microelectrodes, and application to the analysis of actual plating rinse tank systems.

Introduction

The Department of Energy (DOE) laboratories and plants have been required to modify their operations and procedures so that they are conducted in the best interest of the environment, safety, and health. In addition to current activities, this also includes the remediation of sites which have become contaminated with chemical and radioactive waste. Clearly, a variety of chemical sensors will be needed for these efforts.

Waste minimization for plating operations conducted within the DOE-complex is one specific area of concern. Many of the metal ions involved in plating operations, such as Cu^{+2}, Ni^{+2}, Cd^{+2}, Pb^{+2}, $Cr^{+3/+6}$, etc., as well as several anions, such as CN^-, are highly toxic, and the concentrations of these species which can be discharged to sanitary sewers are strictly regulated, as is solution pH. Currently, for rinse tank systems contaminant levels are usually determined in over-burdened analytical laboratories, which often have turn-around times of days or weeks and can be very costly. To this end, user-friendly chemical sensors which could be used by technicians on shop floors would be of great benefit.

While electrochemical sensors as a class constitute one of the oldest sensor types, they continue to enjoy widespread application. Recent developments in chemically modified electrodes and the increasing use of

ultramicroelectrodes has renewed an interest in them for use as environmental sensors. In our work, we have developed arrays of microelectrodes using both photolithography and more conventional methods (1,2). The use of chemical sensors in the form of arrays enhances chemical selectivity. We have used electrochemical arrays with relatively non-selective individual elements (i.e., each can have a substantial response to more than one chemical component), as well as those employing elements with intrinsically greater selectivity. In the former case, while each individual element may not yield a unique chemical signature, the sum of responses from the various elements can. Data analysis using non-selective element arrays is facilitated using some form of pattern recognition (1,3-5). In this regard, we have found the use of artificial neural networks to be particularly useful for the analysis of "noisy" electrochemical data (3).

For use as sensors for plating waste streams and other environmental applications, our current emphasis is on using arrays with elements having intrinsically greater selectivity for the detection of specific inorganic contaminants. For many of the chemical species of interest, electrochemical techniques exist (for use in the laboratory) which have high sensitivity and selectivity. For instance, specific elements can be designated for anodic or cathodic stripping voltammetry, using mercury thin film or chemically modified surfaces, respectively, for the detection of species such as Ni^{+2}, Cd^{+2}, Pb^{+2}, Cu^{+2}, etc. (6). As a pH sensitive element, hydrated iridium oxide films can be used because they have been shown to have a pH-dependent potential response (7). In addition, we have used ion implantation to create extremely thin modified membranes which can be used as anion ion-selective electrodes (ISE's) (8). For instance, implanting $^{35}Cl^{+}$ into a silver substrate microelectrode produces a Cl^{-} ISE. By combining these individual elements on a single microsensor, it is possible to more fully characterize an environment and detect a variety of contaminants.

In addition, we are developing a compact electronics package, consisting of a potentiostat, signal generator, and microcomputer with a user-friendly "canned" software package to use in conjunction with the arrays. Both modular and integrated designs have been considered. For ease of replacement of parts, or any other necessary maintenance, the modular design is preferred.

This presentation includes a summary of the development of electrochemical sensors for monitoring plating waste streams and other environmental applications. Much of our effort to-date has involved the selection and development of individual elements for incorporation into a microsensor array, defining behavior at microelectrodes, and devising mass fabrication methods for the microelectrode arrays. Mass fabrication implies relatively inexpensive devices which could potentially be disposed of following a prescribed period of use. Application of electrochemical

techniques to an actual rinse tank used for a copper plating bath will be presented. As we are limited in space, other details regarding the use of electrochemical array sensors for environmental applications can be found elsewhere (1-3).

Experimental

Chemicals and Solutions. Chemicals of at least analytical reagent grade quality were used, although in some experiments higher purity chemicals were used. For instance, in order to prepare the calibration curve for copper, ultrahigh purity $CuSO_4$ (Johnson Matthey Puratronic grade) and Na_2SO_4 (Aldrich 99.99+%) were used. For adjustment of the pH of the standard copper solutions to correspond to that measured for an actual rinse tank sample (see below), dropwise additions of 1M solutions of ultrapure KOH and H_2SO_4 (Johnson Matthey, 99.9999%) were made. Unless otherwise stated, solutions were prepared from purified, deionized water (18 MΩ-cm resistivity) from a Milli-Q™ purification system (Millipore, Inc.).

For determination of lead in "natural waters", water from a local San Francisco Bay Aqueduct was utilized. This water (pH = 8.3) is formed by the mixing of fresh water from the Sacramento River and saline water in the San Francisco Bay region.

The copper rinse tank sample was supplied by Allied-Signal, Kansas City Development Plant. The sample was taken following rinsing of 40 ft^2 of copper printed circuit board, and adjustment of the tank conductivity back to the set point of 20 μS using "house" deionized water. The pH of this water was determined to be 3.0 using a conventional glass pH electrode.

In the study of ion implanted chloride ISE's, prior to making measurement, 2 ml of ionic strength adjuster (5M $NaNO_3$, Orion) was added per 98 ml of solution.

Microelectrode Arrays and Individual Electrodes. The general fabrication procedures for electrode arrays prepared by photolithographic techniques have been described previously (1). The exact fabrication details vary somewhat depending upon the array design and materials used. A recent design is shown in Figure 1. Individual microelectrodes in this array sensor were discs 50 μm in diameter. These are shown as the dots at the ends of the "spokes of the wheel" inside the inner ring. The electrode materials for multielement arrays were chosen from the group Pt, Au, Ag, V, Ir, and C. Pt counter electrodes (outer ring) were employed, along with a Pt or Ag pseudo-reference electrode (inner ring), which could also be configured as a Ag/AgCl (no liquid junction)

reference electrode. All materials were deposited via DC magnetron sputtering using either an insulated silicon or ceramic substrate. Photoresist, polyimide, and SiO_2 have been used for masking to define precise electrode areas to be exposed to solution. Electrical contact to the microelectrodes is made through the pads at the top of the sensor chip using a specially designed holder and connector pin fixture.

Another type of multielement microelectrode array was fabricated by flame-sealing together individual glass capillaries that contained filaments of different materials; filament diameters were typically 50 μm (150 μm for Ir). The capillaries were bundled together inside a glass tube, which was then flame-sealed at the end. Following this, the sensing end of the array was ground and polished to expose the microelectrodes. Electronic connection was made through pins which were attached to the individual elements using conductive silver epoxy. These arrays (not shown) resemble those shown in Figure 1, although without the precise geometric registry between the elements attainable using the photolithographic technique.

Individual conventionally-sized disc electrodes (glassy carbon, 3.0 mm dia.; Pt, 1.6 mm dia.) and microelectrodes (Pt and graphite discs 10 μm in diameter) have also been used in this work and were either fabricated in-house (flame sealing procedure, as above) or were purchased from Bioanalytical Systems, Inc. (West Lafayette, IN).

Prior to use, the as-fabricated photolithographic arrays were rinsed with deionized water, acetone, absolute ethanol, and then allowed to air-dry. In all cases, the fused capillary arrays and the individual electrodes were polished to a finish of 1 μm using a series of alumina slurries (in some cases preceded by a wet polish with 600 grit SiC paper for the conventionally-sized electrodes), followed by immersion in deionized water in an ultrasonic water bath for 2-3 min to remove residual particles, and then rinsing with acetone.

Electrode Surface Modification and Experimental Procedure. For anodic stripping experiments various individual micro- and conventionally-sized electrodes were coated with a mercury thin film using standard means for the film deposition (6). This generally consisted of polishing the electrodes to a 1 μm finish using alumina slurries, then cleaning in an ultrasonic bath in deionized water for 2-3 min. Platinum electrodes were additionally immersed in hot concentrated nitric acid for 3 min., then rinsed with deionized water, and finally dried in air prior to film deposition.

Typical mercury thin films were deposited using the following procedure: a solution containing 5×10^{-5} M Hg^{+2} (from mercuric acetate) in 1N acetic acid/acetate buffer was deaerated for 8 minutes. Following this, a mercury thin film was deposited while holding the electrode at -0.9V vs. Ag/AgCl for either 20 or 30 minutes. Solutions higher in Hg^{+2}

concentration (5 x 10^{-4} M) were also occasionally used. During the deposition, when using the conventionally-sized electrodes the solution was stirred using a magnetic stirring bar. The solution was not stirred when depositing films onto microelectrodes. Following film formation, the electrode was held at 0.1V for 2 minutes.

Prior to deposition of Cu^{+2} or Pb^{+2}, the unknown and standard solutions were deaerated for 8 minutes. This was followed by deposition of the metal at -1.0 V vs. Ag/AgCl. Differential pulse anodic stripping voltammetry (DPASV) was the experimental technique used for analysis. Unless otherwise stated, the scan parameters for DPASV were: scan rate, 20mV/s; pulse amplitude, 50 mV; pulse width, 50 ms; and, pulse period, 0.2 s.

In order to increase the mechanical stability of mercury thin films used in stripping voltammetry, coatings of cellulose acetate were applied. For these studies, individual microelectrodes and conventionally-sized electrodes have been used. A thin film of cellulose acetate impregnated with mercury is created by dissolving 1 wt. % cellulose acetate in acetone, dipping the electrodes surface to be coated into this solution, then drying the sides by rolling gently in a lint-free paper towel, and finally, holding end-up in air until dry. Following this, the films were hydrolyzed by placing in 0.07M KOH at room temperature for 40 minutes while stirring, then rinsing with deionized water. This procedure follows closely that of Wang (9). Mercury was then deposited through the pores of the cellulose acetate coating, using procedures similar to those above.

Chloride ISE's were prepared by ion implantation in the following manner. Highly polished Ag substrates were mounted in a 200 keV ion implanter with the sample surface perpendicular to the ion beam. $^{35}Cl^{+}$ ions were mass spectrometrically selected from HCl gas for implantation into the Ag surface. Three sequential ion beams of energies 200, 70, and 33 keV were employed to yield a nominal implant depth of approx. 100 nm. A detailed discussion of the fabrication procedure for these ion implanted ISE's is provided elsewhere (8).

The procedure for the preparation of IrO_2 electrodes for pH measurement followed closely that of Hitchman and Ramanathan (10). Ir electrodes (discs and wires, 0.127 mm dia.) were cycled between -0.25 and +1.25 V (vs. SCE) in 0.5 M H_2SO_4 at 3 V/s for 8000 cycles, ending with a scan at 30 mV/s to the anodic peak. Variations on these scan parameters have also been used, with some resultant variation in pH response (i.e., slope and intercept of the potential vs. pH response). The pH response of these electrodes was determined using a universal buffer (7), which consisted of 0.01M H_3PO_4, 0.01M H_3BO_3, 0.01M CH_3COOH, and 0.10M KNO_3. Dropwise additions of 1M HNO_3 or NaOH were made in order to decrease or increase the pH of this buffer, respectively.

Voltammetric studies were conducted using a Bioanalytical Systems (BAS) Model 100B Electroanalytical System. All measurements were conducted at room temperature. Either a saturated calomel (SCE) or Ag/AgCl reference electrode was used, and solutions were deaerated with Ar or N_2 before each experiment (unless otherwise indicated).

Results and Discussion

As is now well-known, microelectrodes possess several desirable electrochemical characteristics (11-13). With regard to application as sensors, some of the more important of these are: relative immunity from uncompensated resistance, which allows direct use in environments of widely varying resistance; small sample volumes; high rates of mass transfer; high S/N ratio; and, a convenient form of data representation. In addition, microlithographic methods (e.g., photolithography) can be routinely used to fabricate arrays of microelectrodes of almost any useful geometry, using silicon or ceramic substrates. Arrays with several different electrode materials can be fabricated using sequential deposition. As mentioned above, because of the procedures which could be used to mass fabricate microelectrode arrays, low individual cost for these devices could result. Much of our current work, which will be discussed in this report, has been directed toward the selection of appropriate elements for the arrays to be used in our particular applications.

In general, it desirable to make sensor measurements with as little sample pretreatment as possible and to be able to use the sensors in "messy" environments. In some earlier work (2), we use individual microelectrodes and arrays to make measurements of toxic metal ions in natural environments. An example is shown in Figure 2. In this case, a bundle of 10 graphite fibers (each 8 μm in diameter) in one of the fused capillary arrays constituted the sensor microelectrode. A pre-deposited mercury film on this graphite fiber bundle (creating a so-called mercury film electrode, or MFE) was used to analyze for Pb^{+2}. In order to obtain the data shown in Figure 2, Pb^{+2} (from $Pb(NO_3)_2$) was added to San Francisco East Bay Aqueduct water. The stripping voltammogram using this electrode shows a peak for lead at -0.67 V vs. Ag/AgCl. Using incremental additions, a calibration curve of the stripping current vs. lead concentration is obtained, as shown in Figure 2. For this curve, the average of 3-5 independent determinations for each concentration were plotted.

For the results shown in Figure 2, no pH adjustment was made, nor was there any addition of a buffering agent or supporting electrolyte, which is commonly done in DPASV, especially when conventionally-sized electrodes are employed. Using microelectrodes, the ions already present in the natural water environment are of sufficient concentration to mitigate against the effects of uncompensated resistance which can cause increased background currents. Also, because of favorable mass transfer, no stirring

or other solution agitation is required during the deposition or stripping steps.

Similarly, we have used a MFE on both conventionally-sized and micro-platinum electrode substrates to analyze for uncomplexed Cu^{+2} in an actual rinse tank sample. In addition, we have used the mechanically more stable cellulose acetate/mercury films on microelectrodes. Both sizes of electrodes, and types of coating yield linear peak (stripping current) vs. Cu^{+2} concentration curves. An example curve obtained using the cellulose acetate/mercury sensing electrode is shown in Figure 3. As demonstrated here, the concentration of Cu^{+2} in the rinse tank can be obtained graphically from the measured stripping current peak value. In practice, the determination will probably be made using an automated standard addition method.

Beside increasing the mechanical durability, these polymer layers serve another function. Namely, they can exclude large organics or other surfactants which may adsorb onto the mercury surface (or other sensor electrodes) and inhibit response (9).

It should be noted that platinum is often not the ideal substrate to use for anodic stripping voltammetry. This is because platinum has a solubility of about 0.01 wt. % in elemental mercury (6), and therefore, it is available in the film to form intermetallics with other amalgamated metals, such as copper. When this occurs, the signal due to copper could be diminished. Iridium has a much lower solubility in mercury than does platinum ($<10^{-6}$ wt. %) (14) , and therefore would make a better substrate. Current work is focused on this as a base material. Because of their sensitivity for analysis of the metal cations fundamental to plating processes, an MFE element of some form, most likely the mechanically more stable polymer-modified film, will be incorporated as one element of our multielement arrays.

A final point concerns solution agitation during deposition. When we deposit mercury films on conventionally-sized electrodes, or in the initial metal deposition step, the solution is stirred to increase mass transport. When using microelectrodes, stirring the solution is usually not necessary because of more favorable mass transport characteristics in this case (11-13).

The peak current observed in stripping voltammetry is directly proportional to the deposition time used to preconcentrate the analyte into the mercury film (6). Figure 4 shows characteristic responses for three different systems: a conventionally-sized Pt/MFE used to evaluate the response for a 5 ppm Cu^{+2} solution, as well as an actual rinse tank sample of about the same concentration; and, a micro-Pt/MFE and the 5 ppm standard solution. The expected linear response is obtained in all cases.

Sample pH can also have an effect on the results of stripping voltammetry analysis. It is also a variable of environmental concern, and the pH of industrial discharges are restricted to certain ranges. Therefore, it would be desirable to incorporate a pH-sensing element in the microelectrode arrays to be used for analysis of plating waste. As is well-known, the glass electrode is typically used to measure pH in aqueous systems. Clearly, this cannot be integrated into an array of microelectrodes of the type we have proposed. It also has an upper temperature range of about 100°C. A more mechanically stable solid-state system system is needed which can be micro-patterned onto the arrays.

Recently, there has been considerable interest in the use of membranes formed from oxides of various metals for use as solid-state pH electrodes (7, 10, 15, 16). These oxides include TiO_2, IrO_2, PtO_2, Ta_2O_5, RuO_2, and several other materials. These materials show open-circuit potential pH sensitivities ranging from about 46 to more than 80 mV/pH (7, 15), depending upon the material and the oxidation state of the metal in the film. For IrO_2 , the pH response is assumed to arise from a redox reaction mechanism (involving different oxidation states of iridium) tied to proton ejection from the hydrated oxide films (15). Of the various systems investigated, the IrO_2 electrode has arisen as the most promising alternative to the conventional glass electrode because of its stability, smaller redox interferences, and range of linear pH response.

Using an iridium microelectrode, we electrochemically formed an anodic oxide film on the surface using potential cycling (see experimental). As shown in Figure 5, a linear potential vs. pH calibration curve in standard buffers was obtained for this electrode. We also used this electrode to determine the pH of the same rinse tank sample which we analyzed for Cu^{+2} in the anodic stripping experiment discussed above. The pH of the rinse tank sample was determined to be about 3.2, a value extrapolated from the measured potential response. This agrees closely with the pH of 3.0 measured using a conventional glass electrode. The reason for the small discrepency is not known and is under current investigation.

It is clear that such micro-IrO_2 pH-sensing elements could easily be integrated into a multielement sensor array. Methods such as d.c. magnetron sputter deposition using an IrO_2 target (17), or ion implantation of oxygen into an iridium substrate could be used to pattern such elements.

There are also numerous anions which are important for plating bath operation and of environmental concern in rinse tank systems. With regard to environmental concerns, cyanide ion is of obvious importance. Therefore, we would also like to include anion-specific elements in the multielement arrays. As for the pH element, commercial sources for such ion-selective electrodes (ISE's) exist. Solid-state membrane ion-selective electrodes are commonly fabricated from single crystals, disks cast from

melts, sintered materials, and pressed polycrystalline pellets (18). For instance, a AgCl membrane fabricated using such methods in contact with a silver substrate constitutes an ion-selective electrode for the chloride ion. Conventional methods do not, however, readily lend themselves to fabrication of multielement microelectrode arrays of the type under development.

We have fabricated a solid-state membrane chloride ion-selective electrode using ion implantation. We have found that if chloride ions are implanted into a silver substrate, a solid-state membrane ISE can be produced which shows (approximately) the expected Nernstian response in solutions containing chloride ion over several decades of Cl^- concentration. The responses of three separate chloride ion implanted ISE's to Cl^- in solution (concentration range 1-1000 ppm) are shown in Figure 6. Note the very good reproducibility of the response between different implanted specimens. The slope ($dE/d\log[Cl^-]$) is -51 mV when the full concentration range in Figure 6 is considered; and is -54 to -58 mV for the individual electrodes when data in the range 10-1000 ppm is considered. While the results reported here were obtained using electrodes of conventional size, this method of preparation obviously readily lends itself to the fabrication of multielement microelectrode sensor arrays.

In addition, the potential response of the ion implanted ISE compares quite favorably to that of a commercially available Cl^- ISE (Figure 6, inset). Because we have precise control over the implantation energies and doses, we can tailor the thickness of the implanted layer. For the ISE's shown in Figure 6, the thickness of the implanted layer was about 100 nm. These very thin layers result in rapid response times (<1.5s).

Different combinations of substrates and implanted ions will yield ISE's selective toward different ions, such as CN^-. Ion implantation readily lends itself as a technique to the mass fabrication of arrays of micro-ISE's. Further details regarding the preparation and properties of ion implanted ISE's are provided elsewhere (8).

Finally, the electrochemical sensors are complete with the development of a user-friendly compact electronics system with "canned" analysis software. These systems will contain a potentiostat, microcomputer, an analysis chamber containing the multielement microsensor array, and a sampling and analysis procedure incorporating flow or sequential-injection analysis (19, 20). Our present concept for such a system is shown in Figure 7. It is a modular design which, as mentioned above, would facilitate any necessary maintenance and scheduled replacement of sensor arrays.

Conclusions

Electrochemical sensors readily lend themselves to the analysis of plating baths and associated rinse tanks. For these systems, we are developing techniques for monitoring for specific chemical species of environmental concern and process control, such as Cu^{+2}, Cd^{+2}, Pb^{+2}, pH, and various anions. In this effort, we are developing multielement microelectrode arrays using state-of-the-art microlithographic techniques. Chemical and physical methods transform the as-deposited sensor elements into ion-specific sensors. Specifically, techniques such as ion implantation and polymer modification have been shown to be valuable in the precise tailoring such elements for this purpose.

In the present work, examples have been presented of the application of electrochemical sensors for the analysis of an actual plating bath rinse tank, and several other applicable systems. Our work to-date has been focused on the development of individual elements to be included in array sensors, and upon methods which could be used for mass fabrication of arrays. The advantages of the use of microelectrodes in such arrays has been demonstrated by us and others. Advantages of these devices include low detection limits, large dynamic ranges, small sample volumes, to name a few. The multielement microelectrode arrays will be interfaced to a user-friendly, compact electronics and data analysis system, which is also under development. We believe that these systems will also find use in numerous other areas of environmental monitoring and process control.

Acknowledgements

Work performed under the auspices of the U.S. Department of Energy by the Lawrence Livermore National Laboratory under contract number W7405-ENG-48.

References

1. R. S. Glass, S. P. Perone, and D. R. Ciarlo, Anal. Chem. 62, 1914 (1990).

2. R. S. Glass, K. C. Hong, K. Ashley, and V. E. Granstaff, "Versatile Electrochemical Microsensors for Environmental Monitoring," Proceedings 1991 Annual Meeting of The American Institute of Chemical Engineers, Symposium on Electrochemical Sensors, paper No. 164c, Los Angeles, CA, November 17-21, 1991. Lawrence Livermore National Laboratory Report UCRL-JC-108143.

3. R. S. Glass, K. C. Hong, E. M. Johansson, and F. U. Dowla, manuscript in preparation.

4. W. P. Carey, K. R. Beebe, B. R. Kowalski, D. L. Illman, and T. Hirschfeld, Anal. Chem. 58, 149 (1986).

5. D. S. Ballantine, S. L. Rose, J. W. Grate, and H. Wohltjen, Anal. Chem. 58, 3058 (1986).

6. J. Wang, *Stripping Analysis*; VCH Publishers: Deerfield Beach, FL, 1985.

7. A. Fog and R. P. Buck, Sensors and Actuators 5, 137 (1984).

8. R. S. Glass, R. B. Musket, and K. C. Hong, Anal. Chem. 63 (19), 2203 (1991).

9. J. Wang and L. D. Hutchin-Kuma, Anal. Chem. 58, 402 (1986).

10. M. L. Hitchman and S. Ramanathan, Analyst 113, 35 (1988).

11. R. M. Wightman, in *Electroanalytical Chemistry*, Vol. 15; A. J. Bard, Ed. Marcel Dekker: New York, 1989.

12. S. Pons and M. Fleischmann, Anal. Chem. 59, 1391A (1987).

13. M. Fleischmann, S. Pons, D. R. Rolison, and P. P. Schmidt, *Ultramicroelectrodes*; Datatech Science: Morganton, NC, 1987.

14. R. R, De Vitre, M. -L. Tercier, M. Tsacopoulos, and J. Buffle, Anal. Chim. Acta. 249, 419 (1991).

15. W. Olthuis, M. A. M. Robben, P. Bergveld, M. Bos, and W. E. Van Der Linden, Sensors and Accuators B 2, 247 (1990).

16. P. H. Huang and K. G. Kreider, NBS report NBSIR 88-3790, 1988.

17. M. J. Tarlov, K. G. Kreider, S. Semancik, and P. Huang in *Process Sensing and Diagnostics*, J. J. Ulbrecht, ed., AIChE Symposium Series, 267 (85), 36 (1989).

18. Koryta, J.; Stulik, K. *Ion-selective electrodes,* 2nd ed.; Cambridge University Press: New York, 1983.

19. J. Ruzicka and E. H. Hansen, *Flow Injection Analysis*, 2nd ed., John Wiley and Sons, New York, 1988.

20. T. Gubeli, G. D. Christian, and J. Ruzicka, Anal. Chem. 63, 2407 (1991).

Figure Captions

Figure 1. Multielement microelectrode array sensors fabricated via photolithographic procedures.

Figure 2. DPASV calibration curve for lead in East Bay aqueduct water using micrographite array electrode coated with a mercury thin film.

Figure 3. Calibration curve for Cu^{+2} determination in a rinse tank sample using a cellulose acetate/MFE on a glassy carbon substrate.

Figure 4. Stripping response as a function of deposition time for: (a) a 5 ppm Cu^{+2} solution using a conventionally-sized Pt/MFE; (b) the same electrode as for (a), only analyzing a copper rinse tank sample (AC-16); and, (c) a 5 ppm Cu^{+2} solution using a micro-Pt/MFE.

Figure 5. Potential response vs. pH for an IrO_2 microelectrode. Also shown is the determination of the pH in an actual copper rinse tank sample.

Figure 6. Potential vs. $[Cl^-]$ response for an ion implanted ISE. Inset shows comparison of the response of an ion implanted ISE to a commercially available electrode (Orion Model 94-17A).

Figure 7. Compact, modular electrochemical plating rinse tank sensor system under development.

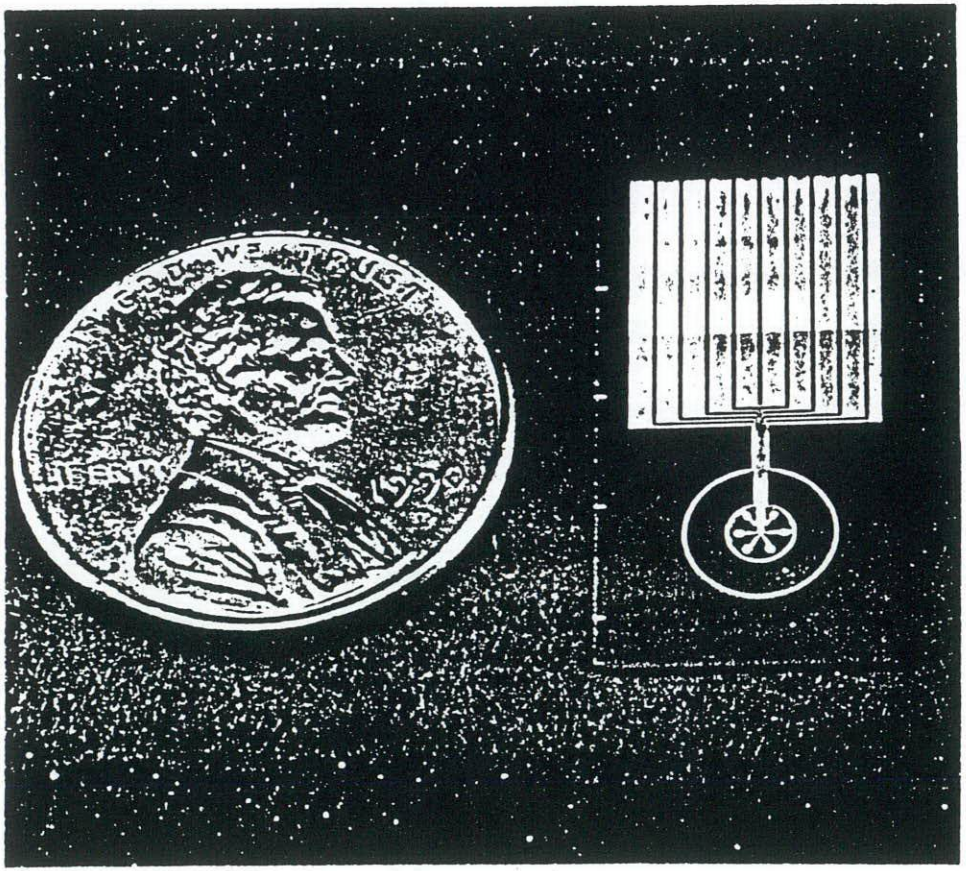

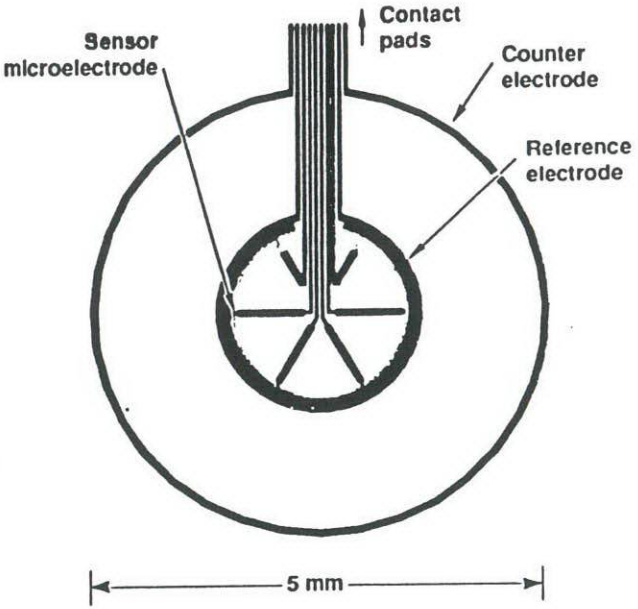
Contact pads
Sensor microelectrode
Counter electrode
Reference electrode
5 mm

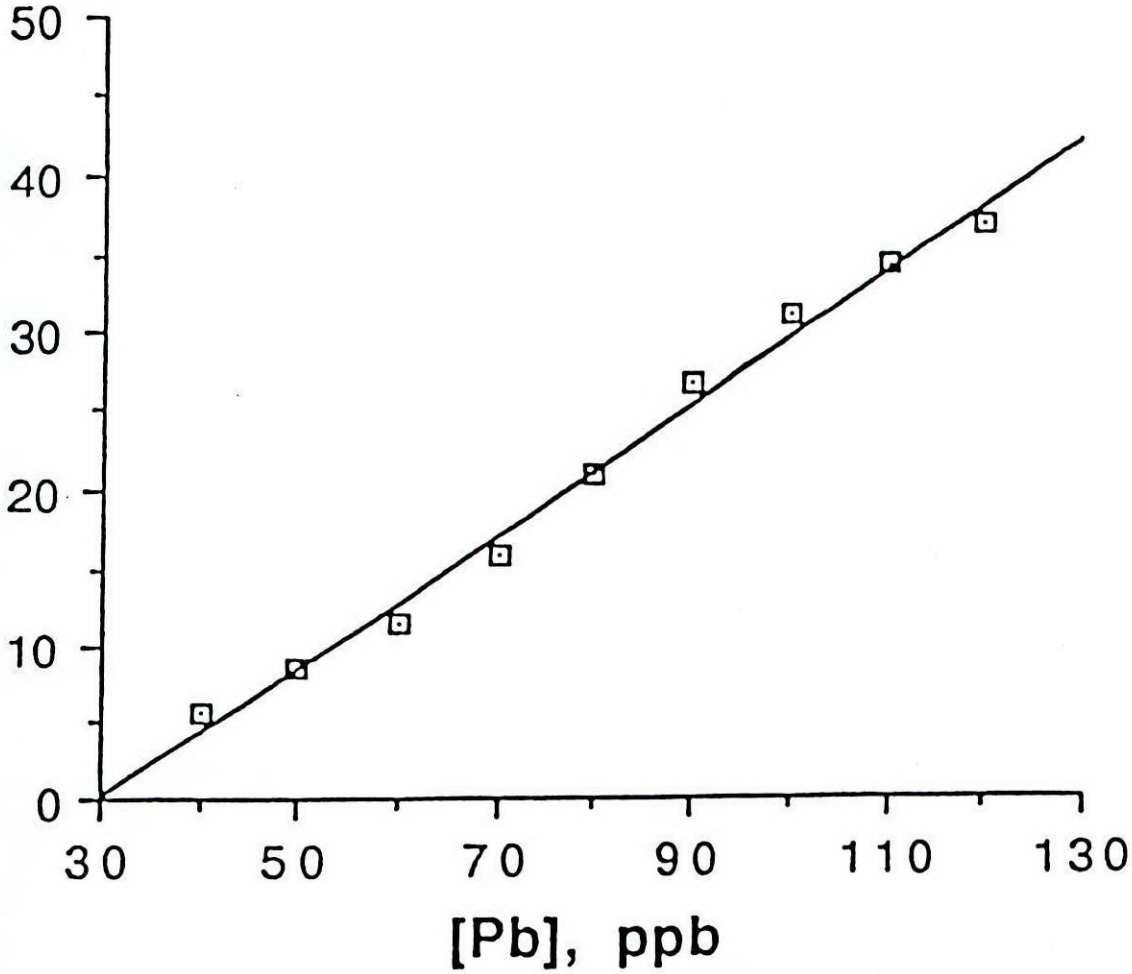
50
40
30
20
10
0
30
50
70
90
110
130
[Pb], ppb

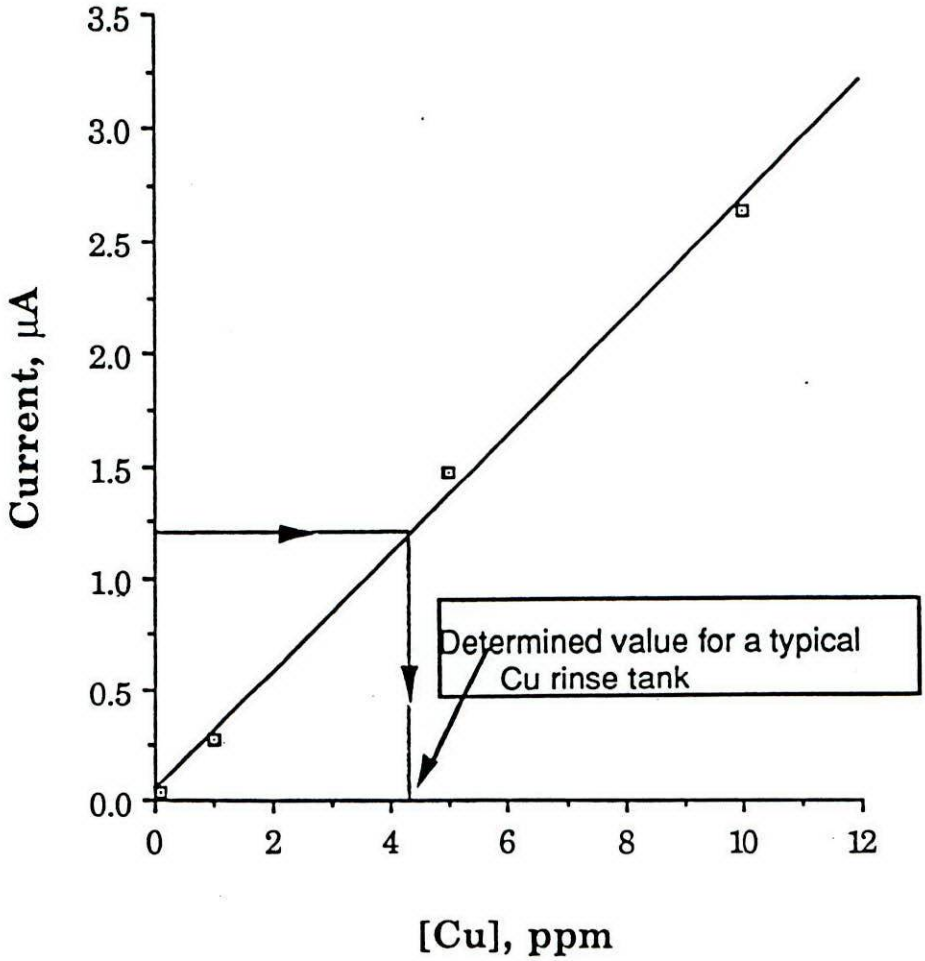
Current, μA
3.5
3.0
2.5
2.0
1.5
1.0
0.5
0.0
0
2
4
6
8
10
12
[Cu], ppm
Determined value for a typical
Cu rinse tank

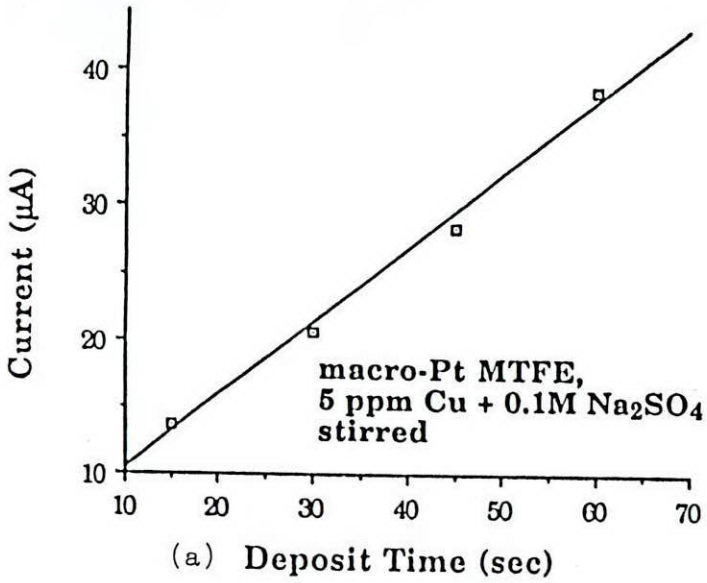
Current (μA)
40
30
20
10
10
20
30
40
50
60
70
macro-Pt MTFE,
5 ppm Cu + 0.1M Na_2SO_4
stirred
(a) Deposit Time (sec)

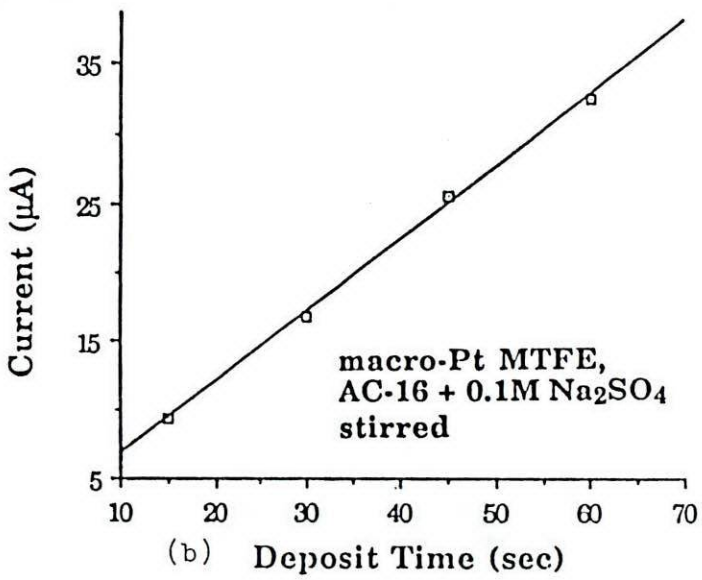
Current (μA)
35
25
15
5
10
20
30
40
50
60
70
macro-Pt MTFE,
AC-16 + 0.1M Na_2SO_4
stirred
(b) Deposit Time (sec)

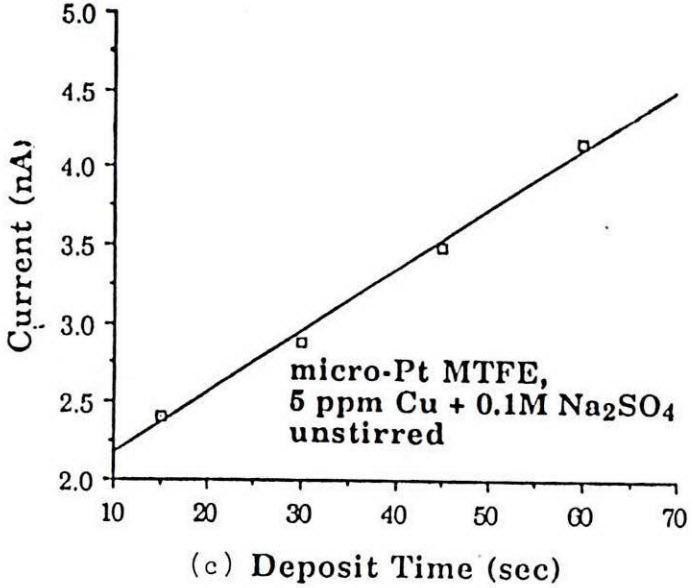
Current (nA)
5.0
4.5
4.0
3.5
3.0
2.5
2.0
10
20
30
40
50
60
70
micro-Pt MTFE,
5 ppm Cu + 0.1M Na_2SO_4
unstirred
(c) Deposit Time (sec)

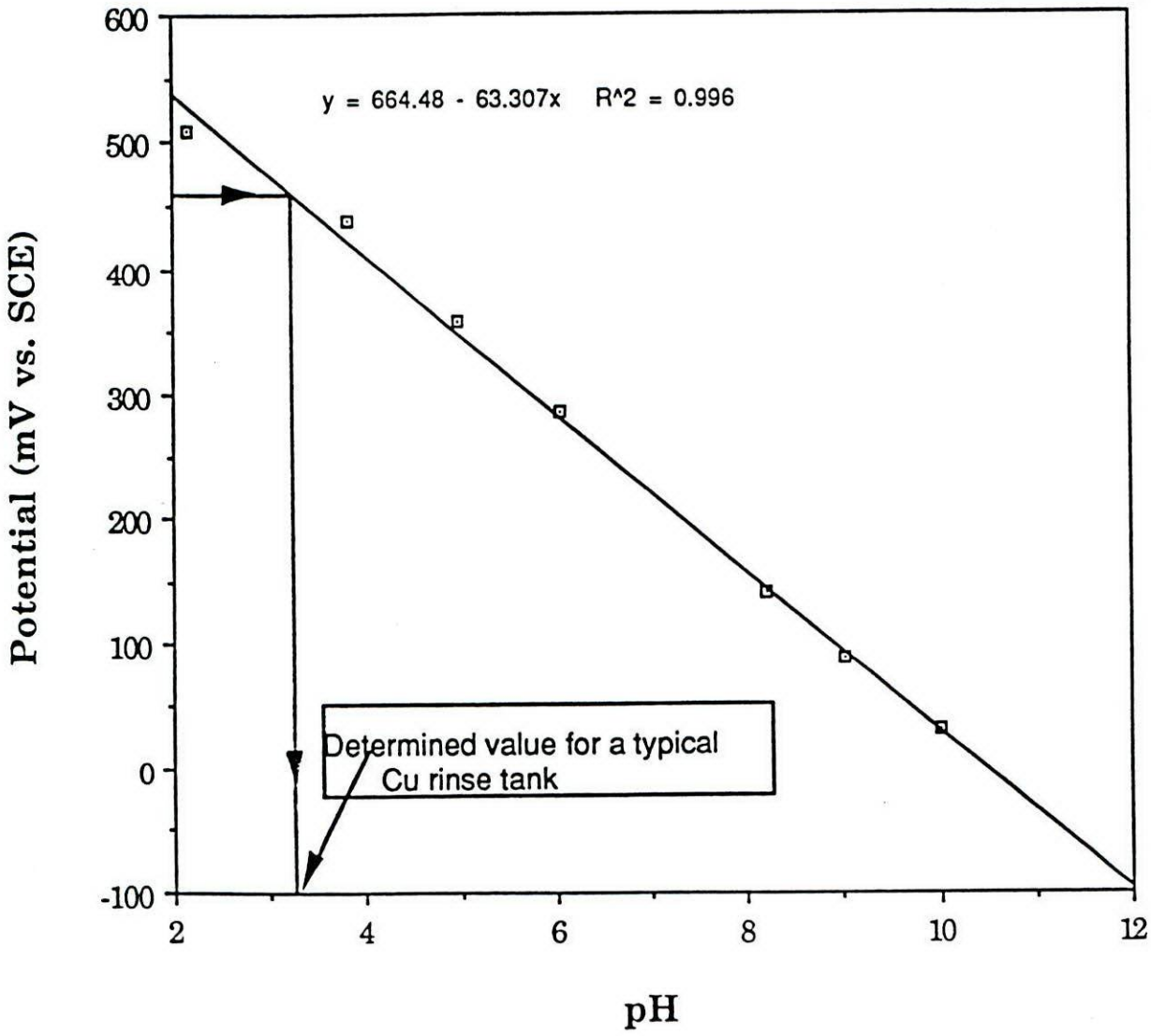
y = 664.48 - 63.307x R^2 = 0.996
Determined value for a typical Cu rinse tank
Potential (mV vs. SCE)
pH
600
500
400
300
200
100
0
-100
2
4
6
8
10
12

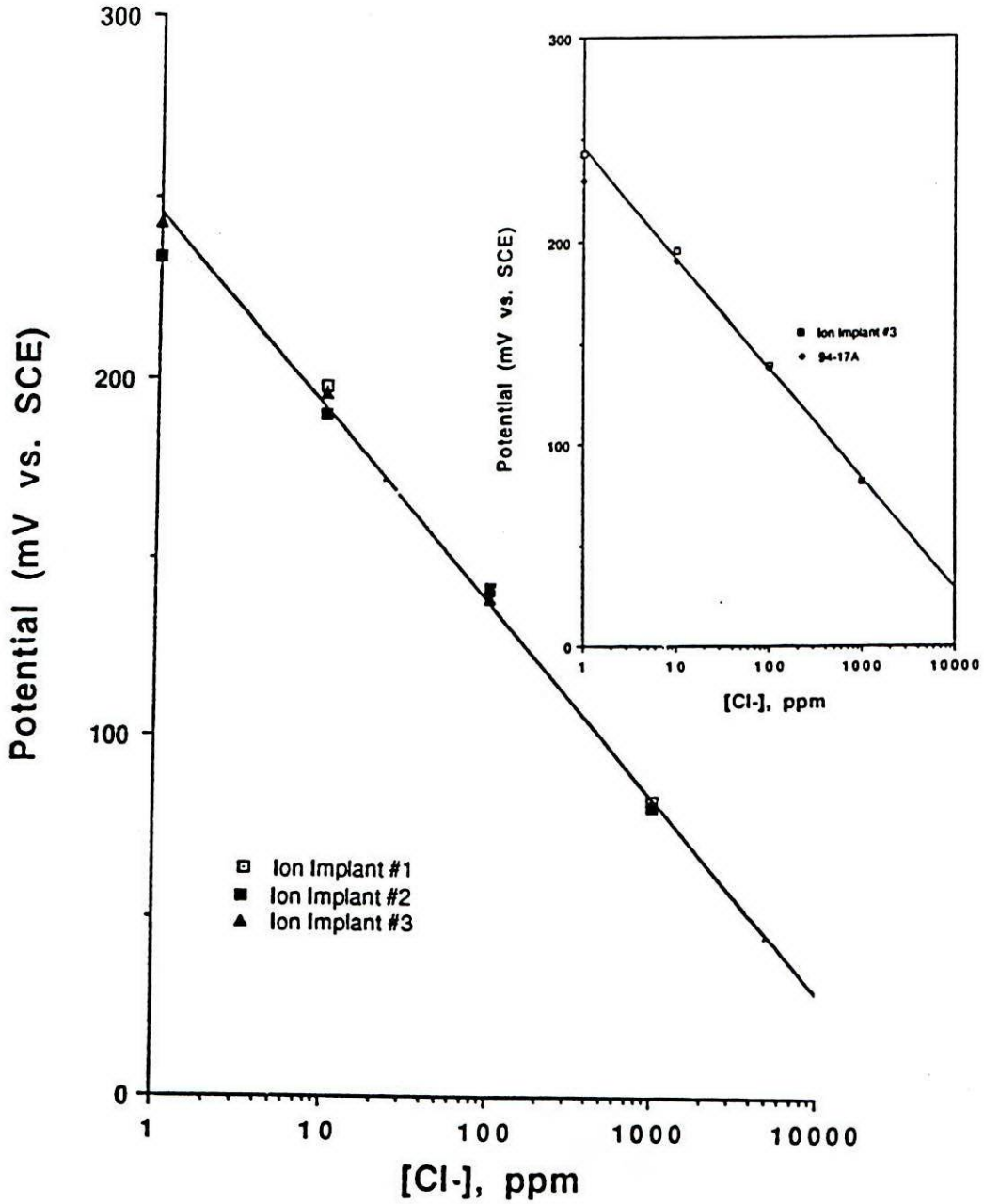
300
200
100
0
Potential (mV vs. SCE)
1
10
100
1000
10000
[Cl-], ppm
Ion Implant #1
Ion Implant #2
Ion Implant #3
Potential (mV vs. SCE)
Ion Implant #3
94-17A
[Cl-], ppm

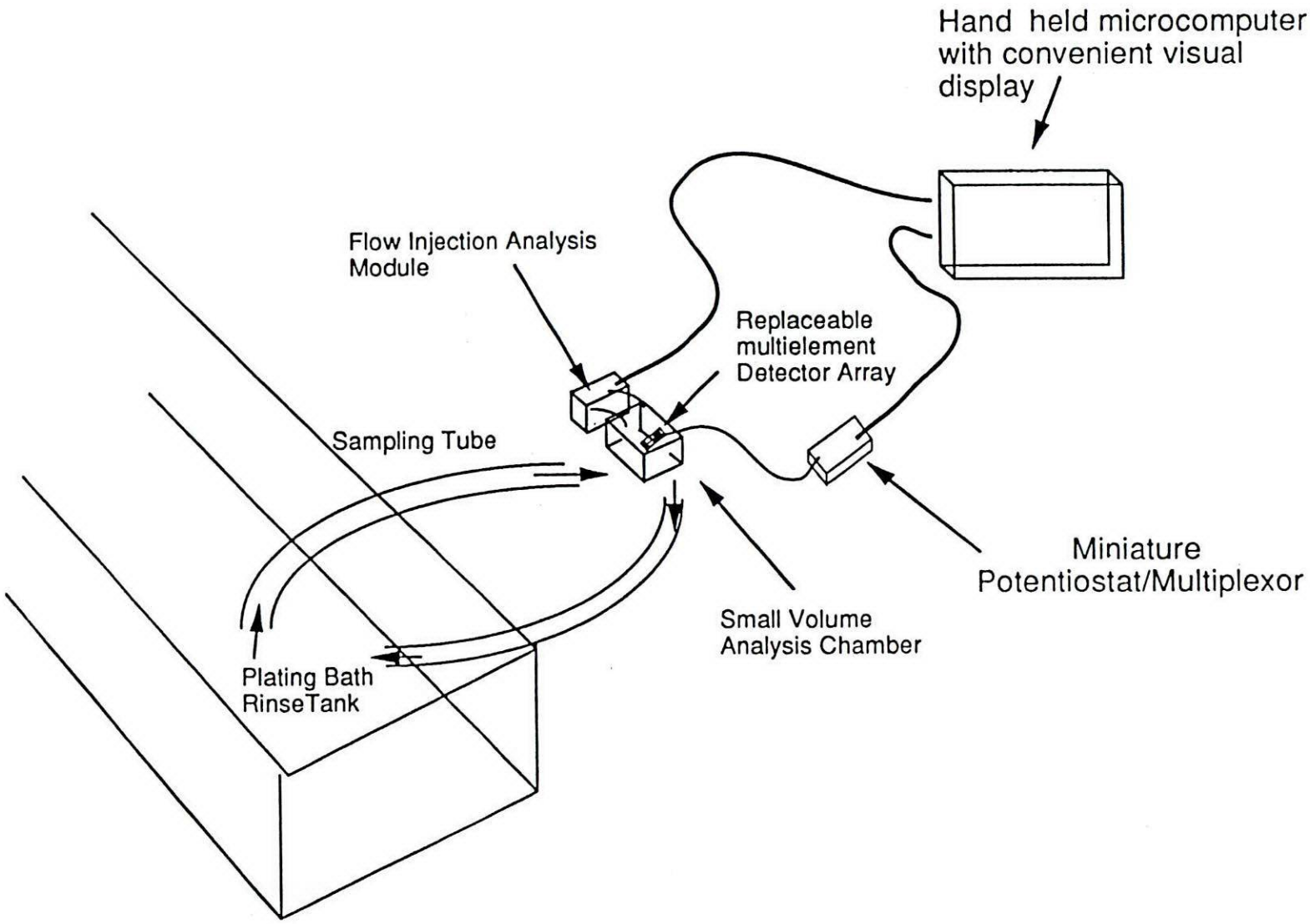
Hand held microcomputer
with convenient visual
display
Flow Injection Analysis
Module
Replaceable
multielement
Detector Array
Sampling Tube
Miniature
Potentiostat/Multiplexor
Small Volume
Analysis Chamber
Plating Bath
RinseTank

Electrodeposition Modeling of Nickel-Iron Alloys in the Presence of Organic Additives

Ken-Ming Yin, B. N. Popov and R. E. White

Center for Electrochemical Engineering
Department of Chemical Engineering
Texas A&M University
College Station, Texas 77843-3122

Abstract

A mathematical model on the electrodeposition of Nickel-Iron (Ni-Fe) alloys with different additives was developed under the potentiostatic condition. The solution chemistry, diffusion, surface reaction, and the additive effect can be rationalized by the model. It is shown because of the surface coverage by additives, the operating potential can be extended to the more cathodic region. Preserved higher concentrations of electroactive species at the electrode interface confine the surface reactions within the kinetically controlled region as compared to the mass transfer limitation in the bath without additives. In consequence, more uniform and bright deposits were obtained. Also, lower interfacial pH was found in the additive contained bath so that metal hydroxide precipitation can be eliminated, which in turn results in better surface appearance. It was also shown that using additives increases the iron content in the alloys.

Introduction

Electrodeposited Ni-Fe alloy is of particular interest for the magnetic properties, protective and decorative coatings. The electrodeposition process is called anomalous codeposition, because the discharge rate of the more noble component is inhibited, causing the appearance of the less noble metal (Fe) at a higher ratio in the deposit than in the electrolyte. The explanation of the deposition mechanism is diverse. Dahms and Croll (1) suggested the preferential adsorption of $Fe(OH)_2$ on the electrode at high pH. The adsorbed $Fe(OH)_2$ inhibits the discharge rate of nickel but does not interfere with the iron deposition. This mechanism was further modified by Romankiw (2) by saying that a very small amount of Fe^{+3} in the solution causes the earliest precipitation of $Fe(OH)_3$, and such film accounts for the selective discharges. Other researchers (3, 4) attributed the under potential electrodeposition of the less noble metal to the appearance of intermetallic compounds on the solid phase. Recently, Hessami and Tobias (5) explained the anomalous electrodeposition by the relative discharging rate of intermediate species $Fe(OH)^+$ and $Ni(OH)^+$ based on the studies by Bockris (6) on Fe and Matulis (7) on Ni. Pulse plating was found to reduce the Fe content, *i.e.*, to reduce the anomalous behavior (8, 9).

Experimental

The plating bath used was kept at a ratio of 10:1 for Ni^{+2} : Fe^{+2} because of the anomalous behavior. The modeling is based on the recipes shown in Table 1. Detailed

Table 1 sulfate plating baths*

[1]	basic solution:	
	nickel sulfate	147.35 g/L (0.5 M)
	iron sulfate	13.89 g/L (0.05 M)
	sodium sulfate	125 g/L (0.5 M)
[2]	basic solution +	
	thiourea	4 g/L (0.05263 M)
[3]	basic solution +	
	sodium saccharin	4 g/L (0.0166 M)
[4]	basic solution +	
	sodium saccharin	2 g/L (0.0083 M)
	boric acid	30.905 g/L (0.5 M)
[5]	basic solution +	
	sodium saccharin	4 g/L (0.0166 M)
	boric acid	30.905 g/L (0.5 M)
	2-butyne-1,4-diol	1 g/L (0.0116 M)

* pH was adjusted to 3 by adding 20 % H_2SO_4.

experimental procedure and results were shown in our previous manuscript.

Solution chemistry

The solution chemistry behavior can be studied by determining the equilibrium concentrations at various pH, since the pH value was found to be one of the most important factors for Ni-Fe alloy composition. The concentrations of species were calculated by the element balances, equilibrium condition of associated species, and the electroneutrality condition under a specified pH. In order to get the whole pH spectrum, a suitable amount of NaOH or H_2SO_4 was added and was also determined in the computation. There should be three regions created depending on the pH values (Fig. 1) : 1. All chemicals are completely dissolved; 2. $Ni(OH)_2$ precipitates at higher pH but no $Fe(OH)_2$ precipitation occurs; 3. For both $Ni(OH)_2$ and $Fe(OH)_2$ precipitation occur at even higher pH. The total materials are the sum of 1000 g of H_2O and the introduced chemicals (*i.e.*, basic solution in Table 1). The total volume is assumed to be one liter. The governing equations for different regions are summarized as follows:
Region I
Variables to be determined are $[Fe^{+2}]$, $[Fe(OH)^+]$, $[Ni^{+2}]$, $[Ni(OH)^+]$, $[OH^-]$, $[H_2O]$, $[HSO_4^-]$, $[SO_4^{-2}]$, and $[H_2SO_4]_{ad}$ (or $[NaOH]_{ad}$, depending on the specified pH).
Equations are:

element balance on oxygen

$$[H_2O]_{ad} + 4[Na_2SO_4]_{ad} + 4[FeSO_4]_{ad} + 4[NiSO_4]_{ad} + 4[H_2SO_4]_{ad} = [OH^-] + [FeOH^+] + [NiOH^+] + [H_2O] + 4[HSO_4^-] + 4[SO_4^{-2}] \quad [1]$$

element balance on sulfur

$$[Na_2SO_4]_{ad} + [FeSO_4]_{ad} + [NiSO_4]_{ad} + [H_2SO_4]_{ad} = [HSO_4^-] + [SO_4^{-2}] \quad [2]$$

element balance on iron

$$[FeSO_4]_{ad} = [Fe^{+2}] + [FeOH^+] \quad [3]$$

element balance on nickel

$$[NiSO_4]_{ad} = [Ni^{+2}] + [NiOH^+] \quad [4]$$

electroneutrality condition

$$2[Na_2SO_4]_{ad} + [H^+] + 2[Fe^{+2}] + 2[Ni^{+2}] + [FeOH^+] + [NiOH^+] = [OH^-] + [HSO_4^-] + 2[SO_4^{-2}] \quad [5]$$

equilibrium conditions

$$[H^+][SO_4^{-2}] - K_1[HSO_4^-] = 0 \quad [6]$$

$$[Ni^{+2}][OH^-] - K_2[NiOH^+] = 0 \quad [7]$$

$$[Fe^{+2}][OH^-] - K_3[FeOH^+] = 0 \quad [8]$$

$$[H^+][OH^-] - K_4 = 0 \quad [9]$$

Note the element balance of hydrogen is not needed because it can be derived by algebraic combination of other balances. Depending on the pH value specified, either variable $[H_2SO_4]_{ad}$ or $[NaOH]_{ad}$ is determined.

Region II

Variables to be determined are $[Fe^{+2}]$, $[Fe(OH)^+]$, $[Ni^{+2}]$, $[Ni(OH)^+]$, $[OH^-]$, $[H_2O]$, $[HSO_4^-]$, $[SO_4^{-2}]$, $[Ni(OH)_2(s)]$ and $[NaOH]_{ad}$.

Equations are:

element balance on oxygen

$$[H_2O]_{ad} + 4[Na_2SO_4]_{ad} + 4[FeSO_4]_{ad} + 4[NiSO_4]_{ad} + [NaOH]_{ad} = [OH^-] + [FeOH^+] + [NiOH^+] + [H_2O] + 4[HSO_4^-] + 4[SO_4^{-2}] + 2[Ni(OH)_2(s)] \quad [10]$$

element balance on sulfur

$$[Na_2SO_4]_{ad} + [FeSO_4]_{ad} + [NiSO_4]_{ad} = [HSO_4^-] + [SO_4^{-2}] \quad [11]$$

element balance on iron: Eq. [3]
element balance on nickel

$$[NiSO_4]_{ad} = [Ni^{+2}] + [NiOH^+] + [Ni(OH)_2(s)] \quad [12]$$

electroneutrality condition

$$\begin{aligned} 2[Na_2SO_4]_{ad} + [NaOH]_{ad} + [H^+] + 2[Fe^{+2}] + 2[Ni^{+2}] + [FeOH^+] + [NiOH^+] \\ = [OH^-] + [HSO_4^-] + 2[SO_4^{-2}] \end{aligned} \quad [13]$$

equilibrium conditions: Eqs. [6], [7], [8], [9], and

$$[Ni(OH)^+][OH^-] - Ksp_{Ni(OH)^+} = 0 \quad [14]$$

Region III
Variables to be determined are $[Fe^{+2}]$, $[Fe(OH)^+]$, $[Ni^{+2}]$, $[Ni(OH)^+]$, $[OH^-]$, $[H_2O]$, $[HSO_4^-]$, $[SO_4^{-2}]$, $[Ni(OH)_2(s)]$, $[Fe(OH)_2(s)]$ and $[NaOH]_{ad}$.
Equations are
element balance on oxygen

$$\begin{aligned} [H_2O]_{ad} + 4[Na_2SO_4]_{ad} + 4[FeSO_4]_{ad} + 4[NiSO_4]_{ad} + [NaOH]_{ad} \\ = [OH^-] + [FeOH^+] + [NiOH^+] + [H_2O] + 4[HSO_4^-] + 4[SO_4^-] \\ + 2[Ni(OH)_2(s)] + 2[Fe(OH)_2(s)] \end{aligned} \quad [15]$$

element balance on sulfur: Eq. [11]
element balance on iron

$$[FeSO_4]_{ad} = [Fe^{+2}] + [FeOH^+] + [Fe(OH)_2(s)] \quad [16]$$

element balance on nickel: Eq. [12]
electroneutrality condition: Eq. [13]
equilibrium conditions: Eqs. [6], [7], [8], [9], [14], and

$$[Fe(OH)^+][OH^-] - Ksp_{Fe(OH)^+} = 0 \quad [17]$$

Diffusion phenomena

The electrodeposition process is described by the mass transport within the diffusion layer and the expression of surface kinetics. Within the diffusion layer, species are

transferred by diffusion and migration. Outside the diffusion layer, the solution is well mixed, *i.e.*, the concentrations are uniform. The diffusion layer thickness characterizes the extent of fluid dynamics (10, 11, 12, 13). The flux of species i is

$$N_i = -z_i u_i \mathrm{F} c_i \frac{d\Phi}{dy} - D_i \frac{dc_i}{dy} \qquad [18]$$

The material balance of species i:

$$-\frac{dN_i}{dy} + R_i = z_i u_i \mathrm{F}\left(\frac{dc_i}{dy}\frac{d\Phi}{dy} + c_i \frac{d^2\Phi}{dy^2}\right) + R_i = 0 \qquad [19]$$

where R_i is the generation rate of i from possible homogeneous reactions. By algebraic manipulation, the following equations follow:

$$-\frac{dN_{Ni^{+2}}}{dy} - \frac{dN_{NiOH^+}}{dy} = 0 \qquad [20]$$

$$-\frac{dN_{Fe^{+2}}}{dy} - \frac{dN_{FeOH^+}}{dy} = 0 \qquad [21]$$

$$-\frac{dN_{SO_4^{-2}}}{dy} - \frac{dN_{HSO_4^-}}{dy} = 0 \qquad [22]$$

$$-\frac{dN_{H^+}}{dy} + \frac{dN_{OH^-}}{dy} - \frac{dN_{Ni^{+2}}}{dy} - \frac{dN_{Fe^{+2}}}{dy} - \frac{dN_{HSO_4^-}}{dy} = 0 \qquad [23]$$

$$-\frac{dN_{Na^+}}{dy} = 0 \qquad [24]$$

Homogeneous equilibrium conditions should also be satisfied within the diffusion layer, *i.e.*, Eqs. [6], [7], [8] and [9]. Finally, the electroneutrality condition should be included. The transport parameters used in the manuscript are listed in Table 2.

Electrode kinetics

The surface reactions can be seen in Table 3. The boundary conditions at the electrode surface are governed by the electrode kinetics. The flux for species i is related to the associated surface electrochemical reactions

$$-\sum_{j=1}^{nr} \frac{s_{i,j} i_j}{n_j F} = N_i \qquad [25]$$

where $s_{i,j}$ is the stoichiometric coefficient of species i in reaction j when the electrochemical reaction is expressed by

$$\sum_i s_{i,j} M_i^{z_i} \rightarrow n_j e^- \qquad [26]$$

Table 2 Mass transfer data

species	z_i	$D_i \times 10^5$ $(\frac{cm^2}{s})$	$c^*_{i,ref} \times 10^3$ $(\frac{mol}{cm^3})$	$c^{**}_{i,bulk}$ $(\frac{mol}{cm^3})$
Ni^{+2}	2	0.72§	1.	0.5×10^{-3}
$NiOH^+$	1	0.72‡	1.	0.1111×10^{-9}
Fe^{+2}	2	0.713§	1.	0.4999×10^{-4}
$FeOH^+$	1	0.713‡	1.	0.8649×10^{-8}
SO_4^{-2}	-2	1.06†	1.	0.1012×10^{-2}
HSO_4^-	-1	1.33†	1.	0.7781×10^{-4}
H^+	1	0.913†	1.	$1. \times 10^{-6}$
OH^-	-1	5.26†	1.	$1. \times 10^{-14}$
Na^+	1	1.334†	1.	$1. \times 10^{-3}$
$\delta = 0.011$*** cm T = 298 K $\rho_o = 1.0$ g/cm^3				

* choose arbitrary for convenience

** calculated according to introduced chemicals

§ Ref. 14.

‡ choose the same as the correspondent metal ion.

† Ref. 15.

*** Ref. 16.

n_j is the number of electrons transferred in reaction j. Because of the surface adsorption phenomena, the Butler-Volmer kinetic expression (15) is modified according to the following assumptions:

- The discharge rates of $FeOH^+$ and $NiOH^+$ are proportional to their respective surface coverage fraction.
- The discharge rates of Ni^{+2}, Fe^{+2}, and hydrogen evolution reactions are proportional to the surface fraction not covered by the organic additives.
- The species adsorption fraction is related to the respective interfacial concentration according to Langmuir isotherm and assuming the vacant active sites are negligible compared to the sites occupied by species.
- The effect of inclusion of additives within the alloys is negligible.

According to the argument, the surface reactions without the additive interference can be expressed

$$i_1 = i_{01,ref}\{\exp(\alpha_{a,1} f\eta_{1,ref}) - \bar{c}_{Ni^{+2},0} \exp(\alpha_{c,1} f\eta_{1,ref})\} \quad [27]$$

$$i_1 = i_{02,ref}\theta_{NiOH^+}\{\bar{c}_{OH^-,0} \exp(\alpha_{a,2} f\eta_{2,ref}) - \bar{c}_{NiOH^+,0} \exp(\alpha_{c,2} f\eta_{2,ref})\} \quad [28]$$

$$i_3 = i_{03,ref}\{\exp(\alpha_{a,3} f\eta_{3,ref}) - \bar{c}_{Fe^{+2},0} \exp(\alpha_{c,3} f\eta_{3,ref})\} \quad [29]$$

Table 3. Electrochemical reactions

	formula	U_j^θ (V)
1	$Ni^{+2} + 2e^- \rightarrow Ni$	-0.23*
2	$NiOH^+ + e^- \rightarrow Ni + OH^-$	-0.3585**
3	$Fe^{+2} + 2e^- \rightarrow Fe$	-0.44*
4	$FeOH^+ + 2e^- \rightarrow Fe + OH^-$	-0.654***
5	$2H^+ + 2e^- \rightarrow H_2$	0.0*

* Ref. 17.
** derived according to Newman (15) as follows

$$FU^\theta_{Ni/NiOH+} - FU^\theta_{Ni/Ni^{+2}} = \tfrac{1}{2}RT\ln\left(\frac{\lambda^\theta_{NiOH+}}{\lambda^\theta_{Ni^{+2}}\lambda^\theta_{OH-}}\right)$$

*** derived according to Newman (15) as follows

$$FU^\theta_{Fe/FeOH+} - FU^\theta_{Fe/Fe^{+2}} = \tfrac{1}{2}RT\ln\left(\frac{\lambda^\theta_{FeOH+}}{\lambda^\theta_{Fe^{+2}}\lambda^\theta_{OH-}}\right)$$

$$i_4 = i_{04,ref}\theta_{FeOH+}\{\bar{c}_{OH^-,0}\exp(\alpha_{a,4}f\eta_{4,ref}) - \bar{c}_{FeOH+,0}\exp(\alpha_{c,4}f\eta_{4,ref})\} \quad [30]$$

$$i_5 = i_{05,ref}\{\exp(\alpha_{a,5}f\eta_{5,ref}) - \bar{c}^2_{H+,0}\exp(\alpha_{c,5}f\eta_{5,ref})\} \quad [31]$$

where $f = \frac{F}{RT}$, $\eta_{j,ref} = V_d - \Phi_0 - U_{j,ref}$, and $\bar{c}_i = \frac{c_i}{c_{i,ref}}$. The surface coverage of $NiOH^+$ can be expressed

$$\theta_{NiOH+} = \frac{c_{NiOH+,0}}{c_{NiOH+,0} + c_{FeOH+,0}} \quad [32]$$

$$\theta_{FeOH+} = 1 - \theta_{NiOH+} \quad [33]$$

by assuming $FeOH^+$ and $NiOH^+$ have equal adsorption equilibrium constants at high surface coverages. In the case with organic compounds involved, the kinetic expressions must be modified. Equations [27], [29], and [31] require multiplication by a factor $(1 - \theta_{add})$, where θ_{add} is the total coverage by additives. The surface coverage of $NiOH^+$ is now

$$\theta_{NiOH+} = \frac{c_{NiOH+,0}}{c_{NiOH+,0} + c_{FeOH+,0} + \sum_i k_i c_{add,i}} \quad [34]$$

k_i is the ratio of adsorption constants between additive i and metal hydroxide ion. $c_{add,i}$ is the concentration of additive i. θ_{FeOH+} can be similarly defined. The kinetic parameters are listed in Table 4.

Numerical procedure

The governing equations and associated boundary conditions can be cast into a three point finite difference to be solved by BAND algorithm (15). The species concentrations, solution potential and surface coverages of additives can then be determined. The

Table 4 Kinetic parameters

reactions	$\alpha_{a,j}^{\S}$	$\alpha_{c,j}$	n_j	$i_{0j,ref}^{\ddagger}(\mathrm{A/cm^2})$	$U_{j,ref}^{\dagger}(\mathrm{V})$
1	1.0	1.0**	2	0.3472×10^{-11}	-0.23
2	1.0	1.0***	2	0.2384×10^{-5}	-0.3585
3	0.5	1.5****	2	0.3473×10^{-10}	-0.44
4	0.5	1.5*****	2	0.9120×10^{-6}	-0.654
5	1.0	1.0	2	0.4310×10^{-10}	0.0

§ $n_j - \alpha_{c,j}$

‡ Estimated parameters

† Eq. [19] in Ref. 18.

** Ref. 19

***chosen the same as reaction [1]

**** Ref. 6.

***** chosen the same as reaction [3]

parameters for exchange current densities $i_{0j,ref}$ and relative surface adsorption constants k_i were estimated using DBCLSF from IMSL Library based on the minimization of residues between the experimental and calculated data. The experimental data includes the nickel and iron deposition rates from atomic adsorption analysis and the polarization curves from the potentiostat. The logic is as follows:

1. From experimental data for bath 1, exchange current densities can be estimated.
2. For given exchange current densities, relative adsorption constants of thiourea and saccharin can be estimated from experimental data of bath 2 and bath 3 respectively.
3. Finally, the relative adsorption constant for 2-butyne-1,4-diol can be estimated from data in bath 5.

Results and Discussion

The solution equilibrium behavior as a function of pH is shown in Fig. 1. At the studied plating bath (pH=3), $Fe(OH)^+$ concentration is about two orders of magnitude higher than $Ni(OH)^+$ because of the larger solubility product constant of $Fe(OH)_2(s)$. $Ni(OH)_2(s)$ precipitates at about pH=6.6, which is more than two units earlier than the start of precipitation of $Fe(OH)_2(s)$. It is interesting to know that once $Ni(OH)_2$ precipitates, $Ni(OH)^+$ will decrease due to less nickel ion available for complexing. From Fig. 1, it seems the theory that preferential precipitation of $Fe(OH)_2$ causes the selective discharge of iron species becomes unlikely. Because of the general small value of solubility constant, the solid phase will establish completely with only a small change in pH. In actual plating process, it is more likely $Ni(OH)_2$ will precipitate instantly on the electrode before $Fe(OH)_2$ with increasing pH. Experimental data show that at higher potential $Ni(OH)_2$ precipitates at the edge areas. The porous $Ni(OH)_2$ structure was confirmed by EDS spectrum, which was due to the higher current density and higher H_2 evolution

rate there. Such current distribution on a vertical plate was discussed by Landau in a theoretical work (20).

The total current density profiles (Fig. 2) show organic compounds increase the polarization. Without additives, the suitable operating potential range is very narrow, and the mass transfer limitation is felt no sooner. However, in the baths with organic compounds, current was inhibited and delayed to more cathodic potential so that the favorable kinetically controlled region was expanded. It is shown the effect is most significant in bath 5. Experimental data also shows the best surface appearance is obtained from plating bath 5. Discharge rates of Fe and Ni are shown in Figs. 3 and 4. Generally, additives decrease both the discharge rate of Fe and Ni, but the inhibition on Ni is greater. The selective inhibition depends on the surface coverage of additives, the respective electrode kinetics for each reaction and the mass transfer of each species. Since iron deposition is more mass transfer influenced, the surface coverage effect will be less on iron than on the deposition of nickel where kinetically controlling is apparent. Because of the selective suppression, iron contents are higher when organic compounds were added (Fig. 5). The typical composition profile was confirmed by many other investigators.

Experimental results on the effect of boric acid are intriguing. It is found that boric acid can increase the Fe contents in the alloys (21, 22, 23). Although boric acid is commonly accepted as a buffer agent, its capability to adjust the pH is doubted. Because of its small equilibrium constant, the buffering effect can not be significant until pH=9. Hoare (24) mentioned boric acid merely masquerades as a buffer, but actually is a homogeneous catalyst in nickel watts bath. Horkans (23) believes boric acid functioned as a surface adsorption agent in Ni-Fe plating. Our experimental results on Ni-Fe deposition show a better surface appearance in bath 4 than that in bath 3. Also, deposits from bath 4 have a higher Fe content than in bath 3 (please see our previous manuscript). Our previous experimental polarization curves and present theoretical study seem to support the adsorption assumption of boric acid. Within the diffusion layer, only minor influence on pH was found by the dissociation of boric acid. However, if one assumes boric acid participates in the adsorption, then selective inhibition of nickel and the increased iron content are expected.

Fig. 6 shows the interfacial proton concentration in different baths. The depletion of H^+ in basic bath is evident, which explains the many burned black areas on the edge where metal hydroxide precipitation is most significant. In comparison, with organic compounds added, lower pH can be preserved so that surface leveling can be more effective. It should be pointed out that according to Dahms and Croll's hypothesis (1), higher pH at the electrode interface induces a $Fe(OH)_2$ film which in turn favors the selective discharge of iron. However, the present study shows $Ni(OH)_2$ precipitates earlier than $Fe(OH)_2$; lower pH at the interface and higher iron alloy content are obtained in the presence of organic additives.

Figs. 7 and 8 show the interfacial Ni^{+2} and Fe^{+2} concentrations. Higher electroactive species are preserved at the interface in additive included baths. Therefore, a wide range of potential can be applied without concentration depletion. Although the effective reaction rates are reduced by less available active surface area, higher interfacial concentrations avoid the mass transfer limitation. Also shown in Fig. 8 the effect of adsorption on preserving iron concentration is not as effective as on nickel concentration.

This is because adsorption is more effective for the kinetically controlled reaction.

Conclusion

The effects of organic additives on the electrodeposition of Ni-Fe alloys can be assessed by a mathematical model that include the surface coverage phenomena, the associated solution chemistry and electrode kinetics. Fe content is increased because of the preferential inhibition on nickel deposition. Lower pH and higher concentrations of electroactive species can be preserved at the interface in the presence of organic compounds, which accounts for the brightening and leveling effects. Also, because of the larger polarization, wider operating potential can be used with no concentration depletion.

Acknowledgments

The authors are grateful for support by Sandia National Laboratories and AESF project RF-83.

Notations

c_i	concentration of species i, mol/cm^3
$c_{i,0}$	concentration of species i at the solid-solution interface, mol/cm^3
$c_{i,bulk}$	bulk solution concentration of species i, mol/cm^3
$c_{i,ref}$	reference concentration of species i, mol/cm^3
D_i	diffusion coefficient of species i, cm^2/sec
F	Faraday's constant, 96487 C/mol
$i_{0j,ref}$	exchange current density at reference concentrations for reaction j, A/cm^2
i_j	partial current density due to reaction j, A/cm^2
$[i]$	bulk equilibrium concentration i, M
$[i]_{ad}$	introduced concentration of chemical compound i, M
k_i	relative adsorption constant of additive i to metal hydroxide ion
K_i	equilibrium constant of chemical reaction i
$M_i^{z_i}$	the symbol of species i with charge z_i
nr	number of electrochemical reactions
n_j	number of electrons transferred in reaction j
N_i	flux of species i, mol/cm$^2 \cdot$ sec
R	universal gas constant, 8.3143 J/mol·K
R_i	generation rate of species i, mol/cm^{3}sec
$s_{i,j}$	stoichiometric coefficient of ionic species i in reaction j
T	absolute temperature, K
u_i	mobility of species i, mol $\cdot$ cm^2/J $\cdot$ sec
$U_{j,ref}$	theoretical open-circuit potential of reaction evaluated at reference concentrations, V
U_j^θ	standard electrode potential for reaction j, V
V_d	potential of the working electrode, V
y	normal coordinate, cm
z_i	charge number of species i

Greek letters

$\alpha_{a,j}$	anodic transfer coefficient for reaction j
$\alpha_{c,j}$	cathodic transfer coefficient for reaction j
δ	diffusion layer thickness, cm
$\eta_{j,ref}$	electrode overpotential with respect to reference open circuit potential, V
θ_i	surface coverage fraction of i
λ_i^θ	property expressing secondary reference state, g/mol
ρ_o	pure solvent density, g/cm^3
Φ	solution potential, V

References

1 M. Dahms and I. M. Croll, *J. Electrochem. Soc.*, **112**, 771 (1965).

2 L. T. Romankiw, in "Electrodeposition Technology, Theory and Practice," L. T. Romankiw Editor, The Electrochemical Society Softbound Proceedings Series, PV 87-17, Pennington, NJ (1987).

3 M. J. Nichol and H. I. Phillip, *J. Electrochem. Interfacial. Electrochem.*, **70**, 233 (1976).

4 S. Swathirajan, *J. Electrochem. Soc.*, **133**, 671 (1986).

5 S. Hessami and C. W. Tobias, *J. Electrochem. Soc.*, **136**, 3611 (1989).

6 J. O'M. Bockris, D. Drazic and A. R. Despic, *Electrochimica Acta*, **4**, 325 (1961).

7 J. Matulis and R Slizys, *Electrochimica Acta*, **9**, 1177 (1964).

8 Z. Kovac, *J. Electrochem. Soc.*, **118**, 51 (1971).

9 D. L. Grimmett, M. Schwartz, and K. Nobe, *J. Electrochem. Soc.*, **137**, 3414 (1990).

10 L. J. J. Janssen and J. G. Hoogland, *Electrochimica. Acta*, **18**, 543 (1973).

11 H. Y. Cheh, *J. Electrochem. Soc.*, **118**, 543 (1973).

12 N. Ibl, *Surface Technol.*, **10**, 81 (1980).

13 D. Gangasingh and J. B. Talbot, *J. Electrochem. Soc.*, **138**, 3605 (1991).

14 D. J. Pickett, "Electrochemical Reactor Design," Elsevier, New York (1977).

15 J. Newman, "Electrochemical Systems," Prentice-Hall, NJ (1991).

16 J. O'M. Bockris and A. K. N. Reddy, "Modern Electrochemistry," Plenum Press, New York (1970).

17 A. J. Bard and L. R. Faulkner, "Electrochemical Methods: Fundamentals and Applications," Wiley, New York (1980).

18 S. Chen, K.-M. Yin and R. E. White, *J. Electrochem. Soc.*, **135**, 2193 (1988).

19 R. Tamamushi, "Kinetic Parameters of Electrode Reactions of Metallic Compounds," Butterworth, London (1975).

20 U. Landau, in "Electrodeposition Technology, Theory and Practice," L. T. Romankiw Editor, The Electrochemical Society Softbound Proceedings Series, PV 87-17, Pennington, NJ (1987).

21 N. Nakamura and T. Hayashi, *Plating and Surface Finishing*, August, 42 (1985).

22 S. Biallozor and M. Lieder, *Surf. Tech.*, **21**, 1 (1984)

23 J. Horkans, *J. Electrochem. Soc.*, **128**, 45 (1981).

24 J. P. Hoare, in "Electrodeposition Technology, Theory and Practice," L. T. Romankiw Editor, The Electrochemical Society Softbound Proceedings Series, PV 87-17, Pennington, NJ (1987).

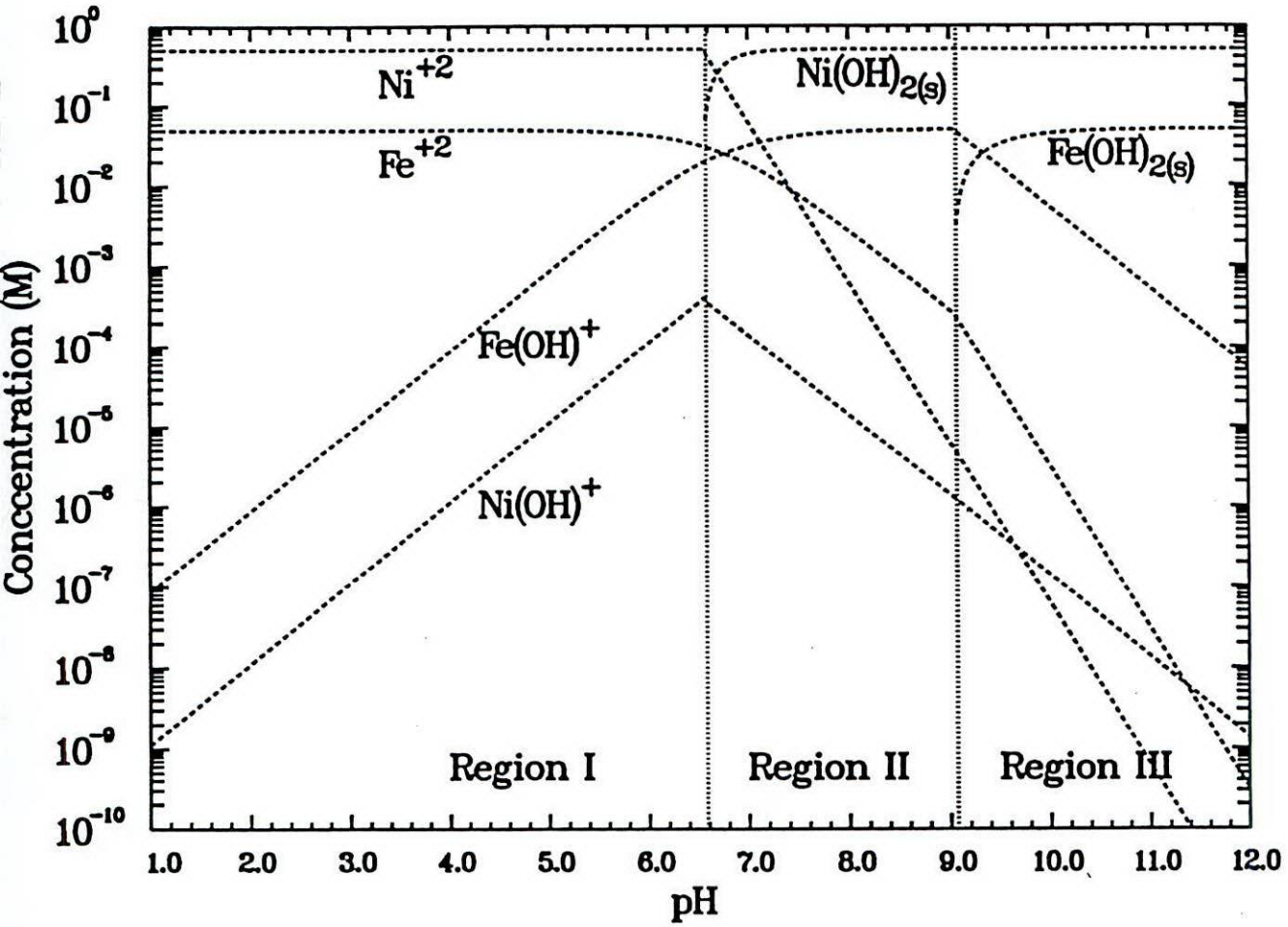

Fig. 1 Solution equilibrium as a function of pH.

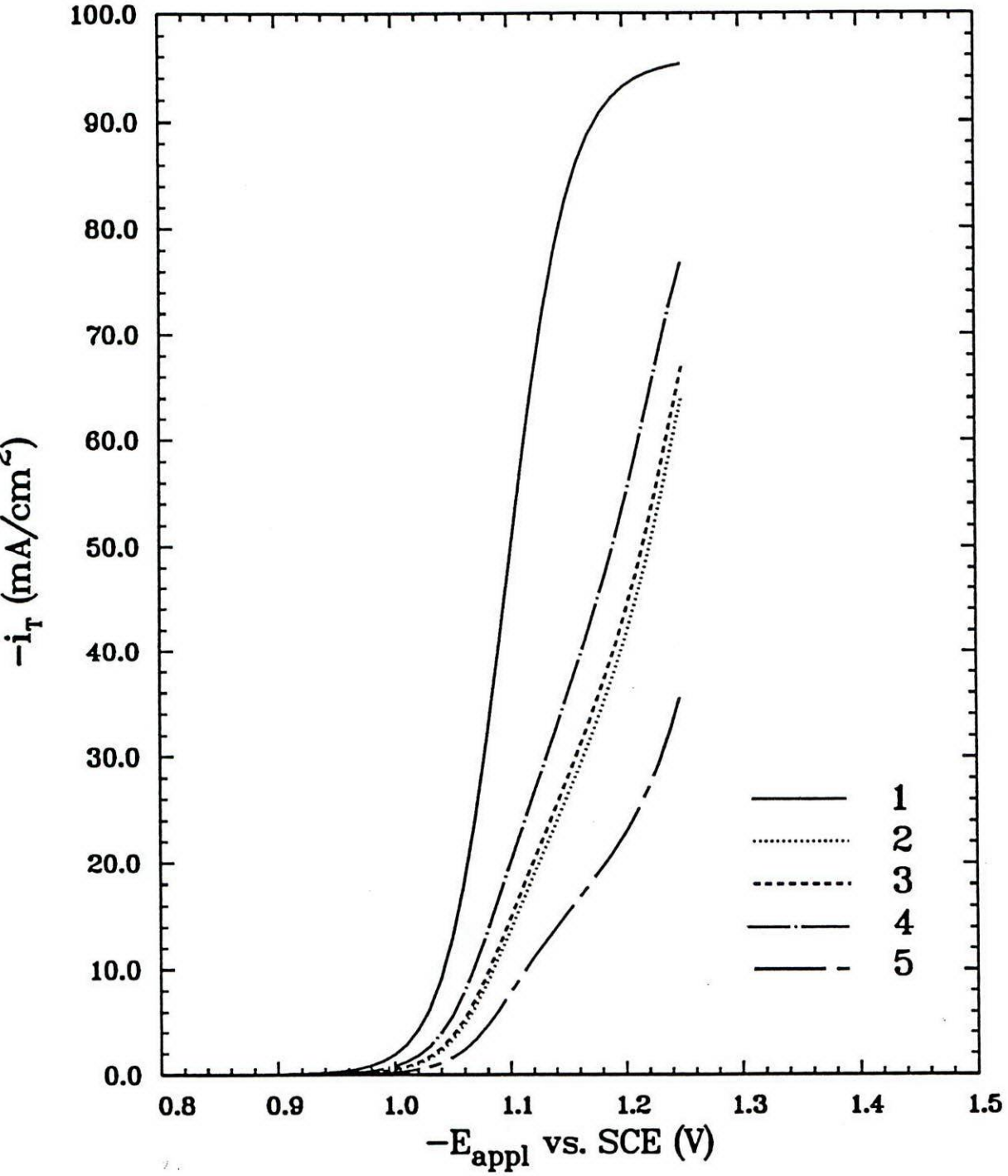

Fig. 2 Polarization curves of Ni-Fe deposition in different baths.

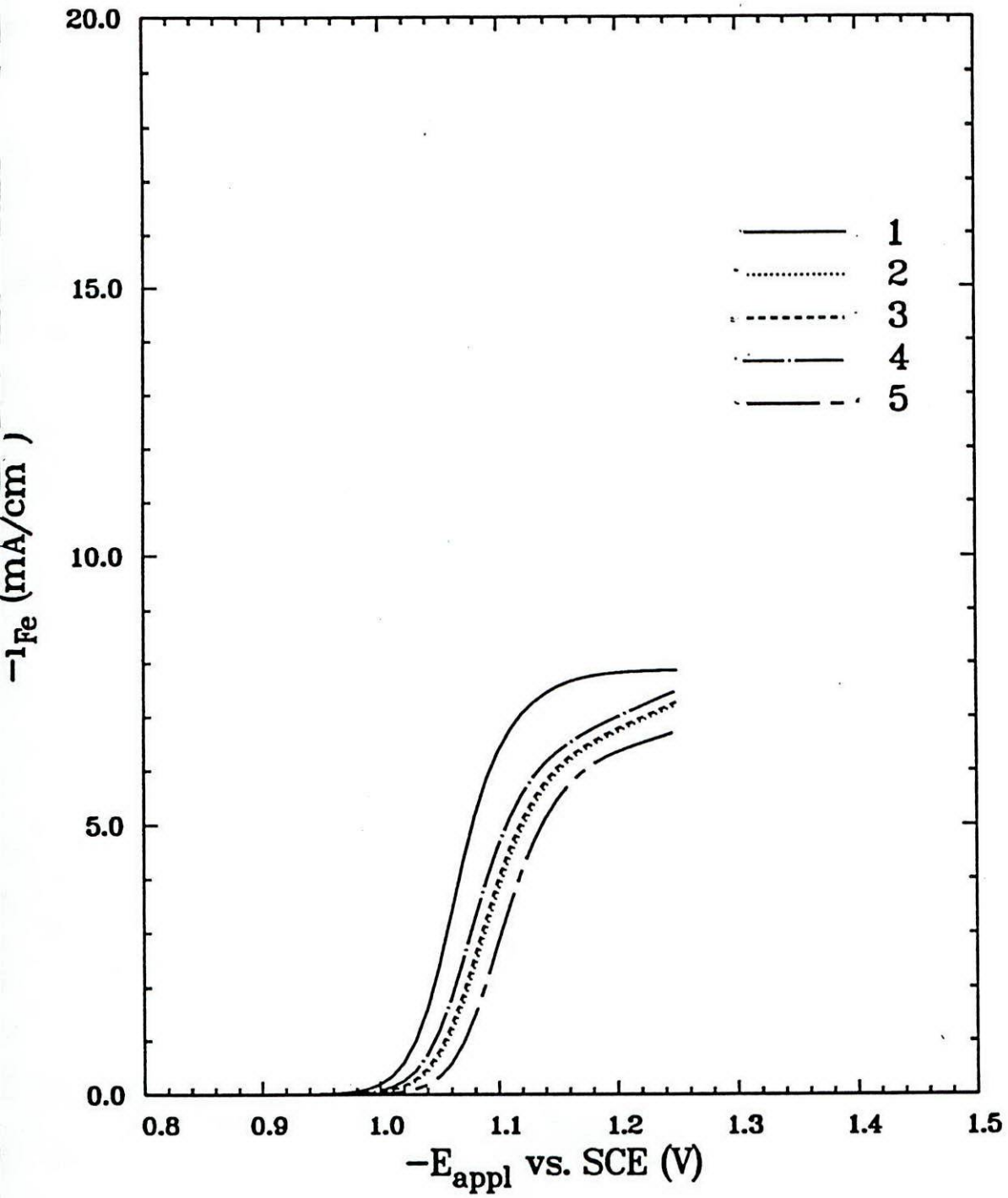

Fig. 3 Iron deposition rates in different baths.

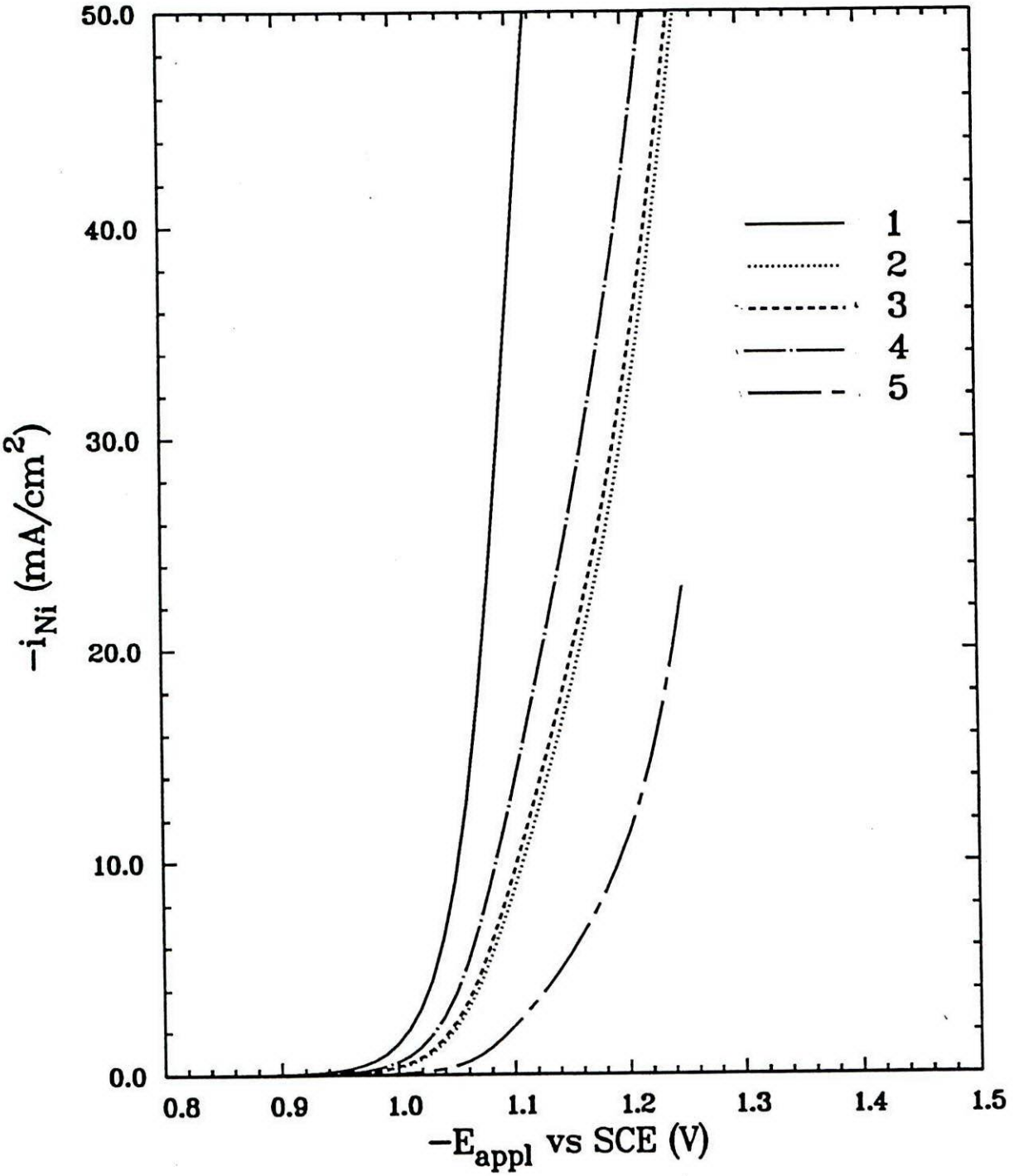

Fig. 4 Nickel deposition rates in different baths.

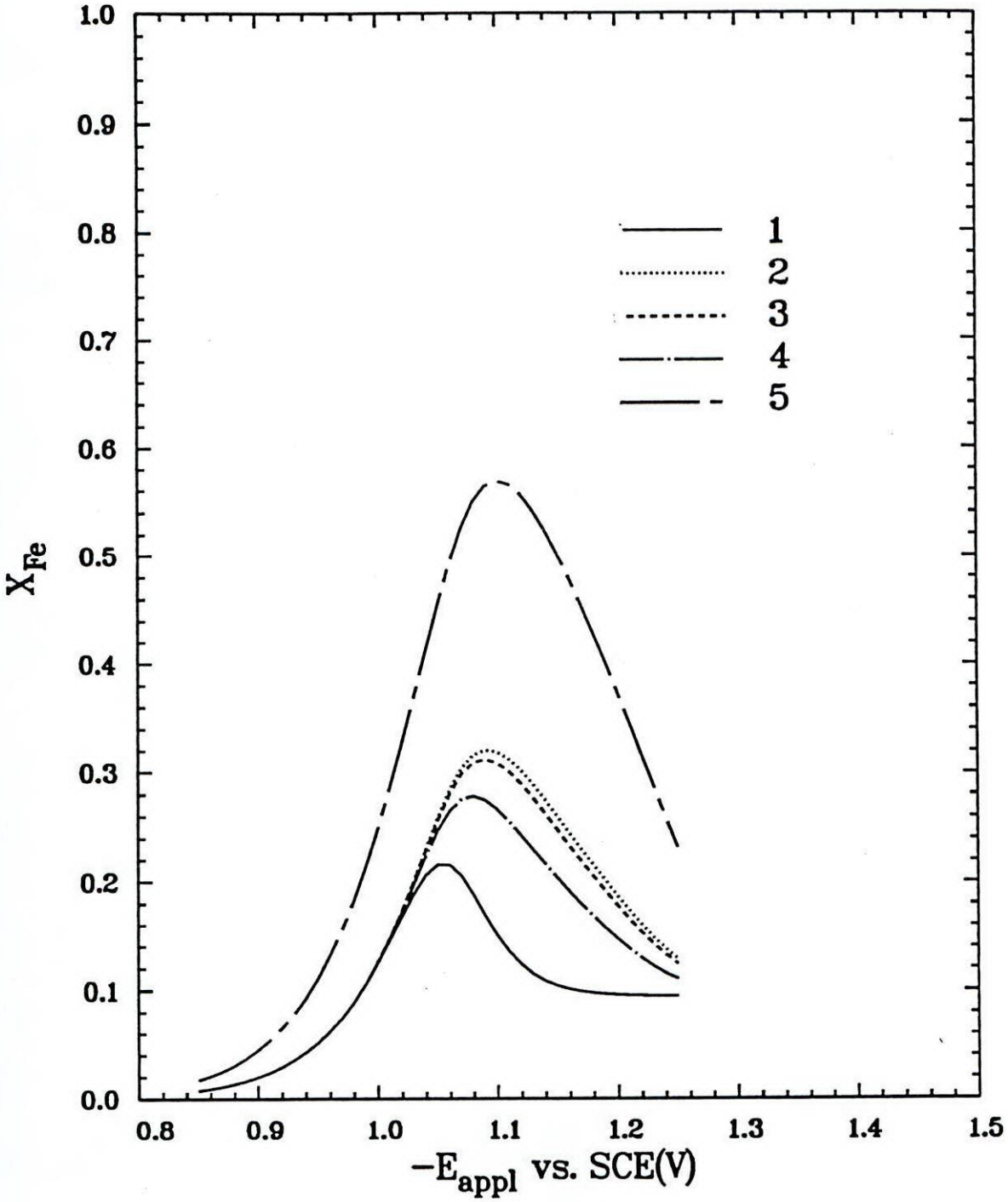

Fig. 5 Iron contents as a function of potential in different baths.

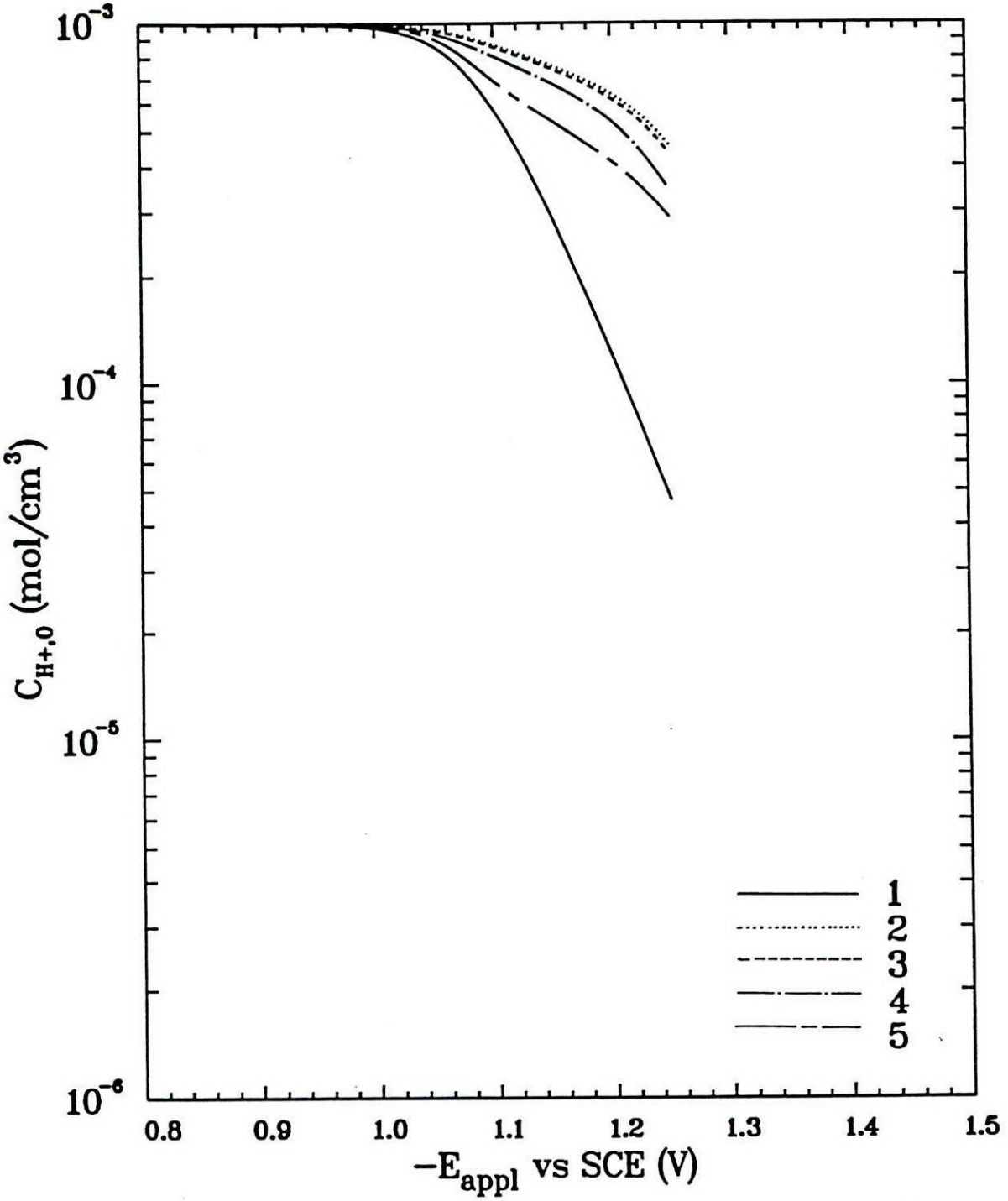

Fig. 6 Interfacial proton concentrations in different baths.

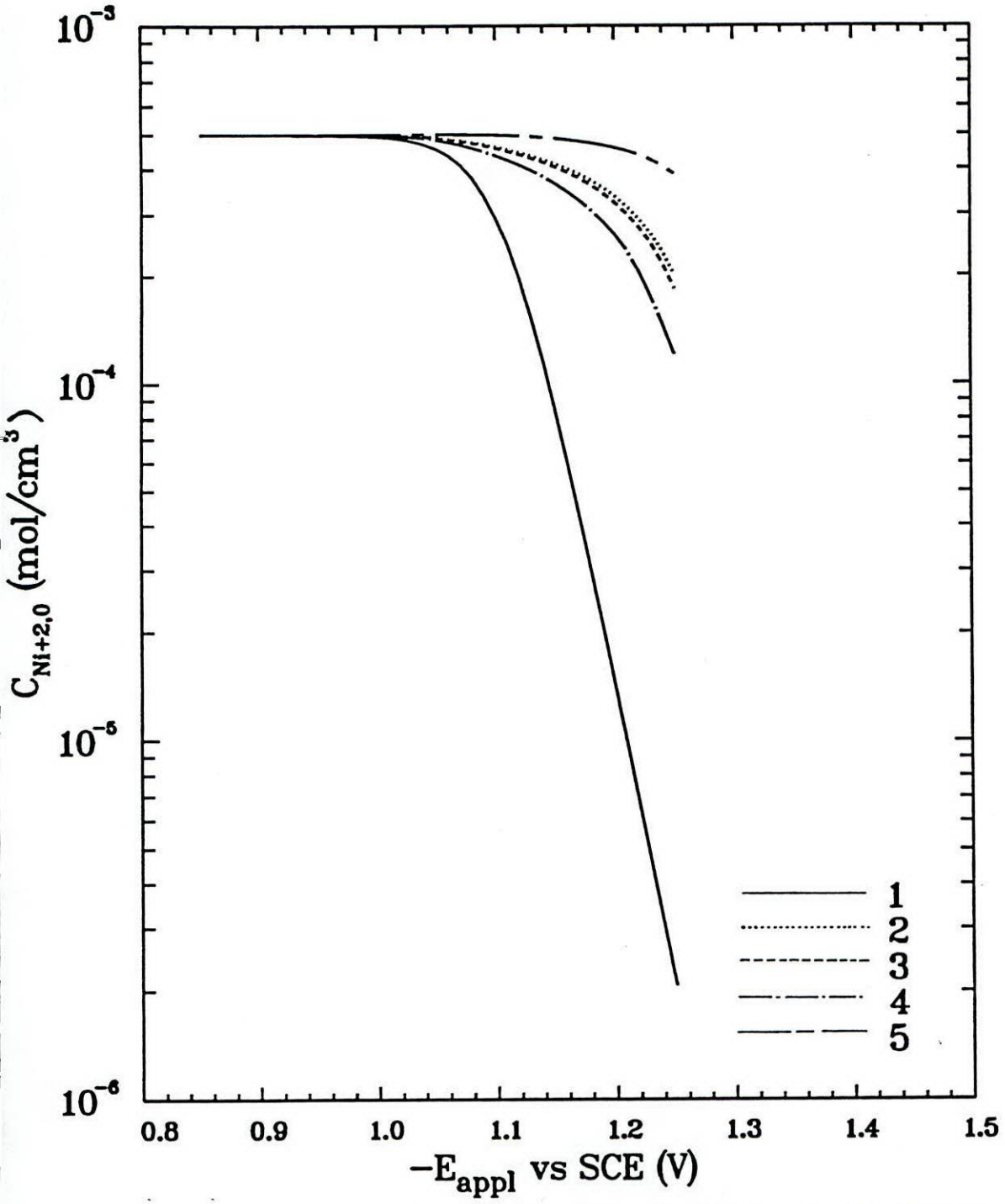

Fig. 7 Interfacial nickel concentrations in different baths.

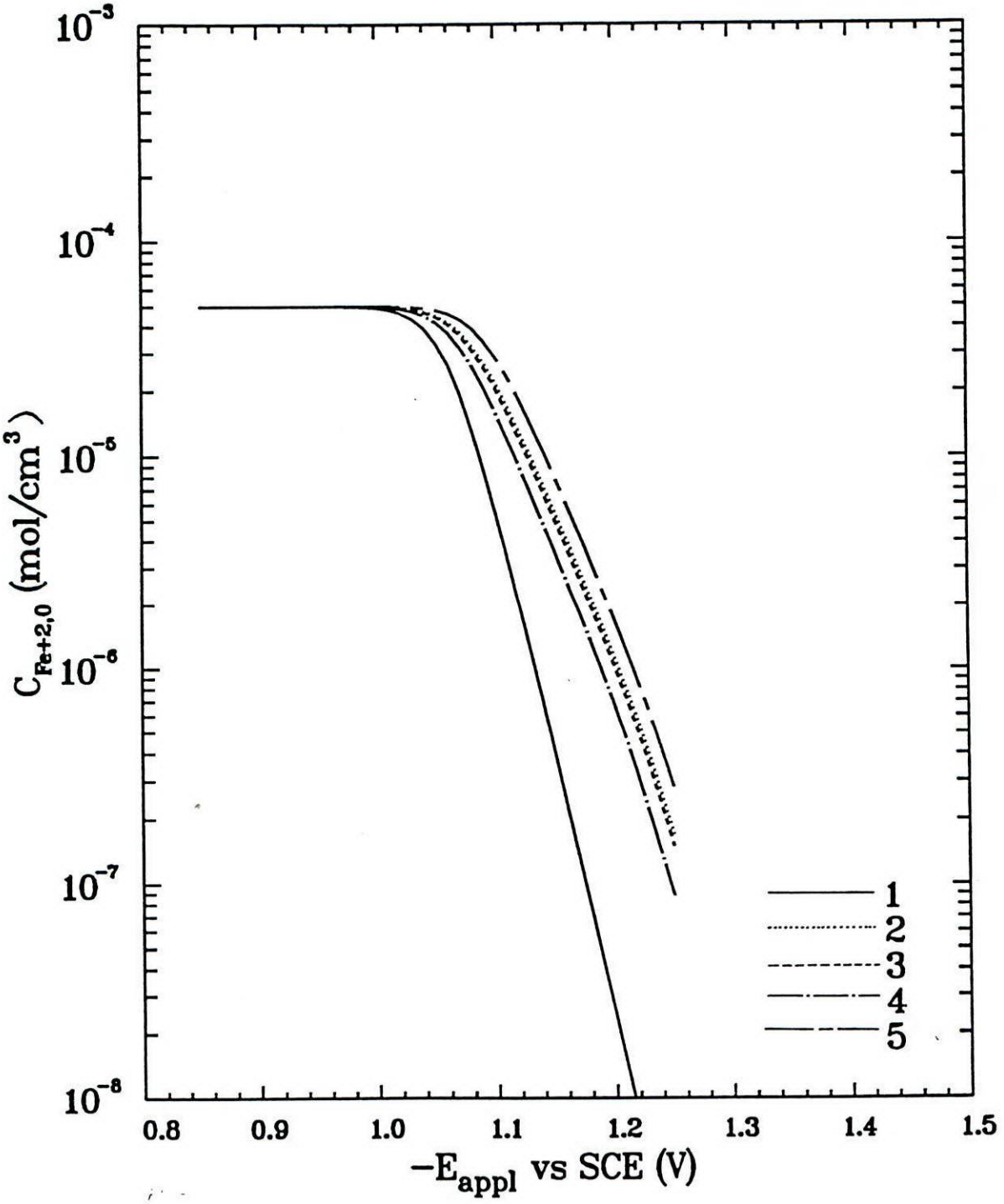

Fig. 8 Interfacial iron concentrations in different baths.

Micro-Finish Hard Anodized Coatings on Aluminum

Chris Steffani

Materials Fabrication Division
Lawrence Livermore National Laboratory

For AESF SUR/FIN 92

Atlanta, GA

June 22-25, 1992

ABSTRACT

The production of thin hard anodized coatings on Single Point Diamond Turned (SPDT) 6061-T6 aluminum has been studied. The investigation centered on producing a surface finish of less than 10 microinch after anodizing. By starting with a 2 microinch (AA) surface finish and controlling time, temperature, current density and solution chemistry, coatings with surface finishes of 8 microinch and a thickness of .0003", are obtained. Surface roughness from several anodizing solutions is compared. The operational life of a PTFE sliding seal against a coated cylinder bore is used as verification of finish quality.

* This work was performed under the auspices of the U. S. Department of Energy by Lawrence Livermore National Laboratory under contract No. W-7405-Eng-48.

INTRODUCTION

Aluminum alloys are used extensively for various aerospace assemblies and components because of a combination of high strength and low density. In addition it has the ability to be machined or formed to a wide range of configurations. Some of the assemblies made from aluminum include reciprocating pumps used to transfer liquid or gaseous materials.

During pump use, friction occurs from a combination of surface contact and the forces required to maintain a seal between piston and cylinder wall. This results in piston and/or cylinder wall wear and eventually component failure. Because aluminum sliding against aluminum has a high coefficient of friction[1], lubricants and coatings are used to minimize this wear.

To further reduce friction and improve the seal between piston and cylinder wall, rings, seals and wipers are used. These may be composed of various materials that include elastomers, polymers, metals, or intermetallic compounds such as oxides or carbides. There are several problems associated with the use of friction reducing seals and coatings. Some applications require ultra clean operation which prohibit most lubricants. Certain types of seals can produce compatibility problems, i.e., corrosion or galling.

One technique for increasing the wear and corrosion resistance of aluminum, is the application of an inert oxide coating. This surface treatment combines oxygen and aluminum to form one of the hardest substances known: Al_2O_3. This oxide coating has many advantages, including resistance to heat, erosion, and moderate chemical solutions[2]. It also has a very low coefficient of friction.

These anodic coatings are formed by electrolytic oxidation of an aluminum surface while immersed in a suitable electrolyte. Many formulations have been used, but the most prevalent are the sulfuric, sulfuric-oxalic, and the oxalic. In some instances electrical current manipulation is used to increase the density, thickness and/or hardness of the coating[3]. The surface finish of these coatings depend on the condition of the surface before anodizing and the processing conditions[4]. One method of reducing surface finish after anodizing is to lap or hone the coating. This has produced finishes down to a less than 2 microinch.

INVESTIGATION

An aluminum piston, conventionally machined to a finish of 32 microinch was fitted with PTFE sealing rings[5]. This piston was then placed into a matching aluminum cylinder, as part of a reciprocating pump. The assembly was then leak checked using a vacuum pump equipped with a helium mass spectrometer. The leak rate was initially excessive (>80 l/min) and grew successively worse with continued piston travel.

To reduce the leak rate, a smoother finish was machined into the internal cylinder bore using a lathe fitted with a diamond tool. This reduced the surface finish to 1-2 microinch, which was well below the seal manufacturers recommendations. A pump assembly was then tested. The results showed an acceptable initial leak rate, but after one piston pass leakage became excessive.

At this point the surface of the cylinder was visually inspected and was found to have numerous scratches. The leading edge of the PTFE seal was also inspected and found to contain minute particles of aluminum. The source of the particles was thought to be a residue from the machining process. A new cylinder was machined and then cleaned using an ultrasonic tank and aqueous cleaning agents. The piston was fitted with new seals and installed in the cylinder. Leak testing this cleaned assembly still showed excessive leak rates after one piston cycle.

An microscopic evaluation of the diamond turned surface showed scratches from contact with PTFE sealing surface. These scratches, running horizontally down the cylinder bore, provided leak paths. To make the surface less susceptible to damage from the sealing surface, a coating of some type was envisioned.

The first choice was to coat the internal surfaces with electroless nickel and then SPDT. This has provided excellent surface finishes on a variety of components[6]. After zincating, copper striking, and deposition of .002" of electroless nickel, the can was SPDT. Leak test results looked excellent (<8 l/min).

At this time it was discovered that copper of any kind was incompatible with the material that would be used in the pump. Without a copper strike, the only alternative to provide adequate adhesion on this alloy was heat treatment[7]. The heat treatment step could not be done because the 6061-T6 aluminum cylinder had to remain in the T6 condition, to retain its mechanical properties.

The next choice was to coat the internal surfaces of the cylinder by hard anodizing. The first coating was applied to a rough machined cylinder using a chilled (32°F) sulfuric acid solution (15% weight) to a thickness of .002". This increased the 32 microinch finish to 82.

Since this finish was too rough, a hand lapping operation followed. The time required to decrease the surface finish in the cylinder bore to an acceptable level was over 4 hours. The remaining lapping compound and alumina particles were removed by ultrasonic cleaning. It was decided to discontinue this approach because of the time required to produce the required finish. Another worry was the lapping residue, which if not completely removed, could clog the small pump delivery lines during operation.

In an effort to reduce the surface roughness caused by the hard anodizing, several test specimens were anodized for various lengths of time. As expected, Figure 1 shows that shorter anodizing time produces much less surface roughness and of course a thinner coating. The project designers felt that the coating thickness should be no less than .0003", which should withstand moderate contact wear[8]. This thickness was obtained after 10 minutes at 36 ASF. This produced a surface finish of about 21 microinch, twice the seal manufacturers recommended value. In an attempt to reduce this finish, other chemistries were examined.

Because of the myriad of solutions that will electrolytically form oxide coatings on aluminum, the next most widely used chemistry was chosen for investigation. This is a sulfuric/oxalic process that was developed commercially[9]. Several test specimens were hard coated in this bath for various times. The surface finish results are shown in Figure 2. This process increased the surface roughness from 2 to 14 microinch in 10 minutes.

With these results a new cylinder was prepared and run for 10 minutes. The internal surface finish increased to 15 microinch after anodizing. After assembly the piston was able to make several passes before the leak rate became excessive. Because of the success of this chemistry change, another process, that had originated in Germany and Japan, was tried. This solution contains (45 gm/l) oxalic acid and is operated at 60°F and 25 ASF.

From this formula a new solution was prepared and test samples were processed. Several differences were noted including higher starting voltage (45 volts vs. 20 volts) and a coating color of translucent yellow instead of grey. The results (Figure 3) show that this produced a 12 microinch finish in 14 minutes. With this data, a cylinder was SPDT and then anodized for 14 minutes. This produced a coating that averaged .0002" thick which had a surface finish that varied from 8 to 18 microinch. This variation was due to the coating being thicker at the open end of the cylinder.

The cathode up to this point had been a 1" diameter aluminum tube, which was also the source of air agitation. To try and remedy the thickness disparity, a "conical" cathode was fabricated. The conical shape was to increase the current density where the coating was thin, and reduce the surface finish where it was thick. After anodizing the surface was inspected and the conical cathode had produced an elliptical coating. A new parallel cathode was fabricated allowing only 1/2" of clearance between electrode surfaces. The results of using this "parallel" cathode provided a uniform coating.

Variations in the surface finish of the cylinder were noted after the use of the 1" cathode. These were attributed to current density variations. To find the optimal current density, samples were run at current densities varying from 40 to 10 ASF. To minimize any thickness disparity all samples were run for 360 amp min/ft^2. The results, shown in Figure 4, show an optimal anode current

density of 18 ASF. The .0003" thickness is reached in 18 minutes at this current density.

Solution temperature is known to have an effect on the porosity of anodized coatings[10]. To determine its impact, another set of samples was coated using various solution temperatures ranging from 70 to 30°F, with a constant 360 amp min/ft^2. The results in Figure 5, show a decrease in surface finish as the solution is cooled to 32°F. The voltage required to maintain a constant current density also increased with reduced temperature. This and the fact that the coating is less soluble at reduced temperature is most likely why the surface finish is reduced[11].

The three anodizing methods are compared in Figure 6. The large reduction in surface finish is easily seen on this chart. When the coating thickness is factored in, the decrease in roughness between the suluric and the oxalic is about 65%, and between the sulfuric/oxalic and the oxalic 46%.

With these results a SPDT cylinder was coated using 45 gm/l oxalic acid solution cooled to 32°F. The anode current density of 18 ASF with an anode to cathode distance of 1/2". Air agitation was supplied to circulate the solution and prevent localized overheating. After processing for 20 minutes the coating was found to have a surface finish of 8 microinch. The thickness was .0003".

This cylinder was then assembled with a matching piston and subjected to the cyclic pump test. The leak rate was very low and the pump cycled over 70 cycles before any seal degradation. Most of the degradation was from flattening of the seal face as opposed to scratching.

Microphotographs of the anodized surface, showed a visible reduction in the surface roughness. This is attributed to the reduced solvent action of the cooled oxalic process. To determine coating density, several coated samples were weighed, stripped and reweighed. This mass, divided by the volume of the oxide was used to determine density. A value of 3.2 gm/cm$_3$, is greater than that obtained from a sulfuric acid solution[12].

CONCLUSION

Thin oxide coatings on SPDT aluminum surfaces are produced in oxalic acid. When produced on a SPDT surface, the finish obtained is much smoother that from a sulfuric acid or sulfuric/oxalic solution. The sliding life of a PTFE sealing ring inside a coated cylinder can be greatly enhanced by this coating. The optimal anodizing conditions are:

45 gm/l oxalic acid
18 ASF anode current density
1/2" anode to cathode distance (minimum cathode current density)
32 degree F. solution temperature
20 minute run time

Figure 1

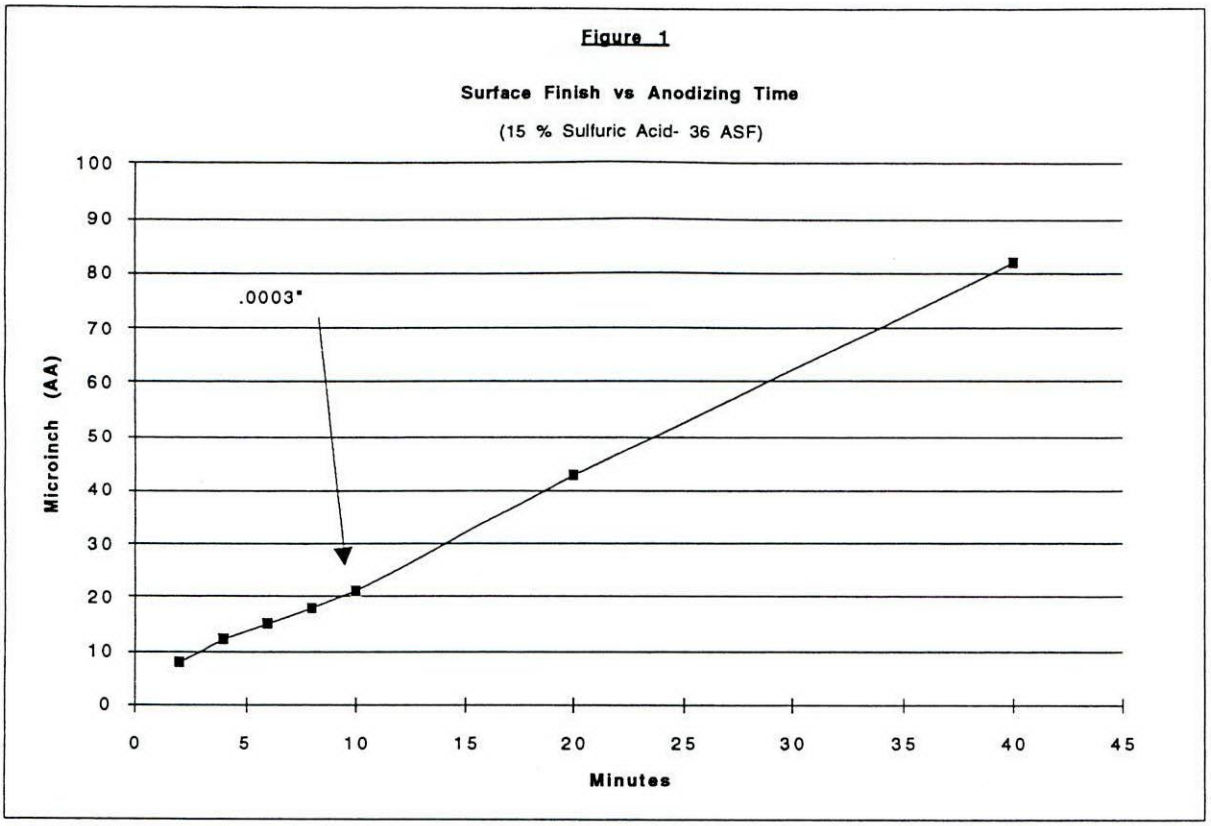

Figure 2

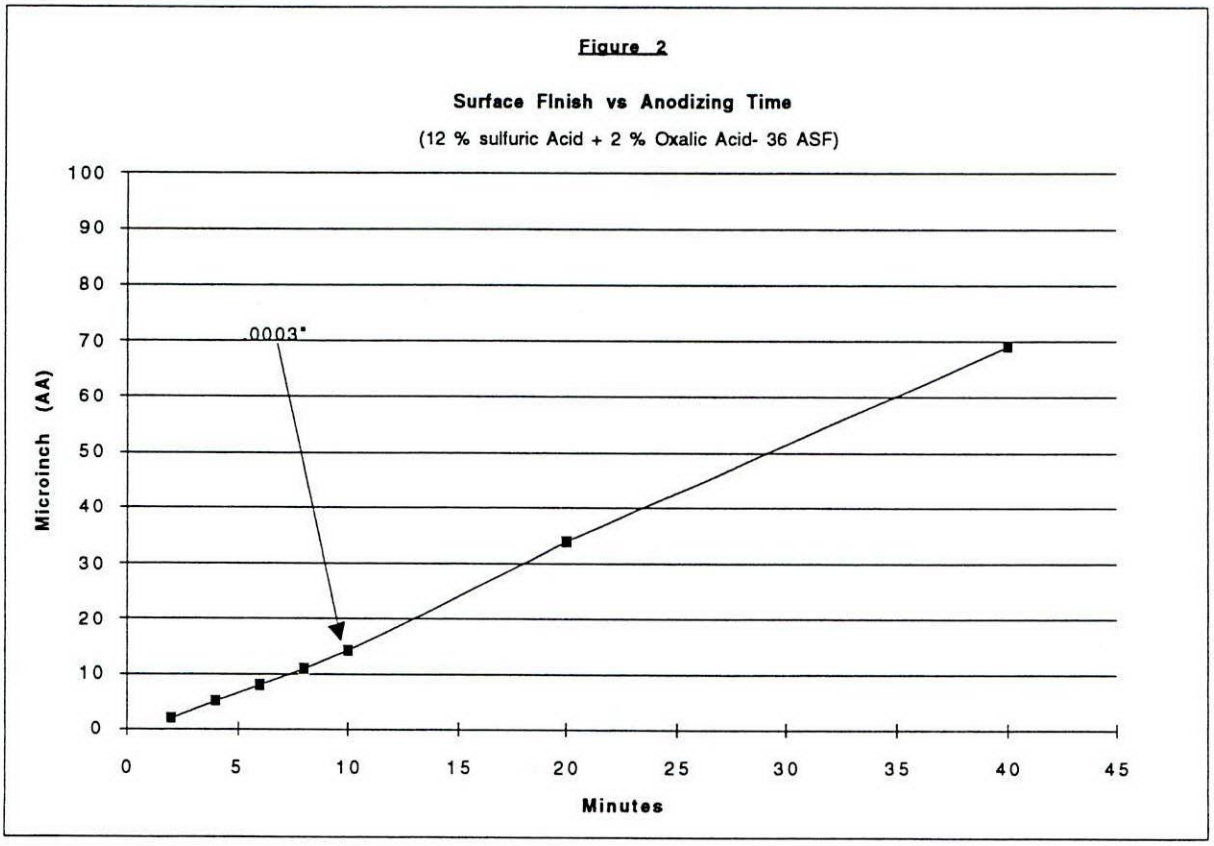

Figure 3

Surface Finish vs Anodizing Time

(4.5% Oxalic Acid- 25 ASF-60 deg. F.)

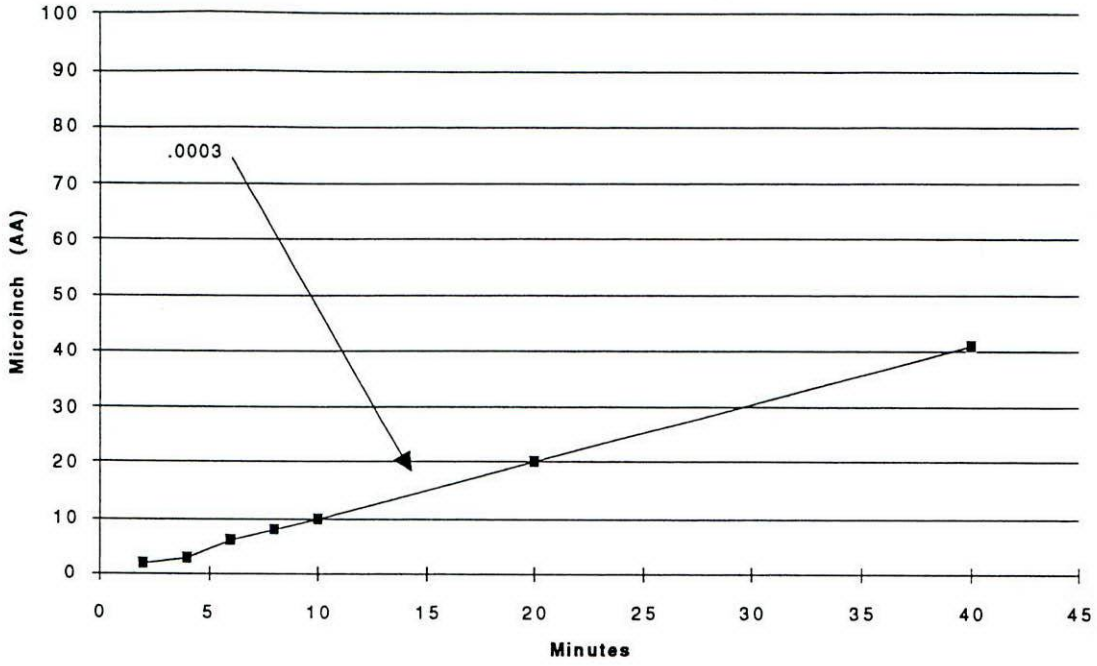

Figure 4

Surface Finish vs Anode Current Density

(4.5 % Oxalic Acid-360 AmpMin.)

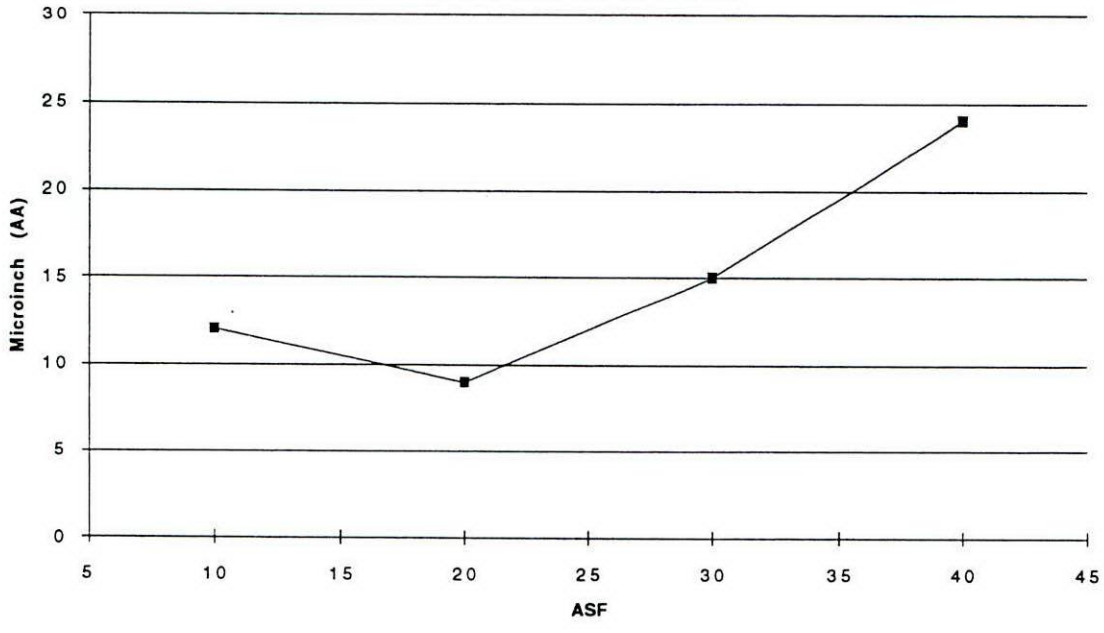

Figure 5

Surface finish vs Solution Temperature

(4.5 % oxalic Acid-25 ASF)

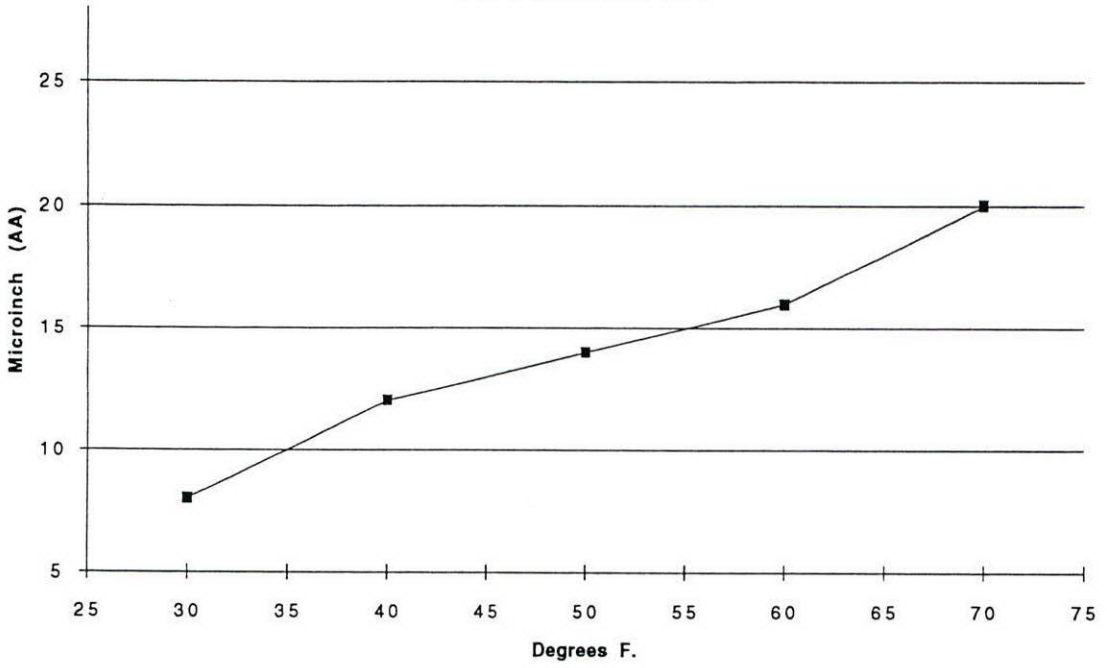

Figure 6

Surface Finish vs Anodizing Method

(360 Ampere Minutes)

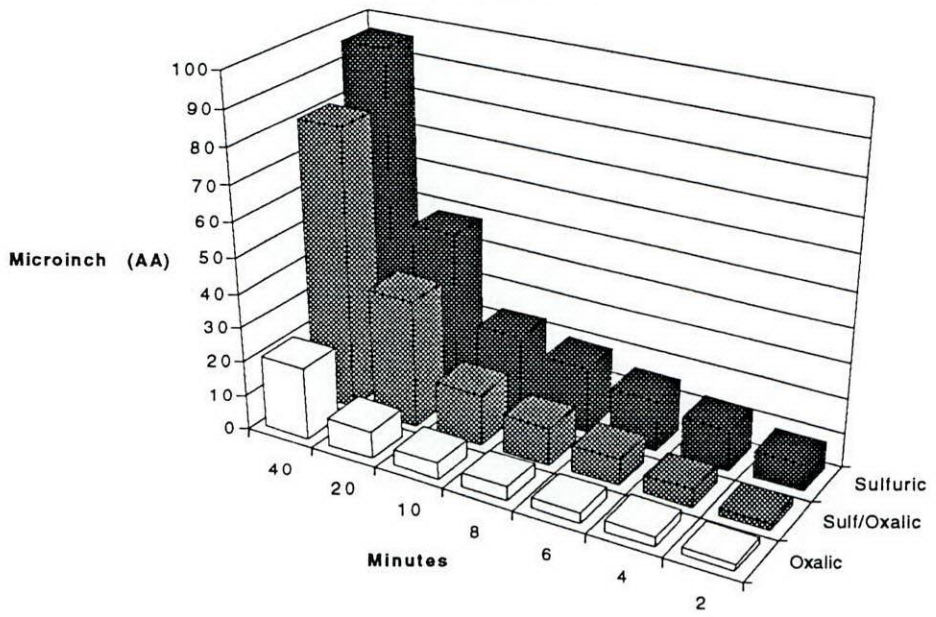

References

1 *Handbook of Tables for Applied Engineering Science*, 2nd Ed., R.E. Bolz and G.L. Tuve, Ed., CRC Press, 1987.

2 *Electroplating Engineering Handbook*,3rdEdition, A.K.Graham Editor, (461-464).

3 Sanford Process Co., U.S. Pat. 4,128,461 (1978),4,133,725 (1979).

4 Aluminum Company of America, Bulletin 14-A.

5 Ball Seal Company.

6 J.W. Dini, "Electroless Nickel: An Important Coating for Diamond Turning Applications". *Proceedings Electroless Nickel Conference II,* Products Finishing Magazine, Cincinnati, OH.

7 J.W. Dini, H.R. Johnson, "Quantitative Adhesion Data for Electroless Nickel Deposited on Various Substrates" UCRL Pub.

9 ANSI/ASTM B 580 - 73, Anodic oxide coatings on aluminum.

9 ALUMALITE 225, Aluminum Company of America.

10 Miyata, A., Isawa, K., Furuichi, A. and Takamura, K., *Rept. Inst. Phys. Chem. Res.*, Tokyo, 1961, 37, 142-48.

11 G. Bailey, G.C. Wood, "The Morphology of Anodic Oxide Films Formed on Aluminum in Oxalic Acid.", *Trans. Inst. Met. Fin.*, Vol. 52, (1974).

12 Spooner, R.C., "Anodic Treatment of Aluminum in Sulfuric Acid Solutions"., *J. Electrochemical Soc.*, 102, (4), 156-62, (1955).

THE HOT-COLD IMPREGNATION OF ANODIZED ALUMINIUM INFLUENCES THE IMPURITIES ON THE POROUS-LAYER BARRIER OF THE SEALING BATH

Xavier Albert Ventura
Electroplating Consultant
Camprodón, 1,1º,1ª, 08012 Barcelona, Spain.

ABSTRACT

An electrochemical method has been developed to rapidly evaluate the quality of anodized aluminum coupons. The test has been optimized for quality control applications via a sample test fixture which allows standard sample coupons to be conveniently interchanged. The feasibility of strengthening anodic films by limiting or preventing the growth of film cracks, was investigated. Oxide films were subject to internal stresses caused by a variety of factors, including the presence of anodization and film thickness. It is thought that these internal stresses influence the growth of cracks resulting from strech-ing of the film. The appearance of cracks in the anodic oxide films is acom-panied by an increase in stick-slipping, peeling of the film and adhesion to the exposed metal. The hot sealing process is accomplished with water at 90ºC, at high temperature with salts and afterwards, water vapour, autocla-ve type, but the cold sealing process is done at ambient temperature, using nickel fluoride salts to seal parts.

Aqueous Dissolutions

Aluminum belongs to that group of metals which have a very negative electro-de potentials and which evolve out hydrogen on contact with aqueous electro-lytes.

Bethume and Loud had calculated the Al electrode potential from thermodyn-amic data.

Electrodes of reaction	E (V)	$\frac{dE/dT}{mV/K}$	$\frac{dE/dT}{mV/K}$
$Al^{+3}+3e^- \rightleftharpoons AL$	- 1.662	1.375	0.504
$AlF_6^{3}+3e^- \rightleftharpoons Al + 6F^-$	- 2.069	0.67	- 0.20
$H_2AlO_3^- + H_2O+3e^- \rightleftharpoons Al+4OH^-$	- 2.40	- 0.06	- 0.93

Latimer also found from thermodynamic data values that dissagreed little with the ones above.

Hayrosky found a value of 1.33 V at 15ºC for the usual potential of the Al electrode, through electrochemical testing. He used Al amalgam at 0.1 % and worked in Al Cl_3 dissolution to avoid hydrogen emission and oxide formation. He atributed this electrode to the reaction

$$Al + 3OH^- \rightleftharpoons Al(OH)_3 + 3e^-$$

Plumb and Haygard found for the usual electrode potential the value -1.324 V,

using an Al electrode constantly renewed and thus with a maximum oxide coating.

Non-Aqueous Dissolutions

Wallace and Bruins measured a potential of 1.150 V per Al/0.1 cell with Al Cl_3-Acetamide AgCl at 90ºC and observed the hydrogen evolution due to the high acidity of the molten $AlCl_3$ acetamide electrolyte.

Anodic Oxidization

Unlike the electrocoating processes in which the layer increases towards the electrode outer part, in anodic oxidization the layer growth is towards the inner part of the metal and therefore consuming it. If we concentrate on the faradic conversion of Al to oxide, we observe that for each gram of metal consumed, 1.889 grs. of oxide is obtained. The coating relation is defined as the oxide amount formed per gram of reacted aluminium, which experimental value -double weighting measurement- show us the efficiency of the anodic process.The classification of the anodized layer during the formation process, can be made in accordance with the dissolvent amount of the electrolyte in that layer.

Non-Porous Layer

The non porous layers are those which do not retain dissolvent in the formed oxide layer and, therefore, are compact, dielectric and thinner. The layer thickness initially depends on the applied potential and temperature. In a dielectric enviroment if the potential applied is high enough, a strong discharge is produced,thus perforating the layer. We call this effect layer's breakage.

The electrolytes causing this type of breakage are aqueous disolutions of borates, tartres, succionates, citrates, phosphates and carbonates. The breakage potential for the non porous layers, oscilates between 500 and 700 V and refers to tickness between 7.000 to 10.000 Å. If the applied potentials are lower, the current's density becomes almost zero and the layer's growth is gradually slowed down until becoming non-existent.

The velocity formation in the initial layer increases lineally in relation to the current density and the coating relation value near to the theoretical value of 1.889 as for a process that has not secondary reactions.

Porous Layers

Porous layers are those which do not hold dissolvent in the formed oxide layer. They are gelatinous and therefore, thick and soft. In the porous layer the coating relation has a value of 1.35 to 1.46 due to the existing competitive effect of dissolution against that of oxide formation. The porous layer because of its physical characteristics cannot serve the purpose of being a protective layer. The insolubility of the porous layer is achieved through sealing. This seems to transform the superficial layer in small crystallines nuclei of hydratated oxide which several authors believe to be

boehmite. However, most probably what happens is the formation of a defective variety of pseudoboehmite $Al_2O_3 \times H_2O$ (x between 1.8 to 2.5).

Disolving Electrolytes of the Aluminium Oxide Layer

In this case, the growing layer is competing with the dissolution of the superficial layer. In coating achieved this way, two layers can de differentiated:

- .The first, in touch with the metal, presents the same characteristics as a non-porous layer of thickness 100-700 Å.
- .The second, belongs to the type of porous layers and its thickness varies between 30 μ for a thin, porous film and 100 μ for a thick porous film.

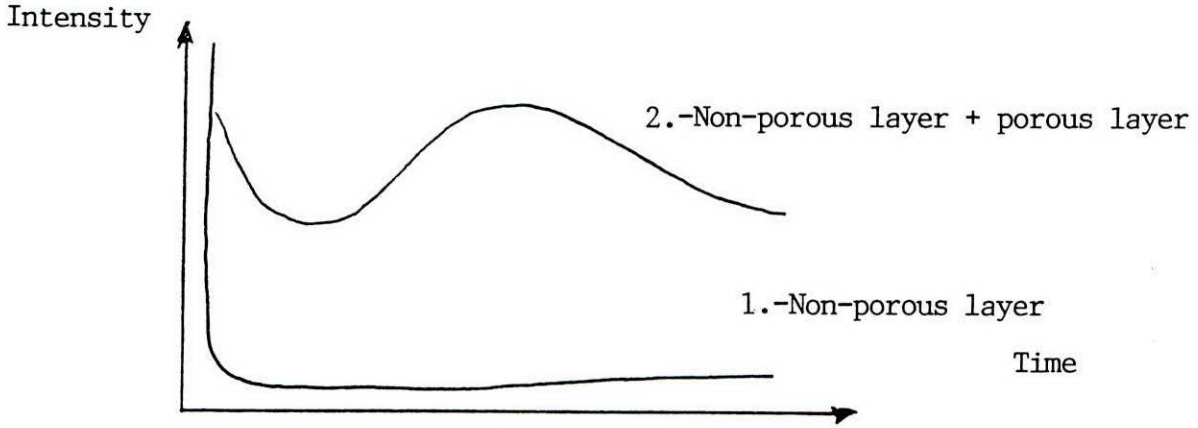

Process 1, is that of forming a non-porous layer and as its thickness increases so does its resistance, because it is dielectric and therefore intensity decreases until practically becoming nule.

In process 2, both layers are formed. Initially, the formed layer is non-porous and because of it, the obtained curve is similar to the previous one but goes inmediately through a maximum due to the formation process of the porous layer and both in competiton with their dissolution reach a point in which become equally even and from then on their intensity remains constant.

Electrochemical Process

Anodizing is that on the anodic half-cycle, at each electrode, film formation takes place and that on the cathodic half-cycle film reduction does not take place and the continous film growth can occur.

On the anodic half-cycle the main reaction is clearly oxide film formation expresses simply as:

$$2\ Al + 6\ OH^- \rightleftharpoons Al_2O_3 + 3H_2O + 3e^-$$

As the voltage is increased some film dissolution occurs, leading to conventional porosity

$$Al \longrightarrow Al^{+3} + 3e^-$$

$$Al_2O_3 + 3\ H_2\ O \longrightarrow 2\ Al^{+3} + 6OH^-$$

or

$$Al_2O_3 \longrightarrow 2\ Al^{+3} + 1\tfrac{1}{2}O_2 + 6e^-$$

and some direct oxygen evolution may occur:

$$4OH^- \longrightarrow 2H_2\ O + O_2 + 4e^-$$

A side reaction also takes place at higher voltage but probable not to any significant extent, oxidation of sulphate

$$2\ SO_4^{-2} \longrightarrow S_2\ O_8^{\ 2-} + 2e^-$$

On the cathode half-cycle hydrogen evolution is the main reaction

$$2\ H^+ + 2e^- \longrightarrow H_2$$

with the reduction of sulfate as a minor side reaction

$$SO_4^{2-} + 8H^+ + 6e^- \longrightarrow S^o + 4\ H_2\ O$$

or

$$SO_4^{-2} + 10\ H^+ + 8e^- \longrightarrow H_2S + 4H_2O$$

Its occurrence is clear from both the smell of H_2S and the presence of sulphur in anodic film present as S or S^{2-} and quite distinct from SO_4^{-2} which is usually trapped residual sulphuric acid electrolyte (4-8).

Two other reactions, theoretically possible at higher voltages, do not in practice occur and can be disregarded. They are alumina reduction

$$Al_2O_3 + 6H^+ + 6e \longrightarrow 2\ Al + 3\ H_2O$$

and aluminium electrodeposition

$$Al^{+3e} + 3e \longrightarrow Al$$

Any process improvement based on the electrochemistry will normally relate to elimination of the sulphate reduction reaction and two possibilities exist. Firstly, the overvoltage for sulphate reduction could be raised or the overvoltage for hydrogen evolution lowered, thereby making sulphate reduction less favourable. Secondly, allowing sulphate reduction to take place but directing the sulphur or shulphide thus formed away from the film preferably as some soluble species.

Experimental

The majority of the work to be discussed was carried out on commercial purity aluminium. Samples measuring 50 mm x 50 mm were cut from the sheet.

The following pre-treatment was employed, prior to nickel flouride cold sealing and hot water sealing.

Cleaning: All samples were cleaned for 10 minutes, at 50-65ºC, in a 50-60 gr/l solution of propietary alkaline cleaner.

Rinse.

Etching: Samples were etched for 10 minutes, at 60ºC, in a propietary long-life solution, containing 60 ml/litre etch bath -approximately equal to 50 grm/l of free caustic soda.

Rinse.

Desmutting: First, the surface was wiped with cotton wool under tap water, then dipped in 20 % nitric acid, at room temperature, for two minutes.

Rinse.

Anodizing: Direct-current anodizing was performed at a constant current density of 1.5 A/dm^2, in an electrolyte containing 165 gr/l sulfuric acid in deionized water at 20ºC.

Equal phosphoric acid 40 gr/l temperature 25ºC current 1.5 A/dm^2.
Equal oxalic acid 90 gr/l temperature 25ºC current 2.6 A/dm^2.
Equal cromic acid 30 gr/l temperature 60ºC current 1.2 A/dm^2.

Rinse: After anodizing, the samples were rinsed two more times in deionized water.

Cold sealing: Cold sealing took 15 minutes at 25ºC in a 6 gr/l Ni $F_2.4H_2O$ solution, at a pH of 6.

The two final rinses removed excess chemical from the surface.

Hot sealing in deionized water with cobalt acetate, 1 gr/l, time 40 minutes, temperature 96ºC.

Finally samples were rinses once more in deionized water at 60ºC.

Pores and Cells

It was found with the help of an electronic microscope, that the porous layer showed a structure similar to cells, thought to be caused by the action of the dissolvent on the simple cells of oxide, formed on the pores base.

The oxide dissolution on the barrier layer, its followed by the current going through it, thus as the dissolution temperature becomes higher, the dissolution power also increases, this being the direct cause for the remaining pores. Futhermore, as the current circulates through the single pores, a cylindric cell with a rough hemisphere ending and a cylindric central pore is formed, in concordance with the electric field. As the layer formation increases, the sell shape alters until touching the six cylinders around it, becoming a hexagonal prism, at the same time modifying the pores shape and obtaining six projections toward the hexagon's vertices.

Observation with an electronic microscope showed its structure, which was identical in all anodic layers obtained with cromic, phosphoric, oxalic and cromic acids.

In the figure below, it is showed the explained scheme of anodized aluminium.

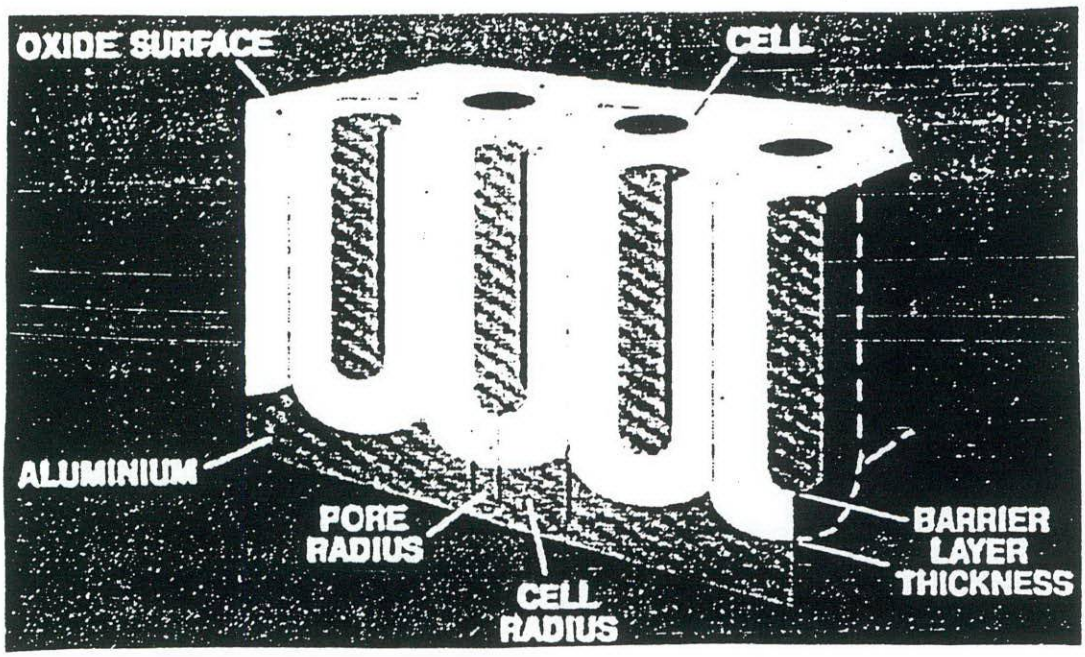

Let us see different micrographs of an 0.1 micron anodic film membrane

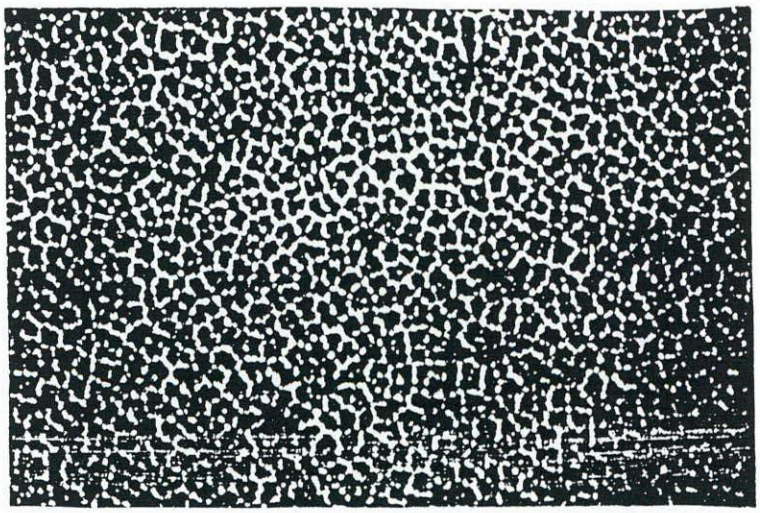

A fracture section micrograph of the 0.2 micron anodic film membrane

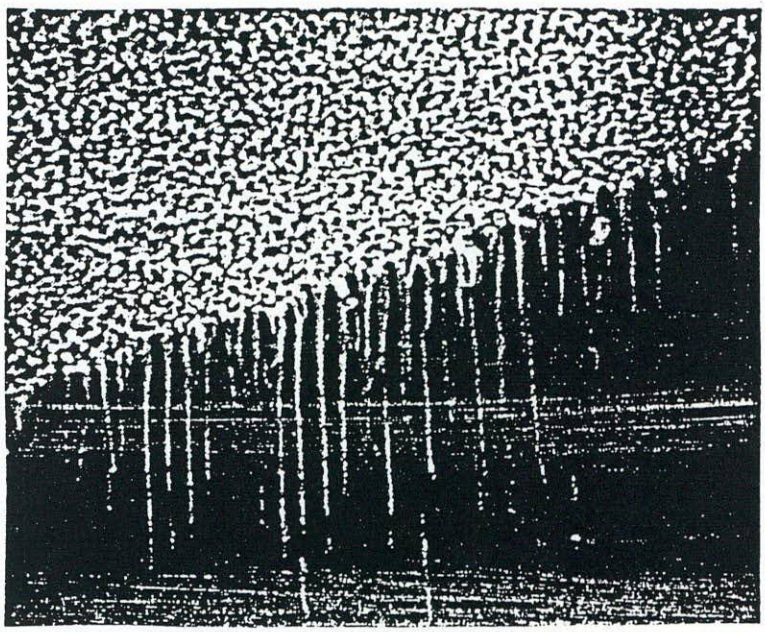

In the micrograph below of the 0.02 micron asymmetric anodic film, it can be seen how oxide penetrates and fills the pores

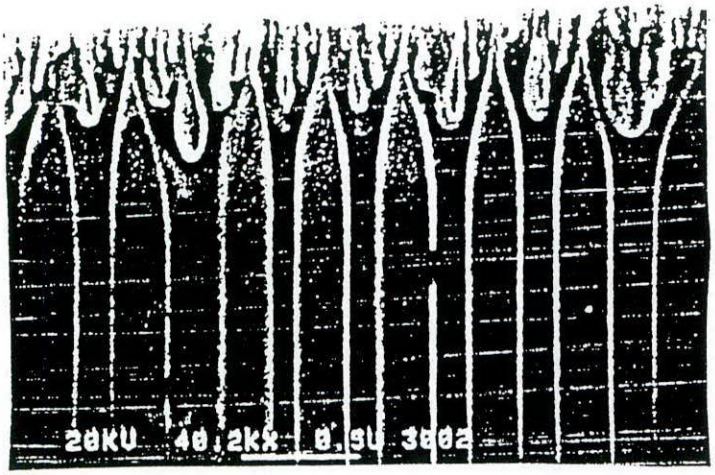

It has been possible to verify the initial cell formation in a layer anodized with phosphoric acid at 40 V. At first, single rows of cells are formed at both sides of the grains, precisely on the parts of the natural oxide film which are less resistant to the electric current. In time, more and more rows of cells are formed along the electric path, until the total reticulate structure is completed. The current strength variations at the beginning of the anodizing process in sulphuric acid, shows that after decreasing the current to a minimum, which coincides with the formation of an uniform film of increasing thickness, the current density after 4 or 5 seconds -at the moment pore formation takes place- reaches a balance state after more or less 15 seconds.

It is represented graphically below

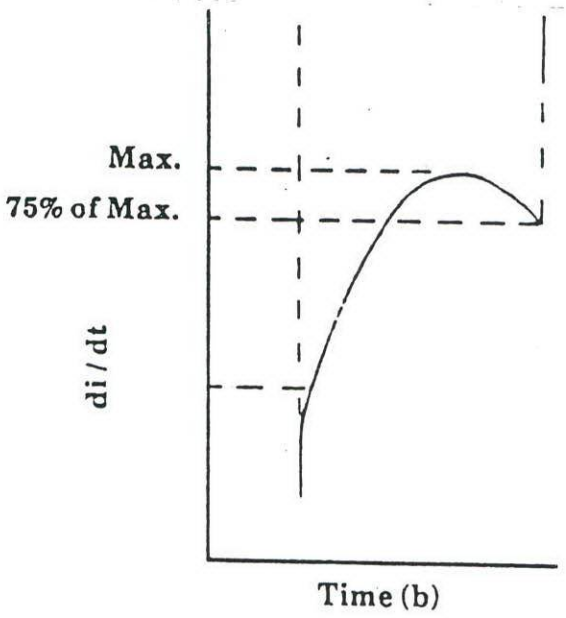

The graph below shows pore size distribution by the number of pores with different parameters, like polycarbonates, polytetrafluoroethylene, mixed cellulose esters, cellulose acetate and polyamide.

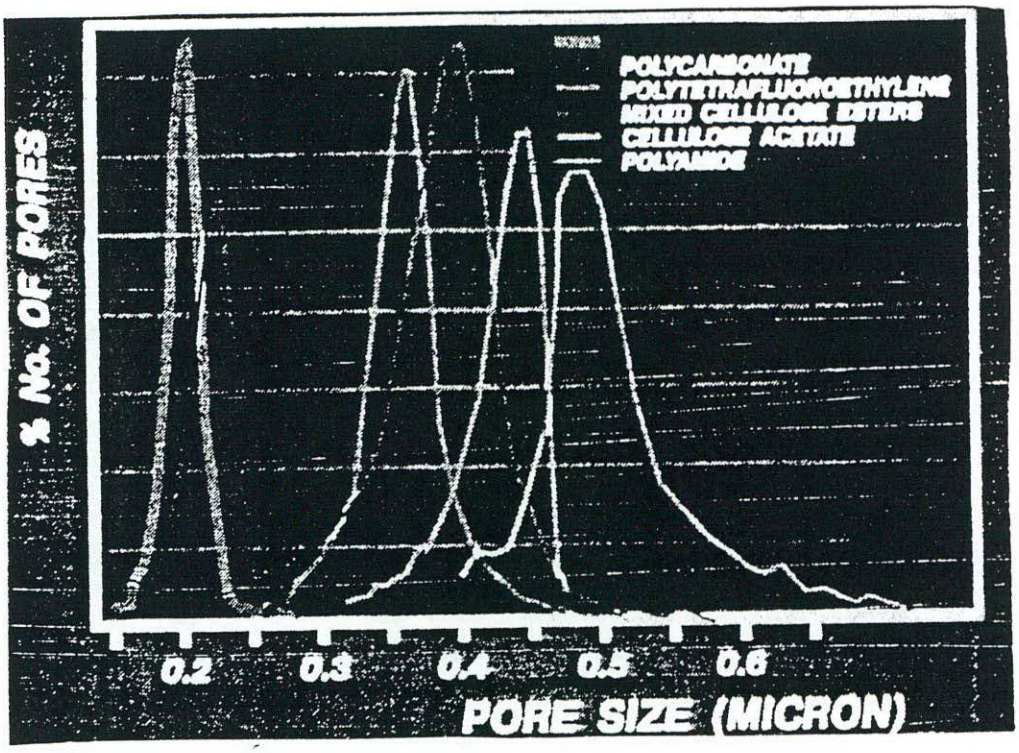

To conclude the table below ilustrates the result obtained with pore size distribution, micron measurements, concentration, temperatures and current intensity and voltage.

ACID	CONC. (g/l)	TEMP. (°C)	CURRENT (A/m^2)	VOLT. (V)	ANION DOPED (wt %)	PORE SIZE (nm)	THICKNESS (μm)
SULPHURIC	165	20	150	18	15	18	>100
OXALIC	90	25	260	55	3	45	>100
PHOSPHORIC	40	25	150	160	7.5	160	75
CHROMIC	30	60	120	100	0.1	120	25

REFERENCES

1. YAFFE, B.S. 'Standars and Specification for Anodised Aluminium', Metal Finishing, pags. 29-35, April, 1986.

2. Barkman, E.F. 'Evalutaing Anodic Coating', paer nr. A-10, Aluminium Finishing Seminar, March 19-21, 1973.

3. Military Specifications MIL-A-8625 E, 'Anodic Coating for Aluminium and Aluminium Alloys', April 25, 1988.

4. 'Dedignation for Aluminium Finisher', Publication 45, Seventh Edition September, 1980, The Aluminium Association.

5. Kalantary-Gabe-Ross, 'Sealing Tests and the Ageing of Cold Sealed Anodized Aluminium' , July,1991, Plating and Surface Finishing.

6. J. Albort Ventura, 'Aluminium Plating by the Seimplex Method', Interfinish 91, Tel-Aviv.

7. Xavier Albert Ventura, 'The Hot-Cold Impregnation of Anodized Aluminium', Euro-Asia Interfinish 91, Tel-Aviv.

8. Xavier Albert Ventura, 'The Electric Double-Layer of Aluminium', 1986, Madrid.

9. Xavier Albert Ventura, 'Increasing the Crack Resistance of Porous Anodic Oxide Film of Aluminium',Surfin 88, Los Angeles.

10. Hidetoshi Takaichi, 'Sealing Bath and Bath Stability at Cold Sealing Method for Aluminium Anodized Film', Okuno Chemical Industries Co. Ltd.

11. Jean Royo, 'Anodization des Alliages Legers Phenomenologie Principes' Congres National de l'Electrolyse et des Traitements de Surface', Paris, 1987.

12. Gabe, D.R., 'Anodizing with Alternating Current: The Process of the Future', IPTME, Loughborough University of Technology, U.K., World Congress on Aluminium, 1990, Modena, Italy.

13. Cowieson, Davies and Furneaux 'Anodizing Process for the Production of Inorganic Microfiltration Membrane Rig', Alcan International Limited, The institute of Metal Finishing, Brighton, 1989.

MECHANICAL PROPERTIES OF ANODIZED ALUMINUM COATINGS

R.S. Alwitt, Boundary Technologies, Inc., Buffalo Grove IL 60089
R.C. McClung, Southwest Research Institute, San Antonio TX 78228

Mechanical properties of anodized coatings on 5657 alloy have been studied. Stresses were measured after each process step and after exposure to different humidities and temperatures. Stress is tensile after anodizing and compressive after sealing. Prolonged exposure to low humidity causes the stress to become strongly tensile; the effect of humidity on stress is reversible. Oxide cracking due to differential thermal expansion depends on environmental and metallurgical factors. Plastic deformation of metal occurs under the oxide cracks.

I. INTRODUCTION

This work is part of a program to obtain information about properties of anodized aluminum coatings that are important to its application as a thermal control surface in a space environment. Since there is no atmosphere in space to support conduction or convection, heat rejection by radiation is the only means to achieve thermal management. Anodic oxide coatings have the high emissivity and low absorptivity that is required for good thermal control. The optical properties are stable in the intense ultraviolet radiation, atomic oxygen, and vacuum of the low earth orbit environment (1). Because of superior optical properties, sulfuric acid anodized 5657 aluminum alloy has been selected as a candidate material for use on Space Station Freedom for certain radiator surfaces (2). Anodic coatings also will be used for thermal control on external structural alloy surfaces.

A potential problem is that anodic coatings may crack under some conditions at elevated temperature. There is concern that extensive cracking of the radiator coating could impair optical properties and reduce heat rejection efficiency. Thermal cracking occurs because the coefficient of thermal expansion of aluminum is about five times greater than that of aluminum oxide. If metal and oxide were each free to expand at some elevated temperature, the metal expansion would be five times that of the oxide. The intimate bond at the metal/coating interface prevents this equilibrium state from being achieved; the metal is constrained to expand less and the oxide is forced to expand more. At a sufficiently high temperature the resulting tensile stress in the coating is large enough to crack the oxide. At low temperatures the forces are reversed and the oxide is placed in compression by metal contraction.

Radiator panels are fabricated by adhesively bonding the anodized sheets to a honeycomb core. This operation is performed at a temperature between 250 and 350°F (120-175°C), depending upon the adhesive used for bonding. Tensile stress in the coating may become large enough at these temperatures to cause cracking.

Expansion and contraction from temperature cycling may result in thermal fatigue. Over the projected 30-year operating life of Space Station Freedom there will be 175,000 orbital cycles, and during each cycle the space station passes in and out of the sun's radiation. During an operational cycle the temperature extremes of the radiator surface are likely to be about +10° to +75°F (-12°to +24°C). Normal operation will be interrupted from time to time, and then a "deep" cycle will occur, during which temperatures may range between -135°F to +120°F (-93° to +49°C). The deep cycle frequency will be between 0.1

and 1%.

Several years ago, NASA initiated a project with the overall goal to specify process conditions that will produce anodized radiator panels that withstand fabrication without cracking, and for which there is a high confidence of 30-year operating life with acceptable optical properties. The major parts of our involvement with this program are as follows:

a. Determine coating physical properties (elastic modulus, coefficient of thermal expansion).
b. Measure coating stress for different process and environmental conditions.
c. Characterize the effects of coating, metal, and environment on oxide cracking.
d. Develop thermal fatigue models to predict coating performance in low earth orbit.

In this paper we present observations of coating stress and cracking that may be of general interest, here in our earthbound environment.

II. EXPERIMENTAL

Aluminum specimens were anodized and sealed, and then exposed to various controlled temperature and humidity atmospheres. Coating stress was measured after each process step, and also during environmental exposure. In separate experiments, cracking of the coating induced by elevated temperature was studied. This was characterized by T_c, the temperature at which cracks first appeared, and also by the crack density at temperatures above T_c.

Most results were obtained with 5657 alloy sheet. Stress measurements were made using strips of 10 mil thick H28 temper sheet 0.25"wide x 8" long. Behavior under thermal strain to induce cracking was studied using 2"x2" coupons cut from 25 mil H242 temper sheet. Some reference is made to results with other alloys.

The process sequence was chemical polish → anodize → seal. The strips for stress measurement were coated on one side with a polymer masking compound after the chemical polish. The polishing solution was a mixture of concentrated nitric and phosphoric acids (Bright-Dip) used at 97°C, with an immersion time of 20-30 sec. Anodizing was in 20% H_2SO_4 at 22°C and 15.0V. The average current density was 15.2 mA/cm^2 (14.2 A/ft^2). Anodizing time was varied to cover a thickness range from 0.3 to 1.2 mil, with most coatings either a nominal 0.5 or 1.0 mil. Sealing was in hot water for 5 min or 20 min. The 2"x2" coupons were sealed at 95°C but, to simplify temperature control during the stress experiments, those strips were sealed in boiling water.

A. Stress Determination

Stress was determined using beam bending analysis. An Al strip is clamped at one end and anodized on one side. Stress in the coating causes the beam to bend - concave if the stress is tensile and convex if compressive. The magnitude of the stress is proportional to the deflection. The average stress in the coating is calculated using Eq. [1]:

$$\sigma_c^{bent} = \left(\frac{E_s}{1-\nu_s}\right)\left(\frac{t_s}{3l^2m(1+m)}\right)\delta \qquad [1]$$

where $m=t_c/t_s$ and subscripts c and s stand for coating and metal substrate, respectively. E is the elastic modulus and ν is the Poisson's ratio, t is thickness, l is anodized length, δ is the tip deflection of the strip (reference point: zero stress position). The term $E/(1-\nu)$ is the biaxial modulus, and must be used when the width of the strip is greater than its thickness. A more complete form of Eq. [1] is given in ref. 3.

To measure process stress the specimen was suspended vertically with its upper end clamped and the lower end free to move in response to stress changes. The specimen was processed by first raising the anodizing bath to immerse the strip, performing the anodization, then lowering that bath, rinsing and allowing the strip to air dry. Then the seal bath was raised and lowered in the same way. Initially, and after each step, the position of the specimen tip was measured by a laser beam scanning horizontally in the plane of the tip. Deflections were typically of the order tenths of an inch. The length and thickness values needed for the stress calculation were measured directly.

To measure stress during long term exposure, the specimen was transferred to a horizontal clamp attached to a plate on which there was a scale to measure the tip position visually. The plate was placed in a glass desiccator in which a controlled humidity could be maintained by placing a selected desiccant in the chamber. Indicated humidities were either measured with a hygrometer or are nominal handbook values, and are given in ppm (v/v) water vapor. For measurements at temperatures above ambient, the desiccator was placed in an oven. In one experiment, coating stress was measured at 10^{-6} torr in a vacuum chamber with a viewing port.

B. Coating Cracking

The 2"x2" coupons for testing at elevated temperature were anodized on both surfaces, so no deflection occurred during heating. Stress at temperature was calculated using Eq. [2]:

$$\Delta\sigma_c^{unbent} = \frac{E_s(\alpha_s-\alpha_c)\Delta T}{(1-\nu_s)\left(2m+\frac{1}{n}\right)} \qquad [2]$$

where α=coefficient of thermal expansion, $n=[E_c(1-\nu_s)]/[E_s(1-\nu_c)]$, and the other symbols are as defined for Eq. [1]. The value for α_c, obtained in separate experiments, was found to be close to that for bulk alumina (4). Values for E_c were calculated from σ vs T measurements with one-side anodized strips (4).

Baseline T_c values were obtained within 2 days after anodizing by heating coupons in ambient air. Between about 100 and 200°C, temperature was raised in 10°C intervals, the coupons were held for at least 10 min at each temperature, and examined visually for cracks after each step. The test was limited to 200°C because at that temperature the metal deformed. Measurements were made on sets of three duplicate coupons. Other experiments were done in which coupons were placed in controlled atmosphere after the anodizing process, and subsequent heating was either in this same atmosphere or in ambient. Although the range in T_c for a particular coating/alloy was rather broad, at least ±15°C in replicate experiments, it served as a general indicator of cracking tendencies with a possible link to cracking during long-term thermal cycling (3).

To determine the effect of thermal cycling, coupons were hung from a chain that moved between heated and cooled chambers in a sealed enclosure. The

humidity was kept at a low level by maintaining a flow of dry air (175ppm) or dry nitrogen (50-80 ppm) through the enclosure. Temperature on the hot side was controlled to within 0.2°C. Coupons were viewed for crack observation through a window located in a short buffer zone between the hot and cold sides. Each cycle took 9.4 minutes.

III. RESULTS AND DISCUSSION

A. Stresses

1. Process Stress - Fig. 1 shows typical values for the stress in nominal 0.5 mil coatings with 20 min seal at each step in their history. The stress after anodizing (σ_a) does not depend on coating thickness; there is some dependence on process conditions and particular alloy, but σ_a is always tensile and relatively small. The stress after sealing (σ_s) is always compressive and increases with seal time. There is a dependence on the ratio of coating to substrate thickness (m), with σ_s most compressive for small values of m. In our experiments, σ_s ranged from -3 to -8 ksi.

2. Effect of Humidity - The ambient humidity has a profound effect on coating stress, as illustrated in Fig. 1. The stress shifts from compressive to tensile when the humidity drops below about 2000 ppm (9%RH at 25°C). The tensile stress increases as humidity drops, and reaches its highest value of 16 ksi at 10^{-6} torr vacuum. In dry atmospheres there is little dependence of σ on coating thickness or seal time. The stress increase is accompanied by a

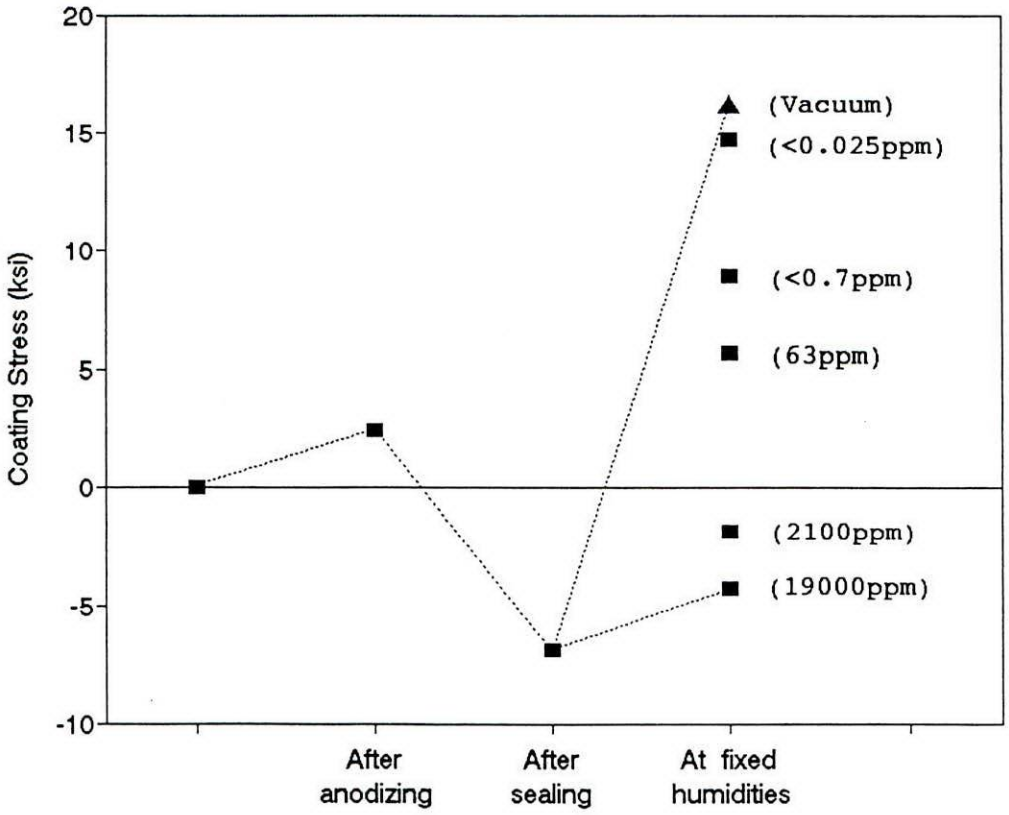

Figure 1. Stress history of 0.57 mil oxide coatings with 20 min seal.

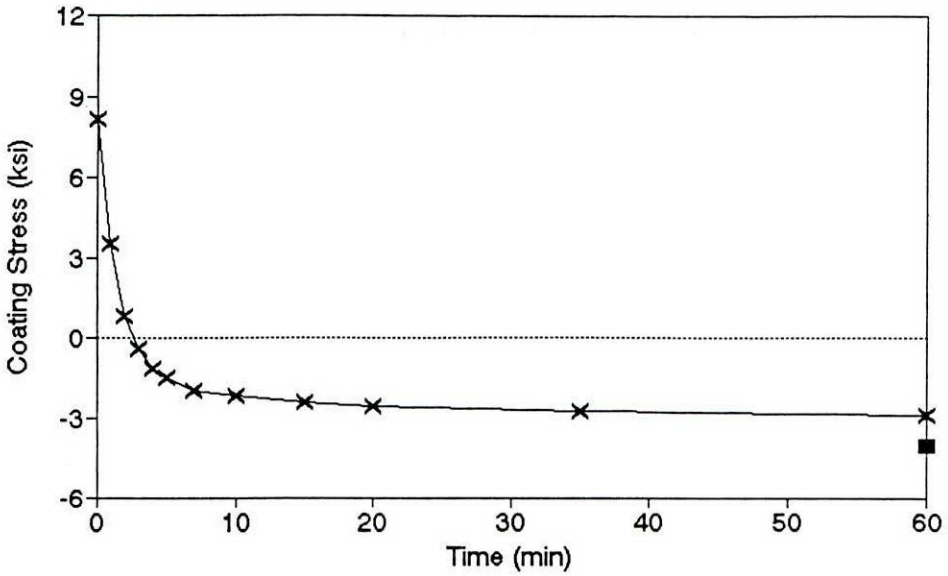

Figure 2. Stress vs time after re-exposure to ambient humidity from 0.7 ppm humidity. Coating is 1 mil thick with 20 min seal. Final stress measured after 149 hours in ambient humidity is shown as filled squared (▪).

loss of coating weight, presumably loss of water. For example, for a 0.9mil/20min seal coating stored over P_2O_5 (humidity < 0.025ppm), σ = 14 ksi,an increase of 16-18 ksi from ambient humidity, and the weight loss corresponds to 1.1% of coating weight (10% of total water content).

The change in stress with humidity is reversible. Fig. 2 shows that upon re-exposure to ambient humidity from 0.7 ppm, the stress becomes compressive within several minutes and the original value is restored within hours.

3. Effect of Temperature - Fig. 3 shows a typical measurement of specimen deflection vs temperature, measured at ambient humidity. The temperature was raised in steps of 3-5°C and held for 1-1.5 hr at each step. The same result is obtained by heating at an approximately steady rate of about 4-5°C/hr. Cooling to room temperature was not controlled, and most of the temperature drop occurred within a few hours. From Eq. [1], stress is proportional to deflection, so it follows from these measurements that the stress increase is proportional to temperature, and the stress change is reversible upon decreasing the temperature. This behavior was observed up to 70°C, the highest temperature used in these measurements. It was found that the temperature dependence of stress, $\Delta\sigma/\Delta T$, is smaller at low humidity than at ambient humidity.

The elastic modulus of the coating (E_c) can be calculated from $\Delta\sigma/\Delta T$. (4). The modulus is found to be independent of coating thickness and seal time. At humidities of 590 ppm and higher, E_c appears to be constant at an average value of 19,700 ksi. At humidities of 63 ppm and lower, the average modulus is 11,200 ksi.

B. Cracking with Step-wise Heating

With 25 mil 5657 sheet, the average baseline T_c value is 132°C for 0.5 mil oxide, and 116°C for 1 mil oxide, with a range of about ±15°C for each. No

dependence of T_c on seal time was found. Using Eq. [2], the corresponding ranges for failure stress are 35 to 49 ksi for 0.5 mil and 26 to 39 ksi for 1 mil oxide. It was generally found that thicker coatings cracked at lower stresses.

Cracks commonly were in the rolling direction and extended across the coupon. Visually the cracks appeared either linear or smoothly curved, but at low magnification, say 100x, they were seen to undulate in response to local variation in stress and/or material properties. It was not uncommon for cracks to propagate in response to an evident local defect, and sometimes in a non-rolling direction. An existing crack stopped the advance of a new crack; cracks never crossed. Cracks that developed between 120° and 190°C were 1-2 μm wide.

Long term exposure at different humidities - Anodized coupons were stored for 4-5 weeks in different environmental conditions and then tested for cracking. These tests are summarized in Table 1. After storage, the first three sets of coupons listed were returned to ambient atmosphere for stepwise heating. Long term dry storage (2-5 ppm) at moderate temperatures has no effect on cracking; T_c and crack density are the same as for the baseline condition. It was shown earlier that dry storage increases coating tensile stress, but that after returning to ambient the stress quickly returns to the usual compressive value. Remaining at the higher stress level for extended time apparently has no permanent effect on the oxide. On the other hand, cracking occurs at a lower temperature and with increasing density as storage humidity is increased. Slow reaction between the oxide and water vapor apparently degrade oxide mechanical properties.

The last two data sets in Table 1 show results for coupons stored in dry atmosphere at elevated temperatures. Cracks were seen in the coatings when they were removed from the test chamber and they were not subjected to further step-wise heating. It appears that at elevated temperature a slow change occurs in the coating at low humidity that can initiate cracks.

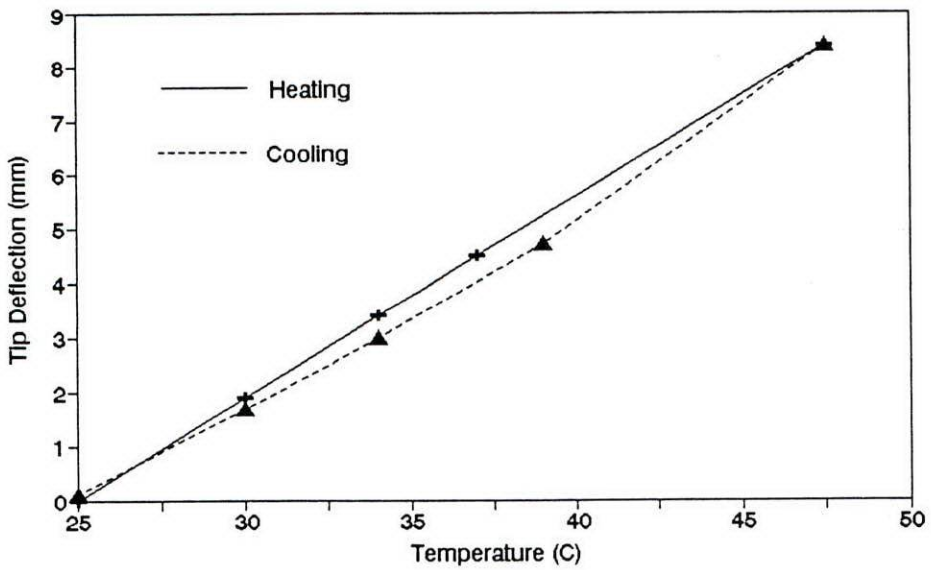

Figure 3. Deflection vs temperature in ambient humidity. Coating is 0.54 mil thick with 5 min seal.

Table 1. Effect of Storage Environment on Cracking

Storage			Coating	T_c	cracks/3 coupons at T (°C)
Time (wk)	Temp. (°C)	Humidity (ppm)	(thickness/seal time)	(°C)	
5	30	2 - 5	0.5mil/5min	130 - 140	0 (100°C) 29 (200°C)
5	amb.	amb.	0.5/5	< 100	40 (100°C) 72 (200°C)
5	30	90%RH	0.5/5	70 - 80	120 (100°C) 360 (200°C)
4	70	90	1/5	-	8 (70°C)
4	80	90	1/5	-	13 (80°C)

In Fig. 4 we plot each of the temperature-humidity conditions from Table 1 and show its effect on cracking tendency. It is likely that the process that causes easier cracking at elevated temperature and low humidity is different from that responsible for the degradation at moderate temperature and high humidity . However, as a guide for operations, it may be convenient to think of the interaction of storage temperature and humidity as shown schematically in Fig. 4.

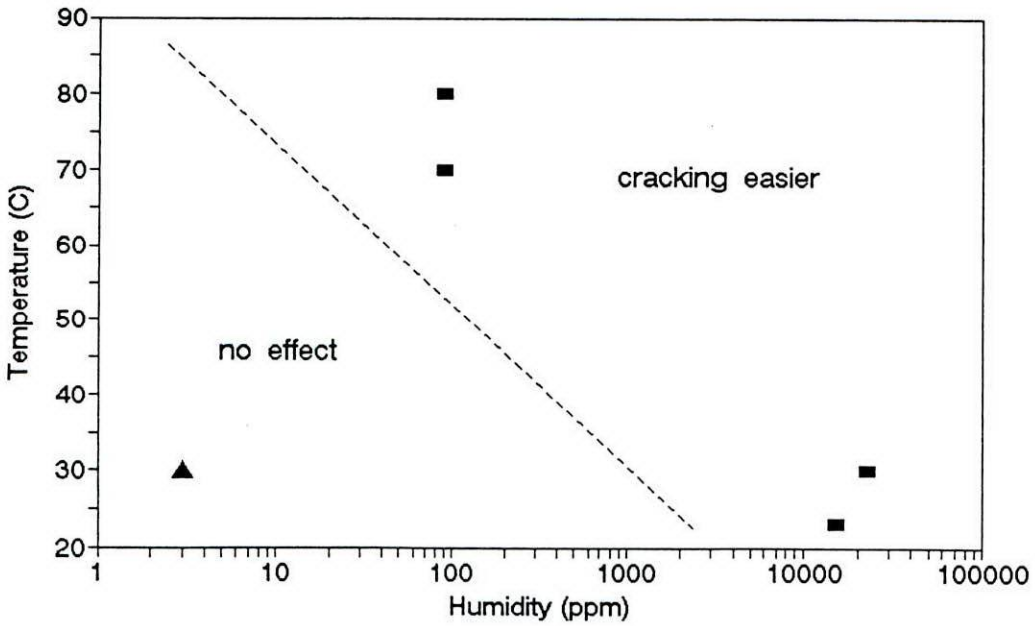

Figure 4. Effect of storage temperature and humidity on cracking: conditions producing enhanced cracking (■) or having no effect (▲).

C. Cracking During Cyclic Heating.

Table 2 is a summary of cyclic test conditions and observations. In each test there was an incubation period before cracks appeared. The cycles at which cracks initiate, N_i, was different for each coating thickness but did not depend on seal time. The subsequent increase in crack density was proportional to log(cycles). Final crack densities did not seem to depend upon coating thickness or seal time, so the end of test crack densities reported in Table 2 are the ranges for all coupon sets in the test.

During tests 4 and 5, sets of coupons were left in the hot chamber for the test duration. The 70° and 80°C results listed in Table 1 are the "static" coupons that accompanied test 4 in Table 2. The cycled coupons were at these temperatures for only half the time of the static samples, but they had up to 3 times the crack density. Thus, a cyclic fatigue process does occur in these oxide coatings that enhances cracking.

A detailed analysis of these tests is found in ref. 4. Here we point out qualitative features of the results. Comparing test 1 with tests 2-4, crack initiation is promoted at 70°C by a dry atmosphere. Tests 4 and 5 illustrate the strong dependence of cracking on T_{max}. Comparing tests 3 and 4, T_{min} has no effect on cracking. This is not surprising, since aluminum oxide is quite strong in compression.

Most of the cracks developed during these cyclic tests were small, about 5mm long and only 0.2 μm wide, which distinguishes them from the longer and wider cracks obtained in the T_c tests. Only for the 1 mil/20 min coatings did some early cracks develop during cycling that extended across the specimen.

D. Deformation of Metal Substrate

When using 10 mil sheet, it was observed that cracks that developed on one surface left a shallow indentation on the opposite surface. Examination of the metal after stripping the oxide revealed that severe plastic deformation had occurred, resulting in a groove in the metal along the crack length, and the indentation was due to necking of the sheet along the crack. Similar grooves developed in thicker sheet, but the deformation did not extend to the other surface. A finite element analysis showed that occurrence of a crack in the coating by thermal loading induced a very large tensile stress in the substrate under the crack, exceeding the nominal yield strength of the alloy (4). Substrate yielding is the origin of the groove.

Table 2. Thermal Cycle Tests
0.5 and 1 mil coatings with 5 or 20 min seal

Test	T_{max}	T_{min}	Humidity	Cycles			cracks per 3 coupons
				total	N_i		
	(°C)	(°C)	(ppm)		0.5mil	1.0mil	
1	70	25	ambient	2300	>2300		0
2	70	25	175	1900	1600	1200	2 - 14
3	70	-40	50	4800	1000	1200	12 - 21
4	70	25	80	4300	1400	300	10 - 24
5	80	25	50	6100	300	<100	32 - 44

Grooves were found under all cracks that were examined, and were about the same width as the crack in the oxide. In addition, a zone of plastic deformation extended for a considerable distance on either side of the groove.

E. Metallurgical Factors

1. Temper - Metal temper affects crack width and density. Whole hard 20 mil 5657 sheet was annealed at several conditions and then anodized. Subsequent heating at 175°C for 20min produced the following crack characteristics:

anneal	approx temper	cracks/coupon	crack width
none	H19	4	2-5 μm
260°C/6 hr	H25	9	1
288°C/6 hr	H24 (est.)	15	<1

The inverse relation between width and density of cracks suggests that total energy release during cracking may be independent of temper, but the distribution of the energy release over the surface depends upon metal yield strength - the lower the yield strength, the more evenly distributed the release.

2. Alloy - Table 3 lists commercial alloys that have been examined during this study and their T_c values. Allowing for the approximate nature of T_c, there is still a real difference among alloys with regard to cracking tendency. The failure of brittle materials, such as oxides, is presumed to initiate at defects. For the anodic oxide coatings it was thought that the precipitate particles from the metal that are incorporated into the oxide would serve as the defects to trigger fracture. However, one of the lowest T_c values was obtained with 4N metal, which has no significant density of precipitate particles. Particles are found in the coating on 5657 alloy at a density of about 2×10^5 cm^{-2} and are mostly 0.4-5 μm in size, with a few particles as large as 25-100 μm. With 1100 alloy, which has a higher density of particles, no cracks were produced up to 200°C. At this temperature the stress in 0.5 mil oxide is greater than 65 ksi. Further study of this puzzling behavior is in progress.

Table 3. T_c of Commercial Alloy Sheet
0.5 mil/5 (and 20) min coating

Alloy	Temper	Thickness (mil)	Test Sets (3 coupons per set)	T_c (°C)
5657	H242	25	9	132
5657	H25	25	1	130
5657	H25	20	1	130
3002	H25	25	1	175
3002	H18	12	4	171
6061	T6	20	1	> 200
1100		10	1	> 200
1199	H19	20	4	115

IV. CONCLUSIONS

1. Coating stress is tensile after anodizing and compressive after sealing.
2. Coating stress responds to a large decrease in humidity by shifting from compressive (humid) to tensile (dry). This is the major determinant of coating stress in dry environment, rather than the coating process conditions.
3. The response of stress to humidity is reversible.
4. The response of stress to a temperature increase is different at low and high humidities. At low humidity, the slope $\Delta\sigma/\Delta T$ is about half its value at ambient humidity.
5. During stepwise heating of coatings on 25 mil 5657 sheet, cracks initiate at a stress as low as 26 ksi for 1 mil oxide and 35 ksi for 0.5 mil oxide.
6. With some alloys, cracks did not occur at temperatures corresponding to stresses greater than 65 ksi (>200°C). Reasons for this high crack resistance are being sought.
7. Long term storage at ambient or higher humidity degrades the oxide so that it cracks more easily upon heating. Dry storage at moderate temperature prevents this degradation.
8. Anodized coatings exhibit cyclic fatigue under thermal cycling in dry atmosphere at relatively modest temperatures. Crack generation is dependent on T_{max} but not on T_{min}.
9. The formation of oxide cracks by heating is accompanied by plastic deformation of the substrate to produce a groove in the metal along the crack line.

Acknowledgements

This work was sponsored by the NASA Lyndon B. Johnson Space Center through the Small Business Innovative Research Program under contracts NAS 9-18087 and NAS 9-18350. The close cooperation of S. Jacobs of NASA, as well as the assistance of F. Maritato, S. Stillwell, and J. Xu of BTI, and J. Dzuik of SwRI in obtaining the experimental results reported here is gratefully acknowledged, as is the assistance of C. Kuhlman of SwRI with the mechanics analyses.

References

1. J.A. Dever, E. Rodriguez, W.S. Slemp, and J.E. Stoyack, "Evaluation of Thermal Control Coatings for Use on Solar Dynamic Radiators in Low Earth Orbit", NASA Tech. Memo. 104335, AIAA paper 91-1327 (1991).

2. S. Jacobs and D.R. Duffy, "Long-Life/Durable Radiator Coatings for Space Station", Soc. Automotive Eng. Tech. Paper 881067 (1988).

3. R.S. Alwitt, R.C. McClung, and S. Jacobs, "Anodized Aluminum Coatings for Thermal Control, Part I: "Coating Process and Stresses", Proc. AIAA Materials Specialist Conf., "Coatings Technologies for Aerospace Systems", Dallas (1992).

4. R.C. McClung, R.S.Alwitt, and S. Jacobs, "Anodized Aluminum Coatings for Thermal Control, Part II: Environmental Effects and Cracking", Proc. AIAA Materials Specialist Conf., "Coatings Technologies for Aerospace Systems", Dallas (1992).

Recycling chemicals on the anodizing line - cost savings and quality improvements

by
Kevin Munns, P.Eng.
Marketing Manager - Eco-Tec Inc.

1.0 Abstract

Aluminum is anodized with simple water-based chemicals that can be treated easily. However, many plants now use recycling equipment to extend chemical life and reduce waste treatment costs. Etching and anodizing solutions are the ones most frequently recycled but technologies are available for other finishing solutions as well. As most recycling approaches involve some degree of purification, anodizers often find that quality improvements go hand in hand with chemical savings. This paper will discuss the technologies available to anodizers and some recent developments that have helped to enhance the anodized surface finish.

2.0 Introduction

Anodizing processes use simple water-based chemicals that can be treated easily. While most municipalities require that the waters leaving the plant be adjusted to the correct pH (acidity/alkalinity) range, many now also specify removal of the suspended aluminum solids. After pH adjustment, the solids can be filtered out of the water and disposed of in a landfill as a non-hazardous waste. Some anodizers have been able to send this solid waste to companies that convert it into aluminum sulfate liquid or alum. Alum can be used by municipal waste treatment plants for phosphate removal.

Although anodizing wastes are simple to treat, many plants use recycling equipment to produce valuable byproducts. Two recycling techniques that are commonly used regenerate the etch and purify the anodizing acid. This is due, in part, to the large amount of solid waste (aluminum hydroxide sludge) that

etching and anodizing generates (Table 1). Recycling reduces this waste, cuts chemical costs and, frequently, improves product quality.

Table 1 - Solid waste from an Etch/Anodize operation

Basis: 1000 ft^2 ($93m^2$) of anodized surface area

Aluminum dissolved in etching (1.5 mil etch per side)	20.3 lb (9.2 kg)
Aluminum dissolved in anodizing (0.7 mil anodic film)	2.1 lb (0.93 kg)
Waste sludge produced (15% w/w solids)	431 lb (196 kg)
Waste sludge produced when etch regeneration is used	64 lb (29 kg)
Waste reduction with etch regeneration	85%

Note: 1000 ft^2 of extrusions will typically weigh about 400 lb. Therefore, without regeneration, a pound of waste sludge is generated for every pound of extrusion. Also, calculations do not apply for hollow extrusions which generate more waste due to the etching of the inner surfaces.

3.0 The technology behind recycling systems

Many recycling technologies can be grouped as being:

- concentration based or,
- separations based

For example, coloring bath chemicals are rinsed from anodized parts with water. The dilute waste that results contains metal salts from the coloring solution. A recycling system here might work by concentrating the rinse water until the volume was small enough to allow it to be added back to the coloring tank. This would be a concentration based process.

In contrast, anodizing solution gradually becomes contaminated with dissolved aluminum as it is used. A system that removes the aluminum would be an example of a separations based technology.

3.1 Concentration based processes

The simplest recycling systems often use concentration based processes. A common pitfall with simple systems is the failure to consider contaminant buildup. Better designs include a purification unit with the concentrating equipment. This ensures that recycled chemicals will not degrade the process solution. Concentration based technologies include:

Evaporation

In order to maintain a water balance in the system (prevent overflowing), it is often necessary to concentrate the purified/recovered chemicals. The most common method used for this purpose is evaporation, which can employ either boiling or non-boiling techniques.

The best known application of the non-boiling technique is the "atmospheric evaporator" which employs the humidification principle. See Figure 1. Liquid is pumped through a heat exchanger into the tower where it drips down through the packing (plastic rings provide a high surface area). A draft of air is drawn up through the tower evaporating the water. Continued circulation of the liquid increases its concentration to the desired level. The design is very simple, inexpensive and ideally suited to smaller applications where the final concentration of the liquid is not too high. The only disadvantage of this simple design is that the energy requirements are 10-20% higher than with boiling evaporators since both air and liquid phases must be heated.

Natural and forced circulation boiling evaporator designs employed in the chemical process industries are also very effective, particularly for higher solution concentrations and capacities. They are somewhat more complex and considerably more expensive than the "atmospheric evaporator" discussed above. These units are often operated under vacuum to reduce the boiling point of the solution and improve heat transfer.

Evaporative recovery systems have been extensively applied in the metal plating industry for some time. Packaged evaporators, both boiling and non-boiling types, are available from a number of vendors.

Reverse Osmosis (RO)

Reverse osmosis uses high pressure to force pure water through a semi-permeable plastic film or *membrane*. Rejecting the dissolved salts, RO produces a concentrated metal salt reject stream (see Figure 2). The membranes are susceptible to fouling and degradation so proper pretreatment of solutions is critical to success. The major operating costs for RO are membrane replacement and energy.

While RO systems have been used to recover nickel from electroplating rinsewater with various degrees of success, they have not been used to a significant degree in the North American anodizing industry.

3.3 Separation based systems

Separations technology can be used in conjunction with a concentrating system (to recover a pure bath chemicals from a rinse, for example) or on its own (to purify a process bath).

Acid Sorption

Certain ion exchange resins (fine plastic beads that have chemically active sites attached to them) have the ability to absorb strong acids (sulfuric, hydrochloric and nitric acid) while rejecting metal salts of these acids. See Figure 3. Water is used to recover the acid from the resin. Recovered solutions contain most of the unused or *free* acid with up to

90% of the metals removed. The most unique feature of the sorption process is that no chemicals or significant amount of energy are required.

The acid sorption process has been packaged into a standard, skid-mounted piece of equipment called an acid purification unit (APU®). APUs have been used to purify acid based process baths and used in conjunction with other purification and concentrating equipment as part of more complex systems.

Diffusion Dialysis (DD)

Diffusion dialysis is similar to acid sorption except an anion exchange membrane is used instead of sorption resin. The ion exchange membrane is permeable to acids but impermeable to metal salts (see Fig. 4). Contaminated acid flows past one side of the membrane, while water flows past the other side. The acid passes through the membrane into the water stream, while the metal salt impurities stay behind. As with acid sorption, no chemicals are required in the separation and energy requirements for solution pumping are small.

A multitude of these membranes are alternately stacked with gaskets and held together in a unit that resembles a filter press. Pretreatment for removal of suspended solids is very important for this process since the space between the membranes is very small and dirt tends to stick to the membranes.

The diffusion dialysis process has not been utilized to a large extent in North America, although it has been used in Japan for some time.

Crystallization

Crystallization processes depend on variations in the solubility of metal salts. Temperature and composition can often be adjusted to cause an metal salt to crystallize from a saturated solution. The salts can be filtered, washed and, often sold. As crystallization systems tend to costly, the number of applications where they are viable is limited.

3.3 Other processes

Some technologies span both the concentration and separations categories:

Ion Exchange (IX)

Ion exchange resins can replace cations (positively charged ions such as aluminum, sodium and most metals) with hydrogen (H^+) or anions (such as sulfate and chloride) with hydroxyl (OH^-). In a water deionizer, an anion exchanger would follow a cation exchanger and the cumulative exchange would yield pure water (H_2O). Cation exchangers are regenerated with sulfuric (or hydrochloric acid) while sodium hydroxide is normally used to regenerate an anion exchanger.

While the most common use of ion exchange is water deionization, a more attractive application in the metal finishing industry is the recovery or purification of finishing solutions. A special form of ion exchange (reciprocating flow), readily identified by its short resin columns, is particularly well suited for chemical recovery applications.

Electrodialysis (ED)

In the ED process, electricity is used to drive ions across ion exchange membranes. A combination of cation and anion exchange membranes can be used to deionize a solution, and recover a concentrate (see Fig. 5). Solutions containing low levels of metals (such as rinsewaters) can be concentrated to allow metal salt recycle. The process is better suited than RO to applications where a high degree of concentration is required.

The major industrial applications of electrodialysis in the U.S. to date have been in the field of water purification.

4.0 Recycling anodizing solutions

Aluminum anodizing is normally done by immersing parts in sulfuric acid and applying current, however, there are a number of other important steps involved. Many of these processes present recycling opportunities.

4.1 The Cleaner:

Before any finishing can be done, grease, fingerprints and other soils must be removed. Alkaline and/or acid cleaners are used.

Cleaning chemicals are discarded periodically as dirt and oils accumulate and cleaning power is lost. Filtration systems have been developed for recycling cleaners based on a technology called ultrafiltration (similar to reverse osmosis), however, they tend to be costly and may well be better suited to large operations such as steel mills. Cleaners normally require neutralization prior to discharge and, where strong alkaline cleaning leads to aluminum dissolution, removal of suspended aluminum hydroxide solids.

4.2 The Etch

Extruded parts show die lines and minor surface imperfections which must be removed in the etch tank. A hot solution of sodium hydroxide (a common ingredient in many cleaners - including household products) removes a thin layer of aluminum and creates an appealing matte surface finish.

Etching is caused by a reaction between the aluminum and caustic soda that produces sodium aluminate and hydrogen gas as follows:

<u>etching reaction</u>

$2Al + 2NaOH \text{ ----> } 2NaAlO_2 + 3H_2\,(gas)$

The etching process is responsible for 80-90% of the aluminum in the waste treatment system, however, etch solutions rarely need to be dumped. Traditionally, chemical stabilizers (complexing agents) are added to prevent the aluminum from crystallizing out in the etch tank. The additives thicken up the solution to the point where enough liquid is carried out on the parts to keep the aluminum level from building up in this "never dump" etch. Water is used to rinse the etching solution off the parts. The rinsewater carries dissolved aluminum and caustic to the plant's waste treatment system.

If stabilizers are not used and the sodium aluminate concentration is allowed to rise too high, it will hydrolyze according to equation (2) to produce alumina tri-hydrate ($Al_2O_3 \cdot 3H_2O$), liberating free caustic soda.

hydrolysis reaction

$2\ NaAlO_2 + 4H_2O \text{ ---> } 2\ NaOH + Al_2O_3 \cdot 3H_2O$ (2)

This reaction, known as the Bayer process , is used in the primary aluminum industry to make alumina. While this converts the aluminate back to sodium hydroxide, it also leads to an accumulation of a rock-hard aluminum hydroxide scale in the etch tank. By seeding the etch solution with alumina crystals in a separate crystallizer tank, it is possible to regenerate the etch solution without having scale buildup.

The basic operation of a regeneration system is illustrated in Figure 6. Etch solution is recirculated continuously between the etch tank and the crystallizer. Hydrated alumina crystals form in the slurry section of the crystallizer and settle out in the clarification section. Regenerated etch solution, with reduced aluminum and increased free caustic levels, flows back to the etch bath directly from the top of the crystallizer. Alumina crystals are withdrawn periodically from the bottom of the crystallizer and dewatered in a centrifuge or filter press.

Over the past ten years many large architectural anodizers have installed regeneration systems based on this process. Regeneration can reduce a plant's solid waste by over 80% while lowering caustic chemical (and neutralization) costs by over 70%. The alumina crystals which are removed can be put to a variety of uses as an alumina substitute. Although these systems are relatively expensive to install, larger plants can recover their costs within two or three years.

One drawback to a regenerated etch relates to its lower aluminum levels. As high aluminum levels promote a more matte finish, there were initially some concerns that a regenerated etch would not yield a finish suitable for the North American market. With several systems now in operation, a regenerated etch is widely regarded to produce a finish that is slightly less matte than a "never-dump" finish but satisfactory for most applications. Recently, however, a new high performance etching process has been introduced that is compatible with regeneration systems. This process, known in North America as Euro-Etch, allows an anodizer to achieve a premium heavy matte finish while reducing etch time, chemical costs and waste generation.

4.3 Other Etching processes

Die cleaning

Extrusion dies are changed frequently and normally must be cleaned before they can be reused. Dies are soaked in hot caustic soda to dissolve the aluminum plug that remains in the die after it is removed from the extrusion press. Although die cleaning is normally done in a small tank found in the repair shop, it is often responsible for several thousand gallons of waste each month.

Neutralization with sulfuric acid is one treatment alternative, however, spent die cleaner can create up to twice its own volume in waste sludge. There are other problems as well. The graphite compound that is used to lubricate the aluminum ingot in the extrusion press leaves a deposit in the die that ends up in the die cleaner. These fine graphite solids, together with alloy smut, settle slowly and tend to clog filter press cloths. As a result, die cleaner is often hauled offsite for disposal.

A crystallization system similar to that used for caustic etching solutions has been modified for use in die shops. A flocculation / clarification / filtration process is used up front to remove the suspended solids. The chemistry is also modified to a high speed formulation often used in the aerospace industry for chemical milling of aluminum sheets. A small amount of water is added during flocculation to dilute the die cleaner. The dilution actually causes the solution to saturate, promoting the crystallization reaction. The extra water is not normally a problem, however, as the high temperature of the die cleaner leads to an adequate amount of natural surface evaporation.

Hydrochloric acid etching

Dilute hydrochloric and nitric acid solutions, often modified with various organic and/or inorganic acids, are used to electrochemically etch aluminum sheet. These baths become contaminated with dissolved aluminum and must be dumped frequently and treated.

Usually these baths are fairly dilute, making purification by cation exchange a practical choice. Cation exchange requires chemical regeneration, however, efficiency can be increased by using an APU to recover the used regenerant. In a new process, the units have been integrated together to improve efficiency and reduce cost. Several of these systems are now being used by manufacturers of lithographic plates to purify electrolytic etching (graining) baths. Typical results are summarized in Table 2. The aluminum chloride byproduct produced by these systems has been utilized by municipal sewage treatment plants for phosphate removal. This process has also been used with the hydrochloric acid based etchants used for aluminum capacitor foils.

Table 2: Recovery of lithoplate etchants - typical results

Stream	[Al]	[HCl]	[H_3BO_3]
	(g/L)	(g/L)	(g/L)
bath	4.7	7.0	10
byproduct	13.5	1.5	-

4.4 The Bright Dip

Concentrated phosphoric acid solutions, usually with additions of nitric acid, diammonium phosphate and copper, are used to chemically brighten aluminum parts. After brightening, the adhering solution must be rinsed off immediately with water. Due to the high acid concentrations (ie. 70-80% H_3PO_4) and viscosities of bright dip baths, carryout of bath solution on the parts is typically 3-4 times greater than from an anodizing tank. While aluminum contamination of the bath is rarely a problem, there is a substantial loss of bath chemicals.

Most plants collect the rinsewater as a 35% solution for resale as fertilizer. The seasonal and regional variations in demand for the rinsewater reduce the value to between 10-20% of the original chemical cost. The net cost for larger plants can easily reach several hundred thousand dollars per year.

The rinse can be reconcentrated to bath strength with a vacuum evaporator, however, a purification step must be employed to prevent aluminum buildup. A typical system layout is shown in Figure 7. The feed to the cation exchanger

unit or DCU is drawn from the first of a series of counterflowing rinse tanks at a concentration of 10-15% acid strength. Typically 90% of the aluminum is removed by the DCU before the solution flows to the evaporator for concentration to bath strength. The cation exchanger is regenerated with sulfuric acid and the waste, containing sulfuric acid and aluminum, is processed with an APU. Purified sulfuric acid is returned to the DCU for use in the next regeneration cycle.

The aluminum sulfate waste or byproduct produced by the system can be neutralized in the plant waste treatment system or concentrated by evaporation and sold as liquid alum. Typical results are given in Table 3.

Table 3: Typical Results Phosphoric Acid Bright Dip Recovery

Bath	H_3PO_4 (g/L)	Al (g/L)
Bright dip bath	1340	20-40
First (feed) rinse	150-200	3-6
Third (final) rinse	<10	<0.5
Evaporator product	1365	<5

By using the combination cation exchange/APU system the cost of operation is reduced to the point where recovery becomes economical for any plant consuming more than three truckloads per month of 80% acid. Several installations have been installed over the last ten years and, in all cases, acid recovery efficiencies in excess of 85% have been reported.

A number of plants are now using a proprietary bright dip chemistry that employs a high sulfuric acid content. The process offers a number of quality enhancements when compared to ordinary bright dips, however, until recently, recovery has not been possible. The sulfuric acid affects evaporator design due to boiling point elevation and higher corrosivity. The effect of the proprietary additives on the system and additive replenishment have been two other concerns.

Currently an evaporator design has been developed that is compatible with the higher sulfuric level. Work is also underway to evaluate and resolve issues related to the additive.

4.5 The Desmut Tank

Alloying metals such as copper, magnesium and zinc are not usually removed in the etch tank and leave a dark film on the etched parts. This "smut" must be removed with an acid wash. The actual amount of metal dissolved in the acid is quite low so it unusual for a bath to be dumped because of metallic contamination. Water from preceding tanks that is carried in to the desmut bath on the parts occasionally leads to dilution of the acid. Technically, an APU or small evaporator could be used in these cases. The desmut tank generally does not represent a significant waste management concern.

4.5 The Anodizing Tank

Anodizing tanks represent excellent opportunities for purification as the dissolved aluminum levels must be kept quite low. In addition to eliminating a waste problem, continuous purification can enhance the uniformity of the anodized film, making coloring easier.

Sulfuric Acid Anodizing

The anodize (oxide) film itself is produced by passing electricity through the aluminum parts while they are immersed in a cool sulfuric acid solution. Aluminum dissolves during the anodizing process and this causes the conductivity of the solution to decrease. To maintain a desired anodizing rate the voltage must be increased. The extra power generates heat causing the temperature of the solution to increase. A chiller is used to keep the solutions cool, however by the time the aluminum level in the acid reaches 15-20 grams per liter (g/L), further voltage adjustments are not usually practical and the solution must be discarded.

Other contaminants may also cause problems. Iron, copper and lead are all considered undesirable. Excess levels of chloride, nitrate and phosphate also create problems.

Maintaining low aluminum levels by continuous decanting leads to excessive chemical and treatment expense so that this is an ideal recycling opportunity. In addition, constant aluminum levels lead to a more uniform anodic film. This, in turn, helps to ensure color uniformity in subsequent coloring operations.

An APU (acid purification unit) based upon the acid sorption process can be used to continuously remove metallic impurities as well as phosphate from the anodizing bath. The aluminum level can be maintained consistently in a range (6-12 g/L) considered optimal for anodizing. A large number of these units have been installed around the world since the process was introduced in 1976. A typical APU designed for anodizing service is shown in Fig. 8.

The diffusion dialysis process has been utilized in Japan for the same purpose, although its application in North America and Europe has not been nearly so widespread. It is also possible to remove aluminum by crystallization as ammonium alum by adding ammonium sulphate and cooling, but this process has not been employed to any significant extent.

Chromic Acid Anodizing

Anodizing for military and aerospace applications is often done with chromic acid solutions containing about 30 g/L CrO_3. As with all anodizing processes, aluminum is continually dissolved from the film by action of the acid. This decreases the *free* chromic acid content of the bath. Aluminum dissolution may be countered by additions of fresh chromic acid but, once the aluminum level exceeds 12 g/L, the voltage required to work the bath becomes excessive and the corrosion resistance of the coating may suffer. At this point the bath needs to be either discarded or regenerated.

Trivalent chromium is a contaminant that is created by reduction of the hexavalent chromate at the cathode. Trivalent chromium must be controlled as it retards the dissolution of aluminum, essentially inhibiting the formation of an anodic film.

Cation exchange has been used for many years to remove aluminum and trivalent chromium contamination from chrome anodizing solutions. While the concentration of chromic acid in these baths is low enough to prevent severe resin oxidation, manufacturers often recommend macroporous type resins for this application because of their superior oxidation resistance.

Anodic oxidation of the trivalent chromium is also possible. This method has been used by chromium platers for some time. A separate electrolysis tank fitted with a high ratio (eg. 30:1) of lead anodes to iron or stainless steel cathodes will oxidize the trivalent chromium back to the hexavalent state. This process can be enhanced through use of a ceramic diaphragm that separates the anolyte (ie. the solution around the anode) from the catholyte, thereby suppressing further oxidation of chromium in the anodizing electrolyte.

The simple electrolysis process described above will not remove aluminum or other metals to any significant degree. In order to do this it is necessary to employ a cation exchange membrane in place of the ceramic pot. This will allow migration of aluminum cations from the anodizing solution, which form the anolyte, to the catholyte.

Dragout of chromic acid from the anodizing bath into rinses can pose a severe disposal problem. Ion exchange and evaporative recovery processes, originally developed for recovery of chromium plating rinse water, can be similarly applied in anodizing.

Like their plating counterparts, chrome anodizing baths are extremely sensitive to chloride and sulfate contamination. Chloride levels of 0.2 g/L (as NaCl) and sulfate levels of 0.5 g/L (as Na_2SO_4) are considered maximums. For this reason rinsing of sulfuric acid regenerants from the ion exchange resin bed is critical. Remaining sulfate impurities can be removed by precipitation with barium carbonate or barium hydroxide. Chloride impurities can be precipitated with silver oxide or anodically oxidized to chlorine.

Phosphoric Acid Anodizing

Since phosphoric is a much weaker acid than sulfuric acid, it is possible to remove aluminum from phosphoric acid anodizing baths containing about 30% H_3PO_4, by cation exchange. An APU can then be used to recover the excess sulfuric acid used to regenerate the decationizer. An evaporator may be necessary to remove water added to the bath when the phosphoric acid is rinsed from the ion exchanger.

Phosphoric acid anodizing solutions are extremely sensitive to sulfate contamination. A very small amount of sulfate contamination sometimes occurs, sometimes as a result of inadequate rinsing of the cation exchange resin after regeneration. The excess sulfate can be removed by precipitation with barium carbonate.

4.6 The Coloring Tank

Three types of coloring methods are commonly used with anodized materials:

Integral Coloring

This method uses a weak sulfuric acid anodizing solution containing an organic acid to simultaneously form and color the anodic film in bronze and black shades. These baths are more sensitive to dissolved aluminum than conventional (clear) anodizing baths and must be carefully monitored. Cation exchange has been used with integral color baths for many years to remove dissolved aluminum. When used in conjunction with an APU for regenerant recovery, the operating costs of the purification equipment are quite modest.

Electrolytically Deposited (Two-Step) Coloring

Two-step coloring is done after anodizing in a separate tank. Electrolytes are based on nickel, copper, cobalt or tin salts, and frequently contain a weak organic acid. With its low electrical usage, the two-step coloring process has become a popular alternative to integral color anodizing in recent years.

After coloring, the aluminum must be well rinsed before sealing. The coloring solution carried out of the bath on the surface of the parts (dragout) causes an create appreciable loss of metal salts.

Several ion exchange systems have been installed in cobalt based coloring operations with excellent success. Similar ion exchange technology has also been used for many years to recover copper and nickel sulfate from electroplating rinsewater. With tin based processes, the stannous tin tends to oxidize in the rinsewater to the insoluble stannic form and precipitating from the solution and limiting the amount of tin that can be recovered.

Metal recovery from coloring rinsewaters may also be a good application for electrodialysis and reverse osmosis.

Inorganic Dyeing

Various dyes have been developed for architectural applications and are also applied after the anodizing step. Increasingly, dyes are being used after two-step coloring (over-dye) to produce a wide variety of colors.

Coloring systems based on dyes frequently use a simple recovery method of returning rinsewater back to the dye tank to make up for evaporation and dragout losses.

4.7 Chromate Processes

Chromate is used in several aluminum finishing processes, including conversion coating and chrome anodizing. To avoid pollution hazards there has been a recent trend away from chrome based processes, even though these baths are often better understood. Ion exchange has been used for many years to recover/purify chromic acid from plating operations and has recently been applied to chrome anodizing with good results.

Conversion coatings are difficult to recover. Many formulations are proprietary and, while it may be technically possible to recover chromate from the rinsewaters, it can be impractical to re-formulate the bath. In addition, the

amount of chromium involved is usually small and may not warrant the care required to successfully recycle.

4.8 Sealing

This important process closes the tops of the holes in the oxide layer. Sealing ensures that the surface finish will be colorfast and resistant to staining and corrosion. Seals can be based on either hot water or chemicals. Most chemical seals are very dilute solutions that contain a small amounts of dissolved nickel. The low chemical loss from seal tanks does not represent a significant waste treatment problem or warrant recovery.

5.0 Conclusion

With the increased focus on the 3R (reduce, recycle, reuse) approach in all facets of business, anodizers can look to a host of opportunities in their plants that will:

- reduce process chemical costs,
- reduce waste treatment chemical and labor costs, and
- in many cases, enhance product quality.

Recycling is an environmentally pro-active step that demonstrates a responsible corporate image to your customers, employees and to the local authorities. It makes you feel good and it's not bad for the bottom line, either.

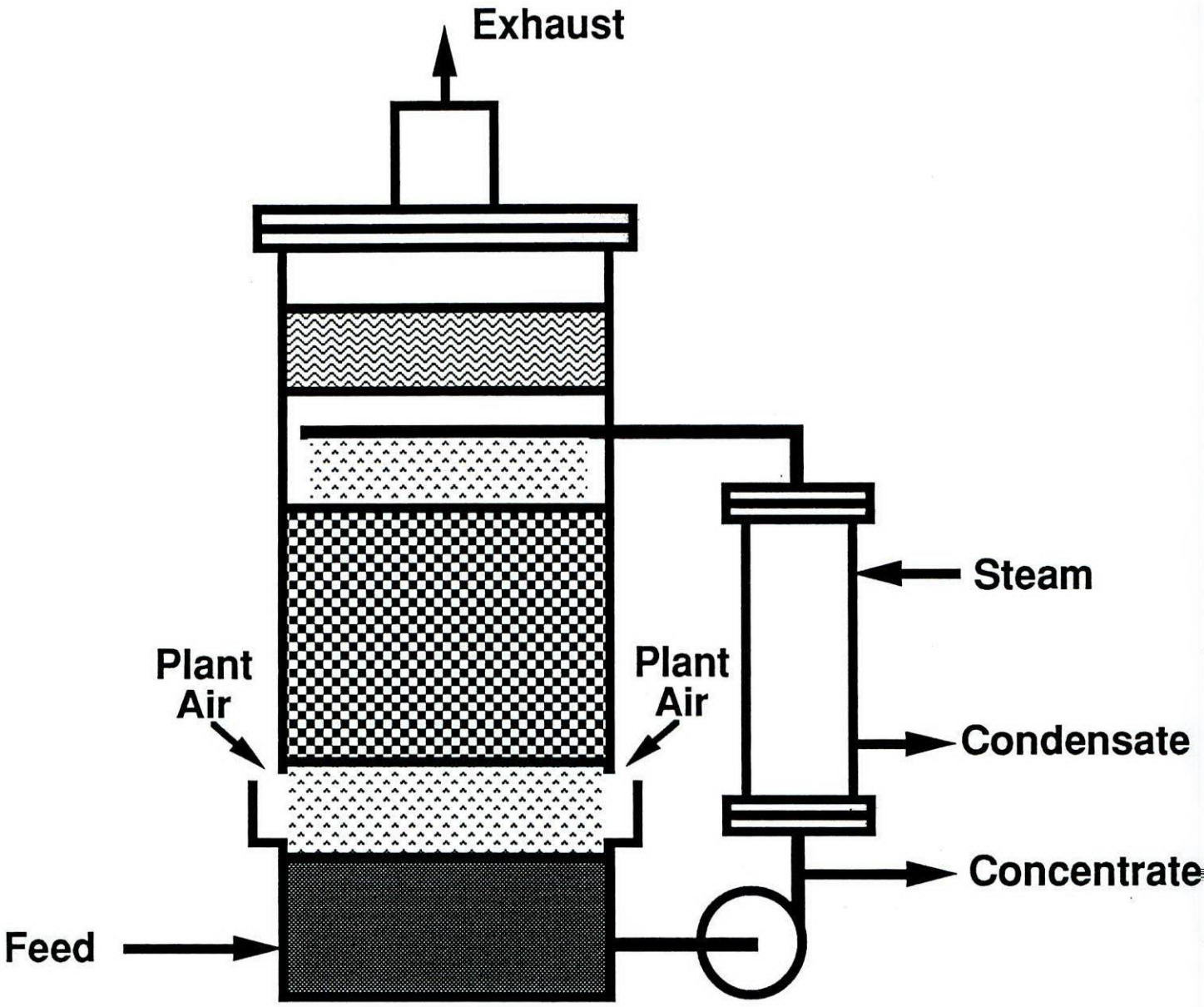

Fig. 1 - Atmospheric Evaporator

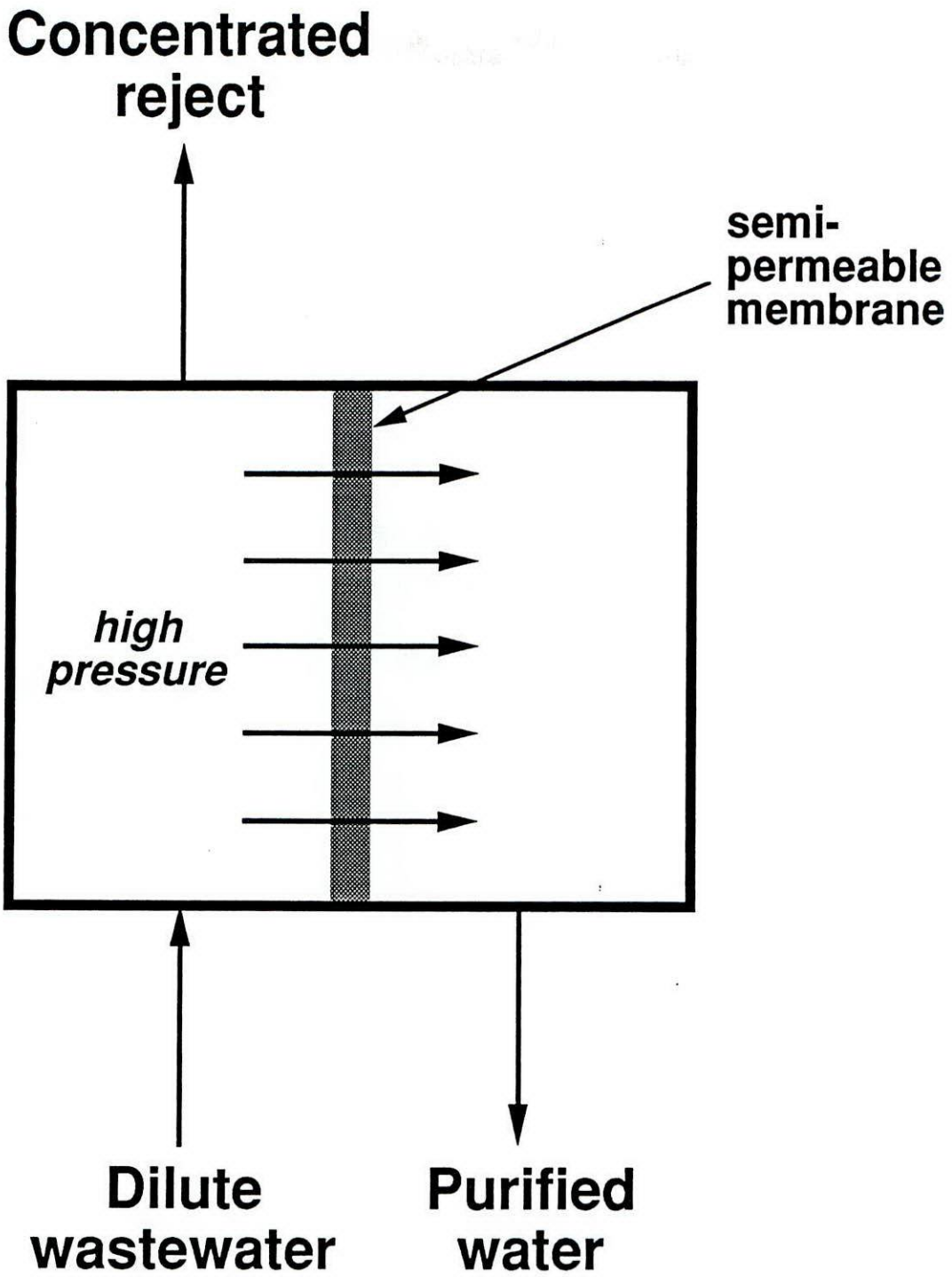

Fig. 2 - Reverse Osmosis

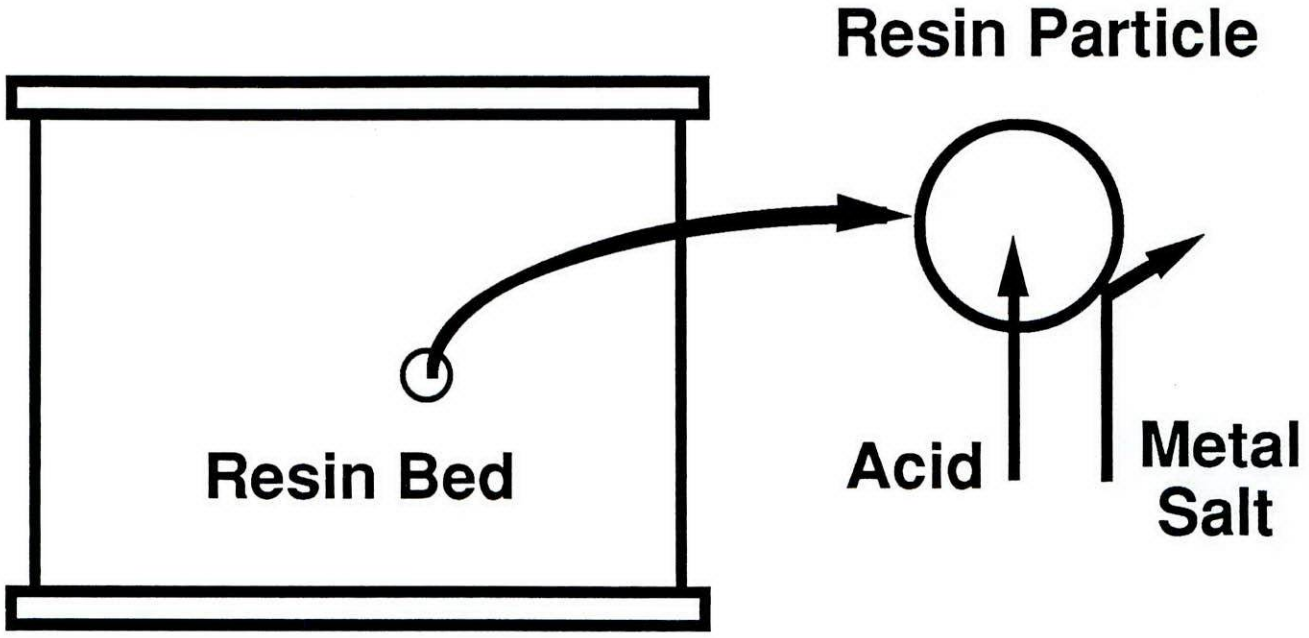

Fig. 3 - Acid Sorption Process

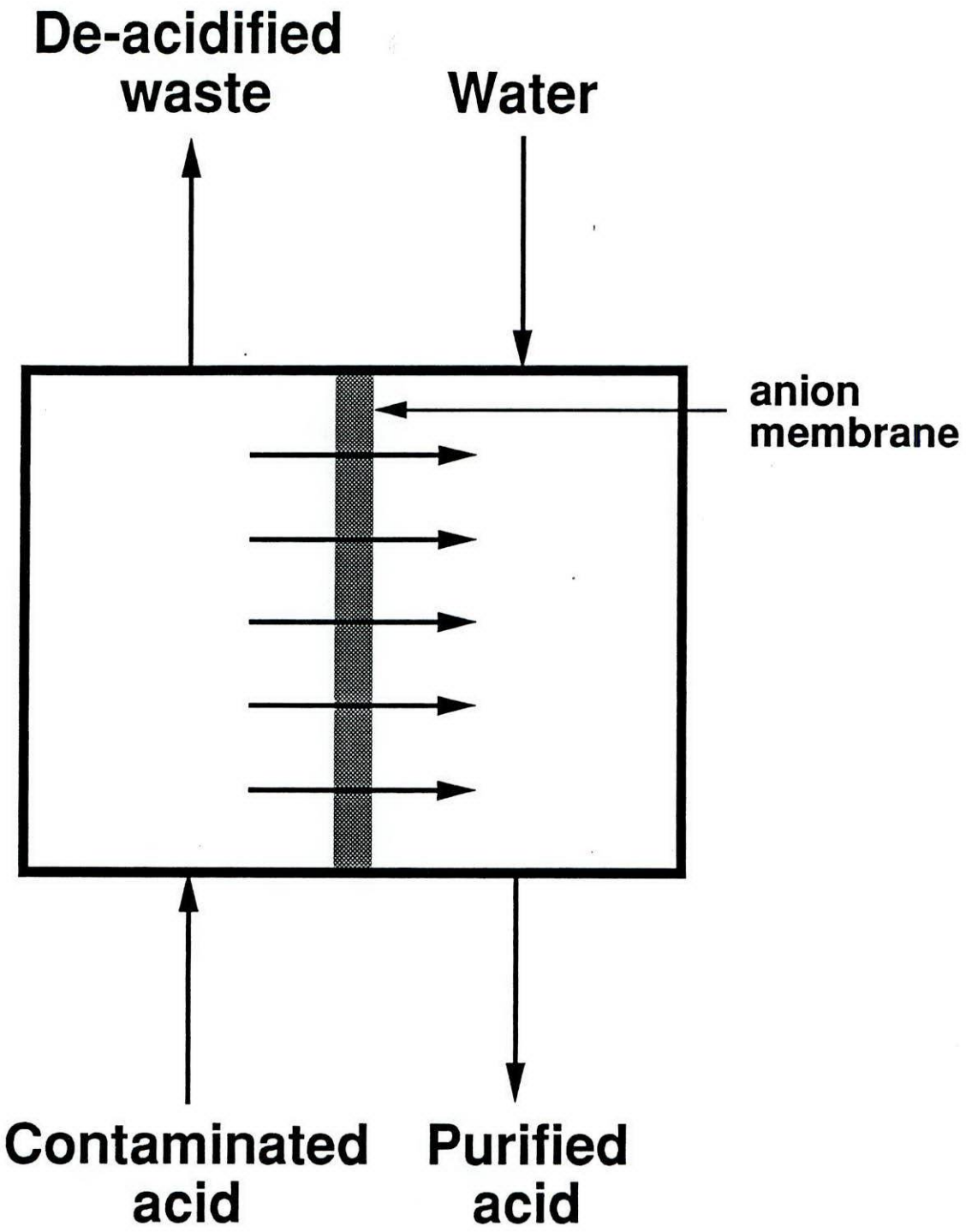

Fig. 4 - Diffusion Dialysis

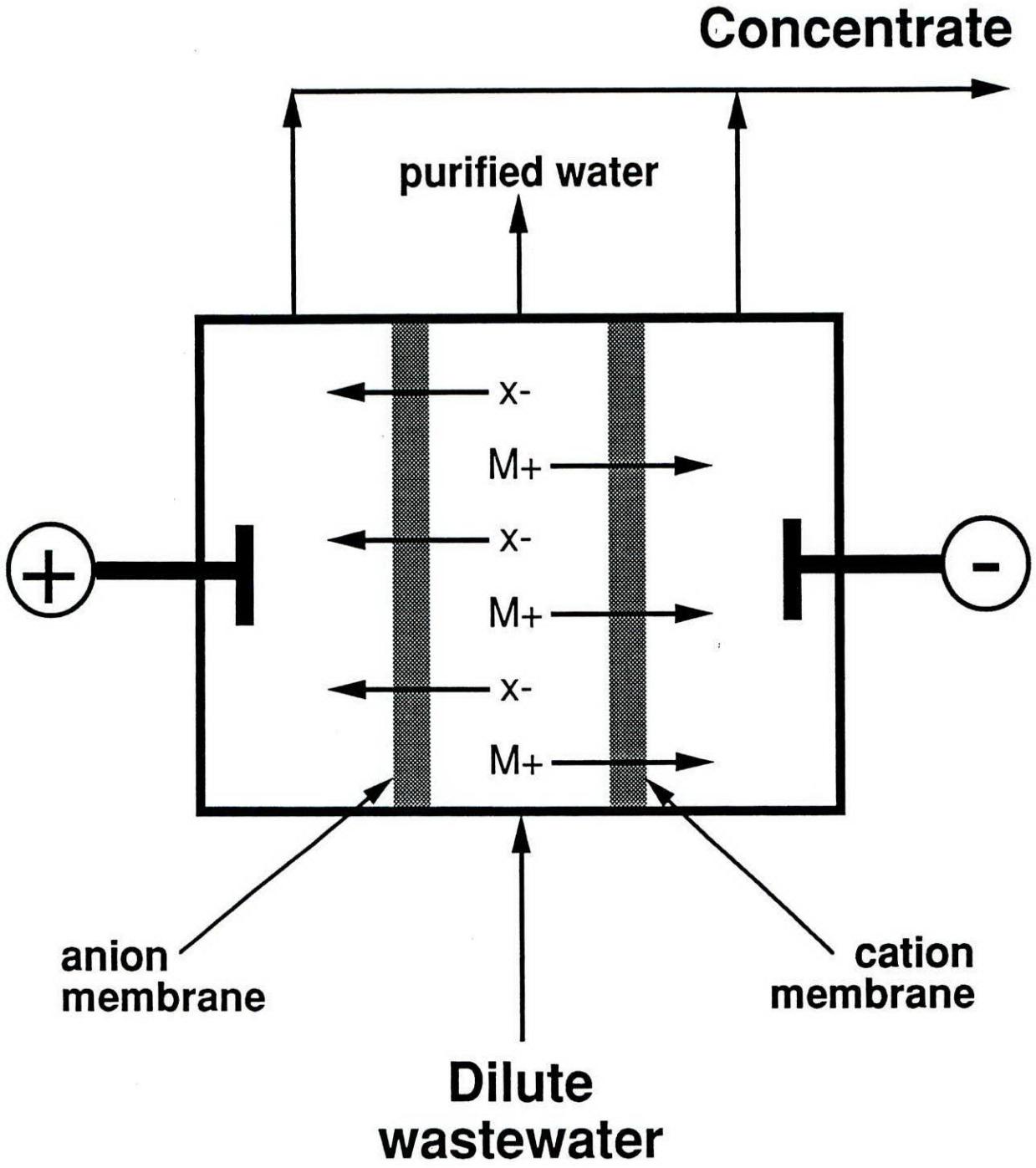

Fig. 5 - Electrodialysis

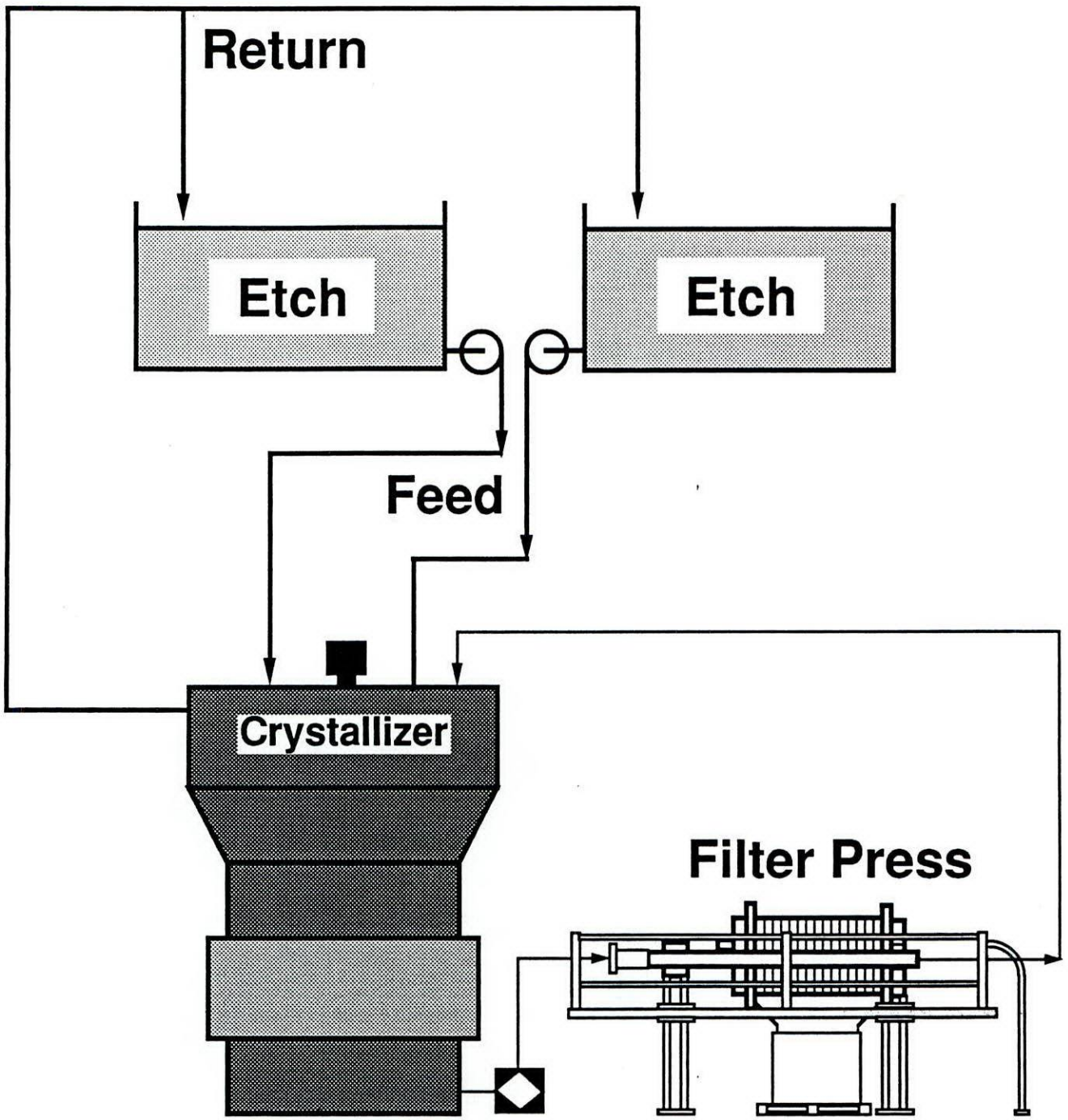

Fig. 6 - Caustic Etch Regeneration System

FIGURE 7 : ACID PURIFICATION

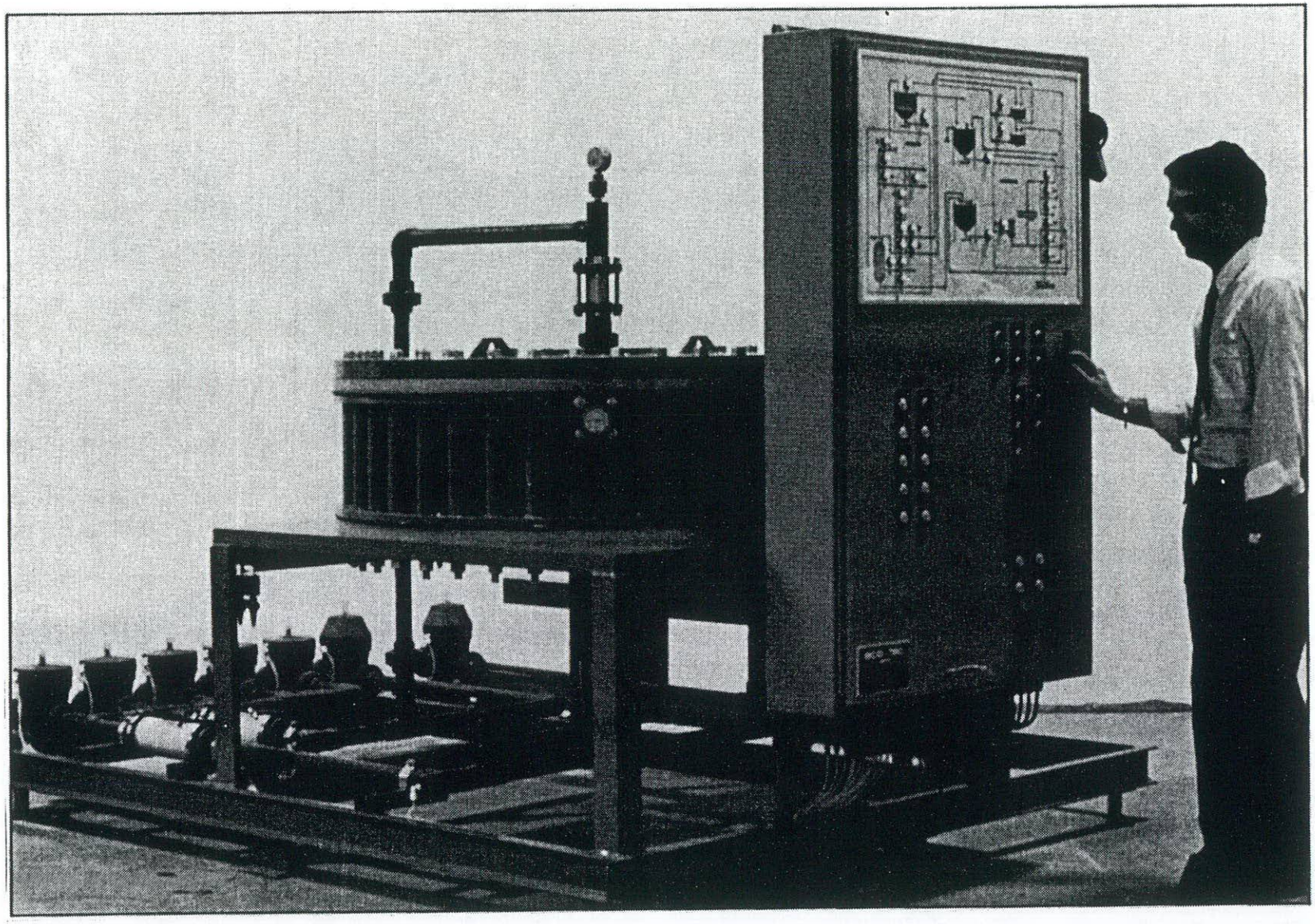

The fully automated Acid Purification Unit uses a unique sorption process to separate dissolved metallic salts from acid. Acid is continuously purified for improved process quality and consistency, at a lower cost. Commonly used for purifying anodizing, pickling and electroplating acids.

AN INTRODUCTION TO PHYSICAL VAPOR DEPOSITION (PVD) PROCESSES©

Donald M. Mattox

Consultant, IP Industries & Technical Director - SVC

For AESF SUR/FIN '92

ABSTRACT

Physical Vapor Deposition (PVD) processes are atomistic deposition processes in which material vaporized from a source is transported in the form of a vapor through a vacuum or low pressure gas environment to the substrate where it condenses and film growth takes place. PVD processes may be used to deposit films of compound materials by the reaction of depositing material with the ambient gas environment or with a co-deposited material. The three basic PVD techniques are: vacuum evaporation, which uses thermal evaporation as a source of depositing atoms, sputter deposition, which used physical sputtering as the source of depositing atoms, and ion plating which uses concurrent ion bombardment during deposition to modify the film growth.

© Donald M. Mattox 1992

INTRODUCTION

Physical Vapor Deposition (PVD) processes are atomistic deposition processes in which material vaporized from a source is transported in the form of a vapor through a vacuum or low pressure gas environment to the substrate where it condenses. PVD processes may be used to deposit films of compound materials by the reaction of depositing material with the ambient gas environment or with a co-deposited material. The three basic PVD techniques are: vacuum evaporation, which uses thermal evaporation as a source of depositing atoms, sputter deposition, which uses physical sputtering as the source of depositing atoms, and ion plating which uses concurrent ion bombardment during deposition to modify the film growth and properties. A fourth technique which can be considered to be a type of ion plating is Ion Beam Assisted Deposition (IBAD) which uses concurrent bombardment from an "ion gun" in vacuum to modify the film growth and properties. The various PVD techniques are shown in Figure 1. Typically, PVD processes are used to deposit films with thicknesses in the range of a few nanometers* to thousands of nanometers; however they can be used to form multilayer coatings, very thick deposits and freestanding structures.

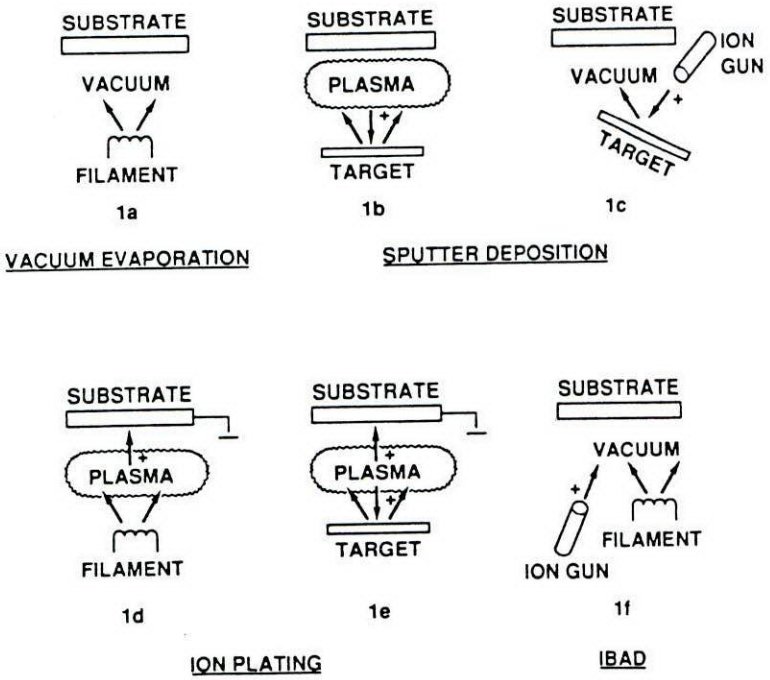

Figure 1: PVD processing techniques: 1a) vacuum evaporation, 1b) sputter deposition in a plasma environment, 1c) sputter deposition in a vacuum, 1d) ion plating in a plasma environment with a thermal evaporation source, 1e) ion plating in a plasma environment with a sputtering source and 1f) Ion Beam Assisted Deposition (IBAD) in a vacuum environment with a thermal evaporation source and ion bombardment from an ion gun.

* 1 nanometer (nm) = 10^{-9} meters = 10 Angstroms (A) = 10^{-3} microns = 0.04 microinches.

© Donald M. Mattox 1992

VACUUM EVAPORATION

Vacuum evaporation is a PVD process in which material from a thermal vaporization source reaches the substrate without collision in the gas phase (1). This means that there is no scattering during transport and the trajectory of the vaporized material is "line-of-sight". The vacuum environment also provides the ability to reduce gaseous contamination in the system to a very low level. Typically vacuum evaporation takes place in the pressure range of 10^{-5} Torr ** to 10^{-9} Torr depending on the level of gaseous contamination that can be tolerated. Figure 1a depicts a simple vacuum evaporation arrangement.

Evaporation and sublimation

The vapor pressure of materials is very dependent on the temperature. Materials that have a high vapor pressure over the solid, such as chromium, sublime. If the material must be molten before the vapor pressure is substantial the material evaporates. Materials that have a high vapor pressure at a relatively low temperature may be vaporized from a resistively heated source such as a filament or boat. For more refractory materials, the material is vaporized using a focused electron beam source. In either case the area of vaporization is rather small resembling approximating a "point source". When vaporizing large amounts of material the source may be replenished using wire or pellet feeds to keep the level of the evaporant constant.

In most cases evaporation of alloys of materials results in a change in composition since the alloying materials usually have differing vapor pressures and thus evaporate at differing rates. In some cases the alloy composition can be retained using "flash evaporation" techniques where small amounts of material are completely evaporated. In the case of evaporation of compounds the composition of the deposited material often differs from that of the starting material because of decomposition and loss of a portion of the more gaseous material i.e. oxygen from an oxide. Thus substoichiometric oxides are normally deposited by vacuum evaporation.

Other vaporization sources

In addition to evaporation and sublimation, other specialized vaporization techniques may be used in a vacuum. Arc vaporization is used to vaporize electrically conductive materials in a high-current low-voltage electric arc. This technique produces high vaporization rates with a high percentage of the atomic vapor being ionized. These ions are accelerated away from the arc and achieve a kinetic energy much higher than thermal energy. In the arc vaporization process molten globules are formed which deposit along with the atomic species. These globules are often detrimental to the properties of the deposit and various techniques are used to try to eliminate them. Laser vaporization (laser ablation) is used to vaporize compound materials and has found particular application in the deposition of high quality high transition temperature (high T_c) superconductor oxides.

Thickness and surface coverage

Since the thermal evaporation is from a point source and the flux has a cosine distribution around the normal to the surface the distribution of the deposited material is determined by

** Atmospheric pressure = 760 Torr. 1 Torr (mm mercury) = 10^3 milliTorr (mTorr). 1 mTorr = 7.5 Pascals (Pa) = 1 micron

© Donald M. Mattox 1992

the source-substrate distance, the angle of the substrate-source trajectory with the surface normal, and the angle of the substrate normal with the depositing flux. In order to increase the deposition uniformity the substrate is generally held in a moving fixture that randomizes the position and orientation of the substrate relative to the source during deposition. Another approach is to use multiple sources to produce an apparent large area evaporation source, although this approach makes thickness uniformity control more difficult.

The ability of vacuum evaporation to cover a surface depends on the surface topography. If the surface is smooth surface coverage will be good. However if the surface is not smooth, geometrical shadowing will prevent good surface coverage. Surface coverage can be improved by randomizing the deposition direction using fixturing that is moveable.

Advantages and disadvantages of vacuum evaporation

Some advantages of vacuum evaporation are:

- high purity materials can be deposited from high purity source material
- source of material to be deposited may be a solid in any form and purity
- line-of-sight trajectories and "point sources" allow the use of masks to define areas of deposition
- deposition monitoring and control are relatively easy

Some disadvantages of vacuum evaporation are:

- many alloy compositions and compounds can only be deposited with difficulty
- line-of-sight and point sources result in poor surface coverage on complex surfaces
- line-of-sight trajectories and point sources result in poor film thickness uniformity over large areas
- film properties depend on the "angle-of-incidence" of the flux of the depositing material
- fixturing with movement capability is necessary to improve surface coverage and thickness uniformity
- few processing variables are available for film property control
- substrate preparation is important to resulting film properties
- source material utilization may be poor
- high radiant heat loads may exist in the system
- the liquid source material may move thus changing the source configuration

Some applications of vacuum evaporation

Vacuum evaporation is widely used to form optical interference coatings, mirror coatings, decorative coatings, permeation barrier films on flexible packaging materials, electrically conducting films, and corrosion protective coatings.

SPUTTER DEPOSITION

Sputter deposition is the deposition of particles vaporized from a surface by the physical sputtering process (2). This PVD process is sometimes called just sputtering i.e. "sputtered films of --". Figure 1b and 1c show sputter deposition configurations.

Physical sputtering

Physical sputtering is a non-thermal vaporization process where surface atoms of a solid sputtering "target" are physically ejected by momentum transfer from an massive energetic

© Donald M. Mattox 1992

bombarding particle. Usually the energetic particle is an ion accelerated from a gaseous plasma. Electrically conducting materials may be sputtered in a direct current (DC) diode plasma configuration. Dielectric materials must be sputtered using a radio frequency (rf) sustained plasma. In the magnetron sputtering configuration a magnetic field is utilized to contain the plasma-generating electrons and produce a high plasma density near the target surface thereby increasing the sputtering rate. There are many sputtering configurations and often the sputter erosion pattern from the target is non-uniform requiring movable fixturing to obtain a uniform deposition over a substrate surface.

Sputter deposition may be performed in a vacuum using an ion gun or in a low pressure (<5 mTorr) plasma where the sputtered particles and reflected high energy neutral particles do not suffer gas phase collisions between the target and the substrate. Sputtering may also be performed in a higher pressure (5-30 mTorr) where energetic particles from the sputtering target are thermalized by gas phase collisions before they reach the substrate surface. The properties of the sputter deposited films depend strongly on the sputtering conditions.

Sputtering targets

The sputtering target is a solid surface and sputtering can be attained over a large area of a surface. Solid targets provide a long-lived vaporization source with rather constant and reproducible vaporization rates. Fabrication of large-area sputtering targets is often costly and the material utilization of the target is poor.

Reactive sputter deposition

By using a reactive gas in the plasma,the deposited material may be made to react to form a compound material. The reaction is promoted by "plasma activation" of the reactive species.

Advantages and disadvantages of sputter deposition

Some advantages of sputter deposition are:

- elements, alloys and compounds may be sputtered and deposited
- the sputtering target provides a stable, long-lived vaporization source
- the solid sputtering target may be mounted in any orientation
- in some configurations the sputtering target provides a large-area vaporization source that can be of any shape
- in some configurations the sputtering source may be a defined shape such as a line or a rod
- in some configurations reactive deposition may be easily accomplished because the reactive species are "activated" in a plasma (i.e. "reactive sputter deposition")

Some disadvantages of sputter deposition are:

- sputtering rates are low compared to those that can be attained in thermal evaporation
- in many configurations the deposition flux distribution is non-uniform requiring fixturing to randomize the position of the substrates in order to obtain films of uniform thickness
- film properties depend on the "angle-of-incidence" of the flux of depositing material
- sputtering targets are often expensive and material utilization may be poor
- most of the energy incident on the sputtering target turns into heat which must be removed

© Donald M. Mattox 1992

- in some configurations gaseous contamination is not easily removed from the system and gaseous contaminants are "activated" in the plasma thus making film contamination more of a problem than in vacuum evaporation
- in some configurations radiation and energetic particle bombardment from the plasma or sputtering target may change the film properties in an uncontrolled manner

Some applications of sputter deposition
Sputter deposition is widely used to deposit thin film metallization on semiconductor material, coatings on architectural glass, reflective coatings on compact discs, magnetic films, dry film lubricants and decorative coatings.

ION PLATING

Ion plating utilizes concurrent or periodic energetic particle bombardment of the depositing film to modify and control the composition and properties of the depositing film (3). Ion plating may be done in a plasma environment where ions for bombardment are extracted from the plasma or it may be done in a vacuum environment where ions for bombardment are formed in a separate "ion gun". The latter ion plating configuration is often called Ion Beam Assisted Deposition (IBAD) (4). Figure 1d and 1e show ion plating in a plasma environment. Figure 1f shows ion plating in a vacuum environment or IBAD.

Source of depositing species
The depositing material may be created either by evaporation, sputtering, or arc vaporization. The energetic particles used for bombardment are usually ions of inert or reactive gas, ions of the depositing material ("film ions") or ions of the reacting gaseous materials (e.g. oxygen or nitrogen).

Source of bias potential
Generally positive ions are accelerated to the depositing material due to a negative potential on the surface. This potential may be applied from an external source or be due to a "self-bias" on the surface. For electrical conductors such as metals, TiN, etc the applied potential may be DC. However if the film material is an insulator the applied potential must be rf in order to prevent a surface charge buildup which will cause the bombardment to cease. A self-bias can be caused to appear on the surface of a dielectric or electrically floating conductive surface by continuously bombarding the surface by high energy electrons.

Reactive ion plating
By using a reactive gas in the plasma the deposited material may be made to react to form a compound material. The reaction is promoted by "plasma activation" of the reactive species and the concurrent bombardment of the depositing material i.e. "bombardment enhanced chemical reaction". Materials such as TiN and SiO_2 are routinely deposited by reactive ion plating.

Film properties
The concurrent bombardment can be used to modify and control the properties of the depositing material. The most common film properties that are modified include: residual film stress, density of the deposited material and composition (stoichiometry) of deposited compound materials.

© Donald M. Mattox 1992

Surface coverage
Concurrent bombardment results in sputtering and redeposition of materials on surfaces that have a complex morphology. This effect, along with gas scattering at higher plasma pressures, can be used to give good surface coverage on complex surfaces such as ones having roughness or which have been patterned to form vias, metallization patterns, etc,

Other sources of concurrent bombardment
Concurrent bombardment of the depositing film can occur without a bias on the surface of the depositing material. For example, bombardment by the reflected high energy neutrals in low pressure sputter deposition and the ions accelerated away from the arc in vacuum arc evaporation can modify the film properties. Ion guns can be used to accelerate ions into a field-free deposition chamber.

Advantages and disadvantages of ion plating
Some advantages of ion plating are:

- in situ sputter cleaning of substrate surface
- surface coverage may be improved over vacuum evaporation and sputter deposition due to gas scattering and "sputtering/redeposition" effects
- bombardment may be used to modify film properties such as adhesion, density, residual film stress, optical properties, etc.
- film properties are less dependent on the "angle-of-incidence" of the flux of depositing material than with sputter deposition and vacuum evaporation due to gas scattering and "sputtering/redeposition" effects
- bombardment may be used to improve the chemical composition of the film material by "bombardment enhanced chemical reactions" and sputtering of un-reacted species from the growing film
- in some configurations the plasma may be used to activate reactive species, and create new chemical species that are more readily adsorbed and to aid in the reactive deposition process ("reactive ion plating")

Some disadvantages of ion plating are:

- there are many processing variables to control
- it is often difficult to obtain uniform ion bombardment over the substrate surface leading to film property variation over the surface
- substrate heating can be excessive
- under some conditions the bombarding gas may be incorporated into the growing film
- under some conditions excessive residual compressive film stress may be generated

Some applications of ion plating
Ion plating is used to deposit hard coatings on surfaces, adherent coatings on surfaces, optical coatings with high densities, and conformal coatings on complex surfaces.

SUMMARY

There are a variety of PVD techniques, each with many variations. Each of these deposition options has advantages and disadvantages. The choice of technique to be used to accomplish a specific coating task depends on a number of factors that must be evaluated for each situation.

© Donald M. Mattox 1992

REFERENCES

1. "Film Formation Methods" Chapter 6 in Coatings on Glass H.K. Pulker, Thin Film Science and Technology Series #6, Elsevier 1984
2. "Sputter Deposition Processes" Robert Parsons, Chapter II-4 in Thin Film Processes II, edited by John L. Vossen and Werner Kern, Academic Press 1991
3. "Ion Plating", Donald M. Mattox, Chapter 13, in Handbook of Plasma Processing Technology: Fundamentals, Etching, Deposition and Surface Interactions, edited by S.M. Rossnagel, J.J. Cuomo and W.D. Westwood, Noyes Publications, 1990
4. F.A. Smidt "Use of ion beam assisted deposition to modify the microstructure and properties of thin films" International Materials Reviews 35(2) 61, 1990

© Donald M. Mattox 1992

AN ELECTROPLATERS VIEW OF PVD PROCESSING

J. W. Dini

Lawrence Livermore National Laboratory

For AESF SUR/FIN 92

Atlanta, Georgia

June 1992

ABSTRACT

This paper provides a comparison of electroplating and PVD processing from the viewpoint of a person who has been involved with the electroplating industry for the past 42 years and PVD processing for the past 12 years. During this recent 12 year period he has served as a manager of groups involved with both electroplating and PVD operations so he has had the chance to closely observe both technologies. After a brief description of each of the coating processes, comparisons are provided with respect to coating choices, deposition rates, properties, adhesion, costs and waste minimization. In addition, examples are provided to demonstrate that by combining the deposition technologies synergism can often be obtained. The conclusion drawn from these comparisons is that both deposition technologies are viable processes and each has its own particular benefits/drawbacks.

*This work was performed under the auspices of the U. S. Dept. of Energy by LLNL under contract No. W-7405-Eng-48.

Introduction

Don Mattox, Technical Director of the Society of Vacuum Coaters, asked me to put this paper together for this session of AESF SUR/FIN 92. Don wanted a view from someone who has been involved with both electrodeposition and physical vapor deposition (PVD) technologies and he is well aware that I have worked both sides of the street on this issue. We can both remember the time when I firmly believed that the only worthwhile coating process was electroplating, while in recent years some folks have accused me of trying to phase out electroplating completely. Hopefully, this paper will show that I consider both processes to be quite viable and that both will continue to play important roles in the coating field.

By way of background I feel I should establish some credentials before embarking on the main body of the paper. I've been involved in the electroplating field since 1950, having spent the first nine years with a consulting firm (PAVCO, formerly Cleveland Supply Co.) that sold brighteners to the plating industry, and the remaining years with research and development laboratories including Republic Steel's Research Laboratory (1959-60), Battelle Columbus Laboratories (1960-62), Sandia Livermore Laboratory (1962-1980), and Lawrence Livermore National Laboratory (LLNL) (1980 to present). In 1980 with the move to LLNL, I assumed the responsibility for groups involved in both electrodeposition and physical vapor deposition processes. Therefore, since 1980 I have been very closely involved with both technologies from both a managerial and technical viewpoint, so I've had plenty of experience with both deposition technologies. I should also add that although most of my time has been spent with R & D laboratories, a number of projects that I've been involved with have been transferred to production, so my views are not just those of a research oriented person.

This review will be broken down into four sections:

1. A brief description of each coating process
2. Comparisons with respect to coating choices, deposition rates, properties, adhesion, costs, and waste minimization
3. Examples where the combined use of PVD and electroplating provided synergism
4. Summary

Description of Coating Processes

Electroplating and Electroless Plating

Electroplating is the deposition of a coating of a metal onto another metal or a non-metal by electrolysis. This is accomplished when metal ions are reduced to the metallic state and deposited as such at the cathode by use of electrical energy.

Electroless plating is a chemical reduction process which depends upon the catalytic reduction of a metallic ion in an aqueous solution containing a reducing agent, and the subsequent deposition of the metal without the use of electrical energy.

Physical Vapor Deposition

Physical vapor deposition (PVD) is a process whereby a material in bulk form is atomistically converted to a vapor phase in a vacuum and condensed on a substrate to form a deposit. PVD techniques fall into three broad categories: evaporation, sputtering, and augmented energy. In evaporation, vapors are produced from a material located in a source which is heated by radiation, eddy current, electron beam bombardment, etc. The process is usually carried out in a vacuum (typically 10^{-5} to 10^{-6} Torr) so that evaporated atoms undergo an essentially collision-less line of sight transport prior to condensation on the substrate which is usually at ground potential (not biased). Sputtering involves positive gas ions (usually argon) produced in a glow discharge which bombard the target material thereby dislodging groups of atoms or single atoms which then pass into the vapor phase and deposit on the substrate. Augmented energy techniques have been employed in more recent times to improve the energy of the deposition process. These include ion plating (D.M. Mattox, U.S. Patent 3,329,601 [1967]), thermionic plasma, and formation of plasmas using hollow cathode discharge sources. Ion plating is a generic term applied to atomistic deposition processes in which the substrate is subjected to a flux of high energy ions sufficient to cause appreciable sputtering before and during film deposition. The ion bombardment is usually done in an inert gas discharge system similar to that used in sputter deposition, except that in ion plating the substrate is made a sputtering cathode. The substrate is subjected to ion bombardment for a time sufficient to remove surface contaminates and barrier layers (sputter cleaning) before deposition of the film material. After the substrate surface is sputter cleaned, the film deposition is begun without interrupting the ion bombardment. Variations in the ion plating technique have given rise to terms such as vacuum ion plating, chemical ion plating, bias sputtering and others which refer to specific environment, sources or techniques.

Comparisons

In this section the deposition technologies will be compared with respect to: coating choices, deposition rates, properties, adhesion, costs and waste minimization.

A. Coating Choices

Electrodeposition and Electroless Plating

Thirty-one metals can be plated from aqueous solutions as alloyed metals (1) and these are shown in Figure 1. Of these, about 16 are commonly plated and these are highlighted in Figure 1. Molybdenum and tungsten can be deposited from aqueous solutions as alloys but not as pure metals. Alloy electrodeposition extends the availability and applicability of coatings from aqueous solutions and about 9 or so alloys have commercial importance (1).

Some metals have been deposited from non-aqueous solutions, the greatest success being obtained with aluminum which is being done commercially. Electrolysis of molten fluorides has been used for preparation of coherent deposits of zirconium, hafnium, niobium, tantalum, chromium, molybdenum and tungsten. Of these, successful production scale has been attained with tantalum, niobium, molybdenum and tungsten, although at present these aren't commercially available.

Many platers also have the capability of doing electroless plating. The metals which are commonly deposited by this process include nickel, copper, gold, palladium and silver. However, the most important of the electroless plating processes from the standpoint of commercial utilization are electroless nickel using sodium hypophosphite and copper using formaldehyde.

Physical Vapor Deposition

PVD offers a much wider choice of coatings and substrates than offered by electrodeposition. As an example, Figure 2 shows the metals that have been deposited in our facility at LLNL and it should be pointed out that other coatings are even possible. Comparison with Figure 1 clearly shows the superiority of PVD in providing a much wider range of coatings. Furthermore, an almost infinite range of alloys and optical coatings can be produced by PVD processes. Also, since the substrate does not have to be conductive as it does with electroplating, almost, any substrate material can be coated via PVD processing.

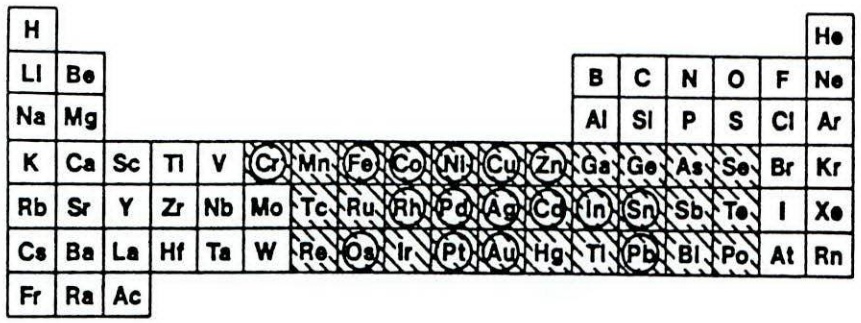

Figure 1: Periodic table showing metals which can be electrodeposited from aqueous solution. Diagonal lines show those metals which have been electrodeposited; circles are those most commonly used.

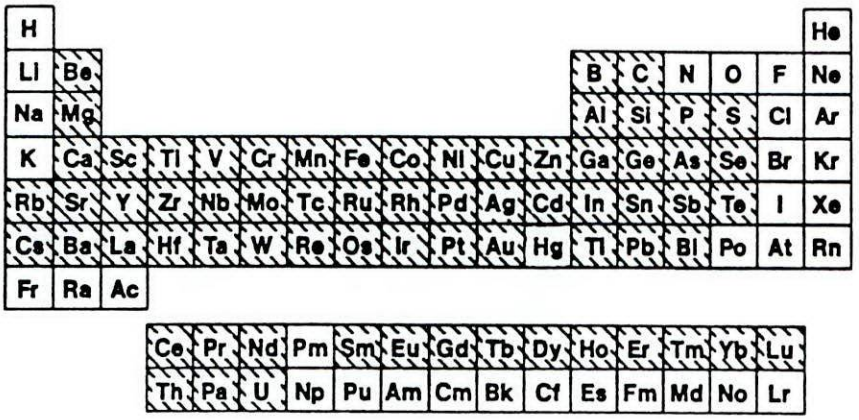

Figure 2: Periodic table showing those metals which have been deposited (diagonal lines) by PVD processes at LLNL.

B. Deposition Rates

Deposition rates for both electrodeposition and PVD processes overlap as shown in Table 1. This means that with specific PVD processes deposition rates can be as fast as those obtained with typical electrodeposition processes. However, very seldom are PVD processes used to produce thick coatings such as those used in electroforming, e.g., 10 mils (250 um), or greater. Most of the time, coating thickness for PVD films is expressed in Angstroms (Å) rather than the familiar term "mil" which is used by platers. For that matter it is my feeling that many platers don't even think in Angstroms (Å) since it is represents such a miniscule thickness. Table 2 provides some conversion factors for comparison purposes. Also, although deposition rates for the two technologies overlap, in many practical cases the deposition rates are faster for electroplating. Therefore, it can be quite difficult for a plater to deposit a coating of a few hundreds or thousands of Angstroms. For example, in the case of electrodeposition of nickel (assuming an efficiency of 95%), a thickness of 0.5 mil (12.5 um or 125,000 Å) is deposited in 23 minutes. This is a deposition rate of 5435 Angstroms/minute and means the plater has exactly 22 seconds to deposit a thickness of 2000 Å.

C. Properties

A wide variety of properties can be obtained with electrodeposits. This is done by using different plating solutions, by varying electrodeposition parameters, or by using additives. One good example is copper, which is deposited for numerous engineering and decorative applications. The range of properties obtainable for copper electrodeposits extends from strengths superior to full-hard wrought copper to properties equivalent to annealed pure copper. For data on the properties obtainable for various electrodeposits, the treatises by Safranek are recommended (2,3). The first edition (2) published in 1974 contains data reported from more than 1300 references while the second edition (3) published in 1986 contains information on 500 additional references.

Property data for PVD films are of a different nature since in most cases the films remain on their substrates and are not "free standing" as is the case with electrodeposits. For example, one can find a multitude of data on stress, hardness, and wear resistance of PVD films but virtually no data on tensile strength and ductility since the deposits are too thin for reliable measurement. Microhardness and scratch adhesion testing are the commonly used techniques for assessing the mechanical properties of thin PVD coatings (4). However, I am told by members of my PVD group at LLNL that property data for "free-standing" PVD films are being obtained and that as a function of time more data of this type will become available.

The structure of PVD films can be shown in three dimensional plots such as those developed by Movchan and Demchishin (Figure 3, Reference 5) and

Table 1

Typical Coating Conditions and Deposition Rates for Electroplating, Electroless, and PVD Processes

Deposition technique	Pressure (Torr)	Substrate temp. (C)	Deposition rate μ/min	mil/hr
Evaporation	10^{-7} to 10^{-5}	up to 250*	1.2-12	0.5-5
Sputtering	10^{-3} to 10^{-1}	up to 500*	0.012-24	0.005-10
Ion Plating	10^{-3} to 10^{-1}	up to 500*	1.2-12	0.5-5
Electroplating	ambient	10 to 100	0.4-180	0.15-75
Electroless plating	ambient	15-100	0.5-2.0	0.2-0.8

*Dependent on rate and material

Table 2

Conversion Factors for Coating Thicknesses

Angstroms	Microns	Platers Terminology	Inches
250	0.025	1 millionth	0.000001
10,000	1.0	40 millionths	0.000040
250,000	25.0	1 mil	0.001

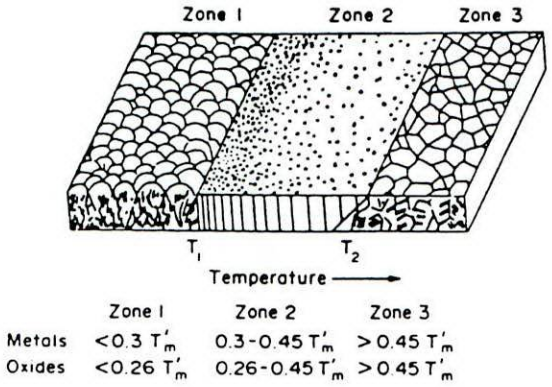

	Zone 1	Zone 2	Zone 3
Metals	$<0.3\ T'_m$	$0.3\text{-}0.45\ T'_m$	$>0.45\ T'_m$
Oxides	$<0.26\ T'_m$	$0.26\text{-}0.45\ T'_m$	$>0.45\ T'_m$

Figure 3: Structural zones in PVD films prepared by electron beam evaporation. From Movchan and Demchishin, Reference 5.

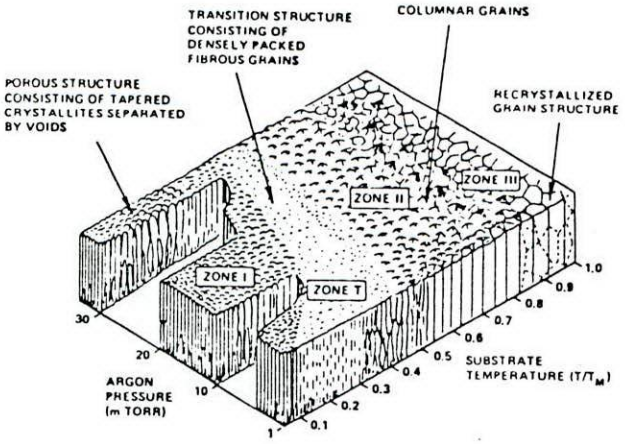

Figure 4: Structural zones in PVD films prepared by sputtering. From Thornton, Reference 6.

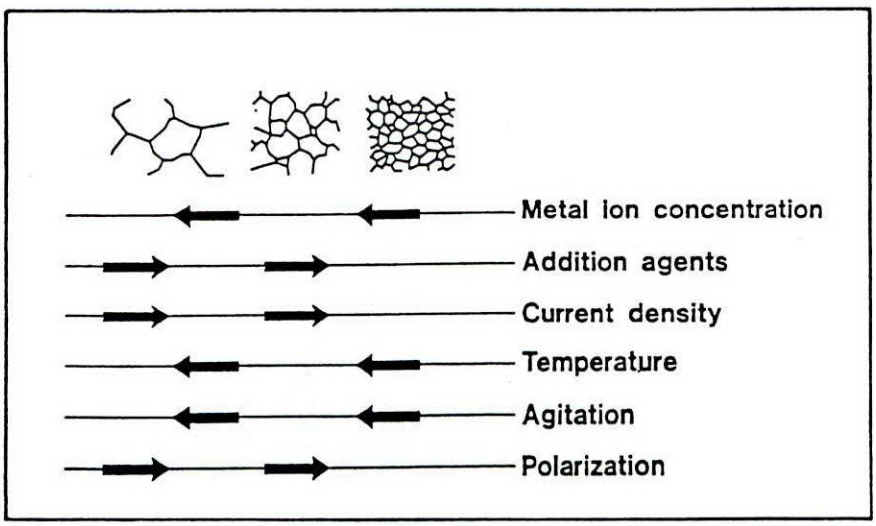

Figure 5: Relationship of structure of electrodeposits to operating conditions of plating solutions.

Thornton (Figure 4, Reference 6). Electroplaters aren't so fortunate since plating processes have more variables that influence structure, e.g., metal ion concentration, addition agents, current density, temperature, agitation, and polarization. Figure 5 pictorially shows how individual plating variables influence grain size of electrodeposits.

D. Adhesion

Excellent adhesion can be obtained with electroplated coatings on many substrates as attested to by a variety of quantitative tests such as ring shear, conical head and flyer plate. Table 3 lists a number of substrate materials and classifies them according to ease of coating with adherent electrodeposits. Those listed under the columns "easy to plate" and "special treatment" can be coated with adherent deposits that will not fail at the deposit-substrate interface. Those listed under the column titled "very difficult" often require extra steps such as heating or the use of augmented energy PVD techniques to provide good adhesion. When thick coatings are required, PVD and electroplating can be combined as discussed below.

With PVD films, adhesion has been reported to vary from poor to excellent (7-9). Sputtering is claimed to provide much better adhesion than the generally weak adhesion provided by evaporation. This is attributed to the higher energy of the deposition species in sputter deposition as compared to that of evaporated atoms (1 to 10 eV vs. 0.1 to 0.2 eV), References 10 and 11. By comparison, electroplating usually develops only a few tenths of an electron volt (11,12). With ion plating, the adhesion is reported to be excellent and better than with sputtering. Again, this is attributed to the highly energetic depositing ions (50 to 100 eV) as well as to the in-situ substrate pre-cleaning and the simultaneous deposition and substrate sputtering due to the continuous bombardment of the substrate during deposition (7,11).

Molybdenum can be used to show how the above generalized statements map with a specific substrate (Table 4). Adhesion of Be deposited on a cleaned Mo substrate via evaporation in a chamber evacuated to 10^{-5} to 10^{-6} Torr was only 31 MPa measured by a Sebastian tester with failure occurring at the interface between the coating and the substrate (13). With electroplating, adhesion of any coating would be no better than this unless special processing was used. For example, Table 4 reveals that good adhesion was obtained on Mo with processes that included hydrogen firing (e.g., gold strike and alkaline ferricyanide). Results with an acid etch/phosphonic acid process were considerably inferior. By comparison, copper deposited on Mo using magnetron ion plating followed by thick electroplating so that ring shear tests could be performed resulted in bond strengths of 216 MPa with failure occurring in the electroplated copper. With substrates such as Mo, Ti, and W the combined use of augmented energy PVD followed by electroplating can provide excellent adhesion of thick coatings without having to resort to severe etching of the substrates or heating after coating.

Table 3

Different Substrates Require Different Treatments to Provide Adherent Coatings

Easy to Plate	Special Treatment	Very Difficult
steel	stainless steels	titanium
copper	aluminum	molybdenum
brass	beryllium	tungsten
	magnesium	niobium
	plastics	tantalum
		glass

Table 4

Adhesion Data for Various Procedures Used to Apply Coatings on Molybdenum

Process	Deposit	Adhesion Results Sebastian MP_a	Adhesion Results Ring Shear MP_a	Location of Failure
Evaporation(A)	Be	31	-	Mo-Be Interface
Gold Strike/H_2 Fire /Electroplate(B)	Au	-	125	Au Deposit
Alkaline Ferricyanide Etch/H_2 Fire /Electroplate(C)	Au	-	90	Au Deposit/ Mo-Au Interface
Acid Etch/Phosphonic Acid/Electroplate(D)	Au Cu	- -	32 37	Mo-Au Interface Mo-Cu Interface
Magnetron Ion Plating(E)	Cu	69	216	Cu Deposit

(A) Be deposit was applied by vacuum evaporation in a chamber evacuated to 10^{-5} to 10^{-6} Torr. From Reference 13.

(B) This process included degrease in perchlorethylene, fire in dry hydrogen (< 2 ppm H_2O) at 1000°C for 10 minutes, immerse in a solution containing four parts NH_4OH (28%) and one part H_2O_2 (30%) for 8 to 10 seconds at room temperature, rinse in distilled water, gold strike to deposit 0.15 to 0.62 mg/cm² (0.08 to 0.32 μm), rinse in distilled water, fire in dry hydrogen at 1000°C for 10 minutes, electrodeposit to desired thickness.

(C) This process included degrease in perchlorethylene, immerse in a solution containing 300 g/l potassium ferricyanide, 100 g/l sodium cyanide for 10 seconds at room temperature, water rinse, electroplate to desired thickness, water rinse and then dry, hydrogen fire at 800°C for 4 hours.

(D) This process included degrease in perchlorethylene, anodic etch in chromic acid (10 percent by wgt) and 71 percent nitric acid (10 percent by vol) at room temperature and 15.5 A/dm² (1 A/in²) for 1 min, rinse, anodic treat in 50 percent aminotrimethylene phosphonic acid (ATMP) - 25 percent by vol, at room temperature and 15.5 A/dm² (1 A/in²) for 4 min, rinse, remove oxide film in chromic acid (10 percent by wgt) and 71 percent nitric acid (10 percent by vol) at room temperature for 1 min, rinse, electroplate to desired thickness.

(E) The magnetron ion plating process included sputter etching in vacuum, magnetron ion plating with 6 μm of copper and then electroplating to final thickness. Base pressure of the system was 5 x 10^{-6} Pa (10^{-8} Torr), etch power was 0.5 watts/cm², and bias power was 0.078 watts/cm² (but tapered to zero after deposition of about 20,000Å of copper).

E. Costs

This topic is not nearly as easy to quantify as those that have already been discussed. There is no doubt in my mind that PVD is more expensive than electroplating; the question is how much more expensive? My own experience plus information from two others will be discussed in the following.

Tom Beat, one of my colleagues who has spent his entire career in PVD and also works closely with outside firms, has provided some interesting information. He is aware of a disc manufacturer in the Silicon Valley who is convinced that to produce the same product (one million discs per month), PVD is ten times as costly as electroplating. Some of the items that contribute to this thinking are the following:

- for PVD a system costs $3 million and you also need a $1 million clean room
- a plating solution costs considerably less than $3 million and plating doesn't require a clean room
- with plating, the work could be processed using 16 hour days and a 5 day work week
- with PVD, the work would require 24 hour days and a 7 day work week
- with PVD every fourth shift would require down time for maintenance and changing of the cathode (deposition) source
- deposition sources are very expensive, e.g., $2000 for a PVD zinc source 6 inches in diameter by 0.625 inch thick ($439/lb compared to $0.72/lb for anode material for electroplating)
- in spite of the expense of PVD, it will be used to replace plating because plating requires 0.5 million gallons of water per day and water is becoming more and more difficult to obtain; also, plating would be replaced because of the hazards of working with and disposing of plating chemicals

Another source I've used is Dennis Koci, who is our resource manager at LLNL. Dennis has been closely involved with costing issues for electroplating and VPL operations during my 12 years at LLNL and he feels that the 10 to 1 ratio is probably a realistic number.

In spite of the above information, I don't know what the actual cost comparison ratio is between the two processes. Clearly, it is a function of many items that can vary from one installation to another. However, above and beyond the issue of capital equipment costs and maintenance which are very expensive propositions for VPL processing, it is evident that the simple issue of having a part coated is more expensive by PVD than electroplating. For example, a chamber has to be prepared, fixturing is often needed, pump down time is required, then the system has to be cleaned and re-configured for the next part. All this takes much longer than the time required for a plater to clean a part and complete the plating operation.

F. Waste Minimization

When comparing the two coating processes and discussing costs, one has to address the issues of waste disposal and waste minimization. There certainly is no question that PVD processing is considerably cleaner and offers savings via waste minimization that are not readily available via electrodeposition processes. Over the past five years we've spent over $500,000 in electroplating on waste minimization issues and this has certainly reduced operational costs because of eliminating or minimizing hazardous wastes which have to be handled and disposed. However, even with the added expense incurred with purchase, operation and maintenance of waste minimization equipment and the costs that still have to be incurred when disposing of hazardous plating wastes, the cost relationships between the two coating processes mentioned above still hold. A strongly influencing factor as already mentioned, which drives the cost of PVD processing is capital equipment and its maintenance. In our PVD facility, we could install only two, or perhaps three new systems for the $500,000 we've spent in plating waste minimization, and the maintenance costs in PVD would most likely exceed those that are required for our operation of waste minimization equipment in the plating facility.

Combining the Two Processes

Synergism can be obtained by combining electrodeposition and PVD. In a number of cases, better coatings and improved adhesion can be obtained when the two processes are combined. Also, for some applications, parts that could not be fabricated by either method itself could be produced when the two processes are combined. A number of references have appeared in the literature attesting to this and some examples will be discussed in the following paragraphs. For an overview and discussion of a variety of combined applications of the two coating processes see References 14-16. A listing of applications includes: metallization systems for hybrid microcircuits (17-19), copper on printed wiring boards (20), plating on difficult-to-plate metals such as W, Mo and Ti (16), a real time monitor for electroless nickel deposition (21), thick (1 mm) copper on glass (22), joining thin Be windows to stainless steel (14,23), fabrication of sputter cathodes by electroplating (24), electroforming parts with precision small inside diameter holes (25), plating on plastics (26), ceramic electronic substrates coated by PVD and reinforced by electroplating (27), molds for plastics, valves and nozzles (28), decorative coatings with various colors (29,30), and pens, wrist watches, jewelry and spectacle frames (31-33).

A. Plating on large molybdenum parts

The Precision Engineering Program at Lawrence Livermore National Laboratory was involved with the manufacture of precise, large-diameter, reflective optics for advanced laser systems by direct machining (34). Specific to

the topic of this paper were a number of Mo parts, including a 1.3 meter diameter ring shaped workpiece with a required form accuracy of approximately 250 Å rms. The parts were to be machined using a single-point diamond tool on a precision lathe under controlled machine and environmental conditions. Because diamond turning can be used successfully on face-centered-cubic metals (e.g., copper and aluminum) but not with Mo, (35-37) it was necessary to coat the Mo parts with thick (0.3 to 0.45 mm), adherent high-quality copper prior to final machining.

As discussed earlier, Mo is quite difficult to coat with an adherent deposit using conventional practices available to the electroplater. As shown in Table 4, the best adhesion was obtained when magnetron ion plating was used to provide the initial coating on Mo substrates. Although good results were also obtained with processes that included hydrogen firing (e.g., gold strike and alkaline ferricyanide), it would have been difficult to find a facility capable of hydrogen firing a part with a diameter of 1.3 m, and the potential warpage on a part of this size as a result of the high temperature (around 1000°C) required during firing could have proven disastrous to the close tolerances required.

B. Thick (1 mm) copper coatings on glass

This is an example of parts that could not have been fabricated unless the two technologies were combined. Thick (1 mm), adherent copper was needed on low coefficient of expansion glass to serve as a heat sink for a laser calorimeter. Another requirement was for 0.4 mm of copper on glass for an x-ray spectrometer system and lastly, diamond machinable coatings approximately 125 μm thick were sought for possible improvements in the optics of systems currently fabricated from metal. By applying an initial thin layer by magnetron sputtering or electron beam evaporation and then thick copper by electroplating, it was possible to fabricate the parts (22).

The conventional technology used by platers for metallizing nonconductors with stannous chloride/palladium chloride activation followed by electroless deposition prior to final electroplating is not acceptable for glass when thick coatings are required. With this process, deposits thicker than around 12.5 μm easily separate from a glass substrate.

The generally accepted criterion for adhesion between an oxide substrate such as glass and a metal film is that the metal must be oxygen active to react chemically with the oxide surface, forming an interfacial reaction zone (38). Metals such as niobium, vanadium, chromium, and titanium, which have a high negative heat of formation have a high affinity for oxygen. Deposition of one of these "glue" or "binder" layers by physical vapor deposition followed by a thin layer of copper without breaking vacuum produces an adherent base for thick electroplating.

The glass substrates were prepared by first fine grinding the surfaces to be coated with 3 μm particles of aluminum oxide followed by an etch in a six percent solution of nitric acid at 100°C. The glass was then placed in the vacuum coating chamber and preheated to 250°C for a minimum of eight hours. Next, the substrates were coated with a "binder" layer of 300 Å of either chromium or titanium using electron beam evaporation. Without breaking the vacuum between the coating steps, the binder layer was overcoated with 4000 to 5000 Å of copper. The parts were then electroplated with copper to final thickness, which in some cases was 1 mm. The electroplating was done at a current density that resulted in zero or slightly compressive stress. A part diamond turned after coating is shown in Figure 8.

C. Joining beryllium to stainless steel

Beryllium windows with a diameter of 0.96 cm and a thickness of 50 μm were joined to stainless steel anode housings for use in sulfur detector units which are compact x-ray tubes designed as a reliable fluorescence excitation source for use in a portable sulfur monitor. They contain a close coupled x-ray fluorescence spectrometer that uses silver L x-rays at 3 keV to excite characteristic x-rays of sulfur present in atmospheric aerosol particles. The sulfur monitor is unique in that the aerosol sampling and analysis are performed in the same unit with quantitative results available in real time.

The beryllium windows were joined to the stainless steel anode housings by using a combination of sputtering and electroplating. The thin Be discs were first coated with gold on their outer edges by sputtering, then placed in a pre-gold plated stainless steel tubular housing. All areas were masked except the sputter coated band on the Be and a companion area on the stainless steel. The Be foil was then joined in place using a thick nickel electroplate. Units fabricated by this combined PVD/electroplating process passed hundreds of hours of testing without degradation. By contrast, use of wet chemical methods, which had been successful with 250 μm thick Be windows (23), dissolved the 50 μm thick Be wafers. A completed unit is shown in Figure 9.

D. Reduced pressure deposition

Plating under reduced pressure was evaluated for both electroless nickel and electrodeposited copper systems. The objective was to reduce pitting of these coatings thereby further enhancing their usage for diamond turning applications. Cursory experiments with electroless nickel showed reduced porosity when deposition was done at around 500 Torr. Detailed experiments with electrodeposited copper at around 100 Torr provided similar results. More information on this work, which is also included in the technical program of SUR/FIN 92 can be found in Reference 39.

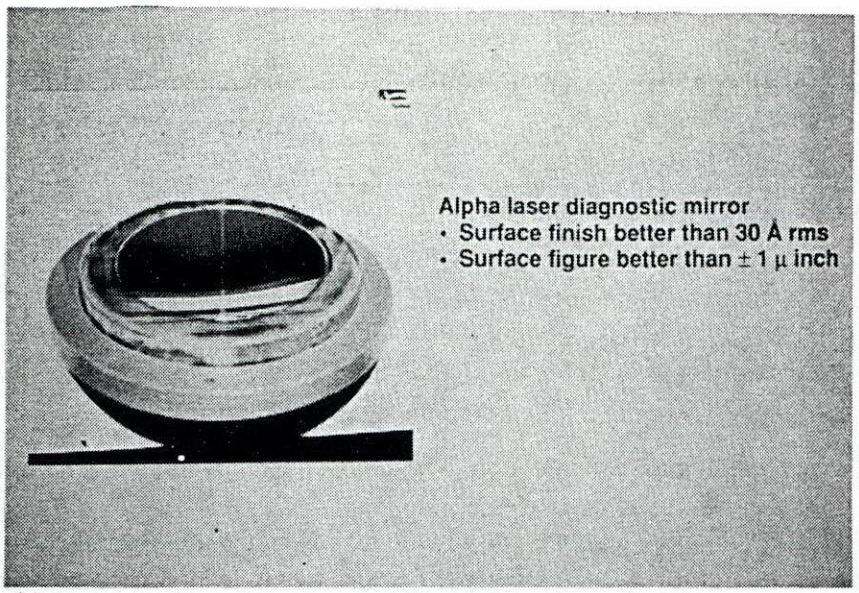

Figure 8: Diamond machined copper deposited on glass using the combined deposition processes. From Reference 22.

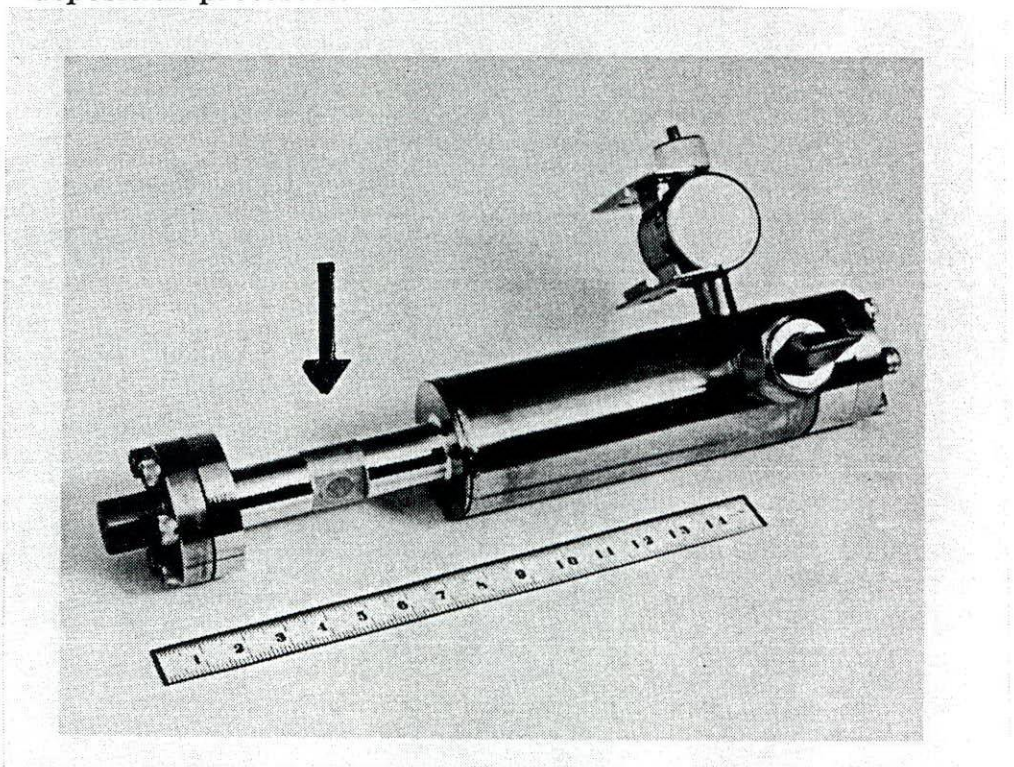

Figure 9: A beryllium window joined to a stainless steel anode housing by using the combined deposition processes of PVD and electroplating.

Summary

This paper has compared two deposition technologies, electroplating and physical vapor deposition. Each of these are extremely important, commercially viable processes and each has particular features that favor it in specific applications.

In terms of coating choices, PVD offers a much wider range than electroplating and PVD coatings can be applied to nonconductors. This isn't to say that electroplated coatings can't be applied to nonconductors, however, special processing is required. Although deposition rates overlap for both processes, thicker coatings (> 125 μm) are more likely to be produced by electroplating. PVD processes favor thin coatings (hundreds to thousands of Angstroms).

A wealth of property data are available for "free standing" electrodeposits but this is not the case with PVD films since these are typically too thin for reliable measurement. Data available for PVD films include stress, microhardness, wear resistance, and scratch adhesion resistance.

Adhesion can be excellent for both coating processes on many substrates. However, substrates such as W, Mo and Ti, with tenacious oxide films can be coated more adherently via augmented energy PVD processing than via electroplating procedures.

PVD processing is much cleaner than electroplating and offers definite advantages from a waste minimization viewpoint. However, even with the added expenses incurred for disposal of hazardous plating wastes and operation of waste minimization equipment, cost of PVD processing is higher than that of electroplating. Sources quoted in this paper suggest that PVD might be as much as ten times as expensive as electrodeposition.

Lastly, combining the two processes often results in synergism inasmuch as parts that could not be fabricated by other means could be produced when the two processes were combined. In other cases, better coatings with improved adhesion have been obtained. A number of examples and references are cited supporting combining the coating processes.

In summary, both PVD and electroplating are viable coating processes; each offers its own unique set of advantages and each has disadvantages. In a number of cases, combining the two processes has resulted in improved product, or parts that could not be fabricated by any other means.

Acknowledgements

I would particularly like to adknowledge the help of Tom Beat who has shared his expertise in PVD processing with me during my years at LLNL. Appreciation is also expressed to the entire PVD group at LLNL for their help in keeping me abreast of this technology.

References

1. J. W. Dini, "Electroplating, Electroless Plating, and Electroforming", Proceedings SUR/FIN 90, Session T, 1193 (1990), American Electroplaters & Surface Finishers Soc.

2. W. H. Safranek, THE PROPERTIES OF ELECTRODEPOSITED METALS AND ALLOYS, American Elsevier Publishing Co., (1974)

3. W. H. Safranek, THE PROPERTIES OF ELECTRODEPOSITED METALS AND ALLOYS, Second Edition, American Electroplaters & Surface Finishers Soc., (1986)

4. P. J. Burnett and D. S. Rickerby, Thin Solid Films, 154, 403 (1987)

5. B. A. Movchan and A. V. Demchishin, Phys. Met. Metallogr. 28, 83 (1969)

6. J. A. Thornton, J. Vac. Sci. Technol., 11, 666 (1974)

7. N. S. Platakis and L. Missel, Metal Finishing, 76, 50 (July 1978)

8. J. E. Varga and W. A. Bailey, Solid State Technology, 14, 25 (1981)

9. P. R. Forant, Metal Finishing 77, 17 (Nov 1979)

10. H. K. Pulker, A. J. Perry, and R. Berger, Surface Technology, 14, 25 (1981)

11. J. J. Cuomo, J. P. Doyle, K. L. Saenger, C. R. Guarnieri and S. J. Whitehair, "High Density Amorphous Carbon Films and the Preparation of Diamond Membranes for X-Ray Lithography", APPLICATIONS OF DIAMOND FILMS AND RELATED MATERIALS, Y. Tzeng, M. Yoshikawa, M. Murakawa and A. Feldman, Editors, Elsevier Science Publishers B. V. (1991)

12. "Sputtering as a Deposition Process", Hohman Plating and Manufacturing, Dayton, Ohio, Bulletin SL-1002

13. A. K. Dua and R. P. Agarwala, J. Vac. Sci. Technol., A3 (6), 2612 (Nov/Dec 1985)

14. J. W. Dini, Plating & Surface Finishing, 72, 48 (July 1985)

15. J. W. Dini, Proceedings 1st International SAMPE Metals and Metals Processing Conference, Cherry Hill, NJ (August 1987)

16. J. W. Dini, Proceedings Third International Conference on Surface Modification Technologies, TMS, Neuchatel, Switzerland (1989)

17. P. L. Blessner, "Feasibility of Electroplated Gold for Hybrid Microcircuits", Bendix Kansas City, BDX-613-1740, (Oct 1977)

18. R. A. Hines and M. K. Raut, Proceedings AES 2nd Design and Finishing of Printed Wiring and Hybrid Circuits Symposium (Jan 1980)

19. W. W. Pcihoda and A. E. Walker, Electronic Packaging and Production, 15, 74 (June 1975)

20. A. Anderson, Plating & Surface Finishing, 68, 44 (Dec 1981)

21. K. K. Kanazawa and S. K. Doss, Plating & Surface Finishing 74, 52 (July 1987)

22. W. C. Cowden, T. G. Beat, T. A. Wash and J. W. Dini, Proceedings of the Electrochemical Society Symposium on Metallized Plastics: Fundamental and Applied Aspects, K. L. Mittal and J. R. Susko, Editors, (Oct 1988)

23. H. R. Johnson and J. W. Dini, Rev. Sci. Instrum. 46, No 1, 109 (Jan 1975)

24. J. W. Weed, W. K. Kelley, and D. M. Sanders, "Fabrication of Sputter Cathodes by Electroplating", Golden West Regional Conference, Santa Clara, CA. (April 1986)

25. W. K. Kelley, W. C. Cowden and G. E. Overturf, III, Proceedings AES Electroforming/Deposition Symposium (Jan 1983)

26. J. H. Lindsay and J. LaSala, Plating & Surface Finishing, 72, 54 (July 1985)

27. E. Flury-Frei, Galvano, 37, No 5, 54 (1990)

28. K. Reichel, W. Brandt and H. Mack, Galvanotechnik, 81, No 2, 426 (1990)

29. H. Erhart, Metalloberflache, 44, No 2, 59 (1990)

30. H. Erhart, Galvanotechnik, 81, No 4, 1216 (1990)

31. Anon., Galvanotechnik, 79, No 7, 2235 (1988)

32. Anon., Galvanotechnik, 80, No 6, 2059 (1989)

33. G. Kienel, Galvanotechnik, 80, No 6, 1937 (1989)

34. S. R. Patterson, "Development of Precision Turning Capabilities at Lawrence Livermore National Laboratory", UCRL-94719, Livermore, CA (June 1986)

35. B. Krauskopf, Mfg. Eng., 92, 90 (May 1984)

36. B. M. Hogan, "Microstructural Stability of Copper Electroplate", Proc. AES 71st Annual Technical Conference, (1984)

37. J. W. Dini, "Perspective on Plating for Precision Finishing", Proc. ASPE Spring Topical Meeting on Metal Platings for Precision Finishing Operations, Tucson, AZ (April 1991)

38. D. M. Mattox, Thin Solid Films, 18, 173 (1973)

39. J. W. Dini, W. C. Cowden, T. G. Beat, L. E. Ryan and W. B. Hewitt, "Plating Under Reduced Pressure", Proceedings SUR/FIN 82, AESF, Atlanta, GA (June 1992)

*** PAPER NOT AVAILABLE IN TIME FOR PUBLICATION ***

Production Techniques for Large-Area PVD Coatings
D.L. Chambers, DC Industries, Columbus, OH

There are various industrial applications using physical vapor deposition (PVD) processes for large-area coatings. Vacuum evaporation has been used for many years to produce mirror and solar control coatings. Sputtering is a well-known process for applying coatings to large sheets of architectural glass. Web materials of both plastic and metal are also coated by PVD in large area applications. This paper compares different PVD applications. Sputtering is especially of interest as a promising production technique that combines economical advantages with improved coating properties. Several products produced by these large area coating systems will be examined. The advantages and limitations of the processes and equipment will be discussed.

*** For copies of this paper please contact the author directly:**

Mr. Doug L. Chambers
DC Industries
1986 Belgrave Drive
Columbus, OH 43220
419/865-1256
Fax 419/865-1932

*** PAPER NOT AVAILABLE IN TIME FOR PUBLICATION ***

High Volume Automotive-Type Aluminum Coating by Ion Vapor Deposition

Graham Legge, Abar Ipsen Industries, Bensalem, PA

Ion vapor deposition (IVD) has been used for several years for the coating of high-strength steel, aluminum, and titanium alloy parts. Aluminum coatings for corrosion protection of numerous aircraft parts are now routinely applied in medium-volume batch IVD coaters. The properties and uniformity of IVD coatings have been demonstrated on many automotive, hydraulic, and electronic parts. The high volume required by these industries, however, has made it difficult to justify batch coating. A new continuous system now makes it possible to produce the volume of parts required for these applications. This paper will review the properties and potential for continuous IVD coating, using case histories developed for several emerging applications.

*** For copies of this paper please contact the author directly:**

Mr. Graham Legge
Abar Ipsen Industries
3260 Tillman Drive
Bensalem, PA 19020
215/244-4900

"TiN Coatings for Wear Resistance and Gold-like Decorative Coatings"

by M. E. Graham and P. Chang
BIRL, Northwestern University, Evanston IL 60201

1. Introduction

Titanium Nitride (TiN) coatings have led the way for providing increased wear resistance and extended life of cutting tools, whether carbide inserts or high-speed steel. Where the earliest applications were for high temperature substrate materials (carbides) and chemical vapor deposition (CVD) was the process of choice, later developments in the physical vapor deposition (PVD) technology, especially in sputtering and cathodic arc deposition, made it possible to achieve similar improvements in performance for high speed steels and other heat sensitive metal substrates. Whereas the CVD process requires temperatures of about 1000°C to apply TiN, the PVD processes can apply the coating at temperatures of 500°C down to only 200°C, depending on the process chosen, and the application. As the deposition temperatures have decreased and the deposition rates have increased, the possible applications for TiN (and other hard coating materials) have expanded greatly.

Because of the gold color of TiN and other similar nitrides such as ZrN, HfN, and alloy nitrides such as TiZrN, applications for use as decorative coatings have developed in jewelry, writing pens, and other personal items. Because of their high hardnesses and relative chemical inertness, these materials are also protective coatings. TiN coatings typically have hardnesses of about 2200 kg/mm^2 (Vickers hardness), which is three times that of fully hardened tool steel. Still other coatings are being developed using alloy nitrides or carbides such as (TiAl)N (bronze) and TiCN (black) that are readily applied by PVD techniques and offer further options for wear and corrosion resistant decorative coatings.

2. Properties

TiN has excellent mechanical properties and finds many uses for wear resistance. As mentioned above, it has a hardness of about 2200 Vickers (VHN) compared to about 700 VHN for hardened M2 steel. It also has a low coefficient of friction (about .1) when sliding against steel. Its ceramic-like nature resists galling when used with steel in a sliding wear situation. In addition to good room-temperature properties, it retains its properties at much higher service temperatures. TiN is stable in air up to about 550°C, and has a melting temperature of 2950°C.

While the properties of the material are impressive, the performance of a coating depends on the deposition process and the substrate material as well. TiN is a good match for steels from the standpoint of thermal expansion coefficient, with a value of about 9 μm/m.°C compared to 10-15 μm/m.°C for steels. Other ceramic materials typically have expansion coefficients closer to half this value.

Since the compound is generally deposited in a reactive process, the composition can be varied somewhat, by controlling the amount of nitrogen available in the process. As the ratio of Ti to N gets closer to 1:1, the golden color deepens and the hardness generally increases. Other deposition parameters have important effects on the coating density, microstructure and internal stresses, which, in turn, effect the hardness, the adhesion and the corrosion resistance of the films.

3. Wear Behavior

The wear behavior of TiN coatings has been studied in recent years at many laboratories including BIRL. We have found outstanding properties when the coating-substrate system is optimized for best performance. Wear testing has demonstrated that TiN coatings can be very successful in enhancing rolling contact fatigue resistance of bearing steels [1]. Pure rolling tests have shown that very thin coatings (0.25 - 1.0 μm) can increase bearing life several fold. Whereas, a 4118 uncoated steel roller showed surface fatigue wear after 10 million cycles, a 0.25 μm TiN coating enabled the roller to run 60 million cycles with no evidence of wear or subsurface cracking. Thicker coatings of 2-5 μm (useful for cutting tools) performed poorly.

In other severe wear tests, involving combined sliding and rolling, the scuffing resistance of coated contact-elements was compared to that of uncoated elements under oil-lubricated conditions [2]. Dynamic test conditions were set so that scuffing failure loads of uncoated steels were quite low. The TiN coated steels generally remained intact to the load limit of the machine, at least one order of magnitude higher load than for the uncoated steel. Such results could be obtained with one or both elements coated, and again, the best results was for coatings that were 0.25-1 μm thick. The thicker coatings did not provide any benefit over the uncoated roller under the test conditions.

Similar tests with substrates of different hardnesses and coatings of different hardnesses (controlled by the deposition conditions such as substrate bias) showed the importance of matching the coating to the substrate for best result [3]. While the scuffing resistance of the hardest TiN film exceeded the machine-load-limit on an Rc62 (Rockwell hardness) steel, it

performed poorly on a softer, Rc45 steel of the same composition (52100). On the other hand, a relatively low-hardness TiN coating tripled the scuffing failure load of the softer steel and similarly enhanced the performance of the harder steel. The combination of hard coating and hard substrate was definitely best, but improvements could be made for both steels if the correct deposition parameters were used.

Analysis of the friction behavior of the TiN coated surfaces has also revealed interesting information about the scuffing behavior of the material. It has been established that the coating allows and sustains the formation of an oxide layer (tribo-chemical reaction products) that lowers the friction and resists scuffing. The uncoated surface cannot resist scuffing at the higher loads [4].

The corrosion resistance of these TiN coatings has also been the subject of investigation. The material itself is relatively inert at moderate temperatures in most common gaseous or liquid environments. Laboratory corrosion potential tests at BIRL and elsewhere [5] have shown that TiN coated steels are two to three orders of magnitude more resistant to corrosion in acid solutions than the uncoated steel. The true measure of its usefulness as a corrosion resistant coating is difficult to assess since its practical performance is limited primarily by our inability to make defect free coatings. Pin holes or other such defects tend to be the controlling factors in many cases, and the comparison given above is for general corrosion of the uncoated steel and pitting corrosion of the coated steel. Deposition parameters, especially substrate bias, which can effect microstructure and density also strongly influence the performance of these coatings.

4. Deposition processes

Today's PVD processes for depositing TiN fall under two general categories: evaporation (resistance, electron beam or cathodic arc), and sputtering. Within these categories there are many variations, but the processes that produce the high quality coatings generally incorporate substantial ion bombardment of the growing film and substrate. This ion bombardment, when properly controlled, produces highly adherent films with good mechanical properties. The ions may be from the evaporated species as in the arc process or as in ion plating processes, or they may be ionized argon gas atoms as in the case of most sputtering processes. This ion bombardment supplies energy to the film that cannot be made available by increasing the substrate temperature and it helps in densifying the microstructure.

All the processes have their strengths and weaknesses, which have defined the areas of application where they are most successful.

The ion plating process is capable of high quality coatings, of good density and good surface quality. A commercially successful process is, however, operated at a temperature of about 500°C, which limits some of its applications. Also, being an evaporation process, it is not as flexible as sputtering for the deposition of alloy nitrides.

The arc process is also capable of highly adherent coatings, and is more flexible in the types of materials that can be deposited. Two difficulties with the arc process are: (1) the development of what are called macroparticles in the coating and (2) the potential for excessive heating in sensitive substrates. The macroparticles are unreacted metal (Ti) in the form of micron-sized nodules. While this has not been a severe problem for some applications such as cutting tools, macroparticles pose problems for corrosion applications and for rolling and sliding wear applications.

The magnetron sputtering approach offers great flexibility in the range of materials that can be deposited and it can maintain low substrate temperatures (< 200°C). The adhesion and coating properties can be very good and the control of microstructure for corrosion applications is very promising. Recent developments in "unbalanced-magnetron" sputtering at BIRL [6] and other laboratories [7-11] have created a large amount of interest in improved microstructure control of sputtered films. Traditionally, the process is thought to be somewhat more expensive than the other two because of target costs and utilization, and the somewhat lower deposition rates. Developments in gas-flow control [12] have enabled rates of 0.5 μm/min. to be achieved with TiN coatings on steel. The evaporation processes generally have the potential for deposition rates an order of magnitude greater than this, but the optimum rate will depend on the properties required in the coating as well as the inherent evaporation capability.

5. Conclusions

TiN coatings (and other hard, highly colored compounds) have great potential for applications in traditional and non-traditional areas. The coatings are very adherent and can be applied to a wide range of substrate materials including metals, ceramics and polymers. Very thin coatings, on the order of a fraction of a micron to a few microns, can provide order-of-magnitude improvements in wear resistance and corrosion resistance. TiN coatings should prove very useful for bearings, sliding surfaces, forming tools, and other wear applications, as well as for decorative coatings with protective requirements.

Cost comparisons, however, must be done very carefully, since they are very application dependent and must take account of both

direct and indirect costs and benefits. The PVD processes can often be cost effective because of reduced pollution/clean-up problems and greater part yield and performance, even though the capital equipment may be more costly than for some traditional coating technologies. Continuing improvements to overcome the recognized weaknesses, make each of the techniques more competitive all the time and increase their range of applicability.

Acknowledgements

The authors would like to acknowledge the support of DoE, Office of Transportation Materials, contract number 00732401, for support of the wear testing of coated surfaces.

References

1. T.P. Chang, H.S. Cheng and W.D. Sproul, **Surf. Coat. Technol., 43/44**, (1990) 699.
2. W.D. Sproul, T.P. Chang and H.S. Cheng, Presented at the AT/DCC meeting, October 28-31, 1991, Dearborn, Mi.
3. T.P. Chang, R.H. Krueger, M.E. Graham and W.S. Sproul, To be presented at Earthmoving Industry Conference, Apr. 7-8, 1992, Peoria, Il.
4. T.P. Chang, M.E. Graham, W.D. Sproul, and H.S. Cheng, To be presented at International Conference on Metallurgical Coatings and Thin Films, Apr. 6-10, 1992, San Diego, CA.
5. B. Matthes, et. al., **Surf. Coat. Technol., 49**, (1991) 489
6. W.D. Sproul, P.J. Rudnik, M.E. Graham and S.L. Rhode, **Surf. Coat Technol., 43-43**, (1990) 270.
7. N. Savvides and B. Window, **J. Vac. Sci. Technol. A, 4(3)**, (1986) 504.
8. D.G. Teer, **Surf. Coat. Technol., 39-40**, (1989) 565.
9. A.G. Spencer, K. Oka and R.P. Howson, **Vacuum, 38**, (1989) 859
10. S. Kadlec, J. Musil and W.-D. Munz, **J. Vac. Sci. Technol. A, 8(3)**, (1990) 1318.
11. W.-D. Münz, F.J.M. Hauzer, D. Schulze, and B. Buil, **Surf. Coat. Technol., 49**, (1991) 161.
12. W.D. Sproul, **Surf. Coat. Technol., 33**, (1987) 73.

*** PAPER NOT AVAILABLE IN TIME FOR PUBLICATION ***

Decorative and Wear-Resistant Coatings by PVD Processing

D. Butrymowicz and J.R. Snyder, Leybold Technologies, Enfield, CT

The increased use of physical vapor deposition (PVD) follows innovations in film performances and higher deposition rates. A wide variety of metals, alloys and compounds are now deposited economically by PVD techniques onto a broad variety of substrate materials and shapes. Some decorative and functional coating applications lend themselves to a PVD-only approach, but finished products commonly combine a cost-effective mix of coating technologies--notably PVD plus plating. As PVD technologies evolve, opportunities emerge for improving profits and performance in established markets as well as for entering new markets. This paper will review existing PVD applications and contemplate future opportunities for plating and finishing.

*** For copies of this paper please contact the author directly:**

Dale Butrymowicz and James R. Snyder
Leybold Technologies
120 Post Road
Enfield, CT 06082
203/741-2267
Fax 203/741-0267

ION VAPOR DEPOSITION OF ALUMINUM

ABSTRACT

In the mid 1970's, McDonnell Douglas developed a process known as Ivadizing (I.V.D.), utilizing the Ion plating technique to apply a uniform, dense and highly adherent aluminum coating. Initial corrosion trials indicated that the Ivadizing process was a suitable alternative to Cadmium.

Since that early development work and with over a decade of service in the Aerospace industry, much has been learned both practically and technically about this process.

The purpose of this paper is to present some of those findings and discuss both the present and future applications for this coating.

Author - B.T. Nevill

Technical Manager

INTRODUCTION

For many year's, Electroplated Cadmium has been the most widely used coating on high strength steels in the Aerospace Industry. Cadmium gave not only good corrosion resistance (cathodic protection), but was cost effective.
There are some major technical drawbacks associated with Cadmium. These include hydrogen embrittlement of high strength steels (due to the plating process), exfoliation corrosion in the countersinks of aluminum alloys, ecology problems (toxic waste), and the solid metal embrittlement of titanium.

In recent years, the ecology issue has become one of the main factors in reducing the amount of Cadmium used in the industry. Tighter legislation imposed to control the disposal of toxic waste and reductions in the permissible level of Cadmium in effluent, has effectively increased the cost of this coating and made it less attractive to the plating shop.

Tests have shown aluminum coatings provide good corrosion protection, particularly in Chloride containing aqueous environments. Aluminum is anodic to steel and gives improved galvanic compatibility with aluminum alloys. Environmental corrosion tests of aluminum and Cadmium coated steel fasteners installed on operational military aircraft were reported to have shown better performance for the aluminum coated fastener. (Ref: Note 1)

A number of alternative processes are available for the application of aluminum coatings, namely metal spraying, cladding and electroplating, etc.. However, Ivadizing (Ion plating) affords the best control of thickness, superior adhesion, excellent "throwing power", low temperature application and good production throughput capabilities. Advances in the vacuum coating industry with rotary racks, specialized tooling and better pumping equipment, has made it much more competitive with the lesser tech coatings.

THE EQUIPMENT

The Ivadizer (coater) is a mild steel vacuum chamber (6' dia x 12') with an inside plating zone of approximately 5' x 10'. Removable stainless steel liners in the chamber help reduce pump down times by allowing the excess buildup of aluminum in the plating process to be removed at regular intervals. The chamber has a mechanical pumping system which consists of a three stage diffusion pump backed by a rotary-vane and booster pump. Correct choice of pumps and careful use of baffles, foreline traps or cold traps, limit the possibility of back migration or back streaming of oil vapour molecules into the chamber.

In addition to the mechanical system, the Ivadizer utilizes a cryogenic system. Briefly, cryogenic pumping is the freezing of gas or vapour out of a vacuum system onto a very cold surface. In this particular operation, the cryogenic pump is used to trap and hold water vapour.

Various racks and fixtures are available to transport work to and from the coater. These dollies are composed of a simple framework with a rail to support the rack (parts tray) and four main leg supports, each with air cushion pads. This facilitates easy movement of loads to and from the coater. The racks (parts trays) are positioned on rollers to allow the components to be loaded and unloaded into the chamber. Rotary pass thru's on the chamber allow the use of rotary rack and barrels to rotate work under vacuum during the coating cycle.

THE PROCESS

Cleaning - As in most metal finishing operations, preparation of the substrate is vital if good adhesion is to be achieved. Oil lubricants, grease or dyes, can be removed using chlorinated solvents or specialized soak cleaners.

In order to minimize surface contamination, and particularly in cases where rust or even scale is present, a dry blasting operation using pure aluminum oxide (150-220 mesh) is necessary prior to vacuum coating. Great care needs to be taken at this stage to minimize surface roughness or irregularities since this would be detrimental to the coating finish and corrosion protection. The components are loaded within 4-6 hours to reduce the possibility of surface contamination. Prior to loading, excess media is removed with dry compressed air.

Gas Cleaning - Once loaded, the vacuum chamber is pumped down to 10-5 torr (45 minute cycle). This allows sufficient outgassing of the chamber, removing previously absorbed gasses and vapours from the coated rack, fixture, and chamber shields. At this point the chamber is backfilled with an inert gas argon to 10 microns. A negative dc (1kv) potential is applied to the substrate (cathode). Positive Ions are produced by collisions between high energy electrons and gas atoms. Bombardment of the cathode (substrate) produces secondary electrons, hence, an avalanche effect is achieved. This process will continue until a normal glow discharge is achieved. This is characterized by the formation of a distinctive light pattern and an increase in current.

The positive ions are attracted to the substrate (cathode) dislodging substrate atoms and removing surface contamination (sputtering). This is not only effective at removing surface contaminants, but is responsible for the graded interface between the substrate and the coating, and hence, excellent

adhesion. The gas cleaning cycle lasts between 10-20 minutes, after which the atomically clean surface is ready for coating.

Coating - The evaporation source (anode) consists of seven intermetallic boron nitride or titanium diboride boats (crucible). Each crucible has an independent wire feed unit and when a high current is applied to the boat, (each crucible has a resistivity of 250-1000 micro-ohm/am), the resistive heat generated melts the aluminum wire which is subsequently vaporized.

Once evaporated, the aluminum atoms are ionized through collisions with high energy electrons or metastable gas atoms (peening ionization). These positively charged ion's are then attracted to and deposited on the negatively charged substrate (cathode).

The speed at which the aluminum wire is fed to the crucible is carefully controlled, so the deposition rate offsets the sputtering rate to give efficient growth of the aluminum film and good adhesion.

The evaporation source is capable of traversing the length of the chamber at a controlled speed, hence, the coating thickness is dependent on the number of passes and speed during this operation.

COATING MICROSTRUCTURE

When investigated with a scanning electron microscope (SEM) the coating clearly shows a columnar structure with the grains extending outward from the substrate. The Ion plating process does help produce strong bonding between the individual columns, however, correct control of gas pressure, substrate bias, temperature and surface roughness (substrate) is necessary to achieve a low porosity coating with a uniform, dense structure.

Figure (1) Sem / Cross Section Aluminum Coating (1060 mag)

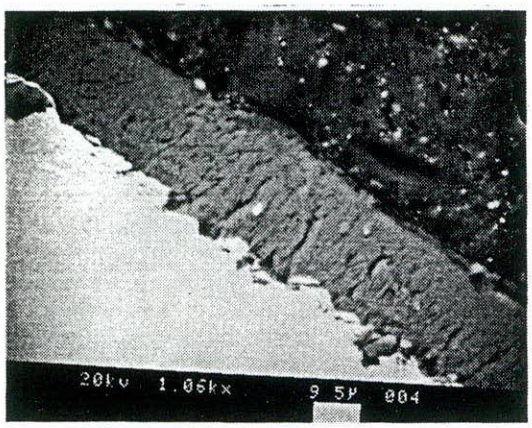

In the "as coated" condition, ion vapor deposited aluminum is very porous. This porosity is reduced by consolidating (burnishing) the coating using a glass media applied at a pressure of 20-30 lbs (psi). This compressing of the aluminum coating yields a more uniform, less porous and more durable coating. However, this is not capable of removing all evidence of microporosity.

To further improve corrosion protection, a chromate topcoat is applied. (Typically 200-250 Angstroms in thickness). This reduces porosity by "sealing" the coating and provides an excellent bond for a paint finish (barrier coat).

UNIFORMITY

The main advantage with the ion plating process is thickness uniformity and excellent "throwing power". This is not strictly a line of sight process with the most complex of shapes receiving complete coverage in one coating operation. This has mainly been put down to the scattering of the metal vapour atoms through their numerous collisions between the evaporation source and the substrate. Also important is the sputtering process which is maintained throughout the coating operation, with metal atoms dislodged (momentum transfer) and re-deposited on the substrate.

Tests carried out by the author (B. Nevill) clearly showed the distance between the source and substrate is vital in providing good coverage. Typically, a distance of 12-15 inches from the evaporation source gave the best results with a 3 to 1 ratio (front to back) coating thickness in one coating operation.

Thru holes can be easily coated although it is difficult to control thickness. The coating will throw into bores to a depth equal to the diameter, although the coating thickness is non-uniform and tends to fade out quickly once the coating has reached half the diameter.

In a recent trial I was able to achieve full coverage in the I.D. of a 24 inch by 6.5 inch diameter tube (open both ends) in one operation. In practice, most complex shapes are turned through 180 degrees in the coating cycle. In many cases this is a cosmetic operation, allowing the movement of hooks and wire fixtures which would normally leave a mark or bare area.

Figure (2) IVD Aluminum Coating Thickness and Uniformity on a Cylindrical Detail

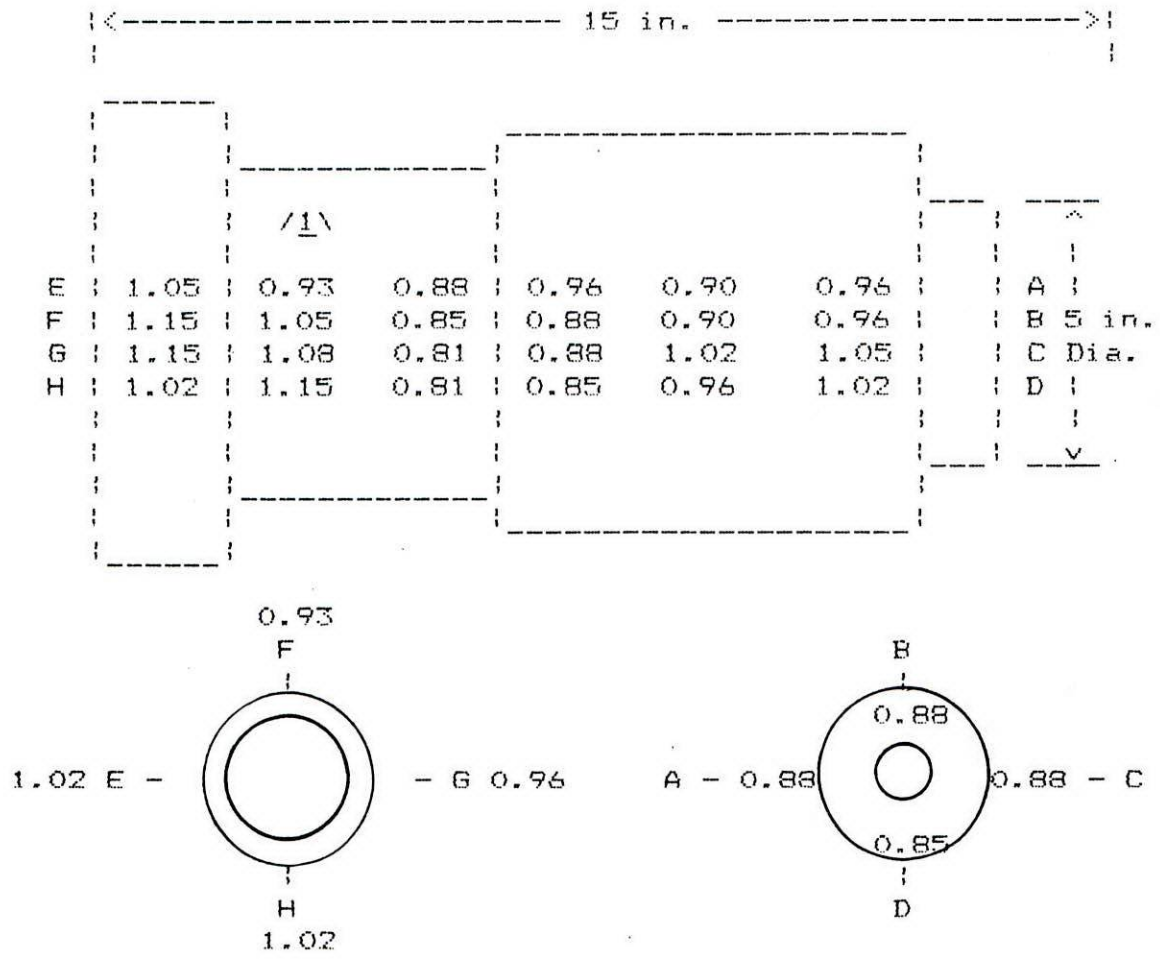

/1\ Coating thickness measurements taken at 90 degree Increments. All readings are in MILS.

Table I

IVD Aluminum Coating Thickness Variation
Throughout a Production Size Load of Fasteners

Fastener Number a,b	Coating Class	Coating Thickness (mils)	Average Thickness (mils)
1	3	0.44,0.55,0.47,0.34,0.62	0.48
2	3	0.77,0.44,0.45,0.62,0.59	0.57
3	3	0.77,0.35,0.44,0.71,0.56	0.57
4	3	0.65,0.35,0.47,0.44,0.35	0.45
5	3	0.87,0.30,0.52,0.44,0.47	0.42
6	3	0.66,0.46,0.56,0.61,0.40	0.54
7	3	0.37,0.32,0.53,0.43,0.58	0.45
8	3	0.61,0.39,0.31,0.30,0.55	0.43
9	3	0.36,0.44,0.50,0.33,0.37	0.40
10	3	0.46,0.58,0.38,0.38,0.38	0.44

a. Fasteners randomly selected from production size run of 150 lb of fasteners/barrel.

b. Hexagon head fasteners are 3/8" diameter x 2.7" long.

Figure (3)

Turbine Blade (Cross Section)

Figure (3)

COATING THICKNESS DISTRIBUTION

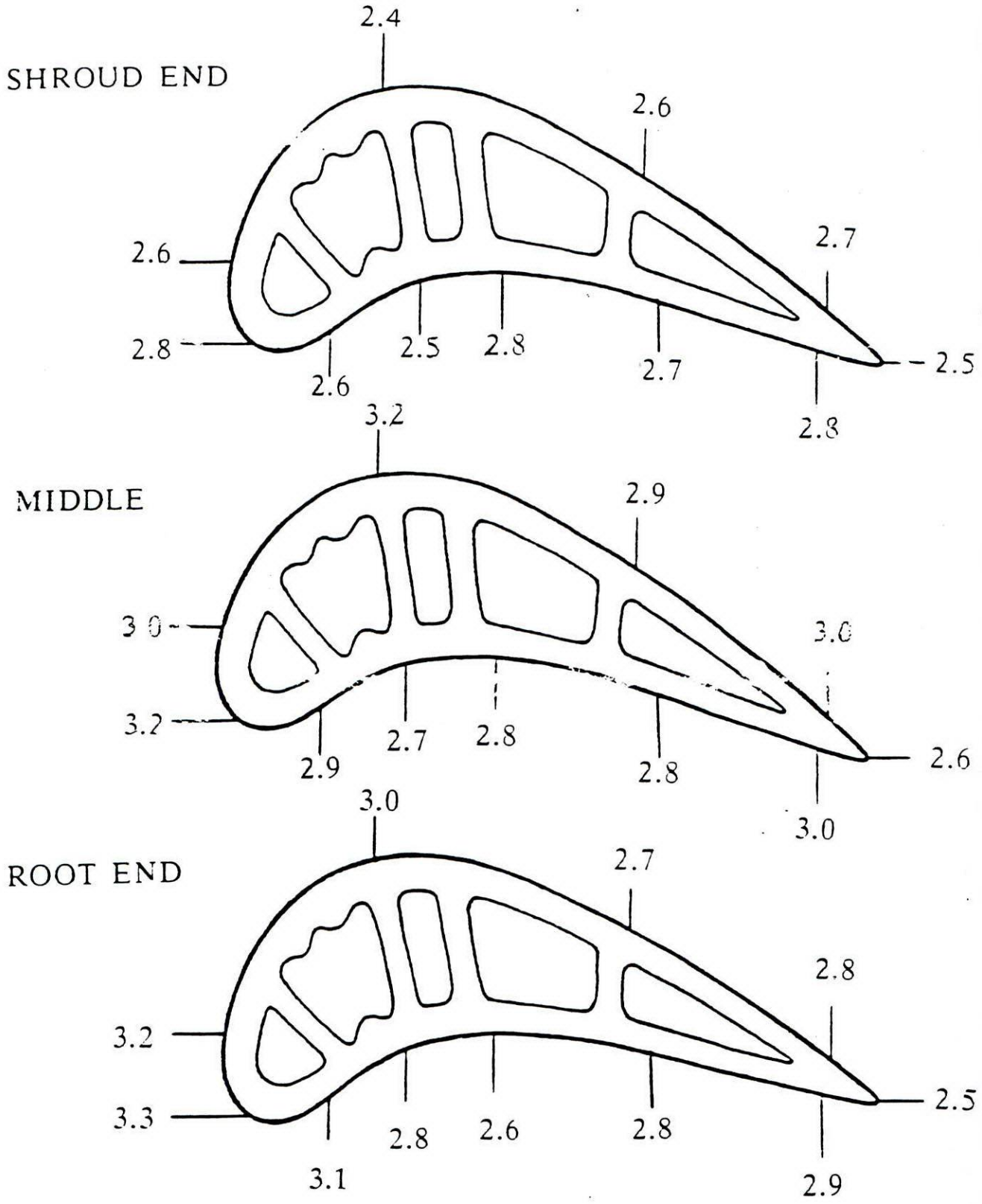

X0.001 I

CORROSION PROTECTION

Many evaluation programs have been carried out, covering the corrosion protection afforded by the I.V.D. process. Typically, these have included neutral salt spray, acidic salt fog, galvanic coupling, synthetic seawater tests and outdoor exposure. It is not my intention to reproduce the extensive data already published by McDonnell Douglas. However, the aluminum coating does tend to act sacrificialy, particularly on steels where the aluminum is anodic. In a recent salt fog trial, steel samples coated with I.V.D. aluminum exceeded 2,000 hours before showing signs of white corrosion. (Coating thickness 25 microns, Type I) A similar trial in seawater was also successful with the I.V.D. coating providing excellent corrosion protection (once chloride had formed on the surface).

Particularly important in most aerospace applications, is preventing galvanic corrosion from dissimilar metal contact. In a recent trial, I.V.D. coated steel reduced the corrosion rate of 7075 (alloy) when coupled and immersed in an aqueous environment. The 7075 alloy acts as the anode in the galvanic cell.

It can be concluded that I.V.D. aluminum does provide equal and in many cases, better corrosion protection than Cadmium in aqueous environments. The degree of protection depends on coating thickness and the level microporosity. Corrosion protection is increased still further with the addition of a chromate topcoat and in many cases, a barrier coat (paint).

Table II

MIL-C-83488

Class	Thickness	Salt Spray In Hours	
		Type I	Type II
Class 1	25 Microns	504	672
Class 2	12.5 Microns	336	504
Class 3	7.5 Microns	168	336

Type I: without chromate conversion
Type II: with chromate conversion

MECHANICAL, FATIGUE PROPERTIES

Since the Ion plating process has no possibility of evolving free hydrogen, it is not necessary to perform lengthy embrittlement relief cycles after coating (typical in the more conventional coating techniques). This has also been the major factor in reducing the problems of stress corrosion cracking. McDonnell Douglas reported no signs of post hydrogen embrittlement or stress corrosion cracking of I.V.D. aluminum coated parts in over 12 years of field service experience. (Ref: Note 1)

The excellent bonding of the coating at the coating/substrate interface and tight knit columnar structure help reduce problems with fatigue. This graded interface has also been important in reducing problems associated with differences in the coefficient of expansion between the coating and the substrate. Also important is the relatively low substrate temp during the coating cycle with typical temp ranging from 90-150 degrees Fahrenheit.

Table III

Effect of IVD Aluminum Coating on Substrate Fatigue Properties

Company	Substrate	Fatigue Test	Effect on Fatigue(a)
Pratt & Whitney (Ref. 27 & 36)	8-1-1-Titanium	High Cycle	None
	6-4-Titanium	High Cycle	None
	410 Steel	Peak Strain	Slight-Same as Nickel-Cadmium
Westinghouse (Ref. 28)	A276 Steel	20 KHz	None
	A276 Steel	20 KHz	
	403 Stainless Steel	20 KHz	
SPS Technologies (Ref. 32)	Steel	Tension-Tension	Slight-Same as "Bright" Cadmium
McDonnell Douglas (Ref. 60)	2024 Aluminum Alloy	6g Symmetric	None
Turbine Support (Ref. 61)	Steel	High Cycle	None

(a) "None" - Less than 3 percent reduction
"Slight" - Less than 5 percent reduction

Table IV

Tension-Tension Fatigue Test of IVD Aluminum and Cadmium Finished Fasteners

Bolt Description (a) and Test Loads	Cycles to Failure (b)		
	Bare	IVD	Cadmium
MS21250-04-018 per MIL-B-8831	135,400	173,000	83,000
Alloy Steel	102,000	109,400	114,000
(Maximum Load - 3,210 lb.	72,200	107,700	125,000
Minimum Load - 321 lb.)	118,800	90,400	128,000
	178,600	102,100	123,000
Average	121,500	116,520	114,600

(a) NAS 1271-16 alloy steel fasteners
(b) Test method - MIL-STD-1312, test no.1 - speed 8,000 cycles per min.

TORQUE / TENSION

The aerospace fastener industry have always been concerned with the problems associated with the installation of I.V.D. coated fasteners. Over the years, this led to the development of aluminum/teflon paints, particularly for application on interference fit fasteners.

Typically, a higher torque is required to install an aluminum coated fastener (versus Cadmium), due to it's higher coefficient of friction. However, this can be greatly overcome using a retyl alcohol lubricant. Applied after the I.V.D. process, McDonnell Douglas reported a 70% reduction in torque required for a given tension load. (Ref: Note 1)

I.V.D. coated fasteners have been in service now for nearly 12 years with very few reports of any serious problems. Indeed, for most parts, the addition of a lubricant has been sufficient, without a need to change installation procedures, tools or hole sizes.

APPLICATION

The larger percentage of business is still in the aerospace sector, divided between commercial and military contracts. I.V.D. still dominates a large sector of the aerospace fastener industry and existing McDonnell Douglas contracts (large wing foils and landing gear, etc.), including various large missile contracts.

Currently, I.V.D. and paint is the prime coating used on all the integral components for the Patriot, Amraam and Lantirn projects, one of the growing areas of business for I.V.D.. Over the last 2 to 3 years, there has been less demand for the I.V.D. coating on fasteners, mainly due to the introduction of the aluminum/teflon paints. Costs and ease of application have been the main factors behind this, rather than technical problems associated with the I.V.D. coating.

More specialized area's include ferrite assemblies (part of a phased array radar system - Patriot) coated with I.V.D. aluminum for wave guide purposes. This has also been applied and proved successful in a similar wave guide set-up used in microwaves. The excellent electrical characteristics (conductivity) exhibited by the I.V.D. aluminum coating has been utilized for electrical bonding purposes and more recently for EMI, RFI shielding. This has led to the most recent development of the I.V.D. process, the coating of plastic/composite materials.

When combined with a barrier coat (paint), I.V.D. has provided both shielding and corrosion protection on a variety of electronic assemblies. Adhesion between the coating/ substrate interface on a plastic/composite material is not the same as a metallic substrate. However, by applying Faraday's law, the author has managed to achieve better bonding on the substrate/coating interface on non-conductors by accelerating the charged particles through a screen. However, these high energy Ion's can damage the substrate, hence, the time of gas cleaning and voltage have to be controlled closely. Work carried out between the Author (B. Nevill) and A. Rashidi (Boeing) on compressed moulded gloss epoxy (1/10" thick) yielded a coating capable of passing a zone 1a lightning strike test. (A primer and urethane base coating was also applied).

Other composite materials (particular fibre wound, yielding partial conductivity) were successfully coated for EMI, RFI purposes. In this case a screen was not used, but great care had to be given to substrate temperature and the pressure in the chamber, otherwise problems with outgassing, delamination and cracking of the substrate material would occur. With only a fine tuning of the process required, the I.V.D. coating of plastics/composites is fast becoming a developing market for the I.V.D. process.

One other successful development over the last 5 years was the coating of permanent magnets using the I.V.D. aluminum process. Since the mid 70's, the predominant material used for the production of permanent magnets was samarium cobolt. However, in the early 80's, a new rare earth based material was introduced, namely NdFeB (Neodymium Iron Boron). This proved to be a cheaper and more powerful source of magnetic energy, however, one of the main disadvantages of this material (NdFeB) was its poor corrosion resistance, particularly in humid or corrosive environments. Standard plating techniques were not suitable, since hydrogen evolved on the surface of the magnet and resulted in a breakdown of the alloy surface and, hence, a poorly adhered coating layer. Also a reduction in the magnetic properties of the material (BH, max.).

Tests carried out by two leading magnet manufacturers showed excellent results for the I.V.D. aluminum in both climatic and corrosive environments. With no hydrogen evolved in the I.V.D. process, excellent adhesion was achieved, yielding a thin uniform coating. This was advantageous, since it minimized air gaps in the magnetic circuit.

A more recent development was the combination of ivadizing and hot isostatic pressing (hipping) as a possible alternative to the more conventional aluminizing process (pack cementation) used on turbine blades. Initially this was isolated to the large blades (LP Blades) for economic reasons. Tests carried out with a leading turbine blade manufacturer concluded that the final diffused coating, produced on a directionally solidified material (MarMoo2) utilizing the IVD/HIP process, did yield a coating of comparable thickness, structure and composition to the present aluminizing process. However, this is still in the development stage with more work necessary to make the IVD/HIP process more viable both technically and commercially.

CONCLUSION

The IVD aluminum coating (ivadizing) has proven itself both in the field and in the test laboratory as a viable alternative to Cadmium.

Development over the last 5 years have proven the versatility of this coating, leading to even greater possibilities for this process.

With more and more demanding applications and an even more need for a safer, cleaner environment, design engineers should not overlook the I.V.D. (aluminum) process.

REFERENCES

Note 1
D.E. Muehlberger and J.J. Reilly - The substitution of IVD Aluminum for Cadmium, October 1988.

Figure (1)
Prepared by MMA Laboratories, California.

Figure (2), Tables I,II,III,IV
Produced by kind permission of McDonnell Douglas Aircraft Company.

Figure (3)
J. Higgins - Evaluation report of the IVD/HIP process. Rolls Royce, Derby, England.

TRENDS IN PRECIOUS METAL PLATING WITHIN THE CONNECTOR INDUSTRY

KEN FLECK, PRESIDENT
FLECK INTERNATIONAL
16400 PACIFIC COAST HWY., SUITE #217, HUNTINGTON BEACH, CA 92649
TEL 310-592-9000 — FAX 310-592-4101

Introduction

Contacts are the "heart" of electronic connectors. The purpose of this paper is to discuss the critical role of coating systems for connector contacts.

The major reason for contact coatings is to provide reliability over the intended life of the connector. To provide this reliability is an exercise in balancing the characteristics of various coating systems to provide:

- Minimum electrical contact resistance
- Wear resistance (e.g., as a function of the insertion/withdrawal cycles)
- Corrosion resistance
- Cost effectiveness

Coatings may be described by the following categories:

- Types of metal coatings

  Precious
  - Gold and gold alloys
  - Silver
  - Platinum group metals
  - Others

  Non-precious
  - Nickel
  - Tin
  - Tin-lead (solders)
  - Others

- Methods of Application
  - Hot Dip (for tin and tin-lead)
  - Electroless (nickel)
  - Electroplating
  - Clad/Inlay metals (for both precious and non-precious metals)

- Processing Methods
  - Barrel plating
  - Reel-to-reel plating

Total Units of Contacts

There were 139.8 billion units of contacts utilized within the U.S. connector industry in 1991.

The top 4 product line categories account for 90% of the units of contacts utilized in the U.S. Contacts utilized in printed circuit connectors account for 34% of all contacts. Contacts utilized in rectangular I/O connectors account for 18%. Contacts utilized in IDC connectors account for 14%. Contacts utilized in IC sockets account for 24% of the U.S. total.

	1991 Units (Billions)
Printed Circuit	47.8
Rectangular I/O	25.1
IDC	19.1
IC Socket	34.0
Other	13.8
Total	139.8

The balance, or Other category, represent contacts press-fit in the backpanel, posts utilized in backplanes, automotive connectors, RF coax, circular connectors, and fiber optic connectors.

Survey Of Contact Coatings

An extensive industry-wide survey at the OEM and manufacturer's level, was conducted for the purpose of assembling data for this paper.

The data to follow in this paper will describe the results of this survey.

This paper will be divided into 4 sections. These sections are:

1. Contact Coatings For Printed Circuit Connectors
2. Contact Coatings For Rectangular I/O Connectors
3. Contact Coatings For IDC Connectors
4. Contact Coatings For IC Sockets

Contact Coatings for Printed Circuit Connectors

There are 19 technology trends impacting the design and use of printed circuit connectors. These are:

Trend #1: Increased Data Rate Speeds
Trend #2: Increasing High Pin Count Populations Required As Pins Per Board Increase
Trend #3: Low Pin Count 2.0mm Connectors — Applications Accelerating
Trend #4: Exploding IC Card/Memory Card/PC Card Applications
Trend #5: Emergence of Hard Metric Connectors In Computer/Telecom
Trend #6: Bus Architectures — Impact Printed Circuit Connector Designs
Trend #7: Futurebus+ Systems For Advanced-Performance Computers
Trend #8: Futurebus+ Selected the 2.0mm
Trend #9: Military Version of Futurebus+
Trend #10: Alliances Between Manufacturers and OEMs
Trend #11: Development and Manufacturing Frequently Occurring In the U.S.
Trend #12: Combus — Standard Communications Bus for SONET Applications
Trend #13: 2.5mm Selected By Combus
Trend #14: PC Board Sizes and Pin Counts Increasing
Trend #15: Pin Sizes and PTH Becoming Smaller
Trend #16: Normal Contact Force — A Controversial Issue
Trend #17: Higher Density — Half Pitch
Trend #18: Trends Driving One-Piece Cardedge Connectors
Trend #19: SMT PC Connectors and Robotics Pick-and-Place Increasing

Additionally, there are 12 technology trends impacting the design and use of backpanels. These are:

Trend #1: Standard Backplanes
Trend #2: Custom Backplanes
Trend #3: Increased Data Rate Speeds
Trend #4: Bus Architectures — Driving Force for Backplanes
Trend #5: Futurebus+ Systems For Advanced-Performance Computers
Trend #6: Emergence of Hard Metric Connectors In Computer/Telecom
Trend #7: Military Version of Futurebus+
Trend #8: Combus — Standard Communications Bus for SONET Applications
Trend #9: PC Board Sizes and Pin Counts Increasing
Trend #10: Increasing High Pin Count Populations Required As Pins Per Board Increase
Trend #11: Futurebus+ Selected the 2.0mm
Trend #12: 2.5mm Selected By Combus

47.8 Billion Units Of Printed Circuit Contacts

Printed Circuit Leads	Gold 100 u in.	Gold 50 u in.	Gold 30 u in.	Gold 20 u in.	Gold 10 u in. & under	Silver Over 200 u in.	Rhodium & Palladium	Tin	Others Ni or None	Total Leads (Billion)
Gov't/Military	0.54	7.73	1.68			0.64	0.83			11.42
Communication		0.54	4.32	3.43	1.71	0.32		1.12		11.44
Computer Peripherals			0.40	1.22	6.69			2.44		10.75
Computer (Mainframes)		0.18	2.48	1.59	0.85	0.21				5.31
Instrumentation	0.18	1.07	0.99			0.74		0.22		3.20
Consumer			< 0.01	< 0.01	0.13	0.21		1.45	< 0.01	1.79
Machinery			0.20					1.33	0.21	1.74
Transportation			0.10			0.11		0.67		0.88
Industrial	0.09	0.27	0.20			0.11		0.12		0.79
Business/Retail/Education			0.10	0.13	0.13		< 0.01	0.12		0.48
TOTAL LEADS PLATED	0.81	9.79	10.47	6.37	9.51	2.34	0.83	7.47	0.21	47.80

To follow is a pie chart showing total printed circuit leads by demand sector.

Each demand sector is then broken down by plating type with a pie chart for each.

Printed Circuit Leads

Total Leads (Billions)

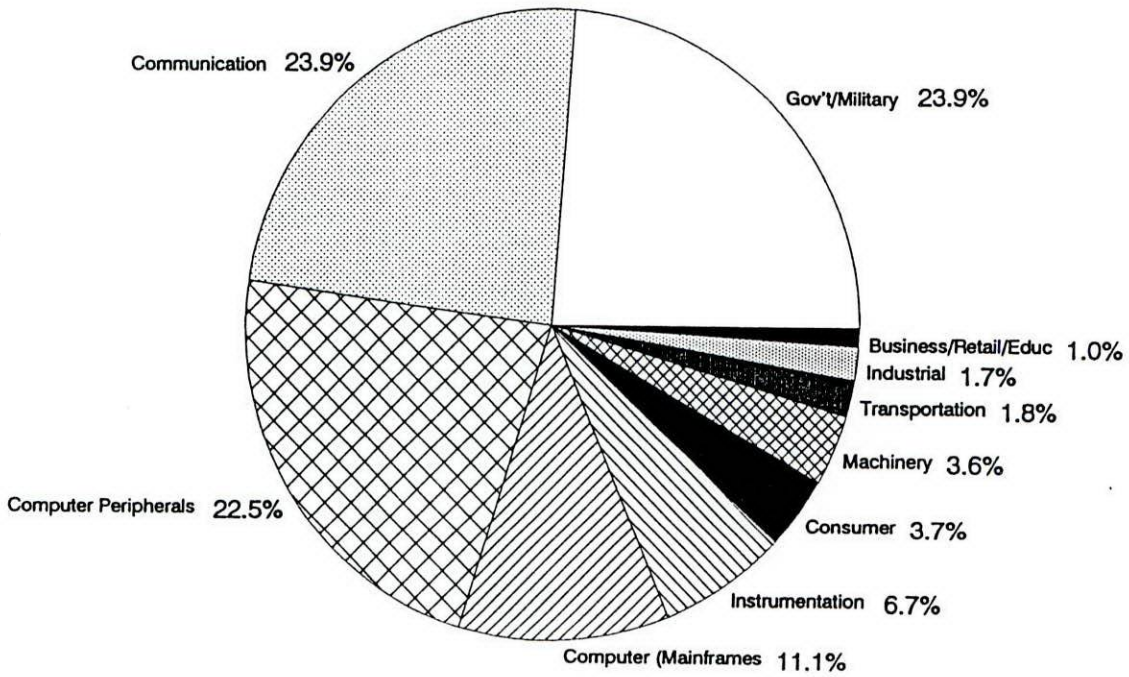

Printed Circuit Leads

Government/Military

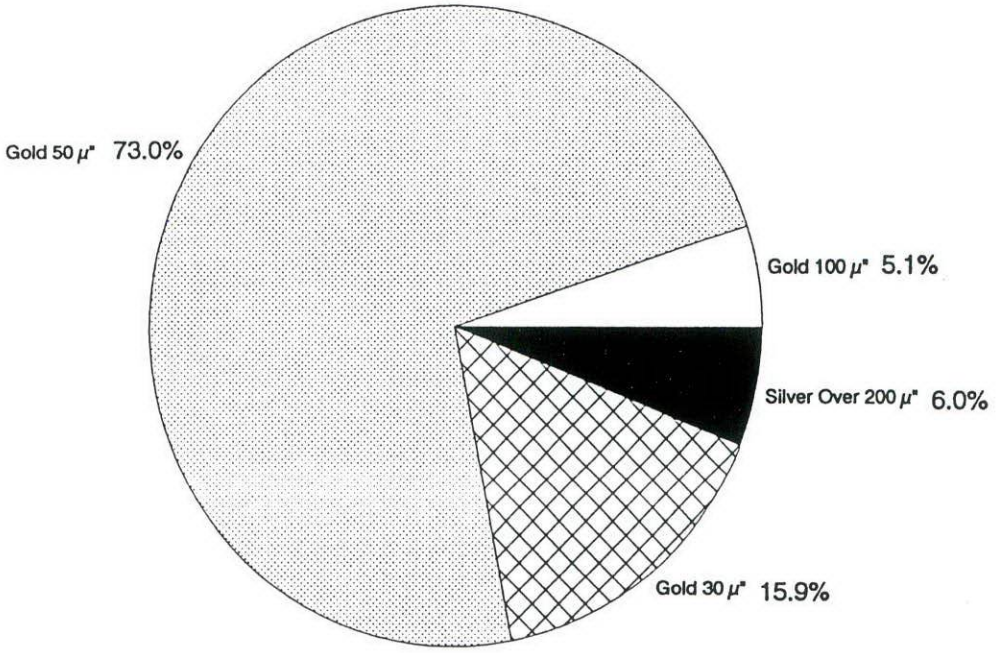

Printed Circuit Leads

Communication

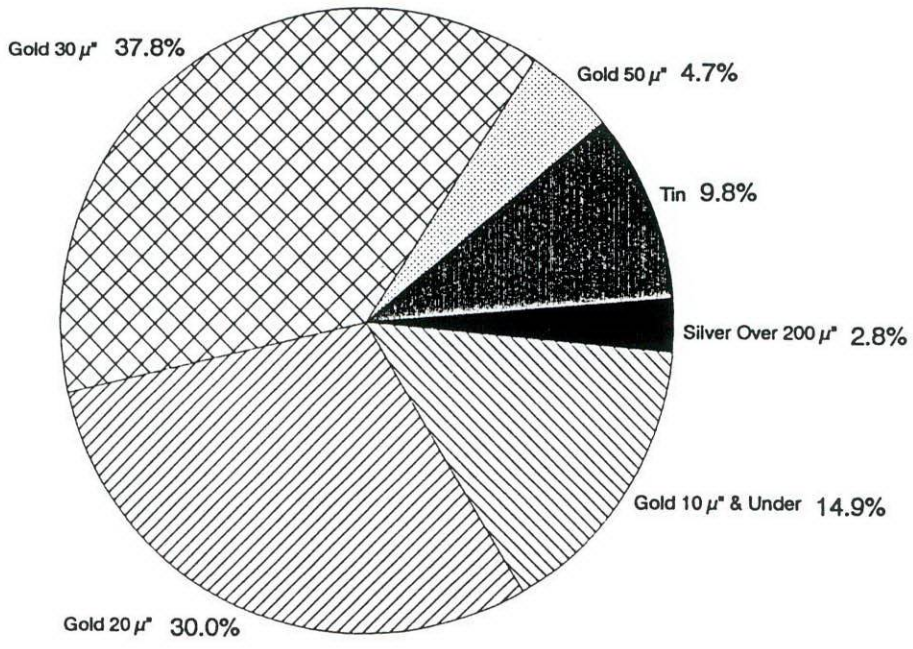

Printed Circuit Leads

Computer Peripherals

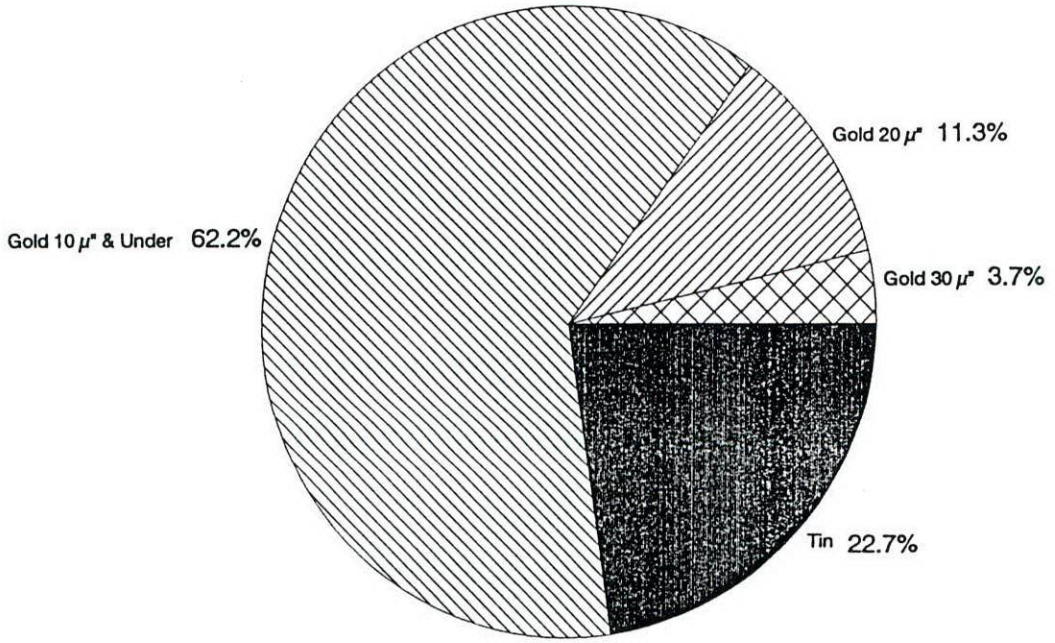

Printed Circuit Leads

Computer (Mainframes)

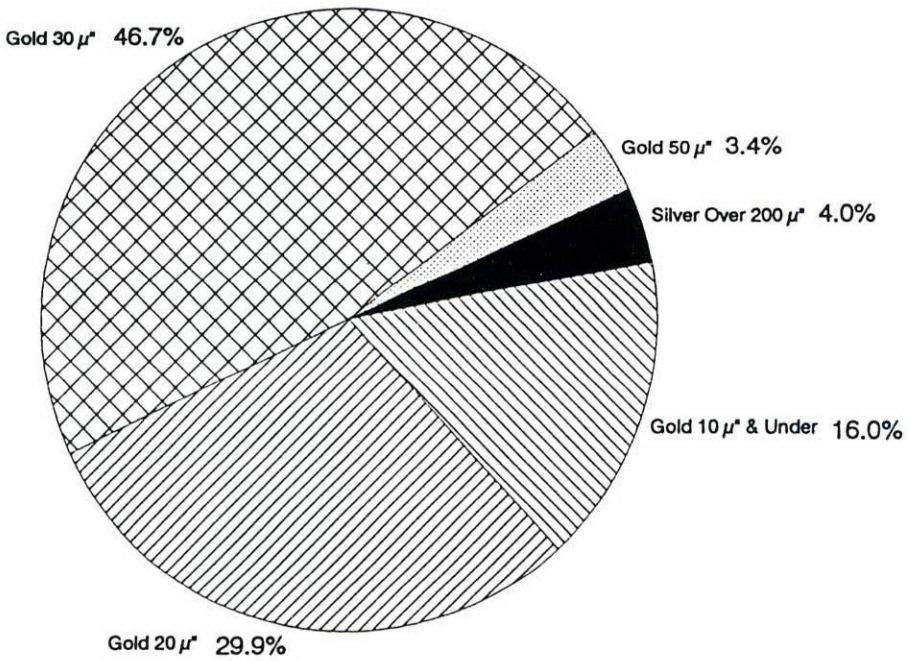

Printed Circuit Leads

Instrumentation

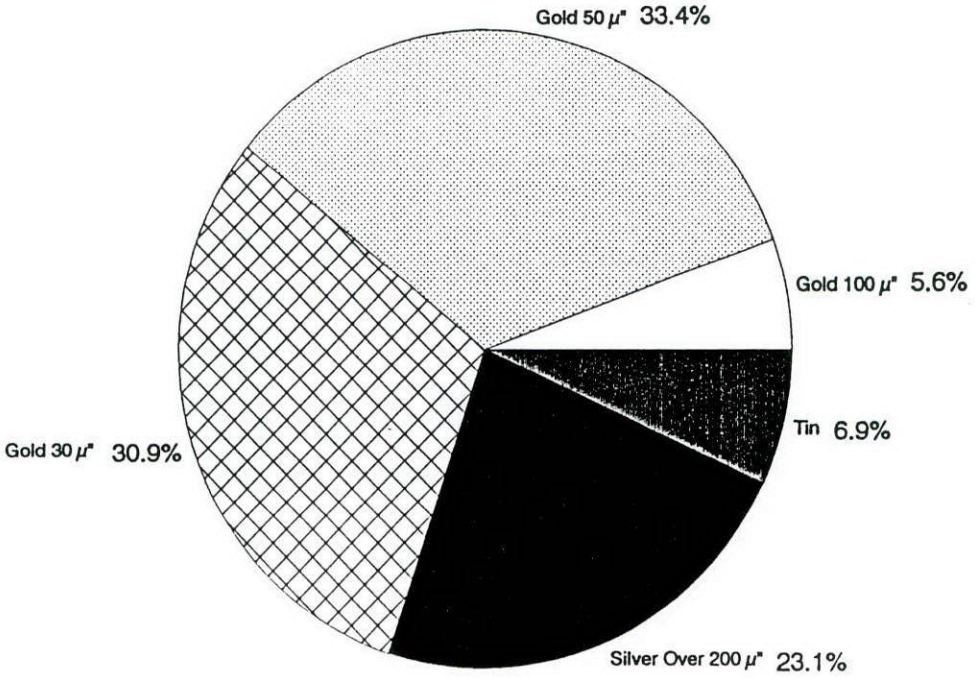

Printed Circuit Leads

Consumer

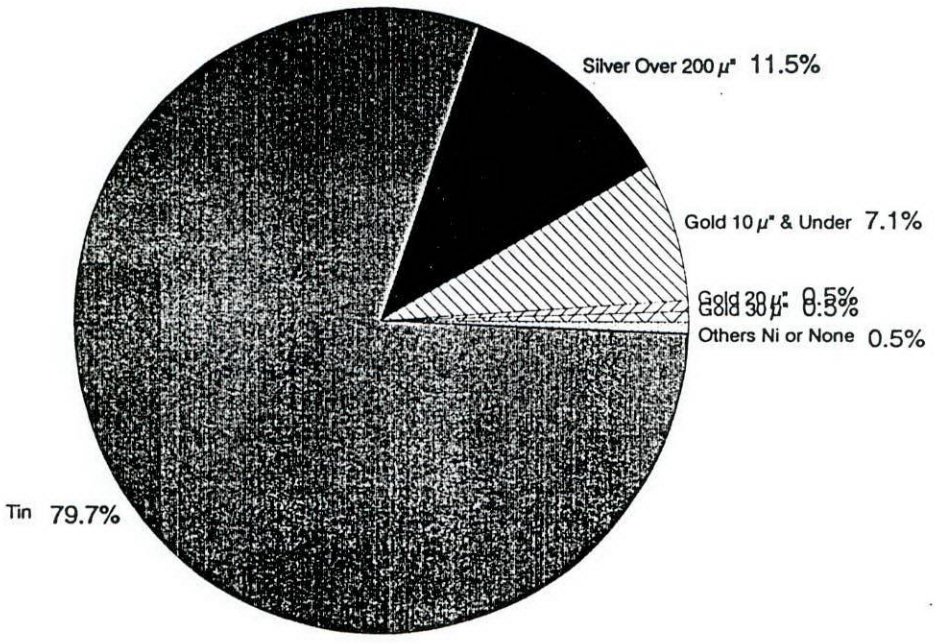

Printed Circuit Leads

Machinery

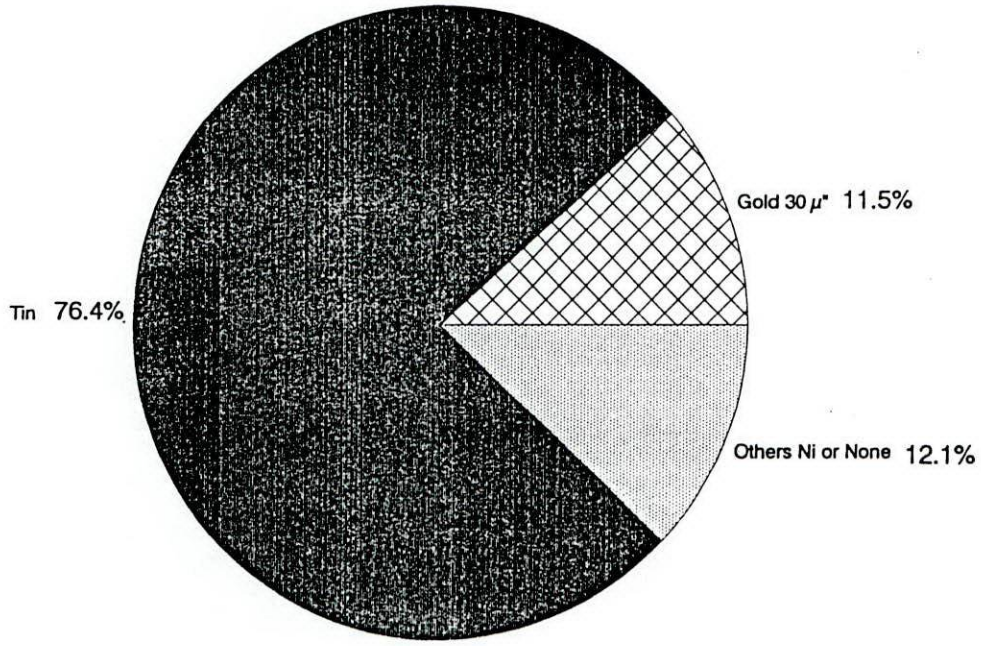

Printed Circuit Leads

Transportation

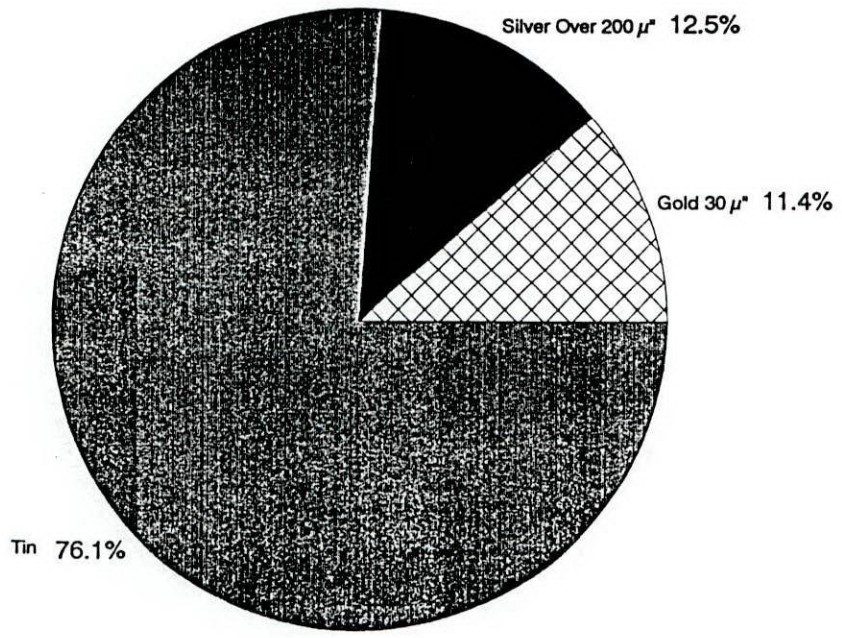

Printed Circuit Leads

Industrial

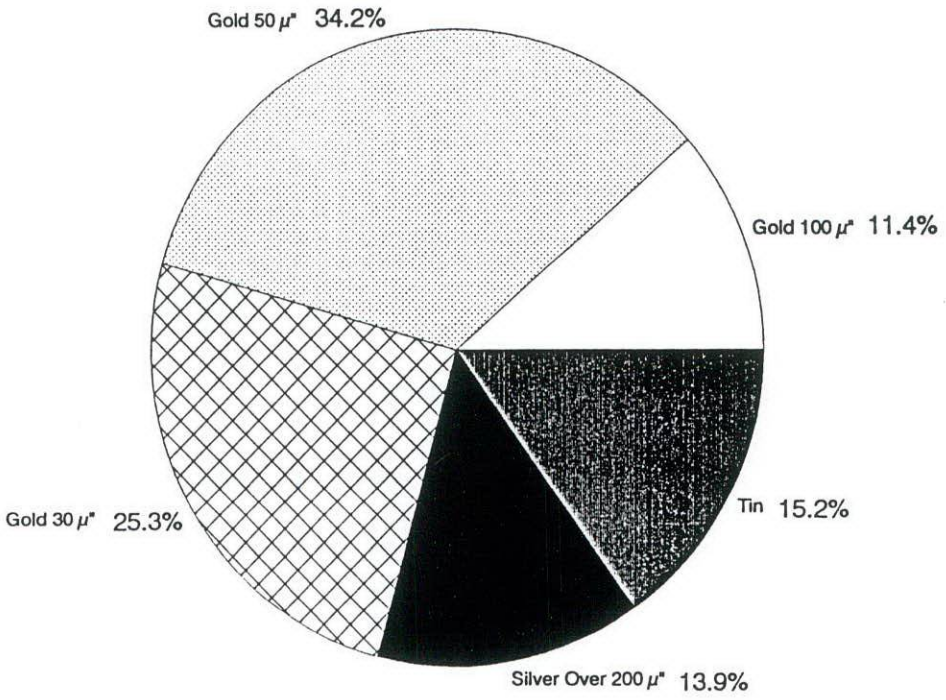

Printed Circuit Leads

Business/Retail/Education

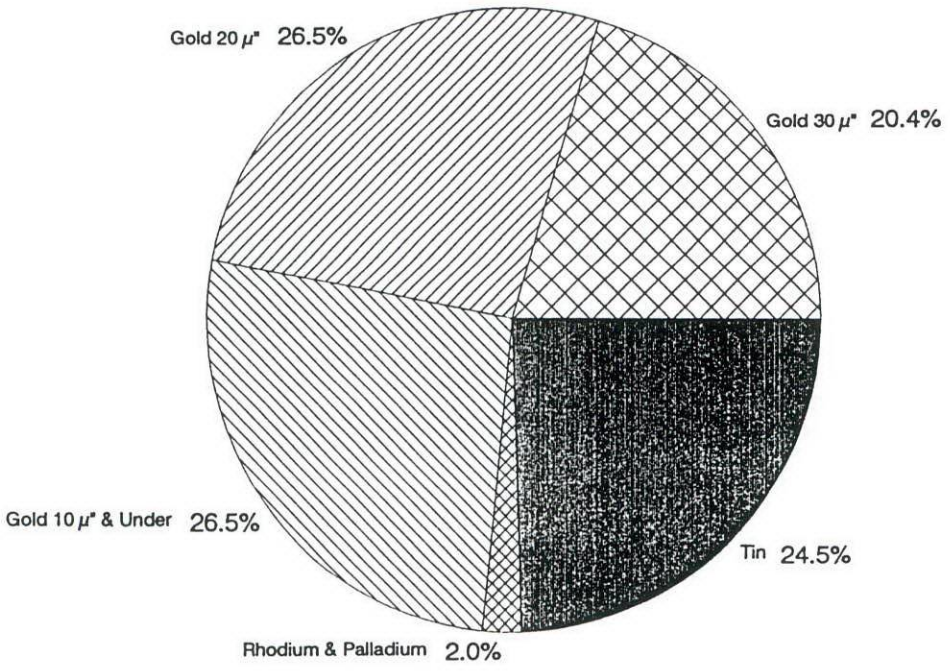

Contact Coatings for Rectangular I/O Connectors

There are 12 technology trends impacting the design and use of rectangular I/O connectors. These are:

Trend #1: Computer Systems Trends Driving High Growth for SCSI Connectors
Trend #2: SCSI I Usage Will Decline
Trend #3: SCSI II Demand to Accelerate
Trend #4: Demand for 3.5" Drives Pushing Aside the 5.25" Drives
Trend #5: Demand for 2.5" and 1.8" Drives Accelerating
Trend #6: De Facto SCSI III Standard
Trend #7: Other Computer and Data Interfaces Continue to Exist
Trend #8: D-Subminiature Is De Facto SCSI-I Standard
Trend #9: Ribbon I/O Connectors Continue Usage as Computer Interface
Trend #10: SMT I/O Connectors and Automated placement Increased to 17 Designs
Trend #11: Shift Away From .100x.100 Grid
Trend #12: Growth Rates Slowing on Many Micro Rectangular I/O Designs

25.1 Billion Units Of Rectangular I/O Contacts

Rectangular I/O Leads	Gold 100 u in.	Gold 50 u in.	Gold 30 u in.	Gold 20 u in.	Gold 10 u in. & under	Silver Over 200 u in.	Rhodium & Palladium	Tin	Others Ni or None	Total Leads (Billion)
Gov't/Military	0.18	2.61	0.56			0.19	0.24			3.78
Communication		0.23	1.83	1.29	0.61	0.12		0.42		4.50
Computer Peripherals			0.22	0.66	3.26			1.21		5.35
Computer (Mainframes)		0.08	1.15	0.72	0.28	0.09				2.32
Instrumentation	0.05	0.35	0.24			0.16		0.05		0.85
Consumer			< 0.01	< 0.01	0.03	0.09		0.80	< 0.01	0.92
Machinery			0.05					0.40	0.05	0.50
Transportation			0.78			0.78		4.34		5.90
Industrial	0.05	0.27	0.20			0.10		0.05		0.67
Business/Retail/Education			0.08	0.09	0.08	0.01	< 0.01	0.05		0.31
White Goods								0.80		
TOTAL LEADS PLATED	0.28	3.54	5.11	2.76	4.26	1.54	0.24	8.12	0.05	25.10

To follow is a pie chart showing total rectangular I/O leads by demand sector.

Each demand sector is then broken down by plating type with a pie chart for each.

Rectangular I/O Leads

Total Leads (Billions)

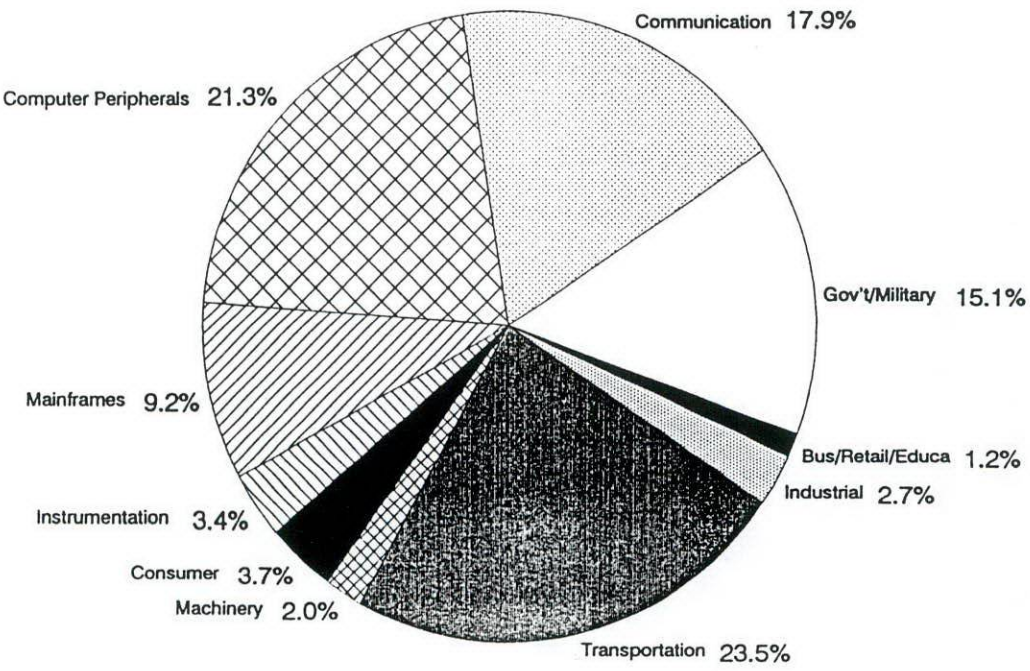

Rectangular I/O Leads

Government/Military

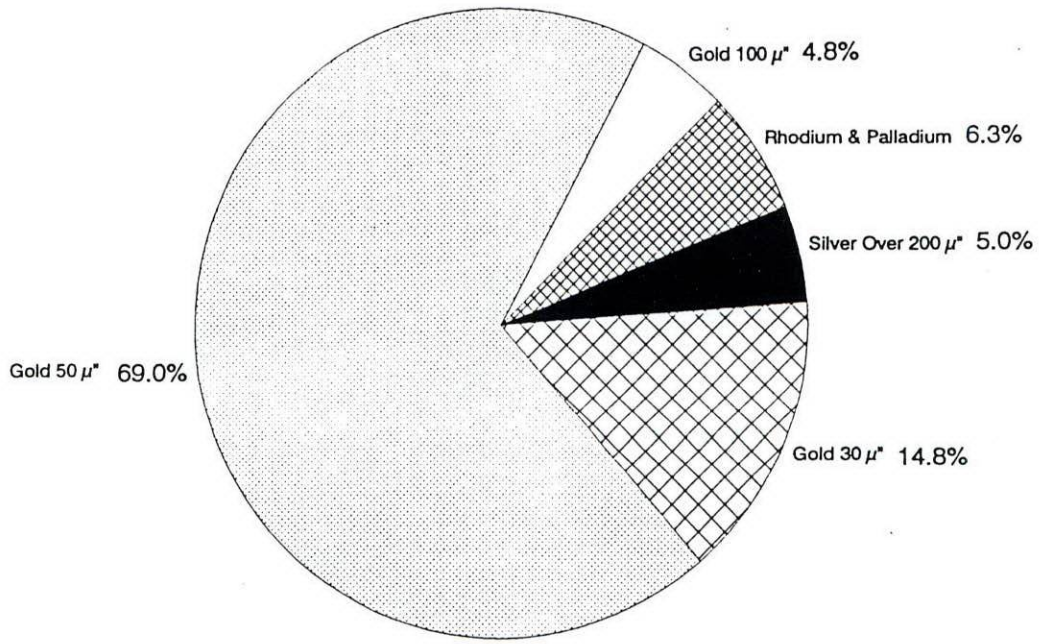

Rectangular I/O Leads

Communication

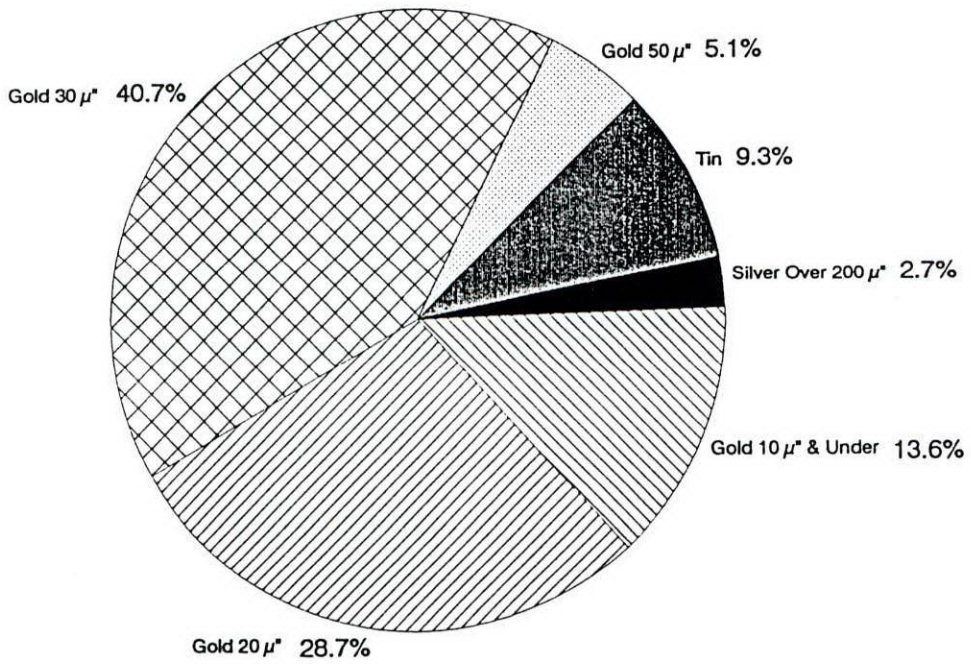

Rectangular I/O Leads

Computer Peripherals

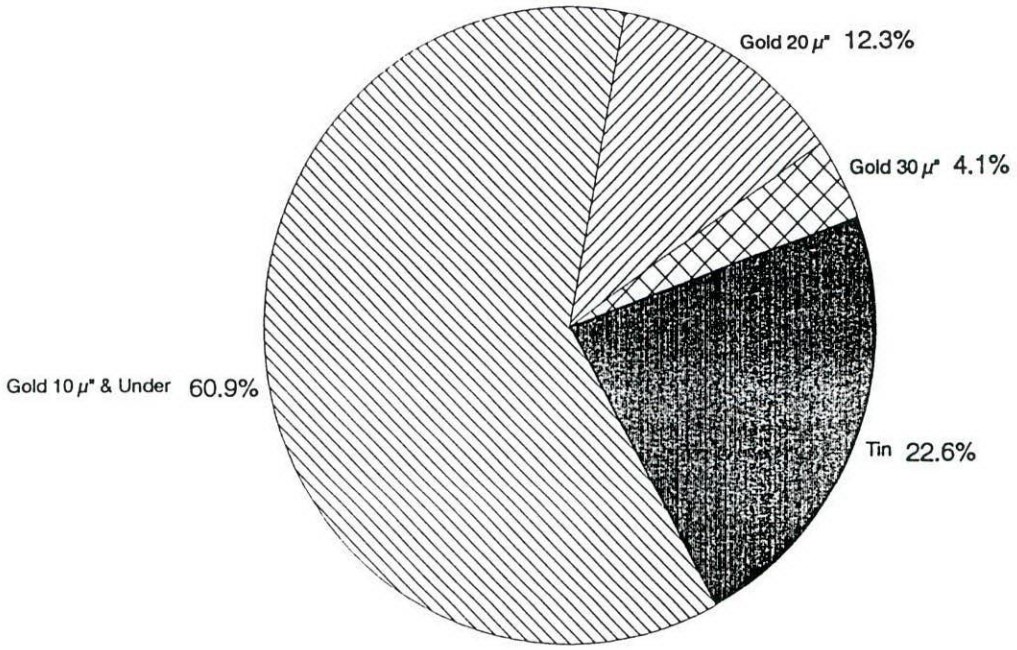

Rectangular I/O Leads

Computer (Mainframes)

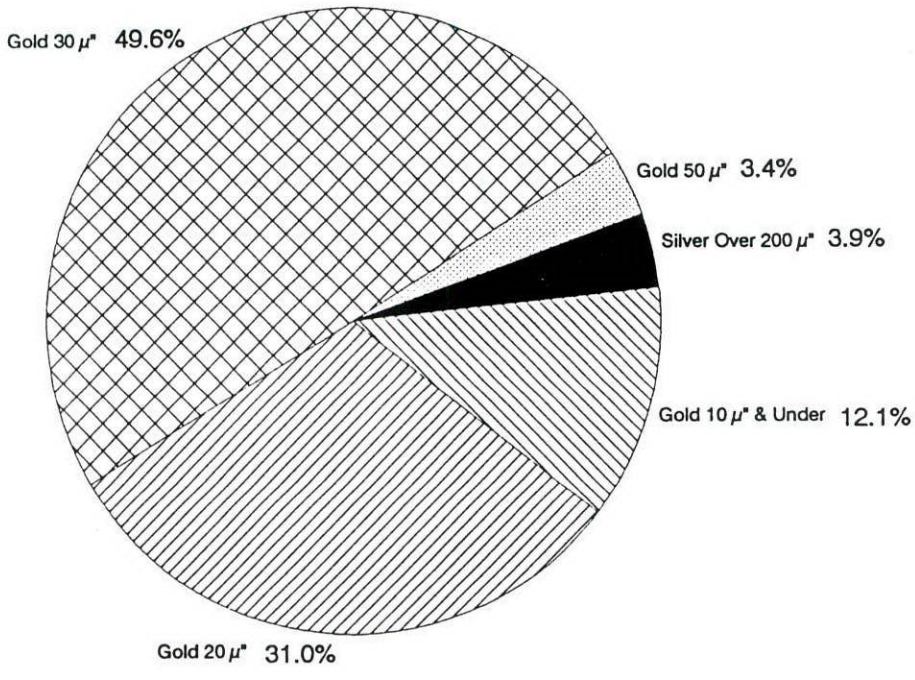

Rectangular I/O Leads

Instrumentation

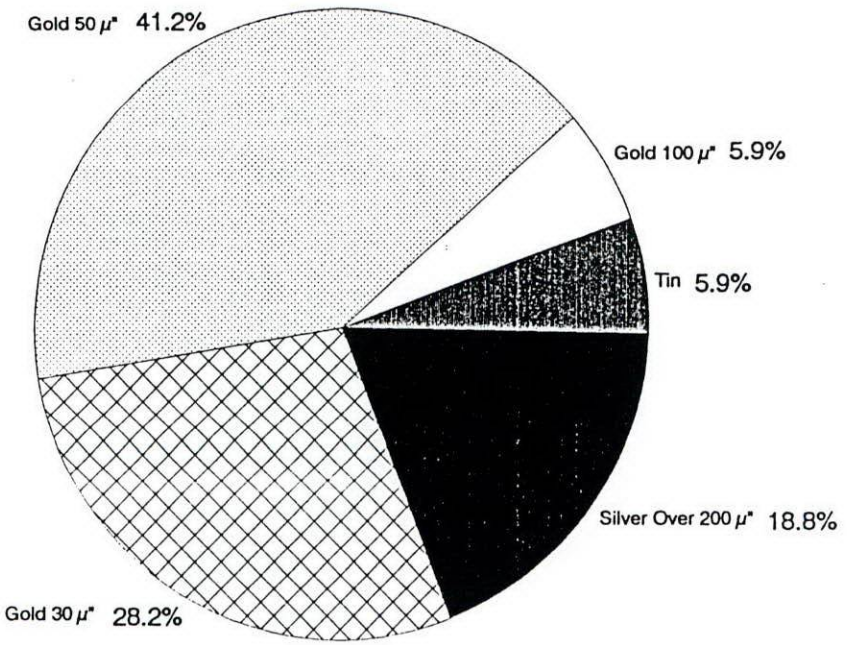

Rectangular I/O Leads

Consumer

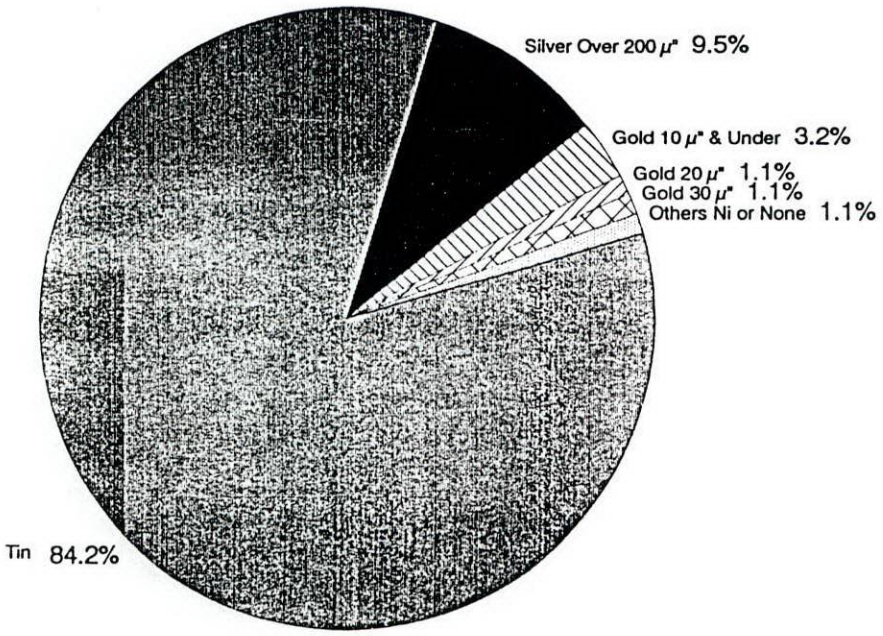

Rectangular I/O Leads

Machinery

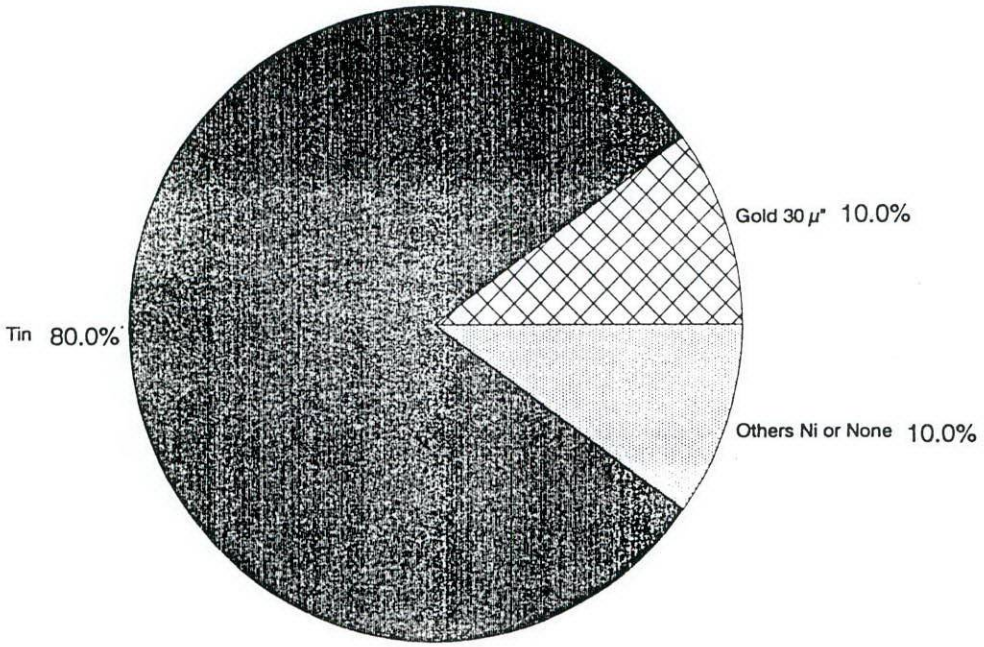

Rectangular I/O Leads

Transportation

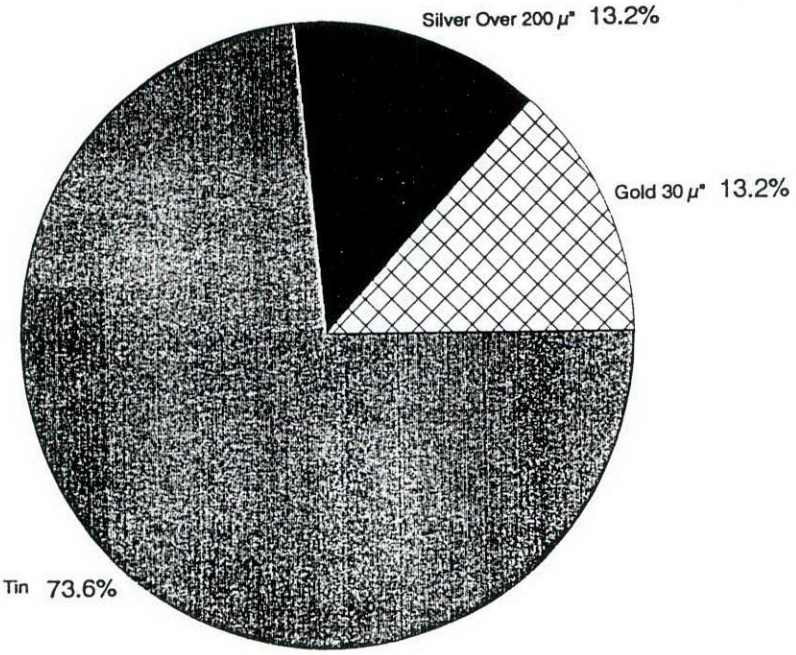

Rectangular I/O Leads

Industrial

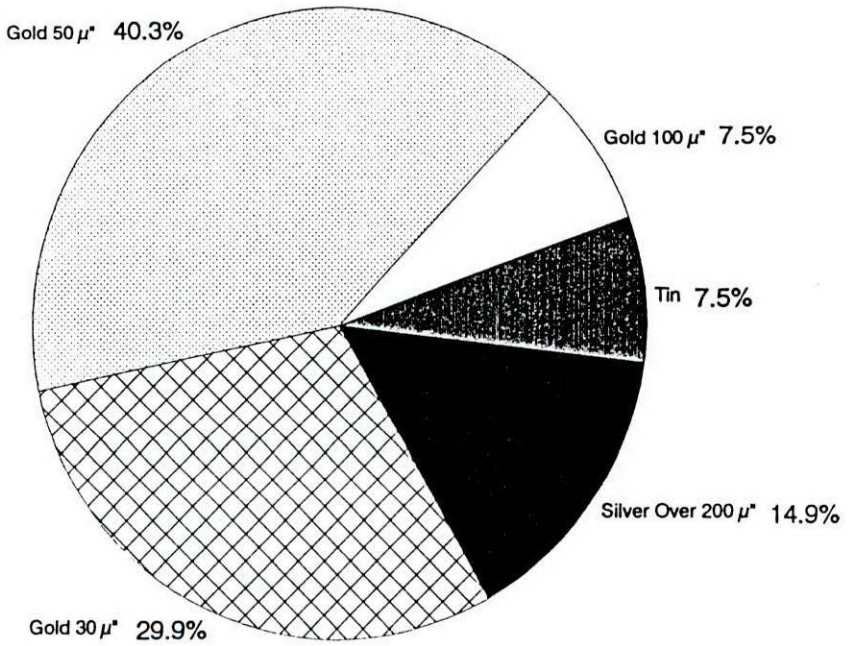

Rectangular I/O Leads

Business/Retail/Education

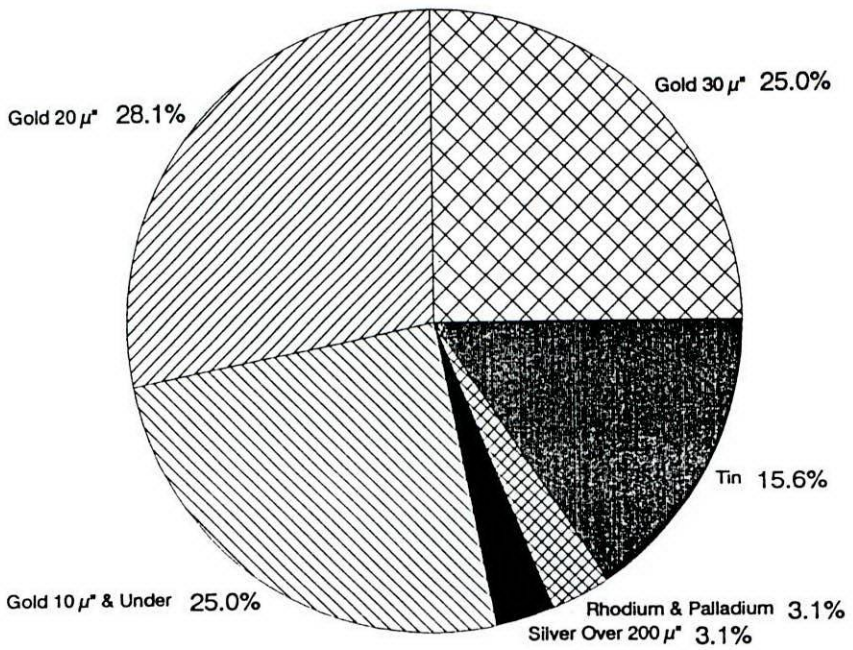

Contact Coatings for IDC Connectors

There are 4 technology trends impacting the design and use of IDC connectors. These are:

Trend #1: Increased Use of Planar/Ribbon Cable
Trend #2: Cost Advantage of Mass Termination
Trend #3: Computer Equipment — A Major Driving Force for IDC
Trend #4: Data Interfaces — Increasing Use of IDC

19.1 Billion Units Of IDC Contacts

IDC Leads	Gold 100 u in.	Gold 50 u in.	Gold 30 u in.	Gold 20 u in.	Gold 10 u in. & under	Silver Over 200 u in.	Rhodium & Palladium	Tin	Others Ni or None	Total Leads (Billion)
Gov't/Military	0.08	0.97	0.21			0.08	0.10			1.44
Communication		0.08	0.65	0.48	0.23	0.04		0.16		1.64
Computer Peripherals			0.33	0.92	4.70			1.85		7.80
Computer (Mainframes)		0.12	1.45	0.88	0.45	0.13				3.03
Instrumentation	0.16	0.97	0.89			0.60		0.19		2.81
Machinery			0.03					0.26	0.03	0.32
Transportation			0.02			0.02		0.16		0.20
Industrial	0.03	0.20	0.15			0.07		0.04		0.49
Bus/Retail/Edu			0.32	0.37	0.37	0.05	< 0.01	0.26		1.37
TOTAL LEADS PLATED	0.27	2.34	4.05	2.65	5.75	0.99	0.10	2.92	0.03	19.10

To follow is a pie chart showing total IDC leads by demand sector.

Each demand sector is then broken down by plating type with a pie chart for each.

IDC Leads

Total Leads (Billions)

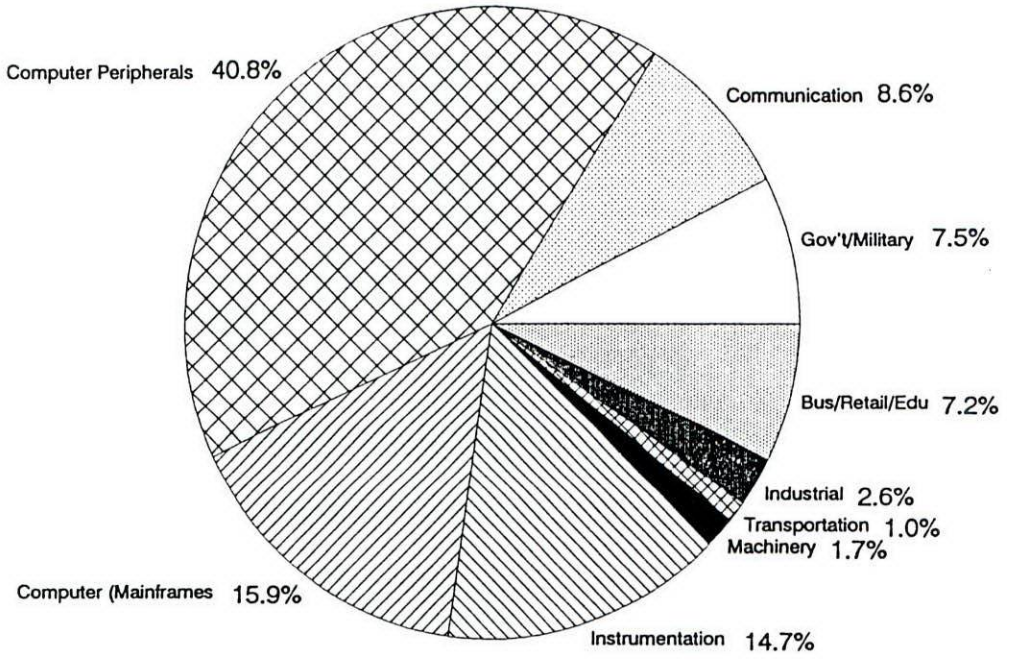

IDC Leads

Government/Military

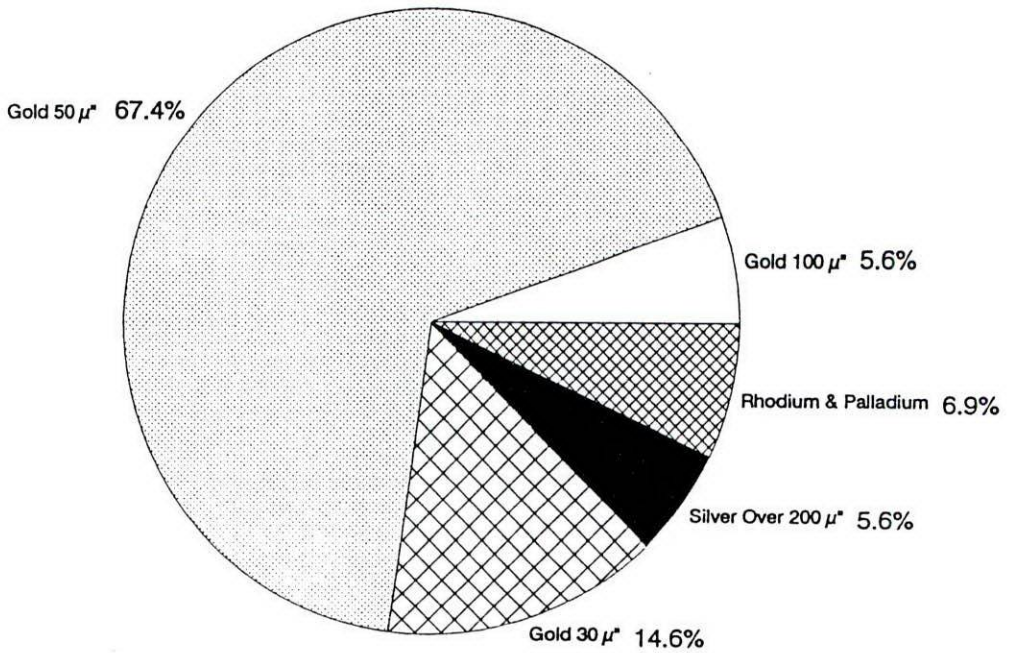

IDC Leads

Communication

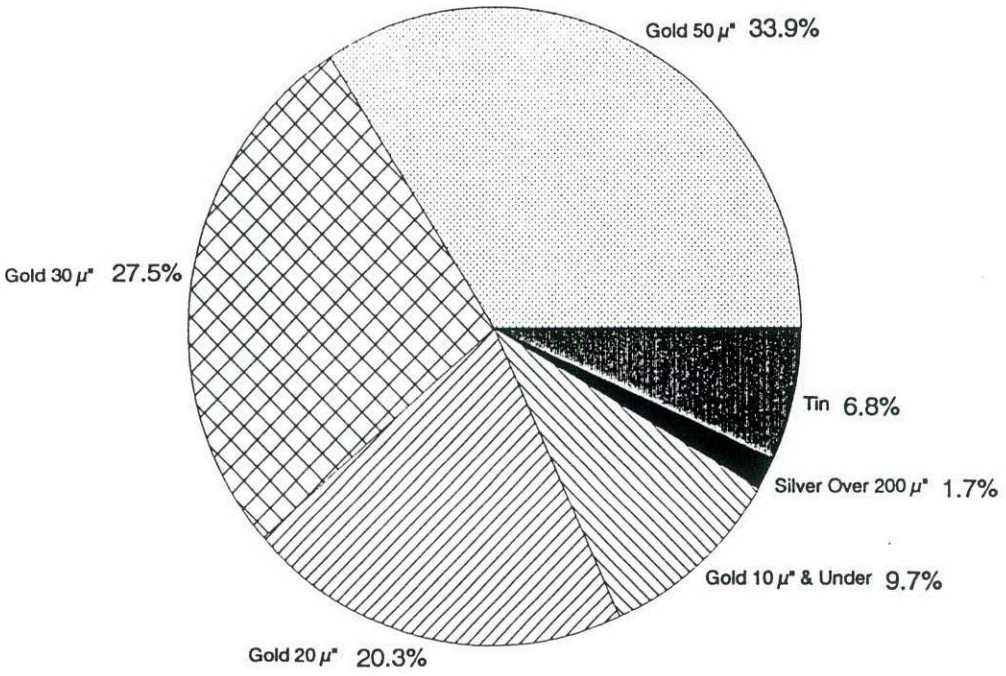

IDC Leads

Computer Peripherals

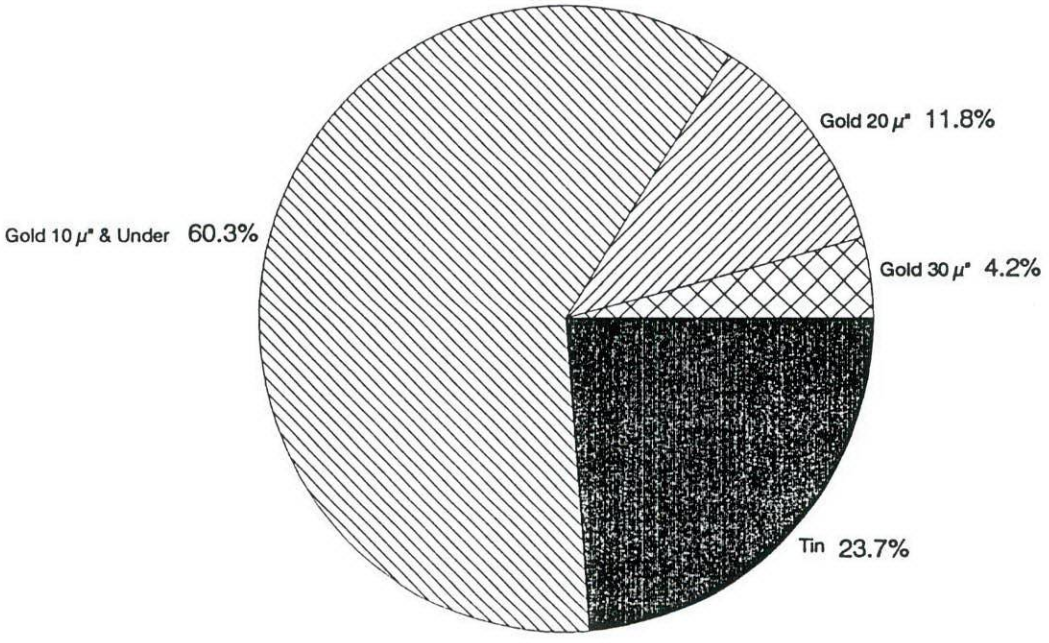

IDC Leads

Computer (Mainframes)

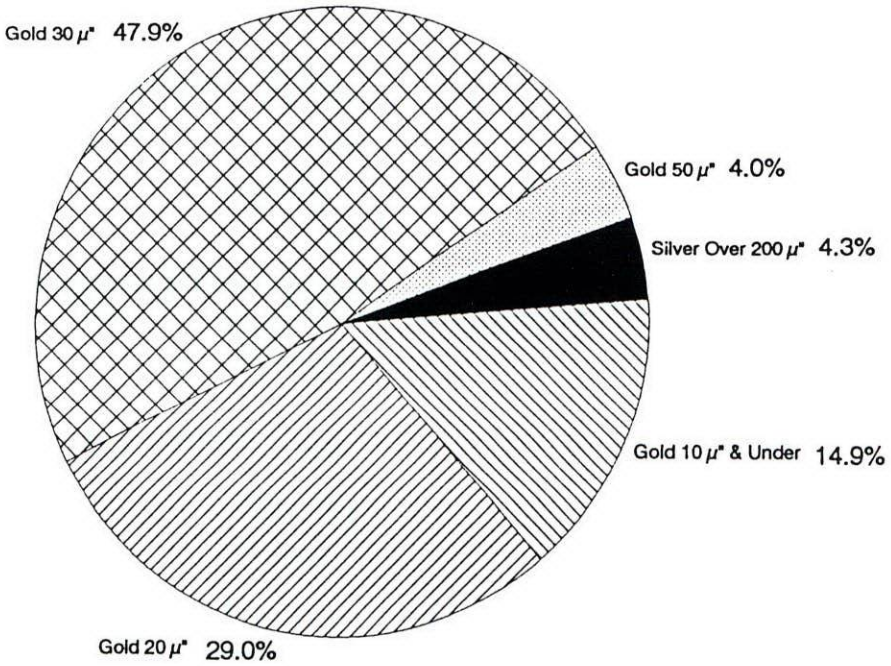

IDC Leads

Instrumentation

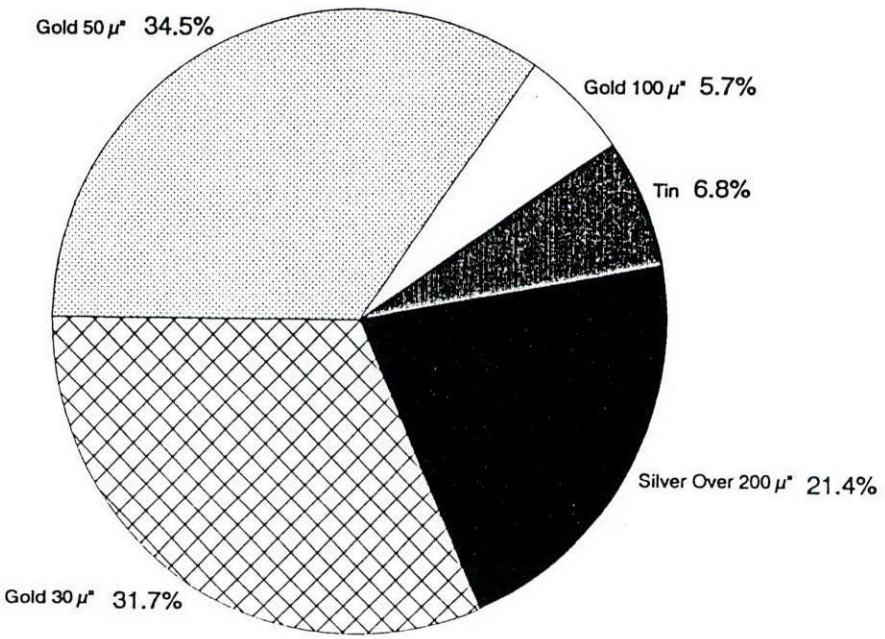

IDC Leads

Machinery

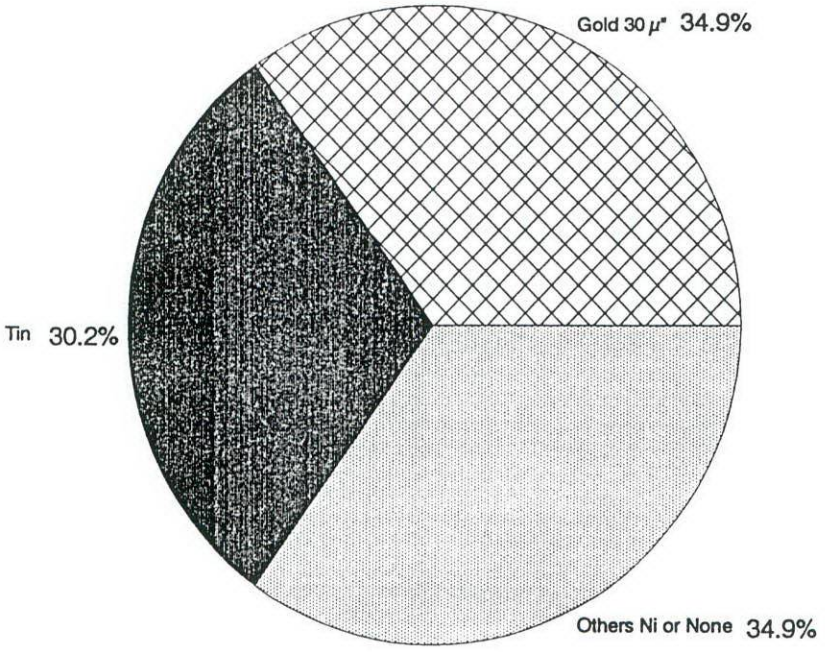

IDC Leads

Transportation

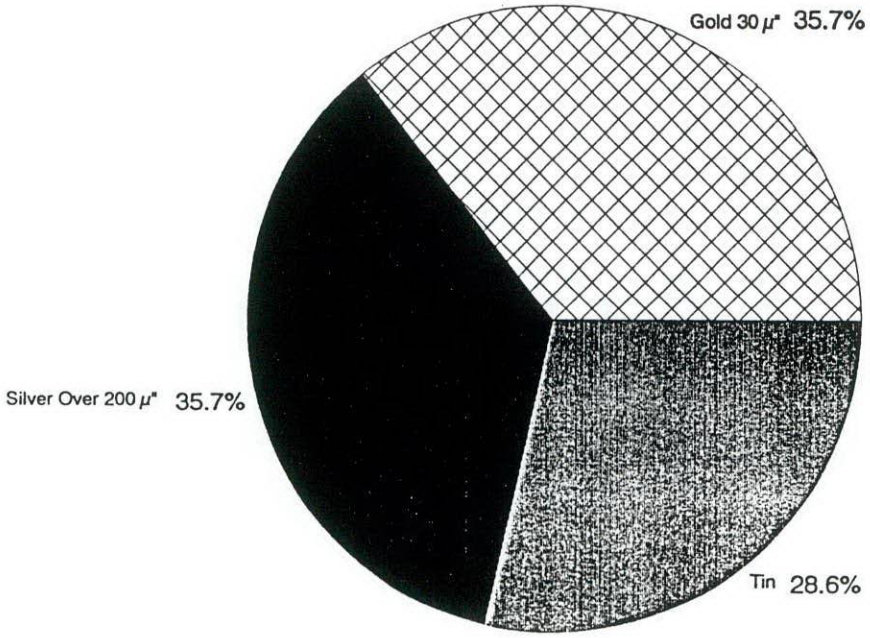

IDC Leads

Industrial

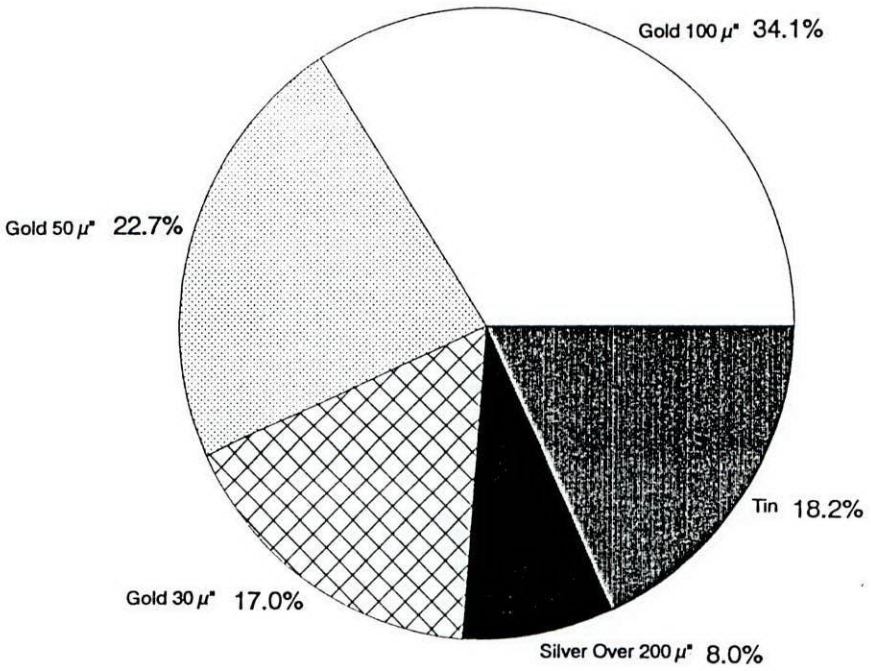

IDC Leads

Business/Retail/Education

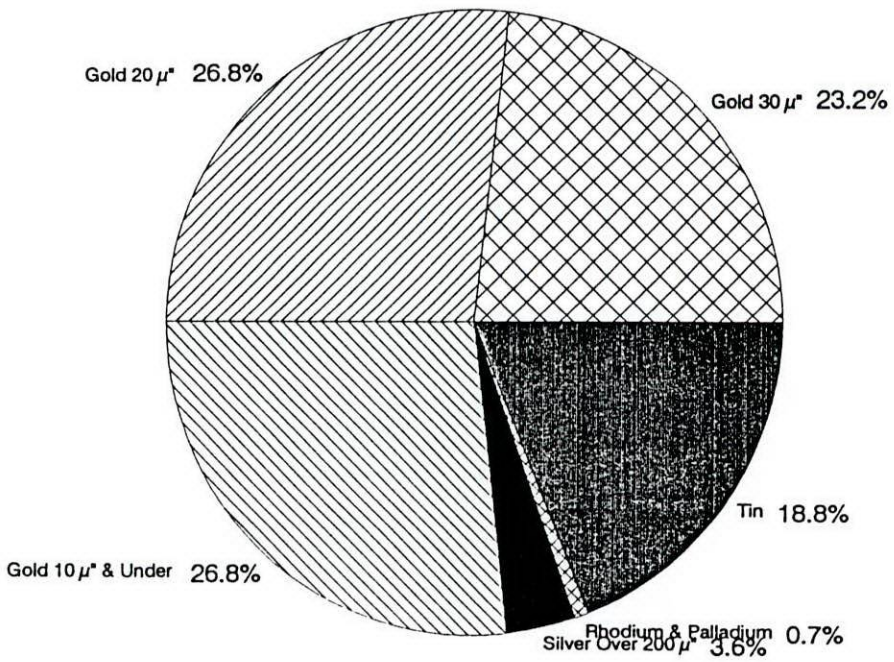

Contact Coatings for IC Sockets

There are 12 technology trends impacting the design and use of IC sockets. These are:

Trend #1: Pin Counts for Integrated Circuits Are Increasing
Trend #2: Smaller, Thinner, and More Pin Count Packages
Trend #3: MCM Penetration to Reach $18 Billion By Mid-1990s
Trend #4: Packaging of Microchips Within IC Cards — Causes Shift to PC Connectors
Trend #5: VSOP Packaging Within Memory Cards — Causes Shift to PC Connector for
Trend #6: Chips Packaged in PCMCIA/JEIDA (PC Cards) — Shift to PC Connector for
Trend #7: Optical Memory Cards Pin-Outs Pin-Outs for Pin-Outs
Trend #8: Microprocessors Associated With Memory Cards
Trend #9: Memory/PC Cards Replacing Hard Disk, Battery Packs, PCBs, Cabling, and
Trend #10: SIMM — Shifts Pin-Outs to PC Cardedge Connectors
Trend #11: IC Sockets Mandated by the Active Device
Trend #12: Shift Toward SMT IC Packages—Also Surface Mounted Sockets

34 Billion Units Of IC Socket Contacts

IC Socket Leads	Gold 100 u in.	Gold 50 u in.	Gold 30 u in.	Gold 20 u in.	Gold 10 u in. & under	Silver Over 200 u in.	Rhodium & Palladium	Tin	Others Ni or None	Total Leads (Billion)
Computer Peripherals			0.62	1.97	10.21			3.98		16.77
Computer (Mainframes)		0.41	4.57	2.56	1.31	0.41				9.25
Communication		0.19	1.40	0.98	0.47	0.09		0.30		3.42
Gov't/Military	0.09	1.08	0.25			0.08	0.13			1.63
Instrumentation	0.05	0.28	0.25			0.16		0.04		0.78
Industrial	0.05	0.23	0.21			0.13		0.04		0.65
Transportation			0.09			0.06		0.07		0.22
Business/Retail/Education			0.10	0.13	0.11	0.03	< 0.01	0.08		0.44
Consumer			< 0.01	< 0.01	0.03	0.05		0.34	< 0.01	0.42
Machinery			0.05					0.32	0.05	0.42
TOTAL LEADS PLATED	0.19	2.18	7.53	5.64	12.13	0.99	0.13	5.17	0.05	34.00

To follow is a pie chart showing total IC Socket leads by demand sector.

Each demand sector is then broken down by plating type with a pie chart for each.

IC Socket Leads

Total Leads (Billions)

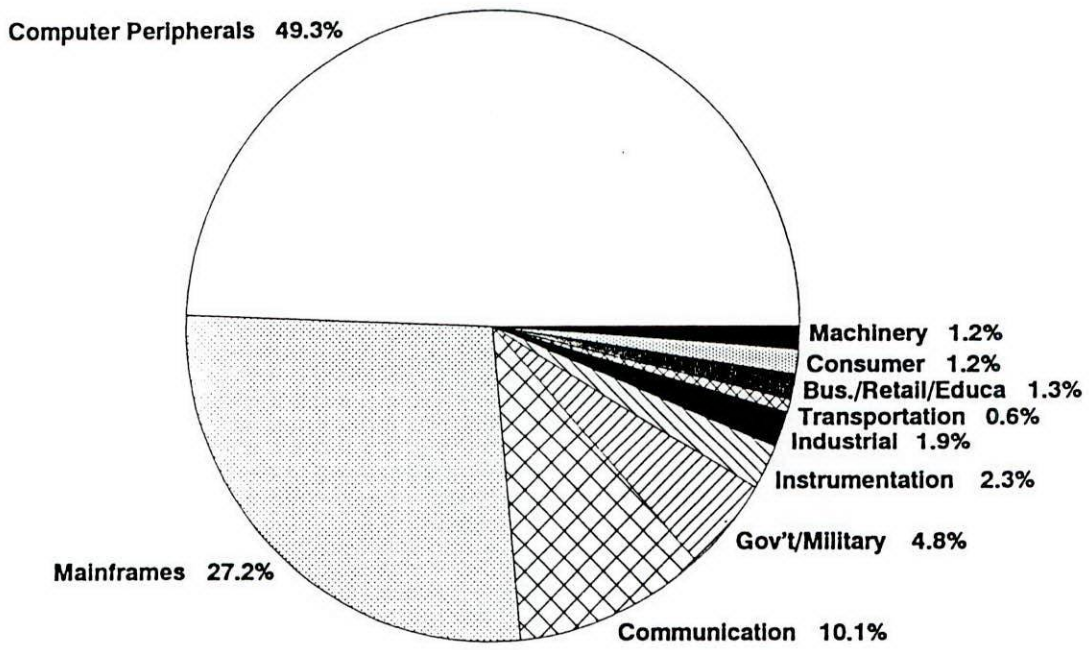

IC Socket Leads

Computer Peripherals

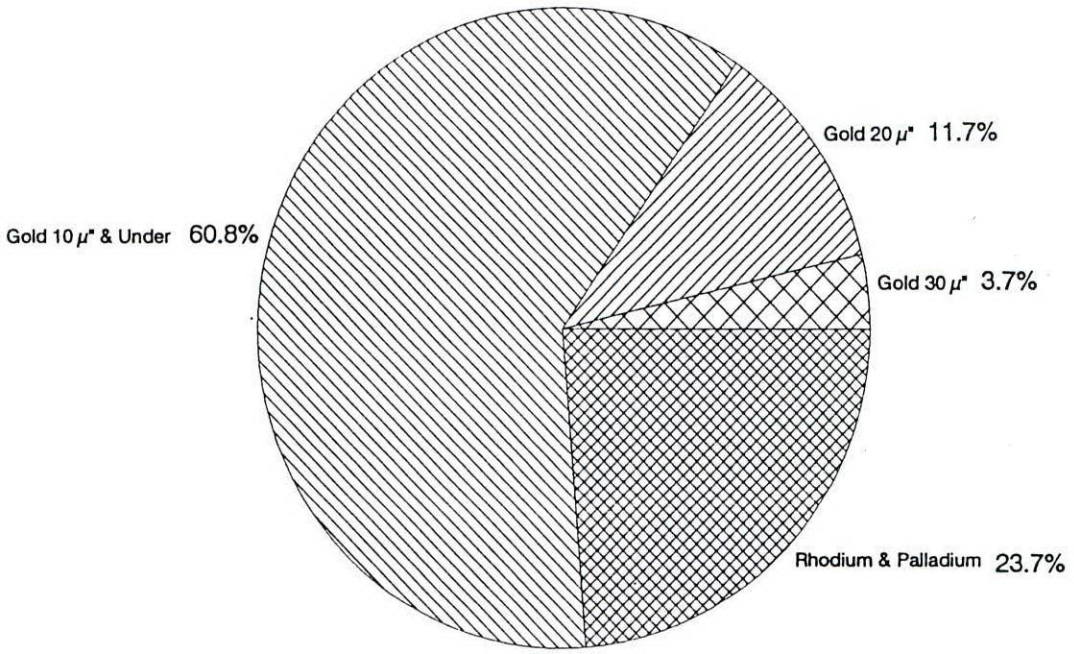

IC Socket Leads

Computer (Mainframes)

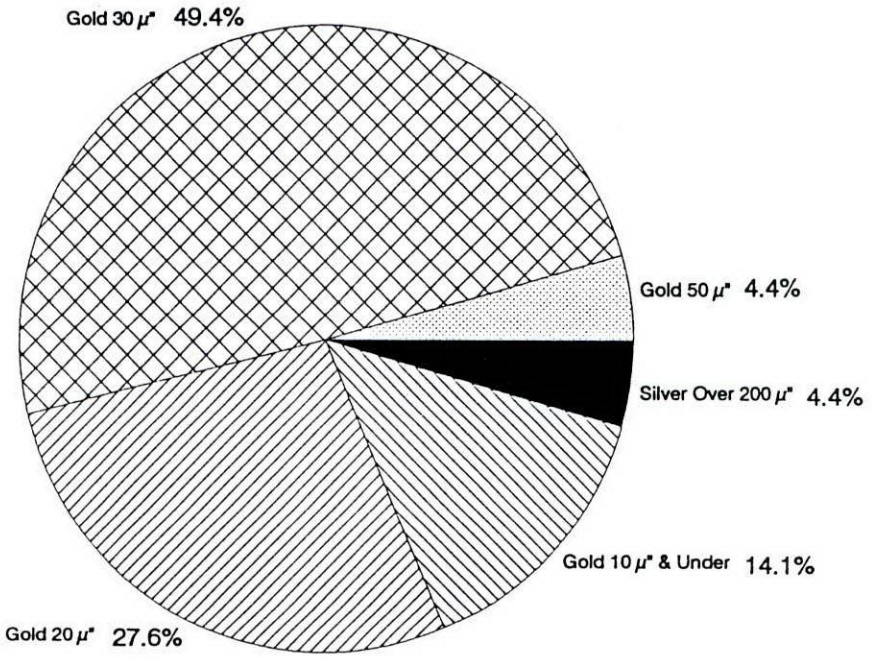

IC Socket Leads

Communication

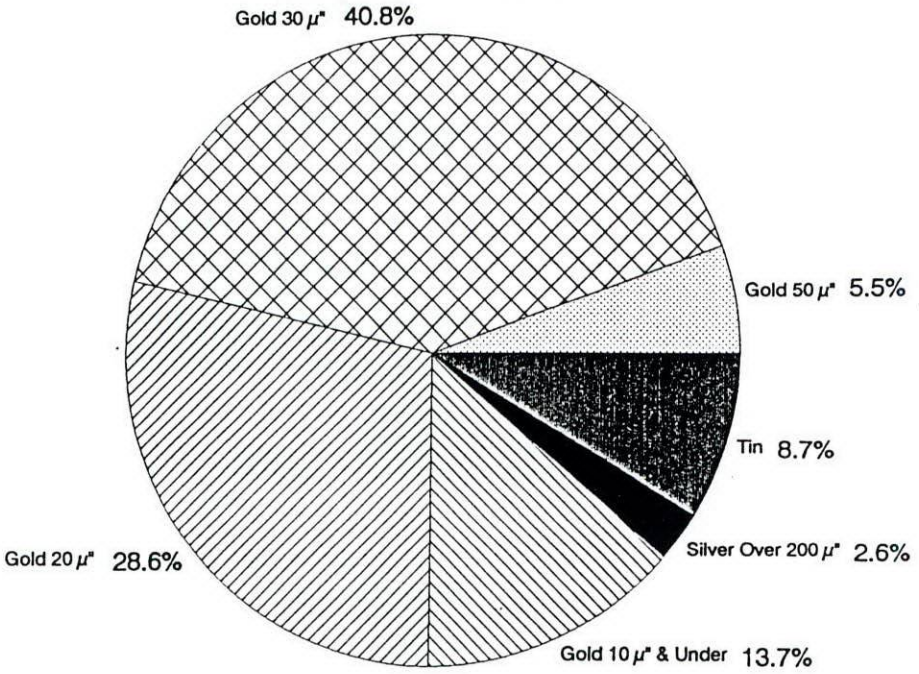

IC Socket Leads

Government/Military

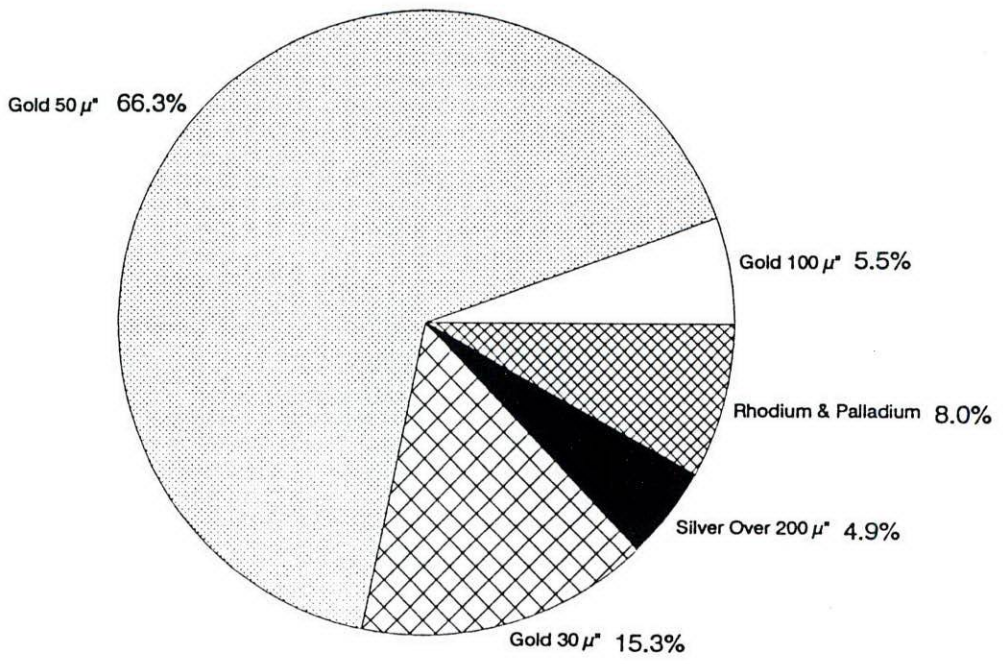

IC Socket Leads

Instrumentation

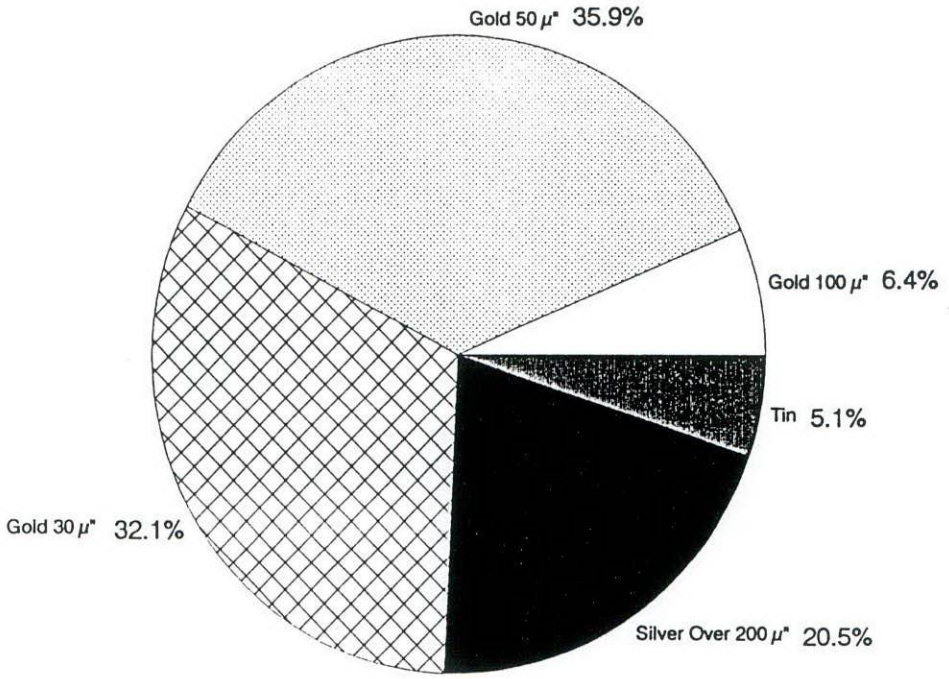

IC Socket Leads

Industrial

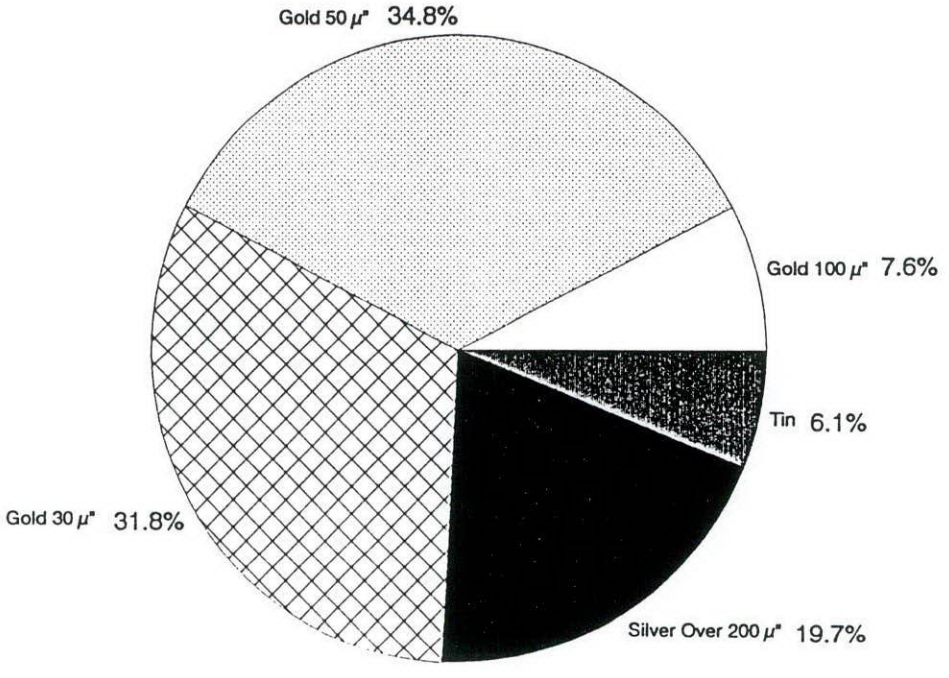

IC Socket Leads

Transportation

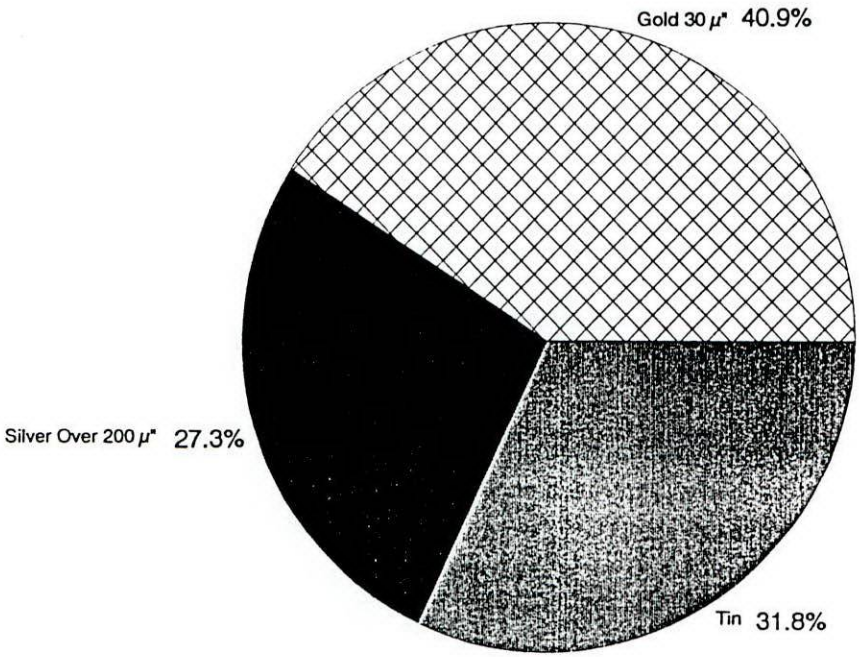

IC Socket Leads

Business/Retail/Education

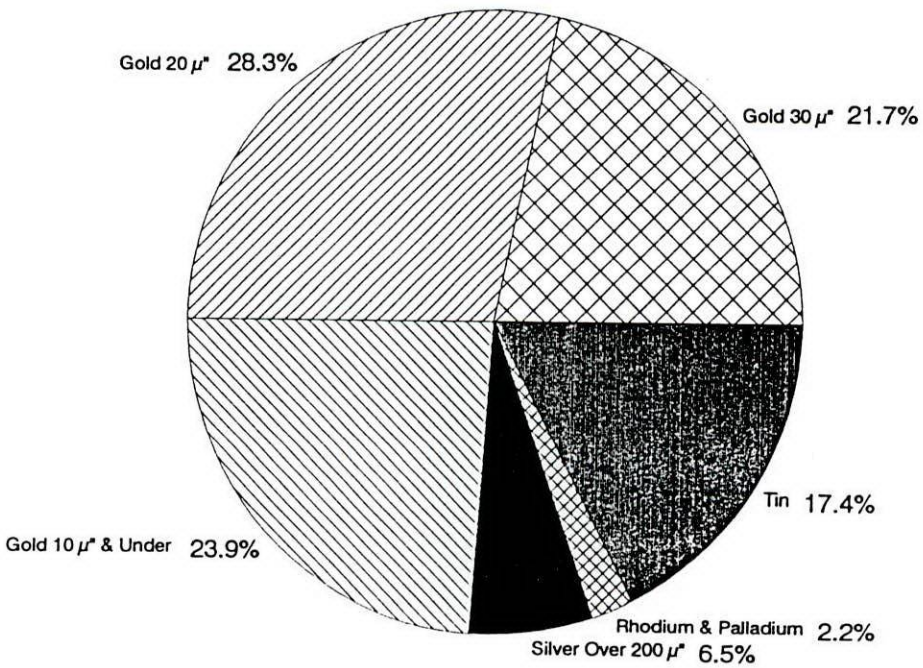

IC Socket Leads

Consumer

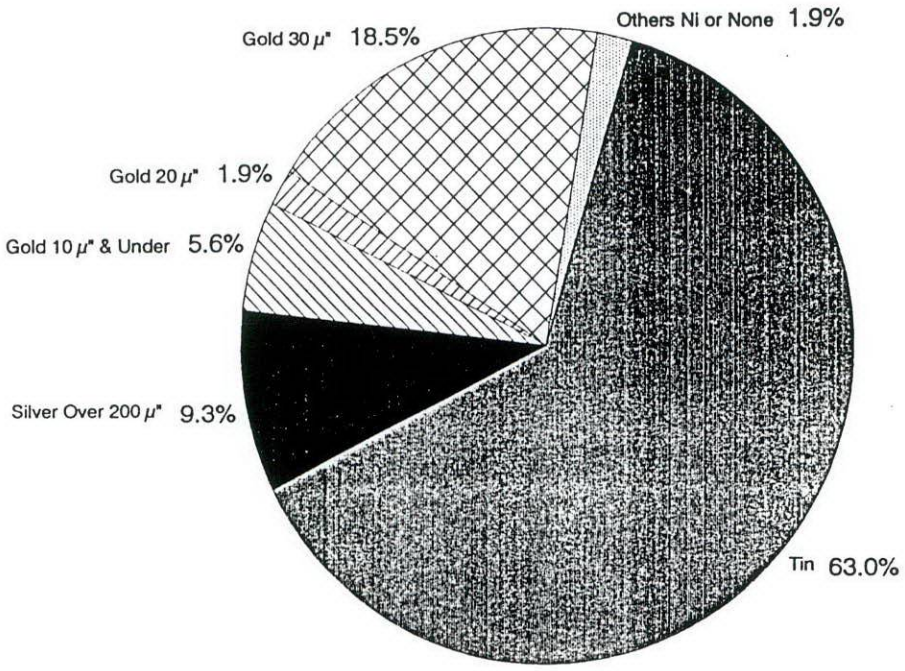

IC Socket Leads

Machinery

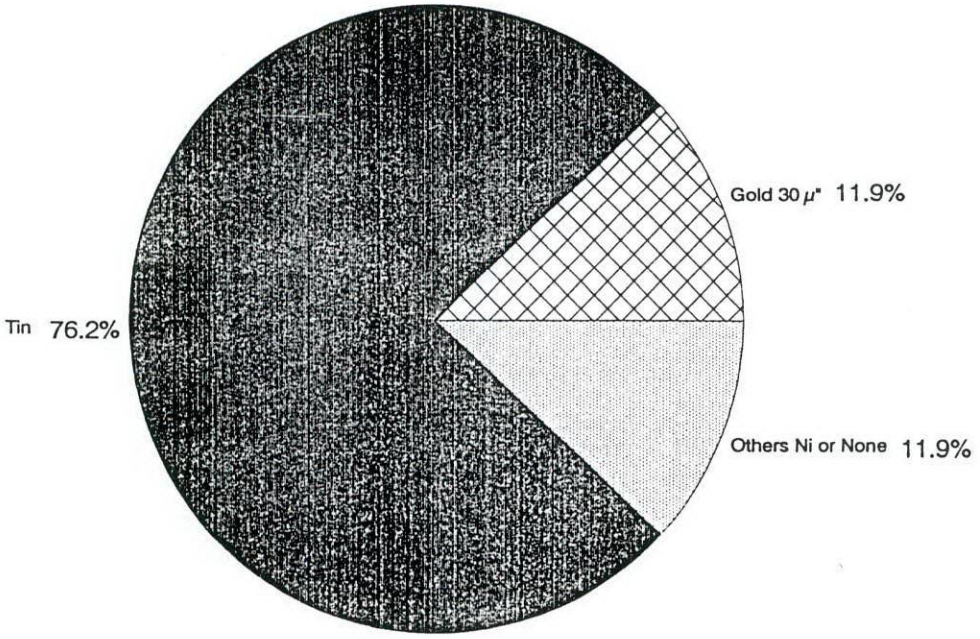

MICROHARDNESS TESTING OF PLATED COATINGS: DEFINING PRECISION AND BIAS FOR ASTM B578

by

Jack Horner, Research Manager
Allied-Kelite Division, Witco

Microhardness testing has been described by ASTM E384, Test Method for Microhardness of Materials since 1969. ASTM B578, Standard Test Method for Microhardness of Electroplated Coatings was issued originally in 1973, as an adaptation of E384 to plated coatings.

Since 1980, ASTM has required that test methods include statements on the precision and bias of each method. To develop these missing parts of E384 and B578, each committee responsible for these documents, E04 and B08, initiated new interlaboratory comparison studies, commonly referred to as round-robins. These studies involve circulating standard materials to each of several chosen laboratories for measurements. Considerable planning and attention to detail are required [1][2]. ASTM Committee E04 has completed their testing and a lengthy statement on precision and bias is now included in E384-89. Work continues in the B578 round-robin which is the subject of this paper.

Scope:

This paper will present a review of work and an update on data received to date from the B578 round-robin. Several more participants have submitted data since the progress was last reported [3] and are included in this status report. The project is still active and ongoing with some volunteering laboratories yet to participate.

Basics in Test Methods and Round-Robins:

Certainly, if a property can be measured and is of sufficient importance to be specified, some standard test method is required. Further, this test method must be accurate and capable of detecting significant changes of the specified property values in sufficient degree to be effective. A test method with known accuracy allows for establishing more realistic limits of acceptance and is a valuable tool in Quality Control.

Accuracy is defined, generally, in terms of 'precision' and 'bias'. While some nuances in definitions exist, the term 'precision' refers to repeatibility and reproducibility - and the term 'bias' refers to the overall difference between a "true" value and the "test" value.

In real practice, even with very rigid test procedures, it is normal to obtain varying results. Within a given laboratory, repetitive tests on the same material, using the same equipment by the same operator will produce results with the least variance (usually). Substituting other

equipment or another operator in the same laboratory increases the variance. When changing all the factors and comparing results obtained in different laboratories, different equipment, but using the same test sample and test method, the variance is at its greatest. To be a useful tool in commerce, manufacturing, and trade, test methods should keep variance to a reasonably low limit in this latter, interlaboratory condition.

Defining the variance by conducting round-robin testing is subject to many secondary effects which can be difficult to control. ASTM E691-87, Conducting an Interlaboratory Study to Determine the Precision of a Test Method, is a good tool and describes many of the problems in planning, conducting, and expressing the results. Practically, the conditions of the round-robin should not be so rigid that only highly-skilled, bona fide experts with the ultimate in skill and equipment would be utilized. Conversely, the use of totally inexperienced operators with poor equipment will throw results, unrealistically, in the opposite direction. What is sought is some condition in between the extremes. Testing has to be done by interested and trained operators using adequate equipment. Putting all the possible problems of conducting a useful and meaningful round-robin into perspective, however, does seem to require experience along with a dash of good fortune. People still are very important in successful round-robins.

Basics in Microhardness Testing

Hardness and Microhardness

Hardness has been defined as resistance to indentation. Microhardness is probably an inaccurate term which actually refers to micro-indentation - a very small "indent"; not a very small "hardness". Hardness is generally measured by forcing an indenter into the surface of a test piece and measuring the depth of penetration or the imprint left by the indenter. Many shapes of indenters have led to many different hardness scales. Two of these have found use in testing coatings: Knoop, which leaves a longer, thinner, rhombic imprint and Vickers which leaves a wider, square imprint. The hardness number is a function of the force used and the depth or imprint of the indenter. When using comparatively low forces, the hardness number will vary with the force until it reaches a substantial level where further increases in force have little effect on the calculated hardness number. To differentiate, many experts classify hardness values as "microhardnesses" when the force is less than 1000 gf; and simply "hardness" at higher forces. Plated coatings are often tested at 200 gf or less, where the force affects the microhardness numbers.

Knoop Vs. Vickers

Microhardness testing of plated coatings is usually done on cross-sections of the test piece. As such, a minimum plate thickness is required so that the indentation is not too close to the edge of the test piece. The Knoop indenter will require less minimum thickness than Vickers. Vickers tests are reputed to be more tolerant of slight

surface variations. Knoop may be used more for plated coatings, but both are fairly common. Modern testing machines allow use of either indenter.

ASTM B578 presently describes only the Knoop indenter; Vickers is described along with Knoop in ASTM E384, but it is not specific for coatings. A user of Vickers for plated coatings could use both specifications. It is of interest to note that B578 round robins are including Vickers and Knoop so that, in a future revision, both can be included in B578. ISO 4516 currently describes both indenters.

Review of Work to Date

While previous round-robins have been part of the history of the working Section, B.08.10.03, on microhardness testing, results and testing were not complete. The present phase is part of the overall plan to answer the need for precision and bias statements and generally to assist in revision and improvement of B578.

There was little doubt that microhardness testing was in need of improvement, especially among those more familiar with the method and in attempts to reproduce published information.

Initially, the general plan was:

1. Circulate prepared and indented specimens to test for error associated with measuring only.

2. Circulate prepared specimens to test for the variance of both indentation and measurement.

3. Circulate plated specimens to test for variance of the whole process; preparation, indentation, and measurement.

Since it was expected that the variances would be affected differently from softer coatings to harder coatings, probably three types of coatings should be used; soft, medium, and hard. Additionally, Knoop could be affected differently than Vickers. Finally, the variance can be affected by the loads used.

Considering these obvious factors, the first stage of this series of round-robins included a soft copper specimen (nobody would donate a heavily plated gold speciment to our cause) and two hard chromium-plated specimens. Instructions were detailed but included:

a. Take 5 readings on each of 5 indents.

b. Repeat for each of 3 specified loads.

c. Repeat for each indenter, Knoop and Vickers.

When the data was collected and analyzed [1] for this stage, the variance suggested that the test method was statistically out of control. The results were rejected and this stage was considered to be a "practice run".

The next specimen circulated was an electroless nickel-plated specimen to represent the medium hardness group. Results of this were reported[2] and tentatively rejected because of a possibly "tainted" preparation.

The present stage is based on circulation of a standard reference material (SRM) electroformed nickel, made available more recently by National Institute of Standards and Technology (NIST). This specimen was prepared, indented, and measured by NIST personnel prior to distribution. Participants measure NIST indents as well as indent and measure their own. This in effect combines the first and second steps of the general plan. Results-to-date were reported at SUR/FIN 91. Since then, data has been received from five (5) additional participants with three awaiting their turns. The data from these last five is added to the previous data and presented here. Total number of participants at the conclusion of this stage should be about twenty.

Data and Results:

Over 5000 readings have been received and analyzed for the NIST SRM specimen. When all the data has been collected at the conclusion of this stage, it will be re-analyzed according to E691-87 which now has a computer disk programmed to do the analyses.

For purpose of this interim or status report, the results are shown in Table I for the measure or "read-only" step and Table II for the "indent-and-read" step. Table III has averaged all the results on the Ni-SRM specimen and compares these to the average reported by the NIST personnel.

Data accumulated this past year has been added to histograms from 14 participants.

Discussion of Results to Date:

Comparison of current results with that of the previous specimens, Cu, Cr, and EN, does show better agreement between laboratories. A major factor in this could be possibly improved technical capability, better interest, and better equipment of the participants. It could also be an indication of more consistent specimens.

Of particular interest, the range still appears to be too broad, especially so with the lighter loads. Fifty (50) gram forces should probably be avoided.

Of spectacular interest, Table III shows how closely the overall averages are to NIST readings whether it is read-only or indent-and-read. From the fairly broad ranges of over 130 units in some cases and the very close

agreement in the averages, this makes a strong statement for using several people and several readings to obtain good results.

Another interesting observation that can be made from Table I and Table II is that a majority of the variance would appear to come from the measurement process, and not the indentation process.

Future Plans:

While the Ni-SRM work is about complete, it should be considered that it is an electroform. The electroplated or coated specimen may not perform in the same manner. Plans are to include plated specimens for the next stage - where the participant prepares the plated specimen, supplied from one controlled piece.

Soft specimens are in the plan; a gold standard has been promised. Soft deposits may prove to be more variable and measuring procedures at very low loads may give additional problems.

Similarly, the hard specimen should be re-done with the present round-robin personnel.

References

1. Horner, J.D., Microhardness Testing of Plating Coatings: Recent Round-Robin Experiences, Testing of Metallic and Inorganic Coatings, STP 947, ASTM, Philadelphia, 1987, p. 96.

2. Microhardness Testing of Plated Coatings: An Up-Date on Round-Robin Results. Presented at SUR/FIN 1991, Toronto, Canada.

3. ASTM #691 Standard Practice for Conducting an Interlaboratory Test Program to Determine the Precision of Test Methods, ASTM, 1916 Race Street, Philadelphia, PA 19103. (Also the source for other ASTM documents mentioned.)

Acknowledgement:

The author wants to thank Witco for permission to publish this paper and for allowing the time spent on ASTM and AESF work. He also wishes to thank all the participants of this Round-Robin who, unfortunately, must remain anonymous. Without their dedication, this type of work would fail.

TABLE I

Microhardnesses of NIST Ni-SRM

B578 Round Robin Results to Date*

Stage I: Read Only
(Indents by NIST)

	$\bar{x}$	Range	s	v
HK_{50}	547	478-593	31.5	0.058
HK_{100}	529	500-548	15.3	0.023
HK_{200}	515	494-539	12.3	0.024
HV_{50}	525	457-590	334	0.064
HV_{100}	519	472-555	24.1	0.047
HV_{200}	513	485-558	19.9	0.039

* March 10, 1992; 19 participants

TABLE II

Microhardnesses of NIST Ni-SRM

B578 Round Robin to Date*

Stage II - Indent and Read

	$\bar{x}$	Range	s	v
HK_{50}	546	481-611	38.8	0.071
HK_{100}	532	478-581	23.5	0.044
HK_{200}	519	476-545	16.2	0.031
HV_{50}	520	457-573	28.2	0.054
HV_{100}	521	474-565	22.6	0.043
HV_{200}	519	486-563	17.2	0.033

* March 10, 1992; 19 participants

TABLE III

Overall Summary

Microhardnesses of NIST Ni-SRM

Comparison to NIST Values

	NIST $\bar{x}$	(1991*) $\bar{x}$	Present** $\bar{x}$
HK_{50}	544	(542)	547
HK_{100}	529	(530)	531
HK_{200}	515	(518)	517
HV_{50}	526	(524)	523
HV_{100}	520	(523)	520
HV_{200}	513	(518)	516

* 14 Participants
** 19 Participants

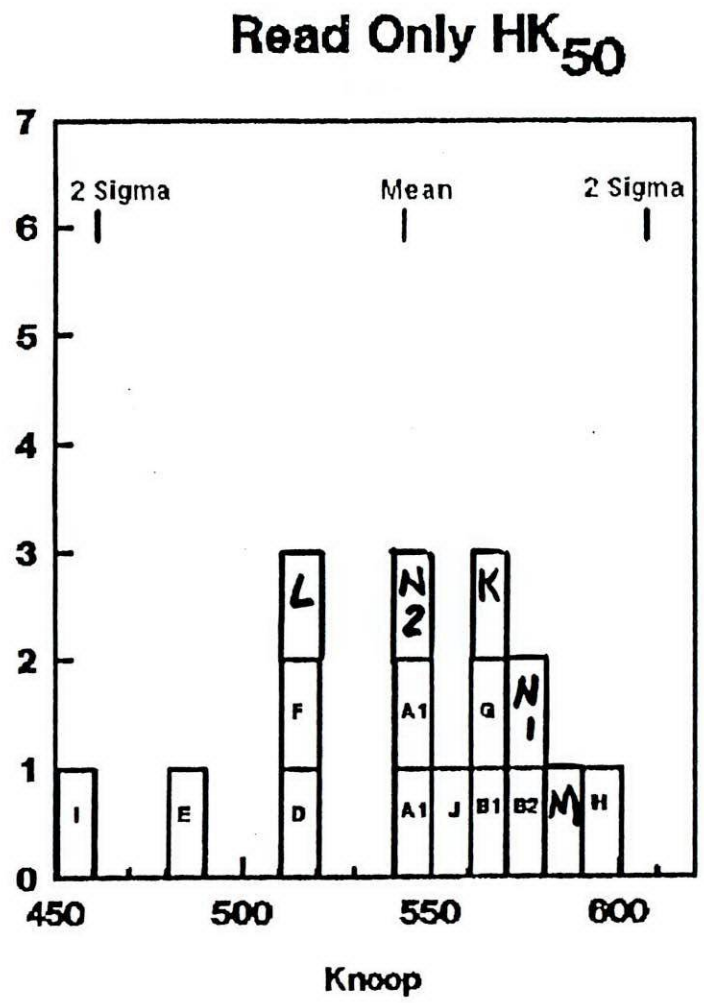
Read Only HK50
2 Sigma
Mean
2 Sigma
7
6
5
4
3
2
1
0
I
E
D
F
L
A1
J
B1
B2
N2
A1
G
K
N1
M
H
450
500
550
600
Knoop

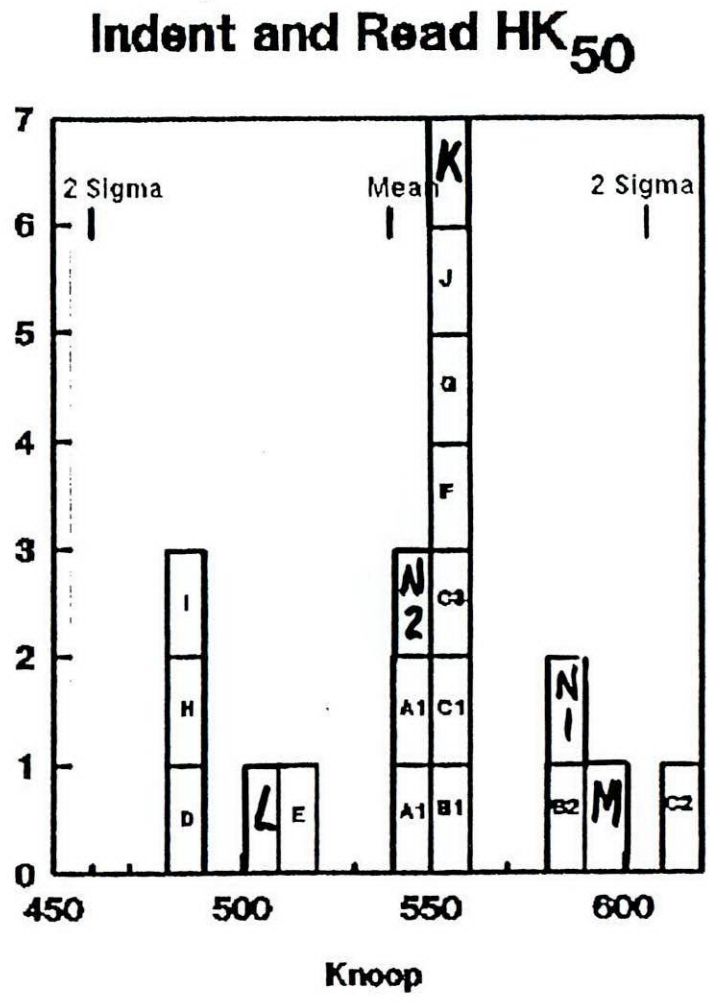
Indent and Read HK50
2 Sigma
Mean
2 Sigma
7
6
5
4
3
2
1
0
I
H
D
L
E
A1
B1
N2
A1
C1
K
J
G
F
C3
N1
B2
M
C2
450
500
550
600
Knoop

Read Only HK_{100}

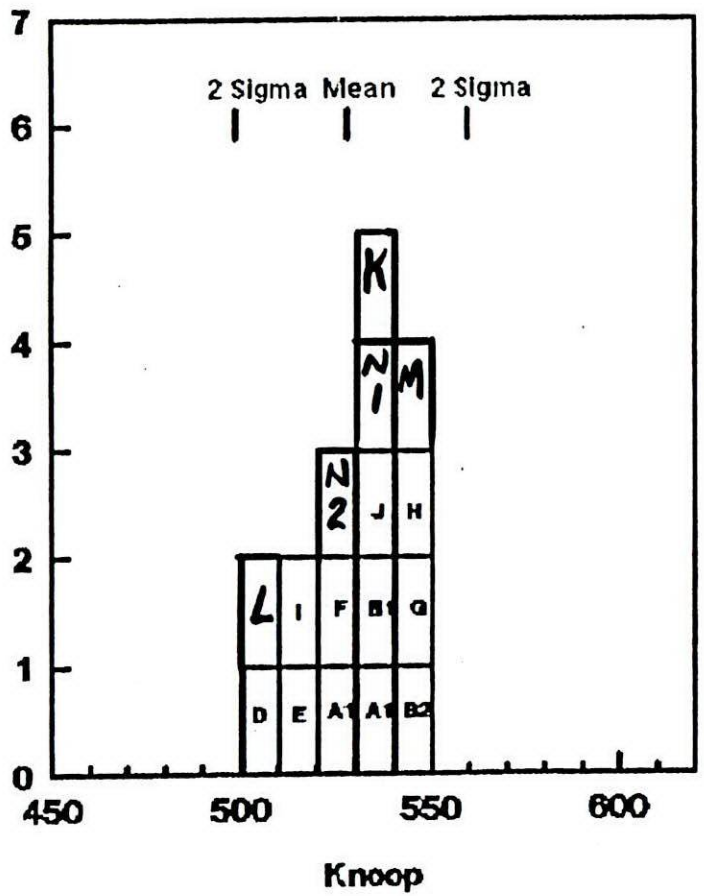

Indent and Read HK_{100}

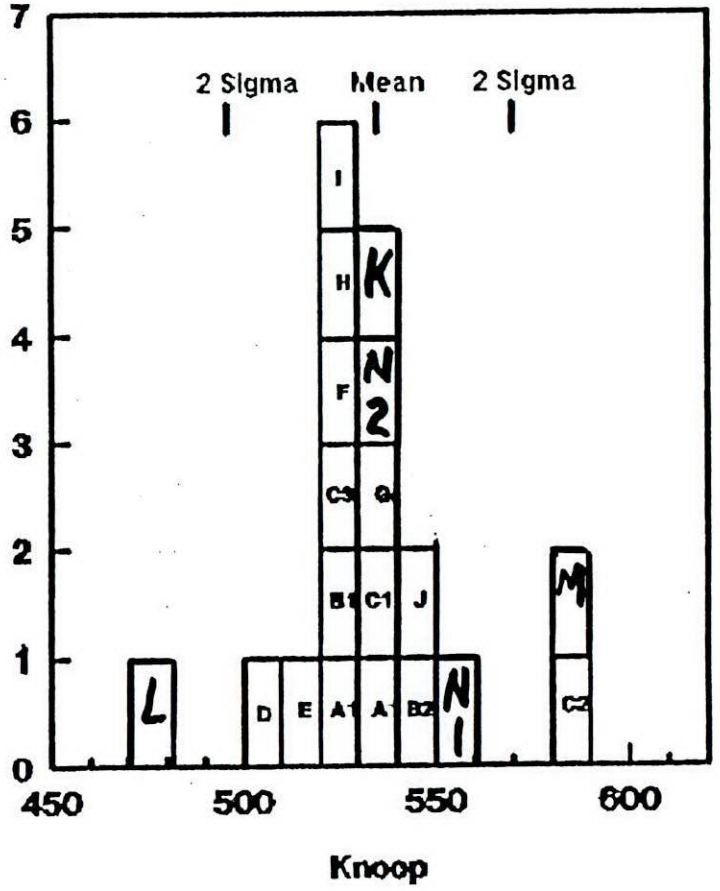

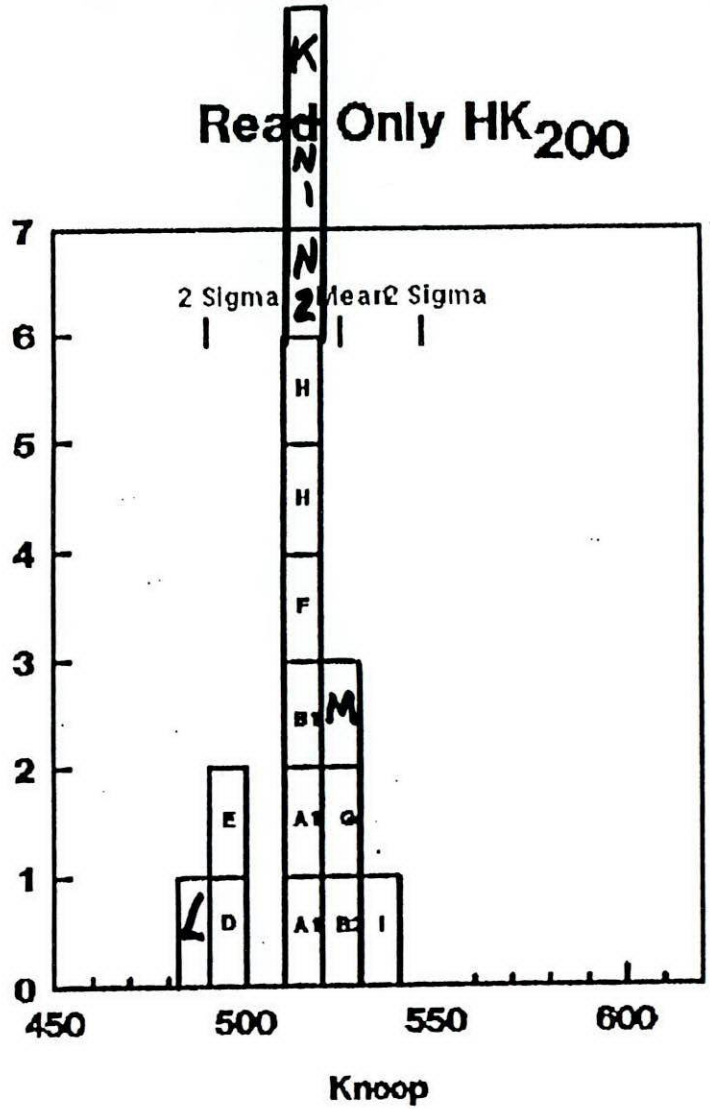
Read Only HK200
2 Sigma
Mean
2 Sigma
Knoop
450
500
550
600
0
1
2
3
4
5
6
7

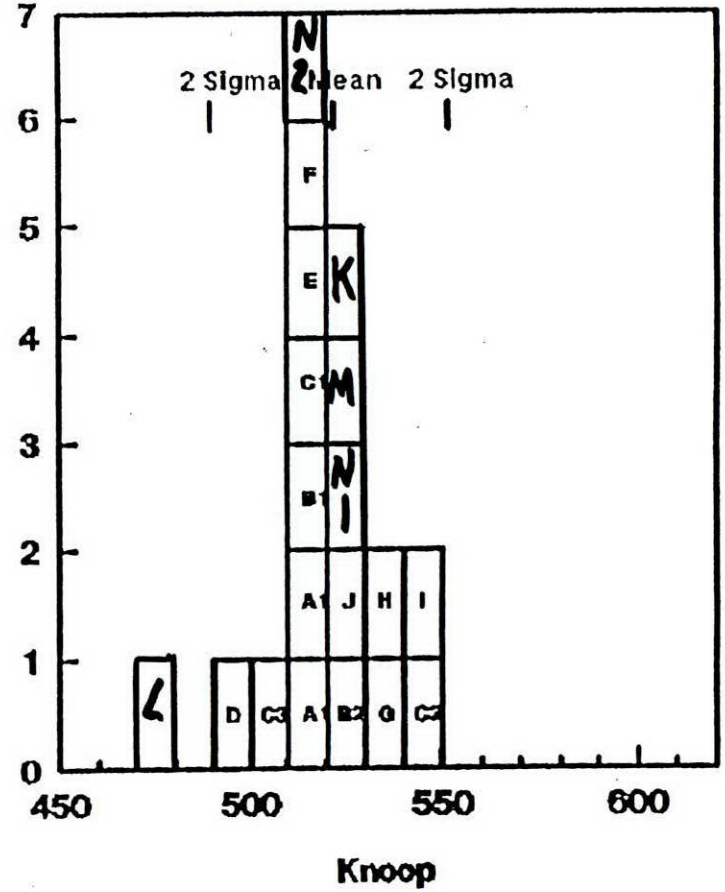
Indent and Read HK200
2 Sigma
Mean
2 Sigma
Knoop
450
500
550
600
0
1
2
3
4
5
6
7

Read Only HV_{50}

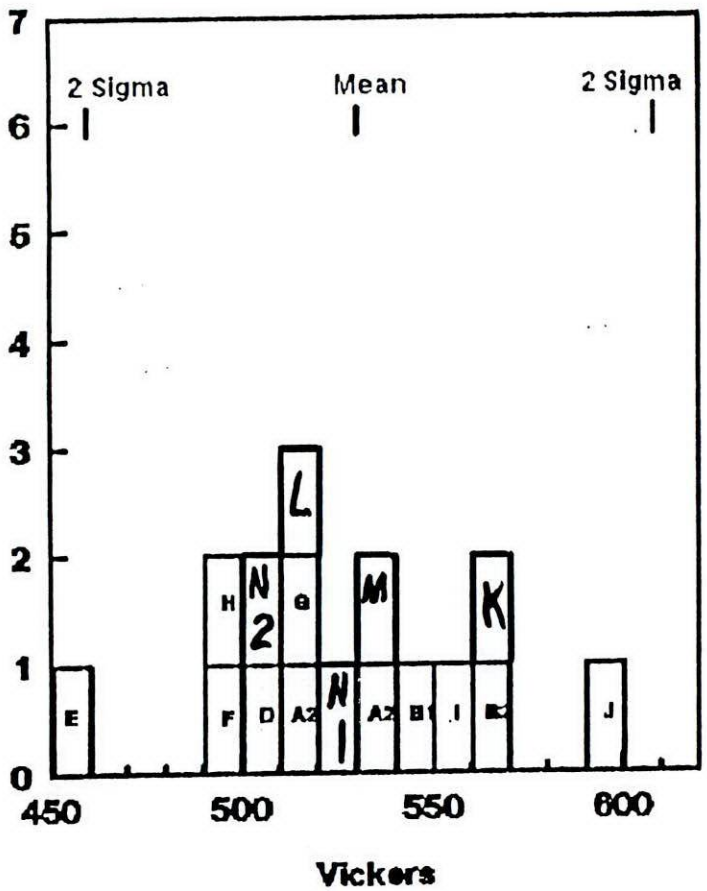

Indent and Read HV_{50}

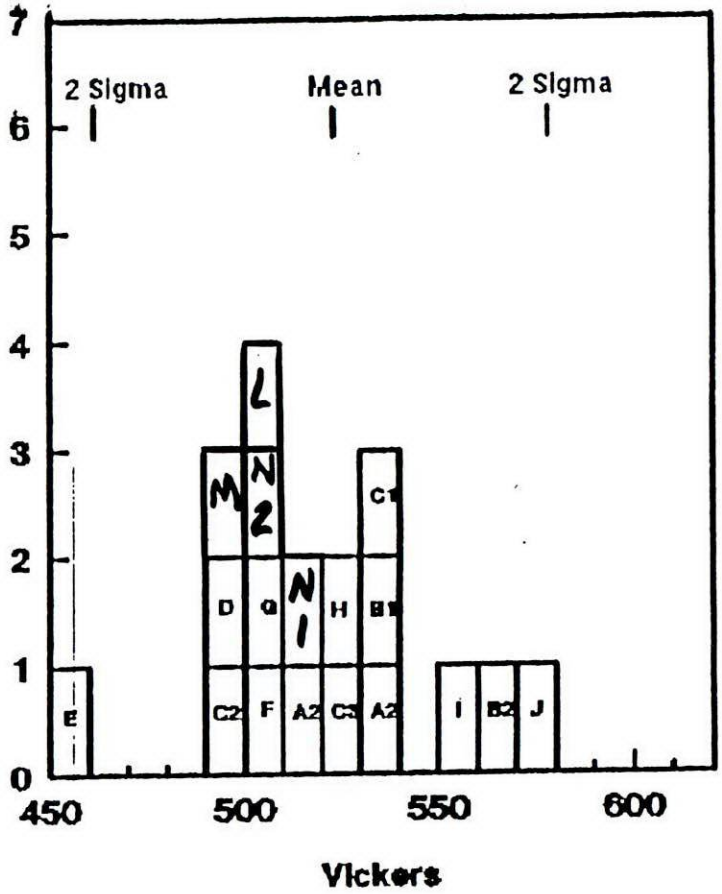

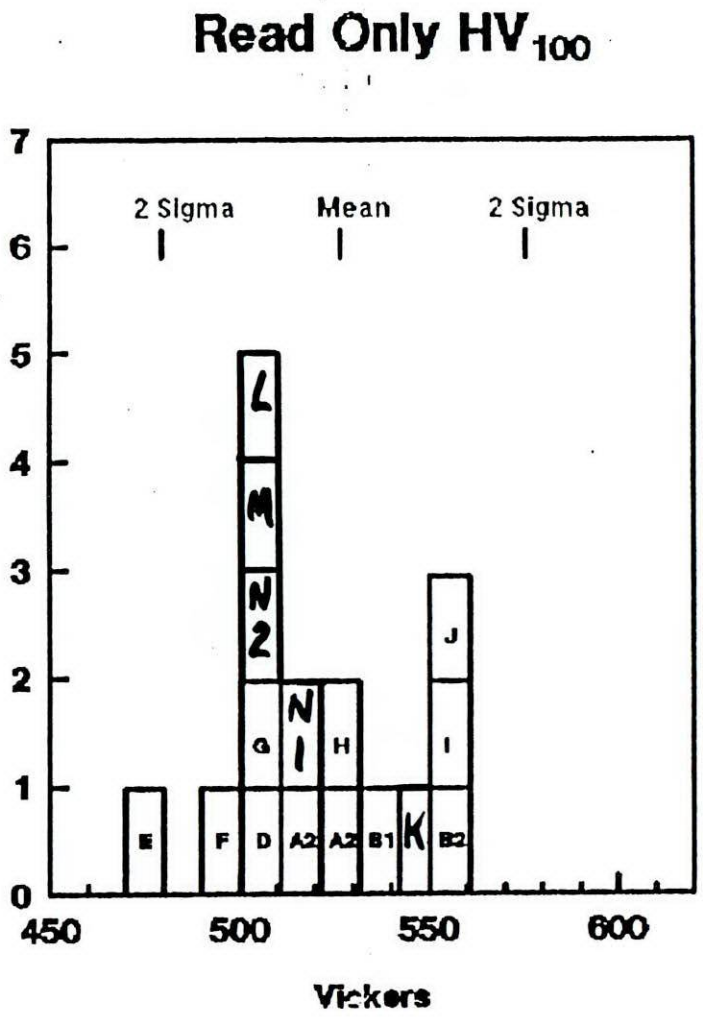
Read Only HV100
2 Sigma
Mean
2 Sigma
7
6
5
4
3
2
1
0
450
500
550
600
Vickers
L
M
N2
N1
G
H
J
I
E
F
D
A2
A2
B1
K
B2

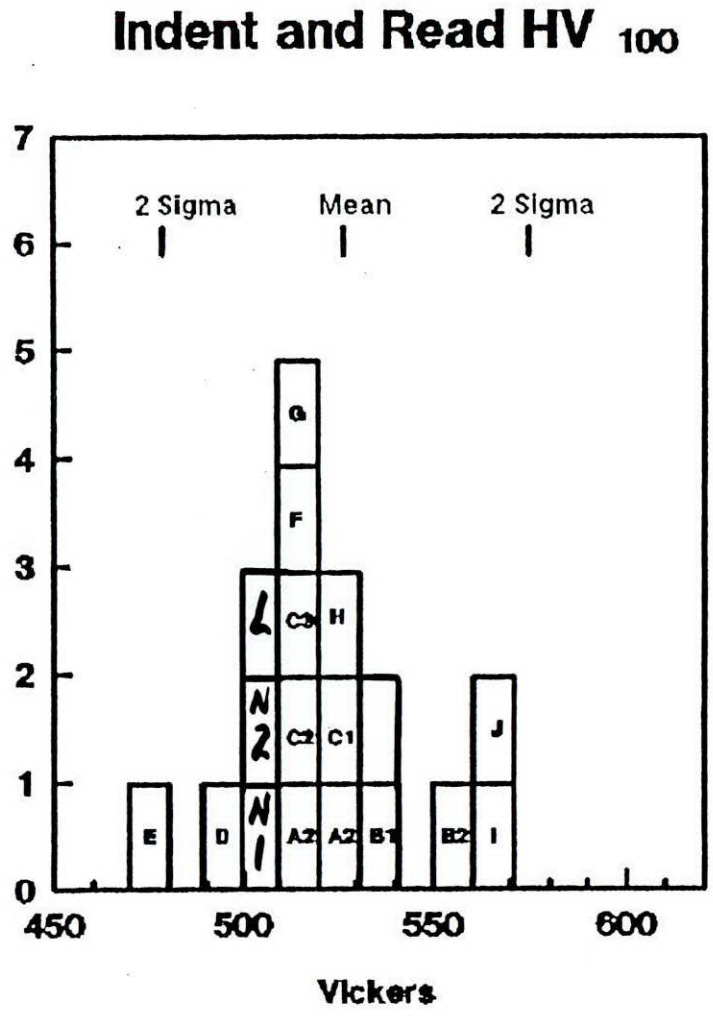
Indent and Read HV 100
2 Sigma
Mean
2 Sigma
7
6
5
4
3
2
1
0
450
500
550
600
Vickers
G
F
L
C3
H
N2
C2
C1
J
N1
E
D
A2
A2
B1
B2
I

Read Only HV_{200}

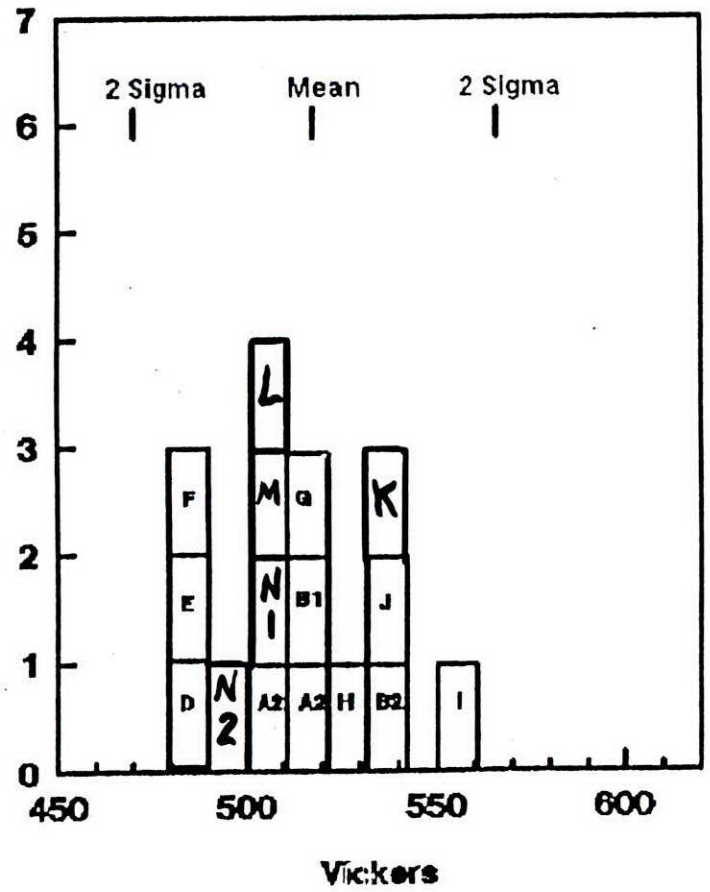

Indent and Read HV_{200}

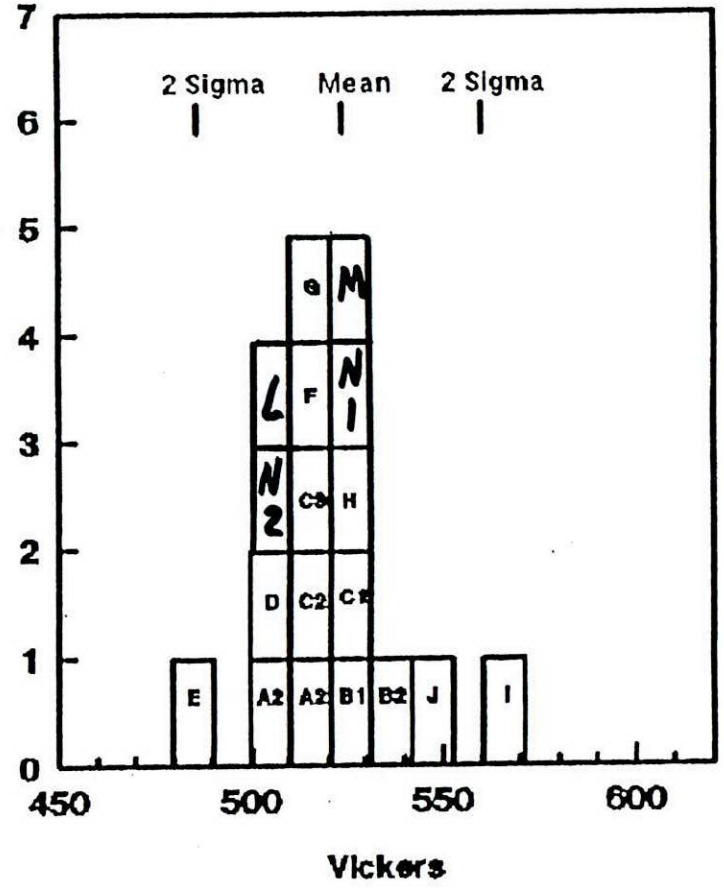

THE RELATIONSHIP BETWEEN VICKERS HARDNESS AND UNIVERSAL HARDNESS

W. Weiler
Federal Institute of Physics and Technology

The Vickers indentor hardness test based on the indentor displacement under test load (universal hardness) is coming in use for an increasing number of applications. The new method is also subject to much discussion among the experts. An important question is the relationship, or the degree of correlation between the new universal hardness test and the classic Vickers hardness test. A clear answer to this question will be presented here, based on the definition of the Vickers and HU (Universal Hardness) numbers and the test piece material deformation process using a Vickers indentor. Existing empirical results will be compared to these answers. It is requested that even the expert reader not skip section 1 on the definition of terms :

1 Definition of terms

1.1 Indentor

For both methods, the indentor is a square based diamond pyramid with a face angle of $\alpha = 136°$.

1.2 Vickers hardness

To measure the Vickers hardness (HV), the indentor is pressed into the material at a defined test load. After a certain period, the test load is removed. The Vickers hardness value is defined as the quotient of the test load F and the surface area A of the residual indentation, which is only resultant of the permanent plastic material deformation component of the test. To determine the indentation area, the indentation diagonals *d* are measured on the specimen surface. Based on the Vickers indentor geometry, the Vickers hardness is defined as

$$HV = \frac{0.102*F}{A} = \frac{0.102*F}{\frac{d^2}{2\sin\frac{\alpha}{2}}} = \frac{0.1891F}{d^2} \qquad (1)$$

The factor 0.102 has been entered to produce the same hardness values after adopting *Newtons* instead of *KILOPOUNDS* as unit for the test load.

This definition and calculation is based on the assumption, that the permanent indentation is a true geometric image of the indentor after load removal. However, for several reasons, this assumption is not justified . While the test load is applied, the indentor is under the same stress as the specimen, and will therefore be subject to elastic deformation. For the following discussion, this fact will be neglected, and the indentor will be viewed as having ideal stiffness because the modulus of elasticity for diamond is very high.

More important is the fact that the stresses in the test piece material at the point of indentation are highly non-uniform due to the non-uniform tension distribution across the indentation area. This also results in locally non-uniform elastic deformations, which are subject to recovery after load removal. The resultant permanent indentation is geometrically distorted, compared to the indentor shape. Elastic deformation is highest under the indentor tip and smallest at the surface of the test piece. The face angle of the indentation is larger than the face angle of the indentor. This distortion increases as the degree of elastic deformation increases in comparison to the total (plastic and elastic) deformation.

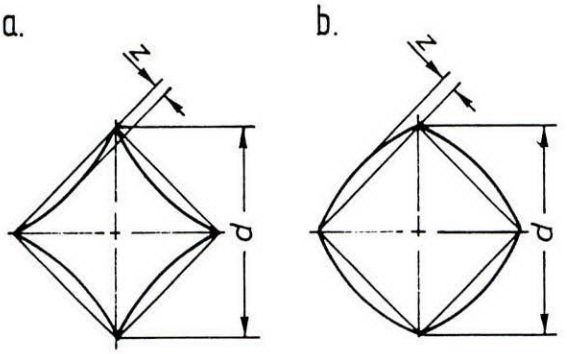

Figure 1. Schematic Vickers indentation
a. for elastic material, b for plastic material

Usually a lower modulus of elasticity and a higher elastic limit will yield a higher degree of elastic deformation.

A Vickers indentation is never a perfect negative imprint of the exact indenter geometry, regardless of material properties. The indentation face angle is always distorted by a few degrees [1], which is primarily dependent on the elastic properties of the test piece material. The indentation outline is also distorted; it is either a pincushion shape or barreled shape (Fig. 1) due to material sinking or ridging during loading, which depends on the degree of plastic flow (cold working) and elastic recovery.

1.3 Universal hardness

Universal hardness HU is based on the indentation with a Vickers indentor and the measurement of the indentation depth , or indentor displacement under test load. The designation Universal Hardness has been selected because the method can be applied to all materials. In related literature other terms referring to this test method, such as HVL [8] or HVT, may also be found. Because the HV test is a different hardness test method, reference to the Vickers method should be avoided to prevent misunderstandings. Also, the indentor has to fulfill different requirements than in the classical Vickers test [2]. The HU test method itself has been previously described, for instance, in [3]. The Universal Hardness is defined as the quotient of the test load and the surface area A of the indentation under an applied test load. Based on the pyramid geometry, universal hardness can be described as a function of test load and indentation depth under test load, with the assumption of an indentor of ideal stiffness.

$$HU = \frac{F}{A} = \frac{F}{4 * \frac{\sin\frac{\alpha}{2}}{COS^2\frac{\alpha}{2}} * h^2} = \frac{F}{26.43 * h^2} N/mm^2 \qquad (2)$$

The universal hardness is expressed in N/mm^2, which differentiates HU from HV. Because equation (2) does not contain a factor to convert the result to kiloponds, values for universal hardness are higher than the classic Vickers hardness numbers by a factor of approximately ten. As the result of the equilibrium between the applied test load and the resistance of the tested material to indenter penetration, the universal hardness also is physically more meaningful. It fulfills, contrary to the classic methods, the definition for technical hardness as the resistance of a material to penetration by another object of harder material.

We must also point out that a hardness test method, which is to measure technical hardness according to it's true definition has to be applicable to all materials. If a test method has restrictions in this regard, it is an indication that the test values obtained by the test method do not fulfill the true definition for technical hardness.

2 Relationship between Vickers hardness and Universal hardness

The relationship can be deduced schematically from figure 2:

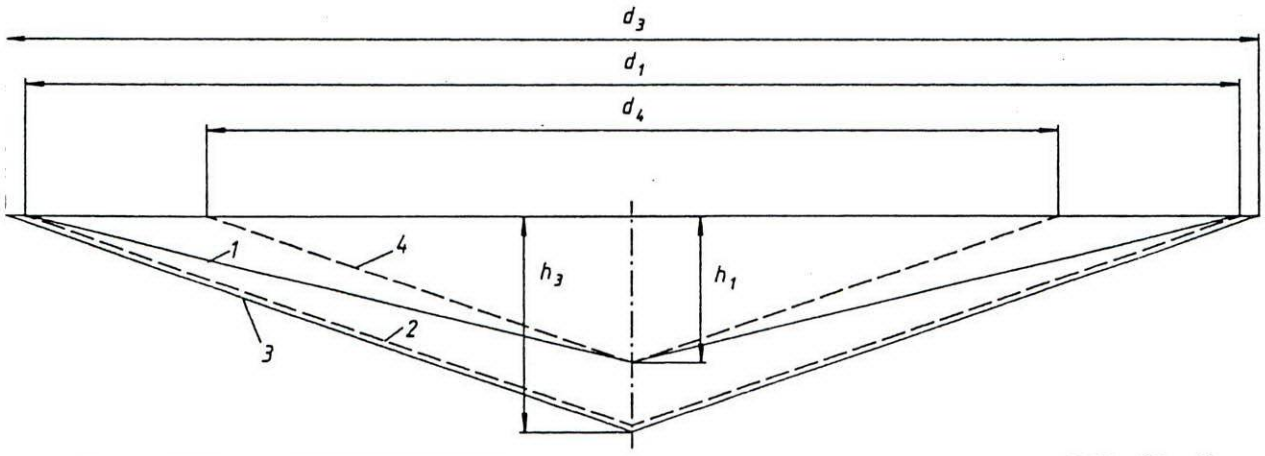

Figure 2 : Schematic representation of Vickers indentation with resultant permanent indentation and universal hardness indentation and evaluation

The permanent Vickers indentation, which is geometrically distorted compared to the indentor shape, is represented by outline 1. Its diagonal d_1 is measured. Using this diagonal, the indentation surface area A_1 is calculated based on the wrong assumption of a geometrically correct indentor image. As figure 2 shows, actually a fictitious surface area is being calculated and represented by outline 2. The defined surface area A_1 and the calculated surface area A_2 are significantly different for the reasons that have been mentioned previously. If instead of the diagonal d_1, the indentation depth h_1 is measured and used to calculate the Vickers hardness, which would then be based on a geometrically correct indentor image, the result would be based on the fictitious indentation outline represented by line 4.

For the determination of the universal hardness, the indentation depth h_3 is measured under test load, and then the surface area of this indentation is calculated. In this case, it is irrelevant to the result whether the indentation depth h_3, or, as is common with plastics [4], the diagonal is being measured. Based on the Vickers pyramid geometry, the following relationship exists

$$d_3 = 7.008 * h_3 \quad or \quad d_3 \approx 7 * h_3 \qquad (3)$$

Substituting equation (3) into equation (2) yields :

$$HU = \frac{F * 1.854}{d_3^2} \; [N/mm^2] \qquad (4)$$

If we disregard the factor 0.102, which stems from the test load conversion, in the HV equation (1), then from the same indentation the Vickers hardness is calculated using the diagonal d_1 and the universal hardness using the diagonal d_3. The difference $d_3 - d_1 = \Delta d$ is the degree of elastic recovery of the diagonal after removal of the load. Therefore, the principal difference between universal hardness and Vickers hardness is based on the degree of indentation diagonal elastic recovery Δd. The following possibilities exist:

1. For materials exhibiting only plastic flow $d_3 = d_1$ and therefore HU = HV.

2. In cases, where the difference between d_3 and d_1 lies within the measurement uncertainty of the indentor displacement measurement system, the values for HU and HV will approximately fall in the same range.

3. In all other instances (which will be the majority of cases) the universal hardness will be lower than the Vickers hardness.
This statement can be proven easily by computing the indentation areas from equations 1,2 and substituting $d_3 = d_1 + \Delta d$ as the diagonal length for the Universal Hardness.

$$\frac{A_{HU} - A_{HV}}{A_{HV}} = \frac{2 * \Delta d}{d_1} \qquad (5)$$

In general, universal hardness and Vickers hardness will therefore always be different. The degree of this difference depends on the degree of the elastic component of the total indentation deformation. This in turn depends on the modulus of elasticity and the elastic limit of the material to be tested. It is therefore impossible to establish a universal conversion formula between Vickers hardness and universal hardness. In reply to the question about the degree of correlation between the Universal Hardness Test and the classical Vickers test for practical applications, the only possibility is to compare empirical test results for a given material at a given material condition. This approach is certainly possible. However, the use of the same indentor geometry in regard to correlation between the test methods will not make this a special case.

3 Comparison using empirical test results

In the appropriate literature, so far only very few test method correlation study results have been published. One has to go back to results on steel [5] (steel specimen having the same modulus of elasticity), which allows the explanation of another "interfering effect" in the interpretation of the test results (Figure 3).

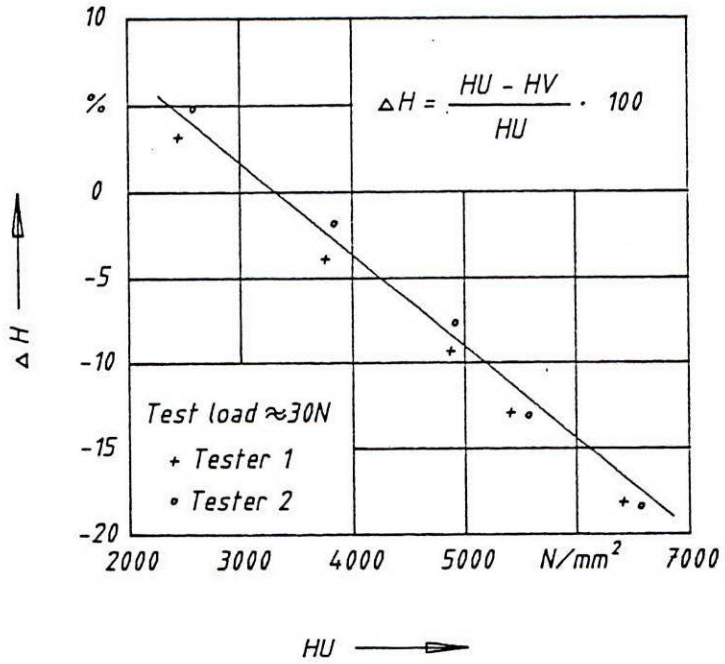

Figure 3. The difference between universal hardness and Vickers hardness for different hardness steel specimen [5]

With increasing hardness of the specimen, the elastic limit also increases. Therefore, the elastic component of the material displacement during indentation increases with increasing hardness. The deviation of the universal hardness from the Vickers hardness follows the increase of the elastic deformation in the described manner. Using a very soft hardness test block, the sign of the reported difference was reversed.

This effect can be explained :
The indentation is relatively large. The elastic recovery under the indentor tip is only in the area of 10%. This corresponds to a degree of diagonal length elastic recovery, which is hardly measurable given the limit of the diagonal length measurement precision for most instruments on the market. In this case using a very soft hardness test block, a significant amount of material pile-up, or ridging occurred around the indentation boundary, as shown in Fig. 4 .
Because of this ridging, the diagonal length was actually measured outside of the true indentation which resulted in a measurement error of the diagonal length on the long side.
The data published as early as 1978 by Dengel and Kroeske [7] also confirm the above statements.

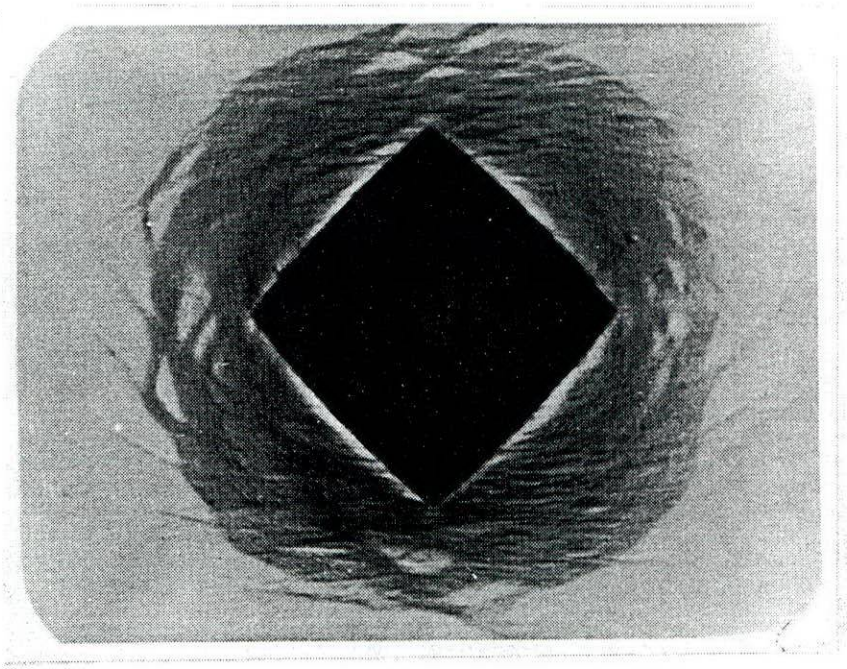

Figure 4. Vickers indenttion, hardness test block approximately 220 HV 10.

In conclusion, it is generally not possible to establish a direct conversion procedure between Vickers Hardness and Universal Hardness, even though both test methods make use of the same indentor geometry.

Literature

1 *Weiler, W.:* Die Bedeutung der wahren Gestalt von Härteeindrücken für die Vergleichbarkeit der Härtemeßverhalten nach Vickers und Rockwell, C Dissertation, TU Braunschweig, 1970 *(The significance of the true shape of hardness indentations for the purpose of comparing hardness measurements according to Vickers and Rockwell, C dissertation, TU Braunschweig, 1970)*

2 *Weiler, W.; Behncke, H.-H.:* Anforderungen an den Eindringkörper für die Universale Härteprüfung, zur späteren Veröffentlichung in Materialprüfung vorgesehen. *(Requirements for indentors in universal hardness testing, intended for later publication in Materialprufung)*

3 *Weiler, W.:* Zur Definition einer neuen Härteskala bei Ermittlung des Härtewertes unter Prüfkraft. Materialprüfung 28 (1986) 7/8 S. 217 - 220. *(Definition of a new hardness scale for determination of the hardness under test load. Materialprüfung 28 (1986) 7/8 pg. 217 -220)*

4 *Müller, K.:* Anwendung einer neuentwickelten Härtemeßmethode auf der Basis des Vickers-Verfahrens. Kunststoffe 60 (1970) 4, S. 265 - 273 *(Application of a newly developed hardness test method based on the Vickers method. Kunststoffe 60 (1970) 4, p. 265 - 273)*

5 *Meyer, R.:* Ein Universal-Härteprüfautomat nach Vickers mit Prüfmessung. VDI Berichte 583 (1986) *(A automatic universal hardness test instrument according to VDI-reports 583 (1986)*

6 *Weiler, W.:* Härteprüfung an Metallen und Kunsstoffen 2. aktualisierte und erweiterte Auflage. Expert Verlag, Ehningen 1989 (Hardness testing on metals and plastics. 2 nd revised and expanded edition. Expert publishing, Ehningen 1989

7 *Dengel, D and Kroeske, E :* Preload-free digital hardness measurement of various materials with the Vickers indentor. VDI Report 308, 1978 , pg. 63-69

8 *Weiler, W. :* Dynamic Loading, A new Microhardness Test Method. ASTM Journal of Testing and Evaluation 1990, Volume 18, Number 4, pg. 229..

The author of this article

Prof. Dr.-Ing. Weiler, born in 1934, studied mechanical engineering majoring in material finishing and materials research, since 1961 active at the Physikalisch-Technischen Bundesanstalt (Federal Institute of Physics and Technology) in Braunschweig , heading the group "Force" since 1974.

Solderability Characteristics of Palladium, Palladium Nickel, Hard and Soft Gold Electrodeposits

I. Kadija
J.A. Abys
E.J. Kudrak
J. J. Maisano

AT&T Bell Laboratories
600 Mountain Avenue
Murray Hill NJ 07974

Abstract

Palladium and palladium alloys are the only serious alternatives to gold as an "electronic finish". In the past, the major impetus for such a substitution has been economic; however, today palladium's technological advantages are generally recognized. This is especially true in the connector markets where the material properties (e.g. hardness, ductility, thermal stability, etc.) of palladium are in many instances superior to hard gold.

Recent advances in plating technologies coupled with a more thorough understanding of the materials properties have expanded the use of electroplated palladium and palladium alloys in the PCB, semiconductor and optoelectronic packaging markets. To assess the suitability for such applications, the wire bondability and solderability of these finishes need to be investigated.

Introduction

Packaging of electronic devices has always been a critical operation in electronics. Its importance has increased in recent days due to high clock speeds and power output. More compact units are being produced with greater functionality with larger numbers of contacts in smaller spaces. With such design requirements, interconnect density and contact quality have become important quality metrics. This has created technical and commercial challanges for the manufacturing processes. Connection among several hundred interconnects, spaced as thin as 60 microns appart (1) must be perfectly executed. The failure rate of such contacts must be kept at a minimum to keep the production cost competitive. For example, an apparently minimal failure rate of 100 ppm in soldered contacts can double the price of device (2).

Silver and gold finishes are typically encountered in higher quality packaging. Wire bonding is applied on both, while soft gold is the preferred choice for solderability. Pure gold's resistance to tarnish has made it a natural selection for dependable solderability. More recently palladium and palladium alloys are being introduced as interconnect finishes becuse they are less expensive and in some instances functionally better than gold (3 and 4). Their superior performance has been already demonstrated in separable contacts (5 - 7). In addition, palladium plating for leadframe packaging application has been in use for some time (8, 9). The lower overall processing cost of utilizing palladium and palladium alloys is a result of process simplification (8) .This has made their broader introduction into packaging our near future technological challange.

Standards such as MIL STD 883, methods 2003 and 2022, were developed to scrutinize interconnect finishes and establish their functional dependability prior to further packaging. Method 2003 is particularly useful in qualification and performance comparison of the finishes. Although it does not provide complete information on soldering performance of coatings, such as wetting time and wetting force, as indicated by Davy (10), it can be used as a gross indicator of functional performance. A particularly useful aspect of the test is the ability to optically inspect a large substrate area and rate coverage quality, at 10x to 20x magnifications.

Military standard 883 was developed for plated solder or thick (50 to 100 microinches) pure Gold (MIL-G-45204C) finishes and are used for failure mode analysis of these finishes. In light of the economic pressure on the electronic market, reduction of gold consumption without compromising functional performance modification of these standards to accomodate reliable alternate finishes may be advisable.

In an effort to categorize existing plating processes, we have performed solderability tests with hard and soft gold, palladium and palladium alloys. Solutions were commercially available as proprietary or standard plating chemistries.

Sample Matrix Selection

The experiment design included Au, Pd and Pd alloy finishes. The desired finish solderability characteristics are outlined in the MIL STD 883 specifications. Soft Gold was used as a control finish. In addition to standardized solderability tests, which included fresh and steam aged coatings, each finish was exposed to heat treatment simulation test at 200C for 168 hours. We also modified the test to include a 5 fold dilution of the rosin flux and OA (Organic acid) flux. Beneficial effect on parts' solderability have been observed when diluted or preheated "R" fluzes are used. In addition, OA flux, which is known to be highly effective, was used to determine finish performance at optimum solderability conditions. The tests were performed with 20 microinches nickel plated 2"x 1.5" copper coupons. The formulation of the plating solutions used in this work are shown in Table 1.

Solutions:

1. Gold Plating Solutions:

Component	Soft Gold (Used for gold flash on GfPd & GfPdNi finishes)	Hard Gold
Au	8 g/l	8 g/l
Co		100 ppm
Conducting Salt	130 g/l	130 g/l
monobasic potassium phosphate	4 g/l	
Brightener salt	30 g/l	30 g/l

2. Palladium Plating Solutions:

Component	Pd Acid Strike (abbr. PdSA)	Pd Plate (for PdP & GfPd test finishes)	Pd Thick & Ductile (abbr. PdTD)	PdLF	PdNi NFS (for PdNi & GfPdNi test finishes)	Pd NFS
Pd	10 g/l	25 g/l	25 g/l	25 g/l	25 g/l	25 g/l
NaCl	60 g/l					
Ni					15 g/l	
Dipotassium hydrogen phosphate		90 g/l	90 g/l	45 g/l		
Ammonium Chloride			80 g/l	50 g/l	80 g/l	80 g/l
Ligand (proprietary)		50 ml/l				
Additive II proprietary brightener			4 ml/l			
Additive IVS proprietary brightener						
Additive VS proprietary brightener					2 ml/l	2 ml/l
Potassium hydroxide		to pH 11.0	to pH 7.5	to pH 7.6	to pH 7.7	to pH 7.7
HCl (33 %)	to pH 3.9		tp pH 7.5	tp pH 7.6	tp pH 7.7	tp pH 7.7

The temperature and current density used to plate the test coupons were 45 C & 20 ASF respectively for all plating solutions. The plate thicknesses examined are listed below:

Plate Finish	Thickness (in microinches)	Plate Finish	Thickness (in microinches)
Pd Acid Strike	5	Gold Flashed Pd	5 Au/10 Pd
Pd Plate	5 & 10	Gold Flashed PdNi	5 Au/10 PdNi
Pd Thick & Ductile	5, 10 & 25	Soft Gold	5 & 10
Pd LF	5 & 10	Co Hard Gold	5 & 10
PdNi NFS	5, 10 & 25		

Table 1

EXPERIMENTAL GOLD AND PALLADIUM SOLUTIONS

Performance Results

Acceptable wettability is defined as 95% or higher solder coverage as detectable at 10 to 20 X magnification. However, even a 100% coverage does not meet acceptance criteria if coarse occlusions or other defficiencies show over the surface. This is particularly critical with finishes that result in formation of intermetallics of higher melting temperature and slower solubility. Surface features and mechanistic details of such intermetallics are discussed later. Method 2003 gives the following 6 parameters to be used as criteria in identifying the quality of finish solderability:

- Wetting
- Porosity
- Non-wetting
- Pinholes
- Dewetting
- Foreign Materials

Acceptance criteria require that in addition to minumum wettability of 95% there is less than 5% of other defects "not concentrated in any particular portion of the soldered surface". The above criteria are based on typical defects observed when soldering. Porosity gives the bond a reduced resistance to aging and corrosion. Foreign materials and intermetallics can reduce bond strength and induce brittleness. Dewetting also reduces bond strength. In each case the "quality percent" was representative of the coverage percent adjusted by the correction factor for other defficiencies. This meant that in some instances, we had 97% coverage but the excessive presence of occlusions had brought down the overall quality to a nonacceptable level of 93%.

In Figure 1, the test results in "Quality Percent" are plotted for the test finishes "As is" (Freshly plated). Pure soft gold, PdThick & Ductile (PdTD), GfPd and PdLF finishes had acceptable solderability. An example of an acceptable PdTD finish after soldering is shown in Figure 2. However, foreign material and occlusion defects were observed more frequently with palladium products than with soft gold (Figure 3). The trend towards increased content of occlusions coincided with the thickness of deposit, e.g. the 25 microinch-plated PdTD shows more occlusions than the 5 microinch-platedPdTD finish. Inferior performance was observed for Co hardened gold and PdNi finishes. For these finishes a strong dewetting effect was observed, as shown in Figure 4.

Figure 5 shows the effect of steam aging, as per MIL STD 883, on solderability. An average quality loss of 2-4 percent was observed. This loss of solderability is significant enough to bring some coatings bellow the acceptance level. Palladium nickel and Co hardened gold again showed inferior performance.

Thermal aging at 200C for 168 hours had a more deleterious effect than steam aging, as shown in Figure 6. With the exception of GfPd and marginally PdTD and LF deposits, all finishes show an inferior performance in solderability as fresh deposits. This aging cycle had a particularly negative effect on soft gold finishes. Figure 7 shows an example of strong non-wetting of soft gold. In contrast to that, Figure 8 shows good solder coverage of the GfPd.

Figure 9 shows the results of fresh finishes for a series of diluted "R" flux tests. Although the overall grading was very similar to the grading for the regular flux tests (Figure 1), two effects were noticeable: the soldered panels were smoother, and the non-wetting showed as smaller but larger number of non-wetted islands. The results for steam aged samples (Figure 10) soldered using the diluted flux show slightly improved performance compared to the full strength flux samples, particularly in PdTD and PdLF finishes.Figure 11 shows the results for solderability of high temperature aged samples. Although the results are inferior to the steam aged samples they are noticeably improved compared to the undiluted flux samples. This was especially true for the PdTD and PdLF deposits. The potential benefit of using diluted flux is still under investigation.

Tests conducted with OA water soluble flux were all successfull. Figure 12 shows the combined results of all finishes. This was expected since it is known that OA fluxes yield a superior solder coverage.

Results Interpretation and Discussion

Some general trends have been observed in solderability performance of the selected finishes. As expected, soft Gold has demonstrated a superior performance in most of the tests, although there was a loss of solderability after high temeprature tests. The surface of the samples was noticeably tarnished. Palladium coated samples showed superior performance after high temeprature tests, which is expected since gold difuses into the substrate much faster than palladium (11,12). The Au and Pd alloys showed inferior performance to the pure metals, showing strong trends towards dewetting. The results are summarized in the Table 2 (attached at end of the paper). Table 3 shows the finishes listed by the quality of their solderability performance based on MIL STD 883.

Table 3. Order of Solderability Performance of Finishes

Best	GfPd
Good	Soft Gold
Fair	PdLF, PdTD
Low Grade	PdP, PdNiNFS, GfPdNi and Hard Gold

However, OA flux enhanced the performance of all finishes.This observation is supported by practical experience.

Conclusion

In this study we have developed set of data which can be used to select solderable gold flashed palladium and palladium finishes for electronic packaging applications. It is particularly important that a thin layer, 5 microinches, of gold combined with palladium gave a superior solderable finish, even after high temperature aging. We are continuing to investigate the interactions of flux, type of finish and the effect of aging. The information developed will be applied to meet wire bonding, wear reliability and solderability requirements for electronic packaging.

References

1. R.R. Tummala and E.J. Rymaszewski, Microelectronic Packaging Handbook, pg. 404, 1990.
2. C. Bloch and J. Ranganathan, Digital: Process Based Modeling, IEEE/CHMT 11th International Conference, Electronic Manufacturing Technology Symposium, 1991.
3. I. Kadija, V. Chinchankar, V.T. Eckert, E.J. Kudrak and J. Abys, Electroplating of Thick and Ductile Palladium- A New Electroplating Technology, SUR/FIN Cinference, July 9-12, Boston, 1990
4. H.K. Strashil, I. Kadija, J. Maisano and J.A. Abys, Electroplating of Thick and Ductile Palladium Nickel Alloy, ibid.
5. E.J. Kudrak, J.A. Abys, I. Kadija and J. J. Maisano, Wear Reliability of Gold-Flashed Palladium vs. Hard Gold on a High-Speed Digital Connector System.
6. E.J. Kudrak, V. Chinchankar, J. A. Abys and J.J. Maisano, Porosity Evaluation of Composite Palladium, Palladium-Nickel and Gold Electrodeposits, SUR/FIN, June 24-27, Toronto, 1991.
7. S. Umemura, K. Yasuda and T. Aoki, Contact Resistance Characteristics of Noble Metal Alloys for Connector Contacts, IEEE Transactions on Components, Hybrids, and Manufacturing Technology, Vol. 14, No. 1, March 1991.
8. D.C. Abbott, M. Mitchell, B. Lockhorst, Texas Instruments, Case Study of a Palladium Finish on Leadframes for Semiconductor Packaging, EAST Conference, November 1991.
9. A. Murata, D.C. Abbott, Technology Trends of Leadframe Surface Finishing,
10. J.G. Davy, How Should Component Lead Solderability Testing be Performed ?, SUR/FIN, June 24-27, Toronto, 1991.
11. W.G. Bader, Dissolution of Au, Ag, Pd, Pt, Cu and Ni in Molten Tin-Lead Solder, Welding Journal, December 1969.
12. W.G. Bader, Soldering to Palladium and Palladium Coatings, Technical Memo, Bell Labs, Murray Hill, 1977.

Fig. 1 -Solder Dip Test, Method 2003
"R" flux, AS IS Finish

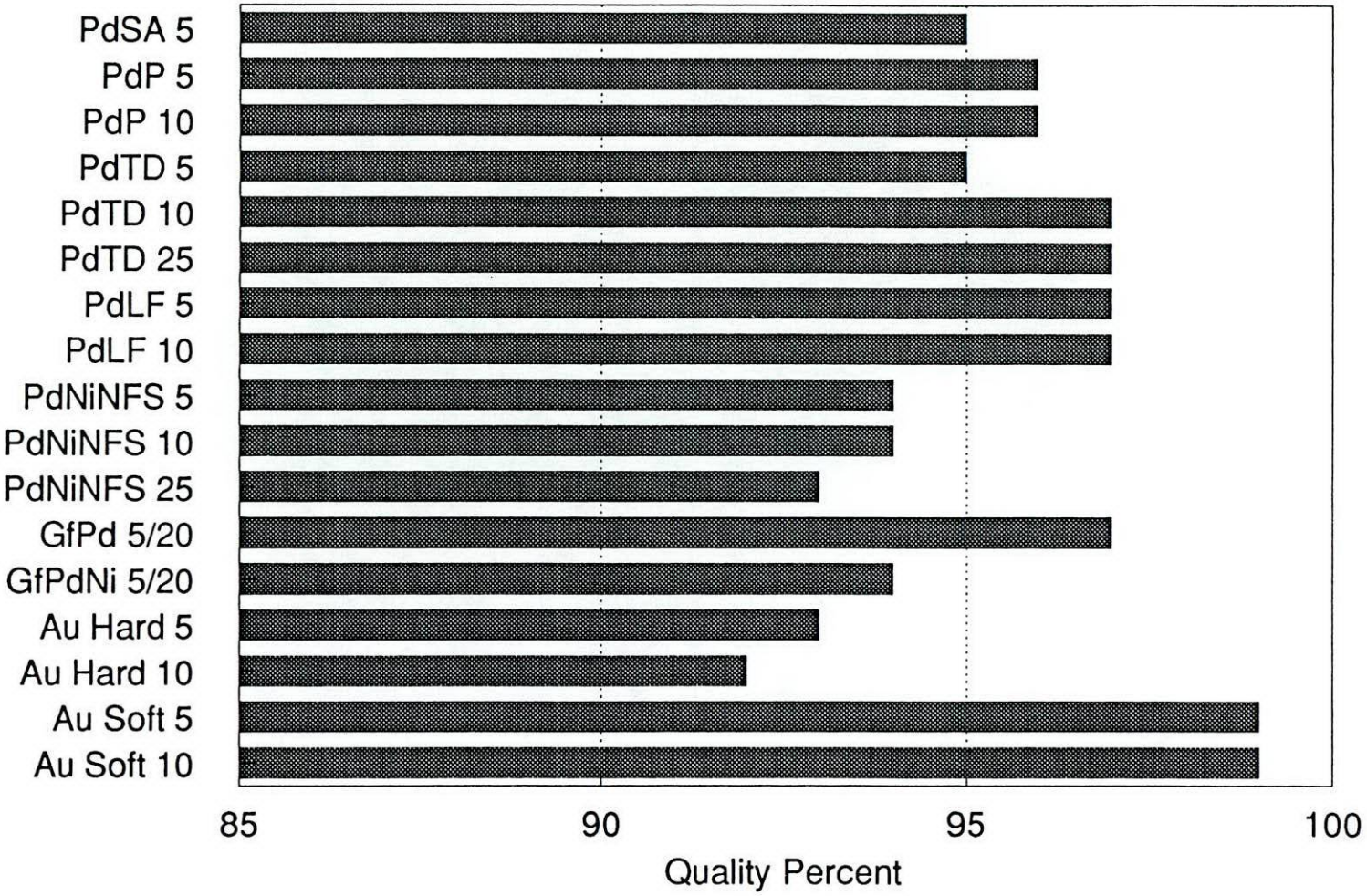

Fig. 2 - Solder Coverage, PdTD 10

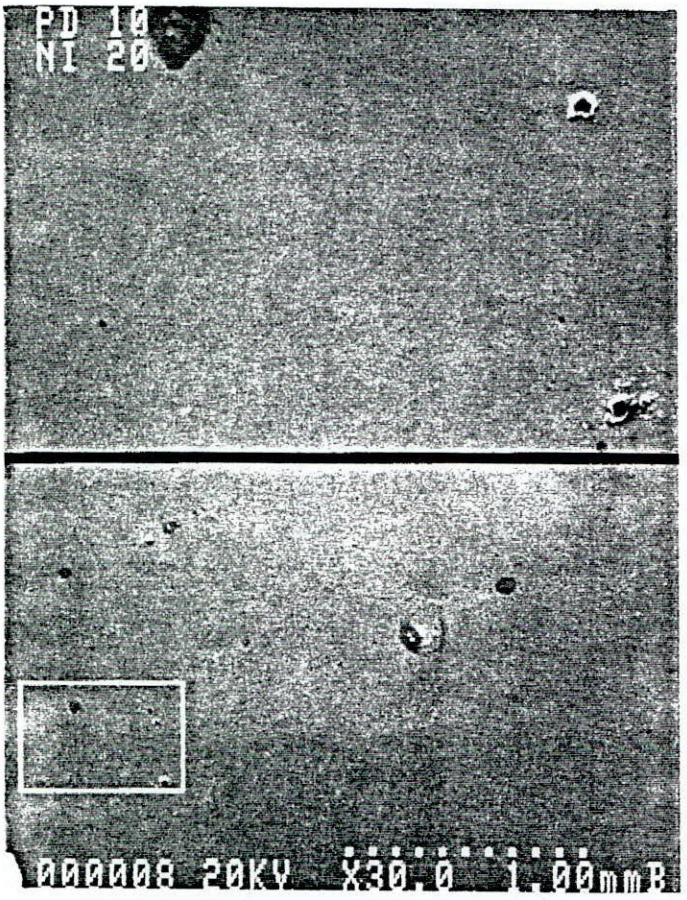

Fig. 3 - Foreign Materials
Undissolved Intermetallics, PdTD 50



Fig. 4 - Dewetting, Hard Gold



Fig. 5 - Solder Dip Test, Method 2003
"R" flux, Steam Aged

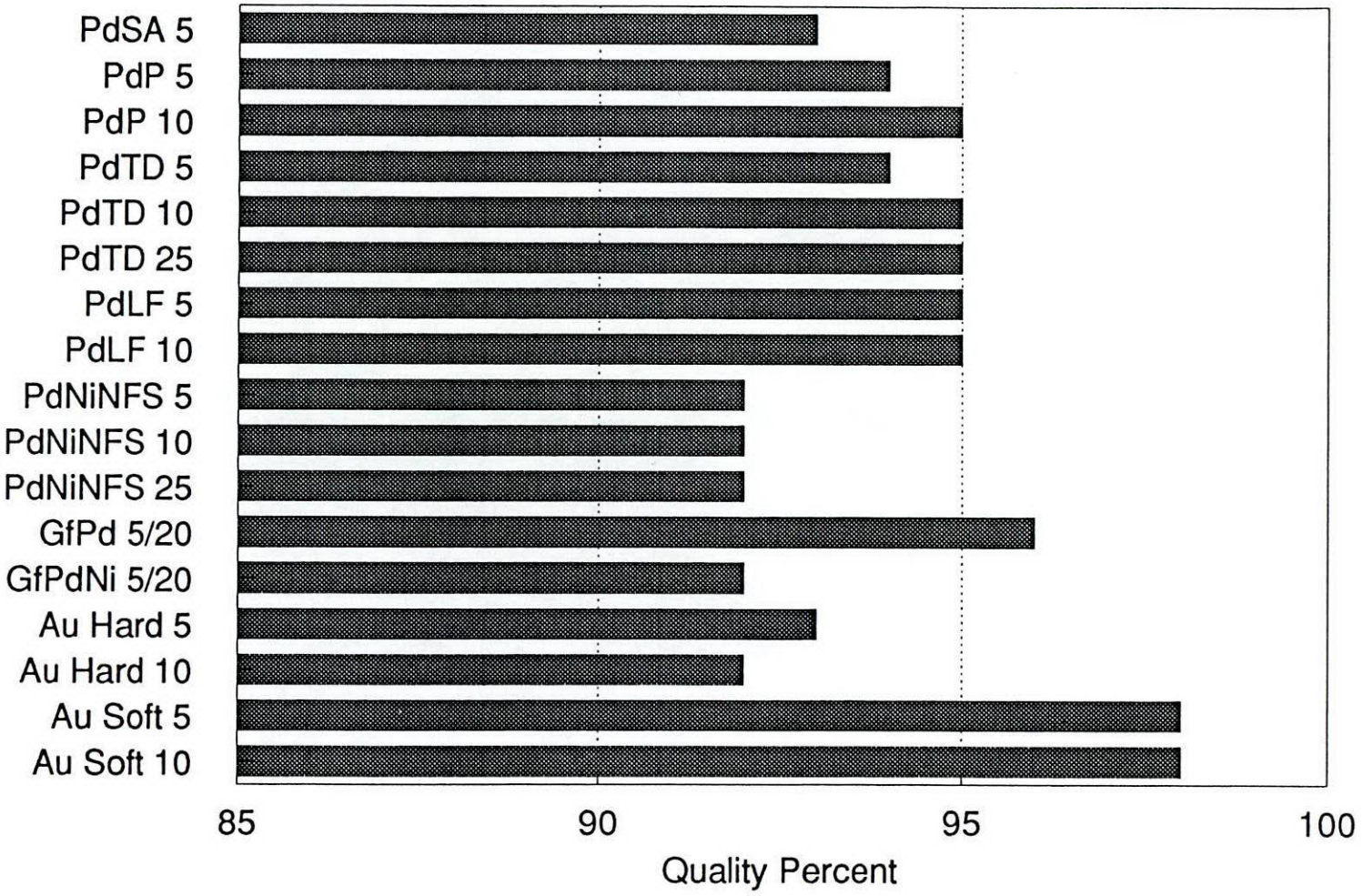

Fig. 6 - Solder Dip Test, Method 2003
"R" flux, 200C, 168 HRS

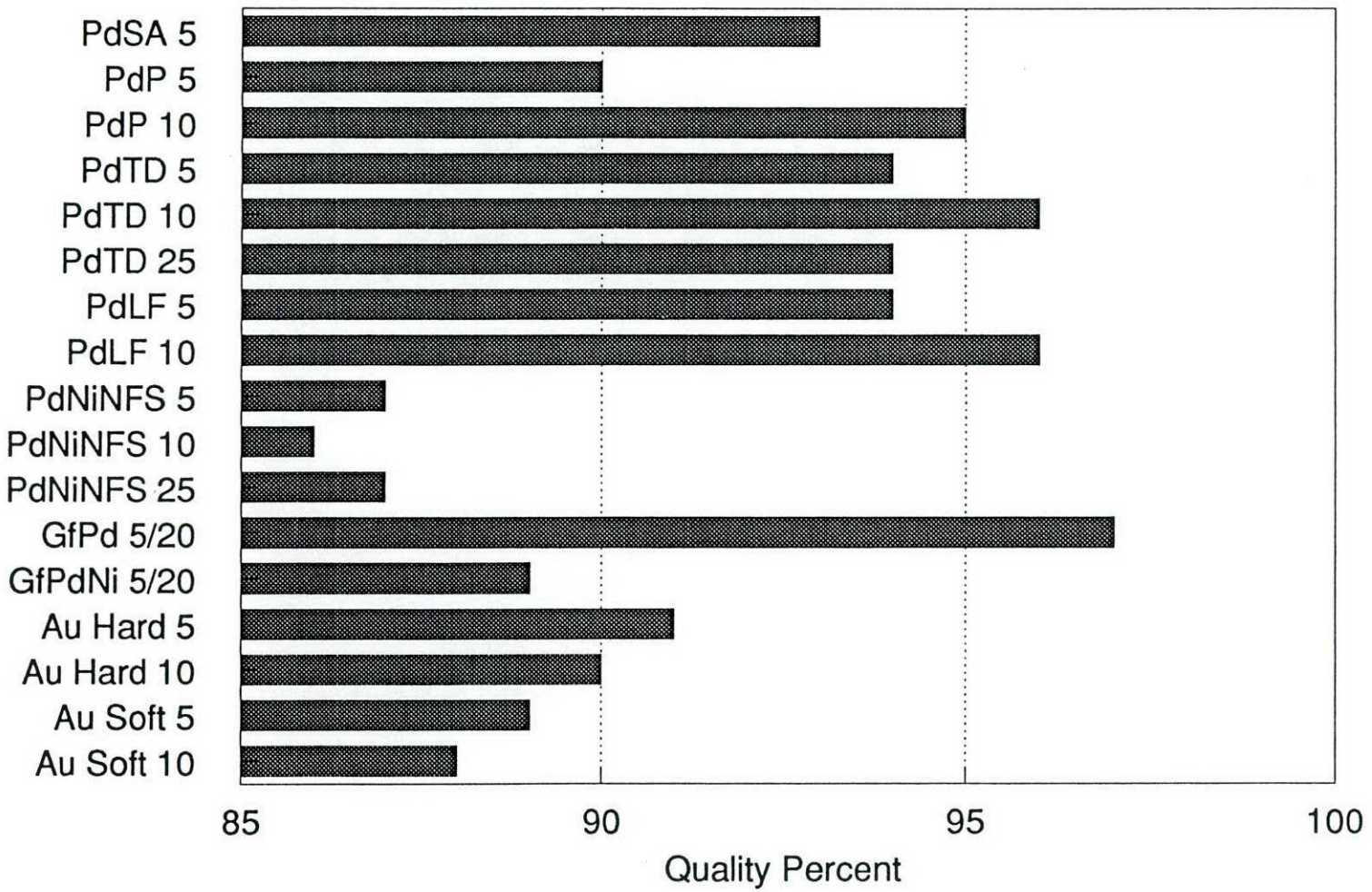

Fig. 7 - Non-wetting, Soft Gold
200 C, 168 HRS

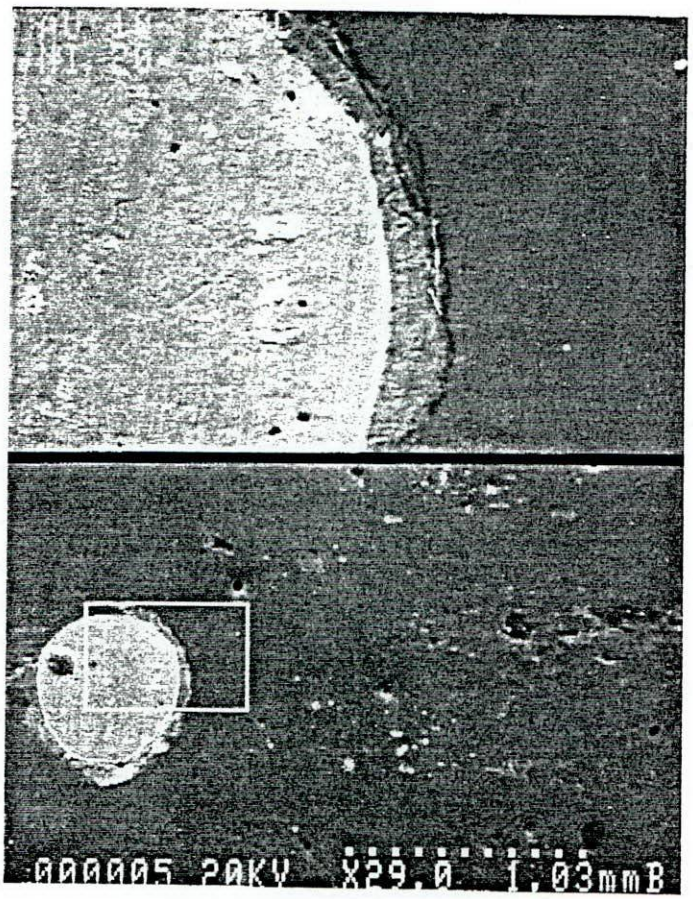

Fig. 8 - Solder Coverage, GfPd
200 C, 168 HRS

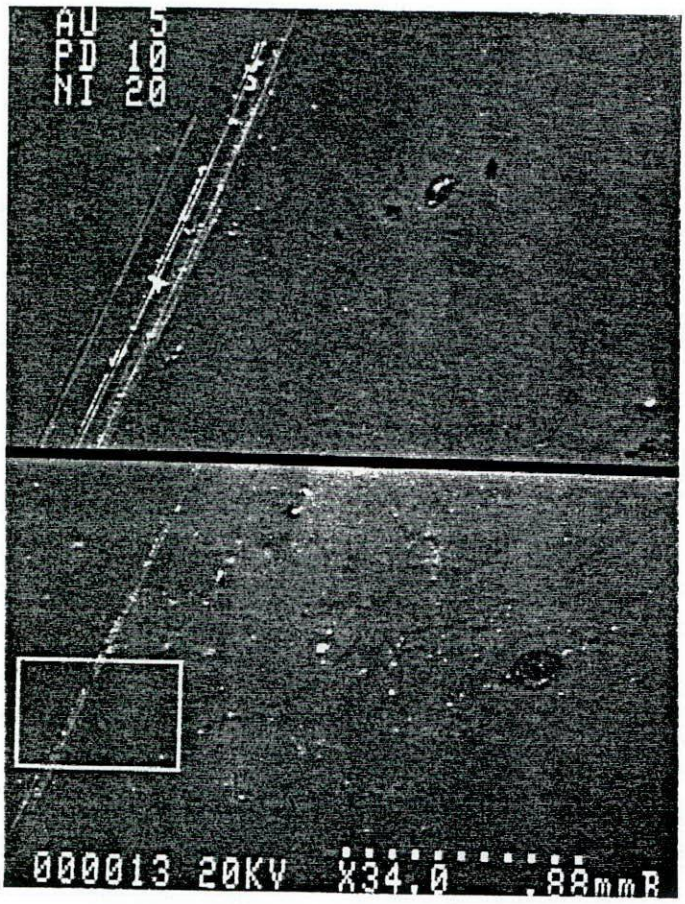

Fig. 9 - Solder Dip Test
"R"/5 flux, AS IS Finish

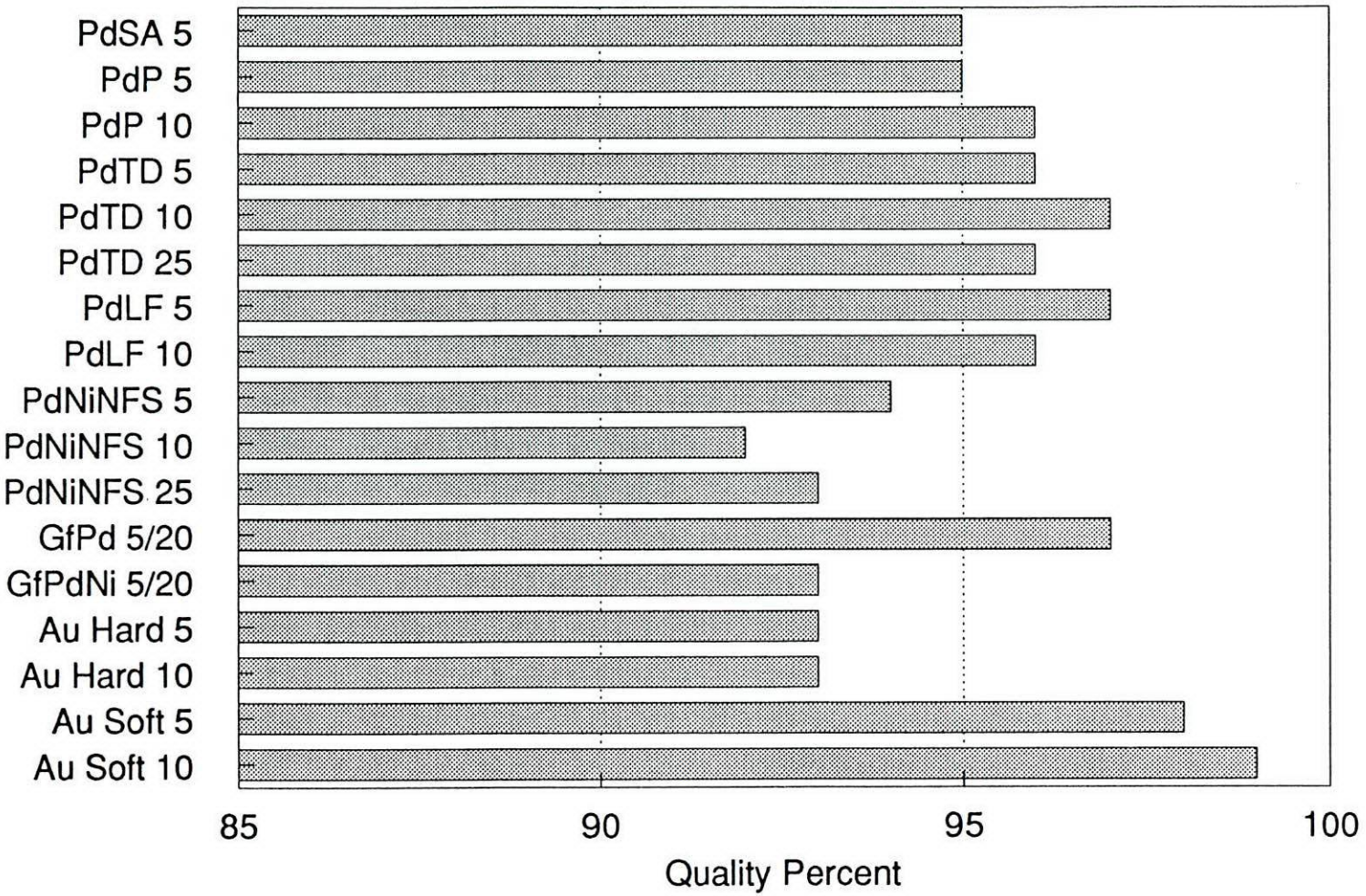

Fig. 10 - Solder Dip Test "R"/5 flux, Steam Aged

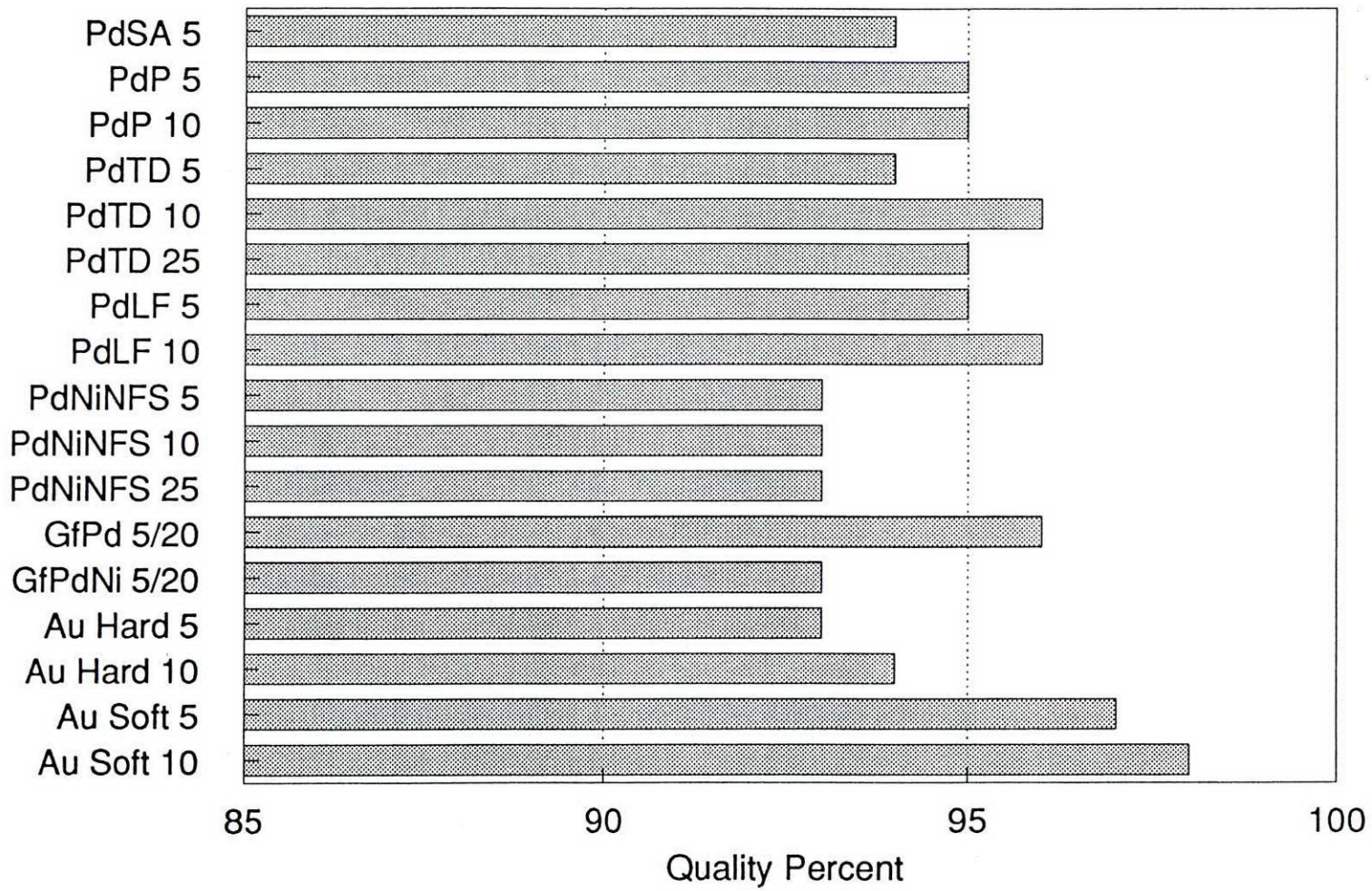

Fig. 11 - Solder Dip Test
"R"/5 flux, 200C, 168 HRS

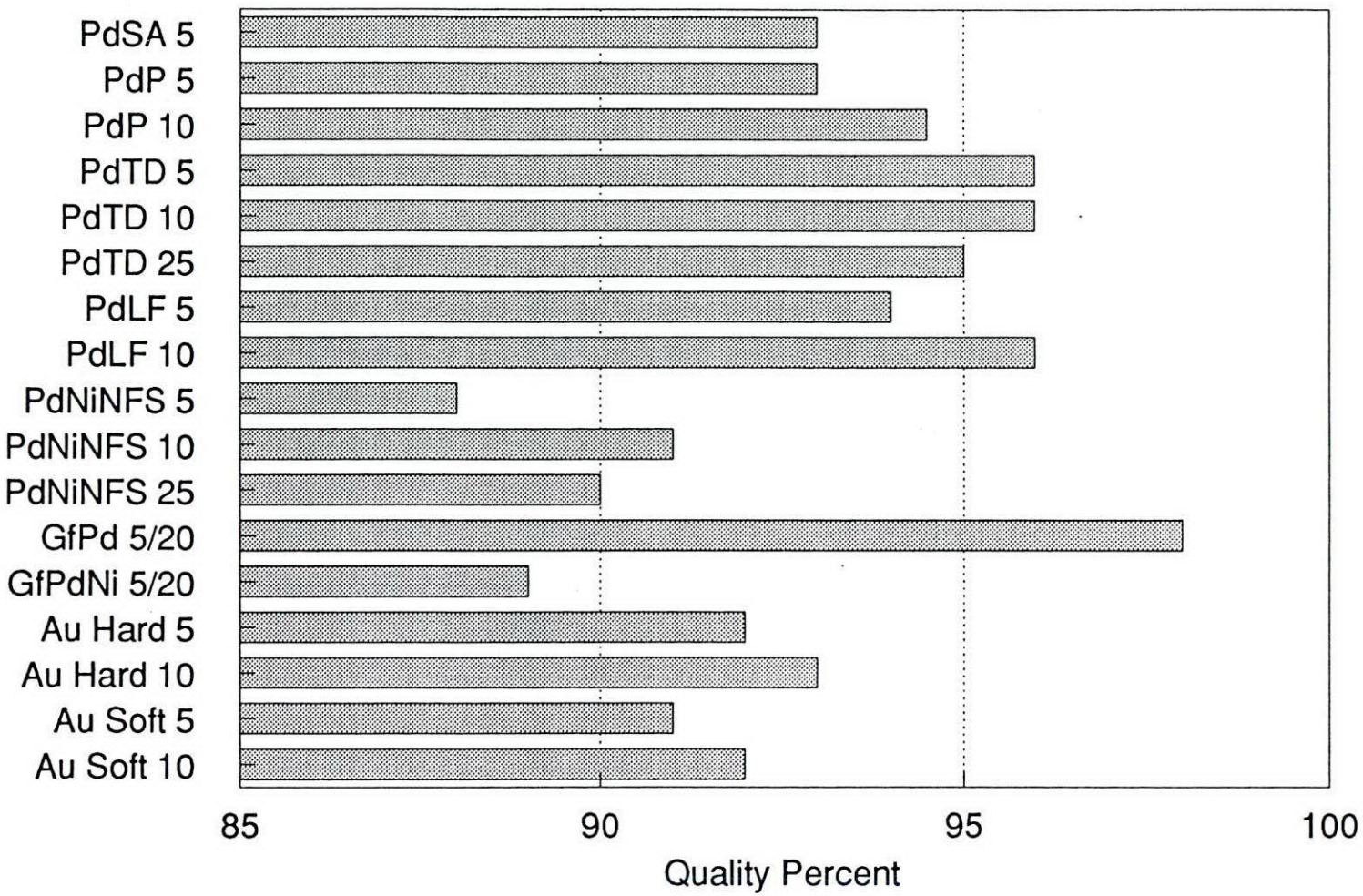

Fig. 12 - Solder Dip Test
"OA" flux, Combined

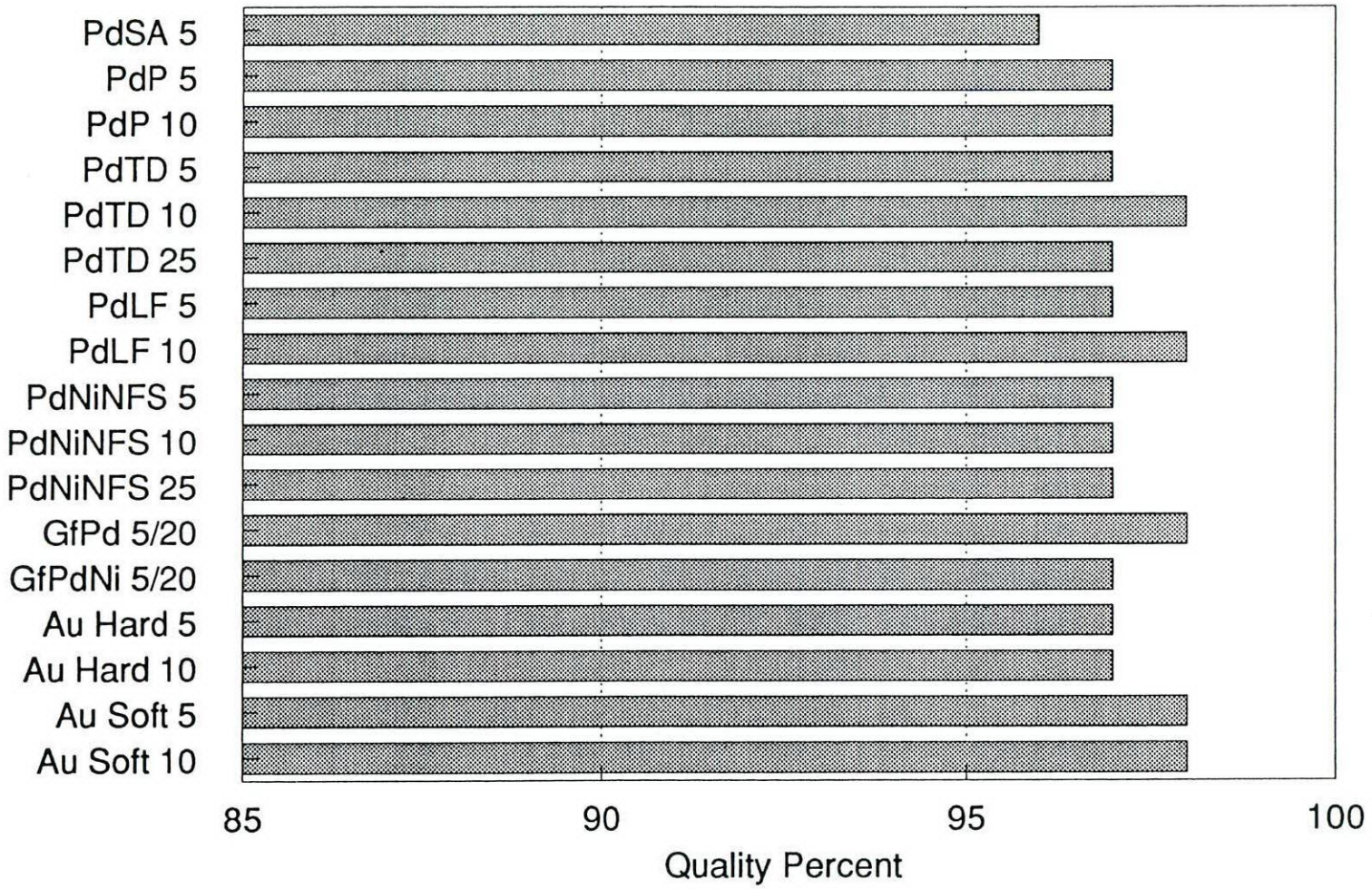

Table 2: Performance Summary and Acceptability

Solution	PdSA	PDP	PdP	PdTD	PdTD	PdTD	PdLF	PdLF	PdNi NFS	PdNi NFS	PdNi NFS	GfPd	GfPdNI	Soft Au	Soft Au	Hard Au	Hard Au
Thickness	5	5	10	5	10	25	5	10	5	10	25	5Au,10 Pd	5Au,10 PdNi	5	10	5	10
"R" Flux, finish "As is"	N	Y	Y	N	Y	Y	Y	Y	N	N	N	Y	N	Y	Y	N	N
"R" Flux Steam Aged	N	N	N	N	N	N	N	N	N	N	N	Y	N	Y	Y	N	N
"R" Flux 200 C for 168 hrs.	N	N	N	N	Y	N	N	Y	N	N	N	Y	N	N	N	N	N
Diluted Flux, finish "As is"	N	N	Y	Y	Y	Y	Y	Y	N	N	N	Y	N	Y	Y	N	N
Diluted Flux Steam Aged	N	N	N	N	Y	Y	Y	Y	N	N	N	Y	N	Y	Y	N	N
Diluted Flux 200 C for 168 hrs.	N	N	N	Y	Y	N	N	Y	N	N	N	Y	N	N	N	N	N
OA Flux	Y	Y	Y	Y	Y	Y	Y	Y	Y	Y	Y	Y	Y	Y	Y	Y	Y

MAGNETIC PROPERTIES AND STRUCTURE OF COBALT HARDENED GOLD

David Kahn
Materials Processing Research
AMP Incorporated
P. O. Box 3608, Harrisburg PA 17105-3608

Abstract

The implementation of an experimental design to investigate the variation in cobalt hardened gold electrodeposition produced a series of electrodeposited **Au**Co alloys which had been stripped from their copper substrates. The magnetic properties of these electroplatings were measured at room temperature using the Faraday method. These measurements showed the presence of two magnetic phases. One phase consisted of a solid solution of cobalt in the gold matrix and the second was found to be a diamagnetic cobalt containing component. The magnetic measurements showed that no precipitates of metallic cobalt were present and that individual atoms and nearest neighbor pairs of cobalt atoms in the solid solution are not magnetic. The diamagnetic phase cannot contain cobalt hexacyanocobaltate $Co_3(Co(CN)_6)_2$, which is found after treatment of the alloy with aqua regia. Also,the second phase can not all be potassium hexacyanocobalte $K_3(Co(CN)_6)$. Subsequent to this the platings were annealed in hydrogen at 800° C to destroy any cobalt compounds in the platings and the magnetic properties were remeasured. These second measurements showed the existence of only one phase, again a solid solution of cobalt in gold. This phase showed superparamagnetic behavior with some remanence and is a magnetic nanocomposite. The amount of the cobalt in the "metallic" and "compound" phase is calculated from the contribution of each phase to the initial slope of the magnetization curve.

Introduction

The use of gold plating containing small amounts of cobalt ~ 0.3 wt. percent(1.0 at %) on electrical contact members is quite common in the electronics industry. Recently the variation in plating efficiency with plating conditions was studied using an experimental design encompassing ten plating bath parameters. One of the results of this effort was 64 **Au**Co platings produced in four experimental blocks. These platings were stripped from their copper substrate and the magnetic properties of these coatings were measured. Since cobalt is a ferromagnetic element and the gold matrix is very weakly diamagnetic, the behavior of the cobalt in the gold alloy should affect the magnetic properties of the samples.

Some of the graphs in this work are presented in the form of the variation of one dependant response on the cobalt content for a number of different samples, although

these experiments are not the usual kind where only one independent variable is changed and the others kept constant. In this designed experiment, ten plating bath variables are determined a priori for each run and their values are one of two levels determined by the experimental design. One of these parameters was the cobalt concentration in the bath. Because of this, the dependence of any measured response on the cobalt content is valid only to the extent that the values of the other variables do not affect the magnetic behavior of the cobalt deposited in the electroplated gold alloy. The measurements of the magnetic behavior of a single sample are not affected by this problem, but this difficulty will arise when the result for one sample is compared to the results for others.

In order to determine the total cobalt content, a portion of the stripped, electroplated **Au**Co platings were annealed in hydrogen at 800° C to destroy any "compound" phase that might be present in the alloy plating and furnace cooled.[1] In this report, the word "organic" is used to identify any second phase in the **Au**Co sample, although as discussed below this phase contains the cobalt in a hexacyanocobaltate salt. The magnetic properties of these annealed samples were also determined. We would expect that these samples are uniform except for the cobalt content, since this treatment probably results in a single metallic phase in the plating. When these annealed platings are dissolved in aqua regia, only a very small amount of black powder remains, which is probably some carbon residue in the plating.

Experimental Method

The magnetic susceptibility of the samples was measured at room temperature using the Faraday method. The magnetic field in these experiments was created by a 12 inch electromagnet(Varian Model V-3900)fitted with specially designed(Faraday) pole caps to produce a nearly constant value of $H\partial H/\partial z$ of 14.964 kOe^2/cm over a vertical distance of 1.8 cm at a magnet current of 168 A. A gold plated pure copper bucket was suspended at this point from a Perkin Elmer AD2B microbalance using a silica optical fiber. The extra force on the sample caused by its magnetization is

$$\delta F_z = m\chi_g H\partial H/\partial z, \qquad (1)$$

where m is the mass, and χ_g is the magnetic susceptibility per gram. A schematic of the experimental setup is shown in Figure 1. The samples used were approximately 20 mg and were weighed using a Mettler Type H15 balance. Since we wanted to measure the magnetic susceptibility over a range of magnetic fields and the pole pieces were calibrated for only one value of the current, the apparatus was calibrated for other values of the current by using a sample of known magnetic susceptibility, cobalt tetrathiocyanatomercurate from SPEX Industries. This calibration was checked by measuring the magnetic susceptibility of a pure gold sample. The magnetic field at intermediate values was measured using the Hall effect monitor furnished with the magnet control system.

In order to check the accuracy of the susceptibility measurements, the saturation magnetization of sample III 8 B Annealed was measured for both directions of the field. These results are shown in Figure 2. Although this measurement requires an extrapolation of the magnetization to an infinite applied field value, the two results agreed to within 0.16 percent. These measurements show that the observed variation in the magnetic behavior from sample to sample is not due to errors in the magnetic measurements, but is due to real variation in the samples.

Experimental Results

As a result of the limited solubility of cobalt in gold, if the concentration of the cobalt is large enough, some of the cobalt would precipitate into small particles. The Au/Co phase diagram is shown in Figure 3.[2] The diagram shows that the solubility of gold in cobalt at room temperature is very low so that any cobalt that might precipitate would be almost pure cobalt and show a corresponding magnetic behavior.

Since cobalt is ferromagnetic with a saturation magnetization, M_s, of 1398 Gauss[3] and gold is weakly diamagnetic with a magnetic susceptibility per gram(χ_g) of -1.42E-07 CGS-EMU[4], any precipitated cobalt will produce a very noticeable magnetic effect. The magnetization of two weight percent cobalt in a cast **Cu**Co alloy is shown in Figure 4.[5] In this case the magnetization is on the order of ten Gauss for an applied field of 3000 Oersted, even though the cobalt particles are small enough to be superparamagnetic. In all of our samples, on the other hand, the magnetization is less than 1.0E-3 Gauss, so that it is clear that cobalt precipitates of any reasonable amount can not be present.

In several instances **Au**Co platings that contained the most cobalt as determined by magnetic susceptibility measurements were examined using X-ray diffraction to see if any crystalline cobalt could be detected. No cobalt peaks were seen although X-ray diffraction probably is sensitive enough to detect a fraction of a percent of metallic cobalt.

A. Annealed Platings

As discussed above, a portion of the thick cobalt plating stripped from the copper substrate, was annealed in hydrogen at 800° C for two hours and furnace cooled. If the magnetization of these annealed platings is measured, the results for all samples are similar. Magnetization curves for samples with the largest(III 8 B) and the smallest(IV 5 B) cobalt content are shown in Figures 2 and 5.

If each cobalt atom in the alloy retained its magnetic character and the magnetic moments were acting independently, we would expect a paramagnetic behavior of the alloy. In this case we would expect that the magnetization at room temperature would be a straight line with a positive slope. We see quite a different behavior in our samples in that the applied field of 20 kOe is large enough to align almost all of the available cobalt

spins so that the magnetization of the alloy is nearly saturated. This can only mean that there is some cooperative interaction between the cobalt spins in the sample. We also notice that there is a small remanence, or residual magnetization, when the applied field is reduced to zero after saturation. The coercive field, i. e. the field in the opposite direction required to reduce the remanence to zero, for sample III 8 B is about 130 Oersted and the coercive field for sample IV 5 B is close to 1 kOe. A portion of this hysteresis is probably due to some iron impurity and is discussed in more detail below, but the majority is real.

The saturation of the magnetization curve would imply the presence of spontaneous magnetization in the alloy, and the existence of a measurable remanence would imply that there is some metastable magnetic behavior. These two results can be explained if almost all of the magnetic units are small enough so that they contain only one domain and in addition, some of these domains are large enough so that the energy of thermal agitation at room temperature is too small to reverse the spin direction because of magnetocrystalline anisotropy.[6] These domains will not become disordered in the time required to make the magnetic measurement and some remanence will be seen.

Since this measurement is made at a known temperature(22-25° C), if we know the magnetocrystalline anisotropy, K_1, we can say something about the size of the magnetic entities. The demagnetizing effects of thermal disorder have been calculated by Neel, and he has derived an upper limit for the volume, V, of a particle that should show saturation but no remanence.[7] Since a particle with a single domain can change its direction of magnetization only by changing the direction of its moment, this shift will occur fast enough so that no remanence is observed if the energy barrier due to the magnetocrystalline anisotropy is less than about 20 times the thermal energy. In this case the inequality

$$K_1V/kT < 20 \qquad (2)$$

must be satisfied for this type of superparamagnetic behavior. Since the cobalt atoms in the alloy have a cubic symmetry, the usual anisotropy value for hexagonal Co does not seem appropriate. If we extrapolate the measured value of K_1 for cubic Co to room temperature, we find a value of approximately -5E05 ergs/cm^3.[8] Using this value we find that the upper limit for the diameter of a superparamagnetic entity at room temperature in the gold is 146 Å. Of course, we are assuming here that the anisotropy constant for pure cobalt is still valid for cobalt in solid solution in the gold.

Since we know the amount of cobalt in our samples, we can compare our measured saturation magnetization with that calculated on the assumption that each cobalt atom has the same magnetic moment that it has in pure cobalt(1.716 μ_B).[9] The calculated value for the saturation magnetization of sample III 8 B Annealed, assuming that each cobalt atom retains its moment is 48.49 Gauss. Since our measured value is only 0.00122 Gauss, we see immediately that the cobalt in the annealed plating can not be in the form of a cobalt

precipitate. Since the cobalt must then be in solid solution in the gold alloy, we can also conclude that most of the cobalt that is dissolved in the gold matrix is also not magnetic. If these hypotheses are true, our next question must be what is then giving rise to the measured magnetism.

Additional information about the distribution of the cobalt atoms in the annealed platings can be obtained by comparing the initial slope of the magnetization curve of each sample with the cobalt concentration in the sample. The data for Block II is shown in Figure 6. This Figure is especially interesting in view of the fact that the cobalt concentration in the plating bath is only one of two values for each sample. The regression of the initial slope on the cobalt concentration shows that the slope increases almost as the third power of the concentration. The reason for this is that superparamagnetism is a cooperative phenomenon and the contribution from any cobalt atom in solution depends on how many cobalt atoms are nearby. This effect has been investigated by Boucaï et al., who find that isolated cobalt atoms in a gold matrix are not magnetic, isolated pairs are also not magnetic at room temperature, but groups of three or more atoms have a magnetic moment and can lead to magnetic ordering at low temperatures.[10]

A plot of data taken from Reference 9 of the variation with cobalt content of the calculated probabilities per lattice site of single cobalt atoms(N1/N), isolated pairs of cobalt atoms(N2/N), cobalt atoms in groups of three(N3/N) and all larger groups(N4/N) is shown in Figure 7. We can see clearly that the probability of finding a group of three or more cobalt atoms is very small for low concentrations of dissolved cobalt and becomes appreciable only for concentrations larger than approximately 0.2 wt. percent cobalt. The total cobalt concentrations in the platings made for this study vary from 0.1495 to 0.691 wt. percent. The probability per lattice site of the sum of N3/N and N4/N is plotted in Figure 8. Here we see that the sum varies as the 2.902th power of the cobalt concentration. This is very close to the behavior shown in Figure 6, which shows a very similar dependence on the cobalt concentration. Similar plots for the other blocks show the same concentration dependence.

The nonmagnetic behavior of single atoms and close pairs of cobalt atoms in the alloy can not explain the total reduction in alloy magnetization that we measure in sample III 8 B Annealed. From Reference 9 the number of cobalt atoms in a mole of alloy included into isolated groups of three or more nearest neighbor cobalt atoms is just the sum of N3 and N4. This number for sample III 8 B Annealed(0.68 wt. %) is 1.322E-03 N, where N is Avogadro's number. In a gram of sample III 8 B Annealed, we have 4.043E+18 cobalt atoms that are magnetic. The ratio of the measured saturation magnetization for this sample to the calculated magnetization if all cobalt atoms carry their metallic moment is 1.32E-04. This means that the magnetic moment of the cobalt atoms in the alloy that are magnetic is approximately 0.0023 μ_B. This shielding of the impurity atom is not too surprising since the Kondo temperature for isolated cobalt gold atoms in gold has been estimated to be 500 K(226.8° C). Below this temperature we expect a shielding of the impurity magnetic moment.[11]

The results discussed above are clearly consistent with an annealed alloy plating containing a random solid solution of cobalt in a gold matrix. The amount of cobalt in these platings has been measured using an inductively coupled plasma emission spectrometer and has been denoted as "total" cobalt.

B. Unannealed Platings

The unannealed platings show a different magnetic behavior. In most of the platings, a plot of the magnetization vs. applied field is similar to the one for III 8 B Unannealed shown in Figure 9. We can see here that the magnetization shows a behavior that is a combination of ferromagnetic and paramagnetic behavior with clear evidence of some saturation but no apparent hysteresis and a magnetization that is on the order of 1.0E-04 Gauss. Since the Langevin function at high field values varies as 1-kT/mH, if we plot the magnetization vs. 1/H, we can extrapolate the points at large fields to find the saturation magnetization. This type of plot for III 8 B Unannealed is shown in Figure 10. The dashed line is the regression line fitted to the five highest field points. The Y-intercept is 143.9E-06 Gauss. The ascending field measurements are given by an "x", and the descending field curve points are denoted by a "o". The superposition of the two curves shows the lack of remanence and the precision of the measurements.

An applied field of 21 kOe should not be enough to saturate the magnetic moments in this sample at room temperature if they were acting independently. The near saturation behavior can easily be explained by the presence of superparamagnetic entities of cobalt atoms in solid solution, whose magnetic properties are not completely quenched by the gold matrix. The calculation of the upper limit for the diameter of particles showing superparamagnetic behavior in the previous section gave a value of 146 Å. X-ray diffraction measurements of the effective grain size for the <111> direction in this sample give a value of 188 Å, while the same measurement for grains with (200) planes parallel to the surface give a value of 130 Å. From these results it is tempting to consider the superparamagnetic entities as individual gold grains containing cobalt atoms in solution in the gold. If for some reason the cobalt atom density is greater in the interior of the grain than it is at the grain boundary, we would expect this uneven distribution of the cobalt in the grains to give rise to the type of superparamagnetic behavior that we observe.

We have shown above that individual cobalt atoms and pairs of atoms are nonmagnetic. The above behavior indicates that the magnetic interactions between nearest neighbor triplets is large enough to cause this superparamagnetic behavior in each grain. The fact that the magnetic character of the cobalt atoms depends on the distribution of neighboring solute atoms can explain the "scatter" in the magnetic data for different samples as shown in Figure 6. If the distribution of cobalt atoms in the gold matrix is affected by the plating parameters, we would observe a magnetic behavior that could be different for two samples even though the average cobalt concentration were the same.

If we expand the plot shown in Figure 9, we see a very small hysteresis as is shown in Figure 11. This hysteresis is very probably due to a small iron contamination, which is very hard to eliminate.

Although most of the unannealed magnetization plots are qualitatively similar to the curve shown in Figure 9, ten of the sixty four unannealed platings have a magnetization curve like that shown in Figure 12. In this case we see a ferromagnetic contribution that saturates at very low fields and a diamagnetic contribution from a second phase. The easily saturated ferromagnetic contribution is again probably caused by an iron impurity in the gold bath. The hysteresis at the low field end of the plot is clear from the deviation of the ascending and descending magnetization curves. This contribution can not be due to the dissolved metallic cobalt, since the data in Figure 9 show that the cobalt magnetization does not saturate at such low fields.

The magnetic susceptibility is equal to the slope of the magnetization vs. applied field. Since the slope for this sample is negative, the magnetic susceptibility must be negative and the existence of a diamagnetic phase is evident. This can not be due to the gold matrix, since the diamagnetic contribution from the gold has been subtracted from all the magnetization curves shown. The curves showing a diamagnetic phase are from those samples that have the smallest amounts of cobalt in the platings. If the samples are ordered in ascending values of the total cobalt content, the ten platings with a behavior like that shown in Figure 12, occur in the eighteen samples with the lowest total cobalt content. These samples have a total cobalt content that varies from 0.150(0.5) to 0.3(1.0) wt. percent. Since the magnetic effect of the dissolved cobalt is proportional to the cube of the dissolved cobalt concentration, the paramagnetic behavior of samples with a low dissolved cobalt concentration should be small by comparison and the diamagnetic phase will be seen. The diamagnetic contribution will not show any cooperative effects and will be proportional to the first power of the "organic" cobalt content.

Although we see the second phase in only ten samples at room temperature, it is likely that this diamagnetic phase exists in all the unannealed samples. In the other samples we would expect the diamagnetic "organic" cobalt contribution to be masked by the larger contribution from the "metallic" cobalt. One method of determining this would be to analyze the magnetization curves in order to calculate the contribution of both phases to the total magnetization curve. An ideal superparamagnetic sample would show a Langevin type behavior, but a number of factors could influence the shape of this curve. Unfortunately the effects of a distribution in particle size, magnetocrystalline anisotropy, demagnetizing effects, and magnetostriction will all cause a flattening of the ideal Langevin curve and can not easily be separated from the similar effect of a diamagnetic contribution.

A more accurate method of determining the diamagnetic phase concentration would be to repeat these measurements at a temperature low enough to saturate the superparamagnetic spins. In this case the contribution to the magnetization curve due to

the dissolved cobalt would become constant and any further change in the magnetization with increased field would be due to the diamagnetic phase only. This is analogous to what we observe for the samples with a ferromagnetic impurity. Many susceptibility measuring instruments use an alternating field magnetometer, and one of these could be combined with a large dc bias field in a low temperature Dewar chamber.

We can estimate the effect of temperature on the behavior of the unannealed deposits by fitting a Langevin curve to the III 8 B Unannealed sample data. If we fit the data shown in Figure 8, using a nonlinear regression routine, we obtain the curves shown in Figure 13. In this calculation the saturation magnetization of the fitted curve was found to be 154.1E-06 Gauss. This is somewhat larger than the intercept value of 143.9E-06 Gauss calculated from the data shown in Figure 10. Since the M vs.1/H plot near small values of 1/H is still curving upward in Figure 10, however, a larger value of the saturation magnetization found from fitting the whole curve is understandable. The value of m/kT determined from the regression calculation is 0.4834. If we change the sample temperature from 299.66 K to 77.36 K, the boiling point of nitrogen, and recalculate the fitted curve, we obtain the top curve shown in Figure 13. As we would expect the sample magnetization approaches much closer to saturation and the change in magnetization at higher applied fields is much less than we observe at room temperature. At this temperature a diamagnetic contribution to the magnetization should be easier to detect. In particular, any downward slope in the magnetization can only come from a diamagnetic phase.

Although low temperature susceptibility measurements are preferable, we can still attempt a separation of the two phases in the unannealed state by using the data at room temperature already obtained in this study. The contribution of the metallic phase to the initial slope of the magnetization can be obtained from the annealed data, since in this state all of the cobalt is dissolved in the gold matrix. If we use the results of the data shown in Figure 6, we can obtain a value for the contribution of the metallic cobalt to the initial slope. The contribution of the organic cobalt to the initial slope can be obtained from the data of Sample IV 5 B Unannealed shown in Figure 12. The chemical analysis of this sample can be understood on the basis that the cobalt in this sample is either completely "metallic" or completely "organic"i.e. all paramagnetic or all diamagnetic. There is no chemical evidence for two phases in this sample. As the data shown in Figure 12 indicates, this sample is clearly diamagnetic. Since this contradicts the assumption that the sample is completely metallic, we use the alternate hypothesis that the sample contains only "organic" cobalt. From the cobalt content of this sample we can obtain the contribution of the diamagnetic cobalt to the initial slope. In order to avoid any complication from ferromagnetic impurities in the samples, the initial slope is measured for applied magnetic fields greater than 4 kOe. Since the sum of the metallic and organic cobalt must equal the measured total cobalt content, we can eliminate one of the unknown concentrations and we have an equation for each sample slope in only one unknown. These equations were solved for each unannealed sample and the results are shown in Figures 14 to 17. The results of a chemical analysis for the composition of the same samples are also shown.

A comparison of the chemical and magnetic results shows a systematic difference in the two results in that the magnetic analysis indicates a smaller amount of the diamagnetic phase in most samples. This may be an artifact arising from the assumptions used in interpreting the chemical data. In these calculations, an excess of the diamagnetic cobalt in the form of $K_3[Co(CN)_6]$ is assumed. Other results discussed below suggest that this assumption is not substantiated for all of the samples measured.

In any event, a separate calculation of the amount of cobalt dissolved in the gold can be obtained from an X-ray diffraction measurement of the lattice spacing of the gold matrix for each sample. This analysis will be reported in a subsequent publication.

Since we observe that this second phase is diamagnetic, we can say something about its composition. This phase is probably the same as the numerous, small inclusions that are observed in TEM observations of cobalt hardened gold.[12] These inclusions have a diameter of approximately 25 Å and could well be clumps of some organic cobalt containing compound. When **Au**Co films are dissolved with aqua regia, a precipitate of $Co_3[Co(CN)_6]_2.xH_2O$ is observed.[13] We have prepared this compound and measured its magnetic susceptibility. Since this compound is paramagnetic it can not comprise the second phase. On the other hand the compound $K_3[Co(CN)_6]$ is diamagnetic, so that the presence of this compound in the plating is possible. These results agree with Mössbauer spectroscopy observations that $Co_3[Co(CN)_6]_2.xH_2O$ can not be present in the plating, whereas the $Co(CN)_6^{-3}$ complex is present in the cobalt-hardened gold electrodeposit.[14] Unfortunately these experiments do not say anything about the positive ions present.These results also agree with Auger spectroscopy results that are consistent with the presence of inclusions of complex potassium hexacyanocobaltate.[15]

A list of some cobalt compounds that may be present in the **Au**Co plating and their magnetic susceptibility is given in Table I. If we assume that the diamagnetic phase is due to $K_3[Co(CN)_6]$ we can calculate the amount of this phase from the second phase cobalt content. The plot of the magnetization vs. H for sample IV 5 B Unannealed is shown in Figure 12. For applied fields above 4 kOe the magnetization is a straight line with a slope of -0.0957E-06 CGS-EMU. From Equation 1 this slope is the magnetic susceptibility per gram of the gold plating.

Sample IV 5 B Unannealed has an organic cobalt content of 0.15(0.5) wt. percent, from which we calculate a magnetic susceptibility of -6.4E-08 CGS-EMU per gram of diamagnetic cobalt. If the organic cobalt phase is potassium hexacyanocobaltate, this would mean that the susceptibility per gram of the compound must be -0.361E-06 CGS-EMU. This number is quite close to the more negative of the two published values for the diamagnetic susceptibility of this compound in Table I. Since the most common impurity in a preparation of this compound would be a small amount of divalent cobalt(paramagnetic) the more negative value would seem more reliable.

A plot of the analyzed potassium content vs. organic cobalt content for the sixty four samples in the four blocks is shown in Figures 18-21. If the organic cobalt is indeed

potassium hexacyanocobaltate, all of the points should fall along the calculated straight lines shown in each Figure. The fact that many of the measured points fall below the line indicates that the potassium content in many of the samples is too low to support the hypothesis. The data for Block IV shown in Figure 21 show that the sample IV 5 B does indeed fall close to the line that is predicted on the basis that the "organic" phase is potassium hexacyanocobalte and is a confirmation of the susceptibility measurements discussed above. Nonetheless, it is clear that not all of the organic phase in other samples is potassium hexacyanocobaltate.

Interestingly the data in all four blocks show that no organic cobalt phase has more than approximately three potassium atoms for each organic cobalt atom, although many have less potassium. This would suggest that the potassium and the organic cobalt are somehow connected. The samples in block I contain smaller organic cobalt concentrations than in the other blocks, and have a greater percentage of samples lying on the all hexacyanocobaltate line. The sample with the greatest cobalt content, III 8 B Unannealed shown in Figure 22, has a potassium/organic cobalt atom ratio of 0.655 for the magnetic analysis data, and 0.423 for the chemical analysis data.

These results suggest that the organic cobalt phase begins with the formation of a compound with a 3 to 1 potassium to cobalt atomic ratio, and then continues with other compounds containing less or no potassium. If this is true, then the organic phase of most samples is not composed of a single compound. On the other hand, since the magnetic behavior of the cobalt compounds resides in the cobalt containing anion, the above analysis of the magnetic data based on the assumption that all organic cobalt has the same magnetic properties may not be too far wrong.

The requirement that the second phase be diamagnetic imposes certain restrictions on the electronic structure of the cobalt in this phase. The diagrams in Figure 22 show the electronic structure of the cobalt atom for various types of chemical binding. The only structure that does not have an unpaired electron, which is a requirement for diamagnetic behavior is the octahedral covalent bonded Co(III) ion. Since cobalt is introduced into the plating bath as Co(II)acetylacetonate(acac) and any cobalt that might be oxidized at the anode to the trivalent state should immediately precipitate as $Co(acac)_3$, the presence of Co(III) in the gold plating might seem surprising. One explanation of this behavior lies in the fact that cobalt has a great affinity for octahedral covalency with strongly electronegative groups such as $(OH)^-$,$(CN)^-$, etc.[16] If an octahedral complex with Co(II) is formed at the cathode, this will be unstable because the one unpaired electron on the cobalt 5s orbital is easily lost to form the Co(III) covalent compound.[17] In this way we can understand the incorporation of Co(III) compounds into the plating at the cathode.

Although all octahedral covalent trivalent cobalt compounds are diamagnetic and possible candidates for the organic cobalt phase, we can not reject all divalent cobalt compounds a priori. The reason for this is presumably the pairing of the odd electron by the formation of a dimer or polymer to form a diamagnetic salt. One well known example

of this phenomena is Adamson's salt $K_6(Co(CN)_5)_2$, which is diamagnetic. The potassium to cobalt atomic ratio in this compound is the same as the hexacyanocobaltate.

The octahedral covalent compounds of cobalt can form quite complex structures. One proposed structure for $Co(CN)_2$ is shown in Figure 23.[18] In this structure the framework consists of $Co(CN)_3^-$
units. In order to preserve stoichiometry, a Co(II) atom must be present in the interior of every other cube. If the cobalt atoms in the framework are Co(III), the framework is now stoichiometric and no other cations are necessary. This new compound would be compatible with the results of both Mössbauer spectrometry and the present magnetic measurements. Although the compound $CoCN_3$ is reported to exist, one author reports that this compound is paramagnetic, which is hard to understand.[19] It may be that the preparations still contain some divalent cobalt as an impurity. At any rate, I am not aware of any published data on the structure of $CoCN_3$.

Conclusions

The structure of the metallic cobalt phase seems unambiguous. Unfortunately, it seems impossible to be more specific about the structure of our organic phase in view of the complicated structures that can be imagined for these cobalt compounds, especially if some of the cyanide units were replaced with OH^- units.

The properties of the metallic and the organic phases in the gold plating play an important role in the mechanical behavior of these platings.[1] Since we can not be sure of the exact form of the diamagnetic compound that is present in the alloy, we can not be more specific. It may be that x-ray photoelectron spectroscopy(XPS) will determine the structure of the diamagnetic phase in more detail. This technique is frequently used to distinguish paramagnetic and diamagnetic phases in transition metal samples.[20]

These results show that the study of the magnetic properties of **Au**Co platings has been very helpful in analyzing their structure. Magnetic force measurements are especially useful in separating the effects of the metallic and organic phases in the electroplate with a minimum of wet chemistry techniques. It would be expected that additional measurements of the magnetic properties of diamagnetic cobalt compounds would lead to more information on the structure of the organic cobalt phase.

I would like to thank Marsha Lower for some of the sample preparation, Sally Keister for the sample preparations and the sharing of her analysis results and Glenn Staudt for many helpful discussions.

References

1. R. De Donker and J. Vanhumbeeck, Trans.Inst.Met.Finishing 63(2), 59(1985).
2. T. B. Massalski ed. "Binary Alloy Phase Diagrams", (ASM,Metals Park,1986) p249.
3. C-W Chen, "Magnetism and Metallurgy of Soft Magnetic Materials", (Dover,New York,1986)p.100.
4. R. C. Weast ed. "CRC Handbook of Chemistry and Physics",(CRC Press, BocaRaton, 1985) 66th ed. p E-117.
5. C. P. Bean and J. D. Livingston, J. Appl.Phys. 30(4),S120(1959).
6. C-W Chen, loc. cit. p69.
7. C. P. Bean, J. Appl. Phys. 26(11),1381(1955).
8. D. Martin, loc.cit. p19.
9. C-W Chen, loc. cit. p38.
10. E. Boucaï et al., Phys. Rev. B3(11),384(1971).
11. M. W. Daybell and W. A. Street, Rev. Mod. Phys. 40(2),380(1968).
12. S. Nakahara, J. Electrochem. Soc. 136(2),451(1989).
13. E. T. Eisenmann, ibid., 124,1957(1977).
14. R. L. Cohen et al., ibid., 126(9),1608(1979).
15. A. J. Bentley et al., Nuc. Instr. Meth. Phys., 218,555(1983).
16. L. Pauling, "The Nature of the Chemical Bond", (Cornell Univ. Press.Ithaca,1960) 3rd ed. p338.
17. L. Pauling, loc. cit. p149.
18. A. Weiss and W. Rothenstein, Agnew. Chem. Internat. Ed.2(7),396(1963).
19. P. C. Selwood, "Magnetochemistry", (Interscience, N.Y. 1943) p173.

20. T. A. Carlson, "Photoelectron and Auger Spectroscopy", (Plenum Press,NewYork,1975) p231.

21. D. K. Kalani, Laboratory Practice 17(6),691(1968).

22. C. R. Kanekar and S. V. Nipankar, Jour. Indian Chem. Soc. 43(6),397(1966).

23. M. Jansen and R. Hoppe, Z. anorg. allg. Chem. 409,152,(1974).

24. H. Leidheiser et al. J. Electrochem. Soc. 126(3),391,(1979).

TABLE I MAGNETIC SUSCEPTIBILITY

Compound	Susceptibility per mole /1E-06 CGS-EMU	Susceptibility per gram /1E-06 CGS-EMU	Temperature K	Reference
$Co(CN)_2$	3825.0	34.47	303	[1]
$Co(CN)_2.H_2O$	4350	33.73	301	[21]
$Co(CN)_6^{-3}$	-18700	-136.51	Amb	[21]
KCN	-37.0	-0.05682	Amb	[1]
$K_3[Co(CN)_5]$	-60	-0.1959	Amb	[21]
$K_3[Co(CN)_6]$	-132	-0.3971	Amb	[21]
$K_3[Co(CN)_6]$	-103.0	-0.3099	--	[22]
$K_4[Co(CN)_6]$	54	0.1454	290	[21]
$KCo[Co(CN)_6]$ $.2H_2O$	11780	33.74	293	[21]
$K_6(Co_2O_7)$	4690	10.098	294.2	[23]
$Co_3[Co(CN)_6]_2$	9260	15.258	290	[24]
CoO	4900	69.08	260	[1]
Co_2O_3	4560	29.636	Amb	[1]
Co_3O_4	7880	35.054	Amb	[1]

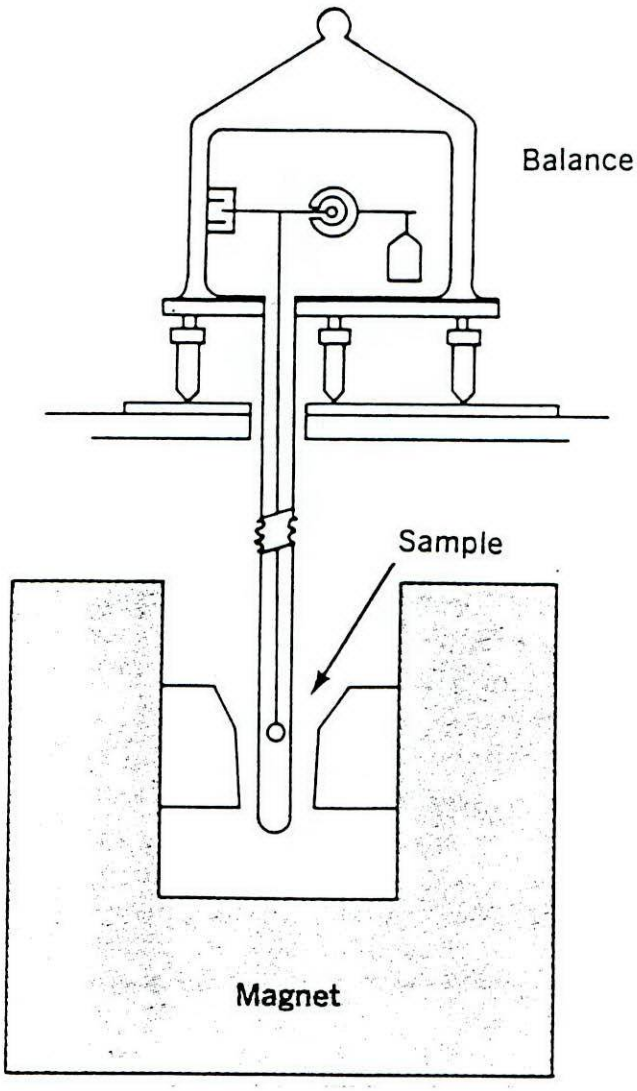

Figure 1. Faraday magnetic susceptibility apparatus.

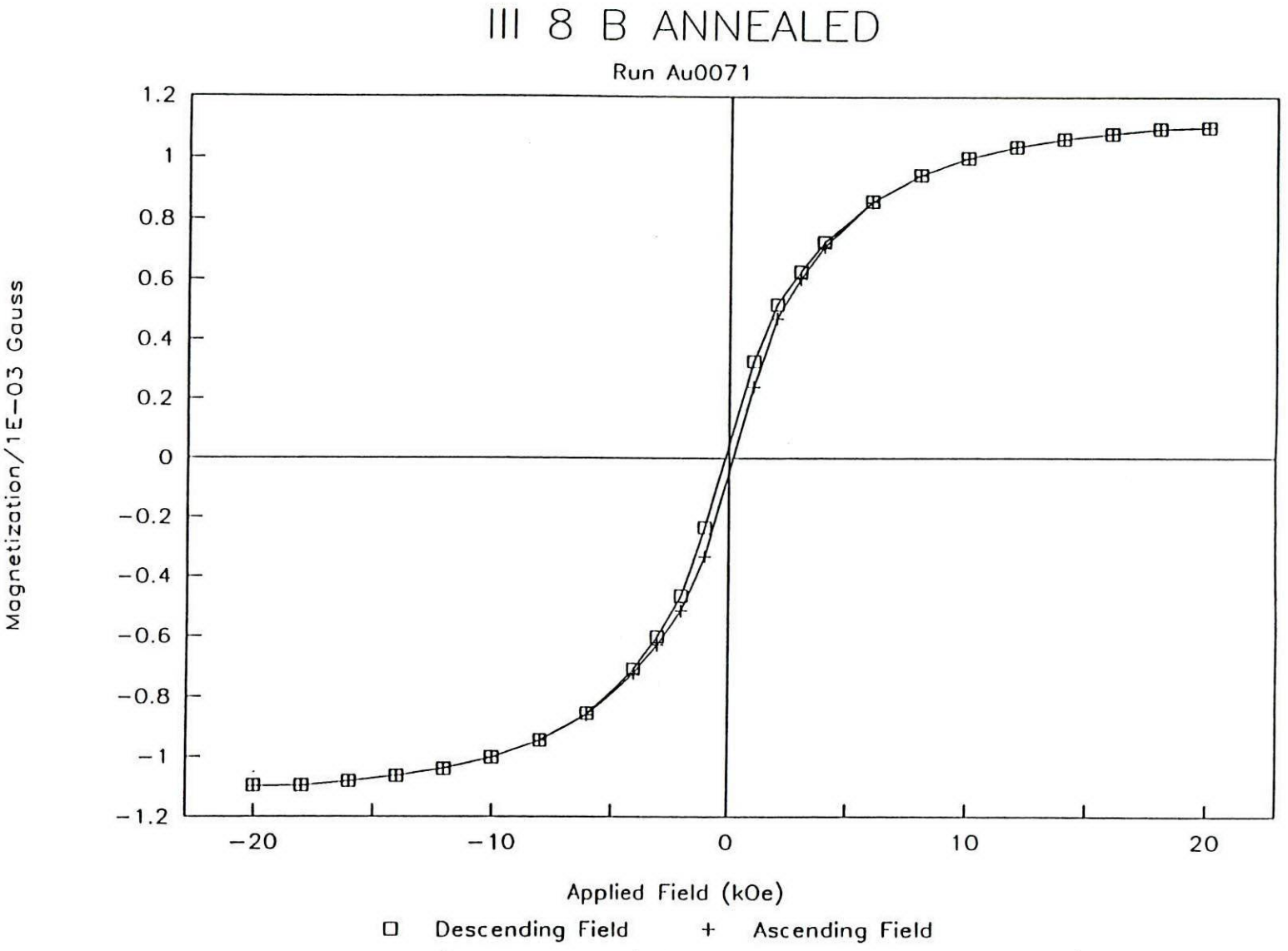

Figure 2. Magnetization vs. applied field for an annealed **Au**Co plating.

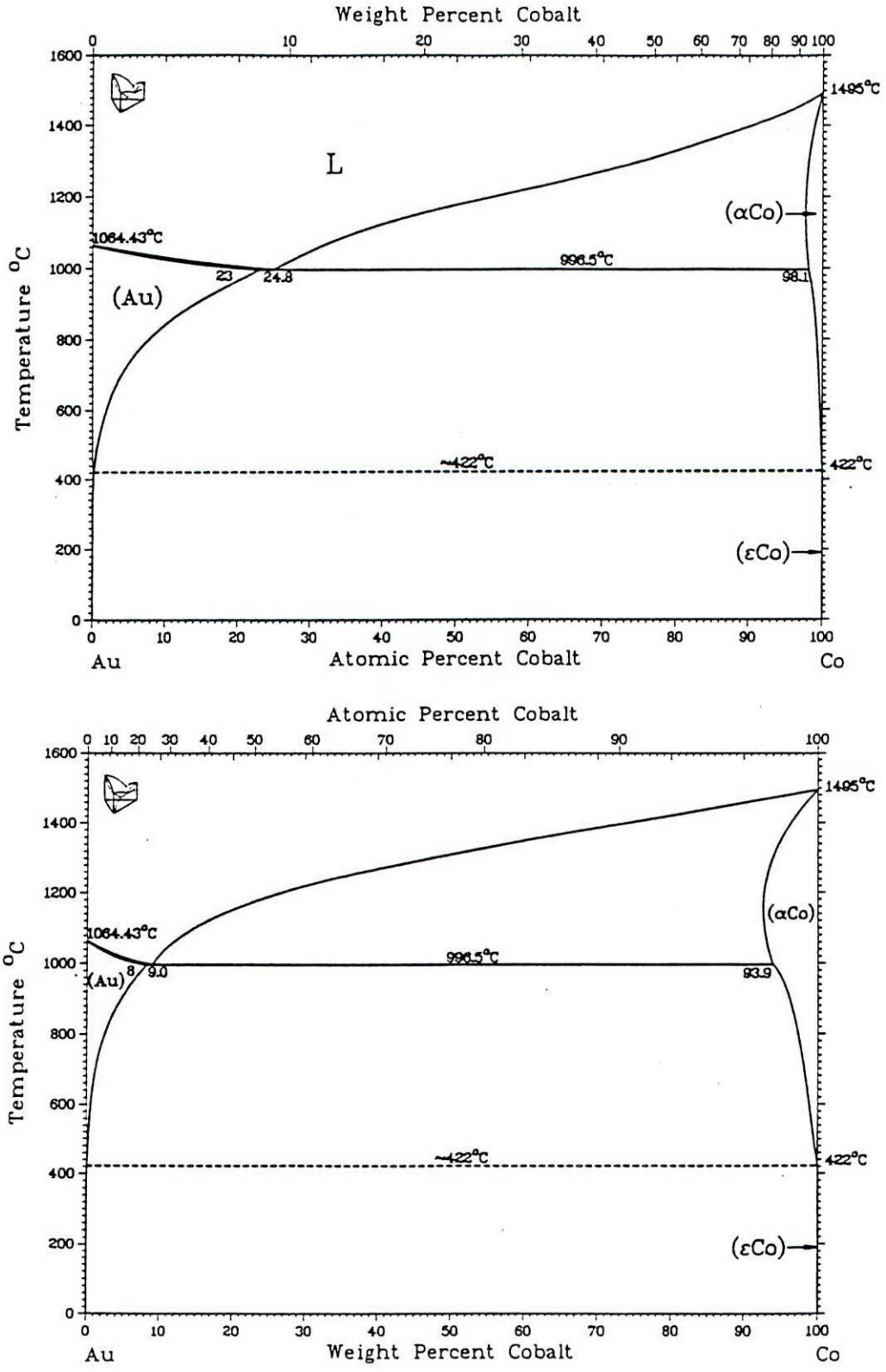

Figure 3. Phase diagram of the Au-Co system. The triangular areas(Au, αCo) at the ends of the diagrams show the maximum amount of one component that can be dissolved in the other at equilibrium. (Reference 2)

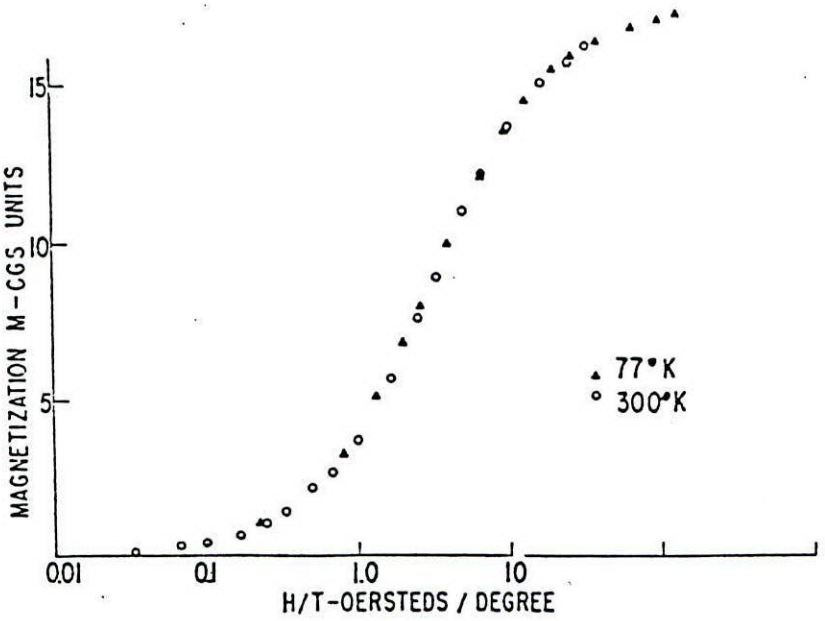

H/T superposition demonstrating superparamagnetic behavior of 27 Å radius cobalt particles formed by precipitation in a copper-2% cobalt alloy (after Becker).

Figure 4. Magnetization vs. applied field for Cobalt particles precipitated from a copper matrix. The shape of the magnetization curve is different from the usual one because the logarithm of the applied field is plotted. (Reference 5)

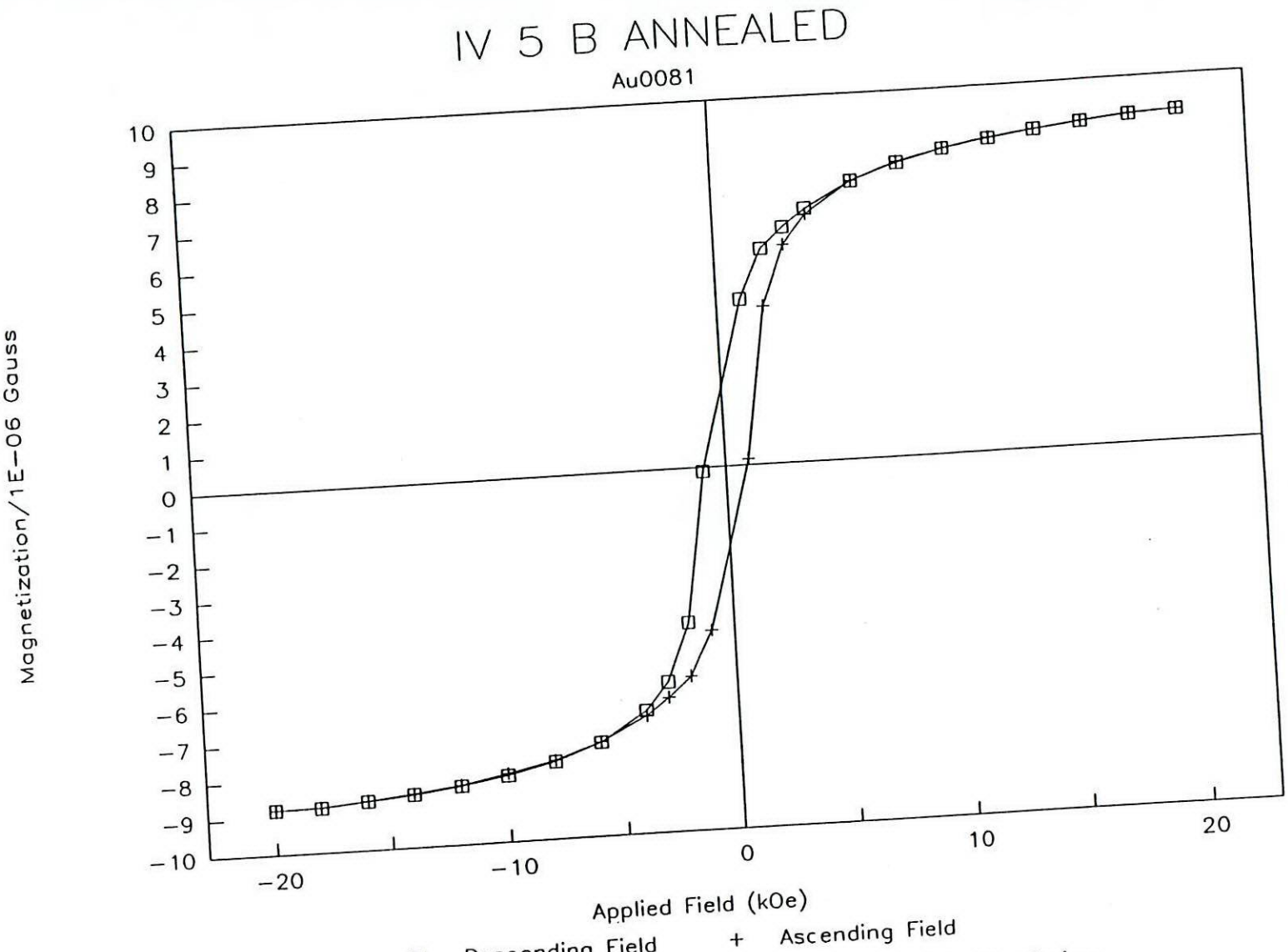

Figure 5. Magnetization vs. applied field for an annealed **Au**Co plating.

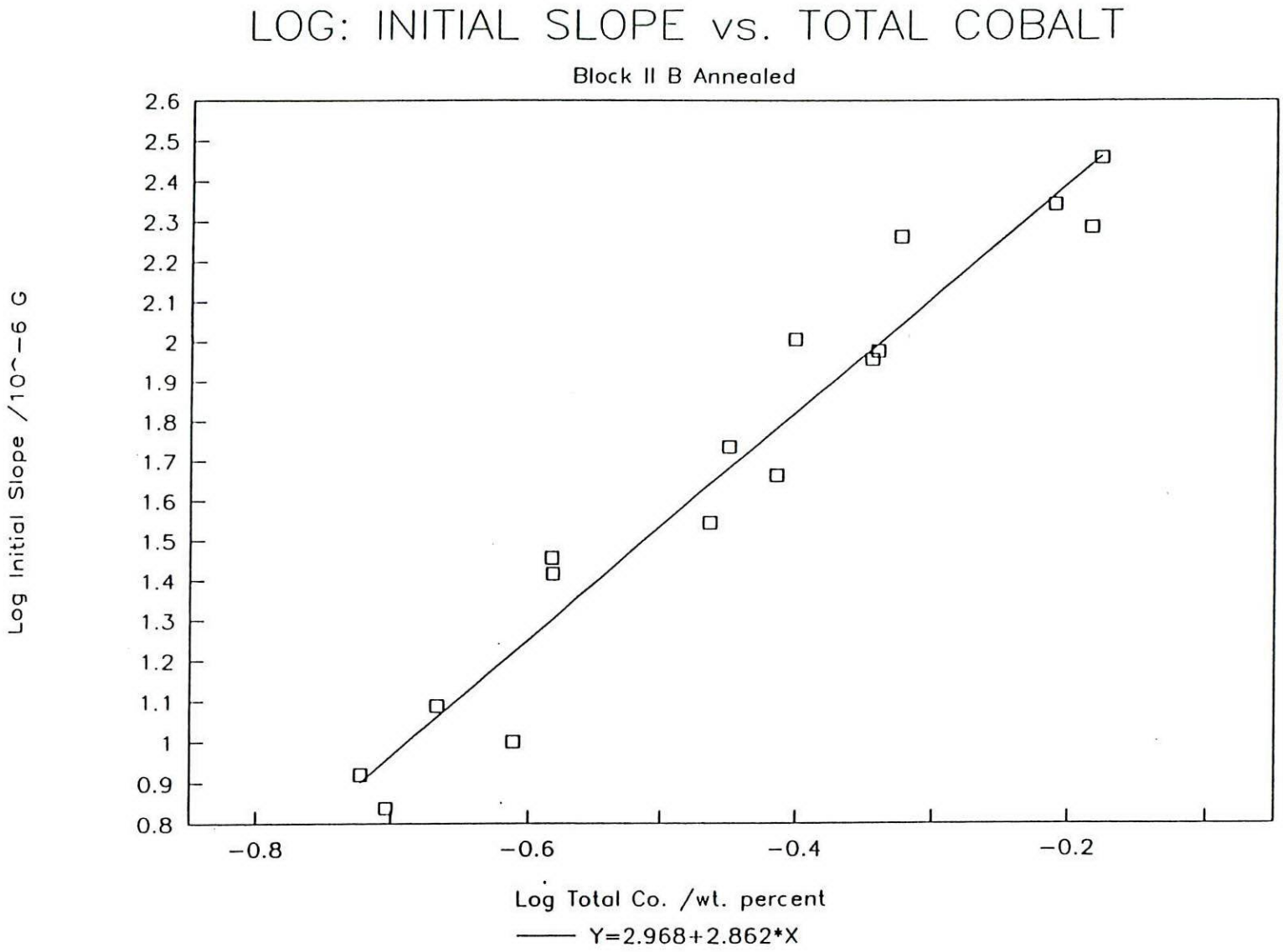

Figure 6. Variation in the initial slope of the magnetization vs. applied field curve with total cobalt concentration for annealed platings.

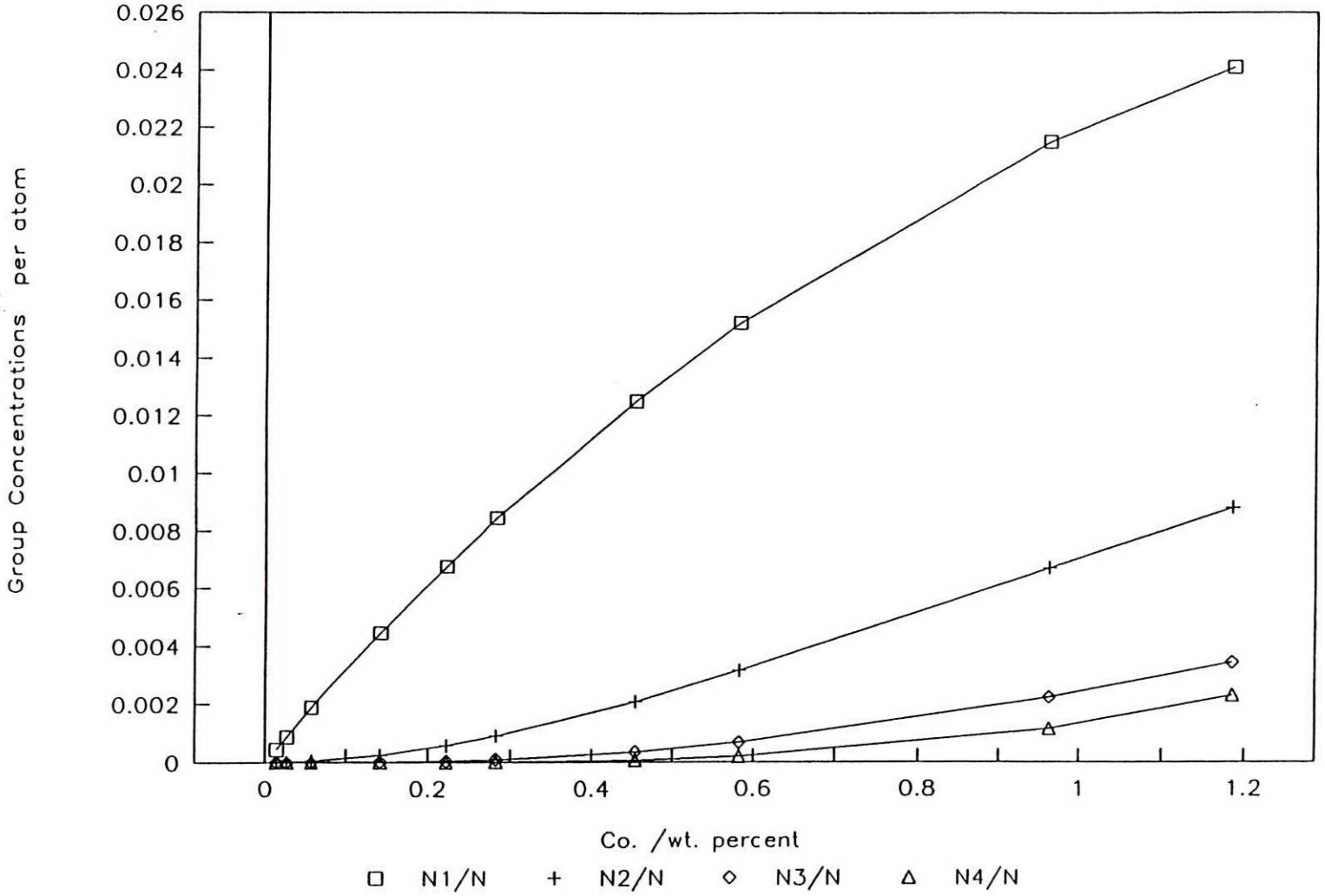

Figure 7. Calculated concentration of isolated cobalt atoms(N1); and two atom(N2), three atom(N3) or more(N4) cobalt atom clusters vs. cobalt concentration.

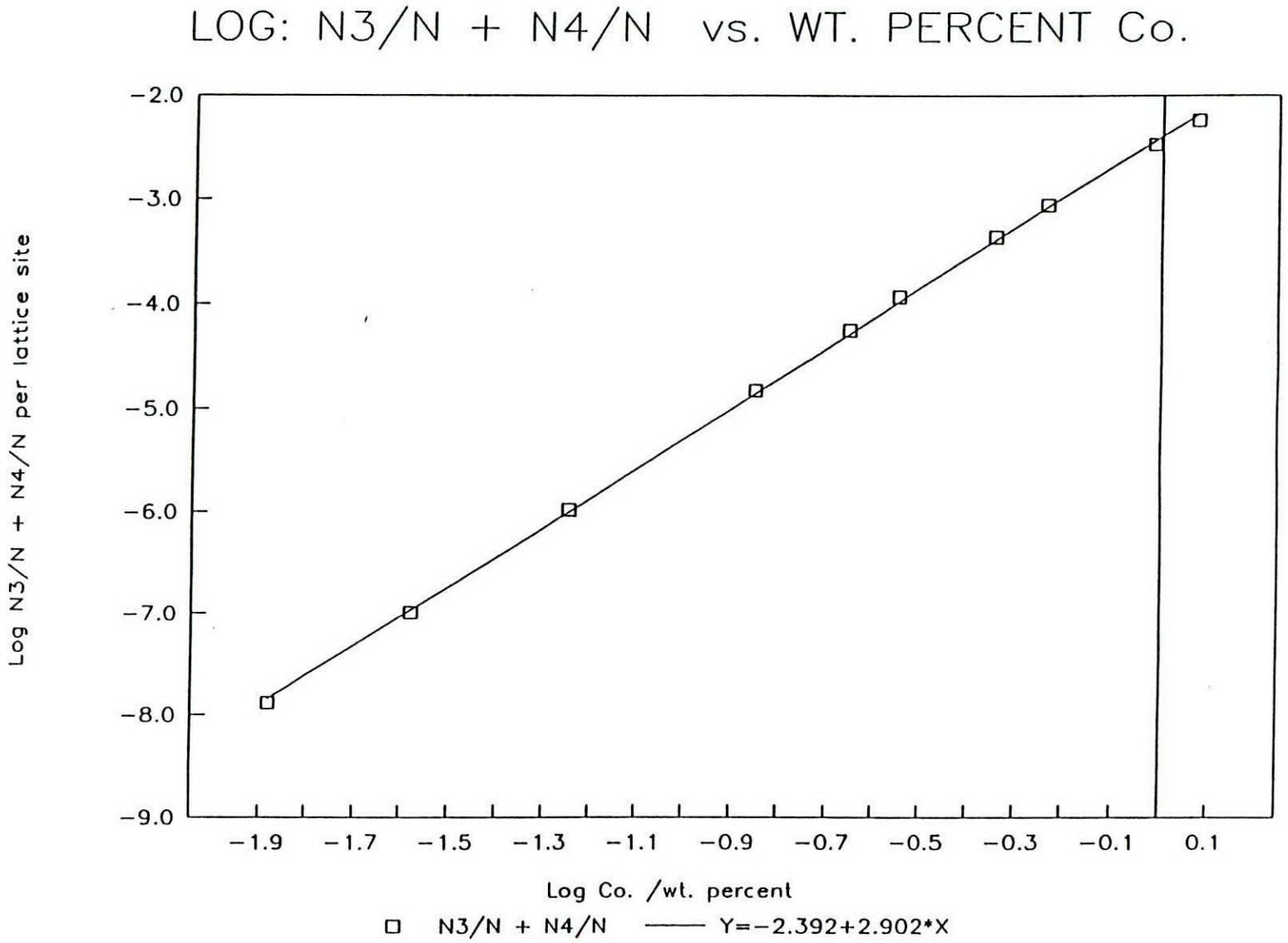

Figure 8. Calculated concentration of three or more cobalt atom clusters vs. cobalt concentration.

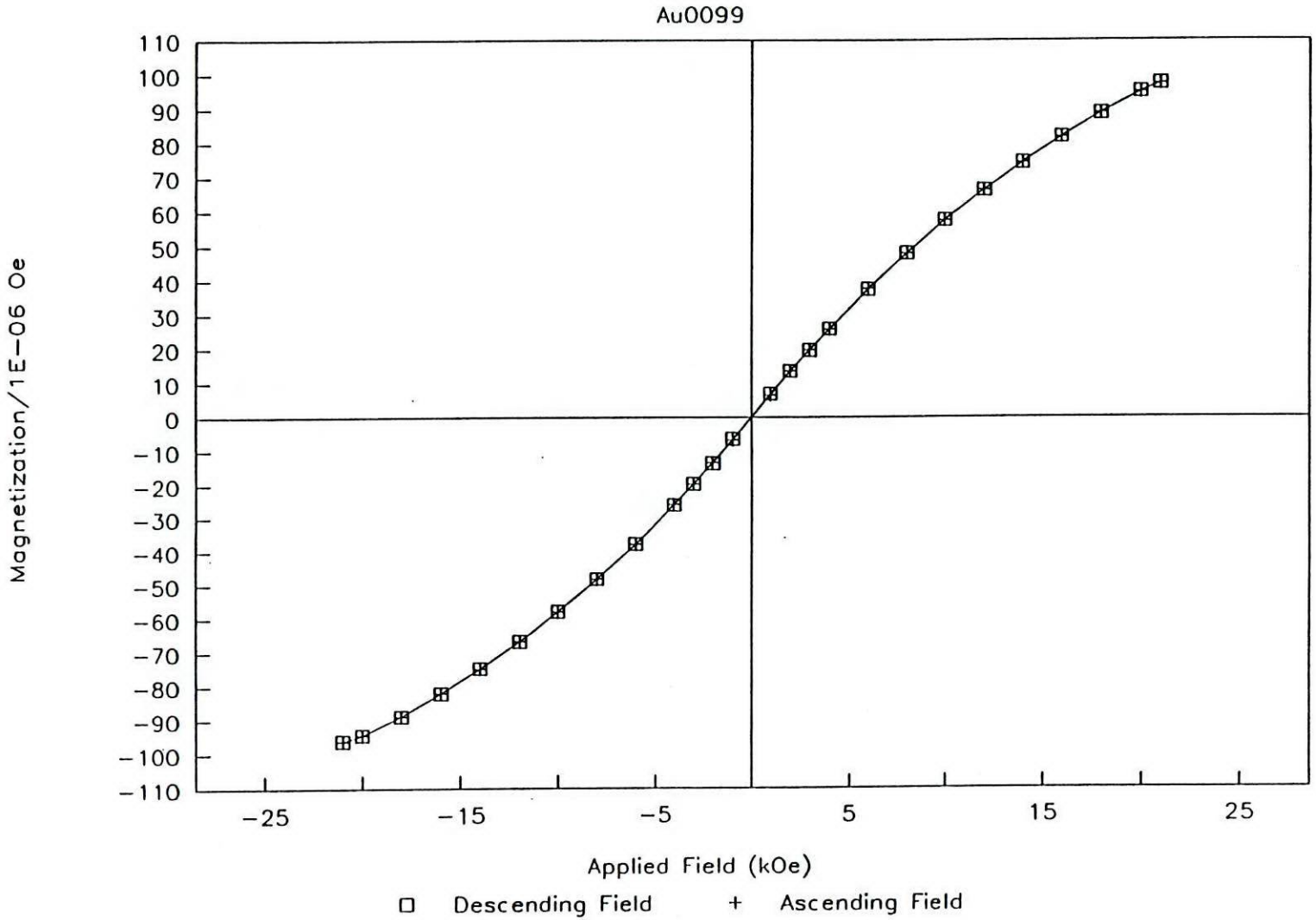

Figure 9. Magnetization vs. applied field for an unannealed AuCo plating.

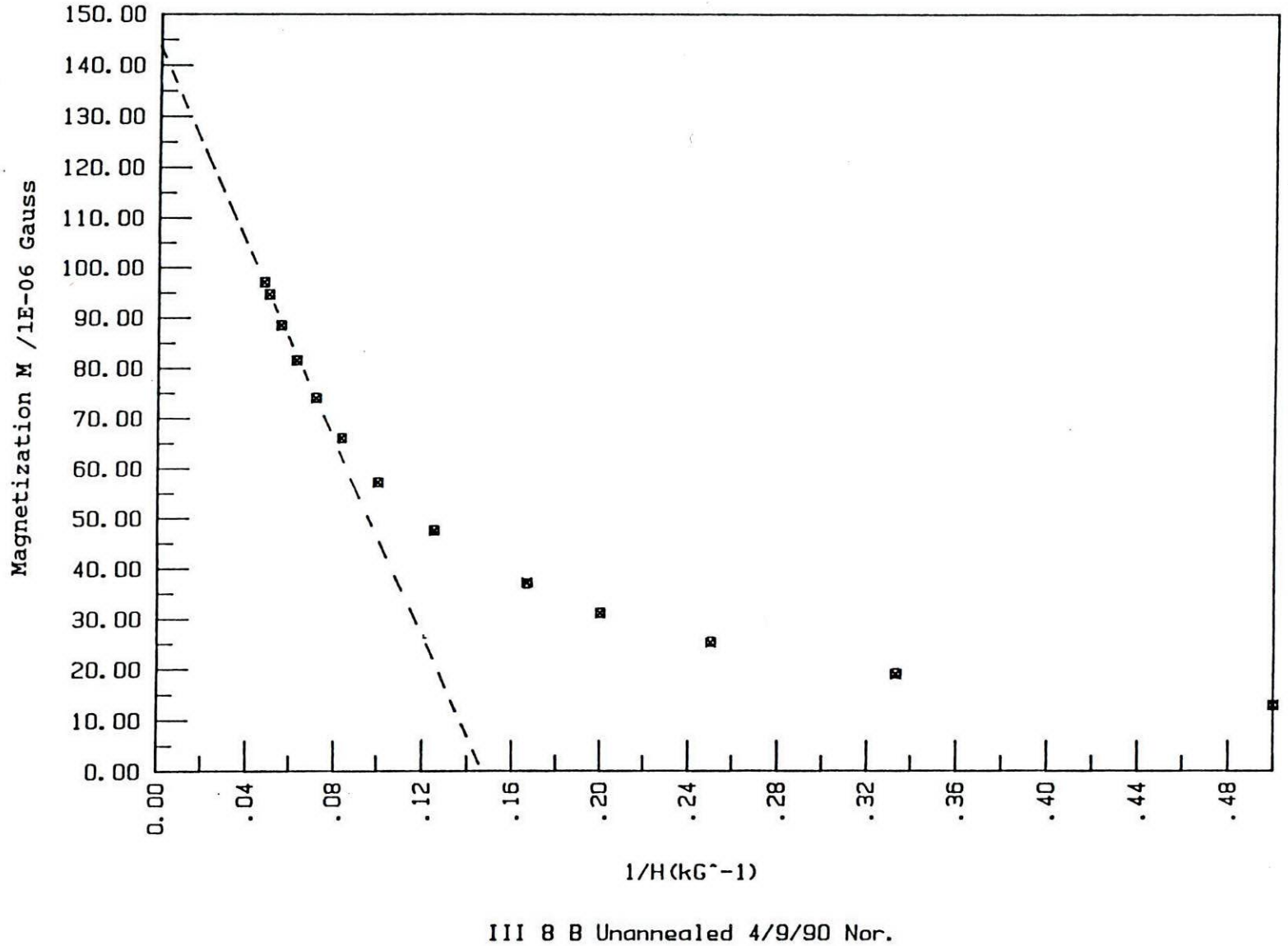

Figure 10. Plot of magnetization vs. 1/H. The method of extrapolating to infinite field is shown. Both the ascending(+) and descending(o) magnetization data are plotted.

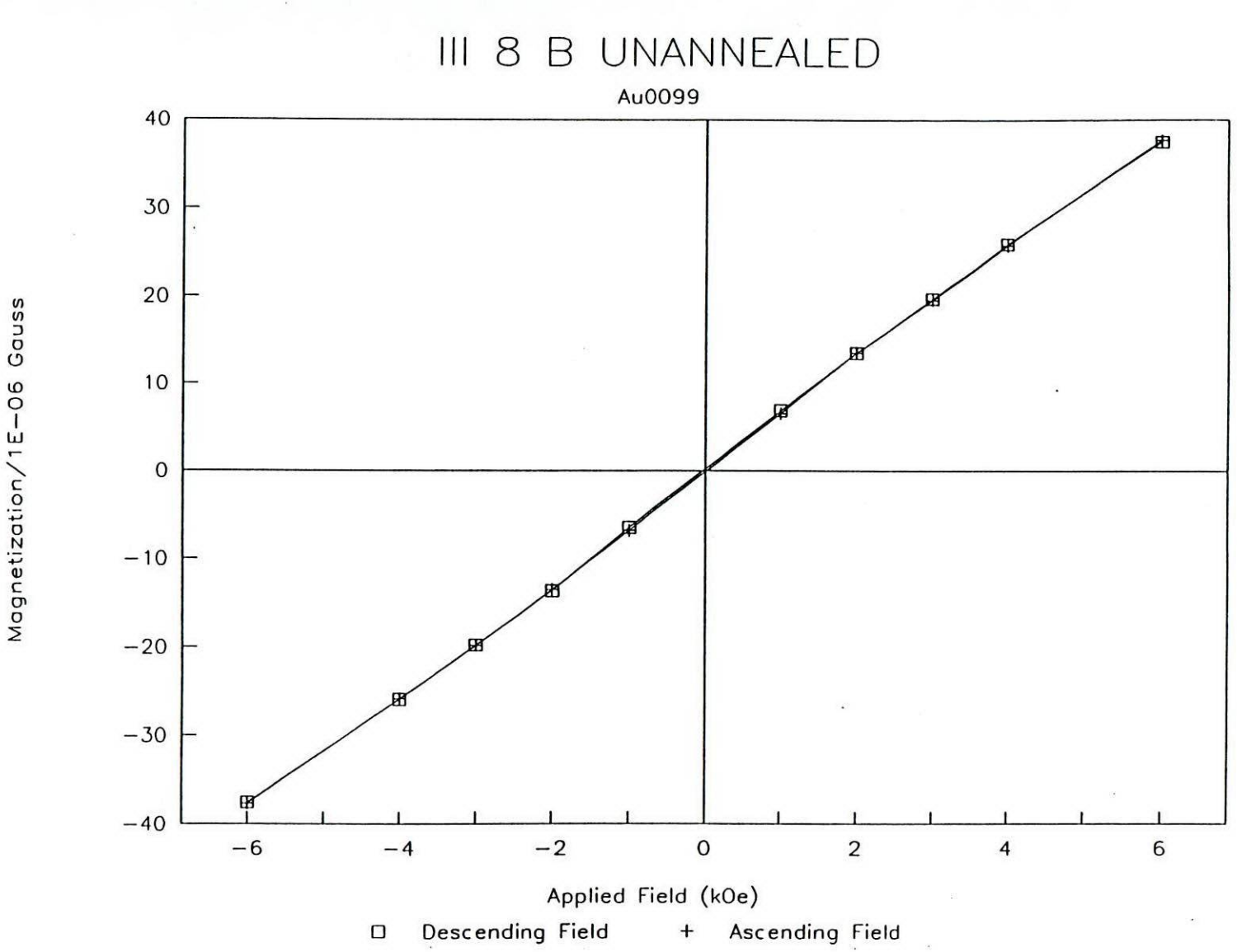

Figure 11. Magnetization vs. applied field for an unannealed **Au**Co plating. This is an expanded plot of Figure 9 to show the behavior at low fields.

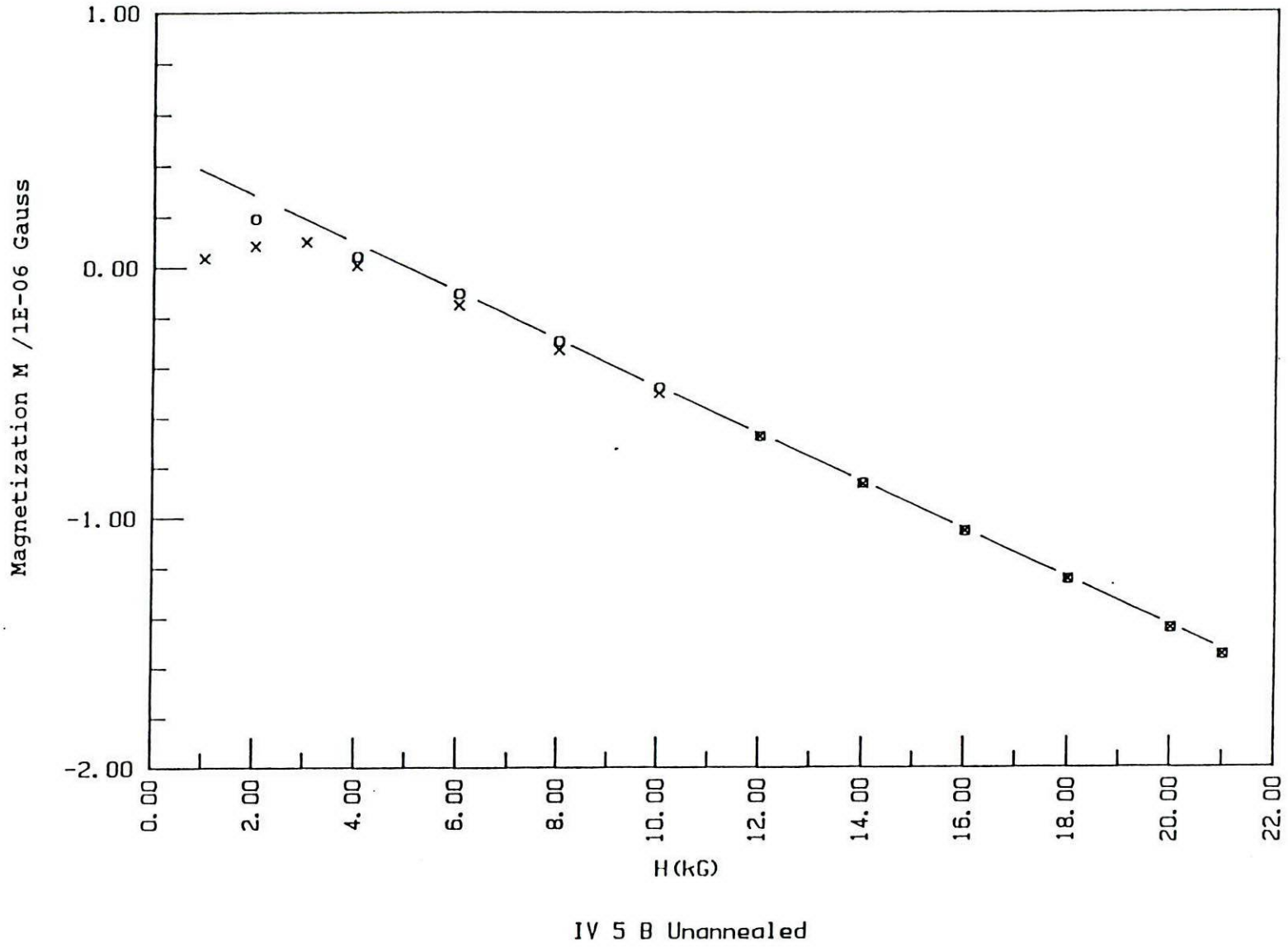

Figure 12. Magnetization vs. applied field for an unannealed AuCo plating. The diamagnetic behavior(negative slope) is evident.

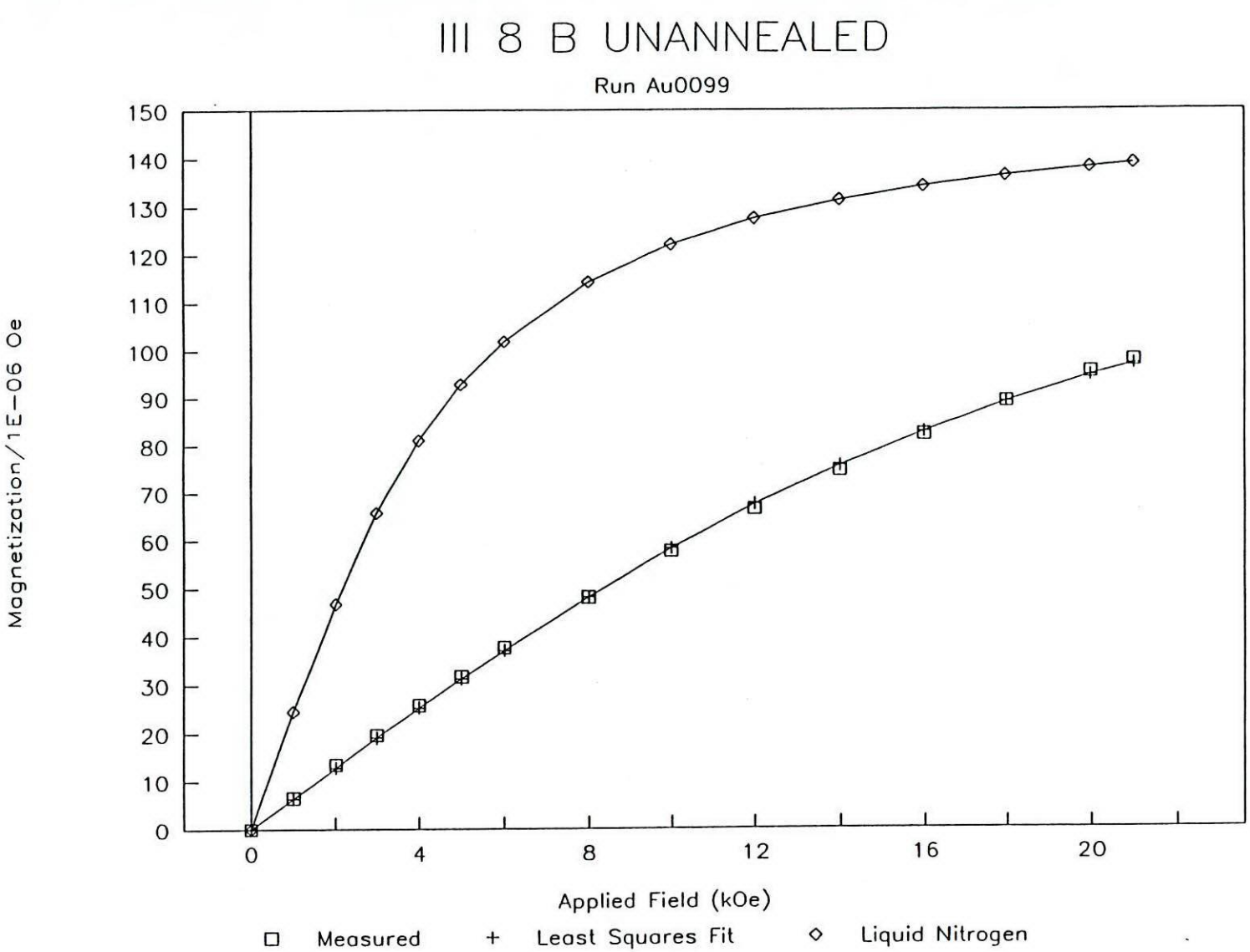

Figure 13. Least squares Langevin curve fit to measured magnetization data and extrapolation of fitted curve to 77 k.

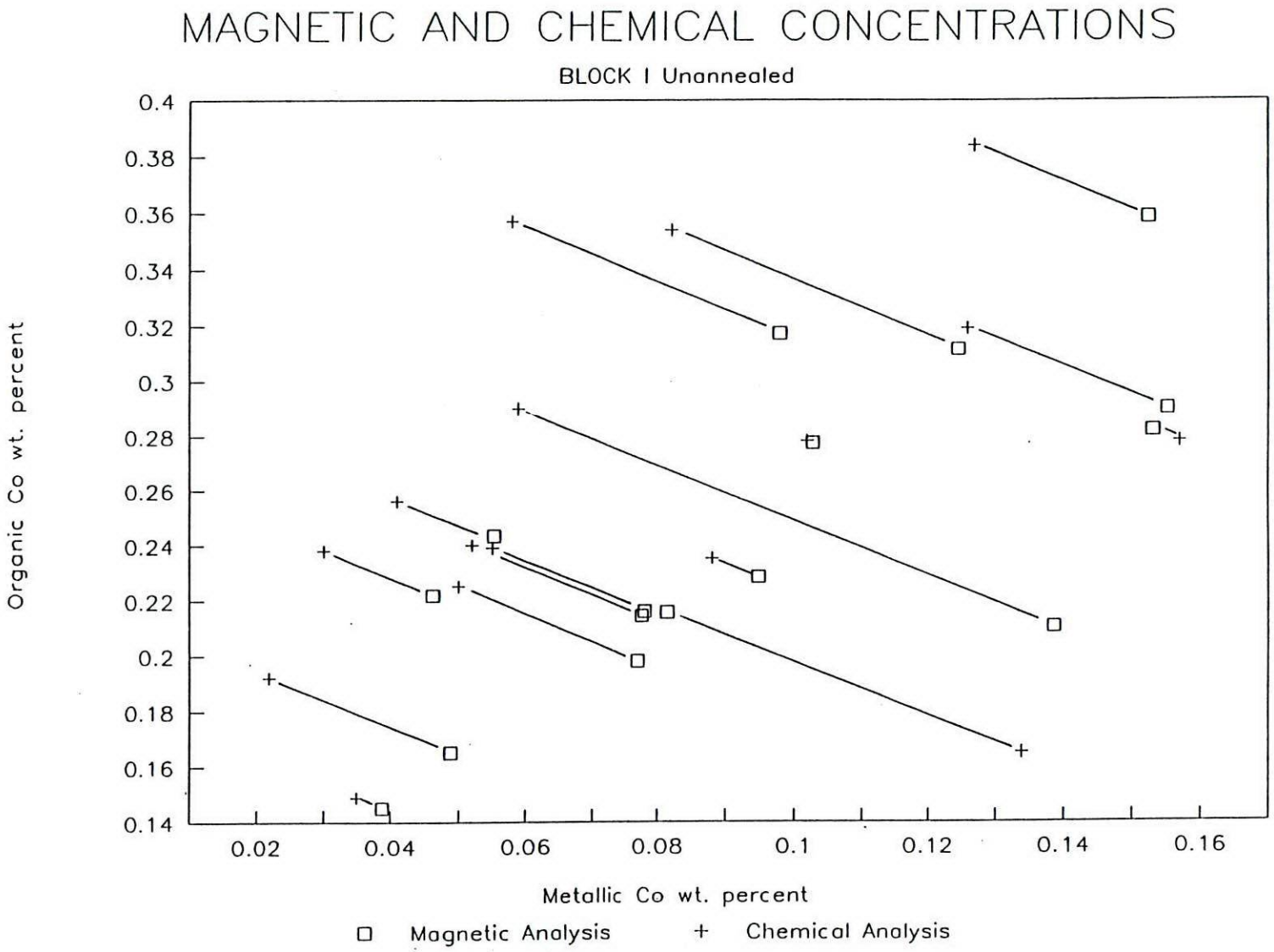

Figure 14. "Organic vs. "metallic" cobalt concentrations using magnetic and chemical analysis. Analyses for the same sample are connected.

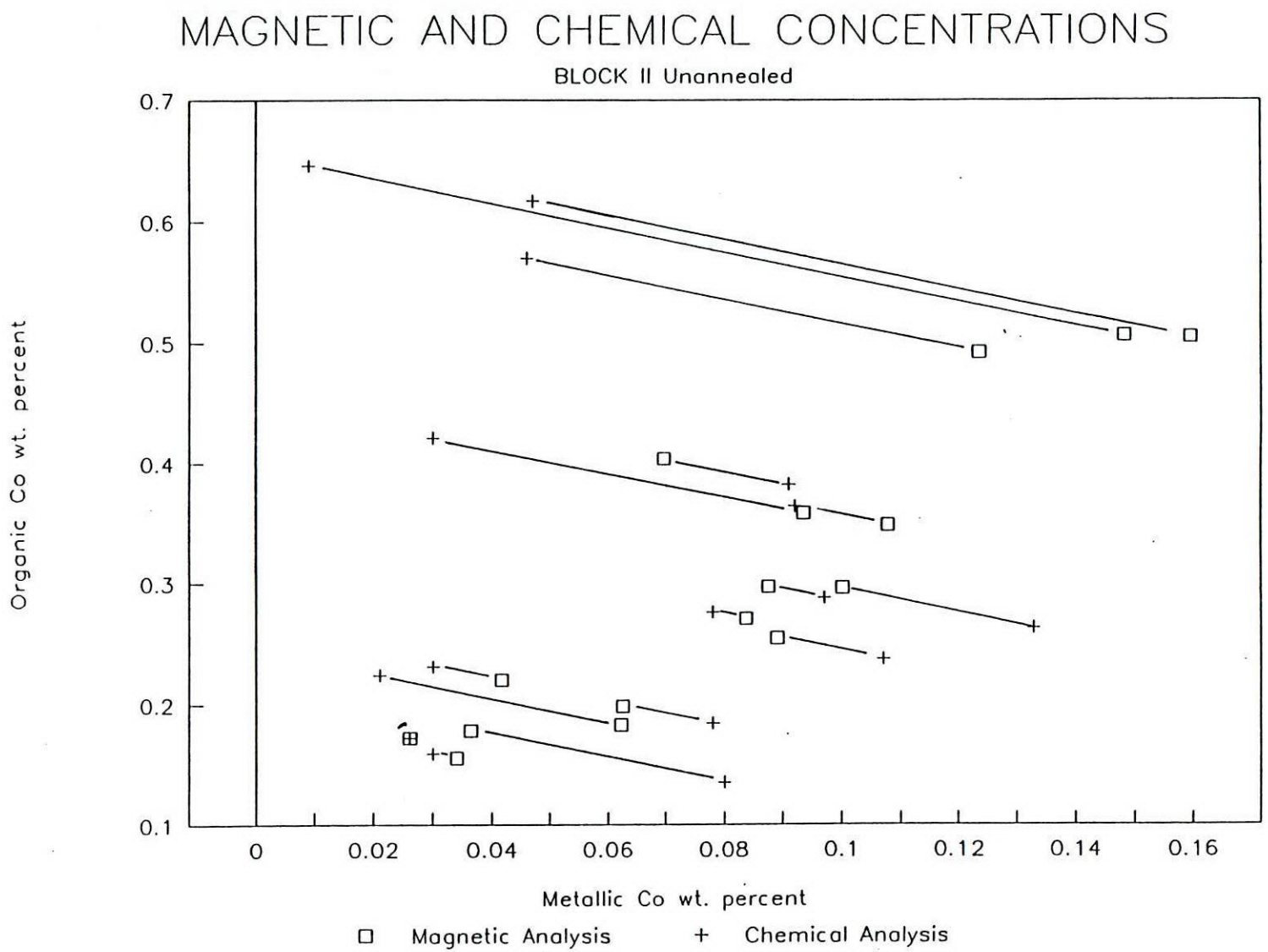

Figure 15. "Organic vs. "metallic" cobalt concentrations using magnetic and chemical analysis. Analyses for the same sample are connected.

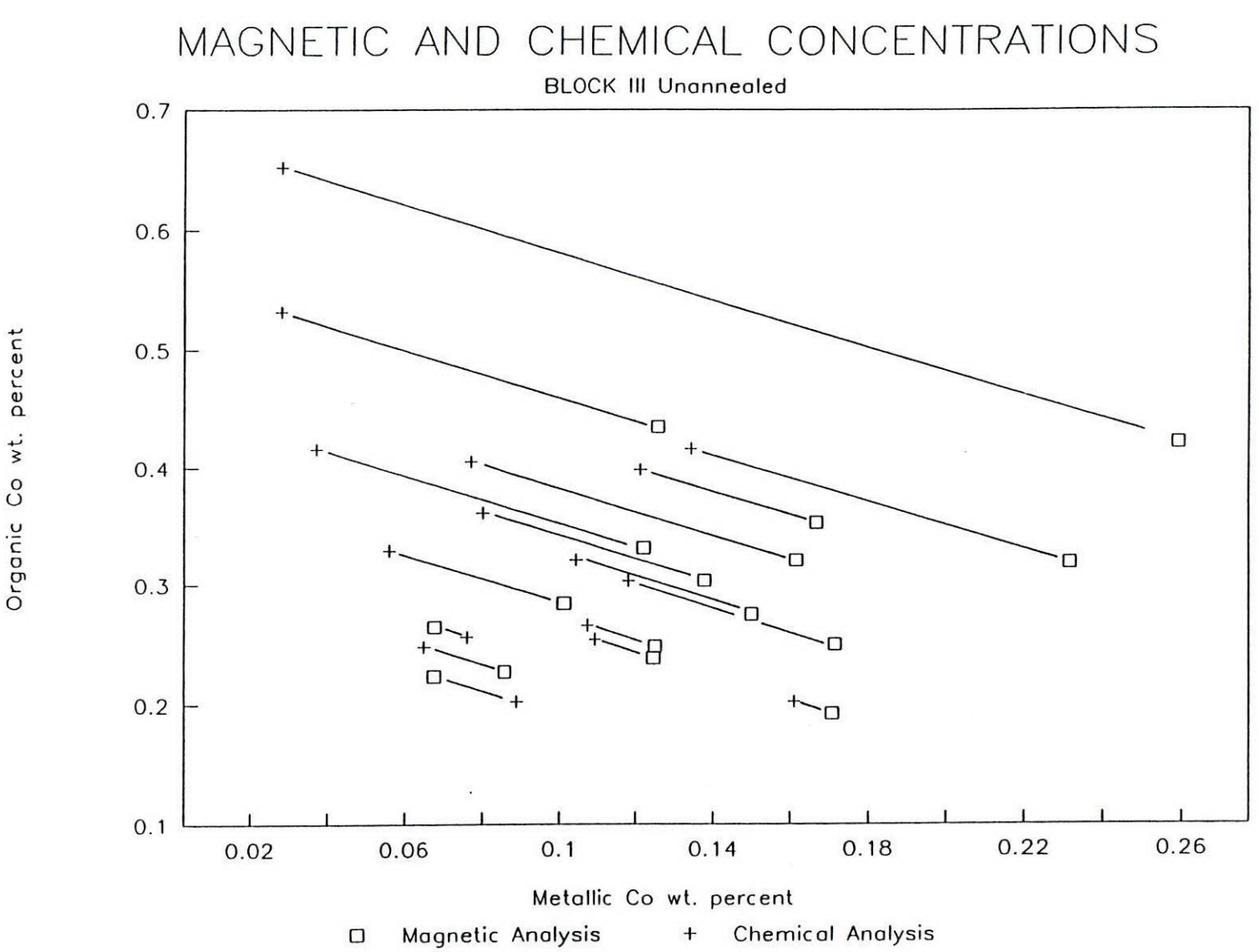

Figure 16. "Organic vs. "metallic" cobalt concentrations using magnetic and chemical analysis. Analyses for the same sample are connected.

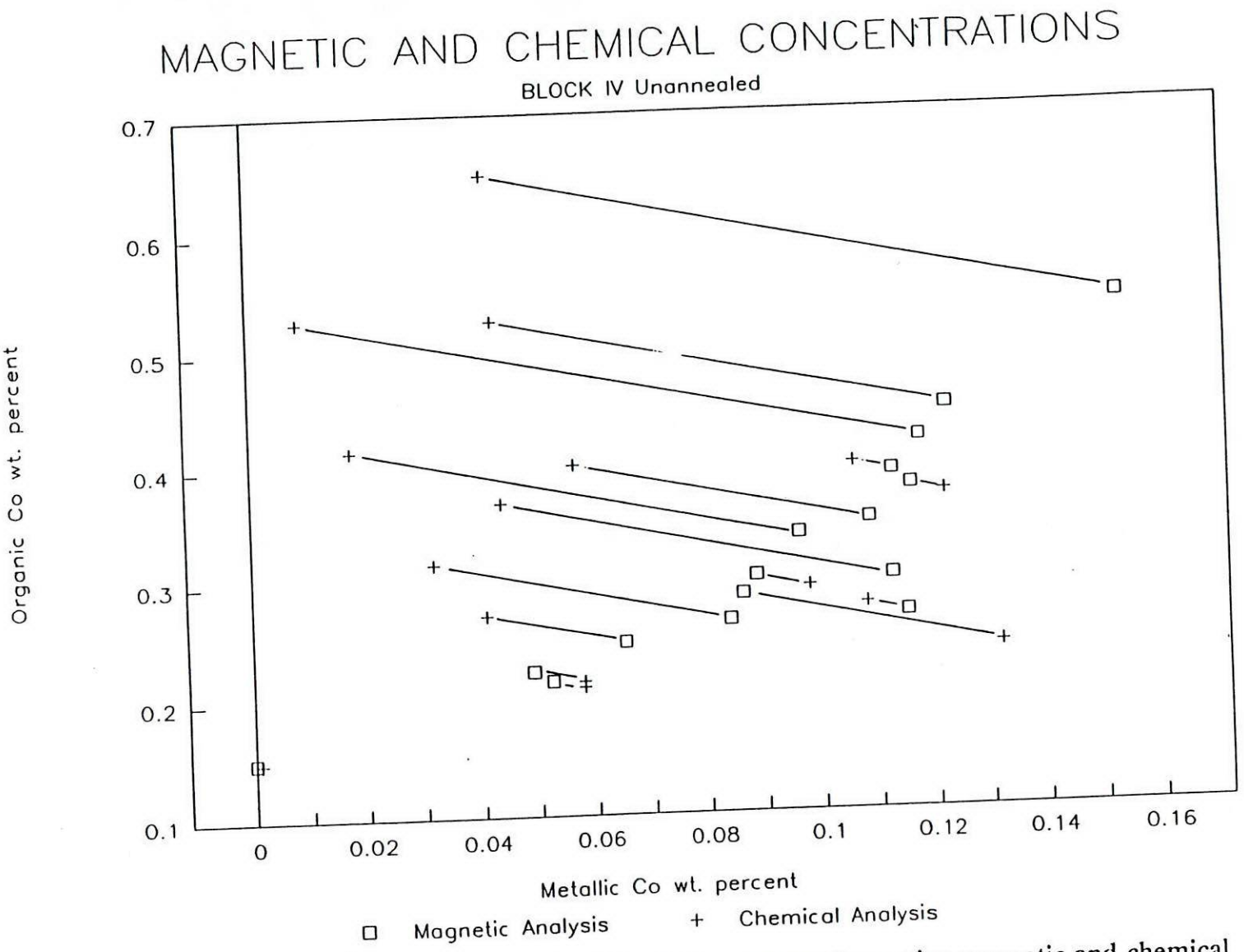

Figure 17. "Organic vs. "metallic" cobalt concentrations using magnetic and chemical analysis. Analyses for the same sample are connected.

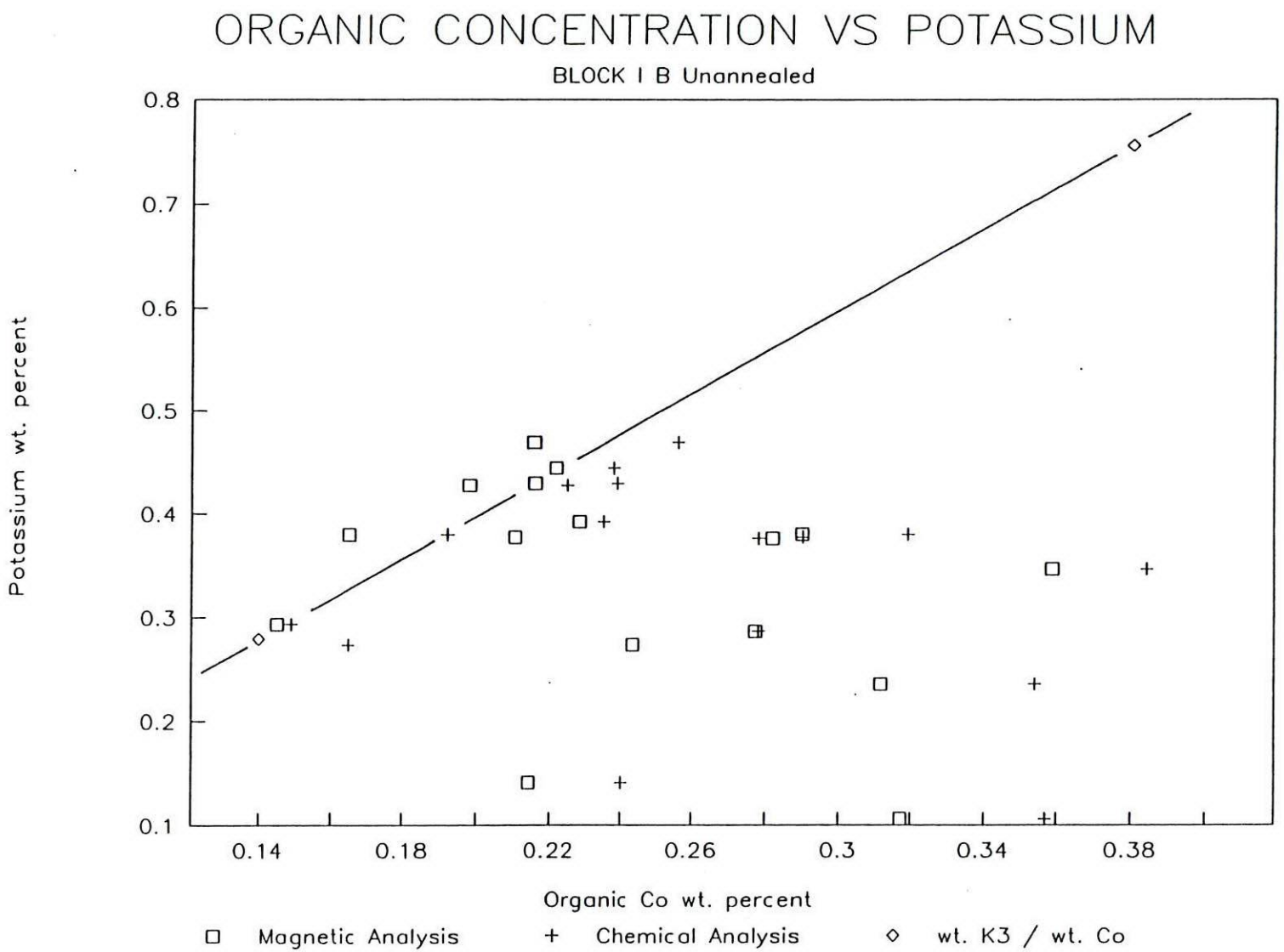

Figure 18. Potassium concentration vs. "organic" cobalt concentration for Block I. If the cobalt were present as $K_3[Co(CN)_6]$, the points should lie on the straight line.

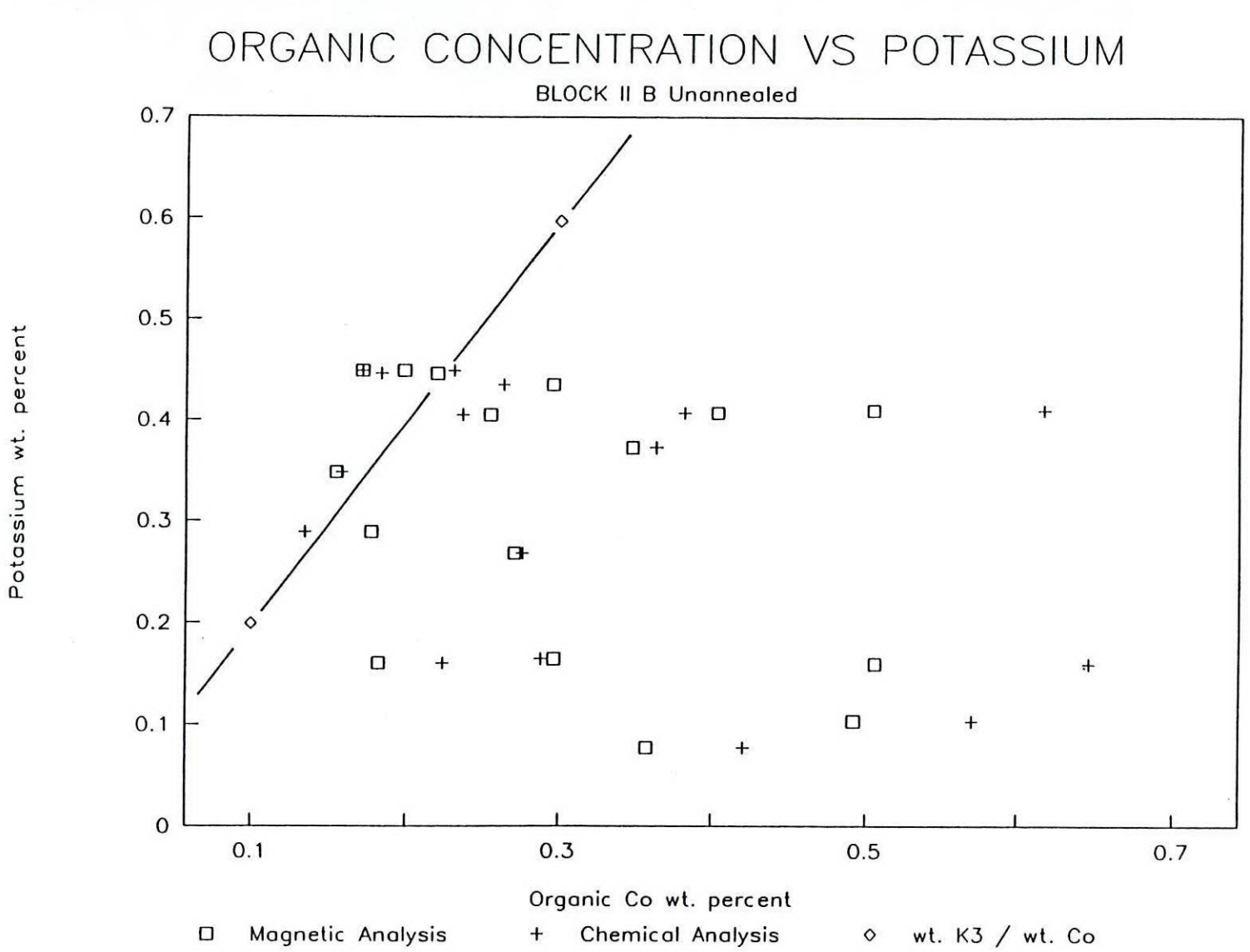

Figure 19. Potassium concentration vs. "organic" cobalt concentration for Block II. If the cobalt were present as $K_3[Co(CN)_6]$, the points should lie on the straight line.

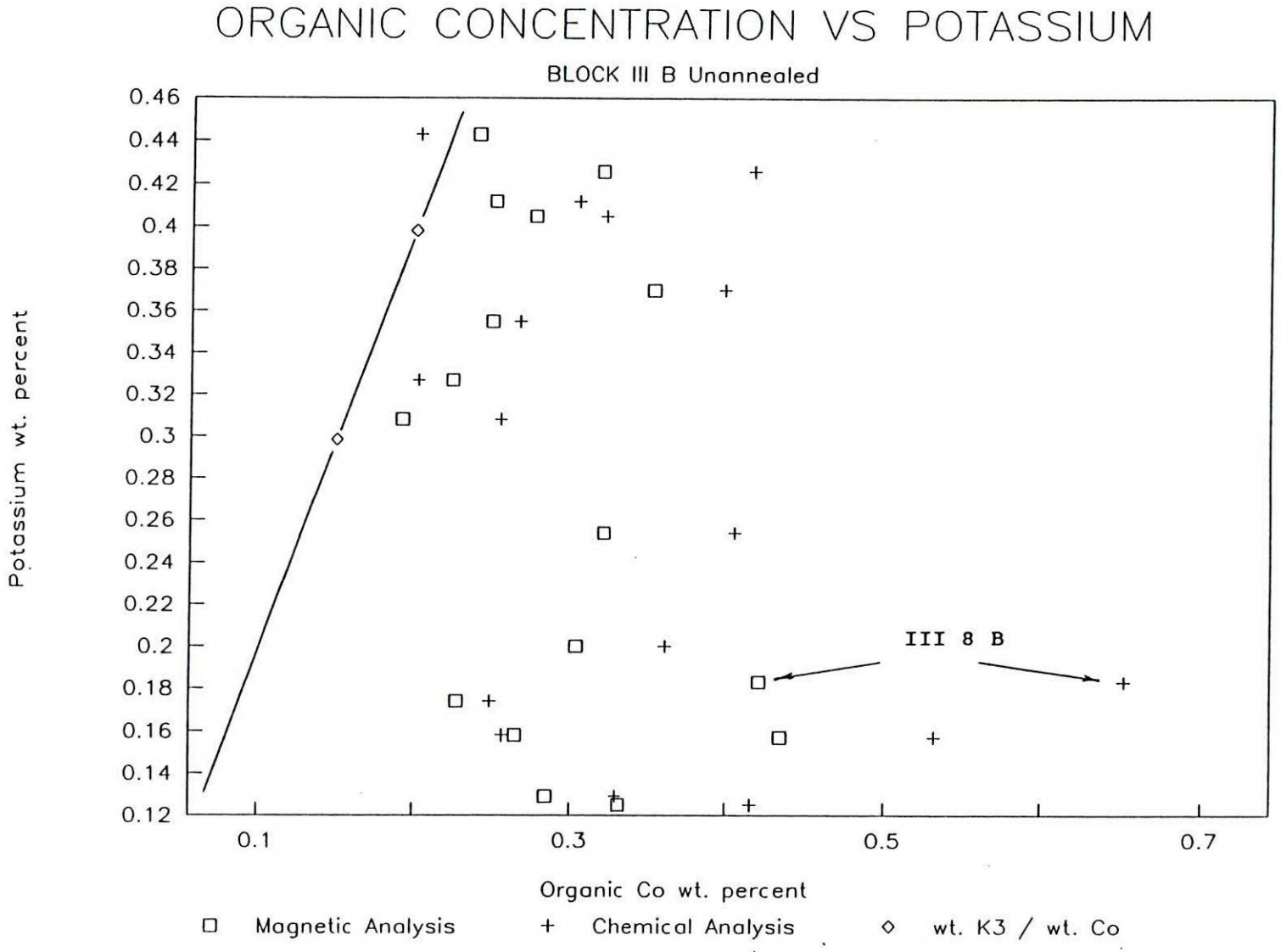

Figure 20. Potassium concentration vs. "organic" cobalt concentration for Block III. If the cobalt were present as $K_3[Co(CN)_6]$, the points should lie on the straight line.

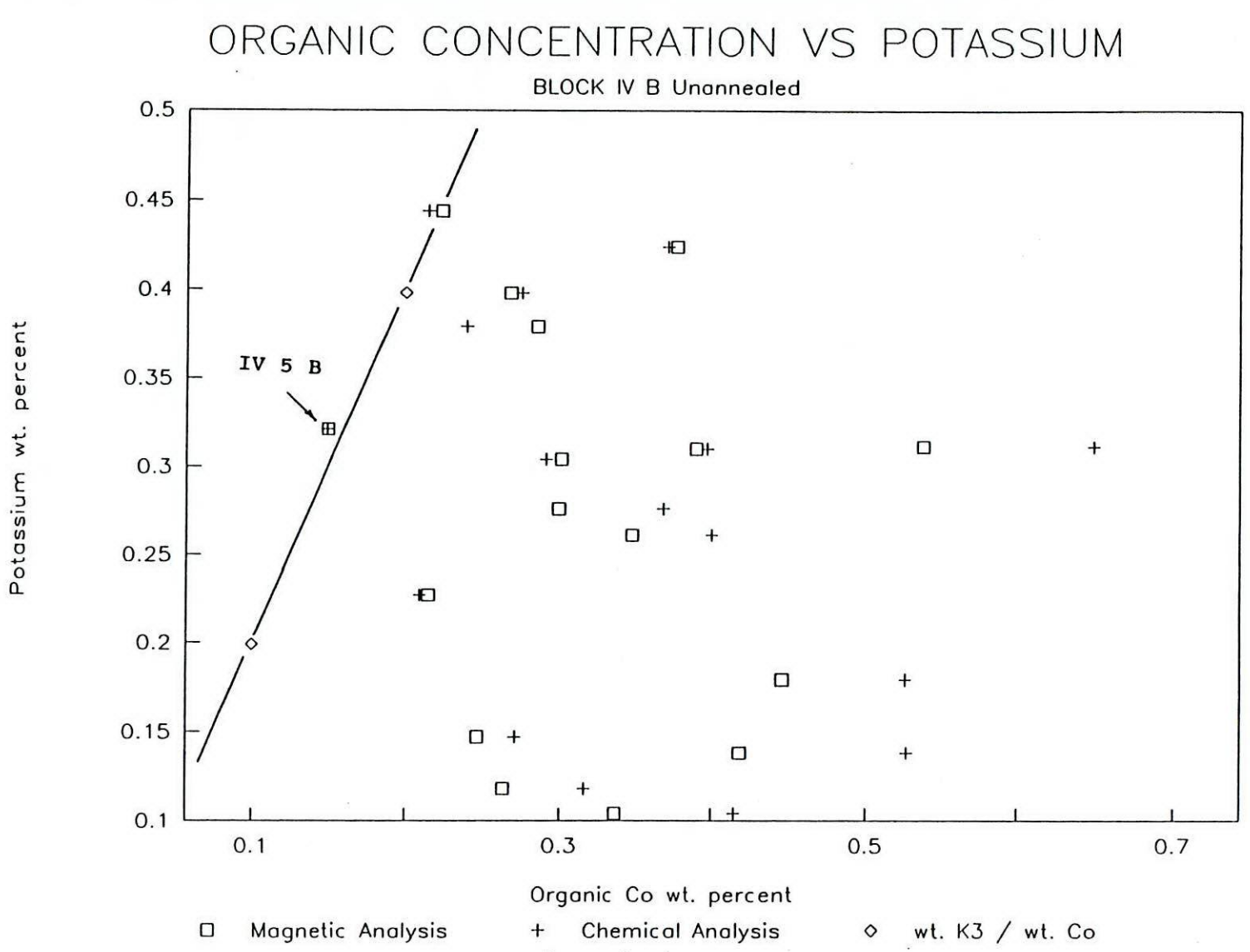

Figure 21. Potassium concentration vs. "organic" cobalt concentration for Block IV. If the cobalt were present as $K_3[Co(CN)_6]$, the points should lie on the straight line.

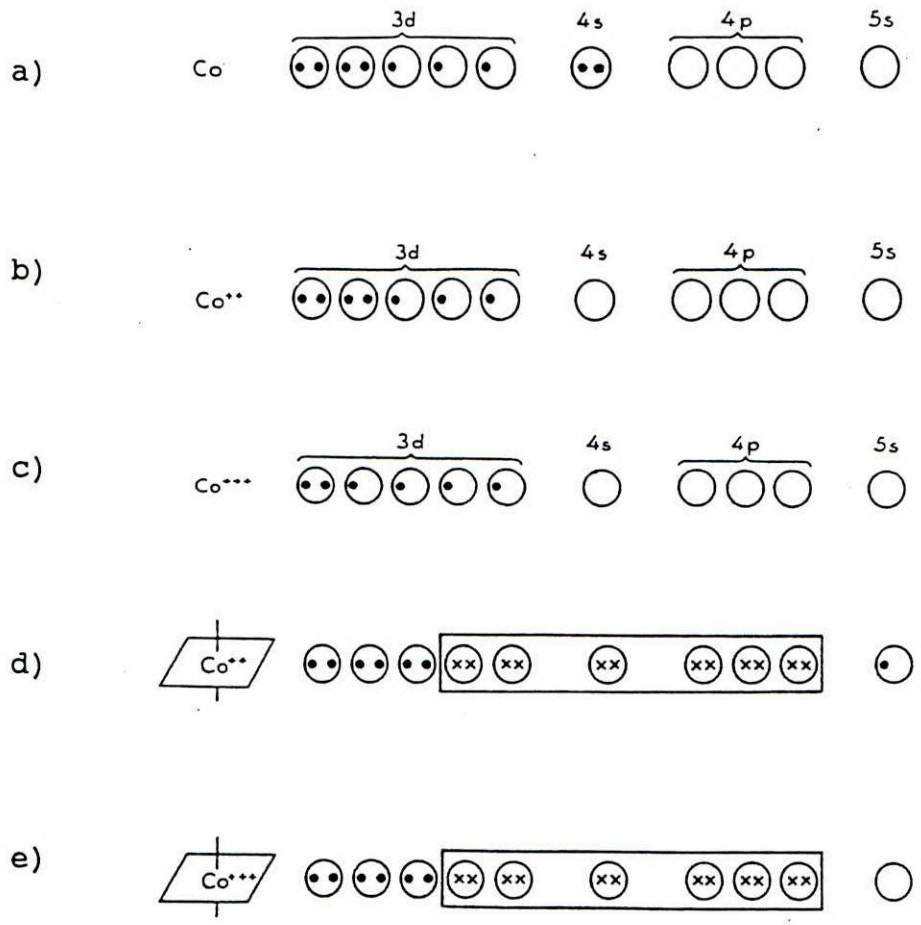

Figure 22. Effect of ionic and covalent bonding on electron distribution on ionic orbitals: a) metallic cobalt, b) Co^{++} ionic, c) Co^{+++} ionic, d) Co^{++} octahedral covalent, e) Co^{+++} octahedral covalent. (•) ionic electron, (x) covalent bonded electron.(Reference 16)

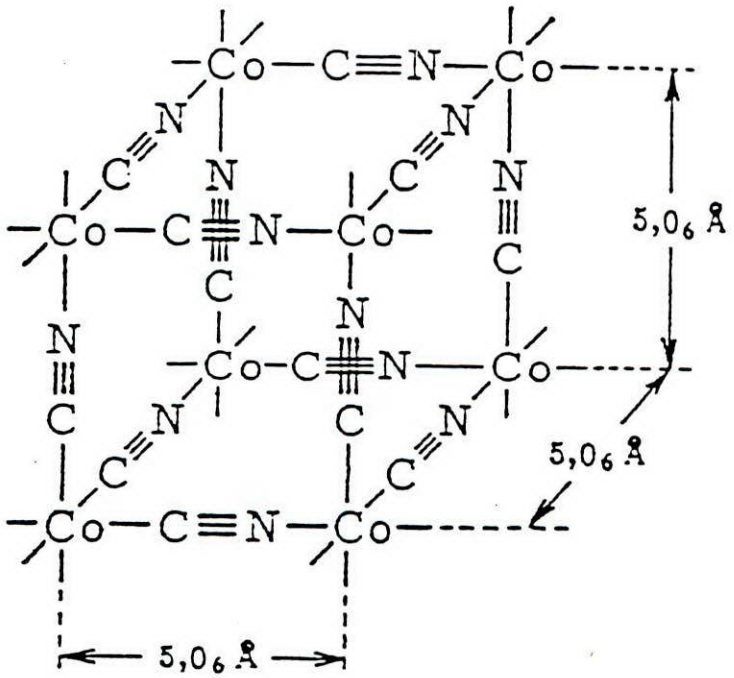

Figure 23. Three dimensional cubic structure proposed for the compound $Co(CN)_2$. The framework consists of $Co(CN)_3^-$ units with additional Co^{++} ions in every second cube. This structure would be stoichiometric without any additional ions, for Co^{+++} ions in the framework. (Reference 18)

SCANNING TUNNELING MICROSCOPY STUDIES OF ELECTROCHEMICAL DEPOSITION

Michael P. Green and Karrie J. Hanson
AT&T Bell Laboratories
600 Mountain Ave, Murray Hill NJ 07974

In this paper we describe the technique of *in situ* scanning tunneling microscopy (STM) and its application to electrochemical systems. The STM can provide real-space, time-resolved, atomic-scale images of topographic changes occurring at an electrode during chemical reactions. We illustrate the technique with experimental examples of the deposition and stripping of Pb and Cu on Au (111) surfaces.

Introduction

With the development of several *in situ* techniques capable of probing the atomic structure of electrode surfaces, the fundamental steps in electrochemical reactions are receiving new attention. These techniques include traditional surface science probes such as x-ray scattering (1) and absorption (2) as well as the newly developed scanning probe microscopies, scanning tunneling microscopy (STM) and atomic force microscopy (AFM). Among these only STM and AFM give direct (real-space) evidence of the surface structure.

The STM operates by rastering a sharpened conducting probe across a sample surface at a distance close enough to allow quantum tunneling of electrons across the gap (3). A three-dimensional piezo-electric actuator maintains this distance, typically 10-20Å, and also provides the scanning motion. The tunneling current, which is exponentially dependent on the gap spacing, is generally held constant by adjusting the perpendicular displacement of the tip in response to changes in surface topography or electronic structure. This displacement, in conjunction with the lateral position information, is used to create a three-dimensional map of the surface. This is usually displayed as a gray-scale image with the shade keyed to the vertical tip position. What this map shows is really the density of surface electronic states near the Fermi level measured at the center of curvature of the probe tip (4); in other words, the extent to which electron wave functions extend from the surface. For most surfaces, especially when atomic resolution is not sought, this accurately reflects the surface topography. In electrochemical systems, however, the interpretation of

the data must be considered carefully; the presence of adsorbates, the electrochemical double-layer, and the changing electrode potential can all affect the tunneling current. However, *in situ* electrochemical STM has an advantage over vacuum-based STM in the ability to control the voltage of the sample and tip independently. This allows chemical reactions to occur selectively, thus allowing imaging of the nucleation and growth of adsorbates in real-time on an intimately close substrate without having the tip structure affected.

The modifications to the STM necessary for its application to *in situ* electrochemistry are relatively straight-forward. Since electrochemistry involves charge transport via the motion of ions, the passage of electrons from the tunneling tip to the sample is still a tunneling process, even when both are immersed in a conducting solution. The main consideration is how to incorporate the STM tip into a standard three-electrode electrochemical cell. We configure the cell so that the tip is maintained at a constant potential with respect to the reference electrode. This allows the tip to be held at a voltage where no electrochemical activity takes place. In practice, this is usually set at the open circuit, or "rest" potential of the tip with respect to the reference electrode. While this creates the least interference to the tunneling signal from background electrochemical current, the varying electric field between the tip and sample could influence reactions being studied, especially if the tip penetrates the "double layer" region, the thickness of which is the effective screening length in the electrolyte. For 0.1 molar solution, the double layer has a thickness very close to the tunneling distance (5). We have looked for effects caused by the changing tunneling voltage and do not find a measurable effect. An additional precaution to minimize electrochemical current noise on the tunneling current signal is to coat all but the very point of the tip with a non-conductive coating. Noise levels can generally reduced to <0.1nA by these techniques.

The utility of using the STM to study electrochemical systems can be demonstrated by considering the deposition of monolayer metal films, especially since there is little known about the microscopic details of the layer formation. We will discuss our recent investigation of the underpotential deposition (UPD) of Pb and Cu on Au(111) (6) to illustrate the technique.

Lead

For the Pb/Au(111) system, we noted that there was a variation between the first and subsequent voltammograms in the UPD current peaks. It has been speculated that this change is due to some modification of the electrode surface (7), but nothing more was known. Fig. 1a shows an evaporated Au(111) film immediately after immersion in the electrolyte (0.05M $HClO_4$ + 5mM PbO), with the potential held at its open-circuit value. Atomically flat terraces separated by monoatomic steps (2.35Å) repeat the morphology imaged in air. Fig. 1b shows the result of the deposition of a Pb monolayer. Although the structure looks similar, terraces in Fig. 1b are a monolayer higher than those of Fig. 1a; the Pb

has deposited in an almost conformal layer. From a previous study of the deposition dynamics (8), we found that the Pb deposits directly into its final close-packed structure via two-dimensional nucleation and growth, and does not pass through a less dense superlattice as some have suggested (9). It was also determined that the growth of the Pb layer progressed outward from atomic steps at terrace edges and around small Pb islands which nucleated on the terrace planes. Removal of the Pb adlayer does not return the smooth Au surface. Fig. 1c shows the roughened electrode surface which results from the deposition and stripping of the Pb layer. It is composed of 20-150Å diameter monolayer-high islands, and ~25Å diameter monolayer-deep pits. Similar topographic changes were found to occur for sweep rates from 0.5 to 1000 mV/s.

In order to see if the roughening was a local effect of Pb deposition, we halted the first potential sweep at submonolayer Pb coverage (θ=0.25ML), and then stripped the Pb to look for roughening in the regions of Pb coverage. Lead deposition was restricted to a ~20Å wide strip at terrace edges and a few islands on the terrace planes; this can be seen in Figs. 2a and b. During the potential hold, the close-packed structures remained stable, but a less dense phase with an apparent height of only 1.3Å slowly covered the Au surface (Fig. 2c). We speculate that this is a $(\sqrt{3}x\sqrt{3})R30°$ Pb superlattice, which is believed to form on Au(111). Upon reversal of the potential sweep, the superlattice phase desorbed immediately; however, few of the deposited islands were removed, nor did the terrace edges retreat to their original positions (Figs. 2d and e). Instead, we observed the development of numerous, small, monolayer-deep pits clustered in a border near the terrace edges and around (and even within) the remaining islands. The pits can be seen most easily in Fig. 2f, after the surface has had a chance to anneal slightly and the very small vacancies have combined into larger, more easily imaged pits. The images of Figs. 2g-i show the results of the second partial (θ=0.33ML) deposition and stripping sequence. The earliest topographic change we observed was Pb deposition into the pits. The terrace edges again extended by about a ~20Å strip of Pb, and more islands nucleated on the terraces. No islands nucleated over the border region which had contained the pits. Removal of this Pb layer again left the Au pitted (Fig. 2i), but as a result of the higher Pb coverage this effect was more pronounced.

We have suggested that these observations can be explained by a model in which the Pb deposition is followed by a surface alloy formation. The diagram in Fig. 3 illustrates how these effects occur. Through a series of Pb-Au place exchanges, both vertical and horizontal, a surface alloy forms in the vicinity of Pb deposits (Fig. 3a-d). Atomic vacancies which remain in the surface after Pb stripping will quickly coalesce into small pits (Fig. 3e), and it is likely that these would continue to grow as the surface annealed. Upon redeposition into these pits, the Pb atoms would be already partially dispersed in the plane, and therefore the alloy forms more rapidly (Fig. 3f). Since the overpotential for nucleation on the alloy is almost certainly greater than on bare Au, no new islands would form over the alloy and a border, protected from island deposition results (Fig. 3g).

In summary, we find that a Au(111) electrode is substantially roughened after a single monolayer of Pb is electroplated and stripped from the surface in a linear sweep experiment. The roughened electrode surface rearranges into 20 to 150Å diameter monolayer islands and smaller monolayer pits. This process is observed on all samples, for sweep rates ranging from 0.5 to 1000mV/s. If a partial layer of Pb is plated and then stripped, pitting and an increased overpotential for Pb deposition are observed only in the areas adjacent to the plated sites. We suggest that these observations are consistent with the formation of a Pb-Au alloy in the surface layer.

Copper

Our *in situ* STM studies of Cu on Au (111) surfaces in sulfate electrolytes showed strikingly different behavior from the Pb system. No evidence of alloy formation was observed and the Cu adlayer was formed by a complicated sequence of intermediate superlattice arrangements. Recent *in situ* scanning tunneling microscopy (STM) (10), atomic force microscopy (AFM) (11), and x-ray absorption spectroscopy (XAS) (12) studies of this system have emphasized the atomic arrangement of the Cu adatoms at various stages of the monolayer formation. Instead of this, we concentrated on larger substrate areas, and imaged continuously during the layer formation stages. This approach allows consideration of the film growth dynamics. At this scale we cannot determine an atomic lattice spacing for the phases we observe, but rely on comparison of our results with those of the previous *in situ* STM, AFM, and XAS studies of this system to assign a structure to the observed phases.

We observe three distinct Cu phases in our STM images during deposition and stripping. They are distinguished as regions of similar patterns of growth of a certain average height above the bare Au plane. The three phases are referred to as phase I (the lowest), phase II (approximately half of a monolayer high), and phase III (one monolayer high). We assign these phases to the ($\sqrt{3}$ x $\sqrt{3}$), the (5 x 5), and the (1 x 1) Cu overlayer structures, respectively, based on comparison with previous *in situ* results (10-12) and on calculations using a hard sphere model for the structures (13). Fig. 4 shows a deposition sequence consisting of a potential sweep from 500 to 30 mV (2mV/s), which was interrupted and held at 75, 65, and 50mV. All images in this section were taken with an acquisition time of 51s, scanning from bottom to top. Three single atomic steps can be seen on the 750x750Å^2 region of the Au surface (Fig. 4a), shown during the initial part of the deposition wave. About halfway up the image, the terrace surface begin to show an additional layer having a height of 0.46 ± 0.10Å which we have termed phase I. This new phase can be seen more clearly in Fig. 4b, which is a closer view of the boxed-in in region of Fig 4a. Phase I deposits initially as patches (arrow **A**), in the center of the plane, and then grows rapidly over most regions of the Au surface. During the ramp from 200 to 75mV, additional Cu is deposited into two different phases having average heights of 1.23 ±0.23Å (phase II) and 2.38 ± 0.28Å (phase III). Phase III appears as small islands (10 to 25Å in diameter) which nucleate in filaments across the surface of the terraces with no apparent

orientation. Phase II, with an intermediate height between phases I and III, is visible mostly between and around the phase III islands, giving a web-like appearance. Other domains of phase II appear, concentrated at the top edge of the steps. This growth pattern gives the appearance of "ribbons," which continue to widen and become more distinct as the phase II domains grow slowly outwards to replace phase I, finally merging until phase I disappears entirely. Thus, during the deposition sequence, we find that all three Cu phases exist simultaneously.

Reversing the direction of the potential sweep (75 to 500mV) strips the Cu overlayer. Images of this process are presented in Fig. 5, with the current voltage data for Fig 5c included as Fig. 5d. Fig. 5a begins at a potential of 175mV, mid-way through the adlayer removal. Between 50 and 175mV (not shown), phase II was stripped and many of the phase III islands disappeared. Phase I is removed with the main anodic current peak at 243mV. A zoomed view of a portion of Fig. 5a is presented in Fig. 5c with enhanced contrast, showing the removal of phase I. From the corresponding electrochemical data (Fig. 5d) it can be seen that phase I lifts in the potential window 230-243mV, and is completely dissolved by the time the current begins to drop. During the remainder of the potential sweep phase III is slowly removed by a process of island dissolution and coalescence. Fig. 5b shows the Au surface and the few remaining phase III islands at the end of the scan, with the potential held at 500mV. We find that these islands are relatively stable at this potential, but that they can be removed if the electrode is cycled through a Au oxidation potential scan.

Future Prospects

Numerous avenues exist in electrochemistry for the application of STM's proven capabilities. Investigations of nucleation and growth structures can be applied to metal deposition on semiconductors and can be expanded to follow the development of bulk plating on both semiconductor and metal substrates. In this regard, the role of additives - surfactants, leveling agents, inhibitors - can be assessed. A study of corrosion mechanisms at the atomic level could greatly increase our understanding of this process. Increased attention will certainly be given to the possibilities of using the tip to perform localized electrochemistry; lithography (by both deposition and etching) and catalysis are likely targets.

References

1 M.G. Samant, M.F. Toney, G.L. Borges, L. Blum, and O.R. Melroy, *J. Phys. Chem.* **92**, 220 (1988).

2 A. Tadjeddine, D. Guay, M. Ladouceur, and G. Tourillon, *Phys. Rev. Lett.* **66**, 2235 (1991).

3 G. Binnig, H. Rohrer, Ch. Gerber, and E. Weibel, *Phys. Rev. Lett.* **49**, 57 (1982).

4 J. Tersoff and D.R. Hamann, *Phys. Rev. B* **31**, 2 (1985).

5 A.J. Bard and L.R. Faulkner, *Electrochemical Methods, Fundamentals and Applications* (Wiley, New York, 1980) p. 506.

6 M.P. Green and K.J. Hanson, *Surf. Sci. Lett.* **259**, L743 (1991).

7 K. Engelsmann, W.J. Lorenz, and E. Schmidt, *J. Electroanal. Chem.* **114**, 1 (1980).

8. M.P. Green, K.J. Hanson, R. Carr, and I. Lindau, J. *Electrochem. Soc.* **137**(11), 3493 (1990).

9 K. Juttner and W.J. Lorenz, Z. Physik. Chem. NF **122**, 163 (1980).

10 O.M. Magnussen, J. Hotlos, R.J. Nochols, D.M. Kolb, and R.J. Behm, *Phys. Rev. Lett.* **64**, 2929 (1990); O.M. Magnussen, J. Hotlos, G. Beitel, D.M. Kolb, and R.J. Behm, *J. Vac. Sci. Technol. B* **9**(2), 969 (1991); O.M. Magnussen, J. Hotlos, G. Beitel, D.M. Kolb, and R.J. Behm, unpublished.

11 S. Manne, P.K. Hansma, J. Massie, V.B. Elings, A.A. Gewirth, *Science* **251**, 183 (1991).

12 A. Tadjeddine, D. Guay, M. Ladouceur, and G. Tourillon, *Phys. Rev. Lett.* **66**, 2235 (1991).

13 M.P. Green and K.J. Hanson, accepted for publication in *J. Vac. Sci. Technol.*.

Figure Captions

Figure 1. *In situ* images of the deposition and stripping of Pb on pristine Au. Shading is keyed to height and five atomic levels are shown. **Image a**: Bare Au. **Image b**: After deposition of one monolayer of Pb. **Image c**: After Pb monolayer is stripped, first cycle. **Image d**: Second deposition of Pb layer. **Image e**: Same region, as Pb is being stripped. (the direction of the STM scan is bottom-to-top). **Image f**: After Pb layer is stripped, second cycle.

Figure 2. Partial Pb coverages. Sequence of images from two sweep-and-hold, plate-strip cycles. Potential sweep is shown at top of figure. **Image a**: Bare Au. **Image b**: Beginning of hold period. Terrace edges extend by 15 - 20 Å and several islands appear. **Image c**: A new phase (arrow) is seen by the end of hold period. **Image d:** At the end of stripping, pits can be seen near terrace edges. **Image e**: A superposition of the original step edge positions (from Image a) over a portion of Image d. **Image f:** Pits are fewer and larger. **Image g**: Pits fill and new islands nucleate. Margins near the top edge of the steps are protected from nucleation at this potential (240 mV). **Image h**: Step positions have rearranged slightly after hold. **Image i**: After second stripping sweep.

Figure 3. Schematic illustration of how a series of place-exchanges between Pb and Au could account for the observations shown in Figure 2.

Figure 4. Cu deposition sequence. Images scanned upwards. **Image a:** Bare Au surface and the formation of phase I adlayer; potential 270-188mV. **Image b:** Zoomed section of image a highlights phase I formation beginning at arrow; potential 230-188mV. **Image c:** Initial growth of phase II on top of step edges and around phase III islands; potential 75mV. **Image d:** Expansion of phase II in "ribbon" domains; potential 65mV. **Image e:** Continued filling of phase II domains leaving patches of phase I, potential 50mV.

Figure 5. Removal of first partial Cu adlayer. Images scanned upwards. **Image a:** Before this image phase II is removed, and here a lower number of phase III islands remain. Phase I is removed at arrow, box indicates area reproduced in image c; potential 200-275mV. **Image b:** Au substrate with several phase III islands remaining; potential 500mV. **Image c:** Zoomed view with enhanced contrast of boxed portion of image a showing phase I removal at arrow; potential 210-260mV. **Image d:** Electrochemical current and potential for image c.

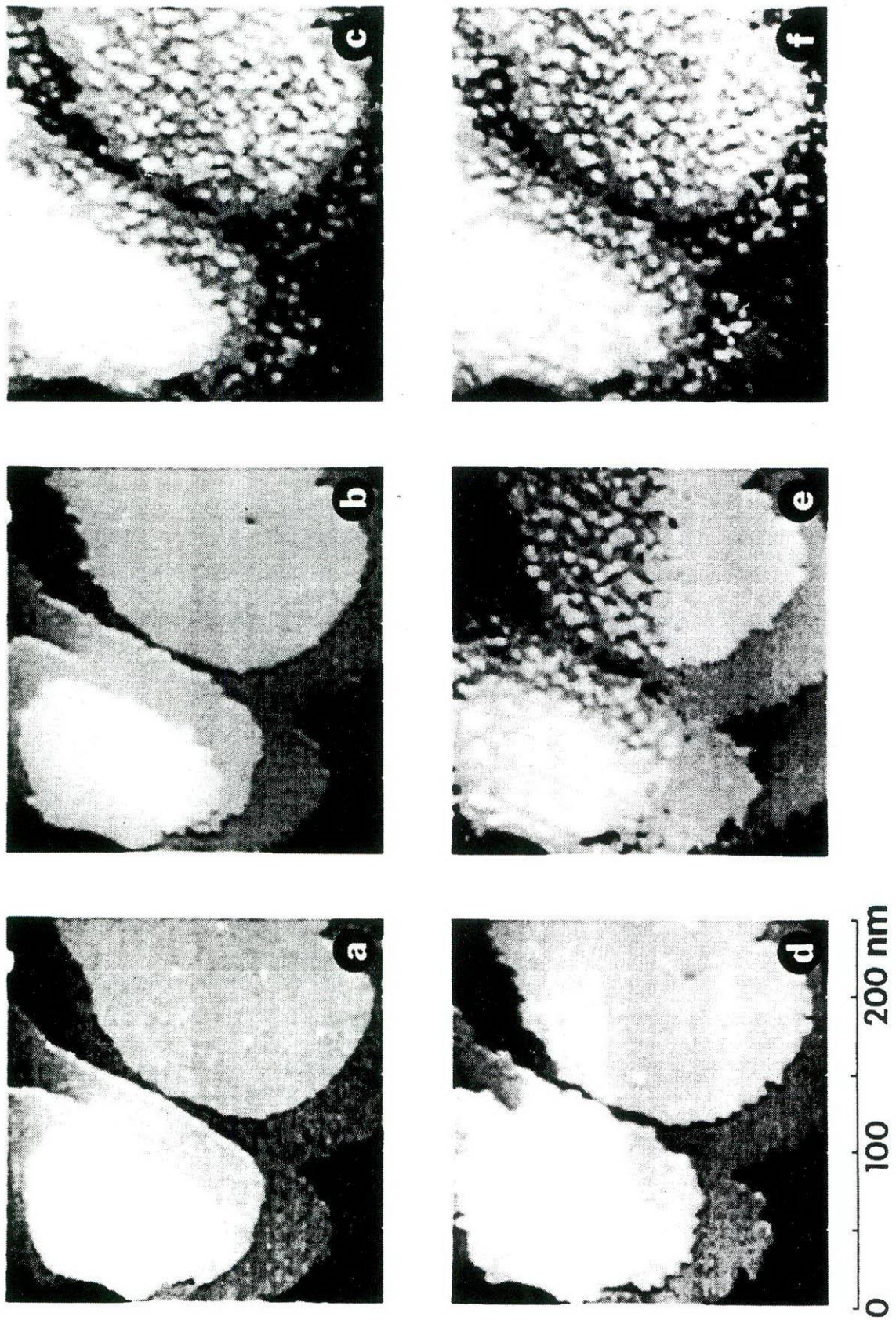

FIGURE 1

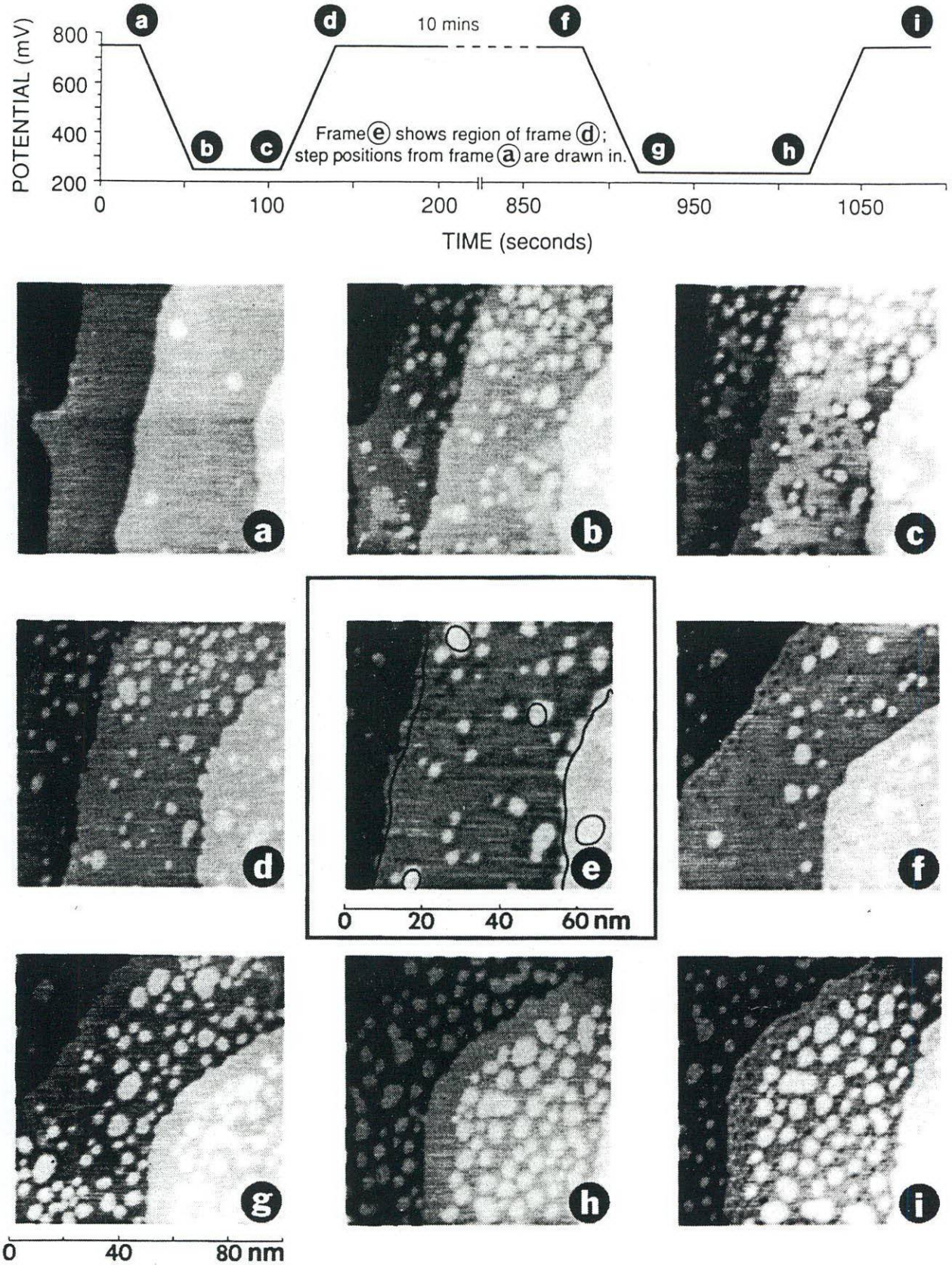
POTENTIAL (mV)
800
600
400
200
0
100
200
850
950
1050
TIME (seconds)
10 mins
Frame ⓔ shows region of frame ⓓ;
step positions from frame ⓐ are drawn in.
a
b
c
d
e
f
g
h
i
0 20 40 60 nm
0 40 80 nm

FIGURE 2

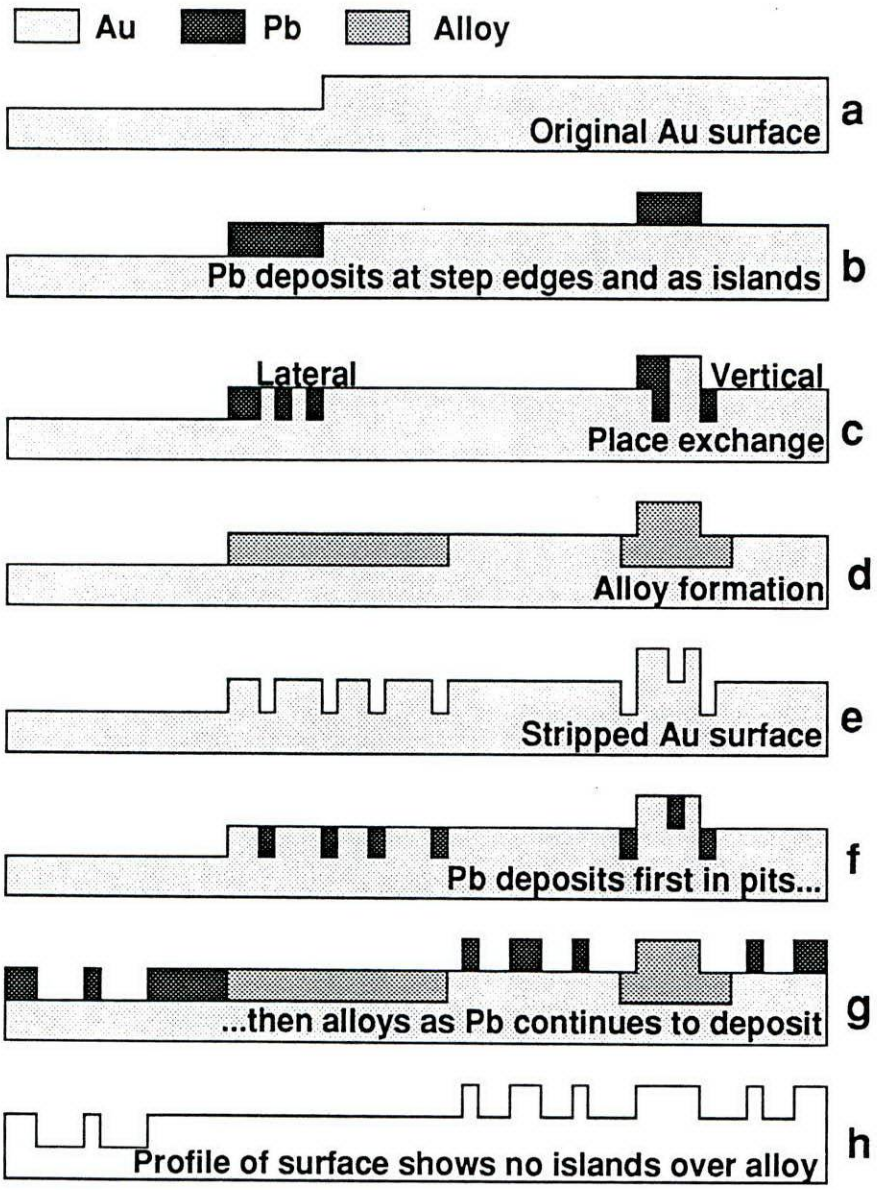
Au
Pb
Alloy
Original Au surface
a
Pb deposits at step edges and as islands
b
Lateral
Vertical
Place exchange
c
Alloy formation
d
Stripped Au surface
e
Pb deposits first in pits...
f
...then alloys as Pb continues to deposit
g
Profile of surface shows no islands over alloy
h

FIGURE 3

FIGURE 4

FIGURE 5

a
0
75nm
b
0
75nm
c
0
40nm
d
Potential, mV
500
400
300
Current, µA
10
5
0
Percent of image c, bottom to top
0
10
20
30
40
50
60
70
80
90

INSURANCE COVERAGE FOR ENVIRONMENTAL LIABILITY

For Presentation To The
American Electroplaters And Surface Finishers Society

February 15, 1992

John S. Vishneski III
Keck, Mahin & Cate
8300 Sears Tower
233 South Wacker Drive
Chicago, Illinois 60606

INSURANCE COVERAGE FOR ENVIRONMENTAL LIABILITY

John S. Vishneski III
Keck, Mahin & Cate
8300 Sears Tower
233 South Wacker Drive
Chicago, Illinois 60606

I. Purpose And Scope Of Paper

The purpose of this paper is to describe the nature of environmental liability currently imposed by federal law and to discuss the prospects companies may have for recovering the cost of such environmental liability from their liability insurance carriers.

This paper does not discuss issues involved in litigating environmental suits brought by the United States Environmental Protection Agency ("EPA") against electroplaters, surface finishers and other companies. Nor does it discuss liability imposed under state statutes or state common law. This paper assumes that such liability has been (or clearly will be) incurred by companies and focuses on the potential for companies to obtain insurance coverage for that liability.

II. Nature Of Federal Environmental Liability

Although there are many federal statutes that impose environmental regulation and liability on American industry, the most far-reaching is the Comprehensive Environmental Response, Compensation and Liability Act of 1980 ("CERCLA"), 42 U.S.C. §§ 9601-9657 (1991). Under CERCLA, liability is retroactive, absolute and joint and several.

The "retroactive" aspect of CERCLA allows the EPA to sue companies for activities that occurred prior to its passage in 1980, typically activities from the 1960's and 1970's. For example, if a company's waste products from 1975 contributed, in 1975, to pollution at a landfill, under CERCLA that company can now be held liable for costs associated with cleaning up that landfill. This is true even if the company disposed of its waste at the landfill in accordance with all laws and regulations in effect in 1975.

Liability under CERCLA is "absolute" in that it is imposed regardless of fault, and even regardless of proximate (or direct) causation. CERCLA operates by creating classes of persons or companies who are typically involved in some way with the operation of a site that has become polluted, such as owners of the site, transporters of waste to the site, site operators, and generators of waste. Persons and companies in these categories are

designated as "Responsible Parties." The statute then imposes liability on everyone in each of these categories.

This liability is not conditioned on any level of fault; that is, whether the pollution was caused by a particular Responsible Party's negligence or intentional action is not a pre-requisit to that Responsible Party's liability under the statute. In addition, liability is imposed on generators of waste even if the pollution was caused entirely by the negligent or intentional acts of a third person. Thus, neither fault nor direct causation is a pre-requisit to liability under CERCLA -- liability is absolute.

Liability under CERCLA is also "joint and several." This means that each person or company that is found to be a Responsible Party is individually liable for the entire clean-up of the polluted site. At the extreme, this means that if a company had just one barrel of waste delivered to a site that was later polluted, that company could now be held liable for the entire clean-up of the site if, for example, the other Responsible Parties were insolvent or could not be found. In most cases, the joint and several aspect of CERCLA liability means that each Responsible Parties' share of the clean-up of a site will be larger proportionally than the amount of pollution attributable to its activities.

III. Comprehensive General Liability Insurance Policies

The environmental liability imposed by CERCLA and similar state statutes may be covered by ordinary general liability insurance. Most American businesses have some form of general liability insurance, usually Comprehensive General Liability ("CGL") insurance, and the coverage language and exclusions in CGL policies are strikingly similar from policy to policy. This results because insurance industry trade organizations draft standard policy forms which are then widely used in practice. The primary purpose of this paper is to discuss the extent to which such standard language may cover CERCLA environmental liability.

The two most important provisions of standard CGL policies with respect to environmental liability are the coverage clause and the pollution exclusion.[1] The standard coverage clause in CGL policies reads:

---

[1] Environmental insurance coverage litigation can become very complex, and numerous issues are raised at and before trial which involve other portions of CGL policies. The coverage clause and the pollution exclusion, however, are usually the central focus of such litigation, and consequently, they are the focus of this paper.

> The company will pay on behalf of the insured all sums which the insured shall become legally obligated to pay as damages because of
>
> A. bodily injury or
> B. property damage
>
> to which this insurance applies, caused by an occurrence
>
> ....
>
> "occurrence" means an accident, including continuous or repeated exposure to conditions, which results [during the policy period] in bodily injury or property damage neither expected nor intended from the standpoint of their insured.

Environmental Liability Insurance Law: An Analysis of Toxic Tort and Hazardous Waste Insurance Coverage Issues, Kenneth S. Abraham (Prentice Hall Law & Business 1991), pp. 288, 291. This version has been in use with little variation since 1966.[2]

The most striking aspect of this provision is the set of events it designates as triggering coverage. Under this provision, the event or circumstance that triggers coverage is bodily injury or property damage that happens during the policy period. For example, if a CGL policy has an effective period of one year from January 1, 1989 to January 1, 1990, it covers liability arising from events of bodily injury or property damage that happen during that year. Moreover, this is true regardless of when the event that caused the injury or damage happened.

This aspect of the standard-form CGL policy has important consequences with respect to coverage of CERCLA environmental liability. As noted above CERCLA liability is usually imposed today for events that happened long ago. For example, the mismanagement of a waste site that resulted in soil contamination may have happened in the 1960s or 1970s. In that case, since the damage to the property happened in the 1960s or 1970s, coverage would be provided by CGL policies from the 1960s and 1970s. Thus, the question of whether insurance coverage exists for CERCLA environmental liability involves the interpretation of old CGL policies, usually from the 1960s and 1970s.[3]

---

[2] From 1966 to 1973, the standard definition of occurrence used the language "including injurious exposure to conditions" instead of "continuous or repeated exposure to conditions." Environmental Liability Insurance Law, p. 299.

[3] The passage of CERCLA in 1980 imposed stringent regulatory requirements with respect to the disposal of industrial waste. Hence, environmental problems of today are typically not the result of waste disposal practices from the decade of the

The primary defense to CERCLA environmental coverage put forward by insurance companies is the 1970 standard-form pollution exclusion. This exclusion, placed in most standard-form CGL policies from 1970 through 1986, reads as follows:

> This insurance does not apply ... to bodily injury or property damage arising out of the discharge, dispersal, release or escape of smoke, vapors, soot, fumes, acids, alkalis, toxic chemicals, liquids or gases, waste materials or other irritants, contaminants or pollutants into or upon land, the atmosphere or any water course or body of water; but this exclusion does not apply if such discharge, dispersal, release or escape is sudden and accidental.

Environmental Liability Insurance Law: An Analysis of Toxic Tort and Hazardous Waste Insurance Coverage Issues, Kenneth S. Abraham (Prentice Hall Law & Business 1991), p. 291. This exclusion is one of the most widely-litigated insurance policy provisions ever drafted.

In most cases, the controversy centers on the meaning of the exception part of the exclusion, "but this exclusion does not apply if such discharge is sudden and accidental." Policyholders seeking coverage for pollution that happened long ago, and that happened without their knowledge, argue that one reasonable meaning of the words "sudden and accidental" is unexpected and unintended. Under this interpretation, CERCLA liability for long-ago caused pollution is covered, provided the policyholder had no knowledge that the pollution was happening at the time of the events causing the pollution.

Insurance companies, on the other hand, typically argue that the only reasonable meaning of the words "sudden and accidental" is quick (or instantaneous), unexpected and unintended. Under this interpretation, coverage is only provided when the pollution from which liability arises happened all at once, such as when a tanker truck carrying gasoline overturns and explodes. Thus, according to insurance companies, most CERCLA liability is not covered because it is the result of waste disposal practices taking place over an extended period of time.

IV. The Division Of Courts With Respect To Interpreting The 1970 Pollution Exclusion

State and federal courts called upon to interpret the "sudden and accidental" language of the 1970 pollution exclusion

---

1980s. Rather, they are the result of the less-regulated decades of the 1960s and 1970s.

have disagreed as to its meaning. This disagreement has important consequences for policyholders seeking coverage for CERCLA liability because insurance law is almost exclusively state law. Thus, disagreement between courts results in coverage being provided in one state, but not in a neighboring state, for the same set of circumstances.

One common set of circumstance under which CERCLA liability is imposed is when a generator of waste has contracted with a hauler who subsequently causes pollution unbeknownst to the generator. In Du-Wel Products, Inc. v. United States Fire Insurance Co., 565 A.2d 1113 (N.J. Super. Ct. App. Div. 1989), appeal denied, 583 A.2d 316 (N.J. 1990), the policyholder was an electroplater who generated a toxic sludge as a by-product of its electroplating process. The policyholder contracted with an independent state-licensed waste hauler to dispose of its sludge at a state-approved disposal site. The policyholder was sued because the waste hauler did not properly maintain the landfill and caused the site to be contaminated. The New Jersey Appellate Court, applying Michigan law, held that since the policyholder had complied with all applicable regulations and had not expected or intended that its wastes would cause the pollution, it was entitled to coverage under its CGL policy, despite the pollution exclusion.

On the other hand, in FL Aerospace v. Aetna Casualty & Surety Co., 897 F.2d 214 (6th Cir. 1990) (Michigan), the Federal Court of Appeals for the Sixth Circuit, interpreting Michigan law, decided a case identical to Du-Wel Products the opposite way. In FL Aerospace, the policyholder produced liquid waste as part of its production process. To dispose of the waste, it hired an independent waste hauler who took it to a landfill, and, because of the hauler's negligence, waste was released onto the soil and contaminated the site. The policyholder had no knowledge that its waste was causing pollution. The Sixth Circuit held that coverage was blocked by the pollution exclusion because the contamination happened over a period of time, and it could not therefore be considered quick or instantaneous as required by the court's interpretation of the "sudden and accidental" language.

Another common set of circumstances under which CERCLA liability is imposed is when a generator of waste or landfill operator believes that its waste disposal system will effectively prevent uncontrolled polluting releases of its waste, but it discovers belatedly that the waste control system did not function as expected. In Just v. Land Reclamation, Ltd., 456 N.W.2d 570 (Wis. 1990), the policyholder operated a waste disposal site, which it expected to contain pollutants from entering into the surrounding soil. The wastes nevertheless contaminated the groundwater surrounding the landfill. The Wisconsin Supreme Court held that to the extent the release of contaminants from the landfill into the ground was unexpected and unintended by the

policyholder, coverage would be provided under the standard-form provisions of the CGL policies in question.

Prior to the Just decision, however, the Wisconsin Court of Appeals decided a similar case exactly the opposite way. In State v. Mauthe, 419 N.W.2d 279 (Wis. Ct. App. 1987), the policyholder was in the business of chromium plating. Periodically but unexpectedly, its pollution control system broke down, causing accidental spills. The court held that the policyholder's standard-form CGL policy pollution exclusion blocked coverage because the spills took place over an extended period of time, and consequently, they could not be considered quick or instantaneous as required by its interpretation of the pollution exclusion's "sudden and accidental" language.

As the above examples demonstrate, different courts interpreting even the same state law have decided identical fact situations in contradictory ways. The problem of inconsistency in the courts becomes even more pronounced when courts from different states are compared. This inconsistency creates a problem for companies deciding whether they want to pursue insurance coverage for CERCLA liability; namely, that there is usually no way to predict the chances of prevailing in such a suit.

V. Other Pitfalls Of Environmental Insurance Coverage Litigation

In addition to the unpredictability of insurance coverage litigation for CERCLA liability, there are a number of factors that cause such litigation to be very expensive.

First, it is important to recognize that insurance companies, with remarkable consistency, have resisted claims for coverage of CERCLA liability under their standard-form CGL policies. If a policyholder makes a claim for such liability, it is very likely to be sued by the insurance company in a declaratory action. This happens because most states require an insurer to defend its policyholders when they are sued for environmental liability and coverage is uncertain, or, the insurer must file a declaratory judgment action seeking a clarification by a court as to the rights and duties it owes under the insurance policy. In order not to be misinterpreted as agreeing that coverage exists, insurers sue. Thus, a great many environmental coverage claims ultimately have to be determined through expensive litigation.

Once in court, there is usually a battle over whether the chosen court is the right venue for the action. This battle takes place because of the inconsistency of the courts in deciding these types of cases. For example, if a policyholder sues an insurance company in a state where prior court decisions are favorable to the policyholder, the insurance company will attempt to remove the action to a more favorable location. These preliminary battles involve expensive motion practice.

After the venue is determined, insurance companies will insist on extensive discovery. They will take depositions of every employee (or retired employee) of the policyholder who had anything to do with the company's waste disposal in an attempt to establish that the policyholder had knowledge that its wastes were causing pollution. Insurance companies also take extensive discovery of site operators and waste haulers, again to try to establish that the policyholder knew that pollution was occurring, or alternatively, that the releases of pollutants happened slowly over a long period of time. This extensive discovery is very expensive.

VI. Conclusion

Electroplating and Surface Finishing companies often face CERCLA liability today because of events that occurred in the 1960s and 1970s. Insurance coverage may be available under standard-form CGL policies for such liability; however, the substantive law relating to insurance coverage for CERCLA liability is uncertain, and the litigation required to determine whether coverage exists is expensive.

ENVIRONMENTAL ISSUES ASSOCIATED WITH FINANCING OF ELECTROPLATING FACILITIES

ROGER A. DHONAU
SEC DONOHUE

INTRODUCTION

The Comprehensive Environmental Response, Compensation and Liability Act of 1980 (known as CERCLA or Superfund) as amended by the Superfund Amendments and Reauthorization Act of 1986 (SARA) is arguably the most significant federal law impacting buyers of industrial property and their financial backers. Under this law, the responsibility and liability for remediation of contaminated sites can extend to one or more of four classes of potentially responsible parties:

1. The current owner or operator of the contaminated property.

2. The owner or operator of the property at the time the contamination occurred.

3. The owner who arranged for disposal or treatment of hazardous substances at the contaminated property.

4. The person or corporation that knowingly transported hazardous substance to the contaminated property.

Any person or company in any one of the these four groups can be held responsible for part or all of the cleanup costs for a contaminated site regardless of their level of contribution to the problem. This liability may also extend back in time to when there were little or no restrictions on waste disposal practices.

In this expensive web of liability, the definition of "owner or operator" is of key importance. Several landmark court cases in the mid to late 1980s held lenders to a given company as liable as the owners for cleanup costs of the company's property.[1] Although restrictions exist limiting lenders liability, there have been enough instances where lending institutions have been saddled with this liability that there is considerable concern throughout the financial industry.

[1] United States vs. Maryland Bank & Trust Co., 632 F. Supp. 573 (1986). Guidice vs. BFG Electroplating, 30 ERC 1665, DC W.PA (1989), and others.

It is obvious that older facilities have a greater potential for environmental problems due to materials and management practices used prior to the institution of modern environmental regulations. The advent of hazardous waste management requirements has placed strict control on management of hazardous materials, but has by no means eliminated the possibility for environmental contamination, even if a facility was in full compliance. Thus, the fact that a facility began operations at a clean site after 1980 and was in full compliance with the applicable regulations, does not preclude the possibility of environmental problems.

THE DUE DILIGENCE PROCESS

In order to protect themselves from environmental liability, lenders are focusing on landowner defense clauses incorporated into CERCLA with the passage of SARA. In accordance with Section 107, a buyer or lender cannot be held liable for contamination caused by past operations if he/she has performed "all appropriate inquiry into previous ownership and uses of the property consistent with good commercial or customary practice in an effort to minimize liability".[2] This environmental due diligence process is required for any financial association, including not only the purchase of industrial property, but other not so obvious activities such as funding expansions or remodeling. Also, if a company seeks financial support for expansions at one facility, all facilities owned by that company may have to be evaluated.

A definition of what is "appropriate" and "good commercial or customary practice" was not incorporated into this law and is the subject of considerable debate. There has, however, been effort made by organizations such as ASTM and the National Registry of Environmental Professionals to set standards for this environmental due diligence process. Consequently, general procedures are gradually becoming established.

Also, the due diligence process is still in the developmental stage, but a general consensus on content is gradually being formulated. It is now widely accepted that the due diligence process is normally completed in one or more of three phases.[3] Phase I serves to determine whether there is a reasonable basis to suspect that theproperty or activities performed by past or present property owner/operators present an environmental risk to the buyer or lender. Phase II is then intended to confirm or deny the existence of suspected

---

[2] 42 U.S.C. Paragraph 9601(35)(B)

[3] Environmental Risks Identification and Management, A.R. Wilson, Lewis Publishers, Inc. 1990

risks identified in Phase I. Phase III studies then serve to determine the extent of the risk and develop a plan to reduce or eliminate the threat posed to human health and the environment. Obviously, if no environmental risks are identified in Phase I, Phase II and Phase III studies are not necessary.

Regardless of the type of property considered, there are several core topics that must be addressed in the Phase I due diligence investigation to determine if an environmental risk is likely. These include:

- ❒ Regulatory compliance history by current and past owners of both the subject and surrounding properties.
- ❒ Current and past waste management practices
- ❒ Property ownership and use history
- ❒ Current and past activities on both the subject and nearby properties that may have affected the site.
- ❒ On-site inspection for physical signs of potential contamination

How these topics are addressed and the level of detail in which they are addressed is highly dependent upon the specific site and the level of risk the buyer/lender is willing to take.

There are probably as many formats and report content standards for due diligence investigations as there are firms offering this service. The generic report outline presented in Figure 1 incorporates the key issues discussed above and represents a minimum which should be addressed in the investigation report. A less comprehensive investigation may subject the lender to an unacceptable level of financial risk.

FIGURE 1

PHASE I REPORT CONTENT

1.0 INTRODUCTION
- 1.1 Purpose
- 1.2 Document Use and Distribution

2.0 SCOPE OF WORK

3.0 SITE DESCRIPTION
- 3.1 Location and Boundaries
- 3.2 Natural Site Features
- 3.3 Cultural Features

4.0 SITE HISTORY
- 4.1 Present Land Use
- 4.2 Past Land Use
- 4.3 Historical Documentation
  - 4.3.1 Zoning Records
  - 4.3.2 Sanborn Maps
  - 4.3.3 Aerial Photos
- 4.4 Property Owner/Facility Records

5.0 SITE CHARACTERISTICS
- 5.1 Site Facilities Description and Inspection Results
- 5.2 Property Grounds Description and Inspection Results

6.0 REGULATORY COMPLIANCE ISSUES
- 6.1 Federal Programs
- 6.2 State Programs
- 6.3 Local Programs

7.0 SURROUNDING LAND USE
- 7.1 Regulatory Compliance
- 7.2 Off-Site Reconnaissance
- 7.3 Other Data

8.0 SUMMARY AND CONCLUSIONS

9.0 LIMITATIONS

ATTACHMENTS

ATTACHMENT A	Site Maps/Area Maps
ATTACHMENT B	Aerial Photos
ATTACHMENT C	Sanborn Maps
ATTACHMENT D	Regulatory Compliance Documentation
ATTACHMENT E	Interview Documents
ATTACHMENT F	Site Inspection Photos
ATTACHMENT G	Analytical Data

ELECTROPLATING FACILITY ENVIRONMENTAL ISSUES

Each industry has its own unique environmental problems routinely encountered during due diligence investigations and the electroplating industry is no exception. Issues associated with the electroplating industry, such as past management of wastes contaminated with heavy metals, are well recognized by both people in the industry and most lenders. Although these particular wastes are indeed a subject of concern, there are other equally important issues associated with either current or past operational practices and materials which could present unacceptable risk to a lender. It is imperative that the presence or absence of environmental contamination stemming from these practices and materials be determined and their associated management practices evaluated in order for the lender to make a rational decision on becoming financially connected to the facility.

The following paragraphs present an overview of the more common of these issues.

Chlorinated Organic Solvents

For many years, chlorinated solvents, such as trichloroethylene and perchloroethylene, were used almost exclusively for removal of organic contaminants from parts prior to plating. These solvents were not only well suited to the task, but were also inexpensive and had the distinct advantage over non-halogenated solvents of being classified as non-flammable. Due to a variety of environmental and human health concerns, their use has diminished considerably in the past few years, but are still quite common.

The vast majority of facilities still using chlorinated solvents manage them very strictly, presenting little risk to an owner, buyer or lender. Unfortunately, these strict management practices are only a recent development. Until the advent of RCRA regulations governing the management of waste chlorinated solvents (1980), it was common practice to simply discharge spent solvents to a convenient drain or onto the surrounding property. Their low cost meant that little or no effort was made to control spills of fresh solvent.

Physical, chemical and biological characteristics of these solvents result in very persistent and troublesome contamination scenarios. Allowing even small amounts of solvents to enter into the facility wastewater management system results in expensive remediation costs. As these solvents have a density greater than that of water, they can accumulate in sumps, low points and/or drain traps throughout the entire wastewater management system. Should sumps or buried piping be cracked, the solvent can drain to the underlying soil and ground water.

This contamination can be then carried off-site by ground water movement or simply by gravity.

In this scenario, the owner would be obligated to clean up contamination on the adjacent property as well as that underlying the plating facility with the cost of cleanup easily exceeding the value of the property. If the owner cannot afford the cleanup, responsibility may then fall on the owner's lending institution. Accordingly, lenders are wary to become associated with an electroplating facility until the absence of such a scenario can be confirmed.

In smaller facilities, fresh solvent was generally purchased in drums which were then stored indoors or outdoors. Until recently, these storage areas rarely had a containment system. If outdoors, spills went directly to ground, resulting in contamination scenarios very similar to that resulting from on-site disposal of waste solvent. If indoors, the spill frequently went to the nearest floor drain and subsequently released to the environment. Similar scenarios have also occurred with tank storage of solvents. Spills and overfilling were quite common and leaks often ignored.

As noted above, disposal of waste solvents was frequently accomplished via discharge to sewer or stream. Although this usually resulted in complete removal of these wastes from the property, it does not necessarily remove the owner/lender from liability. There have been many instances where contamination resulting from such discharges resulted in the owner being responsible for subsequent remediation. Costs associated with such remediation projects are usually very high, frequently exceeding a million dollars.

Lead Tanks

Prior to development of modern plastics, it was common practice to use lead lined wooden tanks to hold acidic plating and cleaning solutions. This practice has resulted in two concerns that must be addressed when evaluating older electroplating facilities. First, misuse or poor maintenance of this type of tank could result in heavy corrosion of the lead lining, resulting in lead contamination in and around the facility.

Secondly, routine spills and leaks resulted in exposure of the wooden support structure to plating solutions. As wood is aggressively attacked by the acid component of these baths, replacement of part or all of the wooden frame was considered a routine maintenance item. Disposal of the damaged wood was often accomplished through on-site burial or burning, resulting in the direct transfer of plating bath constituents to the surrounding environment.

Wastewater Management Systems

Prior to promulgation of regulations governing discharges of industrial wastewater and general public concerns over water conservation, untreated rinse waters, spent cleaners and contaminated plating baths were regularly released from plating facilities. Depending upon the availability of various receptors, this discharge may have been routed to storm sewer, sanitary sewer, stream or an on-site infiltration lagoon. As these discharges contained high concentrations of metals used in the plating operations, as well as a variety of other facility wastes, contamination of these receptors is common and a source of environmental liability. This concern also exists for discharges initiated after installation of pretreatment equipment as metal hydroxide sludges were frequently collected in on-site lagoons.

Long-term discharge of untreated wastewater to stream has, in some cases, resulted in expensive investigation and remediation of the contaminated stream beds. Discharge to an infiltration bed or leach field usually requires remediation, often as a RCRA closure or corrective action. Although less likely, discharge to storm or sanitary sewer may require remediation of soils surrounding the discharge line if there had been significant leaks in the line. More importantly, discharge of heavy metals to a municipal sewer system can result in contamination of the sanitary sludge. Again this can lead to considerable remediation liability for the facility owner.

Obsolete/Unused Chemicals

Over time, most electroplaters have made a wide variety of changes in cleaning agents, bath additives and bath components. These changes, for whatever reason, usually resulted in residuals of the replaced chemicals. Quite often these accumulate in an unused corner and now present a considerable safety risk as well as an expensive disposal problem.

Bench scale testing of new processes and chemicals inevitably results in the accumulation of a wide variety of small containers of unwanted chemicals. Despite their relatively small quantities, these wastes represent a surprisingly high disposal cost due to the extensive handling required. Typical lab-packs used in disposal of miscellaneous bottles of chemicals cost between $2,000-$3,000 per pack with each pack holding only a few hundred pounds of wastes.

Other Issues

Environmental concerns common throughout most industries, such as PCBs and asbestos, should not be overlooked when evaluating electroplating facilities. PCBs were common in a wide variety of electric

equipment manufactured prior to 1970, much of which is still in use. The presence of PCBs in electrical equipment at a given facility does not necessarily mean environmental problems (and associated liability) exist. It simply means that a potential for contamination exists and further evaluation is probably prudent. In addition to electrical equipment, PCBs have unfortunately also been found in hydraulic fluids at many industrial concerns. Although the occurrence is relatively infrequent, cost of remediation under such a scenario can be formidable.

Summary

In summary, there are a multitude of potential environmental pitfalls associated with electroplating facilities. Fortunately, through careful inspection and evaluation, presence or absence of environmental risks can be identified and quantified. With this information, financing can quickly proceed in most instances with little risk to the financial backer. In those instances where significant environmental problems are discovered, the owner then has the opportunity to address the issue in order to allow financing to proceed.

Regardless, these procedures all have the same intention. That is, to perform sufficient inquiry into the environmental status of a property and any activities which have taken place on the property to determine if the site can reasonably be expected to present an environmental risk. Armed with this information, the lender can make a rational decision whether or not to become financially associated with the company seeking a loan.

POLLUTION PREVENTION PLANNING FOR ELECTROPLATERS

Daniel P. Reinke, P.E.
Capsule Environmental Engineering, Inc.
1970 Oakcrest Avenue, Suite 215
St. Paul, Minnesota 55113

Abstract

Many states as well as the EPA are actively working to reduce industrial wastes and emissions through voluntary and mandatory efforts by manufacturers. As part of this work, 17 states have passed legislation requiring companies to prepare written plans that address the sources of wastes and emissions within the facility, options for reducing these wastes, and facility plans to implement these options.

This paper presents general guidelines on what electroplaters and surface finishers need to do to meet these planning requirements, as well as the resources available to assist them in these efforts.

Introduction

With every manifest they complete, large quantity generators of hazardous waste certify that they have a program in place to reduce the volume and toxicity of their waste. In recent years, however, additional regulations have been promulgated that require generators to take a more structured role to reduce their wastes and emissions. These regulations are coming at manufacturers from many fronts.

The benefits of implementing pollution prevention projects are well documented. Large and small companies have realized reductions in the following areas:

- Raw materials costs
- Waste management capital and operating costs
- Regulatory costs and reporting requirements
- Disposal liabilities
- Potential for spills
- Employee health and safety concerns
- Permitting requirements
- Compliance difficulties

In addition, pollution prevention has resulted in improved process efficiencies, product quality, and customer and community relations.

While many companies have jumped on the bandwagon and now actively promote pollution prevention, many others have been slower to realize these benefits. To further encourage firms to conduct these activities, state and federal laws and regulations have been developed. From a political viewpoint, these laws are difficult to oppose. They require manufacturers (polluters) to do something that will ultimately save them money and reduce the impact of their facility on the environment. For this reason it is not unreasonable to expect that further regulations in this field will be forthcoming.

The specific regulations vary in scope and impact. Most laws focus on "pollution prevention." EPA defines pollution prevention as "the reduction, elimination, or recycling of pollutants otherwise discharged into the air, water or land." Pollution prevention can be accomplished through source reduction, reuse and recycling. Massachusetts and Oregon have laws addressing "toxic use reduction," which is more controversial since these laws target the actual materials used in the manufacturing process instead of the emissions and wastes created through the processes. A closed loop hexavalent chrome plating process with a 100 percent efficiency scrubber system may adequately address pollution prevention regulations, whereas conversion to trivalent chrome plating may be required to meet toxics use reduction goals.

Regulatory agencies are also mandating pollution prevention activities through permit requirements. Facilities may only be able to meet tightening emissions and discharge limits by significantly modifying processes. Some platers are changing from cyanide to noncyanide processes while others have installed zero-discharge systems to address wastewater violations.

In addition to regulatory requirements for pollution prevention, there are other factors encouraging certain manufacturers to conduct these activities. Environmental organizations conducting citizen suits against violators of SARA reporting requirements or the Clean Water Act are including pollution prevention planning requirements in negotiated settlements. Environmental certification programs such as the Green Seal may require that member companies have active pollution prevention programs. The Chemical Manufacturers Association requires members to adhere to the Responsible Care program, which calls for continued pollution prevention efforts.

Federal Programs

There are several federal requirements for pollution prevention planning. Under the Pollution Prevention Act of 1990, toxic release inventory reporting forms (Form Rs) must now include questions on pollution prevention activities. Questions are included on source reduction practices used, recycling practices, production ratios and techniques used to identify source reduction opportunities.

Under the new storm water permitting requirements, facilities that report releases on Form Rs that are seeking general permits must include a discussion of pollution prevention activities in the permit application. At this writing, rules were not finalized for facilities seeking individual permits.

In addition, the phase-out of the production of ozone-depleting chemicals represents chemical-specific federal pollution prevention activities. President Bush has recently proposed an accelerated schedule to eliminate CFC production by 1996.

State Programs

As of the writing of this paper, 17 states have passed laws requiring certain facilities to prepare pollution prevention plans. These states include Arizona, California, Georgia, Louisiana, Maine, Massachusetts, Minnesota, Mississippi, New Jersey, New York, North Carolina, Oregon, South Carolina, Tennessee, Texas, Vermont and Washington.

In addition, Georgia's law requires out-of-state large quantity generators who use Georgia's hazardous waste facilities to also prepare pollution prevention plans. The exact requirements of pollution prevention or toxic use reduction plans vary from state to state. In general, however, the laws require the following items to be included in a plan:

certification
policy statement
description of facility and processes
description of wastes and emissions
description of present pollution prevention practices
identification of options
evaluation of options - environmental, technical and economic
selection of options
implementation schedule

Progress towards implementing the plan components is either addressed through plan updates or progress reports. Progress reporting typically allows for an adjustment in waste generation due to changes in production levels. For platers, production levels are usually best expressed in square feet of plated area. Other potential production indicators include machine run time for automatic plating lines and direct labor hours for hand lines.

Preparing a Plan

It may be possible to meet the legal requirements for a pollution prevention plan by one individual sitting down with the necessary data and writing up a discussion of available options. The plan can be set aside on a shelf and no changes made on the shop floor other than those previously planned. In order to reap the benefits of pollution prevention planning, however, you must identify and implement specific activities.

A good plan can be viewed as a business planning document. Preparing a business management plan requires input from sales, operations, legal, and financial groups. Likewise, preparing a pollution prevention plan may require input from purchasing, vendors, marketing, product engineering, quality control, operations, environmental, and maintenance groups. If the plan is to be released to the public, it may also be beneficial to enlist the services of a specialist in community relations to review the plan.

As with a business plan, it is important to establish goals. There are two types of goals that can be set. The first are broad corporate or facility-wide goals, such as the elimination of SARA Form R releases or a 90 percent reduction of hazardous waste generation. Other goals are process specific and are targeted to the individual projects developed in the planning process. Developing goals is beneficial because it helps focus facility efforts. Goals can be included in the policy statements required in some pollution prevention plans.

Developing goals requires the support and commitment of upper management. This support is needed both to initiate and sustain a successful program, and should be periodically reinforced. Reinforcement of management support can be accomplished through employee meetings for smaller companies or through a newsletter or bulletin board postings for larger firms.

Presenting a description of current processes and the wastes and emissions generated from those processes can be difficult. If wastewater from a number of plating operations is combined prior to treatment, you may need to measure the flow and analyze wastewater samples from each process to estimate the amount of sludge resulting from each operation. Another alternative for estimating the impact of various processes on sludge generation is to compare the total (not TCLP) metals concentration in a representative sample of the sludge.

Developing and evaluating options is the key to a good plan. The key to developing options is to review every process in the facility while asking "Why?" Often by asking simple questions, simple answers appear. For a captive shop, product modifications could eliminate the need for plating altogether. For a job shop, changing to trivalent chrome or noncyanide processes may be possible. These basic product changes should be identified and evaluated first before studying process modifications such as dragout reduction and zero discharge systems.

A number of resources are available to assist in developing and evaluating pollution prevention options. Resources include:

employees
trade associations
vendors
consultants
state technical assistance programs (TAPs)
EPA pollution prevention database
regulators
universities/trade schools

The person or team preparing the plan needs to discuss potential options with the individuals whose support will be necessary to implement the recommended options. Enlisting the support of these people will minimize the potential for problems after implementation. The operators and maintenance personnel involved with a particular process are often the most knowledgeable people on that process and can be a valuable source of ideas on how to make that process more efficient.

Once a list of options is developed, these options must be evaluated and selected for implementation. Factors to consider in evaluating options are listed below. The relative importance of these factors needs to be established for each facility to determine which option is best for that facility's operations.

capital cost and availability
operating cost
savings
environmental impact, both short- and long-term
occupational hazards impact
labor requirements or savings
maintenance requirements or savings
energy requirements or savings
technical risk
product changes required and customer approvals
process changes required
additional facility changes required
production shutdown requirements
technical support required and available
implementation schedule

Generally, these factors fall into three general categories -- environmental issues, technical issues and economic issues. Team members should consult the internal and external resources listed earlier for help with the environmental and technical review of options, which usually occurs before the economic evaluation. Those involved in the

environmental and technical review would ask the following questions:

Will it prevent pollution?
Will the option work in this application?
Has it worked elsewhere in similar conditions?
What are the potential problems?
What are the labor and maintenance requirements?
What results have been obtained?

The economic review of pollution prevention options is generally no different than that conducted for any facility capital expenditures. However, for a pollution prevention project, a facility may allow a longer payback or return on investment in an attempt to account for the numerous intangible benefits.

Obtaining the information necessary to conduct the economic review is not always an easy task. The evaluation must include capital and operating costs as well as expected savings. While vendors can supply much of this information, facility personnel also must review the numbers to ensure they accurately represent the expected costs and savings for the facility. This review should again use the internal and external resources identified earlier.

In the review process, certain options may fall out as being obviously beneficial and easily implemented. Other options may have longer paybacks but may have a high priority due to intangible benefits. This prioritization of projects should lead to the development of an overall schedule for implementation of selected activities. The schedule should be realistic and should consider personnel available to complete the projects.

With the information developed in the review process and the overall project schedules, you should be able to estimate expected reductions in wastes and emissions. If these reductions do not meet the corporate or facility-wide goals, additional projects may need to be identified.

The plan should include a discussion of all the options identified and evaluated, as well as the reasons for selecting certain options for implementation. Writing this all into the plan simplifies any plan updates or progress reports that must be completed. Once the plan document is completed, it typically must be certified by the management personnel responsible for the facility.

Specific state regulations should be reviewed to determine the submittal requirements. In some states, including Minnesota and Mississippi, plans do not need to be submitted and are nonpublic documents. In other states, such as Washington and Oregon, you must submit a certification that you have completed your plan or an executive summary of the plan. In New Jersey, Arizona, and Georgia full plans must be submitted to the

regulatory agency. Many states require that the plan be made available to regulatory inspectors. In California the plans must be made available to the general public upon request. Typically states require submittal of periodic progress reports.

Summary

New pollution prevention regulations aside, the procedure of evaluating products and processes for waste reduction opportunities is a logical step for any manufacturer looking to improve cost efficiency. A critical review of your operations allows you step back from daily activities and evaluate where you are going and how to get there. Pollution prevention planning provides a method for realizing the benefits of effective manufacturing processes.

Assessment and Options for Waste Minimization in the Metal Finishing Industry

Clifford W. Walton, CEF, and Kevin J. Loos
University of Nebraska-Lincoln
Department of Chemical Engineering
236 Avery Laboratory
Lincoln, NE 68588-0126

Abstract

An overview of waste assessment procedures and a knowledge of process options for remediation and recycle are necessary for a successful waste minimization program. Factors to consider when constructing a waste minimization program include EPA priorities, constructing an efficient assessment program, elements of previously successful programs, and opportunities relating to both the process and procedure of the particular system. This article describes the basic steps necessary to fulfill all the factors mentioned in order to create a successful and enduring waste minimization program in the metal finishing industries. Some existing and potential technologies are discussed. Finally, available references are presented that may assist in the process of analyzing and constructing a suitable program, including descriptions of selected case studies related to surface finishing.

With the increasing public concern about waste management, more efficient methods for minimization of waste disposal must be implemented. Various federal and state hazardous and solid waste regulations have made it more difficult and expensive to dispose of unwanted by-products, prompting prevention techniques. Some undesirable wastes, such as liquid wastes, have been or will be banned from land disposal completely, while other disposal methods will be restricted considerably. These restrictions have forced a shortage of approved disposal facilities, causing higher disposal costs. Due to the financial and legal incentives of reducing or completely eliminating unwanted by-products, and that generators of these by-products are required to certify that they have instituted a waste minimization program, it has become necessary and beneficial to implement a waste minimization program [1].

By developing a waste minimization program a company can save money by reducing waste treatment and disposal costs, raw material purchases, and other operating costs. Also, successful programs will meet state and national waste minimization policy goals, reduce potential environmental liabilities, protect public health and worker health and safety, and protect the environment [2], as well as promote a better corporate image to the public.

An important step in eliminating or reducing undesirable by-products is to first identify them. Some common by-products generated by metal finishers include industrial treatment sludge containing toxic metals such as copper, chromium and nickel;

Table 1: U.S. EPA Priorities for Waste Management [1, 5]

Rank	Procedure/Process
1	Source Reduction
2	Recycling
3	Waste Separation and Concentration
4	Waste Exchange
5	Energy/Material Recovery
6	Waste Treatment
7	Disposal

spent plating and process baths, including various cleaners; miscellaneous solid wastes such as absorbents, filters, and empty containers; and contaminated solvents [3].

U.S. EPA Priorities

The former U.S. Environmental Protection Agency (EPA) Administrator, William Reilly, announced Pollution Prevention as the environmental goal for the 1990's [4]. Table 1 shows the ranking of priorities for waste management established by the U.S. EPA [5, 6], with particular emphasis on source reduction.

Source reduction is the concept of preventing or minimizing the production of material which must be treated as waste by altering the actual production process or "source." Measures include process modifications, feedstock substitutions, improvements in feedstock purity, improvements in housekeeping and management practices, increases in efficiency of machinery, recycling within a process, and production of valuable by-products.

Recycling is the use or reuse of undesirable by-products as an effective substitute for a commercial product or as an ingredient or feedstock in an industrial process. It can occur on- or off-site and includes the reclamation of useful components from a waste material or the removal of contaminants from a waste to allow it to be reused. It is often less expensive to recycle a chemical than it is to purchase new material and pay for disposal costs. Though a material may no longer meet the specifications for a process in which it is being used; the material may still be suitable for other uses at the facility.

Undesirable by-products that may require unusual treatment or disposal should be separated from other process materials. The EPA rule for a hazardous waste mixture states that mixing a regulated hazardous waste with a nonhazardous waste renders the whole mixture legally hazardous. Therefore, recycling a material requires that the waste remain as clean as possible prior to reuse.

Waste treatment is any method, technique, or process that changes the physical, chemical, or biological character of any hazardous waste in a way that neutralizes the waste, or renders such waste nonhazardous, less hazardous, safer to manage, able to be recovered, able to be stored, or reduced in volume. Disposal is the discharging,

depositing, injecting, or placing of hazardous waste into or on any land or water. If a waste has hazardous characteristics, then disposal in a hazardous waste disposal facility is required. If the waste is treated to eliminate these hazardous characteristics, it can be disposed of in an non-hazardous waste landfill, which is considerably less expensive.

The use of the various options depends on extensive federal and state regulations. Table 2 presents a brief list of the prominent laws and regulations that have an impact on the surface finishing industry. Note that the list cannot be construed as comprehensive and any interested party should contact the appropriate federal, state, or local authority regarding the specifics of the regulations.

Risk Assessment

Risk assessments are the characterization of hazardous waste sources and their adverse effects to humans and the environment due to exposure. For a typical plating shop, a risk assessment would only involve the shop environment and personnel and would not deal with the adverse effects on people and the environment outside of the shop. Risk assessments have become important due to the range of options they offer, each having a specific cost and benefit. Properly conducted risk assessments have received fairly broad acceptance, in part because they put into perspective the terms: toxic, hazard, and risk [4]. If risks can be estimated, they can be incorporated into the costs and benefits of a specific waste reduction program and ultimately into production costs. Without a risk assessment, it is difficult to judge the benefits received for the costs. Specifically, it would be difficult to compare the benefits of a waste disposal program to a waste reduction program. Risk assessment provides an orderly, explicit, and consistent way to deal with scientific issues when identifying the existence of a hazard and the magnitude of the hazard. The National Research Council divided the process of risk assessment into the three components [4]

1. **Hazard Identification**–consists of a review of relevant biological and chemical information bearing on whether or not an agent may pose a specific hazard,

2. **Dose-Response Assessment**–involves describing the quantitative relationship between the amount of exposure to a substance and the extent of toxic injury or disease, and

3. **Risk Characterization**–generally involves the integration of the data and the analysis of the first two components to determine the likelihood that humans will experience any of the various forms of toxicity associated with a substance.

Essential Elements and Common Barriers of Successful Minimization Projects

Various studies of waste minimization programs have identified characteristics of successful programs. Three key elements found were [1]

- Management's active involvement and encouragement at all levels,

Table 2: Some Environmental Laws and Regulations Pertinent to the Surface Finishing Industry (reprinted from [3], 1989)

Regulation	Description
40 CFR 122, NPDES	Federal regulations governing the discharge of wastewaters to surface waters of the United States.
40 CFR 413, 433	Federal regulations specifying effluent limitations, pretreatment standards, and new source performance standards for the electroplating and metal finishing industries.
40 CFR 268	Federal regulations that restrict the disposal of spent solvents and solvent-containing wastes.
CCR Title 23 Subchapter 9	State regulations governing the discharge of wastewaters to surface waters. Includes provisions for issuance of permits and setting effluent limitations.
Local municipal codes addressing discharges to POTWs	Discharge requirements set by local POTWs restricting the concentrations of pollutants in wastewaters discharged to sanitary sewers.
CCR Title 22 Sections 66900 and 66905	Restricts the land disposal of certain liquid and solid hazardous wastes and sets time schedules for implementing the restrictions.
CHSC Chapter 6.95	Requires local government agencies to implement hazardous material management programs requiring local businesses to submit applications for the storage and handling of hazardous materials.
CCR Title 22, Division 4 Chapter 30, Article 6	Sets requirements for generators of hazardous wastes, including restrictions on how long wastes can be accumulated without the storage facility being permitted.
CHSC 25202.9	Requires certification, by waste generators permitted as TSD facilities, that a waste minimization program is in operation and that the treatment, storage, and disposal methods minimize the threat to human health and the environment

CFR - Code of Federal Regulations
CCR - California Code of Regulations
CHSC - California Health and Safety Code
NPDES - National Pollution Discharge Elimination System

- Production personnel strongly motivated to implement and maintain necessary changes, and
- Technologies used were "elegant in their simplicity."

At least one of these elements were missing in each minimization project failure [1].

People involved in implementing waste reduction programs have noted several inhibiting factors which must be identified by those attempting to develop a waste reduction strategy. This identification is necessary so that the resistance can be recognized and overcome. A list of several barriers to waste reduction are [3]

- Lack of information about available waste reduction techniques and the benefits that can be achieved.

  This can be overcome by seeking information on other's successes. For example, the 3M Corporation has had a "Pollution Prevention Pays" program since 1975. In 10 years, the 1,500 projects supported under this program saved the company more than $235 million for pollution control facilities that did not have to be constructed, for reduced pollution control operating costs, and for retained sales of products [1]. Other examples can be found in the case studies published by the U.S. EPA [7, 8].

- Concern for upsetting product quality.

  Both operators and management must be convinced that pollution prevention changes will not adversely affect quality. This requires a commitment to and effective application of a new process or technology, including complete training of operators.

- The "if it ain't broke–don't fix it" attitude.

  The U.S. Navy's hard-chrome plating methods are a good example of ultimately breaking through this barrier. For more than 50 years, the Navy has been using the same methods. During this time, however, improved processes have been developed outside of the Navy. By creating a program to reduce the waste from chrome plating operations, the Navy updated the entire chrome plating process and incorporated these improved methods. The result was a zero-discharge plating process that also produced a more uniform plate while using a considerable smaller tank area [1].

- A reluctance to develop innovative ideas because of the fear of failure.

  Management must take the initiative and absorb all effects of failures. Only then will a commitment from operators and middle managers be made.

- The attitude that a new technology will not succeed because it is outside the company's normal range of expertise.

  This attitude problem can be solved by seeking outside views and help. State programs, consultants, and organizations such as the American Electroplaters and Surface Finishers Society can assist in answering a company's questions.

When developing and implementing a waste reduction program it is essential that management be committed to pursuing waste reduction, be willing to experiment with various ideas, and be prepared to experience failure, as well as success [3].

Waste Minimization Assessment Procedure

The waste minimization assessment procedure begins with the recognized need to minimize waste. The procedure [2] may then proceed through a

1. Planning and organization phase,
2. Assessment phase,
3. Feasibility analysis phase, and
4. Implementation phase.

The planning and organization begins with getting management commitment. Overall assessment program goals must then be set and an assessment program task force organized. Next is the assessment phase, which begins with collecting process and facility data. This data is prioritized and assessment targets are selected. It is necessary to select people for assessment teams who will review data and inspect sites. Generated options are then screened and selected for further study.

After the assessment phase is completed, the feasibility analysis phase is initiated. This includes technical and economic evaluation of the options, after which specific options will be selected for implementation. Outside assistance for technical evaluation may be necessary if the company does not have sufficient expertise. After a final report is drawn up, including recommended options, the implementation step begins. This step includes justifying projects and obtaining funding, procurement (equipment), installation (equipment), training, implementation (procedure), and an evaluation of performance.

The entire process is then repeated selecting new assessment targets and reevaluating previous options. When the waste minimization assessment procedure is administered in its entirety, successfully implemented waste minimization projects will result.

Waste Reduction Opportunities

A waste reduction program can be broken down into two broad areas: procedure and process. The procedure includes employee training, changing methods, preventing spills, and inventory control, while the process includes optimizing solutions, substituting products, concentrating waste, and changing equipment.

The most important aspect of the procedure is employee training. Although management commitment and direction are fundamental to a waste minimization program, commitment throughout an organization is crucial to resolve conflicts and overcome barriers to the program. Employees often can increase the generation of waste, so they can be pivotal in contributing to the overall success of a waste minimization program. Bonuses, awards, plaques, and other forms of recognition often times are the best way to provide motivation and to boost employee cooperation [2].

For example [1], a chemical engineer at a major consulting company spent the early part of her career as an environmental coordinator for a major aircraft manufacturer. Solvents kept turning up in the storm drains and the source was traced to several floor drains in the shop area where workers were pouring used solvent. She then posted signs that read "NEXT STOP IS YOUR FAUCET AT HOME." The violations stopped. When the workers asked her what they could do to reduce waste, she responded, "Act as though your mother were looking over your shoulder [1]."

Some control methods that can be implemented include :

- Minimizing the number of different raw materials and supplies used, such as cleaning fluids, oils, etc. This helps clear-up shelf-life problems and reduces the number of partially filled containers requiring disposal.

- Purchasing container sizes appropriate to the actual use. It can be less expensive to buy smaller containers of perishable materials than to buy bulk quantities, at cheaper prices, that require disposal of the expired portion.

- Reducing the inventory of hazardous materials to a minimum. It must be ensured that containers are being rotated on the shelves so that the oldest materials are used first. This will reduce the disposal of materials whose shelf-life has expired.

These steps will reduce spending on raw materials and waste disposal, as well as the investment tied up in inventory. Such areas as preventing spills and inventory control are simple procedures which can cut significant amounts of waste.

After preparing an inventory of chemicals being used and wastes produced from all processes, an evaluation is needed to determine if the number and volume of chemicals being used can be reduced. Optimizing solutions, taking the waste of one process and adapting it to be used in another, substituting products, less-hazardous for hazardous materials, and concentrating waste are possible modifications [1].

When dealing with a change of equipment, simplicity is best. Typically, on successful projects, off-the-shelf equipment is adapted to a new application, while complex or specialized equipment is avoided. The greater number of modifications attempted at the same time, or the more experimental the equipment is, the greater the chance that problems will occur and the process will be abandoned for more reliable and proven methods [1].

In the surface finishing industry, there are numerous simple approaches. For example, several improved rinsing techniques that can reduce the amount of drag-out loss include [1, 3, 9, 10]

1. **Extended drip times**–The faster an item is removed from the process bath, the thicker the film on the workpiece surface and the greater the drag-out volume will be. Extended drip times are an extremely easy and inexpensive modification to make and works best with cold process baths.

2. **Workpiece positioning**–The amount of drag-out loss can be reduced if the work pieces are oriented so that process chemicals cannot be trapped in grooves or cavities when removed from the process tank. This modification is also easy to implement, but needs to be considered when designing the plating racks.

Improving workpiece positioning is still a fairly inexpensive method to use. Suggestions for orientation include

- Tilting objects so as to avoid table-like surfaces and pockets where solution can be trapped,
- Avoiding the positioning of parts above each other. Offsetting parts eliminates drainage of solution from one part to another part below it.

3. **Spray/fog rinsing**–Spray rinses can be used above heated baths to replenish the loss of process solution due to evaporation. Deionized water should be used for the spray systems and they should be at a flow rate equal to the rate of evaporation. This is another drag-out reduction method which is fairly easy to implement.

4. **Countercurrent rinses**–Countercurrent rinsing involves a sequential immersion of parts in a series of tanks. The parts are immersed countercurrent to the rinse flow. Optimum countercurrent rinsing (cost vs. minimum water consumption) usually employs three tanks operating in series. This method can reduce rinse flows by over 95% compared to single overflow rinses. For a dragout rate from the plating bath of 1 gal/hr, a countercurrent rinse flow of 10 gal/hr would be sufficient, compared to 1,000 gal/hr for a single rinse tank [1]. This method is a high priority method and has now become a standard in the plating industry; however, it is more expensive and more difficult to install on existing plating lines.

5. **Use of drain boards or drip tanks**–Drain boards are used to capture process chemicals that drip from the workpiece when it is being transferred between successive tanks. The board is mounted at an angle which allows drainage of the chemical solution back into the first process tank. Drip tanks serve to capture chemical drips in a tank placed between the process and rinse tank. The drip tanks can then be recycled back into the process bath. These methods are useful if there is sufficient spacing between the process and rinse tank, and the chemicals would otherwise drip onto the floor and enter the wastewater system when the floor is washed down. This method can be expensive to install and is not necessary if the steps discussed previously are administered correctly.

6. **Air knives**–Air knives can be used above process tanks to improve drainage. As the rack is raised from the tank, air is blown across the surface of the work pieces. This air stream improves the drainage of the drag-out solution back into the process tank. The drawback to this method is that it might not be beneficial for a particular part to be completely dry. Part drying can cause much more difficultly when attempting to rinse off certain process chemicals.

7. **Reduce surface tension**–Wetting agents can be added to a process bath to reduce surface tension of a solution and, as a result, reduce volume of drag-out loss. The use of wetting agents in the metal finishing industry has been estimated to reduce drag-out loss by as much as 50 percent. A problem is that wetting agents can produce foaming problems in the process bath and also may affect the chemistry of a bath when such things as catalysts are used.

Table 3: Summary of Recovery Technology Applications [3]

	Decorative Chromium	Hard Chromium	Nickel	Electroless Nickel	Cadmium	Zinc (CN)	Zinc (Cl)	Copper (CN)	Tin (BF_4)	Silver
Evaporation	x		x		x	x	x	x	x	x
Reverse Osmosis			x			x		x		
Ion Exchange	x		x	x						x
Electrolysis					x	x	x	x	x	x
Electrodialysi			x		x	x	x	x	x	x

8. **Use of turbulence or agitation**–Turbulence or agitation in a rinse or process tank can cause better removal of solution from parts. Usually an in-tank filtration system is needed when turbulence or agitation is used in order to remove dirt or non-chemical impurities from the bath. This method can be used with a countercurrent rinse system to help optimize plating line performance.

Waste Reduction Technologies

Evaporation, ion exchange (IX), reverse osmosis (RO), electrolysis, and electrodialysis (ED) have been used to recover chemicals and metals from rinsewaters. General and site-specific factors must be evaluated to determine the best recovery process for a specific situation. Factors include the type of metal to be recovered, drag-out rates, rinsewater concentrations and flows, space requirements, staffing requirements, availability of utilities (such as steam and electricity), and cost for water and wastewater treatment and sludge disposal [1]. Table 3 shows typical recovery technologies related to specific types of plating baths.

Evaporation is the oldest method used to recover chemicals from rinse streams. In this process, enough rinsewater is boiled off to concentrate the solution sufficiently to return it to the particular process. Because of their high-energy use, evaporators are most cost-effective in concentrating rinsewaters that are to be returned to hot baths, such as in a chromium plating process [1].

Ion exchange (IX) uses charged sites on solid resin to selectively remove either cations or anions from the solution. The ions removed are then replaced by equivalent charged ions displaced from the resin. In general, ion exchange systems are suitable for recovery applications where the rinsewater has a relatively dilute concentration of plating chemicals. Ion-exchange systems are not cost-effective when drag-out rates are low and concentrations high [1].

Reverse osmosis (RO) is a demineralization process in which water is separated

Table 4: Some Material Recovery Technology Costs (1985) [3]

Technology	Materials Recovered	Equipment Costs
Evaporation Unit: Capacity of approx. 20 gph.	Rinse water and Chromic acid	$47,000
Reverse Osmosis Unit: Capacity of approx. 100 gph.	Nickel plating chemicals	$27,000
Ion Exchange Unit: Capacity of approx. 20 gph.	Rinse water and Chromic acid	$38,000
Electrolytic Unit: Capacity of approx. 15 gph.	Rinse water and Copper	$25,000

from dissolved metal salts by forcing the water through a semipermeable membrane at high pressures (400 to 800 psig). RO use is limited to moderately concentrated rinsewaters. The cost-effectiveness of RO metal recovery systems varies depending on several factors [1].

Electrodialysis (ED) concentrates or separates ionic species in a water solution through use of an electric field and semipermeable ion-selective membranes. ED has been used to recover cationic metals from plating rinsewaters. The maximum concentration of an ED unit is limited only by the solubility of the compounds in solution, which allows ED to produce a more concentrated solution than IX or RO. ED units are easy to use, economical, require little space, and can operated continuously with little maintenance. However, ED cannot selectively remove ions, resulting in the requirement for periodic plating bath treatments to remove impurities. Along with evaporation, ED has the quickest payback period of a metal recovery process [1].

Table 4 lists some typical costs of applying the described technologies to recover specific materials from a single source wastewater. To achieve savings that justify the purchase of recovery technology requires the waste stream to be fairly concentrated and continuous. Information necessary to determine economic feasibility includes waste stream generation rates, chemical concentrations, and the value of materials to be recovered [3].

Closed-Loop Recovery Systems

In a near closed-loop recovery system which uses such processes as electrodialysis, ion-exchange and reverse osmosis, there are four necessary elements for success [1]. These are

- Rinsewater recycle,

- Chemical recovery,
- Volume reduction, and
- Bath purification.

Rinsewater recycle is important since rinsewater is usually maintained at a low concentration of contamination in order to have good rinsing. Rinsewater can be used again as long as the recycled solution is fairly "clean." Chemical recovery involves recovering chemicals, especially if toxic, from the waste. Recovering chemicals can eliminate the major toxic components from the waste stream and simplifies disposal of any blowdown stream. This recovery is beneficial because it is often less expensive to recycle a chemical than to purchase new material and dispose of it. Recycled materials can also be suitable for other plant processes. Reducing the volume of wastewater can reduce disposal costs. If the volume is reduced sufficiently while the concentration is increased proportionately, it can be feasible to recover useful materials from the waste. Bath purification allows better recycling (less impurities), easier segregation of wastes, and higher efficiency from a process.

Each of the metal recovery processes have specific areas in which they perform best. If a system is needed for rinsewater cleanup, all of the closed-loop systems will be sufficient. Chemical recovery requires the use of ion-exchange or electrodialytic processes. If a system is needed for volume reduction, innovative rinsing or evaporation is acceptable. If a system is needed for bath purification, then electrodialytic processes, porous pot, or ion-exchange will be useful.

It is necessary to identify needs and research a system that will best meet those needs. Every system has advantages and disadvantages, therefore careful consideration must be given to what process will work best in a particular situation.

Summary

When developing and implementing a waste reduction program, it is essential that management be committed to pursuing waste reduction, be willing to experiment with various ideas, and be prepared to experience failure, as well as success. Within a successful waste reduction program three essential elements must be present: active involvement and encouragement of management at all levels, application of the least complex technologies, and motivated production personnel to implement and maintain necessary changes. The second element is especially important because the greater the number of modifications attempted at the same time, or the more experimental the equipment is, the greater the chance that problems will occur and the process will be abandoned for more reliable and proven methods.

Developing a waste minimization program has become a necessity in industry. As EPA regulations on waste disposal become stricter, newer, more efficient minimization methods of waste disposal must be developed. For example, open-loop systems such as chemical precipitation will soon be unable to meet EPA standards. Therefore, near closed-loop systems such as electrodialysis will need to be administered, reducing or eliminating the need for a sludge or precipitate to be disposed of in an appropriate landfill. Waste management methods that reduce or eliminate unwanted by-products

will prove to be more cost-efficient and environmentally sound, traits that will be in high demand in the future.

Acknowledgements

Although the work described in this presentation has been funded in part by the U.S. EPA under assistance agreement number R-815709, to the University of Nebraska-Lincoln through the Great Plains/Rocky Mountain Hazardous Substance Research Center, headquartered at Kansas State University, it has not been subjected to the Agency's peer and administrative review and, therefore, may not necessarily reflect the views of the Agency and no official endorsement should be inferred.

The research was partially supported by the U.S. DOE, Office of Environmental Restoration and Waste Management, Office of Technology Development and the University of Nebraska–Lincoln Water Center.

References

[1] T.E. Higgins, *Hazardous Waste Minimization Handbook*, Lewis Publishers, Chelsea, Michigan (1989).

[2] *Waste Minimization Opportunity Assessment Manual*, U.S. EPA, Washington, DC, EPA/625/7-88/003 (July 1988).

[3] PRC Environmental Management, Inc., *Hazardous Waste Reduction in the Metal Finishing Industry*, Noyes Data Corp., Park Ridge, NJ (1989).

[4] J.J. Segna and R.K. Raghavan, "Approaches to Reducing Environmental Risk Through Pollution Prevention," in *The Environmental Challenge of the 1990's*, U.S. EPA, Washington, DC, EPA/600/9-90/039, pp. 613-23 (Sep 1990).

[5] R.W. Rittmeyer, "Waste Minimization–Part 1: Prepare an Effective Pollution-Prevention Program," *Chemical Engineering Progress*, **87**, 5 (May 1991).

[6] R.J. Avendt, "Waste Minimization–Approaches and Techniques," in *The Environmental Challenge of the 1990's*, U.S. EPA, Washington, DC, EPA/600/9-90/039, pp. 32-40 (Sep 1990).

[7] *Seminar Publication: Meeting Hazardous Waste Requirements for Metal Finishers*, U.S. EPA, Washington, DC, EPA/625/4-87/018 (September 1987).

[8] See **NOTE** below.

[9] *Metal Finishing Guidebook and Directory Issue*, **89**, 1A (1991).

[10] *Guides to Pollution Prevention: The Printed Circuit Board Manufacturing Industry*, U.S. EPA, Washington, DC, EPA/625/7-90/007 (June 1990).

NOTE: Additional technology and case study information can be obtained from

U.S. EPA
ORD Publications
P.O. Box 19962
Cincinnati, OH 45219-0962

Request "ORD Publications Announcement" (e.g., EPA/600/M-91/048) and "Technology Transfer" Newsletter (e.g., EPA/600/M-91/042).

APPLICATION OF MICROCOMPUTERS AS A TECHNICAL RESOURCE FOR IDENTIFICATION OF POLLUTION PREVENTION OPPORTUNITIES IN METAL FINISHING/ELECTROPLATING OPERATIONS

by
Lisa F. Wilk, P.E. and Robert S. Capaccio, P.E., CChE, DEE
Mabbett, Capaccio & Associates, Inc.
5 Alfred Circle, Bedford, Massachusetts 01730

Introduction

With the increasing costs and liabilities associated with waste generation, it has become a necessity for industry to look more closely at its process areas to identify ways in which waste generation can be minimized. Often, this type of evaluation can involve time-consuming iterations of complex engineering calculations. The microcomputer can be a useful tool in conducting an analysis of process operations in order to optimize source reduction and resource recovery opportunities and to minimize end-of-pipe waste generation.

The power and capabilities of microcomputers (also referred to as personal computers or PCs) have advanced significantly since their introduction into the market in the early 1980s. Much of what formerly could only be done on a large mainframe computer that occupied an entire room can now be performed on a desktop or laptop computer. In particular, with the development of "user-friendly" applications software the microcomputer has become more accessible.

Spreadsheet software, although originally designed for financial management, can be readily adapted to assist in engineering design of optimal process layout for implementation of source reduction and resource recovery technologies. This paper addresses the use of spreadsheet software in developing computer models for the analysis of metal finishing/electroplating process operations relative to pollution prevention.

Regulatory Background

The Resource Conservation and Recovery Act (RCRA) was enacted in 1980. As a result of this act, hazardous waste management regulations were promulgated. These regulations originally focused on controlling the symptoms of hazardous waste generation (i.e., what to do with the waste that is generated). However, as management of the significant hazardous waste generation in the U.S. became increasingly more difficult, RCRA was reauthorized in 1984 with the primary objective being waste minimization.

Under RCRA, waste minimization refers to the reduction or elimination of waste generation via source reduction, recycling/reuse, and some forms of alternative treatment.

The term source reduction means reducing wastes at the source of generation. In other words, minimizing wastes by eliminating or reducing their generation in the first place. Examples of source reduction include: product substitution, process modification, product reformulation, waste segregation, inventory control, materials conservation, and general housekeeping improvements. Source reduction is the most effective means of waste minimization, and is therefore the most preferred means of waste minimization per EPA waste minimization policy guidance.

After implementing source reduction, recycling/reuse options should then be considered for remaining wastes generated so as to minimize the amount of waste that must be disposed to other environmental media (air, water, land). Recycling/reuse includes: return to the manufacturer for recycling/reuse, reuse as a lesser grade product in another operation, waste exchanges/clearinghouses (which operate on the premise that one company's waste may be a useful material for another company), and treatment with recycling.

Treating wastes by an alternative means to minimize the quantity and toxicity of wastes generated, and/or to allow recycling/reuse of the waste stream can be considered to be waste minimization. However, alternative treatment is the least-preferred method of waste minimization. In fact, a recent draft policy guidance document issued by EPA proposes to eliminate "alternative treatment" from the definition of waste minimization. Per EPA guidance, alternative treatment can only be considered to be waste minimization if it reduces the volume or the hazard of the waste generated. Treatment that just transfers the waste from one environmental medium to another is not considered to be waste minimization. Concentration is not considered to be waste minimization unless concentrating the material facilitates the recovery of valuable materials from the waste. Also, dilution is not an acceptable means of reducing toxicity.

Although the focus of the RCRA Amendments is on hazardous waste reduction, the recently enacted Federal Pollution Prevention Act (PPA) of 1990 incorporates a multi-media approach to waste minimization (i.e., reduction of wastes to air, water, and land). PPA focuses on source reduction as the means to achieve pollution prevention vs. end-of-pipe pollution controls. Some state laws have broadened the scope even further via toxics use reduction, which focuses on minimizing or eliminating the use of hazardous and toxic chemicals rather than just the waste that is generated from the use of these chemicals (i.e., source reduction vs. recycle/reuse).

Approach to Implementation of Pollution Prevention

In order to implement the most effective pollution prevention techniques at your facility, it is important to initially develop an inventory of current process operations to identify constituents of concern, and sources and quantities of these constituents. The process inventory should be conducted by someone familiar with metal finishing/electroplating process operations as well as available pollution prevention technology. Often, a team approach is most effective.

During the process inventory phase at a facility conducting metal finishing/electroplating operations, information is typically gathered regarding rinsing operations, drag-out/drag-in of process chemicals, bath dump quantities and frequencies, spills, and industrial wastewater pretreatment system operation. The wastestreams for the facility are identified and subsequently prioritized for further evaluation.

The data gathered from the initial process inventory phase can be evaluated utilizing engineering principles to identify: areas of potential source reduction/recycle within the process area to help minimize downstream pollutant loads; areas of potential chemical resource recovery; and areas of potential rinsewater conservation; thereby minimizing end-of-pipe treatment requirements and optimizing reclaim opportunities. With the assistance of spreadsheet applications software, models to aid in this evaluation/analysis can be easily developed on the microcomputer.

The use of these computer models allows a greater number of options to be analyzed in a shorter period of time. Also, the costs for physical/chemical testing, as well as prototype testing can be significantly lowered. In addition to being a useful tool for the technical evaluation of pollution prevention alternatives, the computer can also be used to assist in the economic evaluation of alternatives.

Training

Much like slide rules and electronic calculators, the microcomputer and its associated applications software serve as a tool to assist the user in evaluating pollution prevention options. The microcomputer can perform a greater number of calculations in a shorter period of time, thereby allowing the user to evaluate more options and utilize models to mimic many cycles of an operation. However, engineering and process knowledge are needed in order to effectively utilize the computer as a tool for evaluating these options.

As with any tool, however, the user must be properly instructed on its operation. Computer courses and seminars are available from a number of sources. In addition, disk-based tutorials are often provided with the software applications. Other training resources include computer books, articles in computer journals and trade journals, and videotapes.

Applications Software Capabilities

Most microcomputers are standardly provided with BASIC programming language software. In addition, FORTRAN programming software is available at a relatively inexpensive cost. However, the use of programming language software to develop models can require extensive knowledge of computer programming as well as a significant time commitment for development of the program code.

Spreadsheet software, though originally designed for financial management applications, has been used successfully in process engineering applications. The advantage of spreadsheet software is that it does not require extensive knowledge of computer programming to develop models for evaluating process operations (although most spreadsheet programs have programming options for those familiar with programming techniques). In addition, graphic representations of data can quickly be generated from the spreadsheet input. Also, report formats can be more readily customized.

Basic Spreadsheet Configuration

The standard interface for spreadsheet software applications consists of a row and column structure that looks very much like an accountant's ledger. The spreadsheet is actually made up of several blocks or "cells", each referenced by its row and column location.

Process variables (e.g., process bath constituent concentrations, number of dragout tanks, number of rinse tanks) are entered directly into the spreadsheet. Calculated values (e.g., concentration of constituents in the rinse) are entered as formulas into the block(s) where the result(s) will be shown. These formulas reference cell locations for the process variables rather than specific values, thereby allowing the user to input different values for the process variables without having to alter the formulas.

Additional commands allow the user to quickly copy formulas to several other locations at the same time. The formulas will automatically adjust the cell references when copied. Other more advanced features, allow customized programming and rapid statistical evaluations of data. However, knowledge of these advanced features is not necessary to take advantage of the microcomputers ability to assist in analyzing process operations.

Example Application of Microcomputer for Pollution Prevention

During metal finishing/electroplating operations, the primary source of waste generation is the carryover of chemicals from plating baths into rinsewaters. Typically, these rinsewaters subsequently are treated to remove these contaminants (e.g., metals) prior to discharge to a municipal sewer system or surface water. Conventional treatment systems utilize metal hydroxide precipitation to remove the metals from the wastestream. However, this type of treatment generates significant quantities of sludge that must be disposed as hazardous waste. In addition, although chelated and complexed wastestreams can be isolated for separate treatment to achieve better treatment system performance, the typical metal finishing facility operations generate a variety of metals in the waste stream which can make it difficult, if not impossible, to achieve increasingly more stringent effluent limitations with a conventional system.

Factors that need to be considered when evaluating process operations for pollution prevention opportunities include: minimizing the amount of process chemicals being dragged out of process baths into rinses, and utilizing the minimum amount of water necessary to achieve quality rinsing. By minimizing chemical dragout and water usage, the amount of wastewater requiring pretreatment will be reduced. In addition, opportunities for resource/recovery will be increased. An added benefit of minimizing end-of-pipe treatment requirements and maximizing resource/recovery opportunities is the decreased quantity of sludge generated.

During the analysis of optimal process line layout in terms of most efficient rinsing and dragout minimization, basic chemical engineering principles are utilized to calculate constituent concentrations. By arranging these calculations in a spreadsheet format, several options can be evaluated in a relatively short period of time. The data developed from these analyses can be utilized to evaluate the potential for implementation of advanced pollution prevention technologies such as reverse osmosis, ultrafiltration, evaporation, and ion exchange.

Standard formulas are available in the literature for calculating anticipated dragout quantities and rinsewater concentrations (Kushner, 1981; Carparelli, 1983). Typical parameters that are entered into these formulas or derived from these formulas, include: concentrations in plating baths, dragouts, rinses; temperatures of plating baths and rinses; volumes of plating baths and rinses; number of rinse tanks; rinse tank configurations; rinse flow rates; dwell times; types/shapes of pieces processed; and type of process line (i.e., barrel vs. rack).

For example, this type of spreadsheet format was utilized to analyze options for laying out process lines at a new metal finishing facility in New Jersey. The particular computer model allowed the user to vary the following parameters: number of dragout tanks, number of running rinses, rinse flow rates, chemical constituent concentrations in process bath, dragout factors based on type/shape of piece being processed. Based on these parameters and the engineering formulas incorporated into the spreadsheet, the model would then provide anticipated effluent quality as well as anticipated concentrations in the dragout tanks. This information was then

used to evaluate optimum process layout in terms of source reduction as well as resource recovery. Although this was a new facility, with a minimum amount of available physical and chemical data, reliable predictions were made utilizing the computer model. Significant reductions in end-of-pipe treatment requirements were achieved due to the implementation of pollution prevention techniques.

Similar computer models were utilized to analyze process operations at existing facilities in Massachusetts, Rhode Island, and Maryland. By utilizing computer modelling techniques, savings in analytical costs were achieved due to fewer physical and chemical analysis requirements. In addition, a large amount of data could be evaluated in a relatively short period of time.

Summary

In summary, the microcomputer can be an extremely useful tool in the evaluation of pollution prevention opportunities at your facility. However, it is important to realize that although the microcomputer is a valuable technical resource that can significantly reduce the amount of time required for the evaluation of a number of alternatives, it is still only a tool. Engineering and process knowledge are required in order to effectively make use of the computer as a tool for identifying pollution prevention opportunities.

BIBLIOGRAPHY

Capaccio, Robert S., "Source Reduction and Resource Recovery for the Printed Circuit Board Manufacturer", NEPCON WEST Proceedings, Anaheim, California, February 1986.

Capaccio, Robert S., "Wastewater Treatment for the Electronics Industry", AES Proceedings, San Francisco, CA, February 1983

Capaccio, Robert S., and Stephen Greene, "Waste Minimization Program Strategies", Proceedings of the Fourth Annual Hazardous Waste Source Reduction Conference, October 1987

Carparelli, Frank, et al. "A Rinsewater Analysis and Water Conservation Concepts", Circuit Expo Proceedings, 1983.

Clark, Raymond H., Handbook of Printed Circuit Manufacturing, Van Nostrand Reinhold Company, 1985

Cook, Thomas H., et al. "Experimental and Computer-Simulated Rinses", Metal Finishing, November 1987.

Godfard, S.M., et al., "Spreadsheets for Chemical Engineers", Chemical Engineering, April 1985.

Julian, F.M., "Process Modeling on Spreadsheets", Chemical Engineering Progress, October 1987.

Kushner, Joseph B., and Arthur S. Kushner, Water and Waste Control for the Plating Shop, second edition, Gardner Publications, 1981

Sowa, C.J., "Engineering Calculations on a Spreadsheet", Chemical Engineering, March 1987.

United States Environmental Protection Agency (US EPA), Draft Guidance to Hazardous Waste Generators on the Elements of a Waste Minimization Program, FR 89-13845, June 1989

US EPA, Hazardous Waste Engineering Research Laboratory, Cincinnati, Ohio, Waste Minimization Opportunity Assessment Manual, EPA/625/7-88/003, July 1988

US EPA, Risk Reduction Engineering Laboratory, Cincinnati, Ohio, Guides to Pollution Prevention: The Printed Circuit Board Manufacturing Industry, EPA/625/7-90/007, June 1990.

Wilk, Lisa F., et al., Treatment Technologies for Corrosive-Containing Wastes, Noyes Data Corporation, 1988.

WHAT ARE OUR CLEANING OPTIONS?

L. M. Thompson, R. F. Simandl, H. L. Richards, A. L. Glover
Martin Marietta Energy Systems, Inc.
Oak Ridge Y-12 Plant*
P. O. Box 2009
Oak Ridge, TN 37831-8095

ABSTRACT

Cleaning has always been an important step in manufacturing operations. Cleaning proceeds functions such as machining, inspection, plating, bonding, welding, heat treatment, and painting. If a surface is not properly cleaned or prepared, the results can be disastrous. The majority of industry has used cleaning methods such as vapor degreasing or solvent cleaning with chlorinated solvents such as chlorofluorocarbons, methyl chloroform, or perchloroethylene. These solvents were non-flammable, were considered to have low toxicity, and worked fairly well. However, recent finding regarding these solvents have caused them to fall from favor. Chlorofluorocarbons and methyl chloroform have been implicated as ozone depleting substances and are being regulated as such. Current plans call for a ban on production of these substances in the year 2000 and 2005, respectively. Perchloroethylene has been classified as a suspect carcinogen and has also come under recent guidelines and regulations in the United States. Personnel at the Oak Ridge Y-12 Plant have been actively pursuing substitutes for these solvents. Ultrasonic cleaning with aqueous detergent was originally implemented as a substitute for vapor degreasing at Y-12 approximately 7 years ago. This type of cleaning has been proven to be very reliable and effective. Organic solvents to replace chlorinated solvents have also been investigated for "squirt bottle" or wiping applications. The Y-12 Plant has implemented Solvent 140 (a straight chain hydrocarbon solvent) and a solvent blend (Solvent 140 and dipropylene glycol methyl ether) in these type applications. Results both experimentally and in the field have been favorable using these solvents. As with any cleaning method, there are some drawbacks with these substitutes. The ultrasonic cleaning with aqueous detergent does require a rinse cycle, a drying cycle, and a capital investment. The Solvent 140 and solvent blend are slow evaporators when compared with the chlorinated solvents. However, these substitutes do work. The pros and cons of these substitutes and other possible cleaning methods will be discussed in this paper.

*Managed by Martin Marietta Energy Systems, Inc. for the U.S. Department of Energy under contract DE-AC05-84OR21400.

WHAT ARE OUR CLEANING OPTIONS?

L. M. Thompson, R. F. Simandl, H. L. Richards, A. L. Glover
Martin Marietta Energy Systems, Inc.
Oak Ridge Y-12 Plant
P. O. Box 2009
Oak Ridge, TN 37831-8095

Introduction

Cleaning has always been an important step in manufacturing operations. Without a properly prepared or cleaned surface, paint or plating will not adhere, bond strengths decrease, welds become porous, and parts will stain upon heat treatment. Over the years, industry had begun to depend on chlorinated solvents for their cleaning purposes whether the cleaning operation consisted of vapor degreasing, immersion, or wiping. Typical solvents used in these applications include trichlorotrifluoroethane, methyl chloroform, or perchloroethylene. These solvents were non-flammable, were considered to have low toxicity, and worked fairly well. However, recent developments have caused these solvents to fall from favor. Trichlorotrifluoroethane and methyl chloroform have been implicated as ozone depleting solvents and are scheduled to be banned from production by the year 2000 and 2005, respectively. Currently, there is a movement to have these dates changed to as early as 1995. Perchloroethylene has been classed as a suspect carcinogen, and several regulations are pending on the use of this chemical. All of these solvents are also classed as Resource Conservation and Recovery Act (RCRA) solvents which means that the waste must be handled under strict guidelines. Due to these environmental and health and safety issues regarding these solvents, personnel at the Y-12 Plant have been looking for substitutes and have been successful in implementing substitutes for approximately 95% of their usage.

Initial solvent substitutes are evaluated for cleaning ability, compatibility, toxicity, and usage issues. Cleanliness is normally evaluated using X-ray photoelectron spectroscopy (XPS/ESCA). This technique bombards a surface with X rays and then records the electrons in their binding states which come off of the surface. This technique enables one to look at microlayers on a surface and to identify elements or elements in specific binding states which are present on a surface. Normally ratios of carbon, which is the element most often associated with contamination, to a base metal are calculated and comparisons are made of these ratios (the lower the ratio the cleaner the surface). Compatibility issues are normally addressed using submersion techniques for the materials of interest. Toxicity issues are addressed via our Industrial Hygiene Department and several other sources of toxicity data. Other issues such as equipment requirements and controls are also addressed.

Ultrasonic Cleaning

Substitution efforts at Y-12 have been divided into two main efforts. The first effort was the replacement of large vapor degreasers utilizing chlorinated solvents with ultrasonic cleaners using aqueous detergent and water. Ultrasonic cleaning works by cavitating a liquid and forming small micro bubbles which burst on the surface to be cleaned. This provides mechanical as well as chemical cleaning action. Three variables can influence the effectiveness of ultrasonic cleaning: 1) the frequency of the ultrasonic cleaner, 2) the liquid medium, and 3) the coupling between the cleaner and the liquid.

In most of our operations we prefer using cleaners which operate at frequencies of approximately 20 kilohertz. A frequency of at least 18 kilohertz is required to cavitate the liquid. Many systems operate at 40 kilohertz which is the frequency of choice for cleaning of electronics but does not work well on cleaning of large metal parts. The lower frequencies are required to do a good job on tough oils on large metal parts. Another problem that can occur is that units which may operate at the proper frequency will not couple with the liquid properly. Thus, the micro bubbles are not formed adequately in the liquid. A quick test which will determine if the frequency and the coupling of the cleaner to the liquid is adequate for operations is the aluminum foil erosion test. A piece of aluminum foil approximately 0.001 in. thick is lowered into a tank filled with liquid. After approximately 30 s, holes are actually formed in the aluminum foil from the power of the ultrasonics if the unit is adequate. This test is also good to see where "dead spots" may be in your tank. Dead spots will occur from the sound waves cancelling each other out.

The other critical variable for ultrasonic cleaning is the liquid medium. A comparison of the viscoelastic properties of different mediums[1] show that water has the best properties for use in ultrasonic applications. Thus, aqueous detergents are an excellent choice for your liquid medium. Aqueous detergents can also be handled quite easily with regard to waste treatment options. Aqueous detergents are composed of surfactants and alkaline salts for the most part. Some may also include slight amounts of solvents to aid in their ability to dissolve oils. Surfactants are surface active agents which provide wetting, emulsification, solubilization, and dispersion characteristics. These surfactants can be anionic or nonionic in nature. Common surfactants used are sulfonates, phosphate esters, or ethoxylates. Alkaline salts such as sodium hydroxide, sodium carbonate, sodium metasilicate, sodium EDTA, and tetrasodium pyrophosphates are also used in many detergent formulations. These help to neutralize acidic soils, precipitate hard water ions (soften the water), lower surface tension, emulsify the oils, break apart the solid soils, disperse the solids, neutralize the fatty acids, or break apart fats. There are literally hundreds of detergent formulations using different surfactants or alkaline salts or combinations thereof on the market which can be used in ultrasonic cleaners. One does need to be cautious regarding the selection of the detergent depending upon local sewage discharge controls and also compatibility with materials. Aluminum or soft metals will react with some alkaline materials quite viciously.

Ultrasonic cleaning has been shown to perform as well as, if not better than, cleaning with vapor degreasers, as shown in Figs. 1 through 3. Figure 1 shows the results of a study where samples of Type 304L stainless steel were coated with a rust preventative oil and then cleaned by vapor degreasing or by ultrasonic cleaning. Initially, the samples were cleaned ultrasonically in detergent and water to provide a sample baseline. One of these samples was retained as a control sample. The remaining samples were coated with a rust preventative oil and allowed to sit overnight.

Fig. 1. EFFECTIVENESS OF VAPOR DEGREASING VERSUS ULTRASONIC CLEANING FOR REMOVAL OF RUST VETO.

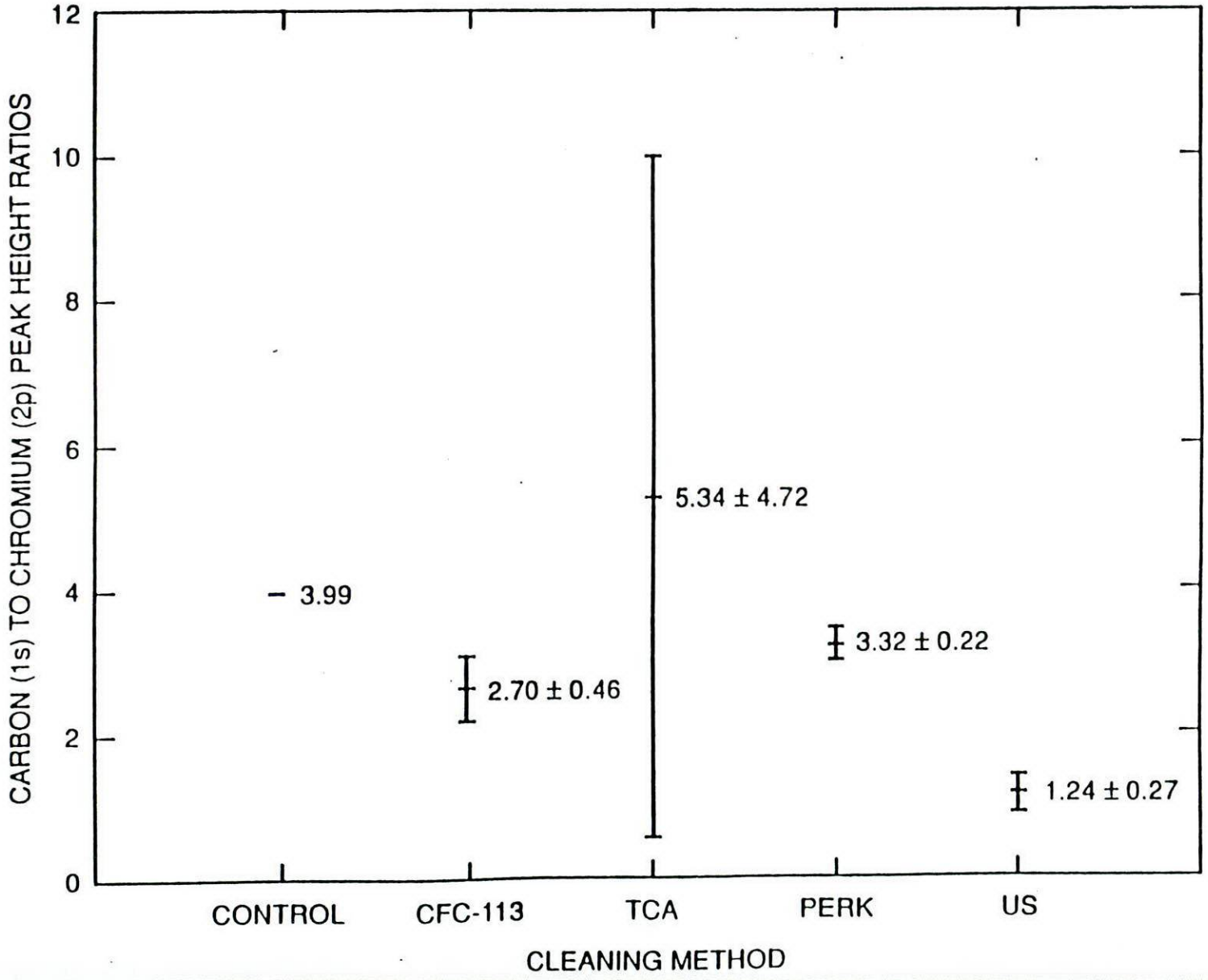

Three samples each were vapor degreased in 1,1,2-trichlorotrifluoroethane (CFC-113), methyl chloroform (TCA), or perchloroethylene (perk) for 15 min. Three samples were also cleaned ultrasonically (US) in aqueous detergent and water for 15 min at 54°C, rinsed in demineralized water, and blown dry with argon. The ultrasonically cleaned samples were much cleaner than the samples vapor degreased in a chlorinated solvent. The samples degreased in methyl chloroform yielded the dirtiest surfaces.

Figure 2 shows the results of a similar study conducted on 4330 V steel which was coated with lapping oil. Again, the ultrasonic cleaning yielded cleaner surfaces with CFC-113 giving the worst cleaning results.

Figure 3 shows the results of another study which was conducted using the same methods as above. This study was conducted on 15-5 pH stainless steel which was coated with a machining coolant known as Trim Sol. Again, ultrasonic cleaning yielded the cleanest surfaces and vapor degreasing with CFC-113 yielded the dirtiest surfaces.

Ultrasonic cleaning has been shown to yield cleaner surfaces than vapor degreasing and the results are more reproducible. This type of cleaning has been used on irons, stainless steels, aluminum, and several other types of metals without any compatibility problems. The waste can generally be discharged to local sewer systems or will biodegrade quite easily.

There are some drawbacks with ultrasonic cleaning. The equipment requires an initial capital investment, a rinse step must be included in the process, and a drying step is also necessary.

Solvent Substitution

The second phase of the substitution program has been the replacement of squirt bottle or specialty type operations with other organic solvents. The main application was the cleaning of parts after machining or prior to inspection by wiping. The contaminants being cleaned from the surface were the usual machine shop contaminants such as machining coolant, rust preventative oil, lapping oil, lubricants, and fingerprints. Initially, possible solvent substitutes were chosen using Hansen Solubility Parameter Theory.[2] Using this theory, solvents which have similar parameters have similar solvent properties. A wide range of solvent types have been tested for the different contaminants which are present. The experimental procedure used was to initially clean samples of 304L stainless steel ultrasonically in aqueous detergent and water in order to establish a baseline level of cleanliness. A sample was retained as a control sample. The remaining specimens were coated with the contaminant and allowed to dry overnight. One contaminated sample was also retained to determine what elements are present due to contamination. Each sample was then squirted with a given amount of solvent being tested and wiped dry. The samples were submitted to XPS/ESCA for analysis. The main element present due to the contamination was carbon. Therefore, a peak height ratio of carbon to chromium (which represents the base metal) was calculated and comparisons were made of this ratio. The lower this ratio the cleaner the surface.

Figure 4 shows the results of the study comparing solvents for the cleaning of rust preventative oil. Solvents such as dipropylene glycol methyl ether (DPM), ethyl lactate, anisole, propylene glycol methyl ether acetate (pm acetate), ethanol denatured with acetone (EtOH/acetone), and isopropanol did not remove the rust preventative oil sufficiently enough to enable the ESCA to

Fig. 2. EFFECTIVENESS OF VAPOR DEGREASING VERSUS ULTRASONIC CLEANING FOR REMOVAL OF LAPPING OIL.

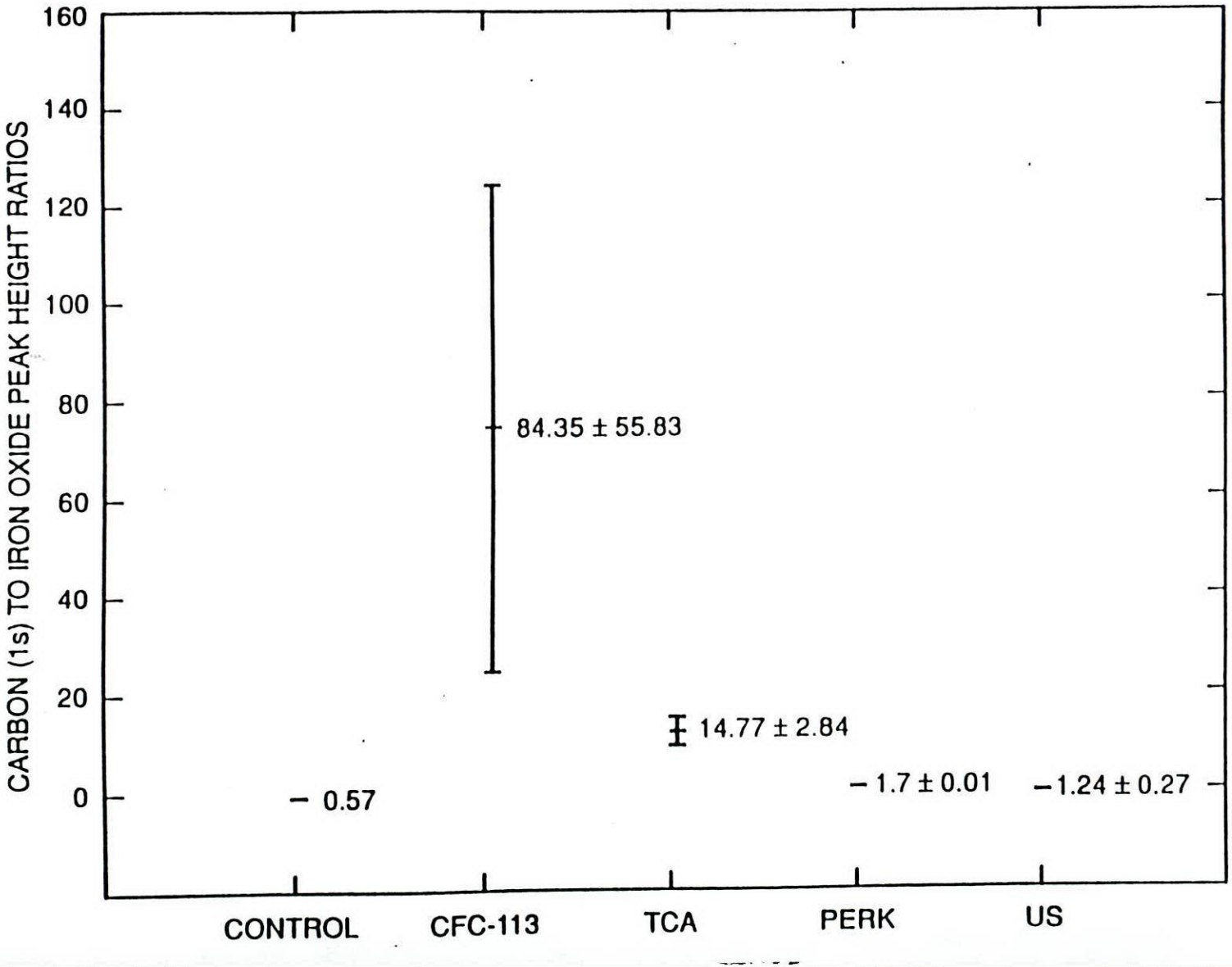

Fig. 3. EFFECTIVENESS OF VAPOR DEGREASING VERSUS ULTRASONIC CLEANING FOR REMOVAL OF TRIM SOL.

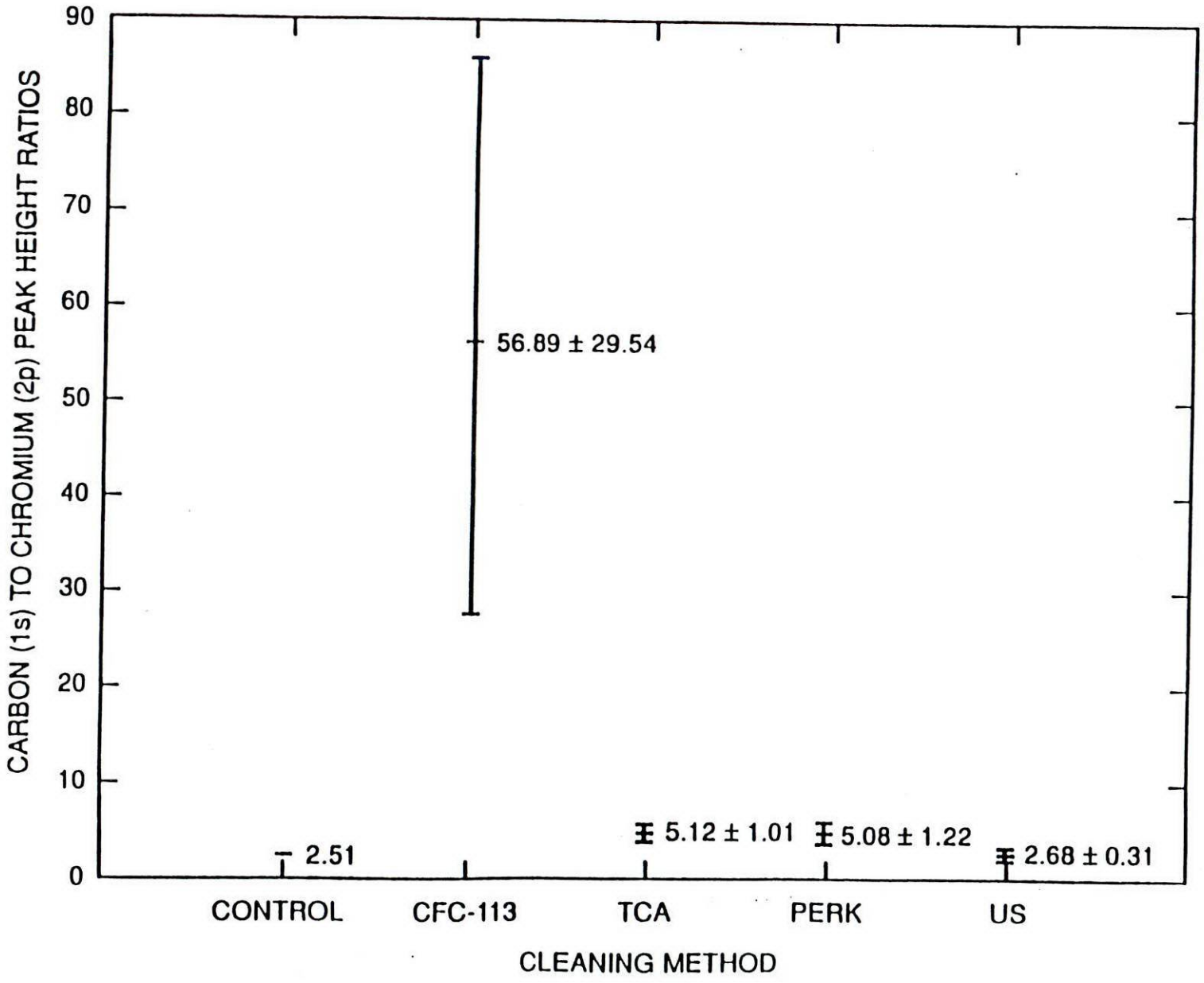

Fig. 4. ABILITY OF SOLVENTS TO REMOVE RUST VETO FROM 304L SS.

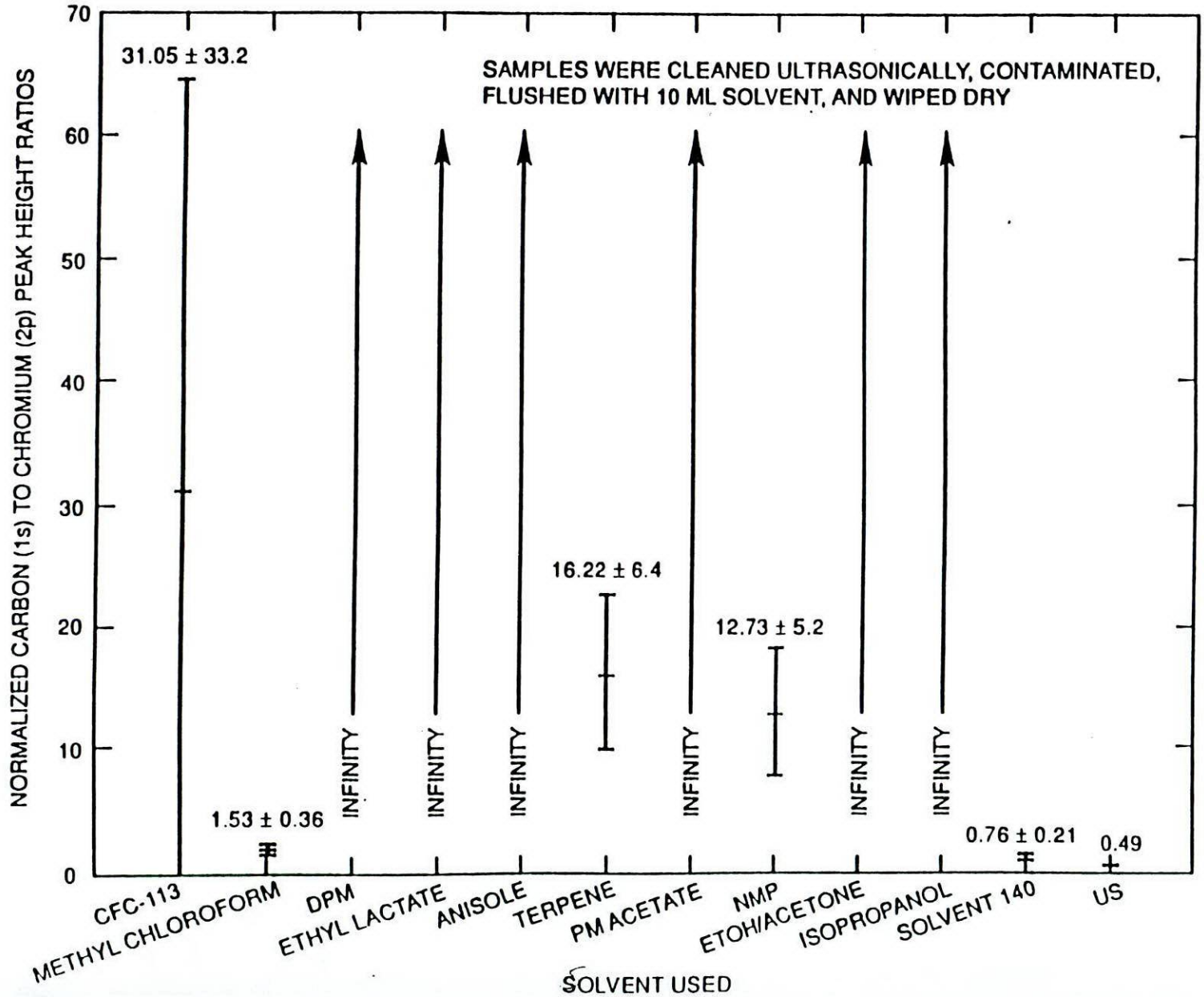

see the metal surface. A terpene-based cleaner and N-methyl pyrrolidone (NMP) worked as well as CFC-113. Solvent 140, which is a high flash mineral spirits, worked as well as the methyl chloroform and better than CFC-113. Ultrasonic cleaning with aqueous detergent yielded the cleanest surfaces.

Figure 5 shows the results of a study comparing the ability of solvents to remove lapping oil. DPM, ethyl lactate, and a terpene-based solvent yielded the dirtiest surfaces followed by anisole, pm acetate, NMP, and Solvent 140. A solvent blend, which consists of 95% Solvent 140 with 5% DPM, yielded the best results of the possible solvent substitutes compared to methyl chloroform and CFC-113. Ultrasonic cleaning with aqueous detergent again yielded the cleanest surfaces overall.

Figure 6 shows the results of a study comparing the ability of solvents to remove a water-based machining coolant known as Trim Sol. Solvents such as anisole, pm acetate, isopropanol, Water Chaser 140, and Solvent 140 yielded surfaces comparable to those cleaned with CFC-113. Surfaces cleaned with DPM, ethyl lactate, and a terpene-based cleaner were somewhat dirtier; and the ethanol/acetone blend yielded the dirtiest surface overall. The cleanest surface was found by cleaning with ultrasonic cleaning with aqueous detergent.

Figure 7 shows the results of a study comparing the ability of solvents to remove fingerprints. The ethanol/acetone solvent mixture and the ultrasonic cleaning yielded the best results overall. Methyl chloroform, isopropanol, and Solvent 140 gave the next best results followed by Water Chaser 140. CFC-113 yielded the worst results and did not appear to remove the fingerprint oils. All of the organic solvents left behind inorganic contamination from the fingerprints such as sodium, nitrogen, sulfur, potassium, chlorine, and calcium.

Due to these results, the Y-12 Plant has changed to a strategy using Solvent 140 and a water displacing solvent blend. Since Solvent 140 is totally immiscible with water, a blend of Solvent 140 with DPM was developed. Adding the DPM enables the solvent to be slightly miscible with water which aids the solvent in its ability to "chase" water-based machining coolants. This also adds the power of a polar solvent to that of a nonpolar solvent. These solvents have low toxicity, are non-RCRA, are easily handled under fire code considerations, and are compatible with materials used at Y-12. Solvent 140 will be used in moisture-sensitive areas of the plant while the water displacing solvent blend will be used in the remainder of the plant. The drawbacks of these solvents are that they are flammable and are slow evaporators which require a change in production operations.

Other Options

There are other equipment options that are becoming available to the market due to chlorinated solvent issues. Vapor degreasers have been developed to use solvents such as acetone, cyclohexanone, and isopropanol and meet the proper fire regulations. Some manufacturers of ultrasonic equipment have also developed explosion proof ultrasonic cleaners which can use flammable solvents. However, use of this type equipment still produces wastes which are considered hazardous under the RCRA regulations.

Fig. 5. ABILITY OF SOLVENTS TO REMOVE LAPPING OIL FROM 304L SS.

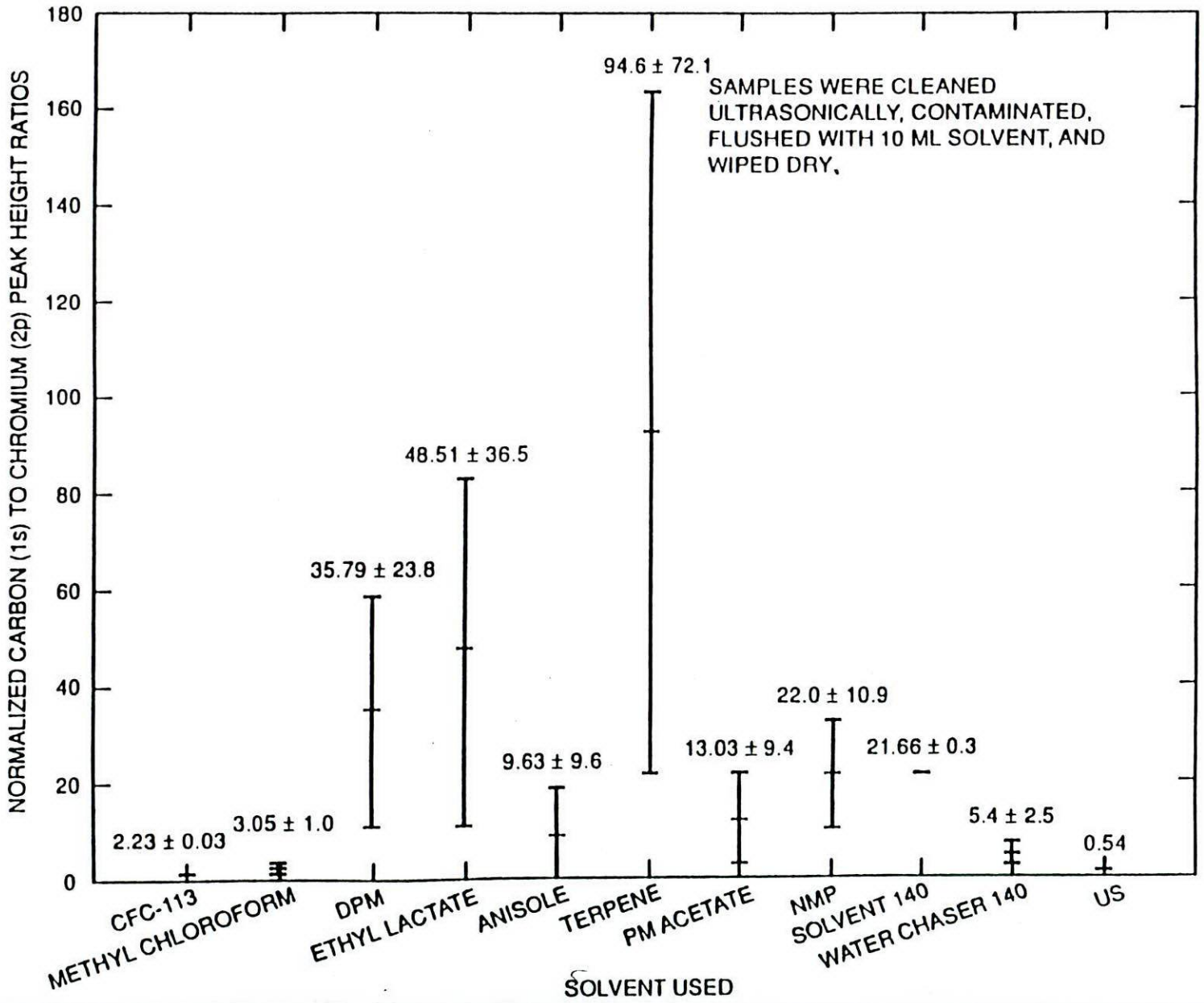

Fig. 6. ABILITY OF SOLVENTS TO REMOVE TRIM SOL FROM 304L SS.

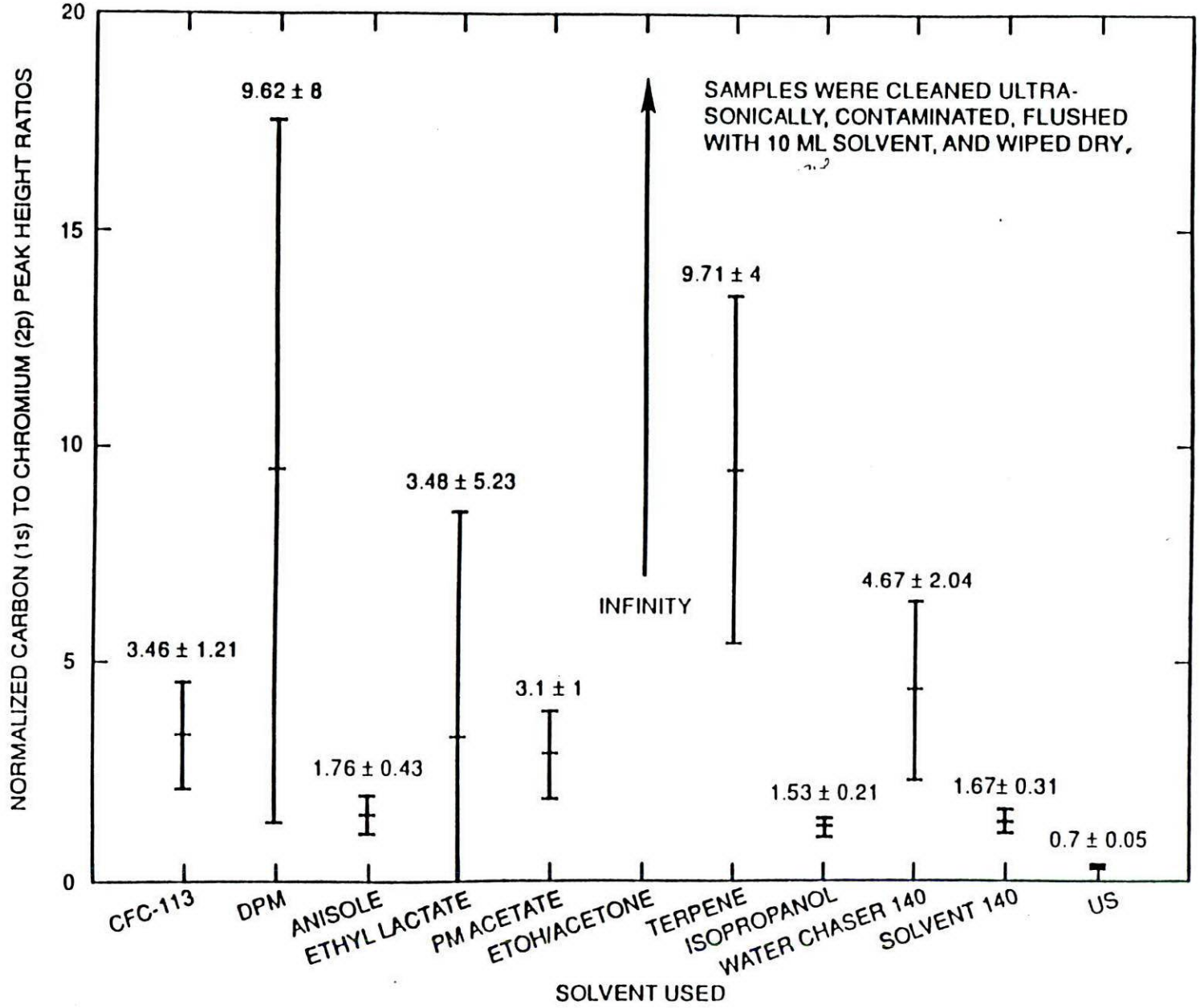

Y-GA 91-4073 ssh

Fig. 7. ABILITY OF SOLVENTS TO REMOVE FINGERPRINTS FROM TYPE 304L SS.

Conclusions

Due to the health and environmental effects, use of chlorinated solvents is rapidly falling from favor. The Y-12 Plant has successfully demonstrated the use of ultrasonic cleaners with aqueous detergent as a replacement for vapor degreasers using chlorinated solvents for approximately 7 years. This type cleaning is reliable and efficient. The drawbacks associated with ultrasonic cleaning include capital equipment investment, required rinse step, and required drying step. Organic solvents such as Solvent 140 and the water displacing solvent blend have also been shown to adequately replace the chlorinated solvents in wiping operations. The drawbacks of these solvents include their slow evaporation rate and flammability concerns. Although there is no perfect solution for substitutes of chlorinated solvents, there are workable solutions.

References

1. Niemczewski, B., "A Comparison of Ultrasonic Cavitation Intensity in Liquids," Ultrasonics, pp. 107-110, May 1980.

2. Hansen, C.M., "The Universality of the Solubility Parameter," IE&C Product Research and Development, ACS Publication, Vol. 8, 1969.

IMPINGEMENT: THE KEY TO EFFECTIVE AQUEOUS CLEANING

INTRODUCTION

Over the years, users of chlorinated solvents have relied on the chemical and vapor-phase properties of these compounds to clean their parts. In most chlorinated solvent degreasing applications, approximately 90% of the cleaning is effected by the chemical action and only 10% by mechanical actions such as work rotation or bath agitation.

With the shift toward aqueous cleaning processes, it is largely the mechanical properties of the cleaning system which are relied on for effective parts cleaning and drying. The primary mechanical methodology used is impingement. Impingement can be defined as the surface impact caused by directing a solution, under pressure, at the part to be cleaned.

In most aqueous cleaning applications, about 90% of the cleaning is effected by mechanical action and 10% by chemical. As a by product of aqueous cleaning's much lesser reliance on chemistry, chemical concentrations are dramatically different from chlorinated solvent degreasers which commonly use 100% concentrations. Aqueous cleaning solutions typically involve concentrations of only 1% - 4% by volume.

This paper discusses the use of surface impingement in aqueous cleaning and stresses its importance in accelerating cleaning and achieving optimum part cleanliness using water based processes.

IMPINGEMENT

The principal mechanical cleaning technique in aqueous cleaning equipment is impingement. Impingement mechanically loosens and removes the soils and contaminants from the product being cleaned. Directing a solution under pressure at the target part creates the impingement or surface impact necessary to obtain the desired cleanliness results.

With the effective use of surface impingement, coupled with several recent advances in aqueous cleaning technology, most cleaning applications can now be successfully accomplished with water based cleaning processes that were traditionally addressed only through the use of chlorinated solvents or chlorofluorocarbons in an immersion, spray or vapor type degreasing system.

Several of these aqueous cleaning innovations are further addressed later in this paper.

Surface impingement, in an aqueous system, can be applied to the product being cleaned through many different methods. They include conventional open air spray, submerged pressure spray, bath turbulation or agitation, rapid solution turn over, product agitation or a combination of these methods. All are designed to create the surface impingement which, in most cases, is necessary for aqueous chemistry to effectively clean the product.

The actual degree of surface impingement can most appropriately be measured in impact per square area, such as pounds of impact. Appendix "A" highlights the theoretical impact against the part showing the relationship of pressure versus volume. In general, impact or surface impingement in a typical open-air spray varies directly with the volume of fluid and the square root of the spray pressure.

In any given impingement based aqueous cleaning system there are several constants that need to be considered to assure optimal results. These include:

SPRAY PATTERN/DISTANCE - For each application there is an optimum spray pattern and operating distance, whether it be an open air or submerged spray system. Nozzle pressure, distance and pattern are largely determined by the configuration of the part being cleaned and the type of soil being removed. A basic design rule in open air spray systems is that "the spray won't clean what it can't see." The spray pattern must be designed for full coverage of the part being cleaned. Parts with hidden cavities or internal pockets do not lend themselves well to open air spray cleaning alone. Nozzle distance is also very important because as the distance between the spray aperture and the part being cleaned increases, the impact tends to decrease depending upon the angle of the aperture.

IMPACT DURATION - The duration of impact or process time per stage is also a very important consideration when designing an aqueous cleaning system. The desired length of impact is largely determined by the type and amount of soil being removed. In most impingement based aqueous cleaning applications the actual cleaning time should take no more than 30 - 90 seconds to obtain optimum results.

PARTS HANDLING - Another important factor that must be carefully considered in today's aqueous cleaning systems is parts handling. Any machine in a manufacturing environment should take into account the primary needs of the production process: Production methods (such as batch, continuous or cellular), production volumes, and the method of part transport through the production process all must be taken into consideration when designing an aqueous cleaning system.

Parts positioning is also an important aspect in the design of an impingement based aqueous cleaning system. The handling system must be designed to accommodate the often complex configurations of the parts being processed. If the parts have intricate internal passages, pockets or crevices that would tend to cup or trap solution, or if there are areas difficult to reach with a cleaning solution spray, part handling becomes very critical. The handling system must assure that all surfaces of the parts are positioned to allow maximum spray impingement. Parts that are not free draining must also be rotated or tilted to prevent cross contamination of the process solutions and to facilitate drying. The part transfer design must also prevent damage to delicate machined parts, and most importantly the handling system must be designed to interface with existing methods of parts loading and unloading.

NOVEL TECHNOLOGIES

A number of novel technologies have been recently developed which, when combined with impingement, greatly enhance the effectiveness of today's aqueous cleaning processes. These include:

CONTINUOUS OIL SEPARATION - Recent advances in oil removal methods for aqueous cleaning solutions have made it possible to deal with high volumes of non-soluble oil entering the cleaning bath. An effective oil separation system can be built as an integral part of the wash solution holding tank. A good oil separation system should be designed to prevent the oil being washed off the parts from circulating through the process pump. This keeps the pump from continuously blending or emulsifying this oil, which would make separation more difficult. Through the use of internal skimming weirs, a constant overflow of the main holding tank can be achieved. This oil laden overflow is then directed to a quiet decanting chamber where a more complete separation can occur. The collected oil then decants naturally from the cleaning solution and is ultimately discharged from the system through gravity separation. Clean solution is returned to the main holding tank which creates the internal skim.

Also note that the aqueous cleaning chemical selected should be a non-emulsifier to facilitate rapid oil separation.

MULTI-STAGE CLEANING - In order to achieve results comparable to chlorinated solvent degreasing with an aqueous system, multiple stages are often required. It is first necessary to determine the final finish requirements of the parts to be processed. Cleanliness is obviously critical but there are other issues to be considered such as detergent residue, corrosion protection, spotting, staining, dryness, and part exit temperatures. These are the questions that must be answered before the optimum aqueous process can be determined.

For heavy oil load applications an example of an effective impingement based aqueous process would be as follows:

Stage #1:	Tap Water Pre-Wash - 160-170° F.
Stage #2:	Mild Detergent Wash - 130-140° F.
Stage #3:	Water Rinse w/Inhibitor - 120° F.
Stage #4:	Forced Air Dry-off - 180°-200° F.

In this example the majority of the oil is removed in the first stage through the use of effective impingement and plain hot water. This arrangement minimizes the amount of oil entering the detergent wash stage, thus greatly extending bath life and reducing chemical usage. Another benefit of this process is that the large amount of oil removed in the tap water pre-wash is more readily separated for removal.

Multiple rinse stages (sometimes with counterflow deionized water) are also often utilized to obtain the desired process results in applications that require stain or spot free parts.

INTER STAGE BLOW-OFFS - Another important consideration in the design of any multiple stage aqueous cleaning system is cross contamination of the process solutions. The machine must be designed to minimize the amount of stage-to-stage carry-over. Simply put, the primary objective is to "keep the process solutions in their own tanks." Carry-over is caused by a number of factors: Residual solution on the parts, ricocheting sprays, residual solution on the transfer conveyor or part baskets, and solution run-out on horizontal track angles or conveyor supports.

There are many methods utilized in the design and construction of the cleaning system to address these issues. However, the best way to minimize carry-over is with the use of inter stage blow-offs. These air blow-offs should be located in the internal vestibules and can be supplied through the use of auxiliary blowers or plant compressed air. A good air nozzle design will significantly reduce solution carry-over on the product and the transfer mechanism.

FORCED AIR DRY-OFFS - There have been significant advances in the methods employed to dry parts after the aqueous cleaning process. One method of particular note is "heated forced air drying."

The use of high velocity forced air impinging against the part surface can reduce drying times to one tenth of the time required with traditional convection type hot air drying processes. High velocity drying also minimizes water spotting and staining, because the majority of the solution is mechanically removed from the product rather than strictly relying on evaporation.

EQUIPMENT DESIGNS - There have been many aqueous equipment innovations recently developed, spurred by industry's need to quickly find alternative methods to clean their parts. One novel example of this is the "Immerso-Jet™" cleaning system. This system is a unique multi-process cleaning and drying system which takes full advantage of all aspects of the surface impingement principle and is specifically designed for use with biodegradable detergents. This machine was developed to provide industry with an effective and affordable alternative to conventional cleaning systems which utilize hazardous cleaning agents. It offers excellent cleaning and drying performance even for parts with complex internal passages or cavities. It is also ideal for delicate, machined parts which cannot tolerate surface marring or water spotting. Its unique elevated sump design and solution diverting system allows multi-stage processing and drying in a single cabinet while effectively preventing cross contamination of the process solutions.

The system combines rotational spray cleaning, immersion cleaning, high energy turbulated cleaning and an efficient forced air part dry-off, all in one compact easy to operate machine. In a single elevated sump, the parts are gently rotated under an open-air spray, the first form of impingement. Once the sump fills, the parts are immersion-cleaned in a turbulated bath for a second form of impingement. The sump drains and the parts are once again open-air sprayed. Subsequent rinse stages and rust inhibition capability can also be incorporated. Upon completion of these wet processes the parts are then dried with forced air impingement, all in the same cabinet.

This unique three way cleaning action has been proven to meet or exceed the cleanliness results of conventional ultra-sonic vapor degreasing methods. With the use of deionized water and an integral high velocity forced air dry-off, the system is also capable of providing a cosmetically appealing spot free finish to the parts being cleaned.

CASE EXAMPLES

HEAT EXCHANGERS - A large manufacturer of automotive radiators wanted to replace several batch type degreasing systems, which were utilizing 1,1,1, - trichloromethane with an environmentally acceptable process. Their needs were obvious. They required good, consistent cleaning results because any oil residual could cause poor brazing and subsequent product failures. They also desired to centralize the cleaning operation, and most of all purchase a system which employed environmentally sound chemistry.

The radiator cores were coated with a light mineral oil, heavily soiled with aluminum fines, and contained a small amount of water soluble oil. The large surface area of the part and the complex tube and fin configuration needed to be addressed in the design of the cleaning system. The extreme surface area would mean that a large amount of oil would be entering the system on a continuous basis. The intricate part design meant that aggressive impingement would be required to obtain the desired cleaning results, and a method would have to be incorporated in the system to minimize cross contamination of the process solutions, since the parts themselves acted as severe water traps.

After process development testing was completed, it was determined that the system solution to successfully address the above issues was an in-line conveyorized cleaning system with a horizontal belt to transfer the parts through the various aqueous process stages. The radiators were supported on the belt at a slight angle to facilitate impingement and promote solution drainage through the tubes. The process selected was a hot tap water prewash, followed by a mild alkaline detergent wash, tap water rinse and a fresh tap water rinse. The water pre-wash effectively removed the majority of the oil from the parts. With the absence of chemical in this stage, the oil was more readily separated with the use of an integral oil decanting system. The oil was then effectively removed from the system on a continuous basis at the rate of 30 gallons per eight hour shift. Special high velocity turbo blowers (inter-stage blow-offs) were provided between each solution stage to minimize carry-over. Residual solution was removed from the individual cores at an efficiency rate of up to 98%.

Through the use of this aqueous system, part cleanliness results were actually superior to their previous process. Significant savings were also realized by streamlining the cleaning operation and in operational/maintenance costs, all while eliminating a serious environmental compliance concern.

TRANSMISSION MODULATOR VALVES - A manufacturer of precision transmission modulator valves was seeking to replace its existing ultrasonic freon degreasing system. Contamination level requirements for this wide variety of intricate, precision machined parts were the most stringent in their industry. They were also concerned about water spotting, part drying and subsequent corrosion protection.

The parts were of steel, stainless, brass and aluminum and were soiled with a wide variety of machining lubricants and fine particulate. This demanded that the cleaning process be extremely flexible in its ability to clean, rinse, inhibit and dry.

As there was a wide range of parts, with most having intricate internal cavities and blind, hard to reach crevices, it was determined that rotational immersion cleaning coupled with aggressive surface impingement would be necessary to meet the critical cleanliness requirements of this application.

The system provides a combination of high energy turbulated immersion cleaning, high impact open air spray impingement, deionized water rinsing, corrosion inhibition and an effective high velocity forced air dry-off.

The machine's programmable controller was programmed to automatically perform up to five different process cycles. All solutions contacting the parts were finely filtered to a level of 5 microns on a full flow basis. These features, along with effective surface impingement, enabled the system to consistency produce parts to a cleanliness level of .03 milligrams per part with a maximum particle size of 10 microns. These results actually exceeded the cleaning capabilities of their former freon degreasing system. Significant operational savings were also realized, since they no longer had to purchase the expensive freon and dispose of the contaminated waste sludge.

ENGINE VALVES - A manufacturer of automotive engine valves had several degreasers in his plant which utilized 1,1,1, - trichloromethane. Although these systems ideally suited their requirements relative to throughput, part cleanliness, corrosion protection and spot free finish, their environmental concerns with the use of this solvent prompted them to seek an alternative process.

The parts were contaminated with metal fines and water soluble oil. Water spotting was a concern, as the following operation was dye penetrate inspection which could mistake a water spot for a surface fracture and reject the part.

To meet this challenging set of requirements, a high volume cleaning process needed to be developed to provide clean, spot free parts utilizing environmentally friendly chemistry.

Through extensive process testing, it was determined that a three stage process would best suit the application. A hot, tap water wash was used in the first stage with a mild alkaline detergent wash in the second stage followed by a deionized water rinse with a morpholine additive to prevent flash oxidation. A high velocity hot air dry-off followed the wet stages.

The material handling requirements also posed a unique challenge. A multiple loop, high speed chain conveyor was incorporated to convey the valves in the optimum attitude for cleaning as well as interface with the automatic part loading and unloading equipment.

This innovative aqueous process successfully met the challenges set forth, providing clean, spot free parts while eliminating the need for chlorinated solvents within their facility.

BENEFITS

In addition to the obvious benefits realized with the use of impingement based aqueous cleaning processes of personnel safety and environmental compliance, there are also several other operational benefits. These include:

* Lower chemical costs,
* In plant waste treatment rather than outside haulaway and disposal,
* Reduced environmental liability,
* Improved part cleanliness, lower contamination levels,
* No need for handling hazardous solvents within the facility, and
* Reduced equipment maintenance, increased "uptime".

CONCLUSION

The effective application of surface impingement in the aqueous cleaning process, coupled with the many innovative technologies discussed in this paper, are critical factors in efforts to successfully replace chlorinated solvent processes with environmentally friendly ones.

AUTHORS

Michael J. Rowny
Ransohoff Company

Stephen D. Temple
Ransohoff Company

MEMBRANE FILTRATION

© Copyright 1992
Thomas J.M. Weaver

Author: Thomas J.M. Weaver
President/CEO
PROSYS Corporation

Abstract:

As Environmental Compliance becomes a critical issue in the successful operation of a metal finishing organization, various treatment techniques are required to meet the compliance demand. Newer treatment technologies have been developed to allow the operators to concentrate on the quality of the product while maintaining discharge compliance. Evaporation, ion exchange, adsorption and numerous filtering methods are employed to aid the operation of the finisher. Clarification, sand filters, polymers and other devices are coupled together to meet the discharge limits. While these various methods are useful, often they do not produce the quality of discharge which will allow the operation to continue without fear of non-compliance.

Membrane separation offers a reliable solution to the problem in many circumstances. Depending upon the physical size of the particle or molecule, and the separation required, various membranes exist with the correct pore size and chemical compatibility to successfully and reliably perform the technique of separation. Using membranes, the "art" of separation is reduced to a physical science. New solutions to old problems are being developed using membranes, as newer membranes, with different materials of construction, are gaining market acceptance.

Although membranes have been on the market for many years, there are many misconceptions as to the applications and the types of membranes which may be used to solve a particular concern. This presentation will define the various types of membranes, evaluate the differences and introduce logical applications for membranes in the waste treatment arena.

Definitions:

(1) Pore Size: The size of the hole in the membrane through which the product can travel. This may be expressed in micron size, Angstroms or molecular weight cutoffs.

(2) Flux: The nominal volume of clean water which can pass through the membrane as rated per square foot of surface area and time, as an example: Gallons per square foot per hour.

(3) General Filtration: Filtration techniques such as filter presses, cartridge filters, bag filters, sand filters and other techniques. Typically, the nominal pore size of this filtration is 10 microns or larger.

(4) Microfiltration: Filtration techniques with a membrane whose pore size is between .1 and 10 microns.

(5) Ultrafiltration: Filtration techniques with a membrane whose pore size is between .001 and .1 microns.

(6) Reverse Osmosis: Filtration techniques with a membrane whose pore size is less than .001 microns.

(7) Crossflow Membrane Filtration: A phenomena of solid/liquid separation by a membrane employing simultaneously superimposed tangential flow across the membrane surface.

Goals of Wastewater Treatment:

The basic goal of wastewater treatment, be it end-of-pipe or treatment at the source, is three fold.

* DISCHARGE COMPLIANCE allows a company to continue to operate and discharge process water without the fear of environmental violations.

* REUSE AND RECOVERY allows the operation to recover many of the valuable assets which would otherwise be lost to the discharge water and the hauling of sludge. Global trends dictate that water itself will become the most expensive resource. Finally,

* ZERO DISCHARGE relieves the company from many of the liabilities associated with the generation of hazardous waste. Although complete recycling is near impossible and extremely expensive, many technical advances have been made on selected waste streams.

INTRODUCTION: Methods

Although compliance, recycling and zero discharge issues are important, the most important goal of treatment is not the treatment itself, but the ability of the company to maintain consistent process quality for its product, while operating within the guidelines of the environmental laws. In an effort to achieve quality, yet live within the discharge guidelines, more and more companies are developing long term plans for the treatment of the generated wastewater, the reuse of the by-products and the recycling of water. Typically, the end result of this process is the implementation of many different technologies. Processes which earn profits are improved, while processes which do not generate operational margins are terminated. Proper control of drag-in and drag-out, coupled with improvements in rinsing techniques are employed to reduce the amount of waste generated, both in chemical losses and water usage. Prior to any purchase of treatment equipment, a complete evaluation of the available techniques is conducted, complete with operational pilot studies. This detailed planning and survey results in the achievement of all the basic wastewater treatment goals.

There are many different methods available for the treatment of wastewater. The methods may be roughly classified into three techniques: SEPARATION, EXCHANGE and EVAPORATION. Each of these methods has applications in which it will operate more efficiently than other methods. Careful consideration of the positive aspects of the methods and the negative aspects of the methods are required to evaluate which method best fits the operational need of the company. It must be noted, that while capital expense is considered one of the most important aspects of the decision, evaluation of pros and cons will highlight other cost impacts which can easily modify a purchase decision.

Evaporation techniques involve the removal of water and volatile organics while maintaining the contaminants for disposal. Typically, this

method has a high degree of operating cost and capital outlay. Yet, there are many critical plating baths where evaporation offers the most economical treatment.

Exchange techniques involve the removal of a specific contaminant using resin or adsorption media. Provided the removal is limited to a single metal, the metal may be recovered. Care must be taken to ensure compatibility between the various plant chemicals and the resins or adsorption material used. Pretreatment and filtration are necessary to insure long term success with the Exchange techniques.

Separation techniques are as varied as evaporation and exchange. The basic separation technique involves the precipitation of the contaminates and separation by gravity, filters and other devices. Membrane filters can achieve remarkable discharge levels while reducing the amount of generated sludge and providing water reuse capability. The proper selection of membranes result in a system which can meet compliance without reliance on balanced flows and waste stream concentrations. Membranes are typically more expensive than clarifiers and sand filters, however, the reliability of membrane systems justifies the expense.

All treatment techniques have a common need for proper segregation and pretreatment. This operation ensures that the operation of the waste treatment system is successful by allowing the system to operate within the design limits of the equipment. As newer treatment processes are developed, segregation allows the operation to implement the technologies with relative ease.

Common chemicals should be gathered together for treatment. In SEPARATION, cyanides must be destroyed, hexavalent chromes reduced, and complexed metal bonds destroyed. These steps must be correctly accomplished or the waste treatment operation will fail. The company must maintain the system, calibrate controllers and ensure the proper operation of all equipment. The long term success of the waste treatment is dependent upon the preventative maintenance and the attention to detail in the operation of the plant. Daily discharge samples should be taken and analyzed to ensure that the system is fully operational.

MEMBRANES: Range and Types

As depicted on Figure 1, Range of Membranes, there are three basic membrane ranges available in the marketplace. Each range of membrane has a specific function in which it will operate repeatably and reliably.

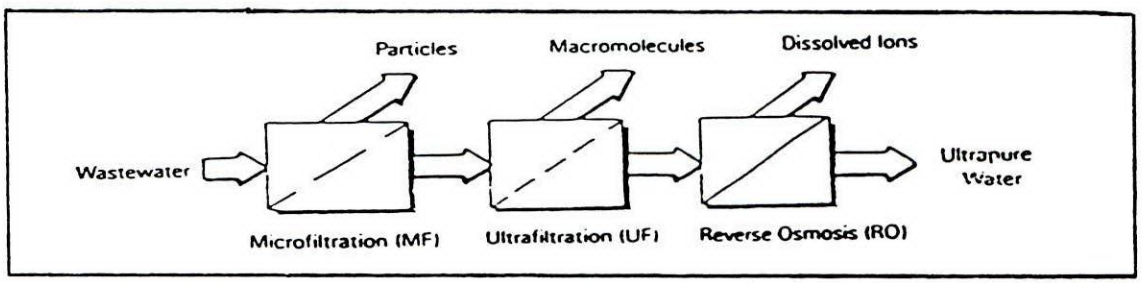

Figure 1: Range of Membranes

Membranes come in different configurations, materials of construction and various pore sizes within the ranges of applications. Each difference must

be evaluated prior to the selection of a system.

Table 1: Membrane Data Sheet

		MF	UF	RO
Pore Size	(microns)	.2 to 10	.001 to .1	<.001
	(Angstrom)	>1000	10 - 1000	< 10
	(mol. wt)	>1M	10K - 1M	<10K
Operating Pressure		30-50#	40-150#	>100#
Configurations				
*	Hollow Fiber		XXX	XXX
*	Tubular	XXX	XXX	
*	Sheet	XXX	XXX	
*	Spiral Wound		XXX	XXX

MEMBRANES: Microfiltration

The typical MF membrane used in the wastewater treatment industry removes, or rejects, particles which have a size of greater than .2 microns. For comparison, 40 micron particles are not visible to the human eye. Thus, the MF membrane has a cutoff 200 times smaller than a visible particle. Yet, this a relatively large hole with respect to the permeation of water. As such, the membrane has a high flux while the operational pressure of the membrane is low.

The MF membranes are typically configured in tubular forms. Hollow fiber, flat sheet and spiral wound configurations are also available. In a tubular membrane, Figure 2, Tubular Membrane Illustration, a large number of membrane tubes are combined in a central housing. The combined membrane area in this bundle is used to determine the nominal flowrate of the

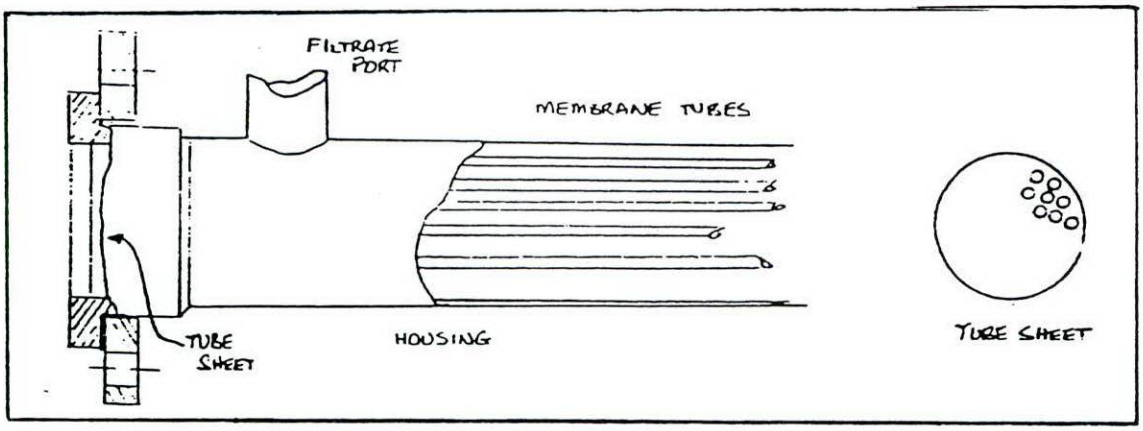

Figure 2: Tubular Membrane Illustration

membrane. It is important to evaluate the amount of area provided with a membrane system, as area results directly in the amount of fluid which may be processed through the membrane.

The primary task of a microfiltration membrane is to remove solids and emulsified oils from a waste stream. For this application, tubular membranes offer the highest degree of reliability. In this operation, the separation process is reduced to a science: if the contaminants are in particle form, the contaminants will not enter into the discharge stream. This statement should not be taken lightly. Membrane treatment is a science, it is not an art which depends on flowrates, sludge blanket levels and many other parameters. However, like the clarifier which depends on pretreatment, the membrane system will only produce compliant discharges if the pretreatment is correct.

A typical process schematic is shown on Figure 3, Membrane Process Schematic. High flows from a centrifugal pump provide the operational

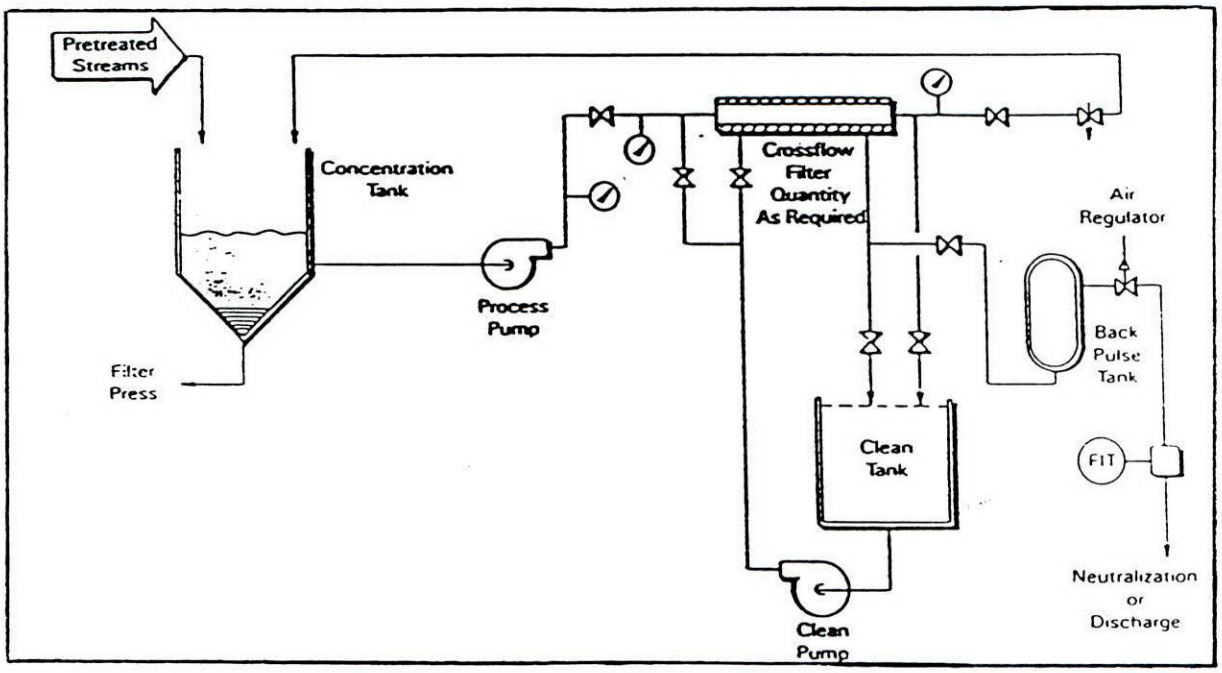

Figure 3: Membrane Process Schematic

pressure for the separation task. A differential pressure is placed across the membrane by means of a diaphragm valve or orifice plate. This resultant pressure gradient raises the trans-membrane pressure and induces the permeation through the membrane surface. As the trans-membrane pressure increases, the permeate flowrate increases. In many instances, as the flowrate of the pump increases, the permeate flowrate increases. As the system generates filtrate, the concentration of the contaminates in the Concentration Tank increases. Removal of sludge is accomplished by the use of a filter press.

There are many factors which determine which MF membrane will operate the most efficiently in a given waste stream. Material compatibility, operating temperatures, pH, membrane configuration and the actual manufacturing process of the membrane are items which should be addressed prior to the selection of a membrane. Manufacturers literature identifies the majority of the key parameters.

With regard to the manufacturing of a membrane, there are two primary methods. First, the membrane is attached to a support structure by means

of solvents or other processes. In this process, the support structure is typically a different material than the membrane. This process yields a very thin membrane. Long term adhesion to the substrate is ensured by always pressurizing the membrane, that is the inner shell of the membrane tube, not the substrate. The second method is that the membrane is part of the substrate, that is, it is the substrate. This method of manufacturing allows the operating pressure to be on either side of the membrane tube.

In wastewater applications, tubular microfiltration membranes foul. In fact, all membranes foul. The fouling of membranes reduces the flowrate of the system. When fouling reaches a level at which the wastewater cannot

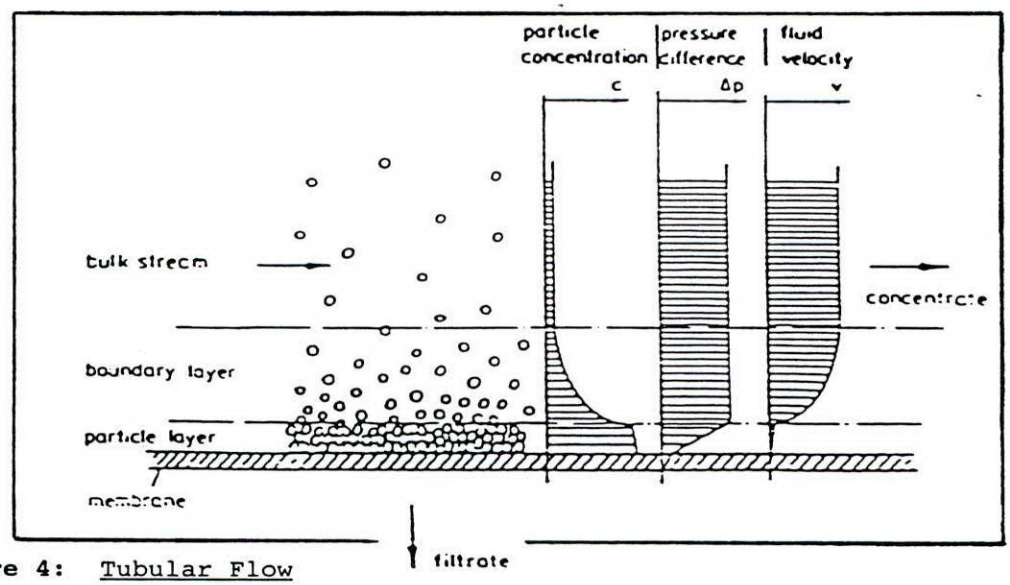

Figure 4: Tubular Flow

be treated in the proper amount of time, the system must be chemically cleaned. As with human skin, cleaning restores the filtration rate of the membrane. There are various methods used to improve the mean-time-between-cleaning. Additions of lime, iron and carbon aid in the scrubbing of the membrane surface, yet it does not prevent the long term cleaning of the system.

There is a physical law in fluid flow which explains why a scrubbing action is relatively ineffective as a method to extend the mean-time-between-cleaning. As illustrated by Figure 4, Tubular Flow, there is no tangential flow at the boundary of the tubular wall due to a continuum of flow, that is, the tangential flowrate at the wall is zero. Yet, the overall tangential flow has long been proclaimed as the reason that the flowrates stay high for long periods of time. Given a high flowrate through the tube, the flow is turbulent. This turbulent flow greatly reduces the thickness of the boundary layer. However, careful examination of the area near the membrane wall indicates that the turbulent flow does not affect the wall. In fact, the only flow in the boundary layer is that of the filtrate passing through the membrane. This action is equivalent to a filter press. As the filtrate exits the membrane, it deposits the contamination on the wall of the membrane. A thin boundary layer of sludge accumulates, cutting the overall pore size of the membrane. This reduces the amount of water which may be passed at a given operating pressure. As such, the flowrate of the system decreases.

In systems which have membranes which are also the support substrate, a reversal of flow disrupts the boundary layer and allows the turbulent flow to remove the contaminants which foul the membrane surface. As illustrated in Figure 5, Backpulsing Operation, this action lifts the foulants into the flowpath of the waste. Many systems are equipped with

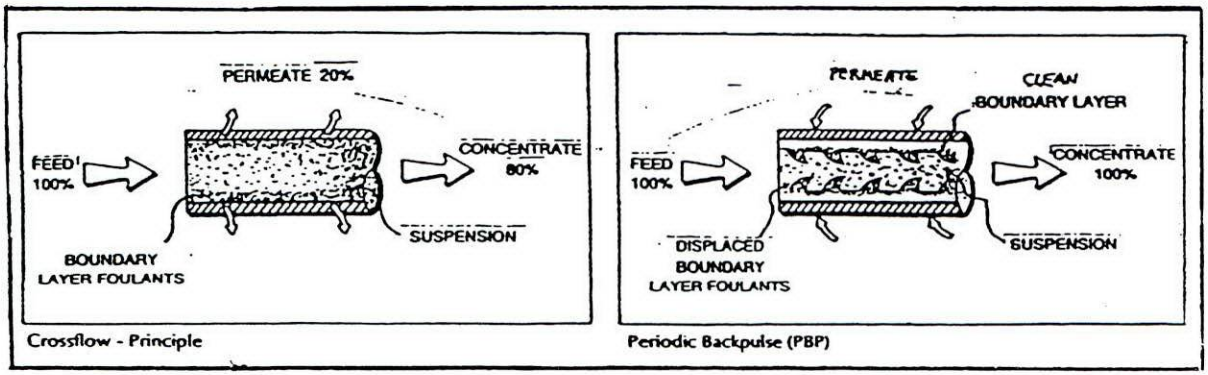

Figure 5: Backpulsing Operation

automatic pulsing units. When pulsing is used, the addition of lime, carbon and iron are not used, other than required to properly pretreat the waste stream for removal of the solids.

Microfiltration membranes offer an excellent upgrade in applications were the operation of the clarifier and sand filter is not meeting discharge limits. These systems may be easily reconfigured with membranes to achieve discharge levels as shown in Table 2, Post Retrofit Discharge Levels. The same

Table 2: Post Retrofit Discharge Levels

		CONCENTRATION ppm		
SYSTEM	SUBSTANCE	INFLUENT	CLARIFIER	MF
Job Shop	Cu	6	.4	.06
	Ni	20	1.5	.09
	Sn	1.5	.15	.07
Captive Plater	Cu	25	.3	.06
Job Shop	Ni	15	1.0	.2
	Cr(T)	60	.5	.15
	Zn	120	1.2	.5
PCB Shop	Ni	2	1.5	.1
	Cu	25	1.5	.03
	Pb	4	.5	.18

pretreatment chemistry is required, however, co-precipitants and polymers are not required for the proper operation of the system. The basic precipitation of metals into hydroxides forms a particle which is large enough to successfully separate with the microfiltration membrane, thus, the removal of the particle is based on science.

MEMBRANES: Ultrafiltration Highlights

Ultrafiltration membranes are tighter than microfiltration. The pore size of UF membranes is between .001 to .1 microns. As a result, the flux rates are not as high per square foot of membrane and the operational pressures to achieve the flowrates are higher than that of the MF membrane. It physically takes more membrane surface area to produce a given flowrate than that of the MF membrane. For this reason, UF membranes are typically spiral wound or Hollow Fiber. UF membranes remove free oils, many surfactants and sub-micron particles. Zyglo oils, dyes and other components may be rejected by the membrane.

Hollow Fibers are similar to tubular except that the operating diameter of the tube is extremely small, resulting in different flow characteristics within the tube. As a result of either the spiral or fiber membrane module configuration, UF systems will not operate with a high degree of solids in the waste stream. If the membrane module configuration is tubular, solids may not be a problem, however, as noted above, for a given flowrate, there will be many modules. In addition to solids, UF membranes in the spiral wound configuration do not operate as efficiently in the presence of emulsified oils. Both the oils and solids tend to block the inlet to the membrane, reducing the transmembrane pressure of the module. This reduces the maximum amount of flow which the membrane will produce.

The UF membranes operate in a similar fashion to the MF membranes, except, UF membranes remove components which pass through a MF membrane. In wastewater applications, it may be necessary to pulse UF membranes to maintain the operating flowrates required. As with the MF applications, membrane manufacturing processes must be understood prior to the implementation of pulsing. With regard to hydroxide removal, there is little difference between a .1 micron tubular UF membrane and a .2 micron tubular membrane. Both membranes remove particles which are greater than .45 microns, the filter size used to determine Total Suspended Solids.

MEMBRANES: Reverse Osmosis Highlights

The Reverse Osmosis (RO) membrane is the tightest of all membranes. The membrane removes salt. It is typically produced as a spiral wound membrane. This configuration provides the maximum surface area available in a membrane module.

Typically, RO membranes produce drinking water or serves as the pretreatment for a De-Ionization process. In waste treatment, RO systems are used to concentrate fluids for reuse. The key in this process is to reduce the amount of salt in the stream. If the process uses city or well water, the RO systems will not only concentrate the desirable components, but it will concentrate the contaminants and salts as well.

Pretreatment of the fluid prior to the RO system is necessary to prevent scaling and unrecoverable fouling of the membrane. Often, MF systems serve as the primary prefilter to the RO system. Utilization of MF waste treatment and RO systems to recover reusable rinse water is a proven application.

RECYCLING AND RECOVERY OF CLEANING SOLUTIONS

© Copyright 1992
Thomas J.M. Weaver

Author: Thomas J.M. Weaver
President/CEO
PROSYS Corporation

ABSTRACT:

The proper cleaning of components in the metal finishing industry is the key for quality in the process. Almost every plating operation commences with a cleaning process. In painting operations, cleaning of the components is essentual to the proper adhesion of the paint. For years, chlorinated solvents have offered a robust solution to the problem of removing oils and greases from the product. Alkaline cleaners have been used to remove dirt and prepare the surface of the product for plating. The basic cleaning operation has been reliable and relatively inexpensive.

As a result of the Montreal protocol, chlorinated solvents are now being phased out in favor of the protection of the ozone layer. The relative ease of cleaning is now being replaced with complex cleaning operations; complex cleaning operations using soap and water. As a result, usage of alkaline cleaners has increased. Newer aqueous and semi-aqueous cleaners are being introduced as the replacement to solvent cleaning. Complete redesigns of components, cutting oils replacements and manufacturing process changes are now being accomplished in an effort to replace solvents.

Aqueous and alkaline cleaners, both the concentrated solution and the rinse water, pose many handling problems not previously encountered with solvent cleaners. Aqueous cleaners require component rinsing following the clean cycle. Companies are finding that the new cleaning processes actually remove dirt and solid material, which the solvents never touched. The cleaners are relatively expensive. And, the aqueous cleaners cause severe upsets when introduced into many waste treatment operations.

An alternative to the discharge of the cleaners now exists. Most cleaners may be selectively filtered to produce a cleaner which is free of oil, grease, and other contaminates while allowing the wetting agents, additives, dispursants and cleaner components to pass through the membrane. This regeneration of the cleaner maintains a fresh cleaner, increases the operational life of the cleaner, reduces the amount of cleaner used in the operation and ensures continuous quality cleaning of the components.

Definitions:

(1) Microfiltration: Filtration techniques with a membrane whose pore size is greater than .2 microns.

(2) Ultrafiltration: Filtration techniques with a membrane whose pore size is between .001 and .1 microns.

(3) Reverse Osmosis: Filtration techniques with a membrane whose pore size is less than .001 microns.

(4) Cleaner: A solution which removes dirt, oil, grease, metal and other contaminates from the product piece of work.

(5) Aqueous Cleaner: A solution similar to Item 4 which contains water, surface active agents, wetting agents, dispersants and other components. Typical aqueous cleaners are caustic solutions and organic formulations.

(6) Semi-Aqueous Cleaners: A solution similar to Item 4 which is comprised of organic acids, such as turpines. This type of cleaner will typically operate at full strength in the cleaner bath without dilution.

INTRODUCTION:

There are many different cleaners and cleaning equipment components available which will replace solvent cleaning. Each process and component manufactured requires different types of cleaning to ensure product quality. As such, the change to aqueous cleaning is complex and time consuming. The bottom line is that solvents are OUT, and aqueous cleaners are IN.

The changeover requires coordination between the manufactures of the cleaning equipment, the company process engineers and the cleaning chemical manufacturer. A battery of items must be examined to determine which method of cleaning will produce the most reliable quality. Temperature, strength of the cleaner, contaminants being removed, rinsing procedures, and material compatibility must be addressed prior to the selection of a cleaner method. In fact, the company must determine "How clean is clean?" Finally, the cleaner must be treated for discharge when it is exhausted.

It may be easy to ignore the treatment of a spent cleaner, especially when the company has an operational waste treatment system. However, the very items which enable a cleaner to clean, make the cleaner one of the most difficult components to treat in a wastewater treatment system. Cleaners cause resin beads to fail. Cleaners cause clarifier systems to burp. Cleaners coat sand filters, decreasing the effectiveness of the filtering media. When determining the best cleaner operation for the company, energy and effort must be expended to determine the method in which the spent cleaner will be treated.

As the cleaner loads with contaminates, the reliability of the cleaning process is decreased. Typically, more cleaner is added to the process to extend the operational life of the cleaner. This masks a developing problem in the entire operation. Dirty spent cleaner is dragged from the cleaner tank to the rinse stream. Unrinsed cleaner is dragged to acid baths. Within a matter of a few hours of heavy cleaning, the spent cleaner has contaminated the entire process line.

Conventional waste treatment processes are affected by the cleaners. In a clarification system, gravity is employed to pull the precipitated contaminate from the waste stream. Polymers are added as well as coprecipitating agents to increase the weight of the contaminate and aid in settling. The cleaners are comprised of wetting agents and dispursants. Simply stated, dispursants push solids and contaminates apart so that a component may be rinsed. This action in a clarifier leads to non-compliant discharges. Continual addition of dirty cleaner only makes the problem worse.

CLEANING PROCESS

The cleaning process is simple. Components must be placed in a position so that the maximum amount of cleaner contacts the components and removes the maximum amount of dirt, oil and grease. Depending upon the type of components, there are three effective means to accomplish the cleaning task. Rack mountable components are dipped in a tank, large items are typically sprayed, and small components are loaded into a barrel for the washing operation. Ultrasonics or other means may be used to agitate the cleaner solution to ensure that all the cracks and crevices of the component are properly cleaned. Depending upon the cleaner, the entire operation may be conducted at elevated temperatures.

Following the cleaning operation, the components must be throughly rinsed prior to further operations. Rinsing can be as complicated as the cleaning step. If all the cleaner is not removed, the product may spot. Some processes require dry parts. As with plating operations, the rinsing of the product following cleaning uses large amounts of water. In some companies, the wastewater treatment system is operating at maximum capacity. Increased water usage only aggrevates compliance issues.

Consider the Cleaning Tank in Figure 1. The process typically starts with a fresh batch of cleaner and water. As the process continues during the course of the day, new cleaner is added to the tank to maintain the strength of the cleaner. Oil, grease, contaminates and other components are removed from the work by the cleaner. Water is added to maintain the level in the cleaning tank. Dragout is comprised of oil, grease, cleaner, water and other items to the rinse stream. Experience

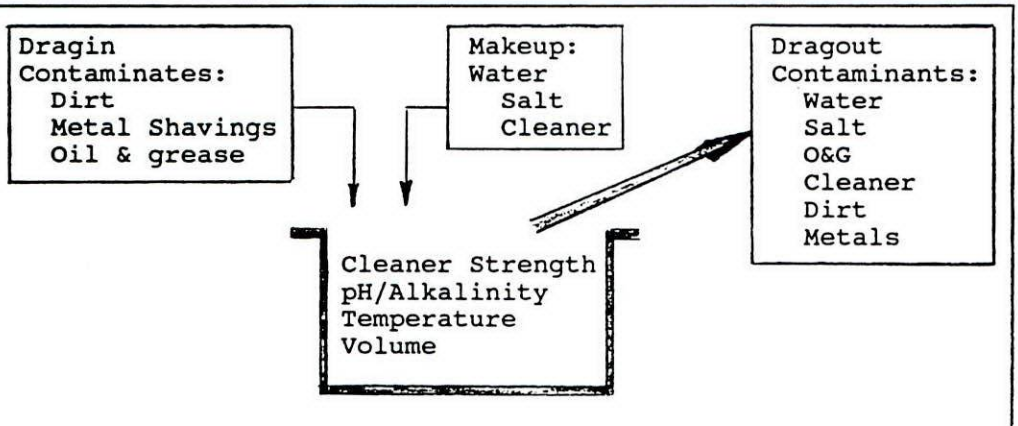

Figure 1: Cleaning Tank Mass Balance

dictates that components are cleaned more reliably and with a higher degree of quality if the cleaner is clean. If fact, the rinsing operation performs better with clean cleaner. As the cleaner continues to operate, the cleaner gets dirty. Floating oils start to appear as the solubility limit of the cleaner is exceeded. Solids buildup in the cleaner tank and settle to the bottom. Clean parts are pulled out of the cleaner tank through a veil of oil. As the cleaner degenerates, the quality of the dragout worsens. The rinse water turns cloudy. In barrel operations, the rinse water may start to look like the cleaner bath.

This operation is not cleaning. This operation is wasting capital

funds, operator time and product which will be rejected by quality control functions. As stated previously, this operation will result in wastewater treatment operations which cannot provide compliant discharges. However, these problems describe many cleaning operations. Complicating the issue is the treatment of the concentrated cleaners. When the cleaning tanks are spent, the cleaner is dumped to the waste treatment area. The cleaner tanks are throughly cleaned and rinsed prior to generating a new cleaner bath. All the wash and rinse water used is sent to the waste treatment area. Depending upon the treatment method, the cleaners are either slowly bled into the treatment process or the cleaners are hauled to a disposal site.

SOLUTION

Microfiltration membranes can selectively remove the comtaminates of a cleaner bath while allowing the cleaner components and the water to pass through the membrane. **Microfiltration membranes clean the cleaner.** As the MF system operates, the contaminates, which have a larger size than the pore size of the MF membrane, are concentrated. The components of the cleaner pass through the membrane and are returned to the cleaner tank with the filtered water.

As shown in Figure 2, Cleaning the Cleaner, the system operation is rather simple. A small slip-stream of cleaner is directed to a Concentration Tank. The cleaner is then pumped through the MF membrane at the required flowrate and pressure. The cross-flow filtration rejects the contaminates, while allowing the permeate to pass through the membrane, where it is returned to the cleaner tank.

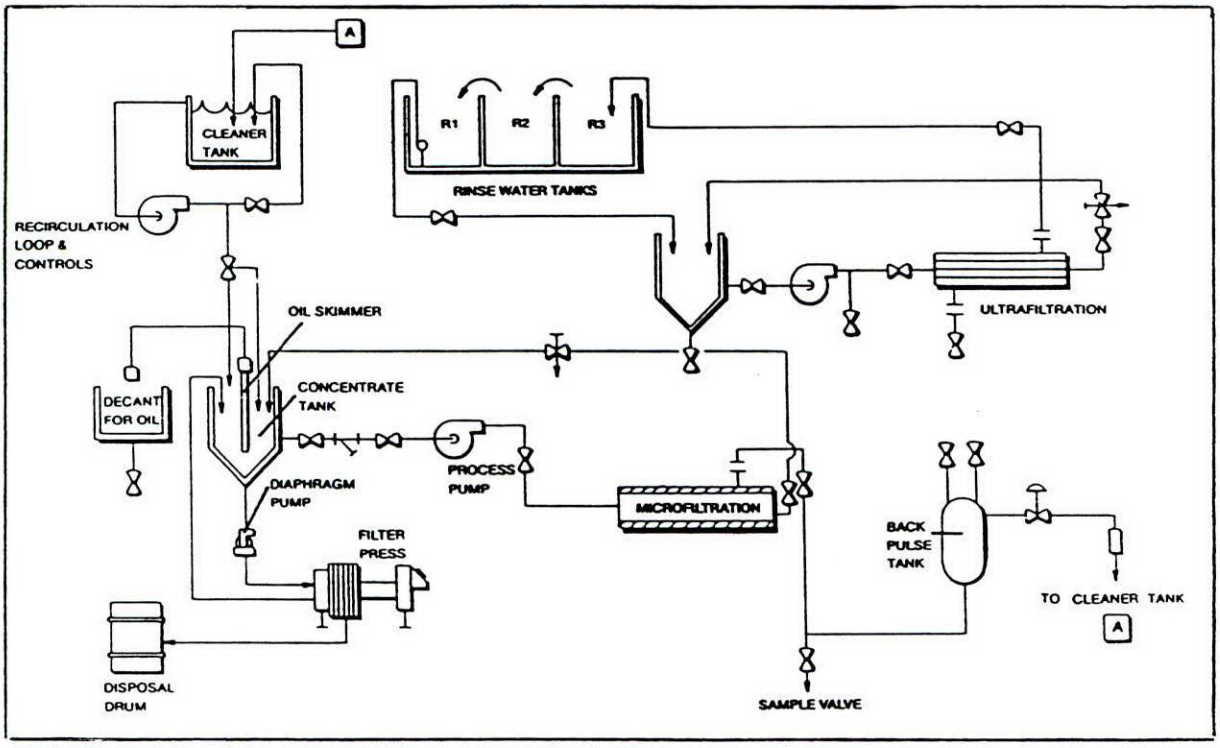

Figure 2: Cleaning the Cleaner

As the contaminates in the concentration tank build in concentration, the ability of the cleaner to hold the oils and solids in solution is exceeded. This results in the cracking of the emulsified oils and the settling of the solids. This separation is further enhanced by decreasing the solubility of the fluid by lowering the temperature. As a result, free oils are removed by an oil removal device and solids are removed by a filter press or bag filter. The net result is that the cleaning tank stays clean, the process quality stays constant and the waste treatment issues are avoided.

Operationally, there are many factors which affect the operation of the cleaner regeneration system. Operating temperature, the size of the cleaner tank, the operational life of the cleaner itself, and the method employed to ensure that the contaminates are removed from the cleaner tank. In addition, cleaner recycle units should not cross-contaminate other types of cleaners. It is important that cleaners stay segregated, as different cleaners are required for different operations.

Figure 3, Recycled Cleaning Tank Mass Balance, illustrates the mass balance of a cleaner tank which is maintained in a clean condition. Many process operations are simplified. The cleaner solution maintains a higher cleaning potential. Rinse water flowrates are not as critical. Downstream tanks are not contaminated with oils and other contaminates. The cleaner operational life is extended.

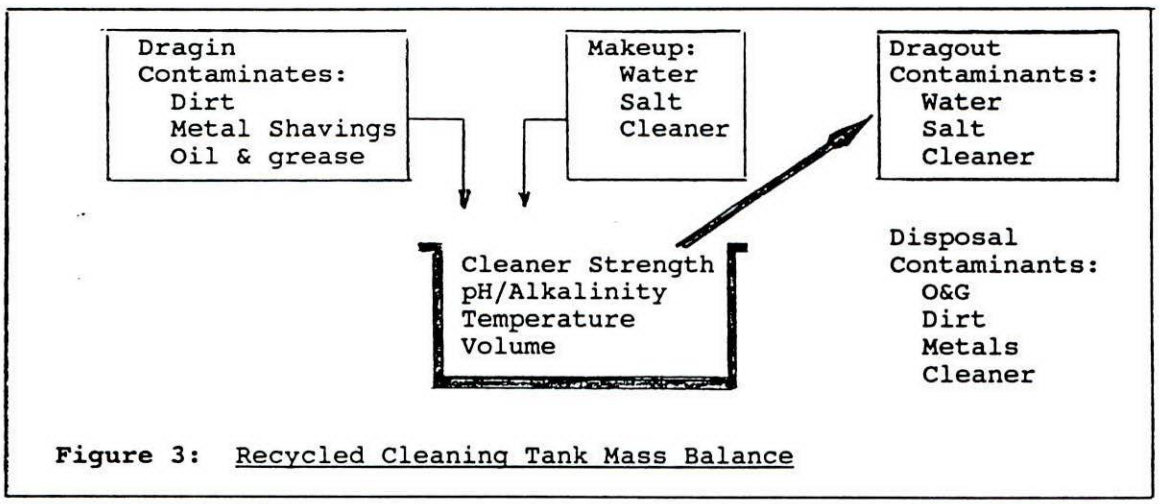

Figure 3: Recycled Cleaning Tank Mass Balance

The recycling of the cleaner bath does not greatly reduce the cleaner addition requirements. The majority of the cleaner is lost due to dragout. When contaminates are removed, the cleaner components which dispursed the solids and emulsified the oils stay with the contaminates. However, the cleaner operates more efficiently when it is clean. When the bath is maintained, cleaner additions are conducted when the alkalinity drops below an acceptable level.

As indicated in Figure 3, salt buildup will occur in the cleaner tank. Consideration should be given to providing RO or DI water when making up fresh cleaner baths or when increasing the operational level of the cleaner tank. When the cleaner is regenerated, salt may prove to be the limiting factor in the operational life of the cleaner.

Table 1, Aqueous Cleaner Recycle Results, shows results compiled for companies testing and implimenting aqueous cleaner recycle methods using membranes.

Application	Contaminants	Concentration(ppm) Before	After	Disposition
Metal Finish	* Molly Lube	-2200 O&G -TSS Heavy	-26 O&G -TSS Clear	Reuse
Hardware Mfg	* Stamping oils	-200 O&G -TSS Heavy	-40 O&G -TSS Clear	Reuse
Jet Engines	* Cutting oils	-1600 O&G -TSS 176	-308 O&G -TSS 52	Reuse

Table 1: Aqueous Cleaner Recycle Results

When the cleaner tank is maintained in a clean condition, the cleanup of the rinse water may be addressed. In a similar fashion as the cleaner bath, membranes may be utilized to clean the rinse water. Ultrafiltration or Reverse Osmosis offer the pore sizes necessary to selectively remove the cleaner and cleaner additives from the rinsewater itself. As the cleaner is concentrated in the concentration tank, it is possible to return the cleaner to the cleaner bath. DI treatment of the rinse water is possible after the cleaner ingredients are removed.

Turpines and other semi-aqueous cleaners may be addressed by the use of membranes. In this case, the rinse water from the operation is filtered using a microfiltration membrane. This membrane rejects the semi-aqueous cleaner while allowing the water to pass through. The concentrated cleaner bath is typically operated until it is exhausted. Membranes are not selective enough to remove the contaminants of the turpines without removing the actual turpine components.

IMPLEMENTATION

The implementation of the recycling of cleaners is a difficult decision and requires planning. Table 2, Questions To Consider, lists various items which should be addressed prior to the purchasing of any equipment.

The discussion generated by Table 2 highlights many of the concerns when it has been decided to regenerate cleaners. Different cleaners require different systems, as cross contamination of cleaners can adversely affect the process. Multiple cleaners may require multiple systems, however, cost becomes an issue. If the rinse water is not going to be recycled, batch treatment of spent cleaners offers a less expensive alternative to multiple systems. The operating

temperature of the process determines which membrane should be used in the process. Ceramic membranes are available, but they are more expensive than polymetric membranes.

Table 2: Questions To Consider

1. How many cleaner lines are there in the facility?
2. What are the sizes of the cleaner tanks?
3. How often are the cleaners dumped?
4. What is the cost of the chemicals to replenish the cleaner?
5. What is the method of disposal?
6. What is the cost of the disposal?
7. How much labor is required to change the cleaner tank?
8. How many different types of cleaners are used?
9. Is it necessary to use different cleaners?
10. Why are the cleaners dumped?

Sizing of the equipment is important. The flowrate required to maintain the cleaner bath is a function of the dragin, the membrane configuration and the nominal operational life of the cleaner bath without cleaning. If a bath is to be processed on-line, it is important to turnover the bath 3 to 5 times during the nominal operational life of the cleaner. This processing will extend the bath life over 10 fold. If the cleaner is to be processed in the batch mode, the sizing of the system depends solely upon the quantity of the cleaner and the amount of time the system can operate to process the cleaner.

OPERATIONAL RESULTS

Case study 1: An alkaline cleaner of 900 gallons was dumped once every week. The operating temperature of the process was 160oF. The solution was hauled to a disposal site as treatment with a conventional 150 GPM system resulted in non-compliance. A MF system was placed on unit. The solution was maintained for a period of 16 weeks without dumping. The alkaline solution was adjusted periodically to replenish cleaner that was removed from the tank due to dragout or removal with the oil and solids. The company has purchased a unit for the process.

Case Study 2: A company had 12,000 gallons of Soak Cleaner and 10,000 gallons of electrocleaner which was dumped every 4 weeks. The solution was hauled as conventional treatment resulted in non-compliance with regard to COD/BOD. The nine cleaner tanks were in 4 different lines. The company purchased a single MF system for treatment of the solution. When the cleaner gets dirty, the cleaner is pumped to a holding tank where it is allowed to cool. When the solution is cool, the spent cleaner is process through the membrane system and stored in a secondary tank. When required, this tank replenishs spent cleaners. Upon completion of the regeneration, the MF system is flushed with water to avoid cross-

contamination. It is estimated that yearly hauling volumes will be reduced to less than 4,000 gallons.

Case Study 3: A company had a 500 gallon cyanide based cleaner tank which was required to remove heavy stains of the product prior to final assembly. The process parts were cleaned with barrels. Dragout from the components was excessive at best. It was assumed that the dragout of the cleaner accounted for the unexplained waste treatment problems. A regeneration system was placed on the cleaner tank. Within one day of operations at .5 GPM, the rinse water tank returned to a clear color. Over a period of six weeks, the waste treatment system operation improved, with no compliance issues. Upon removal of the recycling unit, all the previous waste treatment issues returned. The company has authorized funds to purchase a recycling unit.

CONCLUSION

Although the change from solvent cleaning to aqueous cleaning is difficult, the change will result in cleaner components. In addition, the change is mandated in an effort to protect the ozone layer. Proper planning and testing are required so that the proper cleaning procedure is placed in operation; a procedure which meets the quality and manufacturing needs of the company. Membrane filtration provides the necessary methods to deal with spent cleaners and rinse water. By implimenting membranes, cleaner life is extended. The cleaner bath maintains a high cleaning potential. Recovery of the rinse water becomes a reality. And the wastewater treatment issues are simplified. Aqueous cleaner recycle units provide a cost effective means to save chemicals, decrease operator attention and avoid waste treatment incidents. The change in cleaning procedures is worth the investment.

CLEANING - EMERGING TECHNOLOGIES

Bob Srinivasan
Technical Director
EPI Electrochemical Products Inc.
New Berlin, Wisconsin

Abstract

Mandated by the EPA in the early '80s and later of their own initiative, the US metal finishing industry has been looking to replace chelated and solvent based cleaners. The availability of specialty polymers and surfactants has led to the development of new liquid cleaners which often meet the above criteria, perform better and last longer than the traditional powder cleaners. They are also easy to waste treat and can be safely fed through automated pumps. This paper will discuss such emerging technologies in cleaning which will be increasingly used during the '90s and beyond.

Background

No discussion on such a topic as "Cleaners - Emerging Technologies" would be appropriate without first reviewing the past technologies of cleaners. Remember, back in the sixties, the U.S. metal finishing industry was promoting the use of phosphated cleaners because of their ability to sequester metal ions and thereby reduce scale formation and enhance detergency.

In the late sixties, however, the phosphates were known to cause eutrophication, a phenomenon wherein the phosphates that were once introduced into the water stream acted as nutrients for water plants and led to their uncontrolled growth, as was the case with the water hyacynth in the Florida Everglades.

The industry then quickly started to look at chelates like EDTA and NTA as alternatives for the phosphates. In turn the metal finishing chemical suppliers developed and proudly hailed the so called "CHELATED CLEANERS" and once again promoted their use all through the seventies as "Non-Phosphated Cleaners". The legacy of the chelated cleaners did not last very long either.

During the Carter era one more government agency was created - the Environmental Protection Agency (EPA). The EPA, which all metal finishers are very familiar with, early on discovered the presence of toxic and carcinogenic heavy metals like zinc, copper, nickel, chromium, etc. in metal finishing plant effluents. So, the EPA quickly moved in the early eighties with regulations to limit the levels of heavy metals in effluents by requiring metal finishing plants to do their own pretreatment before discharge into Publicly Owned Treatment Works (POTW).

The end users of metal finishing chemicals, in the process of pretreatment, discovered that the presence of chelates in effluents interfered with the process of metal hydroxide precipitation, flocculation and settling.

So, here we go again. The use of chelates in cleaners suddenly came under severe attack and it became a taboo to even utter the words "Chelated Cleaners" by chemical suppliers in front of their customers.

Caught in an awkward and totally unprepared market situation, the metal finishing chemical suppliers hurried to reformulate their cleaners to meet the new EPA regulations. In the meantime they sought to differentiate between those evil ingredients which would be considered as "Chelates" versus others, the not so evil ingredients which came to be known as "Complexers". The difference being that a chelator is always a complexer, but not the other way around. Some examples of chelates would be EDTA, NTA, and examples of complexers are gluconates, glucoheptonates and phosphonates. While these are the technical terms, some in the industry refer to the complexers as chelates and call the chelates like EDTA and NTA "Hard Chelates", meaning that their presence in effluent makes it "hard" for the waste treatment and removal of heavy metals.

While the metal finishing industry was trying to deal with the problems associated with chelates and their effect on heavy metal precipitation, the EPA came out equally hard on users of solvents for painting, vapor degreasing, etc. Whereas the heavy metal problems had to do with water pollution, the concern in the case of solvents was over air pollution and worker health and safety.

Unlike the regulations on the use and waste treatment of heavy metals that had a great impact on the electroplating industry, the EPA regulations on the solvents greatly affected the painting industry's processes for the automotive and appliance market. Because the electroplating industry was using far lesser amounts of solvents than the painters, the EPA and OSHA regulations restricting the use of chlorinated solvents are just beginning to take effect and the industry is investigating the alternatives.

Now that I have reviewed some of the background and government regulations limiting the use of heavy metals and solvents by the metal finishing industry, it becomes apparent where the emerging technologies on cleaners are heading. Yes, the metal finishing industry is obviously pursuing technology that will help eliminate the use of chelates and solvents in their cleaners, and in turn, the specialty chemical suppliers in trying to address these problems have come up with some solutions which are discussed below.

Waste Treatable, High Performance, Liquid Cleaners

In the late seventies, the metal finishing industry and its chemical suppliers backed away from the use of chelates in cleaners and reverted to the use of phosphates, as by then the EPA had loosened its regulations on the use of phosphates by this industry because of its low use level as compared to the household and institutional detergents for laundry and dish washing.

Also, in the early eighties, the metal finishing industry started to install in-house waste treatment equipment that could precipitate and remove phosphates from plant effluent. The mere phosphated cleaners, however, lacked in performance compared to those of their predecessors, the chelated cleaners.

Toward the mid eighties, specialty polymers of low molecular weight, polyacrylates, became commercially available and it was discovered that such polymers when combined with the polyphosphates in cleaner formulations offer a synergism that results in excellent water softening and scale inhibition properties often superior to those of the chelates. More importantly, polymers did not tie up the heavy metals or interfere with the waste treatment process.

About the same time, the surfactant manufacturers offered this industry special non-ionics and amphoterics that are soluble in caustic and stable towards high electrolytes. So in using these specialty polymers and surfactants along with liquid alkaline builders, the metal finishing chemical suppliers can now offer non-chelated, high performance liquid cleaners.

These new generation cleaners, either in liquid or slurry form, can be formulated with high surfactant and low builder concentration that makes them work at very low use concentration offering superior cleaning performance and outlasting the bath life of the traditional powdered cleaners.

Another added advantage to the use of liquid cleaners is their ease and safety of worker handling, plus the ability to be fed by automated metering pumps, either at set time intervals or based on the cleaner solution conductivity. Thus, the liquid cleaners, although priced higher than the powdered cleaners, have proved themselves to be highly cost effective and are in increasingly common use not only at major captive shops, but also lately at small job shops in the USA.

Solvent Free, Neutral Cleaners

Traditionally in the metal finishing industry, chlorinated solvents, such as trichloroethylene, 1,1,1-trichloroethane, methylene chloride, etc., have been used or are still being used by some, for vapor degreasing in the removal of buffing and lapping compounds and for paint stripping. All through the eighties, however, the metal finishing industry increasingly started to use liquid buffing compounds in place of the bar cakes, and has been switching over to the use of water soluble synthetics for use in lubricants and cutting and stamping oils, thus replacing the hard to clean heavy animal tallows, fatty acids, and chlorinated and sulphonated oils.

All this is a welcome change for the chemical suppliers, for these above mentioned changes in themselves make it easier now to formulate cleaners for most applications without the use of solvents.

Neutral cleaners that do not contain solvents and which operate at a pH between 8.5 and 10.5, and at a temperature between 120 and 180°F, are increasingly being applied in industrial spray washers for the removal of stamping oils, cutting oils, drawing compounds, etc. Being neutral in pH, the solutions of these cleaners are far less hazardous for the health and safety of operators.

The neutral cleaners are generally used for part washing and do not require post rinsing. The cleaner solution when allowed to dry over the clean parts offers temporary rust protection, while the parts are in process between machining, inspection, fabrication and final finishing.

Because their operating pH is at about the same level as that normally required for plant effluent disposal, spent solutions of neutral cleaners require minimum neutralization and waste treatment prior to disposal.

Recyclable Cleaners

There is an increasing demand in the metal finishing industry for cleaners that would lend themselves to recycling. Chemical suppliers and equipment manufacturers are working together to offer the industry the so called "Never Dump Cleaners".

Under the recycle system, the cleaners will be formulated so that their solutions will allow the oil and grease cleaned off the metal surface to float to the top, where they will be mechanically skimmed off and separated through a centrifuge. Solid particles like buffing compounds, metal filings, etc. will be removed using ultra filtration. The resultant cleaner solution can then be replenished and reused under a closed loop system without ever having to dump.

Conclusion

As discussed during this presentation, much of the technologies that emerged in cleaners during the late eighties had to do with the elimination of chelates, solvents, any known or suspected carcinogens, etc. The driving force and motivation for the invention of such technologies, to a large extent, were due to EPA and OSHA regulations governing the environment and workers' health and safety.

In my view, such regulations will not only continue all through the nineties, but will get far more stringent as we go into the 21st century. Even if we assume for a moment that that is not the case, the metal finishing industry for one thing has clearly seen the profitability of using pollution-free products along with the cost savings from automated feeding, improved quality and reduced liability for their workers' health and safety. As such, I believe the emergence of new technologies in cleaners will continue to focus on a cleaner environment and the safety of our health.

*** PAPER NOT AVAILABLE IN TIME FOR PUBLICATION ***

Waste Minimization Via Source Reduction for the Plater Pt (III). Source Reduction Initiatives: The Prerequisite to Closed-Loop

Dr. D. Paul Piplani, CEF, Acteron Corporation, Redwood City, CA

The astute plating shop owner and/or manager is as committed to integrated waste minimization through systematic waste minimization and treatment as they are to "first time right" parts plating. Consistent plating quality, satisfied customers, and overall competitiveness are the indirect benefits of waste reduction efforts. This paper outlines the important steps for succeeding at wate minimization, waste minimization audit, and utilization of low technology source reduction options. These three steps are essential to lasting waste reduction efforts and are pre-requisites to closing the loop in a cost effective manner.

*** For copies of this paper please contact the author directly:**

Dr. D. Paul Piplani, CEF
Chemist
Acteron Corporation
851 Shasta Street
Redwood City, CA 94063
415/369-5217
Fax 415/364-9748

"ELECTROCHEMICAL PROCESSING FOR THE MINIMIZATION OF WASTES IN THE ELECTROPLATING INDUSTRY" - A CRITICAL REVIEW -

Prof. Dr. Andreas Moebius
Langbein-Pfanhauser Werke AG - D 4040 Neuss/Germany

The enormous demands set on the environmental protection result in an increasing number of processes in the electroplating industry and in the surface finishing technology in general, ensuring a minimization or even avoidance of effluents and sludge.

In this connection, the electrochemical processes of metal recovery and especially of the electrolysis are of great importance because metals are recovered in usable form or, in case of the electrolysis, the concentration of rinse water and its return is possible.

Electrochemical processes can easily be integrated into the electroplating process and in the PCB fabrication so that the formation of metal containing effluents can be avoided or drastically decreased. This is the so-called 'production integrated environmental protection'.

Many papers relate to this topic. These should not be repeated here or referred to, but the integration into the processes of waste avoidance and effluent treatment, resp., will be demonstrated by means of the electrochemical cell. Some examples will show the present state of the art.

For a long time it has been suggested to recover metals from relatively concentrated solutions in simple plate cells or to regenerate spent process solutions (etchants, pickle solutions etc.) in such a manner that they can be returned to the production process. That is relatively easy with regard to precious metals, silver, and copper.

In the case of base metals, however, some precautions have to be observed.

When considering the limiting values required for the discharge into public sewer systems it is obvious that these values cannot be realized by means of simple plate cells.

The reason for this is the transference number of materials. Without additional measures limiting current values are quickly reached with an increased hydrogen evolution instead of the required metal deposition.

An improvement of the material transference can be reached by:

- the turbulence of glass beads, added to the electrolyte which have a positive influence on the diffusion layer at the cathode. That is realized in the CHEMELEC-process.

- the use of porous flow through electrodes in the RETEC-process.

- the ENVIROCELL-process based on stationary particle cathodes with a large surface and a special construction following the concentration profile inside the cell.

- In the past, rotating cylinder electrodes, fluidized bed electrodes or moved bed electrodes have been introduced in pilot plants. The scale up of this type of electrodes is in preparation.

The abrasion from the electrodes, even from fixed bed electrodes of graphite particles, causes some difficulties and requires extensive measures for cleaning of the process solution.

Therefore, simple and cheap electrolytic equipments - without any diaphragms and membranes - are limited to the recovery of precious metals, copper, and sometimes nickel and zinc, from process solutions in closed loops and to relatively concentrated rinse waters from drag-out rinses, cascades or from concentrates from regenerations of ion exchange columns in closed loops.

As many electrolytes, etchants or pickle solution contain chlorides or completely consist of hydrochloric acid, another problem occurs at the direct electrolytic regeneration and metal recovery, resp. - this is the evolution of chlorine at the inert, chlorine-resistant anodes. Sometimes this can be avoided by using other anodic reactions, such as the oxidation of copper (I) to copper (II) in hydrochloric acid containing copper chloride etchants applied in the PCB industry or iron (II) to iron (III) in pickle solutions.

It is essential, however, that the process parameters, such as current density, flow rate, temperature etc. are exactly maintained.

As in the case of the FSL-cell or in similar processes, this is often combined with high pump and cooling capacities. Furthermore, these cells have a chlorine sensor which switches off the cell immediately as soon as chlorine is evolved.

Another possibility is to separate the anode from the chloride-containing electrolyte by cation exchange membranes and to operate the anode in a sulphate-containing sulphuric acid anolyte.

Common anodes evolving oxygen can be used. The selectivity of the known cation exchange membranes is not so high as to completely avoid the diffusion of chloride ions through the membrane.

That is, from the theoretical point of view, not possible with regard to the membrane transport processes.

In case of stagnant anolyte and open anode compartments chlorine forms and, thus, an odour nuisance cannot be prevented.

Rinse circulations, closed cells, and absorption of the evolved chlorine in alkaline solutions can solve this problem but result in higher costs. Similar problems exist in the electrode rinse circulation of electrodialysis equipments when they are used for the concentration of chloride containing rinse water.

A solution to this problem could be the use of special electrode coatings which are applied in a cell for the regeneration of hydrochloric acidic copper chloride etchants from the PCB industry connected with a so-called pre-electrolysis for the "oxygen compensation". This pre-electrolysis corrects the copper (II) content which resulted from the air oxidation of copper (I) to copper (II) during the etching process.

The complete recycling process is offered and supplied by Messrs. Hans Höllmüller Maschinenbau GmbH + Co., Herrenberg/Germany, a member of the Langbein-Pfanhauser Group.

Another fundamental question of membrane electrolyses is the life time of the expensive membranes. It has to be ensured, by suitable flow control, additives and cell design, that the pH-jump lies outside the membrane, thus avoiding the precipitation of insoluble compounds. Particularly multivalent cations can destroy the membrane structure irreversibly.

Furthermore, the constructional design of the cell is important in order to avoid high ohmic drop via the membrane and in the electrolyte (gas bubbles). The Hans Höllmüller GmbH + Co., Herrenberg/Germany supplies a new recycling process for the regeneration of peroxodisulphate-containing etchants. The equipment works with a moved particle cathode (rotating barrel type) for the deposition of the etched copper and a vertically arranged electrolytic cell using the gas lift principle for the reoxidation of sulphuric acid to peroxosulphuric acid in a membrane type cell.

Due to the gas lift principle the ohmic drop is reduced in the gas loaded gap between the membrane and the electrodes allowing a very compact design.

As already reported during the last SURFIN in Toronto, gas diffusion electrodes can also be used for saving energy in such processes. These electrodes have the advantage that they do not evolve any chlorine.

These few examples should demonstrate that electrochemical processes can easily be integrated into electroplating and surface finishing equipment , but it has to be ensured that all processes, the design of the cell,and all accessory aggregates are well adapted.

These measures often lead to relatively expensive and complicated electrolytic equipments. For that reason these processes should be supplied and installed by companies specializing in the field of electroplating technology.

The additional purchase and subsequent installation of the electrolysis process into existing electroplating plants is not the best way and sometimes resulted in disadvantages which could have been avoided.

That means that electrochemical processes should be an "integrated part of an electroplating line". Purchase and operation of electrochemical processes are not as easy as sometimes published.

EVALUATING THE ECONOMICS AND EFFECTIVENESS OF SOURCE REDUCTION OPTIONS IN METAL FINISHING

by

Matthew McCullough, P.E.
McLaren/Hart Environmental Engineering
16755 Von Karman Avenue
Irvine, California 92714

ABSTRACT

A series of simple experiments evaluates several dragout reduction and water conservation technique's effectiveness; a summary of potential cost savings is also presented. The results demonstrate that source reduction and water conservation are readily achievable in metal finishing operations. Dragout reductions and water conservation of 20 percent to over 90 percent are demonstrated using various techniques. Most of these techniques are simply and economically implemented and have broad application in other industries.

INTRODUCTION

Source reduction is the reduction or elimination of waste at the source. Source reduction measures include process modifications, feedstock substitutions, improvements in feedstock purity and administration, increases in process efficiency, and recycling within a process. Source reduction and water conservation are complementary programs that are easily implemented together. This paper discusses and compares techniques to reduce dragout and conserve water for metal finishing operations. The techniques illustrated here are broadly applicable throughout the coating industry. While absolute technique effectiveness can vary dramatically depending on workpiece shape, comparing results for simple shapes provides a relative measure of each technique's effectiveness.

Regulatory Background

The Federal "Hazardous and Solid Waste Amendments of 1984" (HSWA) required industry to implement source reduction and recycling programs. However, no substantial tracking or reporting requirements were imposed. Recently enacted legislation such as California's "Hazardous Waste Source Reduction and Management Review Act of 1989" (SB 14) and the Federal "Pollution Prevention Act of 1990" (PPA) require industry to prepare source reduction plans and reports for various chemicals and manifested wastes. Each act also enables the public to gain access to the information in these reports. The requirements of both bills are similar, although the PPA mandates more specific reporting information. In general, the following information is reported:

- Quantity of the chemical used or waste generated
- Source reduction practices
- Techniques to evaluate source reduction opportunities
- Percentage change in the amount of chemical used or waste generated from previous years.

Regulations affecting water usage are usually adopted only in times of water shortage. Industry in the Western United States is traditionally water conscious and has recently endured a long series of drought years. However, water quality issues have forced water conservation measures in areas throughout the world. In general, source

reduction and water conservation go hand-in-hand. Both programs, when implemented correctly, will effect an overall increase in process and production efficiency. Source reduction and water conservation programs can be implemented through the following general program:

Establish Goals and an Implementation Schedule. State goals and objectives in consistent and quantifiable terms over a realistic time period.

Assess Source Reduction and Water Conservation Opportunities. Inventory waste streams and water usage, evaluate each generating process, and develop alternatives based on technical and economic feasibility.

Track and Measure Progress. Establish systems for tracking progress to demonstrate results, meet regulatory requirements, and provide a basis for technology transfer inside or outside of the company.

DRAGOUT

Dragout is the volume of solution carried out of a process tank by a workpiece. This carryover is usually the major source of pollutants in plating shop wastes and can account for 50 to 90 percent of solution losses. Replacing raw materials and treating and disposing of wastes are costly (see Figure 1); therefore, the economics of shop and operational modifications to reduce dragout are attractive.

FIGURE 1: Dragout Costs[1]

Chemical	Cost ($/lb)			
	Replacement	Treatment[2]	Disposal[3]	Total
Nickel				
as $NiSo_4$	1.02	0.38	0.23	1.63
as $NiCl_2$	1.39	0.39	0.32	2.10
Zinc Cyanide as $Zn(CN)_2$				
using Cl_2 for cyanide oxidation	1.89	0.96	0.34	3.19
using NaOCl for cyanide oxidation	1.89	2.05	0.34	4.28
Chronic Acid as H_2CrO_4				
using SO_2 for chromium reduction	1.05	0.64	0.43	2.12
using $NaSO_3$ for chromium reduction	1.05	0.92	0.43	2.40
Copper Cyanide as $Cu(CN)_2$				
using Cl_2 for cyanide oxidation	2.61	0.96	0.34	3.91
using NaOCl for cyanide oxidation	1.61	2.05	0.34	2.40
Copper Sulfate for $CuSO_4$	0.75	0.38	0.23	1.36

[1] Source adapted from Cushnie Electroplating Wastewater Pollution Control Technology
[2] Based on treatment at a concentration of 100 mg/l in wastewater
[3] Based on disposal at 4 percent solids and $0.10/gal

Dragout reduction is accomplished through two general approaches:

- Modifications to reduce dragout before rinsing
- Water conservation measures to recycle dragout to the plating bath.

Each technique is discussed below.

Modifications to Reduce Dragout Before Rinsing

Dragout loss principles (before rinsing) can be summarized by 10 basic rules (Kushner):

- Keep the concentrations of all dissolved materials at the minimum value necessary to proper bath operation.

- Do not add anything to a plating bath that does not perform a necessary function in the bath.
- Operate the bath as hot as possible.
- Use conducting salts that give the greatest density and the smallest viscosity per unit concentration.
- Use an effective wetting agent in the plating bath.
- When using a fixed time period for withdrawal and drainage, use the largest part of the period for withdrawal.
- Rack solid objects to maximize vertical surfaces.
- Do not rack objects directly above each other; this lengthens the drainage path.
- Tilt all solid objects with plane or singly curved surfaces so that drainage flow is consolidated.
- Rack every object to minimize dragout; every solid object, except a sphere, has at least one position where dragout will be at a minimum.

These rules can be consolidated into four general classifications:

- Velocity of workpiece withdrawal
- The geometry of the workpiece and the position on the rack or fixture
- The drainage time allowed over the process tank
- The viscosity, density, and temperature of the process solution.

Withdraw the workpiece slowly. The faster a piece is removed from a bath, the thicker the surface film and the greater the dragout volume. This effect is so significant that USEPA recommends that the majority of the allowed time for withdrawal and drainage be used for withdrawal only (USEPA, 1982). Decreasing withdrawal velocity or increasing drainage time decreases the volume of solution retained by the part. Since time is directly related to production rates, reducing the dragout volume initially adhering to the part is more advantageous than attempting to drain a large volume from the part.

The velocity of workpiece withdrawal is least controllable with hand-operated lines. On automated lines, withdrawal can be slowed, typically without production loss, by changing the machine motion cycle. No standard rule is available to predict accurately the amount of dragout that can be saved by a given reduction in withdrawal speed; the degree of savings that may be expected depends on specific operation.

Rack the workpiece for maximum drainage. Proper racking of parts is the most effective way to reduce dragout. Improperly racked workpieces can have 5 to 10 times the dragout of properly racked work (Pinkerton, 1984). Improperly racked workpieces suffer because of possible surface damage from insufficient rinsing and damage to subsequent solutions from drag-in.

Pieces should be racked so that no cupped recesses are formed, the longest dimensions are horizontal, and the major surfaces are vertical; they should be oriented so that the smallest surface area of the piece leaves the bath surface last; and each part should drain freely without dripping onto another. Every piece has at least one position where dragout will be at a minimum.

Allow adequate drainage time. Drainage time can considerably impact dragout volumes. A drain time of at least 10 seconds has been shown to reduce dragout by more than 40 percent over immediate rinsing (Bosshardt, 1987).

Most shops make some attempt at drainage before transferring the parts to another bath. Often, however, pieces are transferred while they are still slowly dripping. In hand lines, a drain bar can be placed over the process tank where work can be suspended to facilitate drainage. Hanging and removing racks from the drain bars ensures an adequate drain time; slightly jostling the racks helps shake off adhering solution.

Set solution operating parameters to minimize viscosity and surface tension. Increasing solution viscosity results in a thickening of the film clinging to the workpiece. This increases dragout volume, and that volume will contain more chemicals and complicate rinsing. The temperature of a process solution directly influences viscosity and therefore dragout. Liquid viscosity decreases with temperature and can be described by the Andrade correlation (Reid, et al., 1977):

$$\mu_L = Ae^{B/T} \qquad [1]$$

Where:

- μ_L = Solution viscosity
- A,B = Andrade constants
- T = Solution temperature

The viscosity of water is shown in Figure 2. Since most plating solutions are primarily water, this figure can be used where necessary for viscosity calculations.

Figure 2: Viscosity vs. Temperature

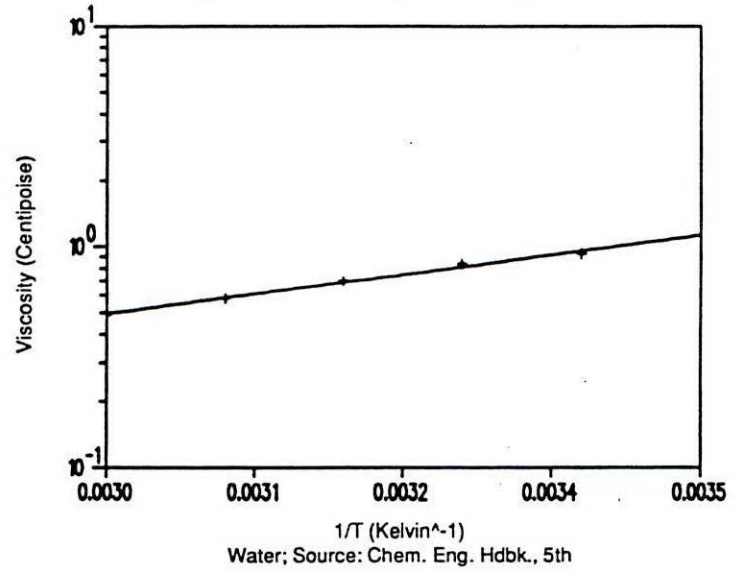

The Andrade equation requires two viscosity temperature data points to determine the constants. If only one data point is available, one way to extrapolate these values is to use the Lewis-Squires approximation shown in Figure 3. Lewis-Squires is based on empirical data that demonstrate that the variation in viscosity with temperature seems to depend primarily on the value of the viscosity. Use the technique by locating the known viscosity value on Figure 3 and then extending the abscissa by the required number of degrees to find the new value of the viscosity.

Some data (Meltzer, 1989) suggest that workpiece drainage dependence on viscosity is approximately described by:

$$Dr = C_1 \mu_L^{-1/2} \qquad [2]$$

Where:

- Dr = Percent drainage
- C_1 = Constant
- μ_L = Solution viscosity

This equation is plotted in Figure 4 for water and a 10-second drainage time. Combining this equation and the Andrade equation results in the following equation for the effect of temperature on drainage:

$$Dr = C_1 e^{-B/ZT} \qquad [3]$$

Surface tension affects dragout similarly to viscosity. To reduce dragout, gravity-induced drainage must overcome the adhesive force between the solution and the metal surface. Wetting agents can be used to lower surface tension of process baths. Lowering the surface tension reduces the amount of work required to remove the liquid and reduces the edge effect (the bead of liquid adhering to the edges of the part).

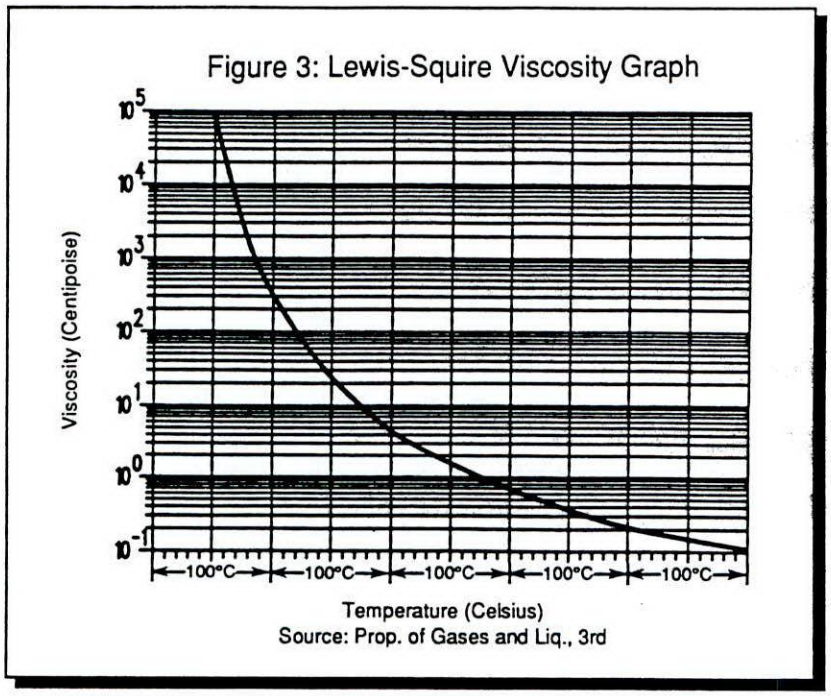

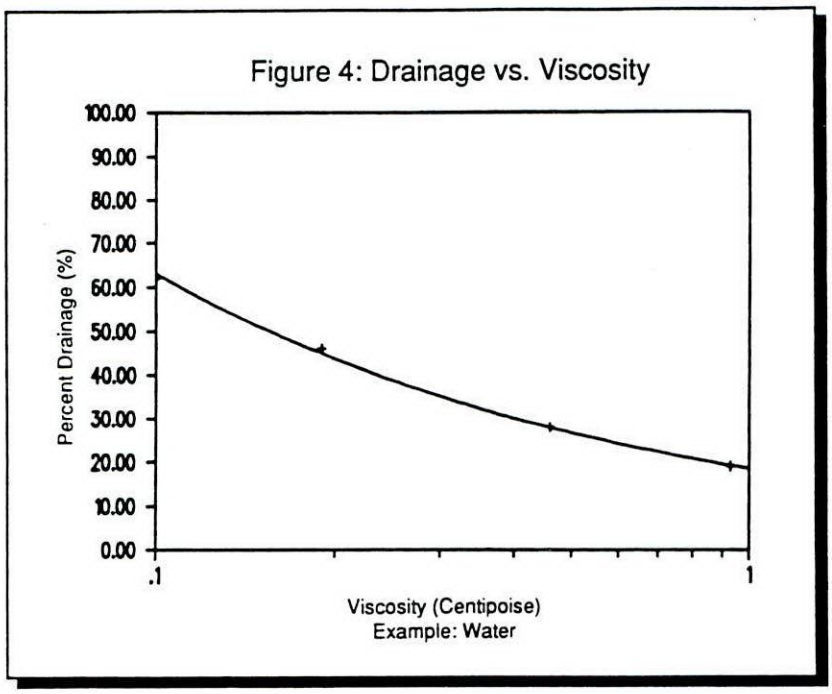

Water Conservation Measures

Water represents the most frequently used chemical in metal finishing. Water conservation designs frequently focus on reducing the amount of water used in the system. However, without sufficient dragout reduction, the quantity of chemicals released to the sewer or treatment plant will not be reduced.

One of the simplest ways to reduce wastewater treatment costs is to reduce the amount of wastewater being treated. Water conservation techniques can usually reduce rinsewater flows by 50 percent or more without impairing rinsability. Reducing flow results in smaller and less expensive equipment; smaller equipment usually reduces the amount of treatment chemicals required and improves efficiency of treatment reactions. Rinsewater flow reduction will have the following benefits:

- Minimizes the size of pollution control equipment

- Maximizes the final effluent concentration levels required to meet permit requirements
- Allows the use of less sophisticated equipment
- Reduces chemical, pumping, mixing, and maintenance costs
- Reduces water costs
- Improves wastewater treatment reaction efficiencies
- Reduces the share of municipal treatment system cost.

Three general principles in rinsing should be considered to make water conservation modifications more successful.

Prolong rinse times for as long as possible. Rinse time has a significant effect on rinse efficiency. For example, for rinse times of 1 to 6 seconds, about 50 percent of the bath solution is drained from the part. If another 10 seconds are added, 70 percent of the bath solution is drained (Meltzer, 1989).

Use deionized water in rinsing operations. Natural contaminants found in water used for production processes can contribute to the volume of waste generated and decrease rinse water efficiency. Any contaminant other than pure water must be removed through purification or disposal and can contribute to waste volumes substantially. This is especially true with hydroxide precipitation and ion exchange systems used for pretreatment. Neither technology discriminates between heavy metals and other constituents. In the case of a hydroxide sludge, as much as 90 percent (dry weight) can be from precipitated hard water ions and other nonhazardous materials (Clarence, 1979).

One concern involved in the use of deionized water is the large volume of reject water from the deionization equipment. However, reject water can be used for a number of secondary and tertiary uses, such as cooling, or as process water for ventilation scrubbers.

Use properly designed rinse tanks. Inefficient rinsing known as "short-circuiting" occurs when only a small portion of the water used actually passes over the product. This reduces tank efficiency. Flow patterns can be studied within a tank using a tracer dye. Tank baffles or relocation of the inlet and outlet nozzles may be required.

Dragout loss from bath solutions and water usage can be reduced significantly through the following water conservation techniques:

Use static rinses where possible. Rinse tanks with no inflow or outflow are called "static," "still," or "dead" rinse tanks. Dragout reduction is accomplished by dilution. The dilution achieved will significantly reduce the amount of water used in downstream rinsing. For a well-mixed tank, the rinse tank dragout concentration is equal to the rinse tank concentration. Therefore, if the rinse tank concentration is kept at 20 percent of the bath concentration, the overall reduction in dragout is 80 percent. The reduction in dragout into the

Figure 5: Evaporation Rate from Bath

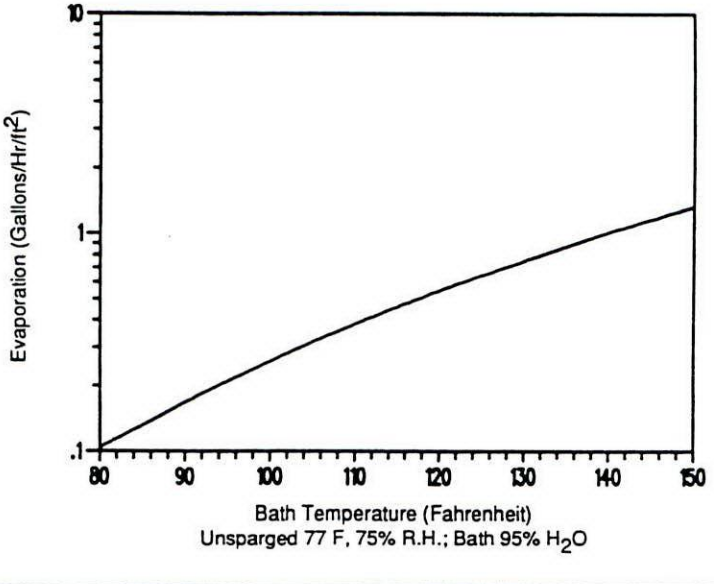

final rinse tank will result in a corresponding decrease in required final rinse water. Concentrations of plating solutions in the static rinse will increase over time until some or all of the rinse is used to replenish the plating bath, and fresh water is added to replenish the static rinse.

As a rule, static rinses are only applicable to plating baths that have a considerable amount of surface evaporation. If the plating bath temperature ranges from 130 °F (55 °C) to 150 °F (65 °C), the evaporation rate is often high enough to use the static rinsate for makeup solution. A plot of water evaporation rates versus temperature is shown in Figure 5.

Figure 6: Evaporation Rate from Bath

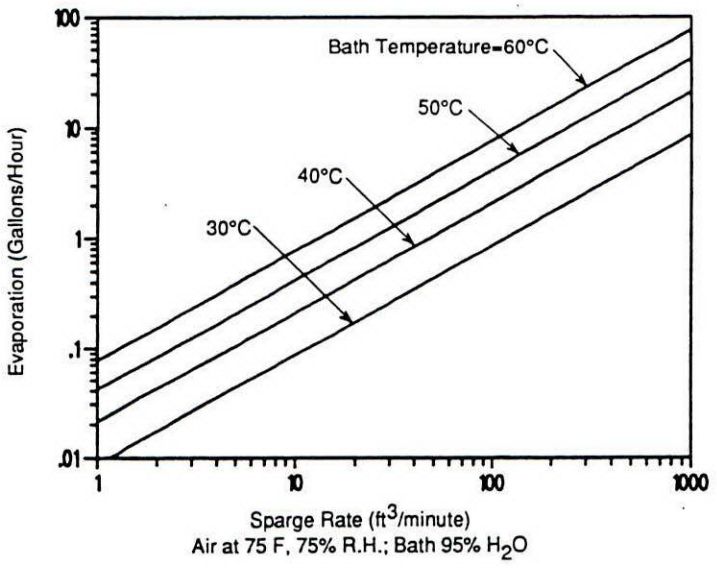

In cooler baths, an evaporator may have to be installed. Evaporators can also be used to concentrate the process chemicals from static rinses. A distinct disadvantage of evaporative techniques is that calcium and magnesium salts originally in the rinse water may be present. This may result in a more rapid deterioration of the bath solution. This problem can be alleviated using deionized water.

Air sparging can be used to increase evaporation rates (see Figure 6). Air sparging will increase bath mixing efficiency as well. However, care should be taken with air sparging because air emission rates of heavy metals will increase.

Figure 7: Counterflow Rinsing

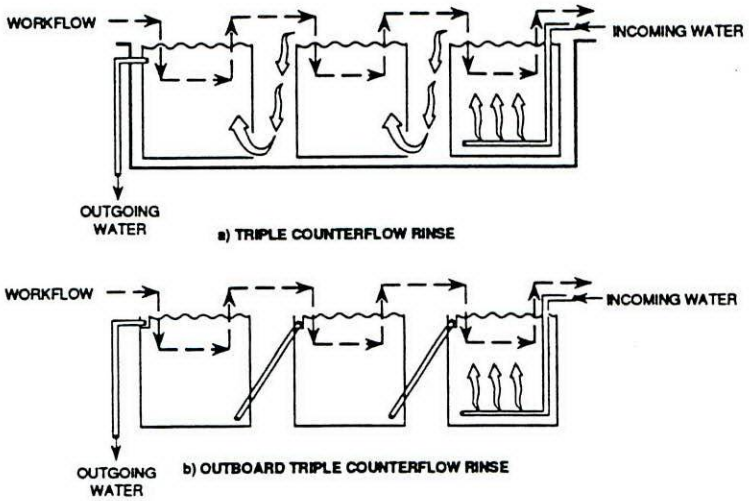

For a well-mixed rinse tank, the required bath evaporation ratio is:

$$E_R = C_p/C_r \quad [4]$$

Where:

E_R = Evaporation ratio, gallons per gallon of dragout

C_p = Concentration of process solution

C_r = Maximum concentration in static rinse tank

Use counterflow rinsing when feasible. Counterflow rinsing is one of the most common water conservation techniques applied in metal finishing. It increases the

contact time between the workpiece and the rinse, thereby increasing rinse efficiency. Fresh water feed is only introduced into the final rinse tank. The overflow from each tank becomes the feed for the tank preceding it in the workflow. This is illustrated in Figure 7. Dragout entering the final rinse tank will be significantly reduced, and the volume of rinsewater required will be reduced by the same degree. Hence, the concentration of dissolved solids decreases rapidly from the first to the last tank.

If all workpieces are completely rinsed and each rinse tank is well mixed, the volume of rinsewater required is:

$$R = (C_p/C_n)^{1/n} \qquad [5]$$

Where:

R = Ratio of rinse water volume to dragout volume
C_p = Concentration of process solution
C_n = Concentration required in last rinse tank
n = Number of rinse tanks

Note: This model does not work well when R falls below 10. Also, the predicted value of R will not be achieved unless there is sufficient rinse time and agitation in the rinse tank.

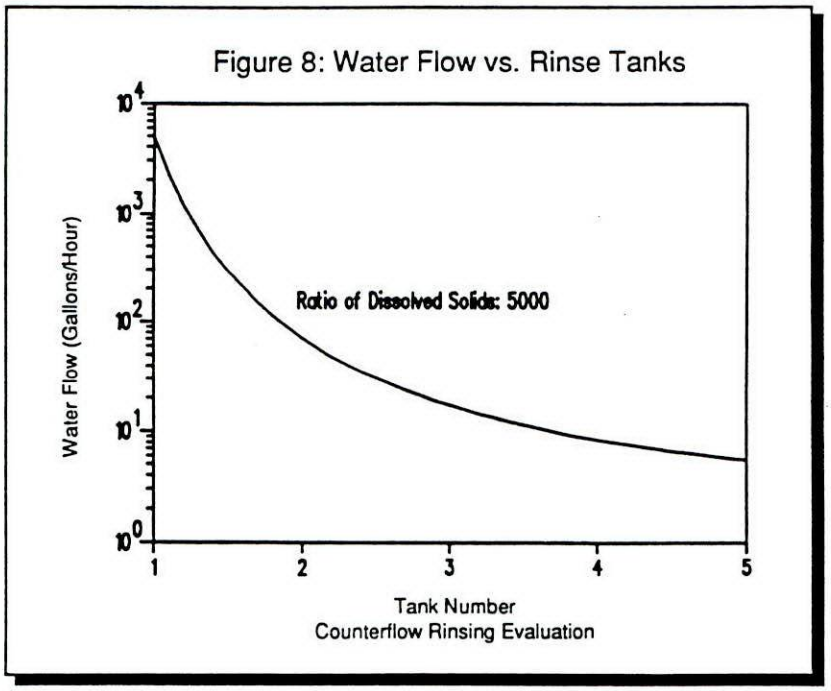

Figure 8 shows the volume of rinsewater required as a function of the number of counterflow rinse tanks for a ratio of dissolved solids of 5,000. For example, if a plating solution contains 250,000 mg/l of dissolved solids and the final rinse must contain 50 mg/l, the ratio of dissolved solids is 5,000. For a single rinse tank, 5,000 gallons of rinse water are required for every gallon of dragout. For a three-rinse-tank counterflow system, only 17 gallons are required for the same rinse specifications.

Use spray nozzle rinsing when evaporation rates are high. Spraying water directly onto a workpiece can rinse off contaminants, using considerably less water than would immersion. Spray rinsing uses between one-eighth and one-fourth the volume of water that an immersion rinse uses (USEPA, 1982). The benefit comes from reducing the concentration in the dragout. For example, if the dissolved solids concentration was reduced from 200,000 mg/l to 100,000 mg/l, the chemical loss and subsequent water usage would be reduced by 50 percent. Spray rinsing is highly effective for flat workpieces; objects with internal surfaces will be rinsed less effectively.

Spray rinsing can be performed in conjunction with an immersion rinse. This permits lower water flows in the rinse tank, since much of the dragout is removed.

A variation of the spray nozzle is the fog nozzle. A fog nozzle uses water and air to produce a fine mist. This uses less water than a conventional spray nozzle. Fog nozzles can be used directly above bath solutions to rinse workpieces as they are withdrawn.

Use air knives when evaporation rates are low. Air knives are high-velocity air that mechanically scours dragout from the workpiece. They can be used like spray rinses, particularly when surface evaporation rates are low. The benefit comes from the percent reduction in dragout. The concentration of the dragged-out solution remains the same.

Care must be taken when using air knives because the workpiece may dry out, condensing salts on the surface. The workpiece can be prevented from drying by using a "foggy" air knife. A foggy air knife uses a slight amount of water to form a high-velocity fog that wets the workpiece.

EXPERIMENTAL PROCEDURES

The effectiveness of various dragout reduction and water conservation techniques was investigated. For the purposes of this investigation, water conservation effectiveness was assumed to be roughly the same as dragout reduction effectiveness; this assumption is generally valid for most applications. Conductivity measurements quantified dragout amounts. Conductivity is directly proportional to concentration and is therefore an indirect measurement of concentration (Smedley, 1963). A Cambridge Scientific Instruments Model 301353 Temperature/pH/Conductivity meter was used for all measurements. All measurements (except for temperature measurements) were made at 75 °F (24 °C).

For viscosity-temperature experiments, the meter was used to measure temperature, and the corresponding viscosity was acquired from available data. The probe was temperature calibrated using a mercury thermometer. All solutions were heated indirectly to prevent contamination.

All rinsing and evaluated techniques used deionized water. The deionized water was measured initially at 10μS/cm.

The workpiece geometries evaluated were:

Flat Stock 1: Rectangular in shape measuring 3 inches (7.6 cm) by 1.5 inches (3.8 cm) by 0.125 inch (0.3 cm). The piece was racked with the longest side oriented vertically.

Flat Stock 2: A T-shaped flat piece measuring 3 inches (7.6 cm) in each direction with each arm 1.5 inches (3.8 cm) by 0.125 inch (0.3 cm). The piece was racked with the longest surface oriented vertically.

Hollow Sphere: A hollow sphere measuring 2 inches (5 cm) in diameter and 0.125 inch (0.3 cm) thick. The sphere contained one drain hole 0.5 inch (1.2 cm) in diameter and one drain hole 0.125 inch (0.3 cm) in diameter. The drain holes were opposed to one another. The sphere was racked with the larger drain hole oriented downward.

For each experiment, the following basic method was followed:

Control Measurements:

(1) The workpiece was immersed in a copper sulfate plating bath and withdrawn in approximately 1 second.

(2) The workpiece was immersed in approximately 35 ounces (1 liter) of deionized water with an

initial conductivity of 10 μS/cm.

(3) The conductivity of the deionized water was measured to quantify uncontrolled dragout.

(4) The workpiece and the conductivity meter were thoroughly rinsed in deionized water.

Experiment:

(1) The workpiece was again immersed in a copper sulfate plating bath and withdrawn in approximately 1 second.

(2) Individual dragout reduction or rinsing techniques were used on the workpiece.

(3) The workpiece was immersed in approximately 35 ounces (1 liter) of deionized water with an initial conductivity of 10 μS/cm.

(4) The conductivity of the deionized water was measured to quantify controlled dragout.

(5) The difference in uncontrolled and controlled conductivity values was calculated as the percent dragout reduction.

RESULTS

The results for each experiment are presented in Figures 9 through 16. All results were regressed with standard curve fitting programs using the least-squares method. This resulted in some values of dragout reduction that are not possible. However, the curves are provided to illustrate the general trend of each technique.

Figure 9: Orientation Effects

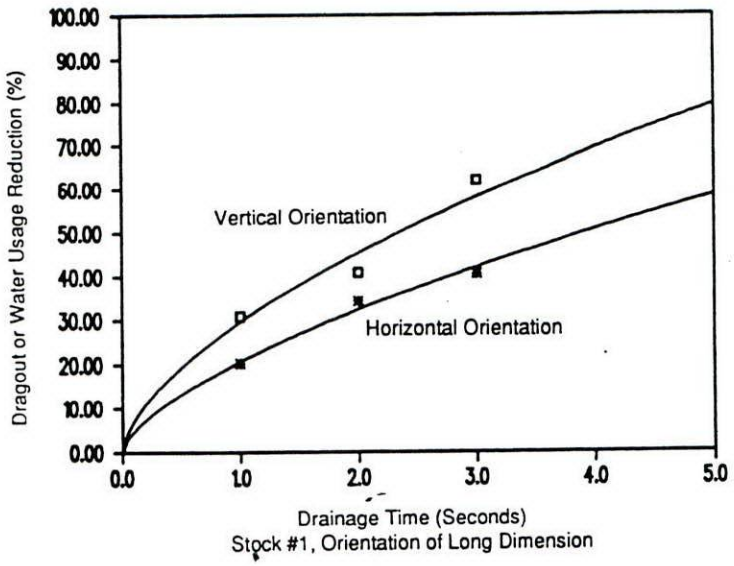

Orientation versus Drainage Time

The effect of orientation versus drainage time was evaluated using flat stock 1, orienting the long dimension both vertically and horizontally. Results are shown in Figure 9.

Vertical orientation resulted in a dragout reduction of over 20 percent after 5 seconds, as expected. This experiment, although limited in scope, is useful in demonstrating the relative effect of piece orientation.

Drainage versus Drainage Time

The effect of drainage time was evaluated for each workpiece. Results are shown in Figure 10. Each piece was

racked with the major surface oriented vertically. The sphere was racked with the larger drain hole oriented down.

Increasing drainage time from 3 seconds to 10 seconds resulted in a dragout reduction of over 20 percent for flat stock and nearly 30 percent for the hollow sphere. The effect of drainage time is more pronounced for the sphere because of fluid retention within the part. After 5 seconds the sphere has drained of standing fluid. This effect skews the data for the sphere slightly.

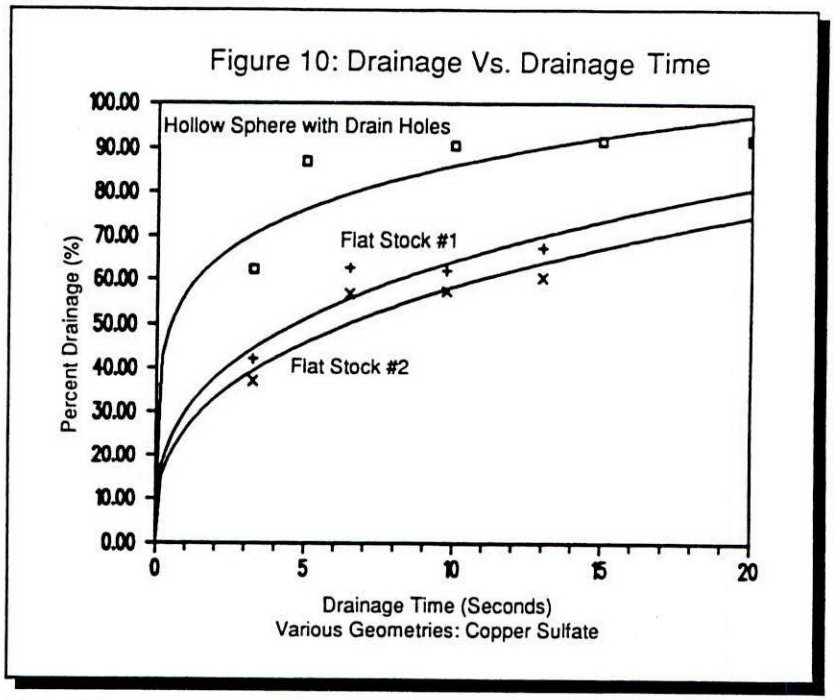

This is one of the most effective and easiest to implement of all the techniques. In hand-operated lines, the installation of drain bars can enhance the implementation of this technique.

Viscosity Temperature Effect

The effect of temperature on solution viscosity and dragout for copper sulfate was evaluated for flat stock 1. Results are shown in Figures 11 and 12. The piece was rinsed as uncontrolled. The solution temperature was measured, and the corresponding viscosity values were acquired from available data.

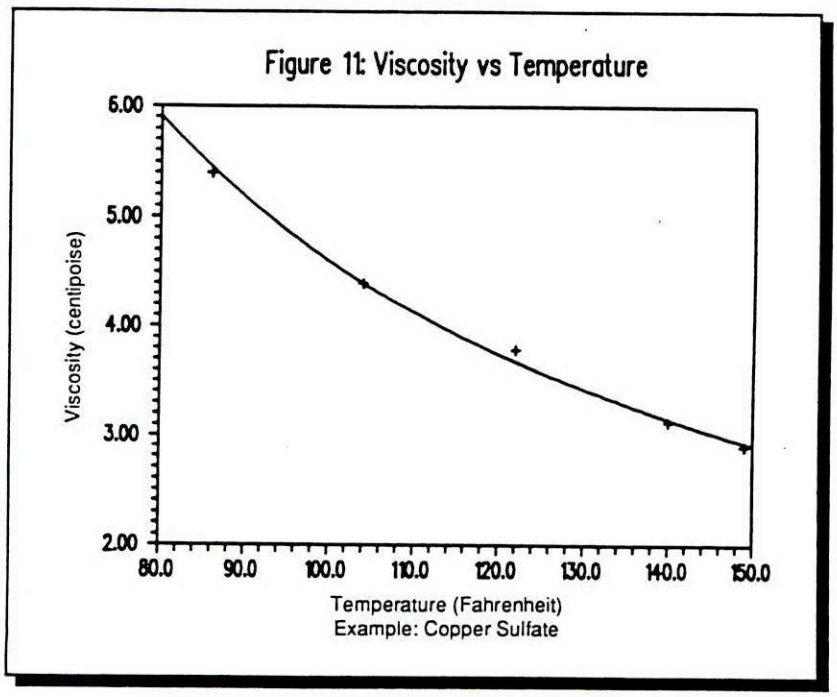

For copper sulfate, increasing the temperature from 100 °F (38 °C) to 140 °F (60 °C) decreased dragout by 12 percent. Raising the temperature of a water-like solution from 100 °F (38 °C) to 140 °F (60 °C) lowers the solution viscosity by 30 percent. This results in a corresponding dragout reduction of approximately 17 percent.

Static Rinse Performance

The effect of a series of static rinses was evaluated using a series of 16-ounce (1-liter) rinse baths. Results are shown in Figure 13. The effect was evaluated for flat stock 1 and the hollow sphere. Each piece was rinsed as uncontrolled. The contact time in each rinse was 10 seconds.

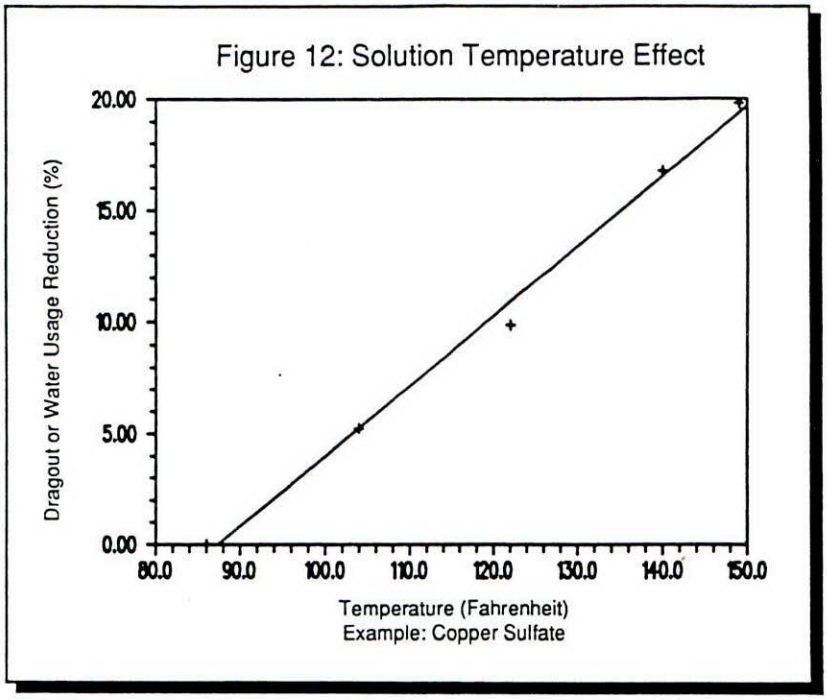

Static rinsing resulted in a dragout reduction of approximately 80 percent for both flat stock and the hollow sphere for a single static rinse. The second and third rinses had increasing incremental effects on the sphere but little effect on the flat stock. The flat stock results can be partially attributed to low initial dragout and resolution of the conductivity meter. The results for the sphere show some influence of the small size (1 liter) of the rinse baths.

Spray Rinse Performance

The effect of spray rinsing was evaluated for flat stock 1 and the hollow sphere. Results are shown in Figure 14. Each piece was rinsed as it was withdrawn from the bath solution.

Spray rinsing resulted in a dragout reduction of over 30 percent for flat stock and only 5 percent for the hollow sphere, after 10 seconds, when compared to drainage alone. The effect of spray rinsing on the sphere is less pronounced because of internal surfaces that are not accessible to the spray.

Hard chromium baths are excellent candidates for spray rinsing. Hard chromium plating is unique in that parts are plated for hours or days rather than minutes as in most plating processes, and the evaporation rates usually far exceed dragout rates. If a part can be rinsed adequately above the tank, subsequent rinse steps can be eliminated and there will be zero discharge from hard chromium plating.

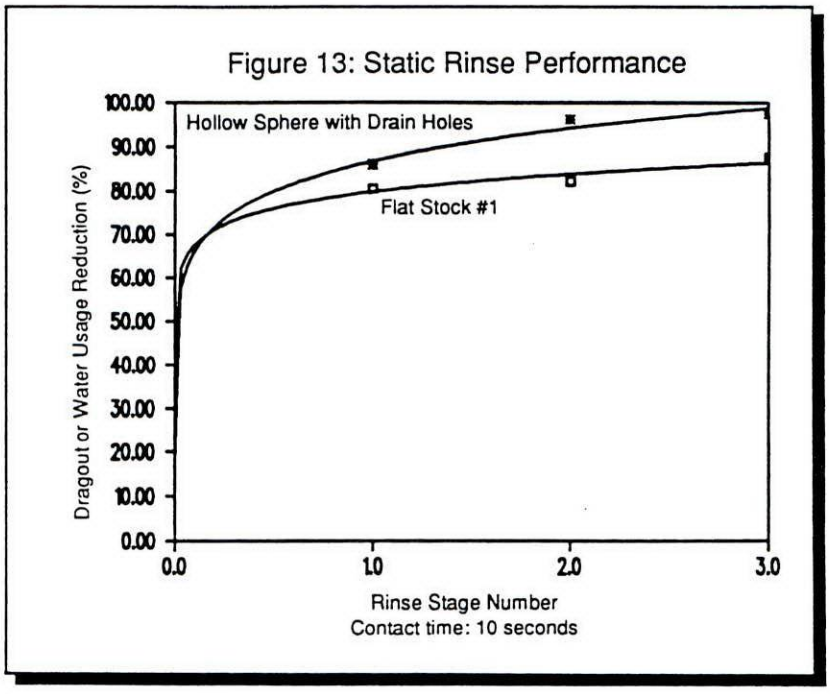

Air Knife Performance

The effect of an air knife was evaluated for flat stock 1 and the hollow sphere. Each piece was scoured as it was withdrawn from the bath solution. Results are shown in Figure 15. No attempt was made to prevent the piece from drying out.

Use of an air knife resulted in a dragout reduction of over 30 percent for flat stock and only 5 percent for the hollow sphere,

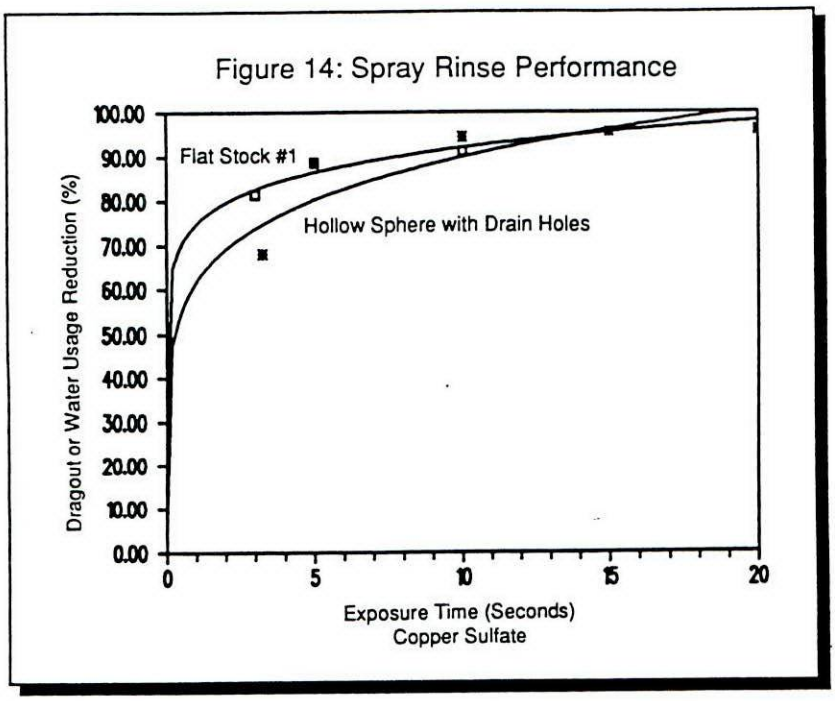

after 10 seconds, when compared to drainage alone. The effect of the air knife on the sphere is less pronounced because of internal surfaces that are not accessible to the spray (as demonstrated in the spray rinsing experiment).

"Foggy" Air Knife Performance

The effect of a foggy air knife was evaluated for flat stock 1 and the hollow sphere. Each piece was scoured as it was withdrawn from the bath solution. Results are shown in Figure 16.

The foggy air knife resulted in a dragout reduction of over 40 percent for flat stock and only 10 percent for the hollow sphere, after 2 seconds, when compared to drainage alone. Again, the effect of the foggy air knife on the sphere was less pronounced because of internal surfaces that were not accessible to the spray, as demonstrated previously. However, the foggy air knife had the greatest effect of the spray rinsing or air knife techniques. This is due to the double action of the air reducing the amount of dragout and the fog diluting the dragout that is left on the piece.

Cost Savings

Cost savings calculations were based on a theoretical small shop plating 3,000 square feet per month each of $CuSO_4$ and $Cu(CN)_2$. The total dragout costs for each solution were \$1.36 and \$5.00 per pound, respectively (see Figure 1). Dragout was then calculated as approximately 100 pounds per month at a cost of \$1,632 to \$6,000. Savings were calculated using technique efficiencies presented in this section. Cost savings for each dragout reduction technique analyzed are shown in Figure 17.

All the techniques discussed can be economically implemented in specific process lines. Careful evaluation of your particular needs and requirements will determine the appropriateness of implementing

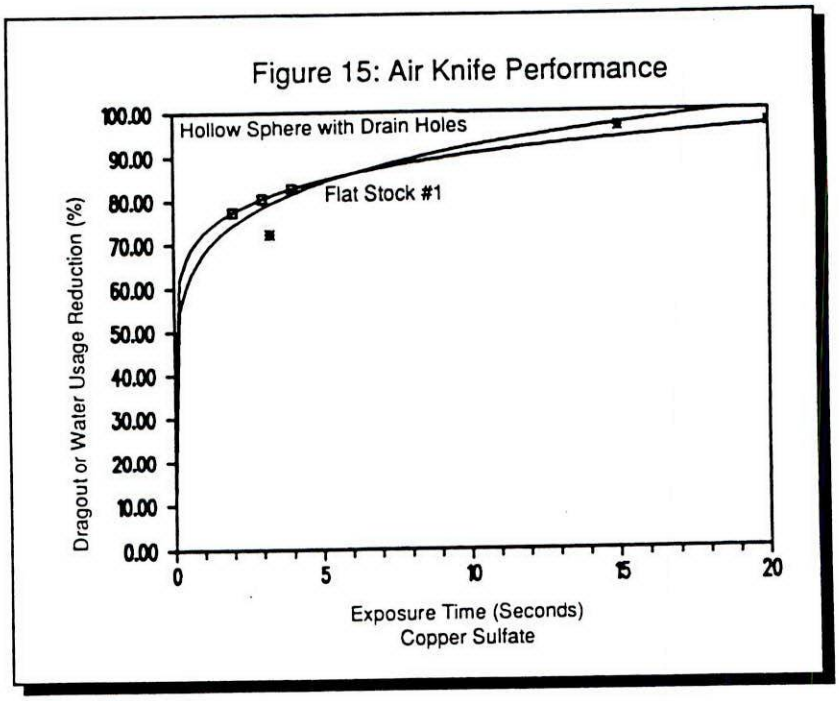

each technique. Several techniques are almost universally applicable.

The foggy air knife is appropriate for most situations and is very economical. The extremely low volume of water used diminishes the need for high bath temperatures. The effect of both dragout volume and concentration reduction leads to high efficiency and a speedy payback period.

Static rinse tanks and air knives are very effective in reducing dragout and thus have a short payback period. Careful process evaluation will determine whether these techniques are appropriate for dragout reduction in a particular shop.

Figure 16: Foggy Air Knife Performance

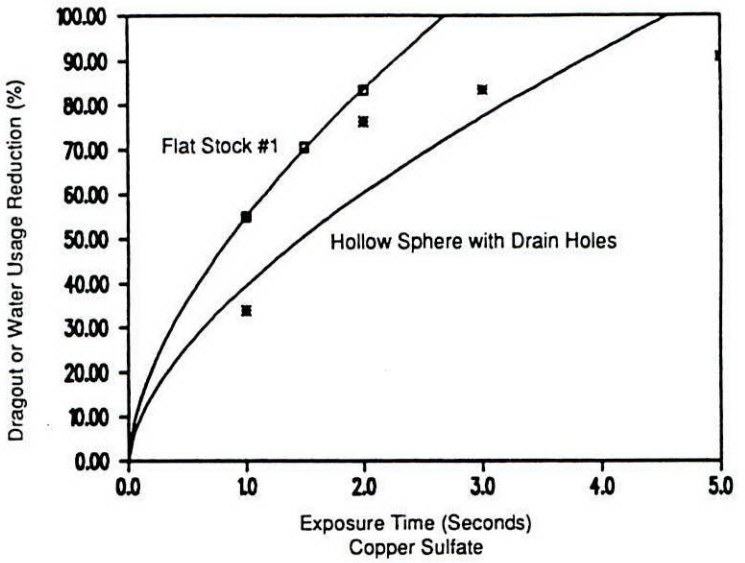

Spray rinsing and increased solution temperature should be closely evaluated prior to implementation. The primary factors influencing implementation are workpiece geometry and solution value. Complex geometries are less amenable to spray rinsing, and solution value universally affects the payback period.

CONCLUSIONS

Implementing a source reduction program can provide significant long-term economic and environmental benefits. The results presented in this paper demonstrate that source reduction is readily achievable in metal finishing operations.

FIGURE 17: Savings From Metal Finishing Source Reduction And Water Conservation[1]

Source Reduction Technique	Dragout Savings ($/yr)		Capital Cost ($)	Payback Period (months)
	Simple Geometry	Complex Geometry		
Adequate Drainage Time	326 - 1,200	490 - 1,800	0	0
Increased Solution Temperature	196 - 720	196 - 720	700[2]	12 - NONE
Static Rinsing (1 tank)	1,306 - 4,800	1,306 - 4,800	1,000	3 - 9
Spray Rinsing	490 - 1,800	82 - 300	200	1 -29
Air Knife	490 - 1,800	82 - 300	125	0.5 - 18
Foggy Air Knife	653- 2,400	162 - 600	125	0.5 - 9

[1] See "Results" for a complete discussion of the basis calculations
[2] Annual energy costs to heat a 100 CFM sparge bath to 140 °F at $0.38/10^6 BTU

Most of these techniques are simply and economically implemented and have broad application in other industries. Maximizing the effectiveness of a source reduction program can be accomplished by addressing some issues in advance:

Proper operator training can significantly decrease operating costs. The easiest way to reduce dragout is through proper racking and drainage. This technique can be easily implemented by the shop staff. Proper training will ensure that the most effective technique is followed.

Careful process evaluation will minimize overall costs. The benefits from implementing a source reduction program far outweigh the costs involved. A careful predesign evaluation process will prevent problems (such as bath contamination) and will minimize shop layout and construction modifications. Careful process evaluation, data collection, and process control are necessary to properly design these systems. All elements of the process, including cleaning and etching solutions, must be predesign considerations.

ACKNOWLEDGEMENT

I would like to thank Mr. Ron Holley, President, and Mr. Dick Mead, Facilities Manager of PSAirmotive, a division of USAir, Inc., for the use of their facilities and for their assistance. This paper would not have been possible without their help.

REFERENCES

1. Bosshardt, R., Reducing Dragout in Copper and Tin/Lead Plating, Minnesota Technical Assistance Program, 1987.

2. Brimi, M.A., and J.R. Luck, Electrofinishing, American Elsevier, New York, 1965.

3. California Department of Health Services, "Reducing California's Metal-Bearing Waste Streams", August 1989.

4. Chang, L.Y., and B.J. McCoy, "Alternative Waste Minimization Analyses for the Printed Circuit Board Industry: Examples for Small and Large Manufacturers," Environmental Progress, 10(2): p. 110-121.

5. Clarence, R., "Methods and Technologies for Reducing the Generation of Electroplating Sludges," Proceedings: Second Annual Conference on Advanced Pollution Control for the Metal Finishing Industry, American Electroplater's Society, 1979.

6. Cushnie, G.C., and A.S. Goldfarb, Removal of Metals from Wastewater, Noyes Publications, New Jersey, 1984.

7. Cushnie, G.C., Jr., Electroplating Wastewater Pollution Control Technology, Noyes Publications, New Jersey, 1985.

8. Dagdigian, J.V., Wastewater Flow Minimization, private communication, 1990.

9. Foecke, T.F., "Source Reduction Opportunities in the Plating Industry," Proceedings: Metal Waste Management Alternatives: Minimizing, Recycling, and Treating Hazardous, Metal Wastes, Pasadena, Californi, September 12-13, 1989.

10. Freeman, H. (Ed.), Hazardous Waste Minimization, McGraw-Hill, New York, 1990.

11. Kushner, J.B., Water and Waste Control for the Plating Shop, Garner Publications, Cincinnati, Ohio, 1976.

12. Meltzer, M.P., Reducing Environmental Risk: Source Reduction for the Electro Plating Industry, 1989, Ph.D. Thesis, School of Public Health, UCLA.

13. Pinkerton, H.L., "Rinsing," Electroplating Engineering Handbook, 4th Edition, L.J. Durney (Ed.), Van Nostrand Reinhold, New York, 1984.

14. Reid, R.C., Prausnitz, J.M., and T.K. Sherwood, The Properties of Gases and Liquids, 3rd Edition, McGraw-Hill, New York, 1977.

15. Rittmeyer, R.W., "Prepare an Effective Pollution Prevention Program," Chemical Engineering Progress, 87(5): p. 56-62, 1991.

16. Smedley, S.I., The Interpretation of Ionic Conductivity in Liquids, Plenum Press, New York, 1980.

17. Steward, F.A., and L.E. Lancy, "Minimizing the Generation of Metal-Containing Waste Sludges", Proceedings: First Annual Conference on Advanced Pollution Control for the Metal Finishing Industry, Lake Buena Vista, Florida, January 17-19, 1978.

18. Tallmadge, J.A., and C. Gutfinger, "Entrainment of Liquid Films," Industrial and Engineering Chemistry, 59(11): p. 18-34.

19. U.S. Environmental Protection Agency, In-Process Pollution Abatement: Upgrading Metal-Finishing Facilities to Reduce Pollution, July 1973.

20. U.S. Environmental Protection Agency, Environmental Pollution Control Alternatives: Economics of Wastewater Treatment Alternatives for the Electroplating Industry, June 1979.

21. U.S. Environmental Protection Agency, Draft Development Document for the Metal Finishing Point Source Category, May 1980.

22. U.S. Environmental Protection Agency, Summary Report: Control and Treatment Technology for the Metal Finishing Industry - In-Plant Changes, January 1982.

23. U.S. Environmental Protection Agency, Guides to Pollution Prevention: The Printed Circuit Board Manufacturing Industry, June 1990.

Silver Recovery with Ion Exchange and Electrowinning

John Lindstedt - President
Artistic Plating Company, Inc.
405 West Cherry Street
Milwaukee, Wisconsin 53212

Michael Doyle, P.E. - Senior Project Manager
Triad Engineering Incorporated
325 East Chicago Street
Milwaukee, Wisconsin 53202

Silver cyanide complexes in wastewater from precious metals electroplating operations can be quite problematic, as the complexed cyanide is somewhat resistant to oxidation by conventional alkaline chlorination. Furthermore, silver is a valuable metal with a high market value and typical precipitation and clarification techniques do not readily allow recovery of the metal. It has long been recognized that ion exchange systems can be utilized to remove the silver cyanide complex from electroplating rinsewater. These metal complexes are strongly retained by anion resins and are difficult to remove with conventional strong base regeneration, so that often the exhausted resin is simply shipped off site for silver recovery by incineration, thereby resulting in high operating costs due to resin replacement. This paper will present the results of bench scale studies which examined the effectiveness of thiocyanate regeneration of the saturated resin for silver recovery. The spent regenerant was then treated by electrowinning to recover the eluted silver in a fairly pure state. Projected capital and operating costs for a 2 gpm regenerable ion exchange system were examined. Operating results of a full scale non-regenerated system are presented.

BACKGROUND

A barrel-and-rack production electroplating facility specializing in high quality decorative and industrial finishes generates a contaminated rinsewater from its silver cyanide barrel plating line. Silver lost by dragout from the plating bath is partially recovered in a drag-out rinse tank. The silver in this tank is recovered by an electrolytic metal recovery unit. Metal parts leaving the drag-out rinse tank are rinsed in a two-stage counterflow rinse running at an average flow rate of 2 gpm. Silver cyanide that is not recovered in the drag-out rinse tank is currently treated in a wastewater treatment facility which utilizes alkaline chlorination for cyanide destruction, hydroxide precipitation, clarification, and filtration for metals removal.

Due to concern over the ultimate environmental fate of the silver cyanide complexes, and the economic loss of the silver metal, a study was commissioned to examine the applicability of ion exchange for silver recovery. The use of ion exchange for the removal of metal cyanide complexes has been reported by Gupta, et. al.[1]. Ion exchange is a process in which soluble, charged ions are removed from solution by exchange with similarly charged ions that are held by electrostatic charges on the surface of a solid (ion exchange resin)[2]. While most conventional ion exchange systems utilize regeneration techniques to recover the exchanged metals in a concentrated form, the metal cyanide complexes are strongly retained by anion resins

and are difficult to remove with conventional strong base (hydroxide) regeneration. For valuable metals such as gold and silver, difficulties with regeneration can be circumvented by simply selling the resin to a metals reclaimer who in turn burns the resin and recovers the precious metals. However, Gupta, et. al. [1] indicate that metal cyanide complexes can be effectively removed from anion exchange resin using thiocyanate as the regenerant. Because of the greater affinity for the thiocyanate anion (relative to hydroxide), the resin will give up the silver cyanide complex under the proper regeneration sequence. Regeneration allows reuse of the ion exchange resin, and can potentially offer significant savings in operating costs since the expensive resin can be reused.

Once removed from the ion exchange resin in a concentrated solution, the silver must be further converted to its elemental form. Electrolytic techniques such as electrowinning have been shown to be very efficient at converting silver cyanide ions to elemental silver.

The goals of this engineering study can be summarized as follows:

1. Verify the feasibility of ion exchange with regard to highly efficient silver cyanide removal from actual rinsewater from an electroplating facility.

2. Determine the effectiveness of thiocyanate regeneration for the removal of silver cyanide from exhausted anion exchange resin.

3. Optimize the regeneration sequence to achieve high silver cyanide capacities following thiocyanate regeneration along with high silver cyanide removal efficiencies.

4. Determine the effectiveness of electrolytic recovery of silver from spent thiocyanate regenerant solutions.

5. Prepare a budgetary cost comparison for thiocyanate regeneration/electrolytic recovery of silver versus resin disposal.

Materials and Methods

Ion Exchange

The bench scale apparatus utilized for the ion exchange studies is shown in Figure 1. An acrylic column was selected in order to provide visual information regarding the potential fouling or staining of the anion exchange resin, and to verify proper bed expansion during backwashing.

Rohm and Haas IRA-400 anion exchange resin was selected based on prior literature reports and field experience. Regeneration sequences and operating parameters were

selected based on suggested laboratory procedures from Rohm and Haas [3]. A summary of the service flow rates and regeneration flow rates and volumes is shown in Table 1. Distilled water was used for regenerant dilution and fast and slow rinse steps. Tap water was used for backwashing the resin prior to each regeneration. Fresh resin was placed in the hydroxide form by regeneration with 10 pounds per cubic foot of four percent sodium hydroxide solution prior to any testing.

Wastewater was formulated by diluting silver cyanide plating bath with tap water to produce a silver concentration of 16 mg/l. This represented a typical final rinsewater silver concentration, although tests were also run at 1.6 mg/l silver to determine the effect of influent concentration on the ion exchange system performance.

Electrowinning

A bench scale electrowinning cell was utilized for the electrolytic recovery testing. A flow rate of 750 ml/min was maintained with a positive displacement pump to produce a recommended hydraulic retention time of 20 minutes. The rectifier amperage was set at 30 amps (2 volts DC). Copper reticulate cathodes with a total of six square feet were utilized in the test cell.

A "typical" spent regenerant solution was prepared as follows:

1.9 gallons silver cyanide plating bath
3.1 gallons distilled water
1600 grams sodium thiocyanate

The spent regenerant was made up to approximate the characteristics determined in the ion exchange bench testing. An artificial spent regenerant using plating bath had to be made up due to the small volume of actual spent regenerant produced in the lab column (1 liter) relative to the quantity needed for the electrowinner (20 liters). While the artificial solution was made up to approximate the silver and thiocyanate concentrations expected (6,300 ppm and 86,000 ppm, respectively), the free cyanide concentration was also high (41,000 ppm). This high free cyanide concentration will not be present in the actual spent regenerant since the resin will be saturated with mainly silver cyanide rather than free cyanide. Therefore, the electrowinning results may be somewhat different in actual practice, though the exact influence of the free cyanide is unknown at this time.

Results and Discussion

Ion Exchange Bench Test Results

One of the primary goals of this study was to verify the feasibility of silver cyanide removal by ion exchange. Figures 2 and 3 graphically depict the low effluent silver concentrations that can be achieved for this particular waste stream--especially with

fresh resin in the hydroxide form (Test Series 1). It is interesting to note that the silver leakage from the column increased substantially following thiocyanate regeneration. Leakage increased from below detection limits (.05 ppm) with fresh resin to 3.7 to 3.8 ppm following regeneration at 30 pounds sodium thiocyanate (NaSCN) per cubic foot of resin. Subsequent regeneration using 50 pounds NaSCN per cubic foot reduced the silver leakage to 1.2 ppm. An additional run using 40 pounds NaSCN per cubic foot followed by 10 pounds sodium hydroxide (NaOH) per cubic foot improved leakage slightly to 0.9 ppm. In general, it appears that a silver leakage of 1 ppm can be expected at a feed concentration of 16 ppm following thiocyanate regeneration at 40 to 50 pounds per cubic foot.

While much of the bench scale testing was conducted with a rinsewater containing 16 ppm silver, there are periods where the silver concentration is much lower. A rinsewater sample was diluted to 1.6 ppm and run through a thiocyanate-regenerated column of resin. The result of this test is show in Figure 3. It is important to note that as the influent concentration is reduced, the silver leakage in the effluent is also reduced. However, overall removal efficiency decreased from 90-95 percent at 16 ppm influent silver to about 75 percent removal at 1.6 ppm influent silver. This relationship between influent concentration and overall removal efficiency has important full scale implications. A regenerable system may be applicable for rinsewaters containing greater than 10 to 15 ppm silver, but lower silver concentrations are best treated with virgin resin which can be removed following exhaustion.

Increased silver leakage following regeneration occurs primarily for two reasons. First, any regeneration procedure leaves some of the saturating ions within the resin. Since ion exchange is a reversible equilibrium, complete removal is virtually impossible. Virgin resin has no silver present and leakage is, therefore, negligible. Once resin has been saturated, some of the ions remaining after regeneration will leak into the effluent during the next service cycle. Leakage can be minimized by applying high dosages of regenerant, but complete regeneration is uneconomical and impractical. Second, because the silver cyanide complex is so tightly held in the resin, a strong regenerant is required to remove the complex. Unfortunately, the resin will also have a high affinity for the regenerant and the equilibrium exchange is shifted slightly away from the resin-silver complex bond. The resin's relative affinity for the silver complex is reduced accordingly, and more silver slips into the effluent during the next service cycle.

Besides silver removal efficiency, another important consideration for any ion exchange system is resin capacity, which can be expressed in pounds of the ion per cubic foot of resin. The service run time between regenerations is directly related to the resin capacity. Resin capacity was determined in the bench studies by making more concentrated "rinse" solution (1,100 to 1,300 ppm silver) in order to force silver breakthrough in a short period of time (5 to 6 hours). Using typical rinsewater would require weeks of continuous testing with hundreds of gallons of rinsewater. Unfortunately, capacity is a function of the influent concentration, so that this technique is somewhat problematic. However, a reasonable estimate of capacity can be obtained

in this manner. The capacity studies indicated favorable ion exchange kinetics and efficient resin utilization, as there was a rapid rise to exhaustion following initial breakthrough. In general, a capacity of about 3 - 4 lbs. silver/cu. ft. of resin was realized with either virgin resin or thiocyanate-regenerated resin. At a bulk resin density of 44 pounds per cubic foot, this capacity corresponds to 7 - 10 percent silver by weight. It is important to note that the resin capacity is also a function of the point at which the column is removed from service. That is, the capacity to complete exhaustion is higher than the capacity to initial breakthrough. By running columns in series, it is possible to fully exhaust the lead column without causing high effluent silver concentrations since the secondary (polishing) column will remove the excess silver.

Finally, the effectiveness of silver cyanide removal from the resin during regeneration is an important consideration in a regenerable system. Gupta et. al.[1] indicate that approximately 85 percent of the exchanged metal-cyanide complexes can be eluted by thiocyanate regeneration. The results from this study are in agreement with this finding.

Figure 4 illustrates the elution of silver from the anion exchange resin during regeneration. The integrated area under the elution curve indicated that 85 - 87 percent of the silver retained in the exhausted resin was removed during regeneration. These results indicate that the resin can be effectively regenerated using sodium thiocyanate. Because of the efficient elution of silver using thiocyanate, the resin capacity remained high during subsequent loading steps.

Electrowinning Bench Scale Test Results

Results of the electrowinning bench tests showed that silver electrowinning was outstanding, with virtually all the silver converted to elemental silver within two hours of testing. Analysis for copper (also present in the silver plating bath as a contaminant at a silver-copper ratio of 4:1) was conducted after 16 hours of electrowinning. Approximately two-thirds of the copper could be removed from solution. It is not known how soon copper equilibrium is achieved, but presumably it is less than 16 hours of operation under the conditions of this test.

An analysis of thiocyanate was run following 28 hours of operation. The electrolytic action of the electrowinner reduced thiocyanate from approximately 86,000 to 69,000 ppm (20 percent reduction). This fairly minimal loss indicates that the treated spent regenerant could most likely be reconstituted with additional thiocyanate and reused. Eventually the dissolved solids content would be problematic and, therefore, only one reuse would be recommended. It also bears mentioning that a considerable amount of ammonia was generated following extended periods of electrowinning. The effect of the ammonia on the treated regenerant is unknown. Since the silver is recovered so quickly, ammonia production can be minimized by minimizing the electrowinning treatment time.

Full Scale Silver Recovery - Preliminary Design and Costs

The two basic flow schemes for ion exchange recovery of silver cyanide complex are shown in Figures 5 and 6. Figure 5 depicts the simplest recovery scheme, in which the silver cyanide is captured on hydroxide-form anion exchange resin. When the lead column reaches silver breakthrough, the column is taken off-line and the exhausted resin is sluiced to a spent resin holding tank. The silver-laden resin is shipped to a reclaimer, and fresh resin is loaded into the exchange vessel, which is then placed in the polishing mode. Fresh resin is always used in the secondary column to achieve the lowest silver leakage possible. Drawbacks of this system are 1) the high cost of resin replacement ($250 to $300 per cubic foot IRA-400), 2) the reclaimer's handling fee (approximately $2 per pound of resin), and 3) shipping costs.

Figure 6 shows an alternative system in which the lead column is regenerated with sodium thiocyanate. The spent regenerant and slow rinse volumes are directed to an electrowinner storage tank. The silver in the spent regenerant is then reclaimed by electrolytic recovery. The secondary (polishing column) is always used with fresh hydroxide-form resin. When this column becomes spent, the resin is removed and sent to recovery. Because of the higher silver leakage that occurs following regeneration, the polishing column is not regenerated and is always filled with virgin resin only. The treated spent regenerant and the effluent from the ion exchange system are directed to the existing wastewater treatment system. The advantage of the regenerated system is the lower operating cost since the resin is reused following exhaustion. Disadvantages result from increased capital cost (additional piping, valves, regenerant storage tanks, electrowinner, transfer pumps, etc.) and greater operational complexity, though operating manhours are minimal due to the long run times between regenerations.
Preliminary budget capital and operating costs for a regenerable vs. non-regenerable ion exchange system were prepared based on the following design considerations:

Rinse Flow Rate = 2 gpm
Silver Concentration = 10 ppm
Shop Production: 16 hours/day
250 days/year
Silver Mass Loading = .16 lb/day
Resin Capacity = 3 lb silver per cu. ft.
Ion Exchanger Size = 2 cu. ft. (6 lb silver)
Regeneration/Replacement Frequency = 6 lb ÷ .16 lb/day ≈ 30 days
Resin Cost = $250/cu. ft.
Silver Reclaimer's Processing Fee = $2/lb resin
Labor to Empty/Refill Vessel = 4 hours @ $20/hr
Sodium Thiocyanate Cost = $1.30/lb
Labor to Regenerate/Electrowin = 6 hours @ $20/hr

A budgetary installed capital cost of a regenerable ion exchange system was estimated to be $30,000. Operating costs were estimated to be $4,500 per year which assumes that the lead (regenerable) column is refilled with new resin twice/year and the polishing column is refilled once/year. The other major operating costs are for regenerant chemicals and labor.

A non-regenerable system was estimated to cost $15,000 (installed). The simplicity of the system results in major capital savings compared to a regenerable system. However, the operating costs are primarily due to the high cost of replacement resin, which can be as much as $6,000/year.

It is imperative to recognize that the operating costs of the two systems are largely a function of the mass loading of silver. Should lower silver mass loadings be realized, the annual operating cost savings that can potentially be obtained with a regenerable system will also be reduced. Given the above design conditions, a regenerable ion exchange/electrowinner system may have a 3 to 4-year payback. However, at lower silver mass loadings, the payback period will increase and a non-regenerable system will clearly be the most cost-effective approach.

Full Scale Ion Exchange Results

Based on the economic evaluation discussed previously, a non-regenerable ion exchange system was installed at the electroplating facility. Due to low silver concentrations that existed in the final rinsewater (less than 10 ppm expected) due to the use of electrolytic metal recovery in the drag-out rinse tank, a non-regenerable system was deemed to be most cost-effective. The results of approximately seven months of full scale operation at a nominal flow rate of 2 gpm are depicted in Figure 7. At an average influent silver concentration of 4.9 ppm, the effluent has averaged .07 ppm, which represents 98.6 percent removal of silver under actual field conditions. Mass balance and spent resin assays indicate that the resin contains 1% - 2% silver by weight. This is somewhat lower than silver content predicted by bench scale testing (7% - 10% by weight), and is no doubt related to the fact that the influent silver concentration is quite low compared to the high concentration (in excess of 1,000 ppm) used in the bench scale treatability testing. Nevertheless, valuable silver is recovered and recalcitrant metal cyanide complexes are removed from solution, while easily-treated free cyanide is passed through to waste treatment.

Summary and Conclusions

The following conclusions may be drawn from this study.

- Bench scale tests have shown that greater than 99% of the silver cyanide can be removed from electroplating rinsewater using strong base anion exchange resin. Full scale system test results confirmed this finding as seven months of operation yielded an average removal of 98.6%.

- The ion exchange resin can be effectively regenerated using sodium thiocyanate at a dosage of 40 to 50 pounds per cubic foot of resin, though subsequent removal efficiency falls to 90% - 95%.

- Bench scale tests indicated that a resin capacity of 3 - 4 pounds of silver per cubic foot of resin could be expected. Preliminary scale results indicate that a capacity of only 0.5 - 1 pounds of silver per cubic foot are actually realized. The lower capacity is probably due to the fairly low influent silver concentration (4 - 5 ppm) that is realized in actual practice.

- Silver can be completely recovered from spent thiocyanate regenerant by using electrowinning. Copper, which is also present in the plating bath, can be practically recovered (67% recovery) using electrowinning. Thiocyanate destruction during electrowinning is fairly minimal (less than 20% destruction), so that regenerant can be reconstituted for reuse.

- Budgetary estimates for a 2-gpm treatment system indicate that a 3 to 4-year payback is possible for a regenerable ion exchange system compared to a non-regenerable system. The higher capital cost of a regenerable system is offset by the savings in annual disposal costs of the anion exchange resin. This payback is applicable for a rinsewater with a 10-15 ppm silver concentration. As the rinse silver concentration decreases, the payback period will increase, and vice versa.

Acknowledgements

This study was funded in its entirety by Artistic Plating Company, Inc. Bench scale treatability was conducted by Triad Engineering, and wastewater analyses were performed by the Artistic Plating Company analytical laboratory.

References

1. Gupta, A., Johnson, E.F., Mindler, A.B., and Schlossel, R.H., "The Use of Ion Exchange for Treating Wastewaters and Recovering Metal Values from Electroplating Operations." AICHE Symposium Series, No. 243, V.81.

2. Weber, W.J. Jr., "Physicochemical Processes for Water Quality Control." John Wiley and Sons, Inc. Publishing, 1972.

3. Rohm and Haas Company. Amberlite Engineering Manual.

FIGURE 1

COLUMN APPARATUS

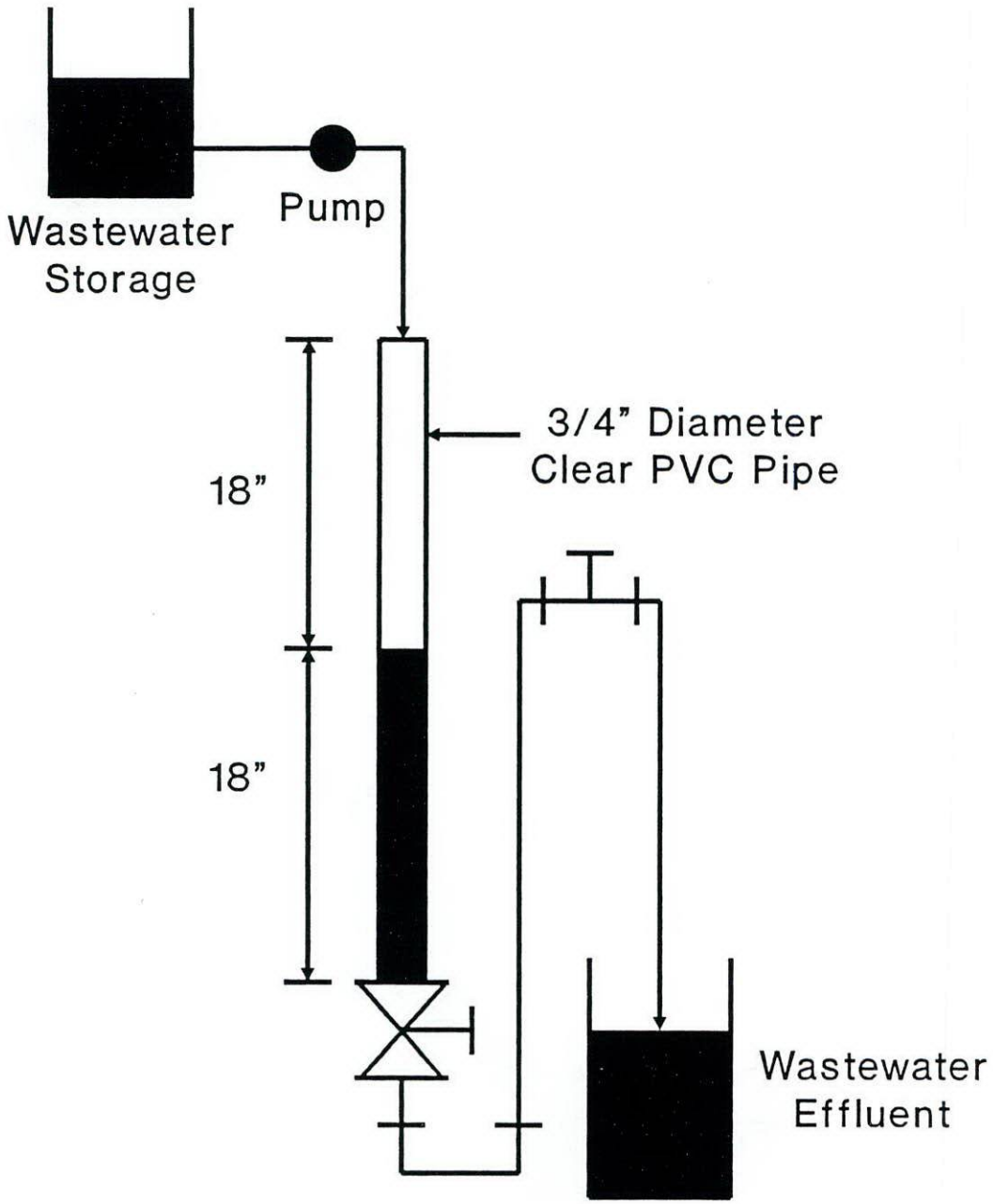

FIGURE 2
SILVER LEAKAGE

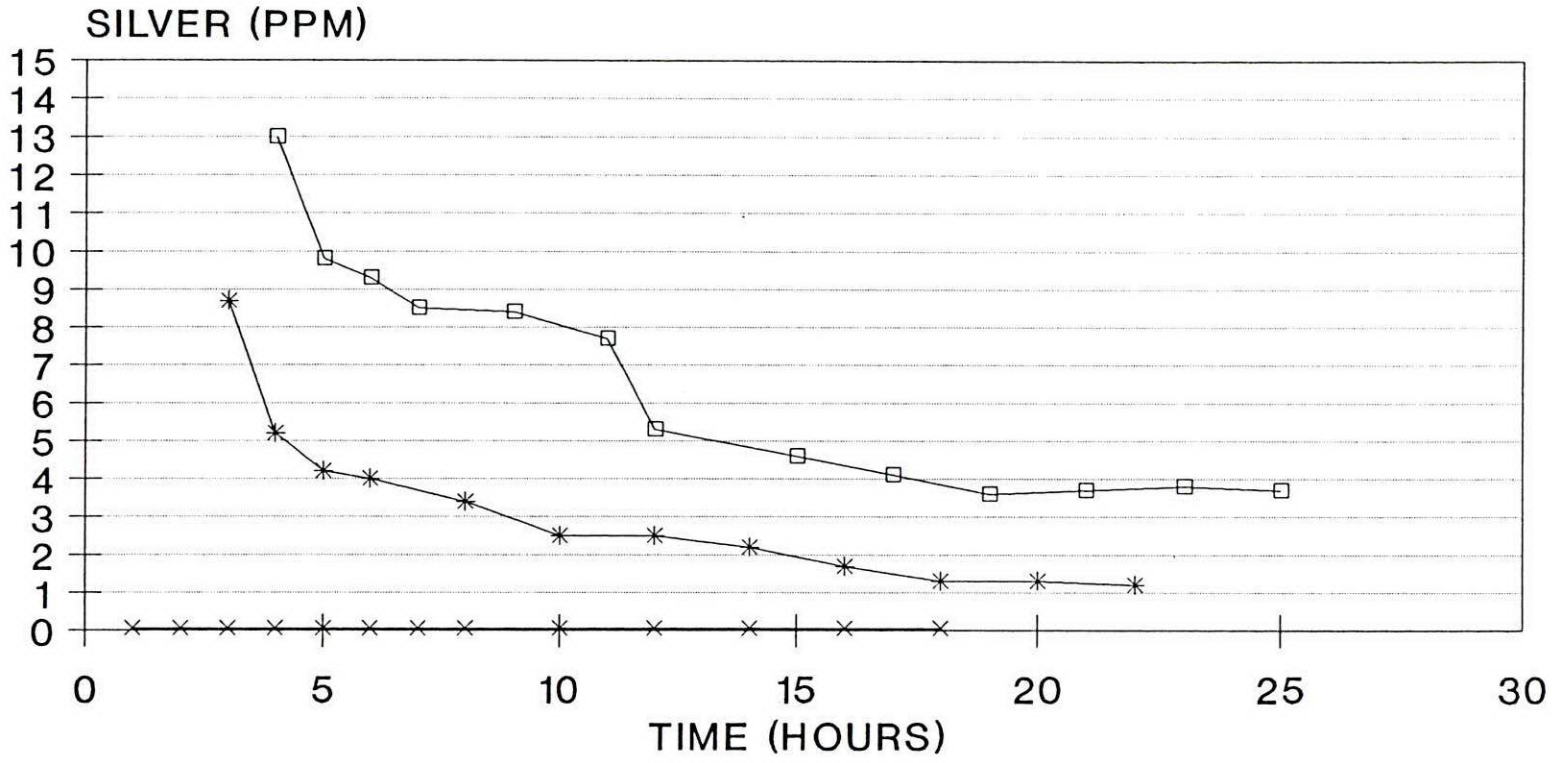

Rinse Concentration = 16 ppm Silver

FIGURE 3

SILVER LEAKAGE VS. INLET CONCENTRATION

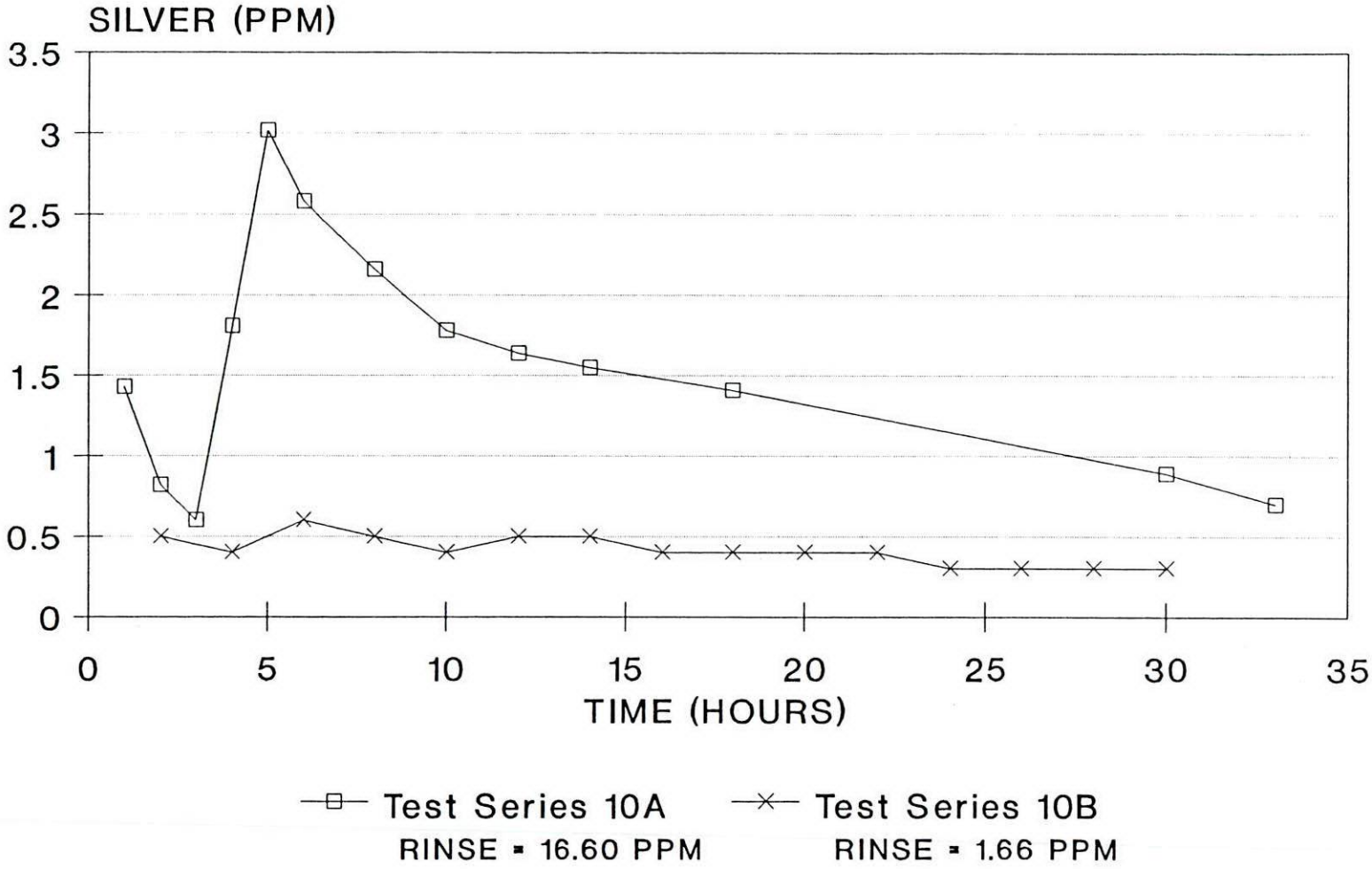

FIGURE 4

REGENERATION CURVE: TEST SERIES 6

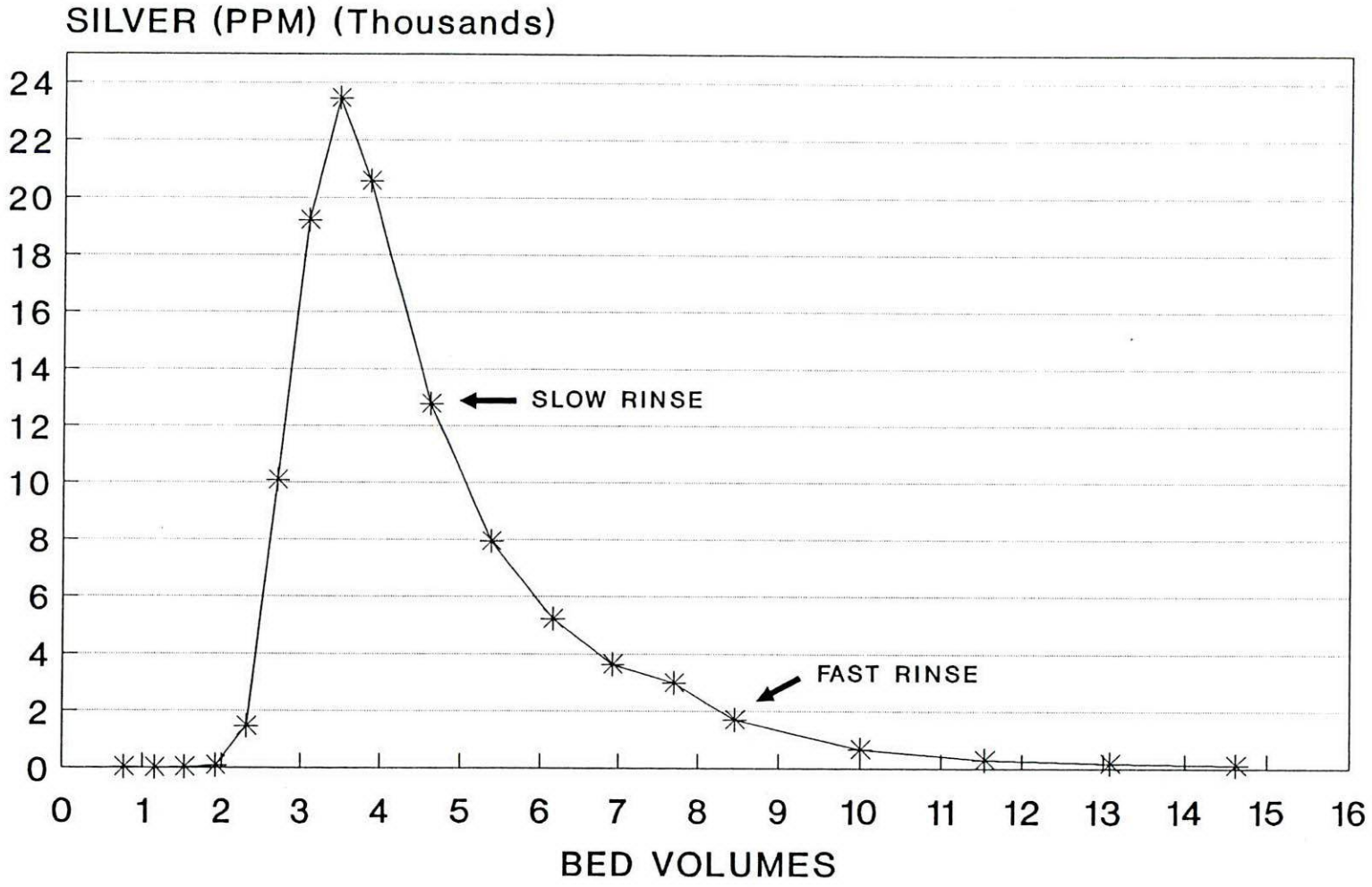

Regeneration at 50 lb NaSCN/cu.ft.

FIGURE 5
SILVER RECOVERY
FLOW SCHEMATIC- NON-REGENERABLE SYSTEM

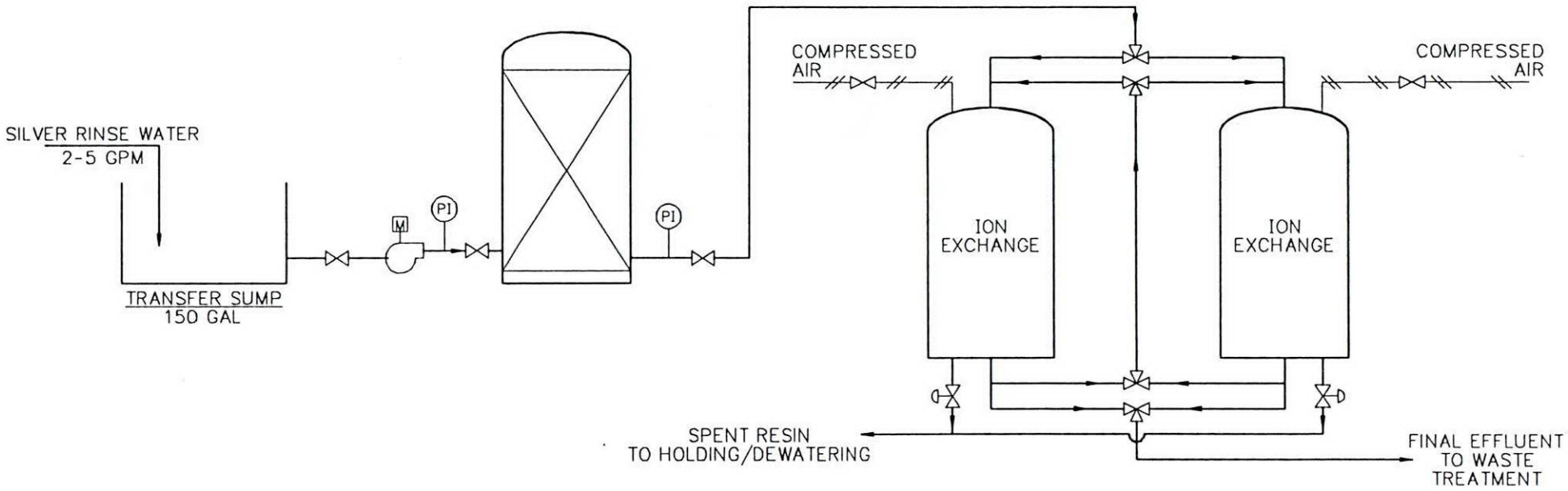

FIGURE 6
SILVER RECOVERY
FLOW SCHEMATIC- REGENERABLE SYSTEM

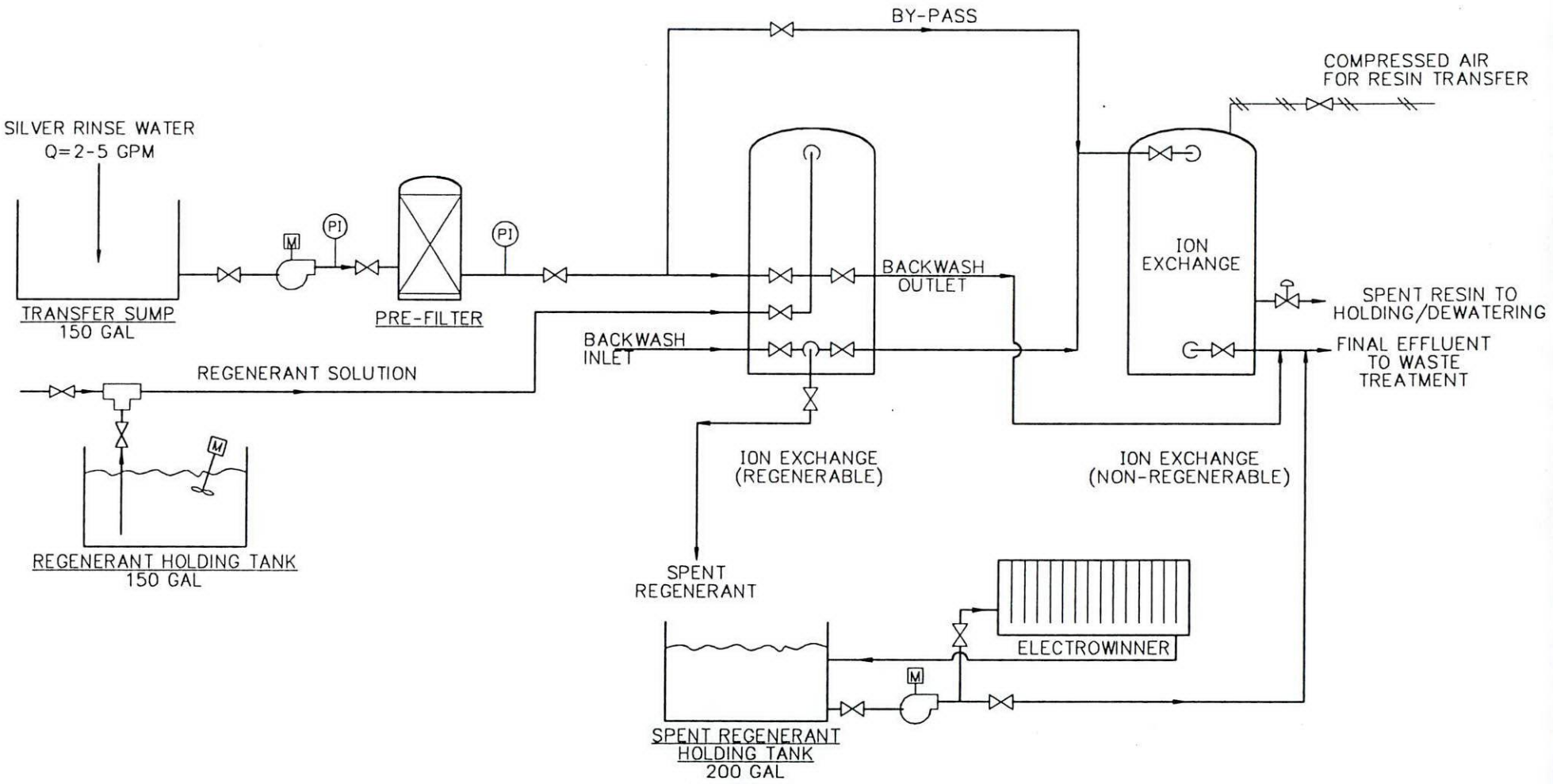

FIGURE 7

SILVER RECOVERY WITH ION EXCHANGE
FULL SCALE RESULTS

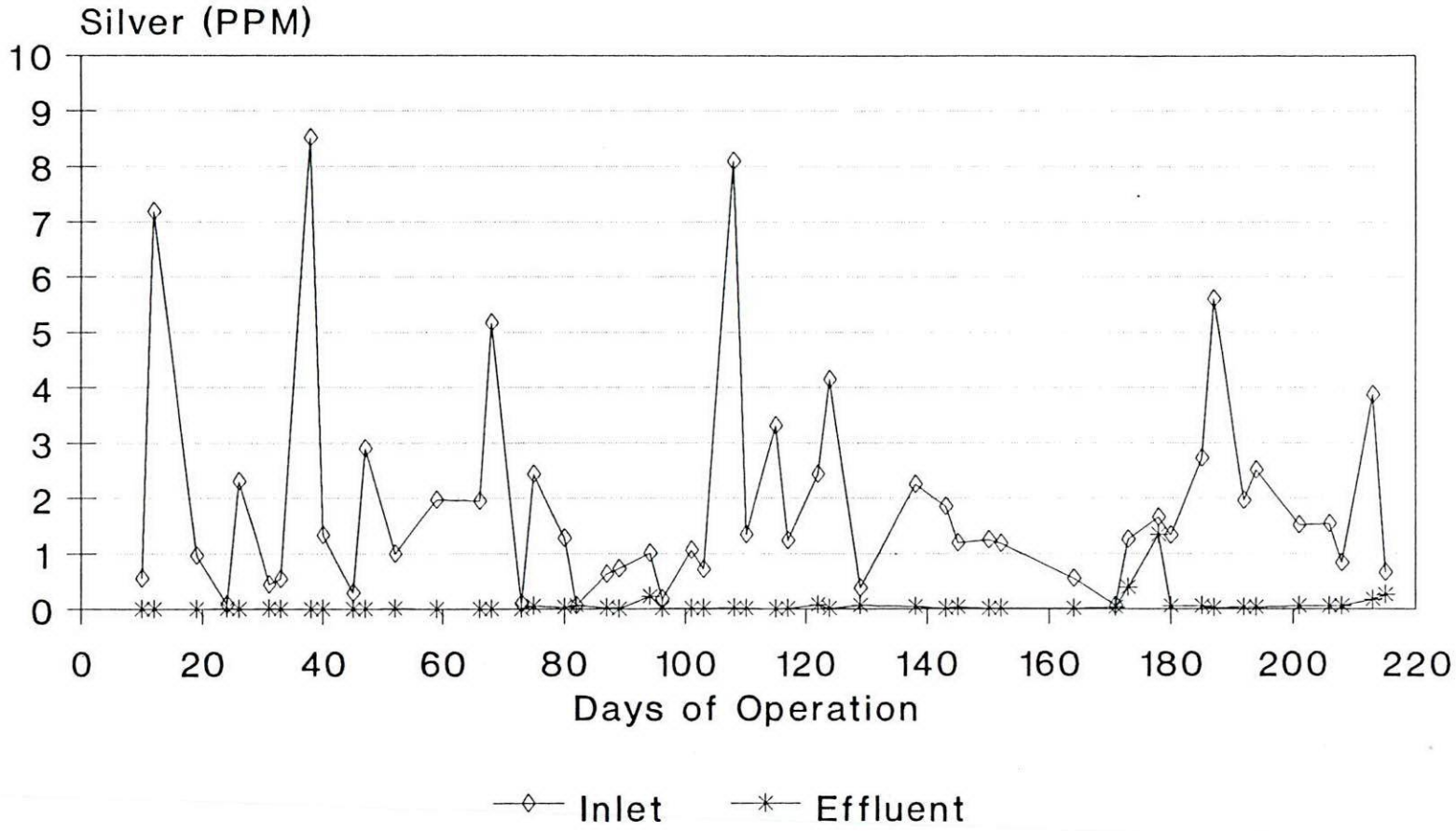

POLLUTION PREVENTION WITH ADVANCED TECHNOLOGIES: A SUCCESS STORY -- WITH A PAYBACK

Michael C. Greene
Bio-Recovery Systems, Inc.
2001 Copper Avenue, Suite 11
Las Cruces, NM 88005

Pollution prevention has always been important to the metal finishing industry. However, in the coming decades that importance will grow, as governments, citizens, and customers create more and more pressure to reduce or eliminate hazardous waste.

Every day, metal finishers are faced with the tough federal attitude toward hazardous wastes. With every hazardous waste shipment that leaves the plant, operators must affix their own signatures to the federally required manifest certifying that "the quantity and toxicity of the hazardous waste has been reduced by the maximum degree economically practicable." In addition, the potential liabilities associated with handling and disposing of hazardous wastes have increased significantly, while the restrictions placed on land disposal of these wastes have increased waste disposal costs significantly. Clearly, treating and disposing of hazardous wastes is no longer the optimal way to deal with them -- metal finishers must find a way to reduce their production of hazardous wastes in the first place.

At the same time, requlatory pressure is increasing to virtually eliminate heavy metals from the wastewater effluent of metal finishing facilities. For example, Milwaukee, Wisconsin, is proposing a one part per billion limit on chromium in wastewater.

As a result, metal finishers must begin to implement wastewater treatment technologies that can do double duty -- that is, technologies that are capable of meeting the stricter effluent standards without producing hazardous waste. Conventional, less advanced methods of treating wastewater cannot always play this double role, but certain newer, more advanced technologies can.

Companies who prepare for the future now by assessing their current waste problems and implementing appropriate advanced technologies will have a competitive advantage -- one built on improved public and customer relations, on cost savings and on reduced liability for dealing with hazardous wastes.

One such company is Alternate Circuit Technology (ACT), a printed circuit board manufacturer in Ward Hill, Massachusetts. By selectively employing state-of-the art wastewater treatment technology where it was most needed, significantly reduced the hazardous waste it generated, met effluent quality standards, and saved money. The company's experience demonstrates both the importance of systematically assessing waste problems and the practicality of using advanced technologies tailored to remedying the problems identified.

The remainder of this paper describes the process used to assess its waste production, the treatment choices it made based on that assessment, and the results of those choices.

The Assessment Process

The first step toward pollution reduction was to thoroughly assess its waste production to determine where improvement was needed. This assessment pinpointed areas where opportunities to significantly reduce waste production existed.

In August 1989, contracted with an environmental services and equipment supplier to perform a Wastewater Characterization Profile of the wet processes in its printed circuit fabrication facility. The study was conducted on site and took about a week and a half. During this time hundreds of wastewater samples were collected and analyzed for metal content (type and concentration). Samples were taken during multiple process runs, both before and after the board entered the process step. Rinse flowrates, bath volumes, and dump frequencies were logged for essentially every process tank. The result was a detailed profile of the types and sources of hazardous wastes produced. A summary of the flow and metal loading, for the facility is shown in Figure 1.

As findings emerged, a team of process engineers and environmental engineers began to develop recommendations to improve waste production levels. Teamwork was important to ensuring that the recommendations would not only solve the waste problems, but would also be practical and realistic. In the end, the team produced a list of recommendations for reducing sludge and lowering the level of contaminants in the wastewater.

Some recommendations focused on reducing or modifying some rinse processes, based on the metal concentration in the rinse. For example, the cleaner/conditioner rinse on the Oxide Line was flowing at 6 gallons per minute (gpm), with an average copper concentration of only 0.212 parts per million. With this low concentration, the team felt that the rinse could still be effective if it were slowed to 3 gallons per minute. This recommendation would reduce the amount of water both consumed from and released into the environment.

The study also showed that the principal sources of copper waste were a small number of rinses and bath dumps, mainly etcher and microetch sources. About 75 percent of the sludge came from the alkaline etcher and microetch rinses and the microetch bath dumps. Therefore, the team recommended that ACT look into wastewater treatment systems designed to minimize waste production. Ion exchange technology coupled with electrowinning is the cleanest solution available -- it virtually eliminates water contaminants without producing hazardous sludge. Proposals were sought for ion exchange and electrowinning systems capable of producing acceptable water and of recovering the metal as metallic sheets suitable for recycle.

System Design

In choosing its new wastewater treatment system, ACT maximized the value of its investments by employing ion exchange/electrowinning technology where most copper waste was produced and for applications in which their existing precipitation system was ineffective.

About five years earlier, ACT had installed a precipitation system for treating wastewater. Understandably, they were unwilling to sacrifice this entire investment by replacing the whole system with ion

exchange equipment, even though doing so would have guaranteed the lowest possible level of waste production throughout the entire system. The company looked for ways to employ both the existing precipitation system and the cleaner ion exchange/electrowinning technology.

The vast majority of hazordous wastes came from the etcher rinse and the microetch bath dumps. Moreover, the precipitation equipment was not very effective at treating the etcher rinse. As a result, the company decided to focus ion exchange/electrowinning technology on these two sources and treat the other metal-bearing wastes with the existing system. The system, ultimately purchased for under $100,000, is diagrammed in Figure 2. Key features include:

- - Two point-source ion exchange units are used to treat about 8 gpm of alkaline etcher rinses, and one is used to treat about 4 gpm of solder bright rinses. The precipitation system continues to treat the other metal-bearing wastes.

- - A single electrowinning cell is used to recover the metal from the ion exchange regenerants and the bath dumps. (The solder bright regenerants containing copper, tin, and lead are electrowon separately from the copper solutions.)

- - Dual-column ion exchange treatment provides redundancy, resulting in low metal effluents consisting less than 0.5 ppm.

- - The compact design uses minimal floor space and required no significant modifications to the existing facility. The modular design allows growth with minimal cost and disruption.

- - Operation is simple and straightforward requiring minimal training and minimal maintenance.

Results

The system began operating in March 1991, and since then has met or surpassed all the goals of the program:

- - Sludge generation has decreased by about 75 percent.

- - Metal effluent levels are well below the limits.

- - The precipitation system is running more smoothly with reduced loading since the ion exchange units took up some of the burden.

- - Executives report that system operators take new pride in their responsibilities now that they are working with cleaner, more advanced technologies.

Waste minimization has proven to be a big financial winner as well. Compared to the previously installed system, the new combination of ion exchange/electrowinning equipment plus the existing precipitation equipment began saving the company almost $100,000 per year (see Figure 3). The new system paid for itself in less than 1 year. Moreover, the $100,000 per year savings figure does not include savings from labor reductions, nor from reduced liability resulting from reduced hazardous wastes going to landfills.

* * *

While the metals finishing industry is comfortable with more conventional wastewater treatment technologies, those technologies are no longer sufficient to take the industry into the environmentally conscious future. ACT's experience shows how more advanced technologies can practically and effectively be integrated into the metals finishing process.

Imagine the delight of the executives in being able to return nearly $100,000 to the bottom line, or use it to invest in process equipment that could further enhance their competitive position. Imagine the delight of the EPA, knowing that 75 percent less ACT-sludge is heading for hazardous waste landfills. And imagine the delight the company's customers, who know their supplier is strengthening their future by meeting and exceeding mandated waste minimization standards. Everyone wins in an effective waste minimization program.

For additional information contact Mr. David Unger, Environmental Engineering Manager, Alternate Circuit Technology at (508)372-0200

Figure 1

FACILITY FLOW AND METAL LOADINGS: ACT

Rinses

Stream	Flowrate (gpm)	Pounds of Metal/Day
Copper Bearing	40	15
Mixed Metal	20	14
Non-Metal Bearing	24	0

Dumps

Stream	Daily Volume (gal)	Pounds of Metal/Day
Copper Bearing	205	10
Mixed-Metal	30	5

From: Wastewater Characterization Profile

FIGURE 2

ACT POINT SOURCE TREATMENT SYSTEM

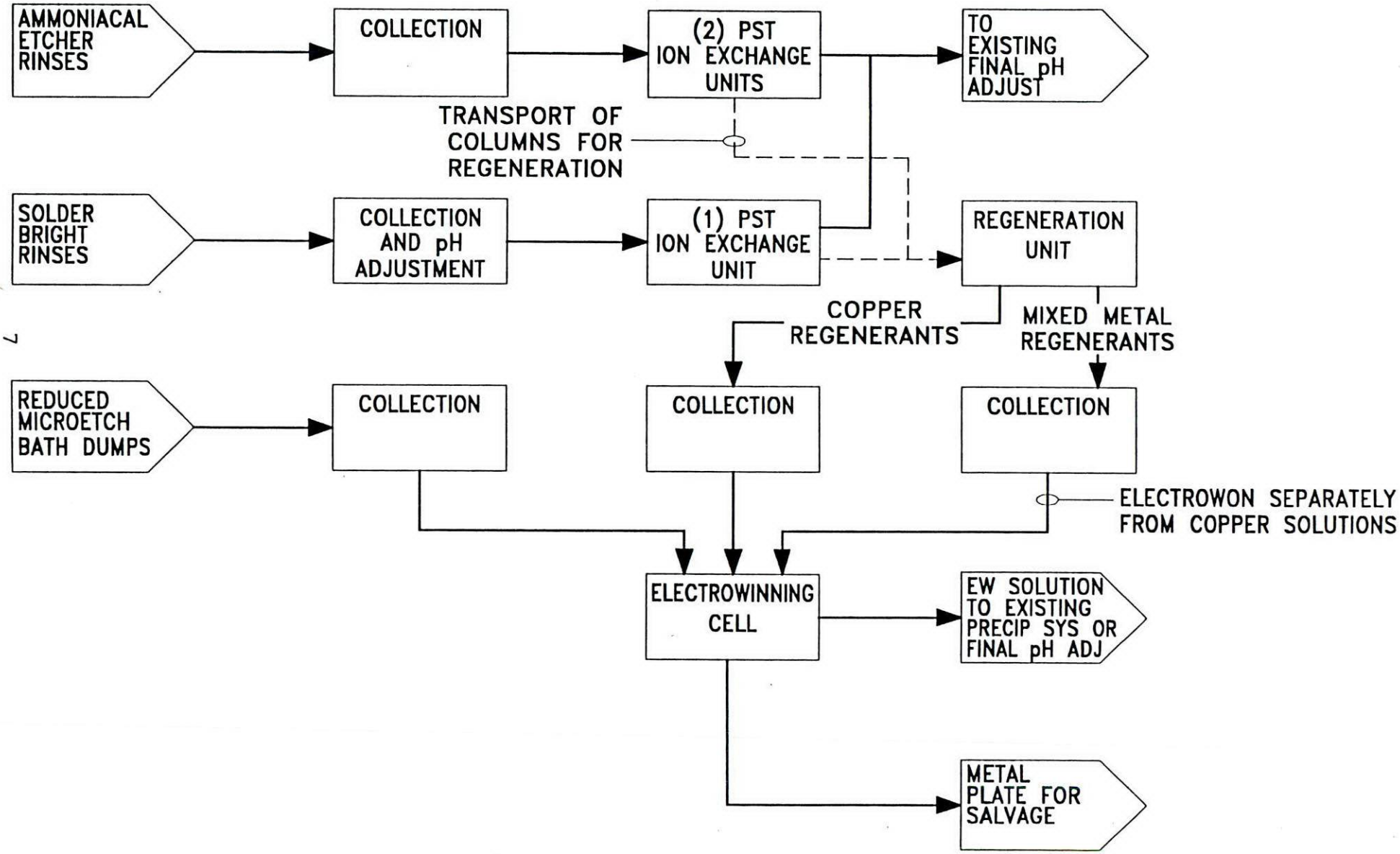

A63-P01 03/19/92

Figure 3

ACT OPERATIONAL COST COMPARISON: BEFORE AND AFTER ION EXCHANGE

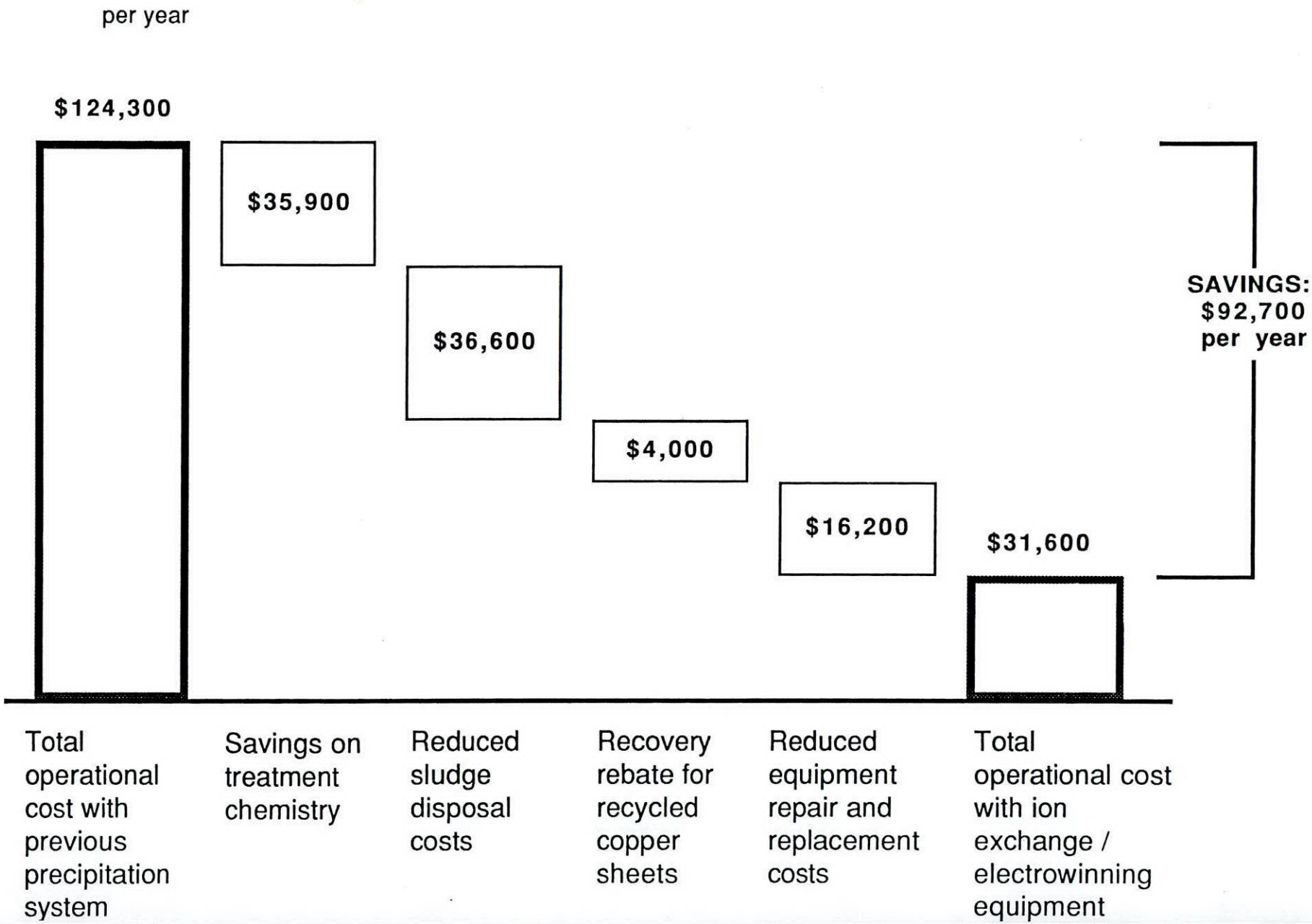

GROWTH MORPHOLOGY AND MELTING CHARACTERISTICS OF ELECTRODEPOSITED AuSn EUTECTIC ALLOYS

G. Holmbom, M. Svensson

Centre for Industrial Microelectronics and Materials Technology, Linköping University, S-581 83 Linköping, Sweden

J.A. Abys, H.K. Straschil

AT&T Bell Laboratories, Murray Hill, NJ 07974, USA

ABSTRACT

Eutectic AuSn (71/29$^{at}/_{o}$) solders have good electrical and heat conducting properties as well as superior thermal fatigue strength as compared to other material used in microelectronics assembly such as SnPb-solders and conducting epoxies. In this study, we have derived a chemistry which has proven to produce high quality AuSn deposits. The deposits have been characterized in terms of phase composition, microstructure, and melting characteristics.

INTRODUCTION

In production of microelectronic devices, there is always a delicate task to choose the technique of mounting the chip to its carrier. This can be done either by soldering or by using epoxy glue. An excellent solder to use in these applications is a eutectic gold-tin alloy (71/29$^{at}/_{o}$, see phase diagram in Fig.1) which has a high thermal fatigue strength and good heat conducting properties as compared to other solders (1-4).

There are several ways to apply AuSn solders, e.g. by using AuSn preforms or by PVD processes such as evaporating or sputtering layers of Au and Sn and, subsequently, diffuse the metals during heating to form the alloy. A third alternative is to electroplate the AuSn solder either as layers or as an alloy. One disadvantage with the preforms is the large amount of material used which can be critical in microelectronics applications. In addition, when Au is used as substrate, a non-eutectic alloy forms due to Au and AuSn interdiffusion. When the alloy gets rich in Au the melting temperature raises rapidly (see Fig. 1). The advantage of PVD and electrodeposition is that the composition can be matched to give a final eutectic composition even if a Au substrate is used. Furthermore, if electrodeposition is used the amount of excess material consumed can be limited to a minimal level.

The problem with electrodeposition of the AuSn eutectic alloy is the difficulties of controlling the alloy composition. In commercially available plating baths the Sn content in the electrolyte

becomes decreasing with time. It has been observed that Sn rich agglomerates form, reducing the available amount of Sn and thus reduces the Sn content in the deposits. The melting point of the alloy raises rapidly due to the steepness of the liquidus line in the AuSn phase diagram (Fig. 1) and, consequently, the properties of the solder change dramatically. The reflow does not occur at 280°C as expected but at higher temperatures, e.g. at 20 $^{at}/_{o}$ Sn the melting occurs at 498°C.

A pyrophosphate based formulation was developed by Kubota et al. (5, 6). This has proven to be stable although the Sn-pyrophosphate has a limited solubility. This bath also produces eutectic alloys within a operating window. The authors are not familiar with the long term stability of this formulation.

The aim of this study is to achieve a process which is stable under production conditions and can plate eutectic AuSn alloys in a reasonably wide operating window. To achieve this goal the plating chemistry was characterized by cyclic voltammetry and the deposits in terms of melting characteristics, chemical and phase composition, and microstructure.

EXPERIMENTAL

To characterize the electrochemical properties of the AuSn cyclic voltammetry was employed on Au rotating disk electrodes at temperatures from 25°C to 60°C and agitation from 0 to 1000 RPM. The counter electrode was platinized titanium mesh and as reference a saturated calomel electrode was used.

The samples were prepared from solutions as listed in Table 1. The anode material was platinized titanium mesh and the cathodes were Cu foil rotating cylinder electrodes. The deposits were prepared under the following conditions: Au concentration ranging from 0.5 g/l to 3 g/l, current density from 5 to 30 mA/cm^2, temperature at 40 and 60°C, and the cylindrical electrode was rotated to achieve controlled hydrodynamics which gave a peripheral speed of 10, 25, and 100 cm/s.

The properties of the plated alloys were characterized in the following way: The chemical composition was measured by atomic absorption spectroscopy (AA). The phase analysis was performed by X-ray diffraction (XRD) and transmission electron microscopy/electron diffraction (TEM/SAD) also utilizing EDS. The microstructure was investigated by TEM. The melting point and reflow characteristics was analysed by differential scanning calorimetry (DSC).

RESULTS AND DISCUSSION

Electrochemical characterization:— The electrochemical reactions were characterized using standard cyclic voltammetry with a Pt counter electrode, Au work electrode and SCE as the reference. The reduction process of the dicyanoaurate ion, $Au(CN)_2^-$, is a two step operation

(REF), where the first step occurs at about -0.96 V and the second at about -1.33 V at a concentration of 1.5 g Au per litre and an electrolyte temperature of 40°C as illustrated in figure 2. These results agree well with e.g. (REF). The first step represents adsorption of $Au(CN)_2^-$ and the second step to the reduction of Au^I to Au^0. The reduction potential is only slightly affected by temperature. The effect of agitation on limiting current density for reduction of $Au(CN)_2^-$ is listed in Table II.

The reduction of stannate, SnO_3^{2-} could not be studied due to the reduction peak being hidden by the hydrogen reduction wave. However, indications show that the reduction potential is about 1.5 V or lower.

Cyclic voltammetry of a bath containing Au (1.5 g/l) and Sn (5 g/l) show a reduction behaviour similar to the pure Au bath on a virgin Au electrode (se Fig. 1b). However, when performing scans in the positive direction from -1.8 V to -0.6 V, an oxidation process is observed at -0.85 V which was not observed for the pure Au system. This oxidation indicates dissolution of Sn which was deposited at low potentials. In addition, when the electrode surface was alloyed by Sn, the potential for Au^I to Au^0 reduction was depolarized and occured at -1.03 V.

Composition:— The alloy composition was measured by atomic absorption spectroscopy. The influence of the ratio of the metallic species in the electrolyte (Sn^{4+}:Au^+), the temperature, the current density, and the solution agitation on the composition of the deposits have been studied.

In figure 3 the effect of the metallic species ratio at different current densities on the deposit composition is shown. The alloy composition is sensitive to the $Au(CN)_2^-$ concentration in the bath but less sensitive to the SnO_4^{2-} concentration. It can also be observed that the Sn content is increased with increasing current density. In a range from about 8 to 12 mA/cm² with low agitation (10 cm/s), the composition is relatively stable around 28$^{at}/_o$ Sn ± 3$^{at}/_o$.

The solution agitation affects the composition as illustrated in figure 4 and the effect of temperature is illustrated in figure 5. The Sn content is reduced by increased agitation as well as increased temperature.

A number of the above observations can be explained by elementary elecrochemistry. The $Au(CN)_2^-$ ions are reduced at a higher reduction potential than the SnO_4^{2-} ions. From cyclic voltammetry (see discussion above) it appears as if the diffusion limiting current for $Au(CN)_2^-$ has to be exceeded for the Sn deposition to initiate. As a consequence, during alloy deposition the partial current for Au deposition is constant and only the partial current for Sn affected by variation in the applied total current. Thereby, the deposition of Au is favoured under conditions where the total applied current is close to the $Au(CN)_2^-$ diffusion limiting current density (i.e. at low current densities) or when the diffusion limiting current density for $Au(CN)_2^-$ is increased by e.g. increased solution agitation or increased temperature.

Crystalline Structure:— The crystalline structure was evaluated by XRD and by TEM/SAD. The eutectic AuSn (71/29$^{at}/_{o}$) alloy is a two phase material consisting of a ζ-phase (Au_5Sn) and a δ-phase (AuSn) as can be seen in figure 1. For alloys with Sn content lower than 16$^{at}/_{o}$ a Au fcc-phase and the ζ-phase are expected at thermal and chemical equilibrium. In a composition range from 24 to 50$^{at}/_{o}$, the ζ and δ-phases are expected while for deposits with Sn content above 50$^{at}/_{o}$ AuSn and $AuSn_2$ are expected and above 67$^{at}/_{o}$ $AuSn_4$ is also expected.

In figure 6, x-ray diffractograms from electrodeposited alloys with compositions at 24, 36, and 48$^{at}/_{o}$ Sn are shown. Both the ζ and the δ-phases are clearly identified. There are, however, peaks shifted in position indicating either stresses or defects in the ζ-phase or, posibly, the existence of a Au fcc-phase. Electron diffraction (TEM/SAD) confirm the existence of the ζ and the δ-phases but do not support the existence of a Au fcc-phase.

The ratio of ζ to the δ-phase is reduced when the Sn-content of the alloy is increased. Figure 7 gives a qualitative perspective of the growing fraction of the δ-phase in a composition range from 24 to 48$^{at}/_{o}$ of Sn in the AuSn alloy. The ratio was taken as the peak height of the sum of the (100) and (101) δ-phase reflections to the (300) and (306) ζ-reflections.

Microstructure:— In the dual phase electrodeposited aloys the ζ and δ-phases exist as 100 to 150 nm large grains as illustrated in figure 8. In the δ-phase grains no defects are observed by TEM and the corresponding SAD patterns are sharp confirming an relatively distortion-free grain structure. In the ζ-phase grains, however, the grains contain numerous lamellas and streaks are observed in the SAD patterns (see Fig. 8a). This indicates the presence of either stacking faults, twins or the existence of a dual phase structure with a very short-range ordering. Up to this point, we have not explained the origin of the distorted structure of the ζ-phase grains.

Melting characteristics:— The melting point and reflow characteristics was studied by DSC. As a reference, a AuSn preform was used as illustrated in figure 9 and 10. The heat of fusion for the eutectic melting of the preform was about 33 J/g. This compares to deposited alloys of eutectic or near eutectic composition as shown in figure 9. The heat of fusion data are within 60% of the preform data for alloys with composition ranging from 28 to 35$^{at}/_{o}$ Sn.

For off-eutectic composition alloys the DSC data looks quite different. For Au-rich alloys no endothermal reactions are observed up to 420°C and for Sn-rich alloys just below 50$^{at}/_{o}$ Sn a reaction is observed peaking at 418°C, indicating melting of the δ-phase. For alloys with Sn content around 70$^{at}/_{o}$ two endothermal reactions are observed, one at 252°C and one at 309°C indicating melting of the $AuSn_4$ and $AuSn_2$-phases, respectively.

SUMMARY

This work can be summarized by the following remarks:

- AuSn alloys can be plated from a slightly alkaline bath with good reproducibility an composition control.

- The alloy deposits with the Au reduction at about -1.0 V on the alloy surface which is depolarized as compared to a pure Au surface where the reduction occur at -1.3 V. The Sn deposition shows to be reversible through an oxidation reaction at -0.85 V

- The composition of the AuSn alloy is sensitive to current density, agitaion, as well as gold concentration and bath temperature. However, operating windows can be defined by bringing the current distribution and the hydrodynamic conditions under control.

- The plated AuSn alloy is crystallographically similar to the bulk material with respect to phase composition. The eutectic alloy consists of a Au_5Sn (ζ) and a AuSn (δ) phase.

- The grain structure of the plated alloy show grain sizes of 100 to 150 nm in size. The δ-phase grains appear defect-free while the ζ-phase grains contain lamellar defects.

- The melting characteristics of the plated alloy indicates good agreement with the bulk material. Heat of fusion of plated alloys are within 60% of preform data within $\pm$ 5at% ot the eutectic composition.

ACKNOWLEDGEMENT

We are greatful to AT&T Bell Laboratories and to the Swedish National Board for Industrial and Technical Development, NUTEK who has supported this work.

REFERENCES

1. C. Wright, *IEEE Trans. Parts, Hybrids, Pack.*,**PHP-13,** 202 (1977).
2. D.D. Zimmerman, *Solid State Techn.*,pp44 (1972).
3. D.R. Olsen, H. M. Berg, *IEEE Comp., Hybids, Manufact.*,**CHMT-2**, 257 (1979).
4. G. Matijasevic, C.C. Lee, *J. Electron. Materials*,**18**, 327 (1989).
5. N. Kubota, T. Horikoshi, E. Sato, *J. Met. Fin. Soc. Japan.*,**34**, 37 (1983).
6. N. Kubota, T. Horikoshi, E. Sato, *Plat. Surf.Fin.*,**71**, 47 (1984).

TABLE I	
Bath constituent	**Molar concentration (mM)**
$Au(CN)_2^-$	5 - 15
SnO_3^-	5 - 15
PO_4^{3-}	35
CO_3^{2-}	35
CN^-	35
Proprietary additive	
pH	11.5 ± 0.05

Table I. Composition of electrolyte for AuSn deposition.

TABLE II	
RDE Agitation (RPM)	**Limiting current density (mA/cm^2)**
100	1.9
250	2.5
1000	4.4

Table II. Limiting current densities for Au in AuSn plating bath on a rotaing disk electrode at 40°C, pH = 11.5 and [Au] = 1.5 g/l.

Figure Captions

Figure 1. Equilibrium phase diagram of the binary Au-Sn alloy. Alloys with composition at the eutectic point at 71^{at}/o (80^{wt}/o) Au is used for soldering purposes.

Figure 2. Cyclic voltammograms obtained from electrolytes with composition as in Table I. The upper voltammogram, scanned from -0.6 to -1.5 V with 1.5 g Au per litre and no Sn added, shows reduction characteristics of the Au component while the lower voltammogram, scanned from -0.6 V to -1.8 V with 1.5 g Au and 5 g Sn per litre, shows reduction of the Au component and oxidation of the Sn component as well as depolarization due to alloying of the electrode.

Figure 3. Effect of $Au(CN)_2^-$ concentration at various current densities on deposit alloy composition. Increased $Au(CN)_2^-$ concentration in bath and decreased current density reduces the Sn content in alloy.

Figure 4. Effect of solution agitation on deposit alloy composition. Increased agitation reduces the Sn content in the alloy.

Figure 5. Effect of bath temperature on deposit alloy composition. Increased temperature reduces Sn content in alloy.

Figure 6. X-ray diffractograms of electrodeposited AuSn alloys with a Sn content of a 24, 36, and 48^{at}/o. The ζ and δ-phases are identified.

Figure 7. Ratio of δ to ζ-phase of electrodeposited AuSn alloys at 24, 36, and 48^{at}/o Sn. The ratio was calculated as the sum of the peak heights of (100) and (101) δ-phase peaks to the sum of the (300) and (306) ζ-phase peaks. The fraction of δ-phase increases with increasing Sn content.

Figure 8. TEM micrograph illustrating microstructure of electrodeposited AuSn alloys of a) 24^{at}/o, b) 36^{at}/o, and c) 48^{at}/o Sn. In a) both ζ and δ-phase grains are observed. The ζ-phase grains dominate and exhibit lamellar features and streaks in SAD patern while the δ-phase appears defect free. In b) only a smaller number of ζ-phase grains are observed. Also in this micrograph the lamellar features and the streaks in the SAD pattern are observed. In c) mainly defect-free δ-phase grains are observed.

Figure 9. Heat of fusion data obtained by DSC of eutectic preform and of eutectic or near eutectic electrodeposited AuSn alloys.

Figure 10. DSC graphs showing melting characteristics of preform and electrodeposited AuSn alloys.

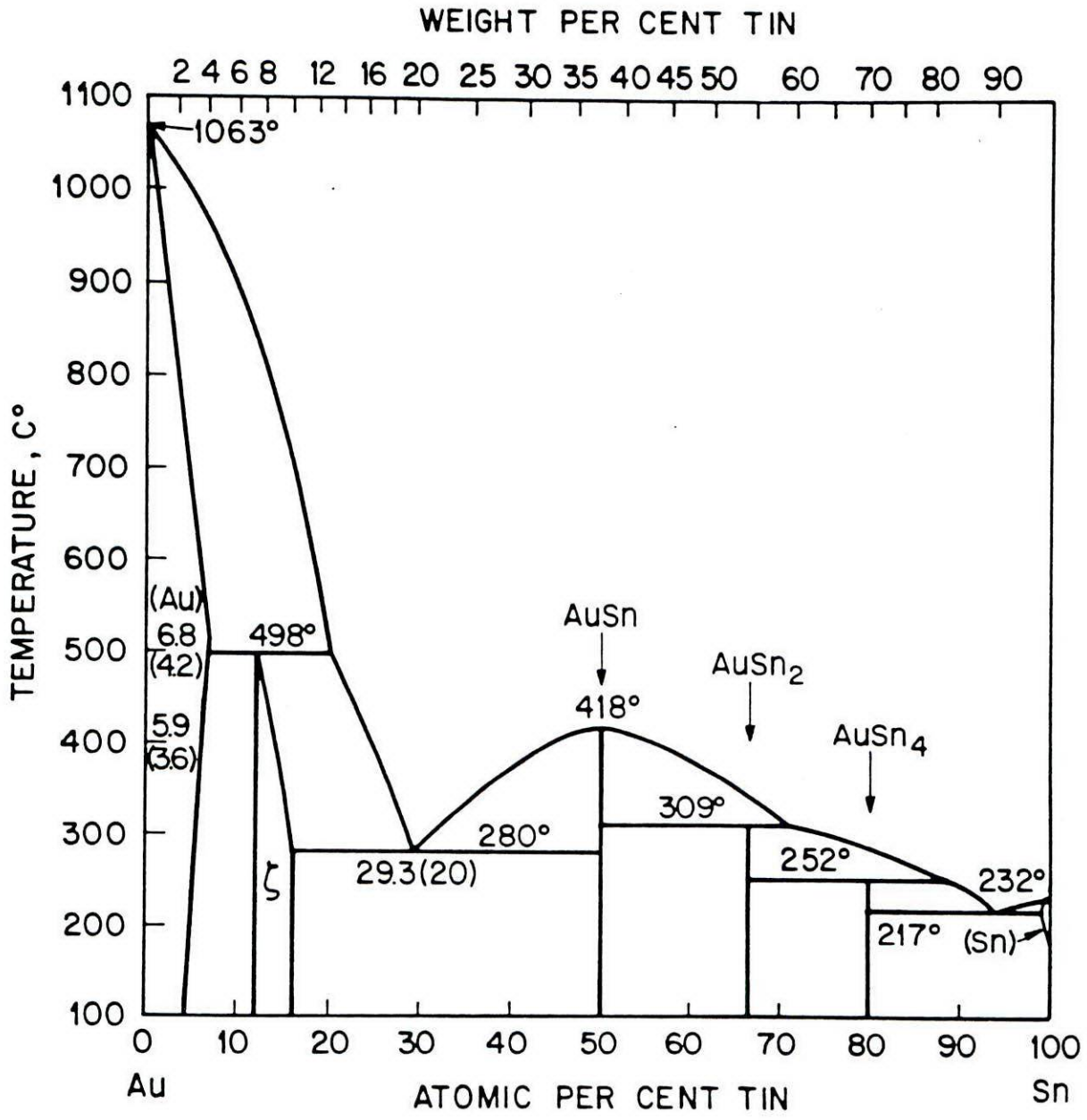

Figure 1. Equilibrium phase diagram of the binary Au-Sn alloy. Alloys with composition at the eutectic point at 71^{at}/o (80^{wt}/o) Au is used for soldering purposes.

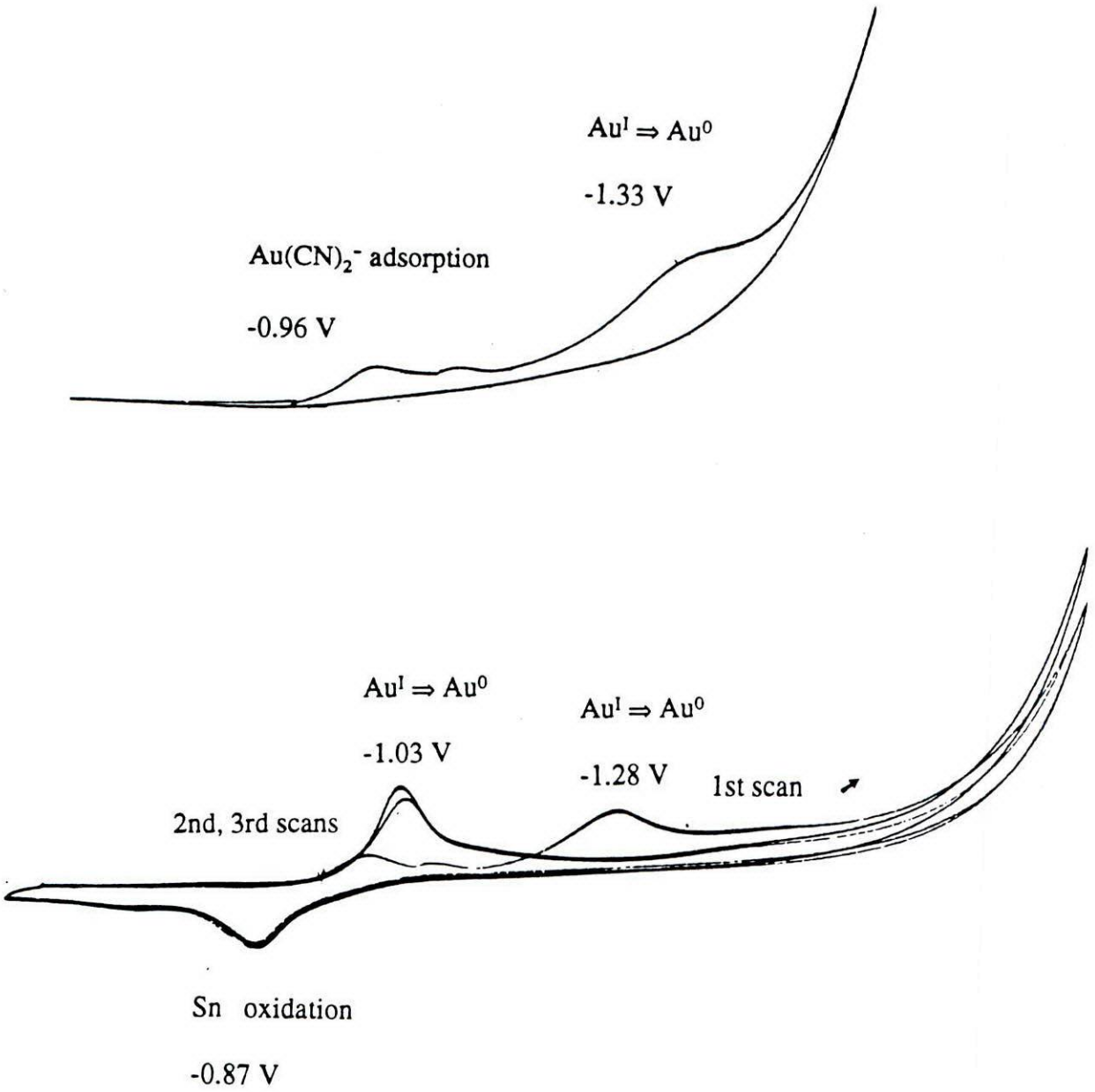

Figure 2. Cyclic voltammograms obtained from electrolytes with composition as in Table I. The upper voltammogram, scanned from -0.6 to -1.5 V with 1.5 g Au per litre and no Sn added, shows reduction characteristics of the Au component while the lower voltammogram, scanned from -0.6 V to -1.8 V with 1.5 g Au and 5 g Sn per litre, shows reduction of the Au component and oxidation of the Sn component as well as depolarization due to alloying of the electrode.

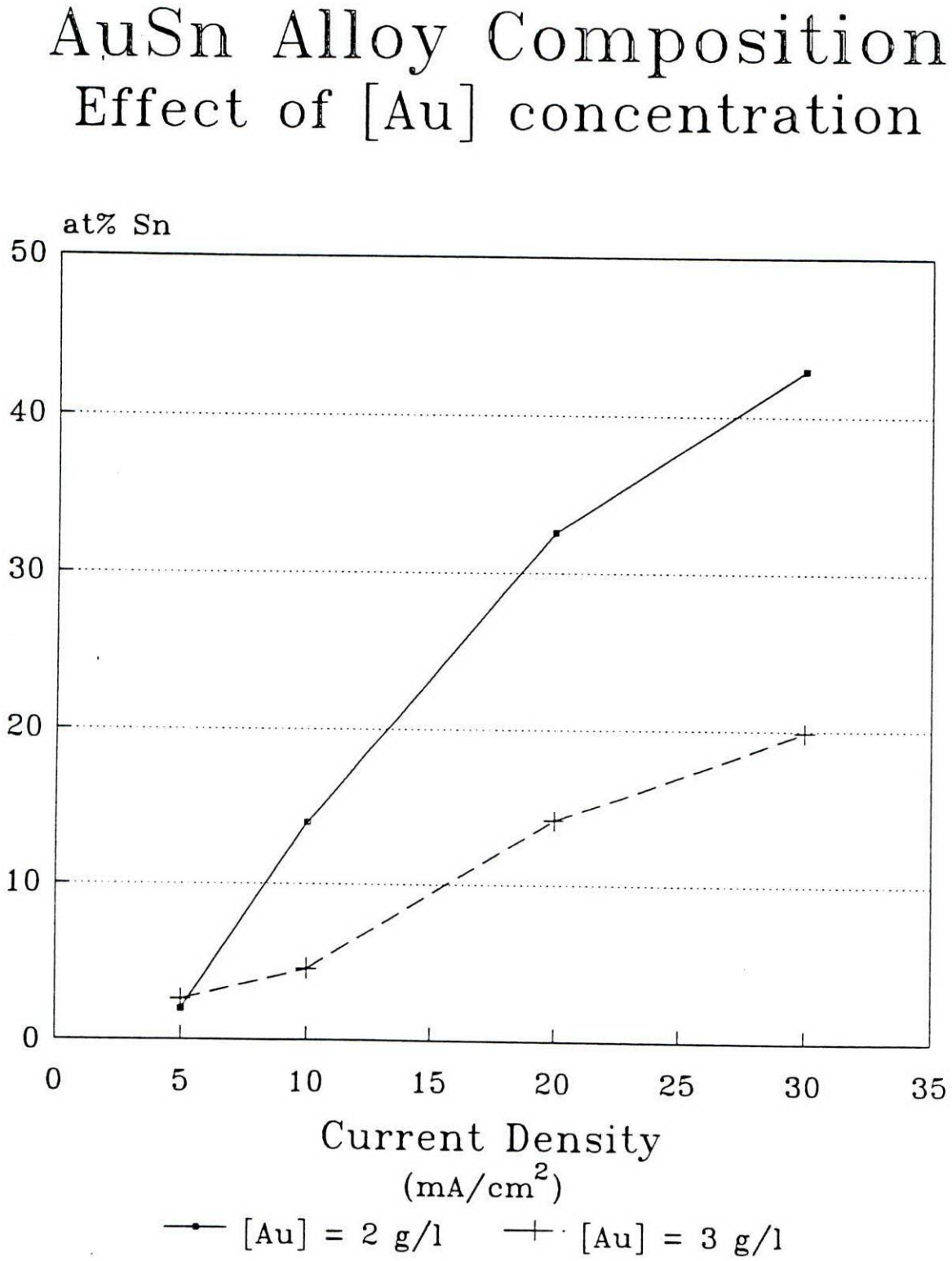

Figure 3. Effect of $Au(CN)_2^-$ concentration at various current densities on deposit alloy composition. Increased $Au(CN)_2^-$ concentration in bath and decreased current density reduces the Sn content in alloy.

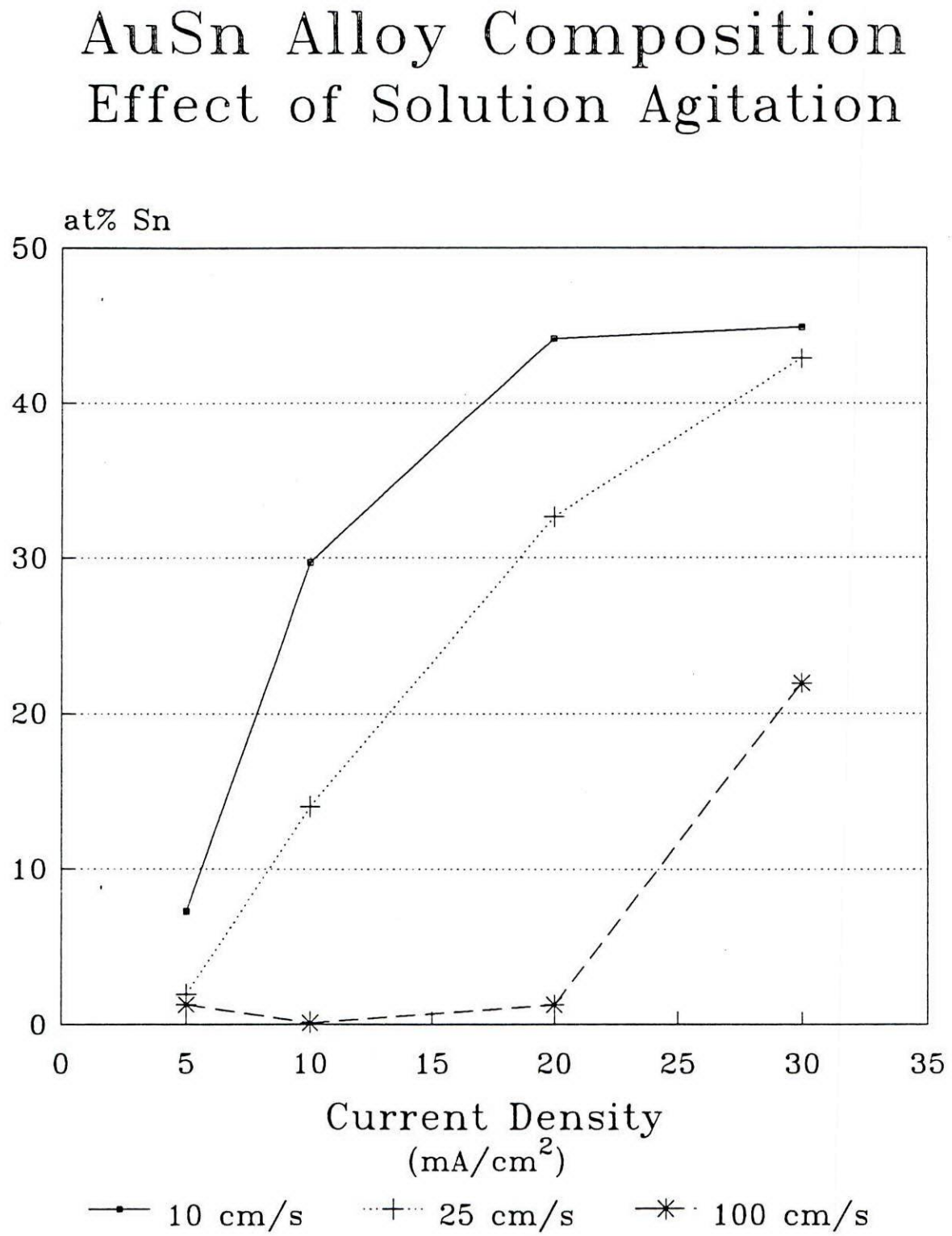

Figure 4. Effect of solution agitation on deposit alloy composition. Increased agitation reduces the Sn content in the alloy.

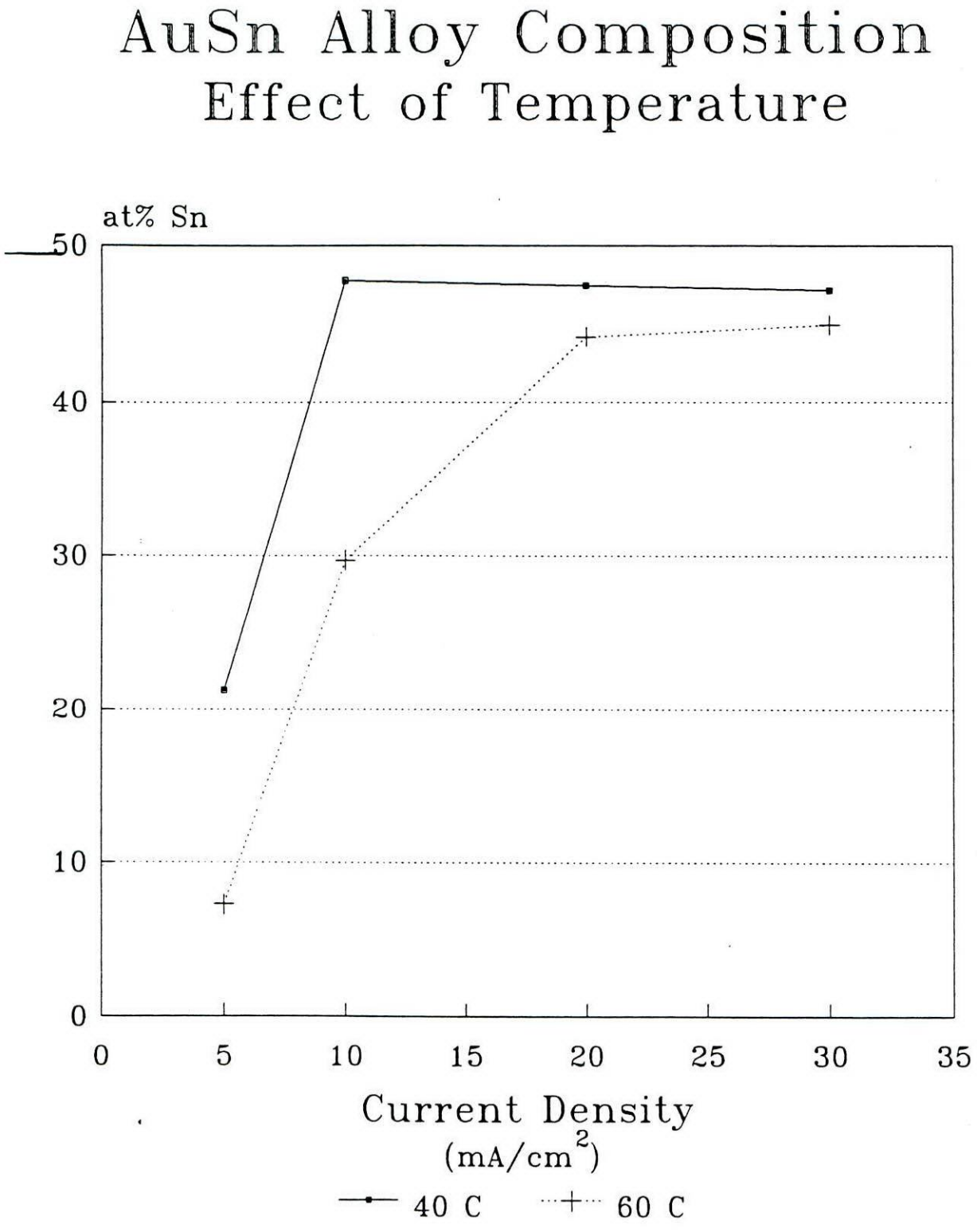

Figure 5. Effect of bath temperature on deposit alloy composition. Increased temperature reduces Sn content in alloy.

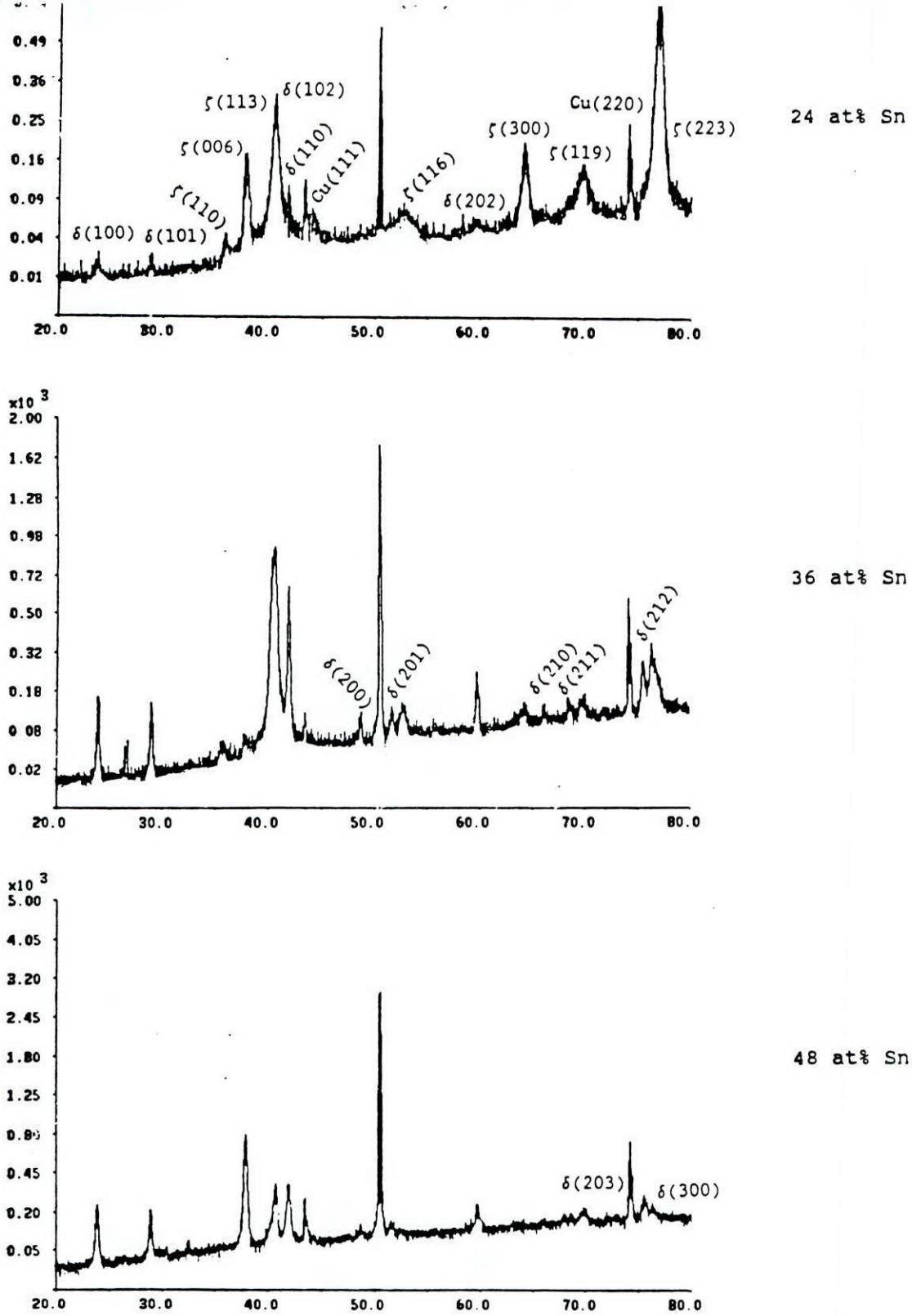

Figure 6. X-ray diffractograms of electrodeposited AuSn alloys with a Sn content of a 24, 36, and 48[at]/o. The ζ and δ-phases are identified.

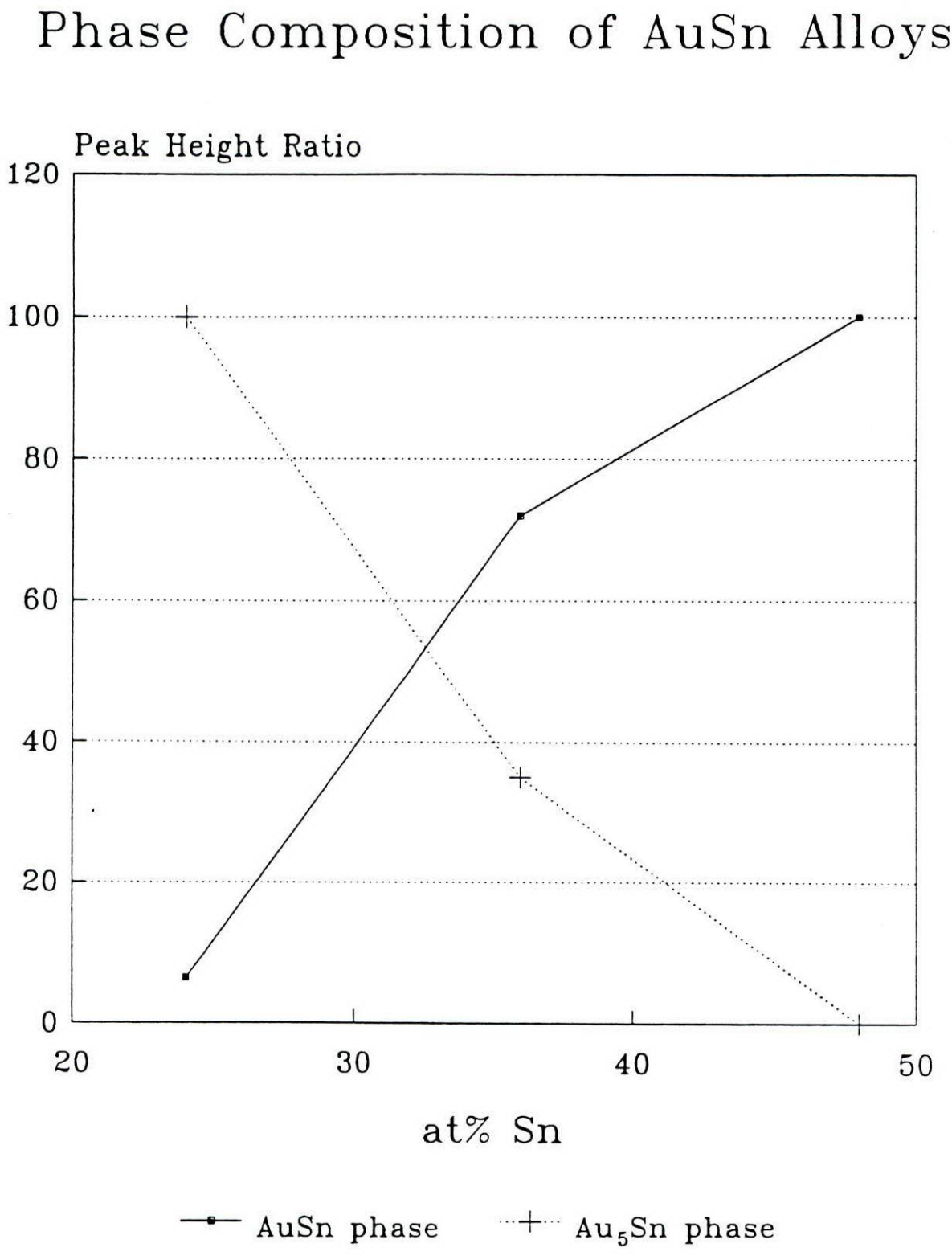

Figure 7. Ratio of δ to ζ-phase of electrodeposited AuSn alloys at 24, 36, and 48at% Sn. The ratio was calculated as the sum of the peak heights of (100) and (101) δ-phase peaks to the sum of the (300) and (306) ζ-phase peaks. The fraction of δ-phase increases with increasing Sn content.

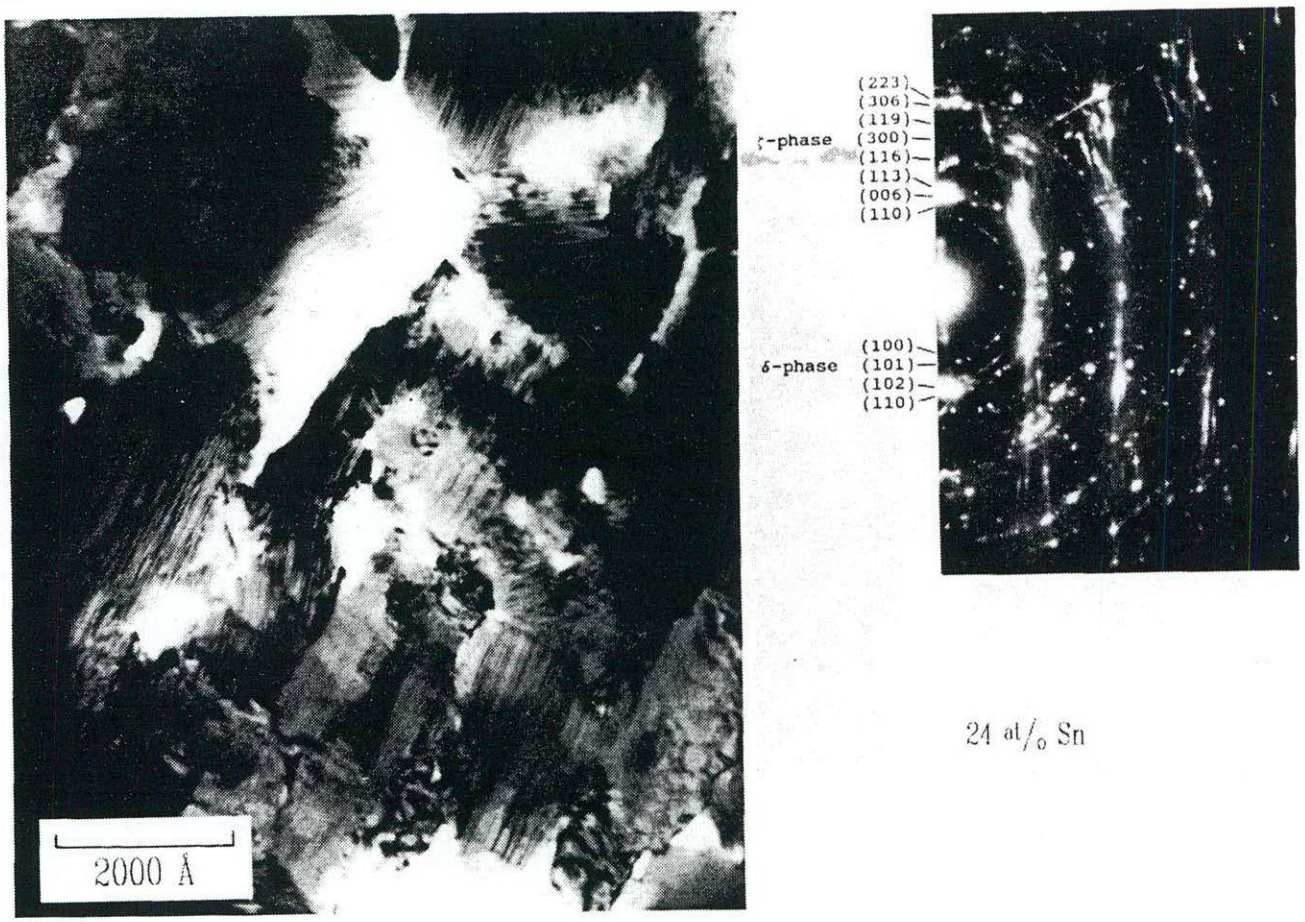

Figure 8a. TEM micrograph illustrating microstructure of electrodeposited AuSn alloy of 24at/o Sn. Both ζ and δ-phase grains are observed. The ζ-phase grains dominate and exhibit lamellar features and streaks in SAD patern while the δ-phase appears defect free.

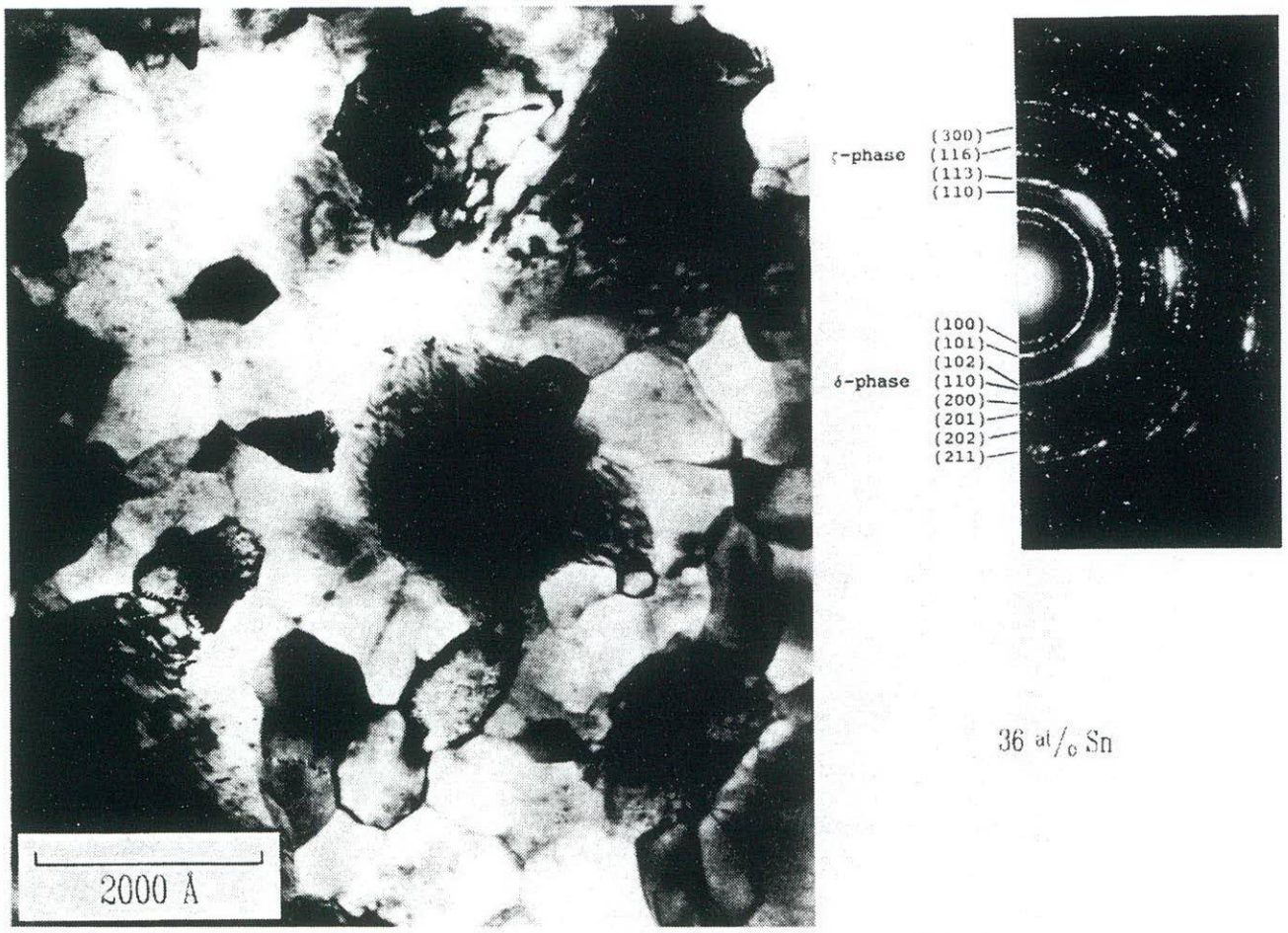

Figure 8b. TEM micrograph illustrating microstructure of electrodeposited AuSn alloy of 36$^{at}/_{o}$ Sn. Only a smaller number of ζ-phase grains are observed. Also in this micrograph the lamellar features and the streaks in the SAD pattern are observed.

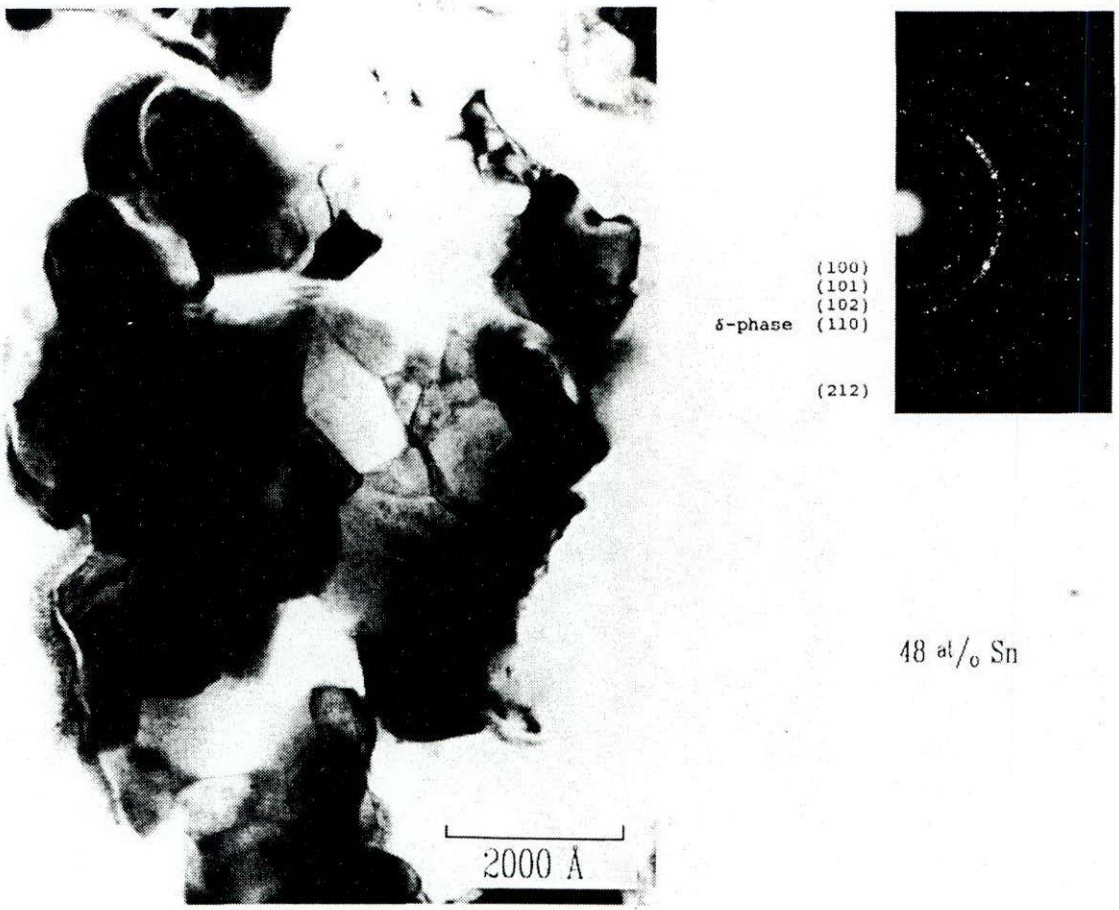

Figure 8c. TEM micrographs illustrating microstructure of electrodeposited AuSn alloy of 48$^{at}/_{o}$ Sn. Mainly defect-free δ-phase grains are observed.

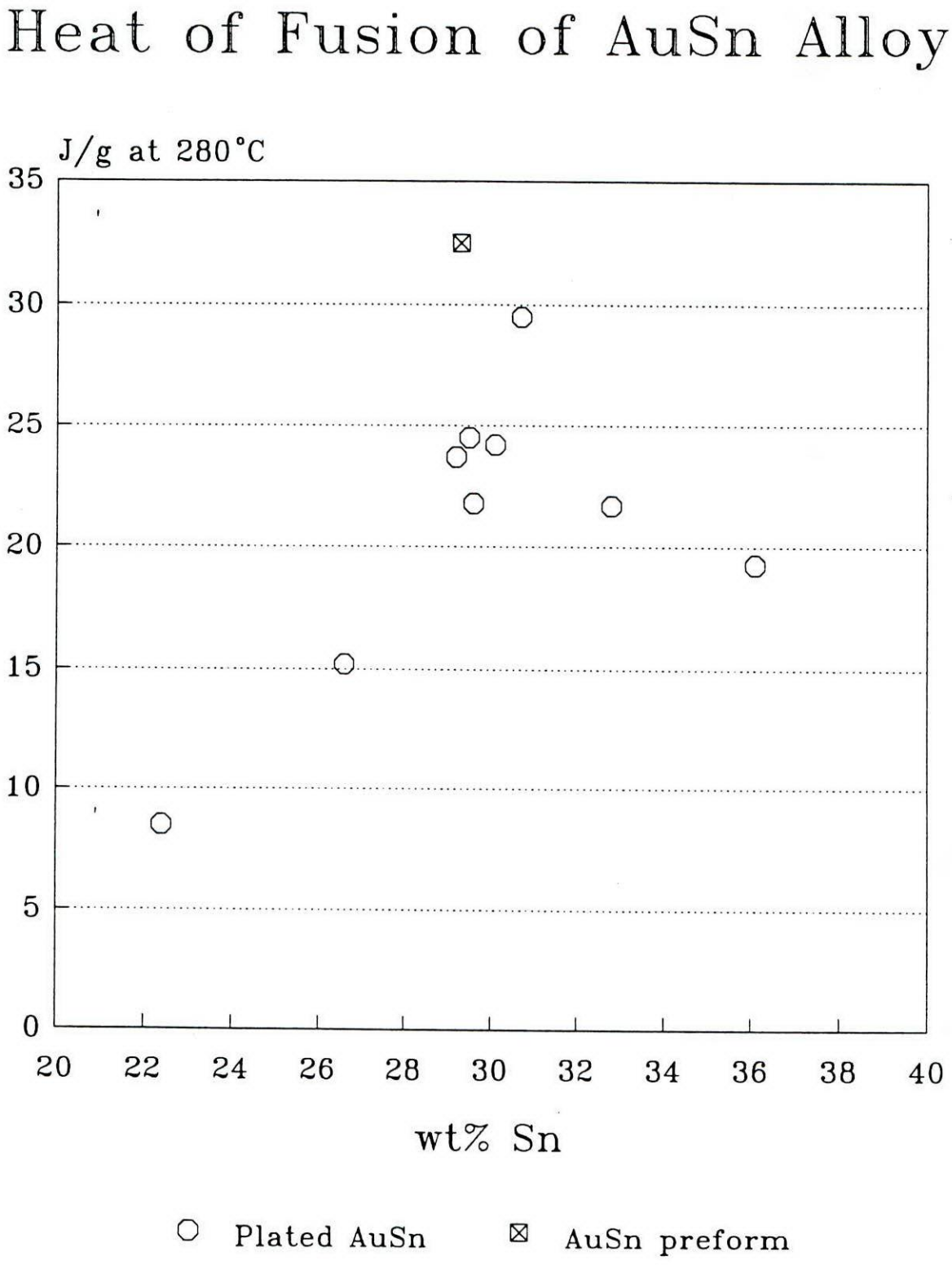

Figure 9. Heat of fusion data obtained by DSC of eutectic preform and of eutectic or near eutectic electrodeposited AuSn alloys.

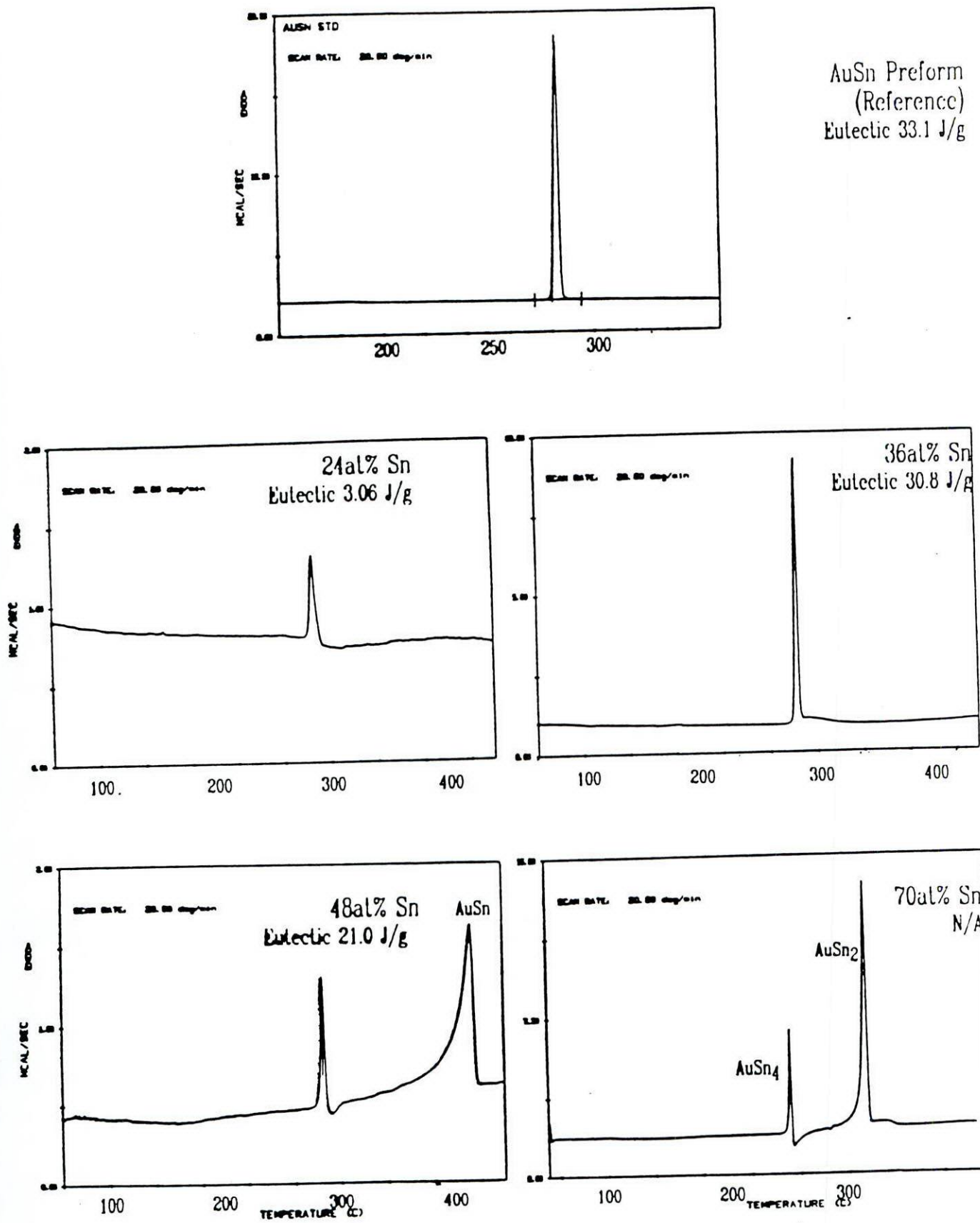

Differential Scanning Calorimetry

Figure 10. DSC graphs showing melting characteristics of preform and electrodeposited AuSn alloys.

NEW AUTOCATALYIC GOLD BATH AND DIFFUSION BARRIER COATINGS

Charles D. Iacovangelo
Physical Chemistry Laboratory
GE Corporate Research and Development
Schenectady, New York 12301

ABSTRACT

Reliability of plated packages after post plating processing steps such as die attach, glass bonding, and lid sealing can be a critical problem causing poor wetting of solder and loss of hermeticity. We have explored three different approaches to obtaining higher reliability gold platings on nickel/tungsten and titanium metallization. These approaches included alloying of nickel and gold, alloying of nickel and cobalt, and discrete barrier layers of palladium or platinum. All three approaches show significant improvement in solder sealing after processing temperatures of 500°C. Of these approaches, electroless palladium or platinum and gold coatings showed superior performance. Critical to the implementation of this approach was the development of a truly autocatalytic electroless gold process for plating on palladium and nickel. Details of this plating composition will be given along with experiments measuring the effect of bath constituents on the activity of selected reducing agents. Experiments with titanium metallized ceramics were conducted with titanium deposited from a molten salt. A brief description of this process will be included.

Introduction

The process of intermetallic diffusion has been shown to be a critical problem in many aspects of microelectronics devices and packaging. [1-10] The thin film thicknesses used in the industry coupled with increasing field temperature use has aggravated this problem. In addition, processing steps such as die attach, epoxy bake, and thermal cycling force the devices to withstand temperatures of several hundred degrees Celsius.

Hall [1] has divided the problems associated with diffusion in microelectronics into three groups; shown in Fig. 1. First, an interface can redistribute its materials to form a weakened or brittle layer. In general, this process can cause loss of strength or delamination. In the absence of intermetallic ordered phases, however, this process can also enhance adhesion e.g. diffusion bonding. Second, the basic material properties of the layer can be altered; eg. resistivity. Third, a surface can be contaminated by diffusion of an underlying material via grain boundaries This can cause problems in joining (eg. soldering, thermo compression bonding or ultrasonic bonding).

The focus of this paper is contamination of the surface gold with the underlying nickel. Nickel diffusion through the grain boundaries in gold [2] during die attach [3,4] has been shown to cause problems with TC wire bonding [5,6], soldering to kovar lead material [7] and soldering ceramic lids for hermetic packages.[8]. Similar problems have been observed with copper underlayers [9-11] where nickel has been used as a barrier for copper. Nickel, however, was later shown [12] to exhibit the problem as well. Although, as outlined, nickel transport through gold causes several problems, this paper will deal principally with the inhibition of solder flow during the lid sealing operation of hermetic packages [8].

Three approaches to suppress the diffusion of nickel through gold were examined in this study. First, the use of a barrier layer material between the nickel and gold layer. The principle

criteria for such a material is that it block the diffusion of nickel, that it not transport to the gold surface, and that it not interfere with the prerequisite functions of the gold and nickel layers. The materials studied were: Pd, Pt, Pd/Ni, and Co. The second approach was replacing the nickel layer with a Ni/Co alloy. Third, forming a Ni/Au alloyed layer between the pure Ni and Gold layers.

Experimental Approach

The effectiveness of the different approaches to suppressing nickel diffusion were examined by analyzing the surface of the gold for nickel and the barrier materials after heat treating in air at 430-500°C for 5-15 minutes. All measurements were done with a PHI 545 Auger microprobe. Depth profiles from the surface toward the nickel layer were obtained by sputtering with 2.5 kilovolt xenon ions at six second intervals. The ion gun was turned off during auger analysis. The sputtering rate was about 100 angstroms per minute. In selected samples, auger data was correlated with lid sealing results carried out as taught by Yang [8]. The criteria used in these tests were the ability of the solder to wet the gold seal-ring and the hermeticity of the sealed package.

Two types of substrates were used in this study. The first was a standard screen printed tungsten cofired alumina leadless chip carrier. The tungsten metallization on the die pad and seal ring were used as the substrate for nickel, cobalt, palladium, gold, and platinum coating. Nickel and cobalt were deposited by a CVD process [13]. Palladium was electrolessly deposited using a Callery First Choice® bath. Gold was electrolessly deposited from two different solutions. Gold over nickel, cobalt, and Ni/Co alloys was deposited from a hydrazine based chemistry [14]. Gold over palladium and platinum substrates was deposited from a DMAB based electrolyte [15]. Platinum was electroplated using a composition described by Reid [16].

The second type of substrate was a 99.5% alumina substrate metallized with a thin film of Ti as a bond layer between electroless platings and the ceramic [17]. These substrates were prepared by coating the ceramic substrate with a paste consisting of Ti powder (400 mesh), 50/50 mole % NaCl/KCl, and water. This paste was spread on the alumina and dried in Argon at 175°C. The package was then fired in 10% hydrogen/Argon at 800-1000°C for one hour. After cooling to room temperature, the paste was lifted from the substrate and the Ti coating cleaned of residual salt with a simple deionized water wash and dried.

Results and Discussion

As outlined earlier, nickel diffusion through a gold overplate during fabrication e.g. die attach, can cause several problems for hermetic ceramic packages. Shown in Figure 2 is a typical Auger surface analysis of a 1.5μm electrolytic gold layer over electrolytic nickel after heat treating for 5 minutes at 430°C in air. This plot clearly shows the presence of nickel which has diffused through the gold layer. A depth profile of the same sample, presented in Fig 3, shows that the nickel on the surface extends for approximately 200Å into the gold layer. This profile is typical of grain boundary diffusion where the nickel diffuses through the grains of the gold to the surface while the actual nickel concentration in the bulk is very small; Figure 1c. Figure 3 also shows that oxygen is associated with the nickel on the surface. It is the oxidation of the nickel on the surface that causes the solder wetting problems and is also the driving force for continued build up of nickel on the surface with time at temperature. In the absence of oxygen, the nickel diffusion is greatly retarded.

Duplex Gold

To suppress the nickel diffusion demonstrated in Fig 2 and 3, the use of barrier layers was examined. Since the principle mode of nickel diffusion has been shown to be grain boundary diffusion, several approaches are possible. One approach is to reduce diffusion by altering the grain structure of the gold. This can be accomplished by plating a thin layer of gold over the nickel and heating the two layers to melt the gold layer and alloy the nickel and gold. This heat treatment in addition to altering the grain structure of the gold, also lowers the nickel activity at the interface between the alloyed Ni/Au layer and the subsequent pure gold layer [18]. This approach,"Duplex Gold", is shown schematically in Fig 4.

To achieve such a layer requires an optimization of heating high enough and long enough to sinter the gold layer while minimizing nickel diffusion into the layer. In general, it has been found that short profiles at high temperatures favor nickel transport over gold grain growth. A more desirable profile has a dwell time of approximately. 20-30 minutes at a reasonable temperature. Shown in Fig 5 is the surface of a thin, 0.5 μm electroless gold layer over electroless nickel after varying heat treatments in a 10% H_2/Ar atmosphere. As shown, the deposit without any heating has a very marked grain structure. With heating, the grain structure is altered. At 550°C the Au layer takes on the appearance of a melted large grain structure. The optimum heat treatment temperature was determined by the ability of the layer to suppress nickel transport. Shown in Fig.6 are Auger depth profiles of electroless gold deposits over "Duplex-Gold" barrier layers formed by various heat treatments. In all cases, the electroless nickel layer was sintered to obtain a clean smooth surface prior to plating and forming the Ni/Au barrier layer. The thickness of the Ni/Au barrier layers were 0.5 μm and pure gold layers were 1.5 μm. Heat treatments were done in 10% H_2 balance argon. The depth profiles were taken after subjecting the parts to 430°C for 5 minutes in air to simulate a typical die attach profile. The scale of Fig 6 is exaggerated over that of Fig 3 to point out several salient features. First, a low temperature heat treatment of 450°C, typical of that used to obtain adhesion, has almost no affect on retarding Ni transport. This correlates with SEM analyses which showed no apparent modification of the gold deposit. In fact, the large number of small grains in the deposit have a sufficient amount of nickel dissolved in the grains to be apparent in the Auger depth profile well beyond a surface contamination. In contrast, the deposits heat treated at elevated temperatures to obtain a barrier layer show no significant nickel in the deposit after some finite distance from the surface. Fig 6 shows that the amount of nickel on the surface and the thickness of the nickel layer decrease with increasing temperature to 700°C. No further decrease in Ni transport was observed after heat treating at 800 and 900°C.

As noted earlier, the goal in reducing nickel transport to the gold surface was to improve the ability of nickel and gold plated parts to accept a solder lid seal. Shown in Table 1 are lid seal results on leadless chip carriers. As shown, parts without a barrier layer (no heat treating of 1st gold) demonstrated poor wetting behavior even with a reduced die attach time of one minute; 50% failure. A clear improvement in seal ring wetting was obtained with increasing the forming temperature of the barrier layers from 600 to 700°C.. Optimizing the heat treatment between 700 and 750°C was difficult due in part to insufficient control of Po_2 and lid seal pressure in the lid sealing facility, and in part due to factors other than nickel transport which can inhibit solder wetting of the seal ring. The results obtained with "Duplex-Gold" parts prepared at 750°C however, were excellent showing consistently 98-100% yield in solder wetting and hermeticity.

TABLE 1. Lid Sealing Results with Electroless "Duplex Gold"

1st Au Heat Treat Temp(°C)	Simulated Die Attach Time at 430°C (min)	# Pieces	Complete Wetting #	Complete Wetting %	Hermetic #	Hermetic %
-	1	10	5	50	NA	NA
-	5	10	2	20	NA	NA
600	1	10	8	80	NA	NA
600	5	10	5	50	NA	NA
650	1	55	51	93	55	100
650	5	20	15	75	20	100
700	1	70	68	97	70	100
700	5	20	19	95	20	100
750	5	200	199	99.5	194	97
750	5	223	221	99	220	98.6
750	5	228	228	100	224	98.7
750	5	150	150	100	148	98.7

Platinum And Palladium Barriers

Figure 6 showed that the "Duplex Gold" process is limited in ability to retard nickel transport. After heat treating at 430°C for 5 minutes the process does allow ~10% nickel ~80A thick on the surface of the gold. Although this has been sufficient to achieve the excellent lid sealing results shown in Table 1, there are parts which demand longer and hotter processing and hence more severe nickel transport. For example, glass seals used to attach lead frames require processing to 500°C for up to 5-10 minutes. As such experiments have been conducted with alternative materials to further retard nickel transport. As noted earlier, one of the pivotal requirements of such a material is that nickel diffuse slower through it than gold and that the material itself not diffuse rapidly through gold. Table 2 lists selected references of diffusivity data along with the estimated distance of penetration based on the following equation:

$$X^2 = 4D't \qquad [1]$$

Where X = the penetration distance(cm), D'= grain boundary diffusivity (cm^2/sec), and t = time (sec).

Table 2 shows that the transport of Pt and Pd through gold is several orders of magnitude slower than nickel. Although there is some variability in the absolute value from different authors, the differences are small compared to the difference between these materials and nickel. Table 2 also shows that the transport of gold into Pt and Pd is slow so that no significant loss of gold would be expected. In order for Pt, or Pd to be viable barrier layers the nickel transport through them most also be slow. As shown, the transport of Ni through Pt is orders of magnitude slower than through gold. No data on nickel transport through palladium was found.

TABLE 2. Grain Boundary Diffusion Data

Material/ Overplate	Do'(cm^2/sec)	Q (KJ/mole)	D'430°C(cm2/sec)	X(μm)	X (μ")	Reference
Fe/Au	$2.7x10^{-5}$	84.0	$1.55x10^{-11}$	1.36	53.69	7
Ni/Au	$3.0x10^{-3}$	113.0	$1.22x10^{-11}$	1.21	47.64	7
Co/Au	$4.8x10^{-4}$	108.8	$3.97x10^{-12}$	0.69	27.17	7
Pt/Au	$1.0x10^{-3}$ $6.6x10^{-8}$	159.2 91.5	$1.49x10^{-15}$ $1.05x10^{-14}$	$1.33x10^{-2}$ $3.55x10^{-2}$	0.53 1.40	19,20
Pd/Au	$6.0x10^{-10}$ $1.6x10^{-10}$	66.6 57.9	$6.82x10^{-15}$ $8.0x10^{-15}$	$2.86x10^{-2}$ $6.00x10^{-2}$	1.12 2.36	21,22,24
Ni/Pt	$1.3x10^{-6}$	125.4	$6.4x10^{-16}$	$8.74x10^{-2}$	0.34	23,25
Pt/Ni	$2.6x10^{-9}$	78.2	$4.0x10^{-15}$	$2.19x10^{-2}$	0.86	26
Au/Ni	$1.4x10^{-7}$	199.6	$1.8x10^{-16}$	$4.68x10^{-3}$	0.18	26
Au/Pt	$1.8x10^{-2}$	159.2	$2.7x10^{-14}$	$5.67x10^{-2}$	2.23	27
Au/Pd	$2.2x10^{-8}$	86.8	$8.0x10^{-15}$	$3.09x11^{-2}$	1.22	22

Based upon this data,a series of experiments were carried out to determine the effectiveness of Pt and Pd as barrier layers. A summary of the data is presented in Table 3. The data in Table 3A were obtained using CVD Ni coated W cofired ceramic substrates. The data in Table 3B were obtained using 2.5μm Ni/P over 2.0 μm copper plated titanium bonded ceramic substrates described earlier. The tabulated data include: barrier metal and thickness, gold thickness, simulated die attach time and temperature, concentration and thickness of nickel on the surface, and surface concentration of Pt and Pd. Selected Auger depth profiles are presented in Fig.7-9. Several salient features are obvious from the data. First, both Pd and Pt are excellent barriers to nickel transport. With the exception of the thin (0.25μm) Pd barrier with thin (0.75μm) gold, all deposits showed marked decrease in Ni transport. From a cost standpoint, it would be advantageous to reduce the gold thickness if Pd or Pt was a sufficient barrier. Comparing samples 1 and 2 (fig 7 and 8) with samples 3 and 4 shows that 0.5 μm of Pd was able to suppress Ni transport with either 0.25 or 1.0 μm of gold. Thinner Pd, 0.25 μm, was not effective with reduced gold thickness. Thin gold deposits had an appreciable amount of Pd on the surface (14-20%) compared to the thicker gold deposits (0-3%). These Pd levels were sufficient to change the color of the gold and to prevent solder wetting during lid sealing. It is clear from these results that Pd cannot be used with reduced gold thickness. Additional testing with nominal 1.5 μm of gold, however, show excellent barrier capabilities. The effect of extending the time of die attach from 5 to 10 minutes is shown in examples 5 and 6. In Sample 5, (0.25 μm Pd) the amount of nickel transport to the gold surface increased from 3 to 9% along with an increase in thickness from 20 to 50 Å. In comparison, Sample 6 (0.5 μm Pd) showed only 2% Ni on the surface. Extending the heat treatment to 485°C for 15 minutes, Sample 12, showed only 1% Pd on the surface. The amount of Ni increased to 12% ~ 180Å thick.

TABLE 3A. Diffusion Through Pt and Pd Barrier Layers, Over CVD Ni Coated Tungsten Substrates

Sample	Barrier Layer Matl	Barrier Layer (μm)	Gold Thickness (μm)	Heat Treat Temp (°C)	Heat Treat Time (min)	Auger Surface Analysis Ni (%)	Ni (Å)	Pd, Pt (%)
1	Pd	0.25	0.75	430	5	20	80	14
2	Pd	0.25	1.50	430	5	3	20	3
3	Pd	0.50	0.75	430	5	0	—	20
4	Pd	0.50	1.50	430	5	6	20	—
5	Pd	0.25	1.50	430	10	9	50	3
6	Pd	0.50	1.50	430	10	2	20	2
7	Pt	0.25	1.0	430	5	3	20	0
8	Pt	0.50	1.45	430	5	—	—	0
9	Pt	0.50	1.45	430	10	—	—	0
10	Pt	0.50	1.45	485	15	4	60	
11	Pt	1.0	1.50	485	15	3	20	0
12	Pt	0.50	1.55	485	15	12	180	1

TABLE 3B. Ni/P Copper, Ti Substrates

Sample	Barrier Layer Matl	Barrier Layer (μm)	Gold Thickness (μm)	Heat Treat Temp (°C)	Heat Treat Time (min)	Auger Surface Analysis Ni (%)	Thickness (Å)	Pd(%)
1	Pd	1.0	1.5	500	15	5	40	2
2	Pd	1.0	2.0	500	15	1	<20	0
3	Pd	1.0	3.0	500	15	2	<20	0
4	Pd	2.0	1.5	500	15	45	20	4
5	Pd	2.0	2.0	500	15	0	0	0
6	Pd	2.0	3.0	500	15	0	0	0

Table 3B shows the effect of increasing the Pd and Au thicknesses up to 2.0 and 3.0 μm respectively. These were carried out over Cu substrates to ensure that copper transport would not be an issue. As shown, with 2.0 μm of Pd and 2-3 μm of Au excellent results were obtained. Ten samples of these thicknesses were subjected to MIL SPEC 883 testing and showed 100% hermeticity.

Shown in Table 4 is the gold composition used to plate these parts. This bath was developed to overcome the poor platability of Pd and Pt with commercial solutions. Details of this bath have been described earlier [28-30]. In the formulation, triethanol amine (TEA) has been shown to improve the initial gold nucleation on Pd and Pt substrates. Carbonate accelerates the oxidation of DMAB and Hydrazine without affecting bath stability. Combining these with a controlled low cyanide activity results in a stable truly autocatalytic gold bath with a high plating rate. Shown in Figure 9 is an S.E.M. of the electroless gold deposit over nickel and palladium substrates.

TABLE 4. Autocatalytic Electroless Gold Formulation

$KAu(CN)_2$	0.005M
KCN	0.035M
KOH	0.80M
K_2CO_3	0.75M
TEA	0.10M
DMAB	0.05M
N_2H_4	0.25M
Lead Acetate	5 PPM

Platinum appears to be an excellent barrier material. Nickel transport after 5 minutes with 0.25 μm of Pt and 1 μm of gold (sample 7) was limited to 3% Ni approximately 20Å thick. Increasing the Pt thickness to 0.5 μm (Samples 8 and 9), showed no Ni on the surface of the gold after 5 and 10 minutes at temperature. Unlike the Pd samples, no Pt was observed on the surface of the gold in any of the samples. Increasing the die attach time and temperature to 485°C for 15 minutes (samples 10 and 11) resulted in no Pt on the surface and only 3-4% Ni 20-60Å thick. It is clear from these results that Pt is an excellent barrier material.

Nickel, Cobalt, and Alloys

It was shown earlier that cobalt diffusion through gold is slower than nickel. As such, replacing nickel with cobalt is a potential alternative but with limited application due to the amount of cobalt transport observed. It should be possible to reduce the amount of cobalt or nickel transport by alloying the metals. This would reduce the activity of both metals in the alloy and lower the driving force for metal transport. Listed in Table 5 and plotted in Figures 10 and 11 are the results obtained from a series of Ni/Co vapor deposited alloys [13]. As shown, decreasing the activity of Ni and Co results in decreased transport of each material. With respect to a 430°C heat treatment, a minimum in transport was observed with a 63 Ni37 Co alloy; approximately 2% Ni 40Å thick and no cobalt on the surface of the gold. Such a result is superior to the best obtained with duplex gold. At higher cobalt levels, cobalt was found on the surface. Ni/Co alloys perform well even under the extremely stringent heat treatment of 485°C for 15 minutes. The minimum transport was observed with a 40 Ni 60 Co alloy; approximately 4% Ni and 1% Co. This results is comparable to the results obtained with Pt barriers with respect to surface Ni concentration. However, a measurable Ni conc. of approximately 1-2% in the Au was observed for several hundred angstroms, compared to 20-60Å with Pt.

It is clear from these results that alloying Ni and Co decreases the transport of each metal over that of pure deposits. The optimum cobalt content to minimize both nickel and cobalt transport was found to be 40-60%. It should be pointed out, however, that from a product standpoint other factors such as ductility, solderability, and corrosion protection must all be considered. Final optimization of the deposits must trade off these factors against substrate migration through the gold coatings.

TABLE 5. Nickel and Cobalt Diffusion Through 1.5 μm Electroless Gold

Sample	Substrate	Heat Treatment		Gold Surface Analysis			
		Temp (°C)	Time (Min)	Ni (%)	Ni Thick (Å)	Co (%)	Co Thick (Å)
1	CVD 100 Ni O Co	430	5	12	120	—	—
2	CVD 70 Ni 30 Co	430	5	6	100	—	—
3	CVD 63 Ni 37 Co	430	5	2	40	—	—
4	CVD 40 Ni 60 Co	430	5	2	40	2	40
5	CVE 30 Ni 70 Co	430	5	1	40	3	40
6	CVD 100 Ni 0 Co	485	15	25	500	—	—
7	CVD 70 Ni30 Co	485	15	8	400	—	—
8	CVD 63 Ni 37 Co	485	15	10	500	—	—
9	CVD 40 NI 60 Co	485	15	4	500	1	42
10	CVD 30 Ni 70 Co	485	15	2	200	5	200

Conclusions

Three different approaches to reducing nickel transport and improving solderability of nickel and gold plated ceramic chip carriers were investigated. Altering the gold grain structure by "Duplex-Gold" plating has been shown to be an effective means of retarding nickel migration. This process has demonstrated consistently high lid sealing yields with both electrolytic and electroless gold coatings. The conditions employed to alter the gold grain structure are critical and depend on the type of nickel and gold deposits being used. Replacing the nickel layer with a Ni/Co alloy has also been shown to retard nickel and cobalt transport compared to the pure materials. The optimum Co appears to be approximately 40-60%. The most effective means of retarding nickel transport was to separate the nickel and gold layers with a barrier layer of either Pd or Pt. Each material is an effective barrier to nickel transport. Palladium, is a much less expensive material than Pt but may have an unacceptable transport through gold. Thus the lower materials cost may be offset by the gold thickness required with Pd compared to Pt. Of the three methods studied, only "Duplex-Gold" plating has undergone considerable reliability testing in engineering and production parts. The other two method show excellent potential but must undergo a battery of reliability testing.

Acknowledgements

The author wishes to acknowledge the extensive work of M. D. McConnel in obtaining Auger surface analysis, the assistance of R. King, O. H. LeBlanc, Jr. and D. S. Park in sample preparations, and C. A. Markowski and J. A. Pagois for preparation of the manuscript.

REFERENCES

[1] Hall, P. M., Morabito, J. M., *Thin Solid Films*, 53, 175, (1978)
[2] Thompkin, H.G., Pinnel M.R., *J. Applied Physics*, 489, 3144, (1977)
[3] Casey, G. J., Jr., Endicott, D.W., *Plat. & Surf. Fin.*, 67,39 (July 1980)
[4] Enidcott, D. W. Casey, G. J., Jr., *Plat & Surf Fin.*, 67, 58 (March 1980)
[5] McGuire, G. E., Jones, J. V., Dowell, H. J., *Thin SolidFilms*, 45,59 (1977)
[6] Hag, K. E., Behrndt, K. H., and Kobin, I., *J. Vac. Sci. Technol.*, 6, 148 (1969)
[7] Swartz, W.E. et al., *Thin Solid Films*, 114, 349, (1984)
[8] Yang, W.M.C., Solid State Technol., 137 (December 1984)
[9] Marx, D. R., Bitler, W. R., and Pickering, H. W., "Atmospheric Factors Affecting the Corrosion of Engineering Metals," ASTM STP 6465, S. K. Coburn, Ed., American Society for Testing and Materials, 1978, pp 48-57.
[10] Turn, J. C., Owen, E. L., *Plating*, 1015, (November 1974)
[11] Panousis, N. T., Hall, P.M., *Thin Solid Films*, 53, 183 (1978)
[12] Brady, T.E., Hovland, C. T., *J. Vac. Sci. Technol.*, 18(2), 339, (March 1981)

[13] Park, D.S., US. Patent 4,664,941, 1967
[14] Iacovangelo, C. D., Zarnoch, K.P., US Patent 4,863,766, September 5, 1989
[15] Iacovangelo, C. D., US Patent 4,978,559, December 18, 1990
[16] Reid, F. H., *Metallurgical Review*, 8, p 192, (1963)
[17] Iacovangelo, C.D., US Patent Appl. RD 20,256
[18] Iacovangelo, C. D., US Patent Appl. RD 17,537, 1986
[19] Nowark, W. B., Dyer, R. N., *J. Vac. Sci. Technol.*, 9(1), 279,1972
[20] Shinha, A.K., Smith, T.E.,Sheng, T.T.,*Thin SolidFilms*, 22(1), 1 (May 1974)
[21] Hall, P. M., Morabito, J.M., and Poate, J.M., *Thin Solid Films*, 33, 107, (1976)
[22] Debonte, W. J., Poate, J.M., *Thin SolidFilms*, 25,441, (1975)
[23] Hirai, Y., Yamamoto, S., *J. Chem. Phys.*, 75(3), 1560, (August 1981)
[24] Murakami, M., DeFontaine, D., and Fodor, J., *J. Appl. Phys.*, 47 (7), 2850, (July 1976)
[25] Chang, Chin-An, Chu, W.K., *J. Appl. Phys.* 52(1), 512, (January 1981)
[26] Van Den Belt, T.G.M., DeWit, J.H.W., *Thin Solid Films*, 109,1, (1983)
[27] McGuire, G.E., Wisseman, W.R., and Holloway, P.H., *J. Vac. Sci. Technol.*, 15(5), 1701, (Sept/Oct 1978)
[28] Iacovangelo, C.D., US Patent 4,979,988, December 25, 1990
[29] Iacovangeo, C.D., US Patent 4,985,076, January 15, 1991
[30] Iacovangelo, C. D. *J. Electrochemical Soc.*, Vol. 183, No. 4, p 976, April 1991

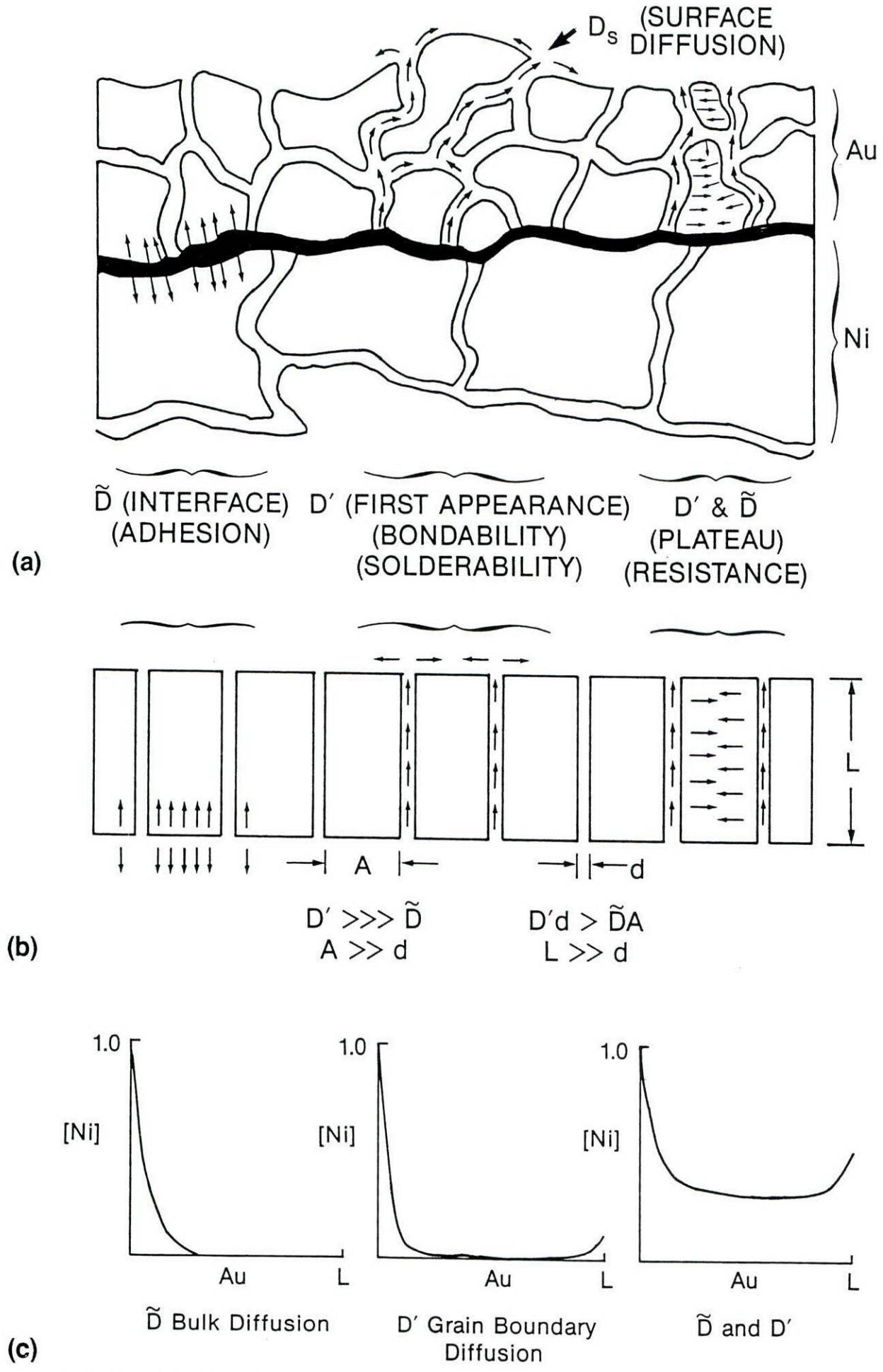

Fig. 1 a) Schematic diagram of the processes involved in diffusion from [1]; b) Idealized model of these processes; c) Idealized Ni acitivty in each layer due to these processes.

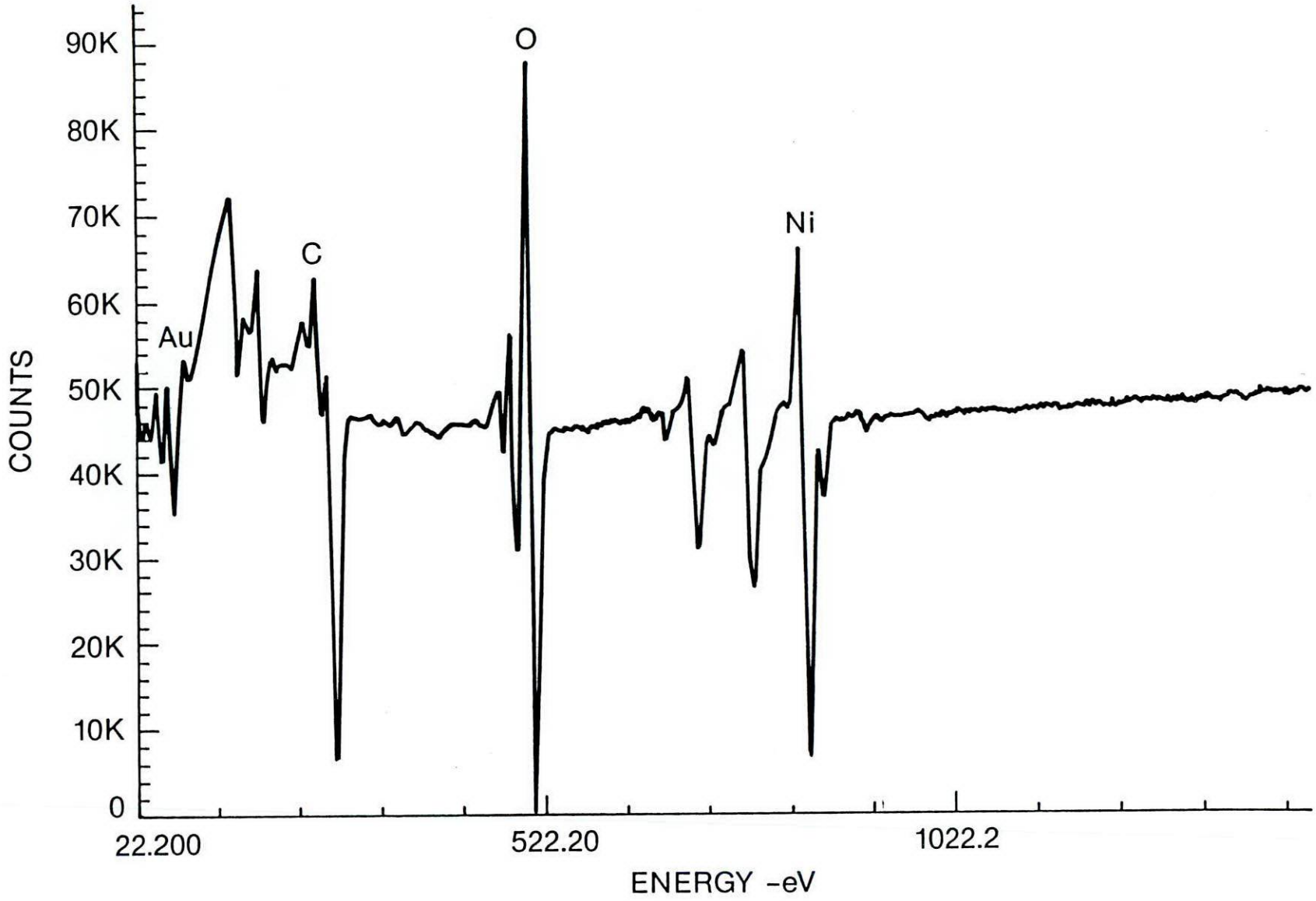

Fig. 2 Auger surface analysis of an electrolytic gold layer over nickel after heat treating for 5 minutes at 430°C in air.

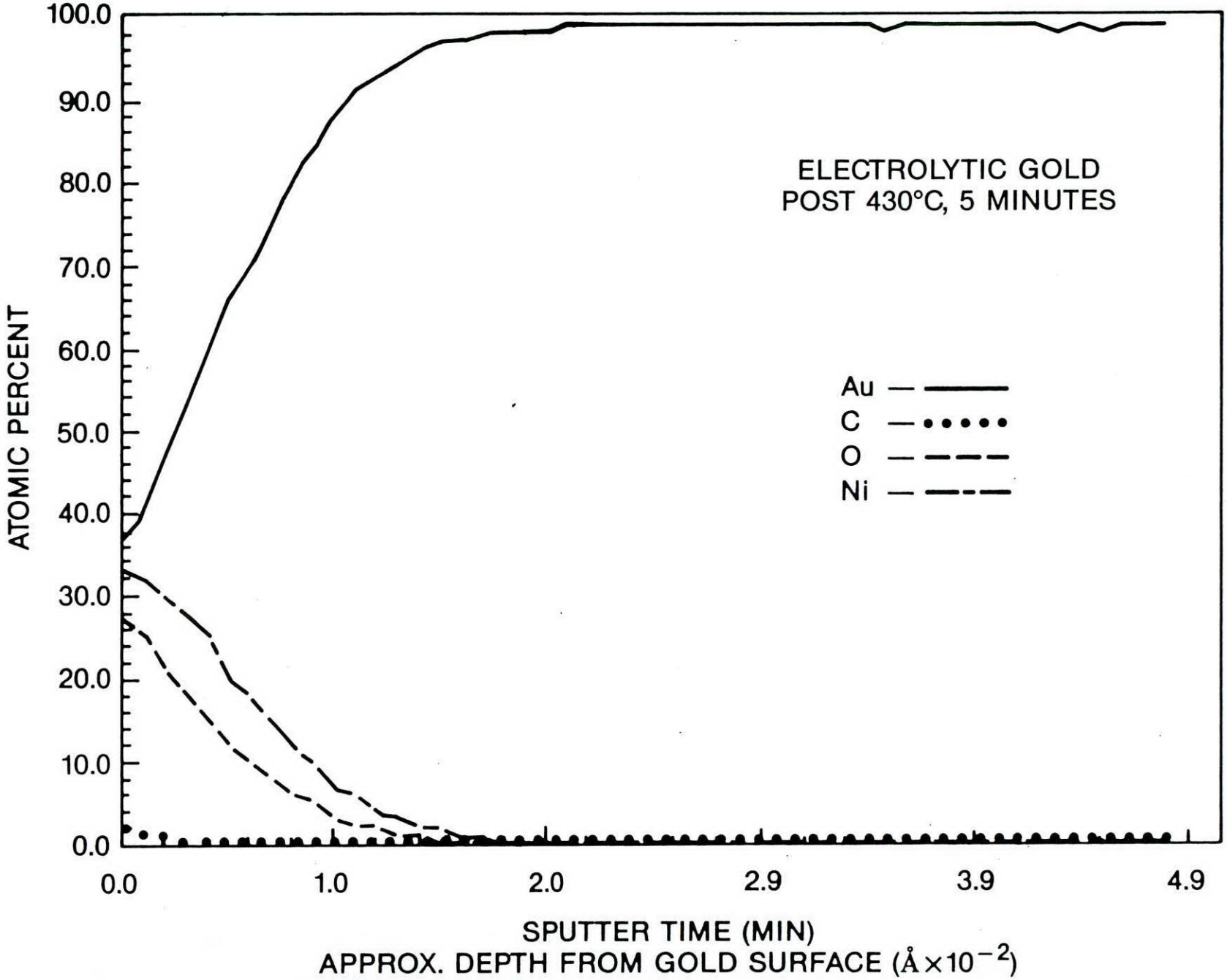
100.0
90.0
80.0
70.0
60.0
50.0
40.0
30.0
20.0
10.0
0.0
ATOMIC PERCENT
ELECTROLYTIC GOLD
POST 430°C, 5 MINUTES
Au
C
O
Ni
0.0
1.0
2.0
2.9
3.9
4.9
SPUTTER TIME (MIN)
APPROX. DEPTH FROM GOLD SURFACE (Å×10⁻²)

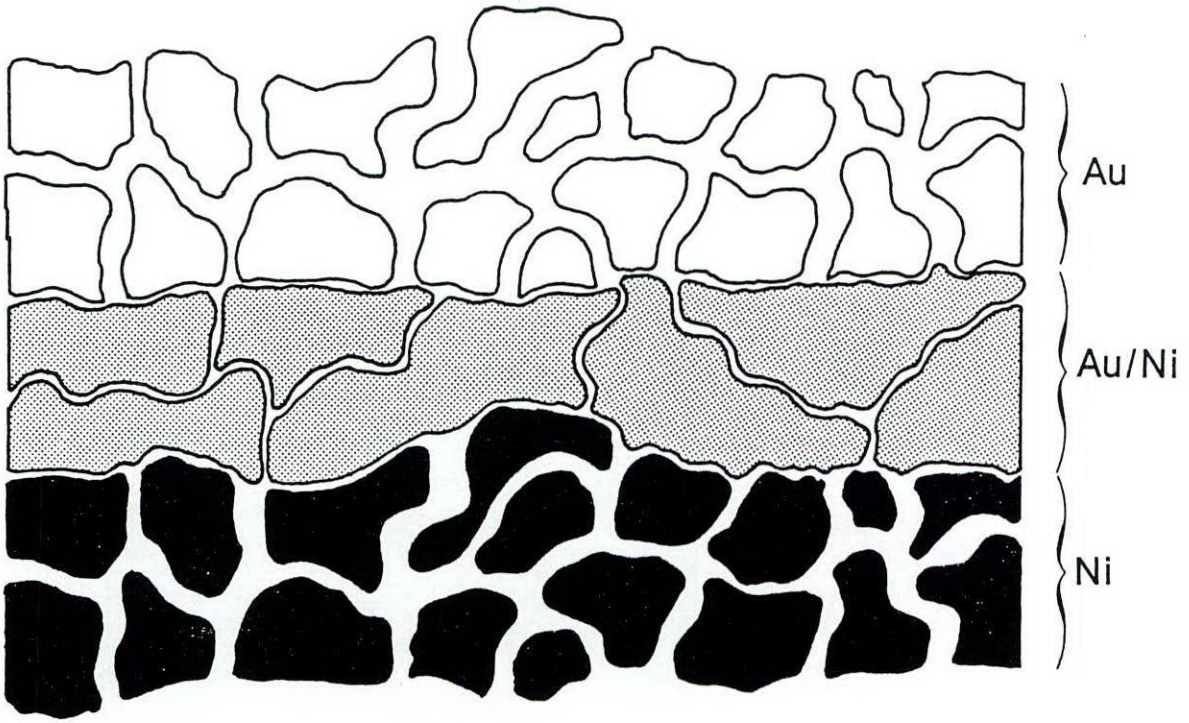

a) SCHEMATIC REPRESENTATION OF "DUPLEX-GOLD" BARRIER

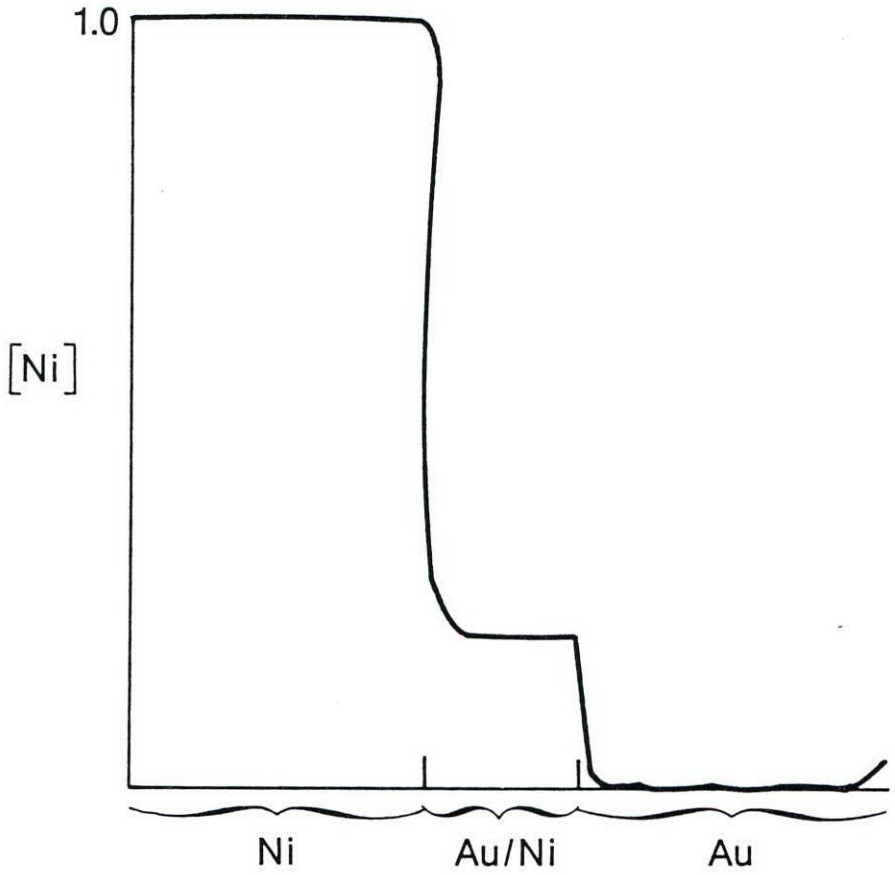

b) NICKEL ACTIVITY IN EACH LAYER

Fig. 4 a) A schematic representation of a "Duplex-Gold" barrier layer; b) Idealized nickel activity each layer due to this process.

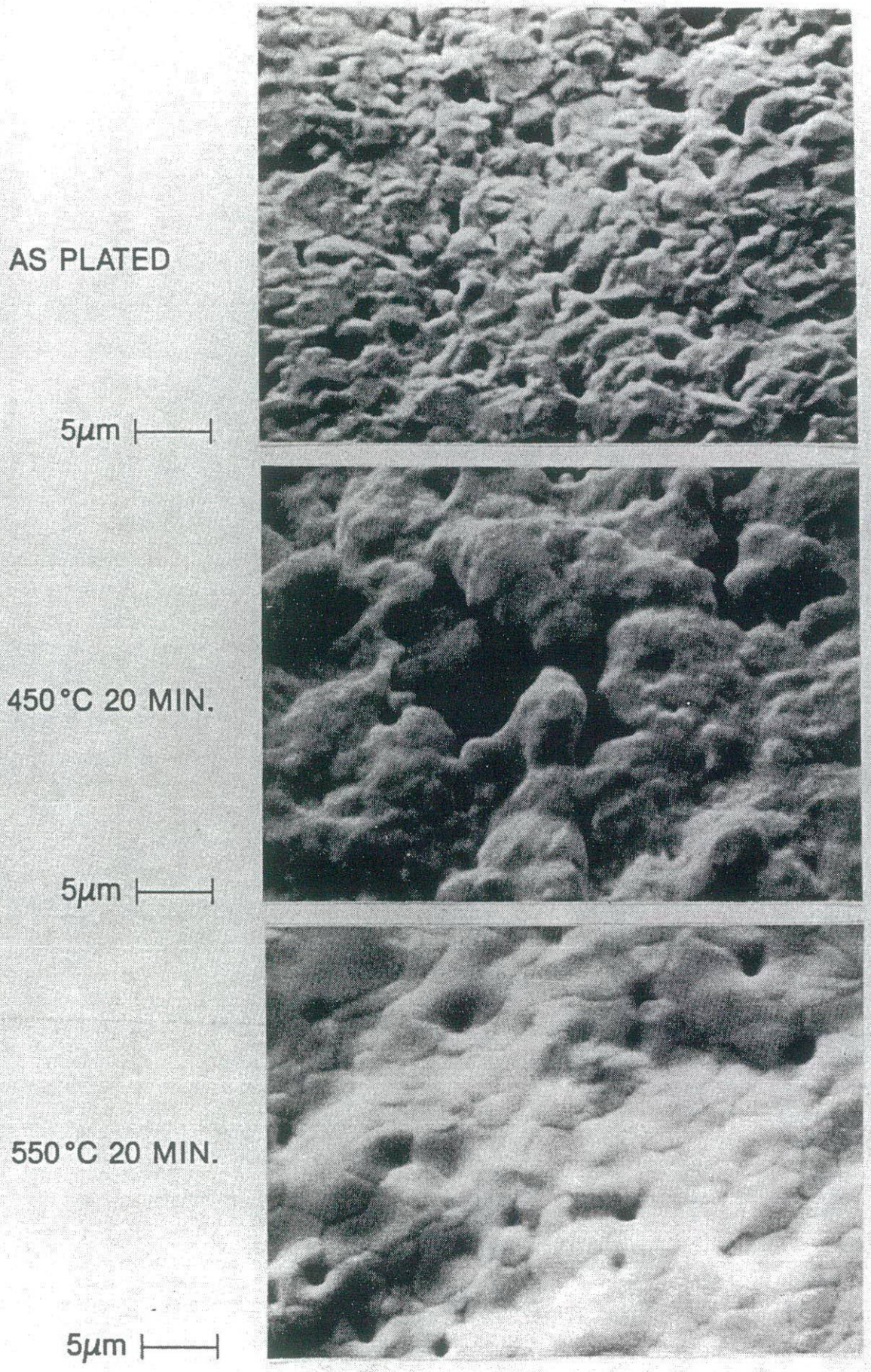

Fig. 5 SEM photomicrographs of electroless gold layers before and after heat treating in 10% H_2 balance Ar.

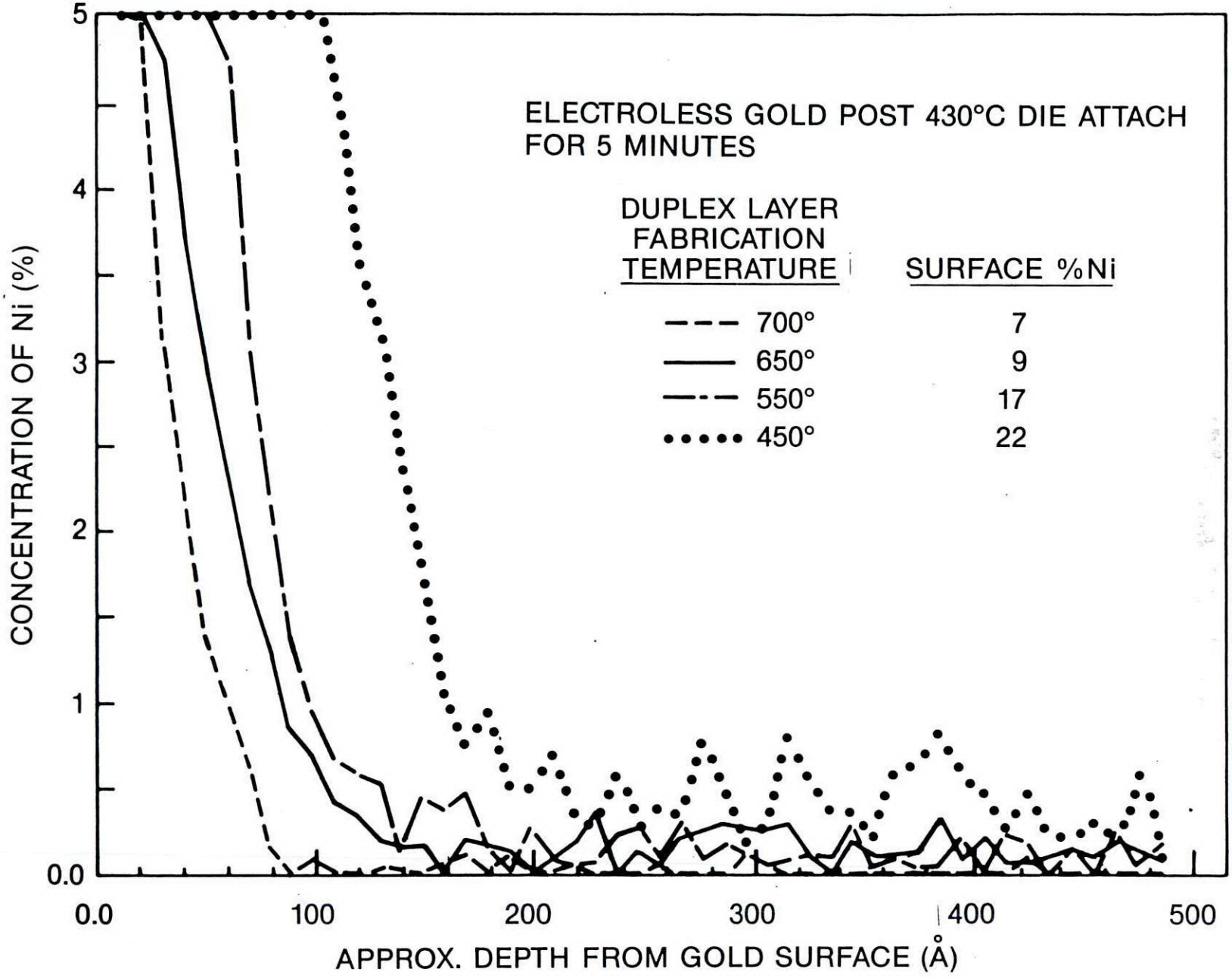

Fig. 6 Auger depth profile of "Duplex-Gold" electroless gold layers prepared at various temperatures. Inset shows the amount of nickel on the surface.

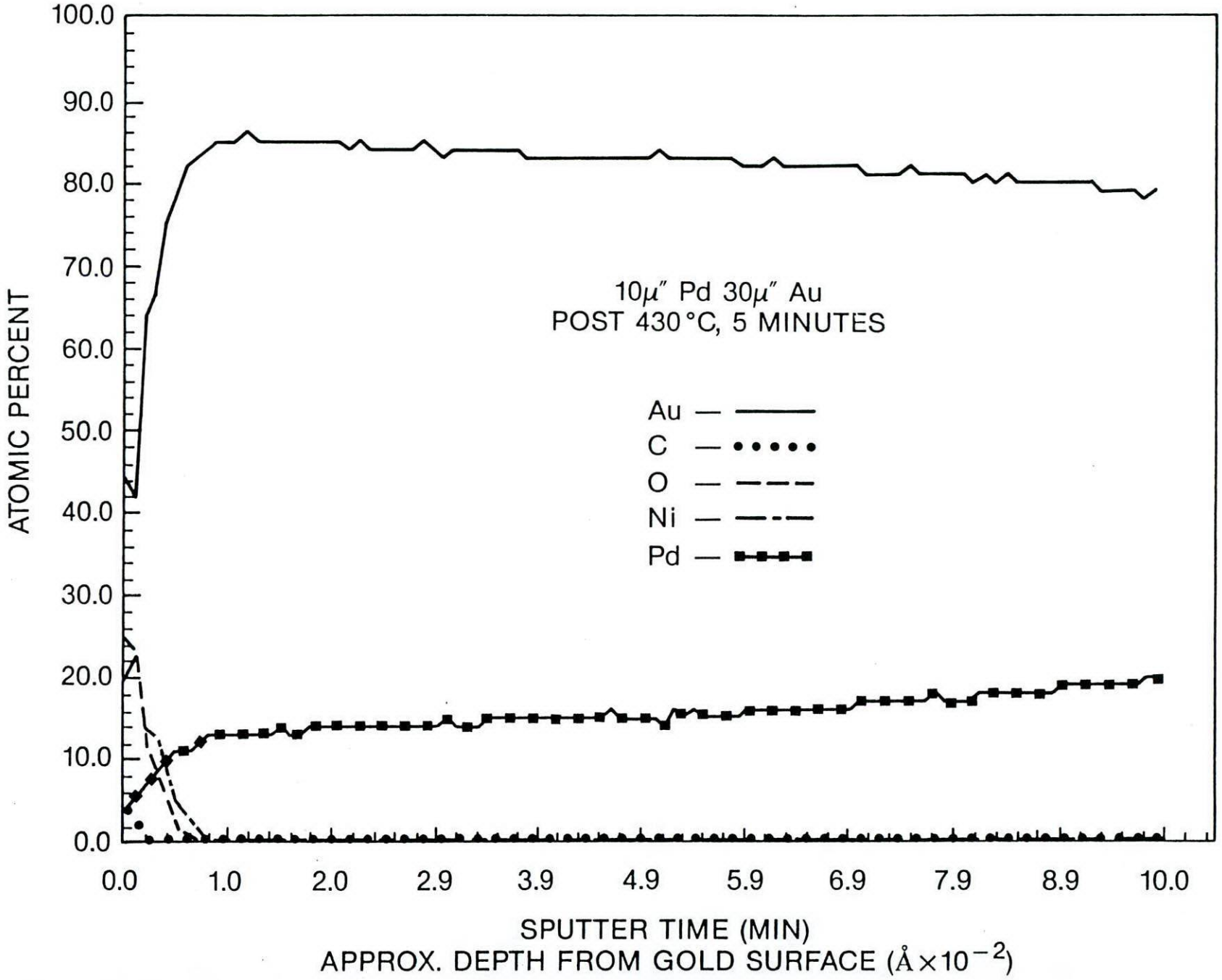

Fig. 7 — Auger depth profile of a 30μ" electrolytic gold deposit over a 10μ" Pd barrier

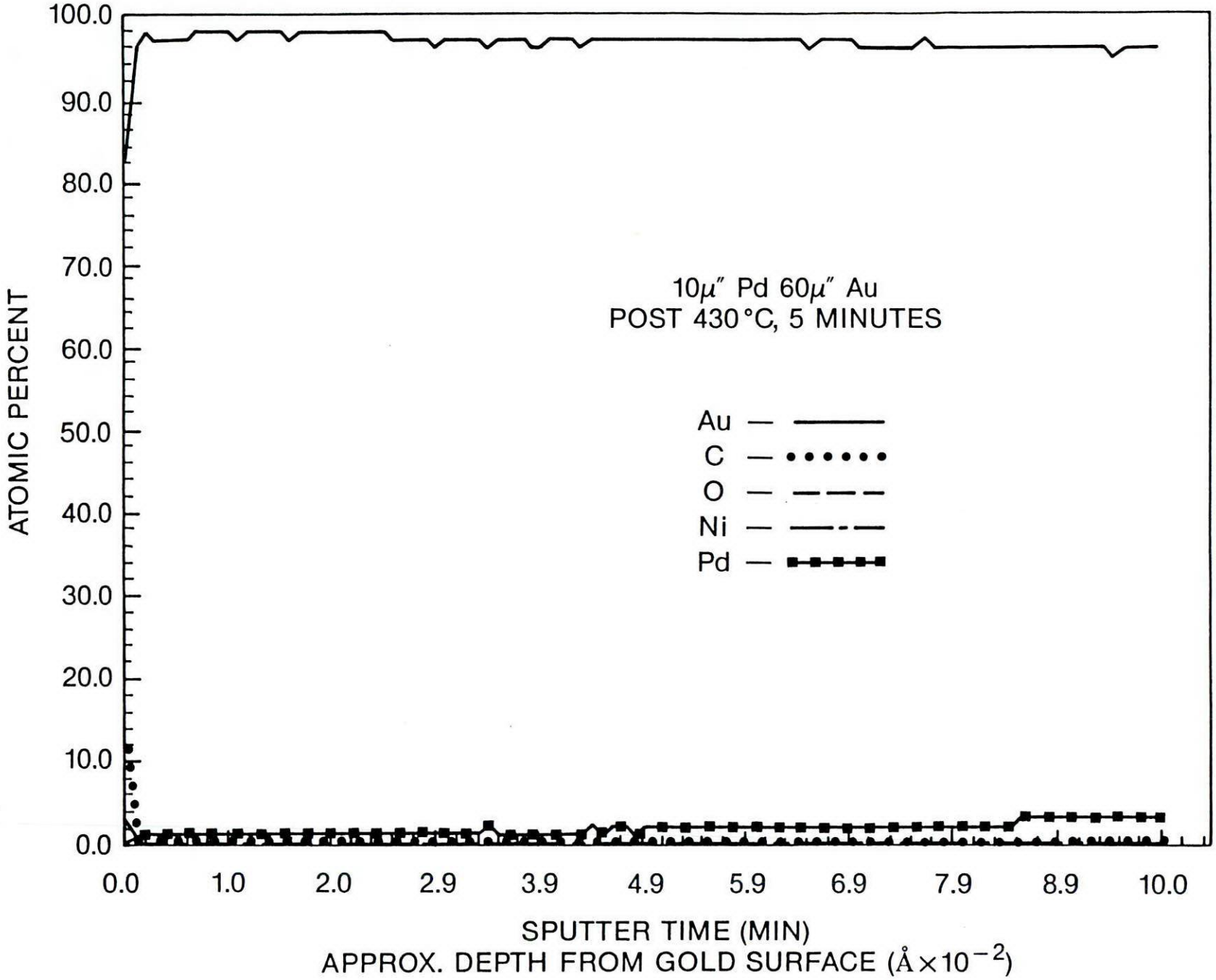

Fig. 8 Auger depth profile of 60μ" electrolytic gold depost over a 10μ" Pd barrier layer (Sample 2).

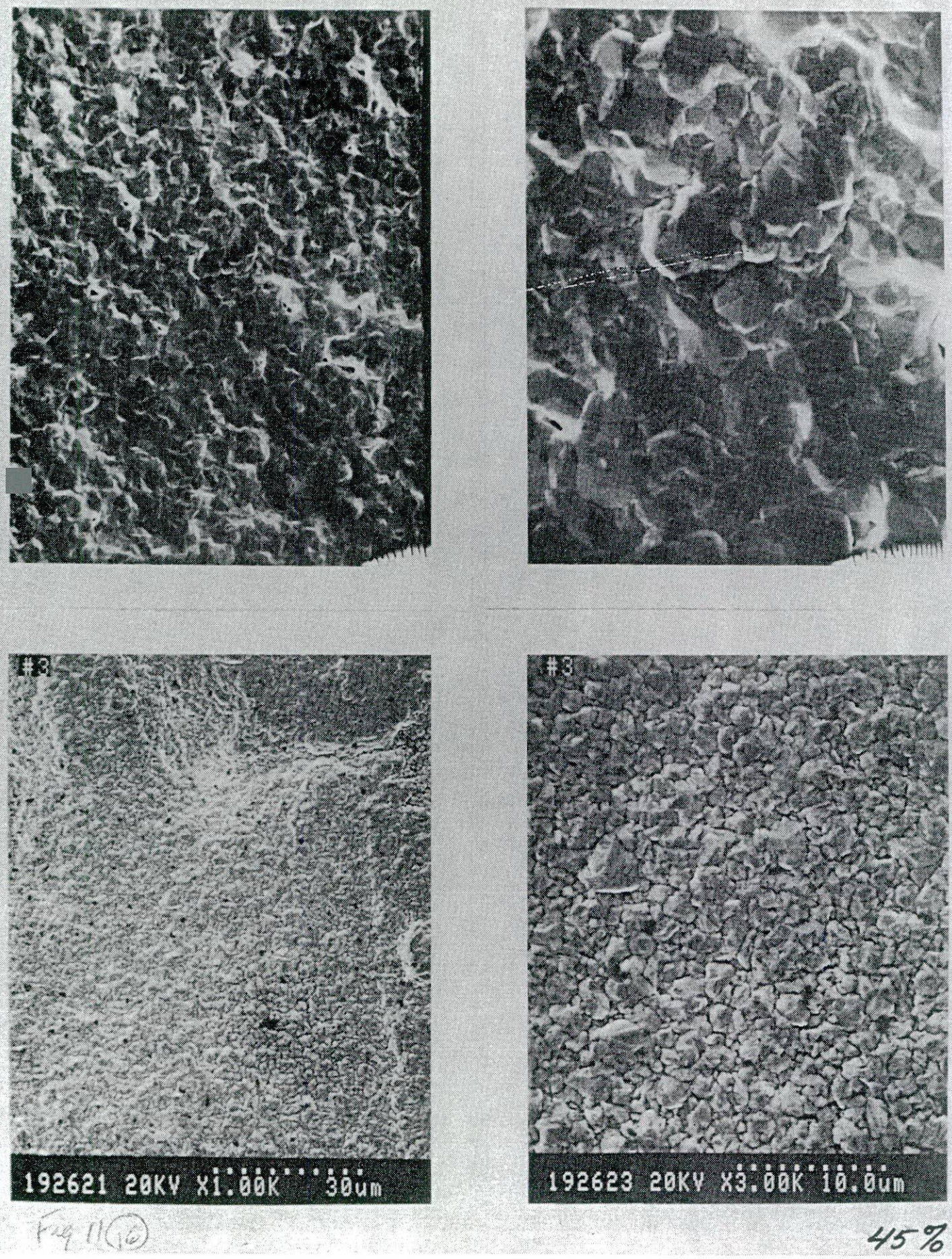

Fig. 9 S. E. M. of electroless gold over Ni (top) and Pd (bottom).

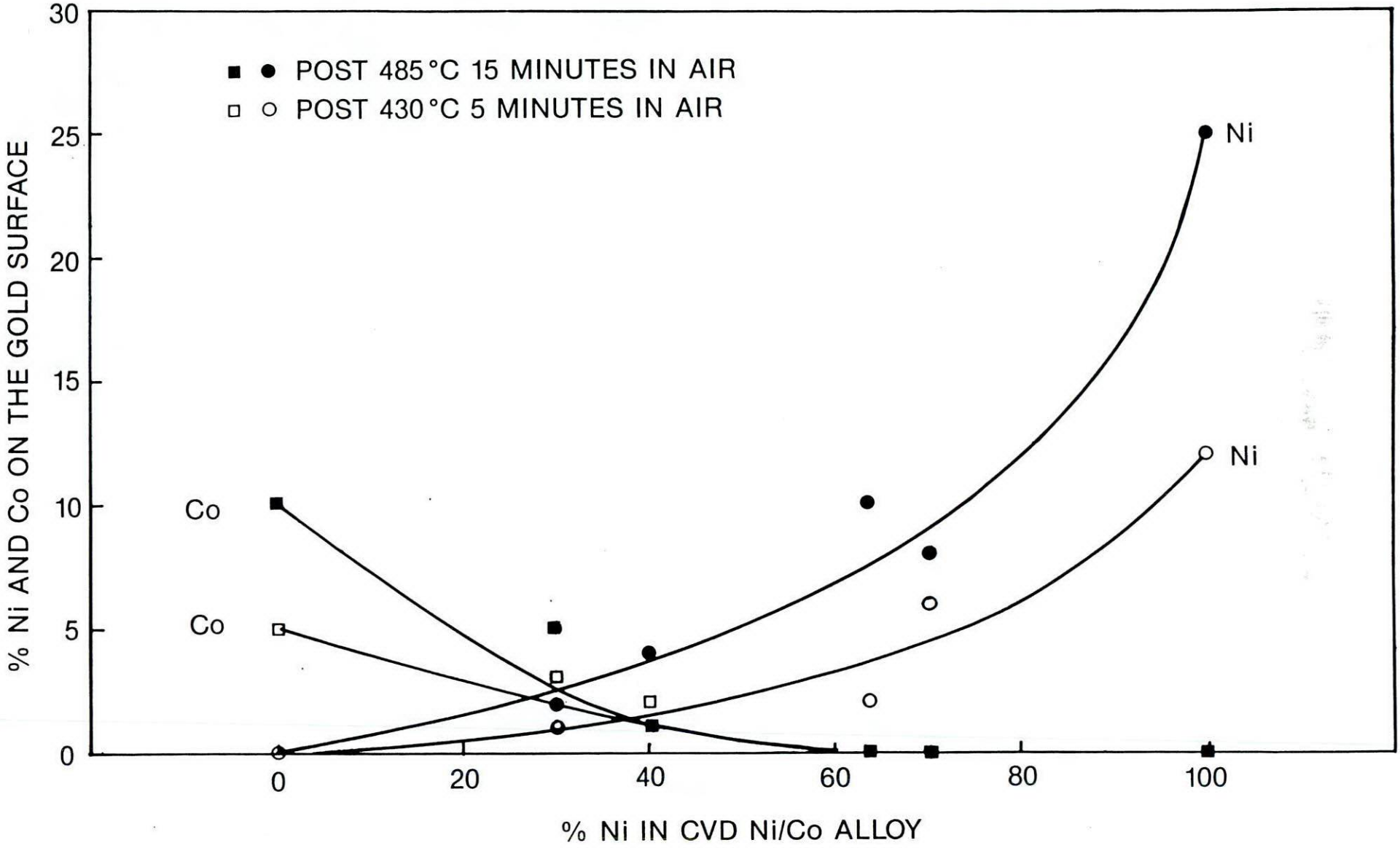

Fig. 10 Nickel and cobalt transport through electroless gold after heat treating at 430°C for 5 minutes and 485°C for 15 minutes.

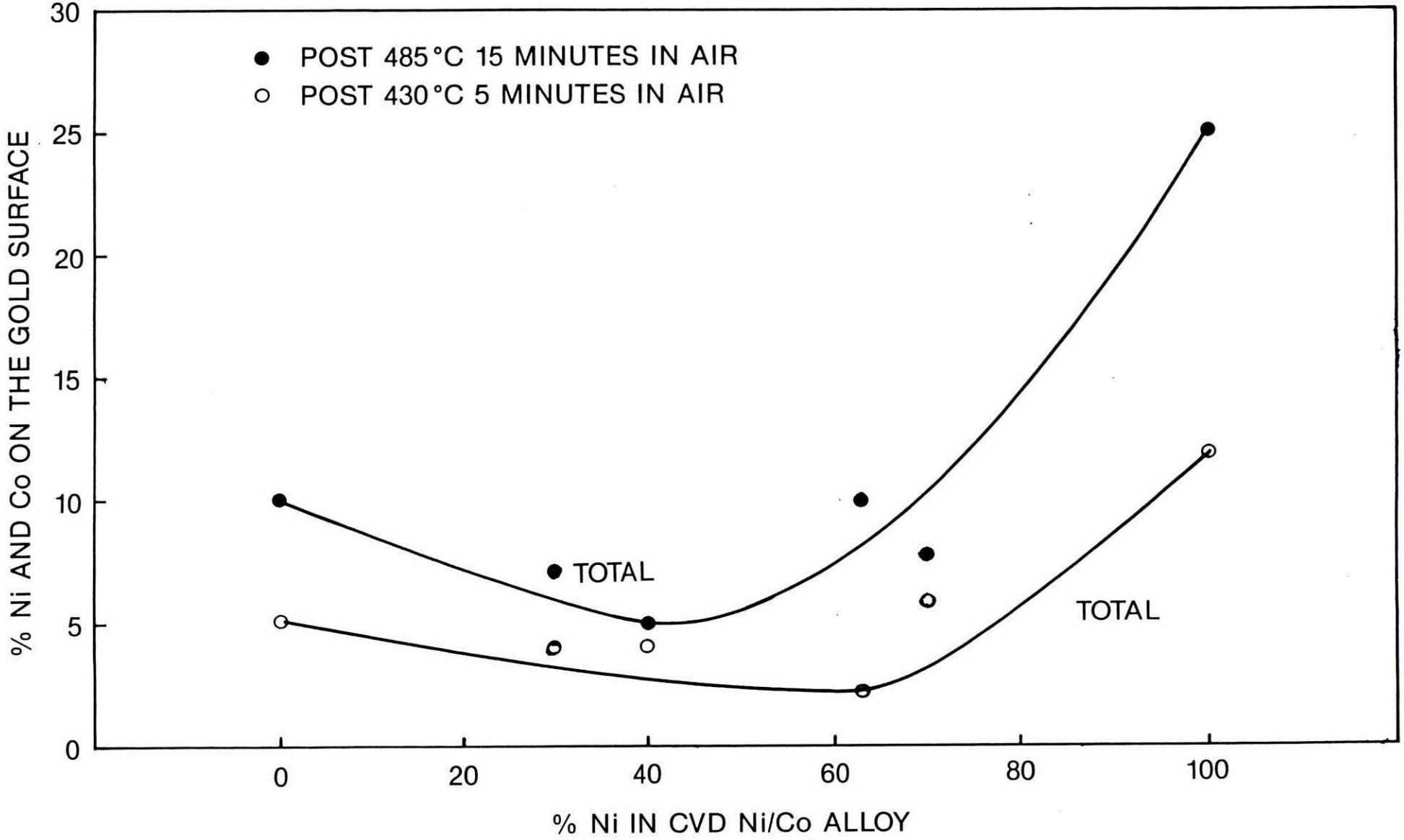

Fig. 11. Total transport of nickel and cobalt from Figure 11.

BUMPING PROCESS ON INTEGRATED CIRCUITS BY ELECTROLESS PLATING

Charles Lin, Ian Yee, and Brad Nelson
Microelectronic Computer Technology Corporation
12100 Technology Boulevard, Austin, Texas 78727

Background

Higher levels of silicon integration and faster switching speeds of advanced integrated circuits demand minimal signal delay and distortion in transmission. These demands are best met when the transmission distance of the interconnects from chip to board or from chip to chip are minimized. To meet these desired goals, the technology used for chip mounting becomes a critical determinant in the performance of the electronic product. Chip packaging techniques such as flip-mounted chips and tape carrier packages (TAB) can advantageously offer high lead count at a fine lead pitch, low profile, improved electrical performance and the ability to collectively bond all I/O's with one operation. These packaging techniques are now being widely evaluated and used in the high density, high performance applications such as packaging display drivers for flat panel displays, low profile smart cards, as well as computers and workstations.

A key component of the standard TAB process and several flip-mounted chip technologies is the anchoring of elevated metallic bumps over the bonding pads in order to facilitate mechanized assembly processes.[1-3] In this paper, we describe a process which uses electroless nickel to selectively bump and metallize aluminum bond pads. The process uses a palladium containing activation chemistry which selectively catalyzes the aluminum but not the passivation or field areas. Since the process is selective only to the pad sites, photolithographic patterning is not required, thus simplifying the bumping of single dies.

Experiments

The test chip used consists of patterned aluminum contact pads with 1μ silicon oxide covering the entire surface except for the via openings over the aluminum pads where the metallic bumps are to be made. The aluminum pads are 1 μ thick, and the via openings are 100μ square with a pitch of 200μ. The native oxide on the aluminum pad was first removed by dipping the sample into an alkaline solution. After the native aluminum oxide was removed, the sample was then cleaned in a dilute sulfuric/hydrofluoric acid

mixture to remove potential metal residues. The etching time was carefully controlled to avoid excess etching of the 1μ thick aluminum. The sample was then activated in a palladium containing acidic solution for 30 seconds. The pH of this solution was maintained at 4. After activation, the sample was rinsed in water to remove extra palladium before going into the electroless nickel plating bath. The bath used for electroless nickel plating was a commercially available bath which has a plating rate about 25μ per hour.

After nickel bumps were formed by the electroless deposition process, a thin coat of gold was selectively applied to the nickel using an immersion gold plating solution. The gold overcoat served as a means of preserving an oxide-free bump surface which is more readily and reliably wetted by a subsequent solder application step. Solder is applied to the bumps by dipping the die in a solder pot containing 60/40 tin/lead. The temperature was maintained at 250°C and the dipping time was about 1 to 2 seconds. No flux or ultrasonic techniques were required; however, a nitrogen inerting technique was found to be effective in improving selectivity.

Results and Discussion

There are two traditional and well known techniques for wafer bumping. In one method, a thin metallic stencil is used as a mask for selective deposition of an evaporated material such as solder. In this method, a stainless steel membrane is precision patterned with via openings by photolithographic and wet etching means. This mask is then clamped to the wafer with the holes of the mask precisely aligned with the aluminum pads. Material can then be evaporated, depositing metal on the wafer only where an opening in the stencil exists. Since the minimum size of the openings is approximately the thickness of the mask, this evaporation technique becomes inadequate as the I/O pitch decreases. Another drawback is that physical alignment of the stencil to the wafer could be troublesome.

The other technology for bump placement is based on electrolytic plating [4]. In this approach, a continuous layer of under bump metallurgy such as Cr and/or TiW is sputtered or evaporated over the entire wafer surface. This layer functions as an adhesion/barrier layer and current-feeding layer for plating. Patterning of the bump sites is achieved by photolithography, using either liquid or dry-film photoresist. Metal, such as gold or solder, is then electrolytically plated up to a desired height. The selective etching of under bump continuous layers, using plated metal as the mask, will then define the final bump geometry. Although the electroplating-based bumping process is capable of realizing ultra-fine pitch I/O's, the process is only suitable whole wafers where the photolithographic patterning of the plating mask can

be readily and economically performed. Once the chips are singulated from the wafer, it becomes very difficult, if not impossible, to apply photoresist, expose, develop and plate.

With electroless nickel deposition on aluminum, the typical activation method used is a zincating process [5-7]. In many applications, however, the low melting temperature and corrosive properties of the zinc, make zinc an undesirable material choice for chip bond pad metallization. The use of palladium as a catalyst is more desirable since it is more corrosion resistant, has a higher melting point, and does not readily form detrimental intermetallics with aluminum. On the other hand, the conventional palladium activation solutions tend to be non-selective. There is a tendency for the entire surface including the passivation layer being activated, especially in the neighborhood of the bond pads. This commonly results in electrical shorts forming as nickel plates up and bridges one or more bond sites. An example is shown in Figure 1.

To activate the aluminum bond pad, the native oxide and any contaminants should be removed from the aluminum surface. Alkaline solutions such as KOH are more aggressive etchants than the acidic ones and are commonly used when there is organic contaminate involved. Although alkaline solution can effectively remove aluminum oxide and metal, in many cases, other constituents such as silicon, titanium and copper which coexist with aluminum will be left on the surface. These metal and smut residues can gradually accumulate as aluminum etching proceeds. Since these accumulated residues have poor adhesion to the aluminum surface, they will affect the adhesion between the nickel and the underlying aluminum. These residues can be removed by acids such as nitric acid, hydrofluoric acid, sulfuric acid, phosphoric acid and their mixtures. Adequate acid rinse after alkaline etching can therefore ensure a clean aluminum surface to which nickel can effectively adhere.

In addition to impurities, care should be taken in controlling oxide and metal removal rate. Improper overetching of the aluminum will damage the bond pad and cause incomplete plating as shown in Figure 2. Overetching can be disastrous when the palladium starts to deposit onto the aluminum. Palladium is a very effective catalyst for hydrogen reduction reaction, once in contact with aluminum in an acidic environment, this property would enhance the anodic dissolution of the aluminum at a very fast rate. Therefore, a weak acidic activation solution or a near neutral rinsing process should be used to avoid aluminum overetching.

Another potential problem with electroless deposition of nickel on aluminum is the incomplete removal of native oxide on the aluminum pads. Nickel will only plate on aluminum areas which are oxide-free and where palladium is deposited. Inadequate removal of the native oxide would result in only partial coverage by nickel over a via. An example of this is given in Figure 3. Such partial plating usually occurs on multiple areas of the same die, repeating a similar tell-tale partial plating pattern.

The key to successful electroless nickel deposition on aluminum is the activation chemistry to be used. Commercially available palladium containing activation solution will cause gross extraneous plating when used as received. Dilution of these kinds of solution will ease the degree of extraneous plating but may cause partial plating to also occur as shown in Figure 4. The use of diluted forms of commercially available activators can result in both extraneous plating and partial plating on the same die. The reduction in process window makes manufacturing yield a serious concern.

After activation, rinsing is important. A proper and thorough rinse will ensure that no activation solution is left on the die surface that would cause either plating in unwanted areas or spontaneous decomposition of the plating bath. We have found that a water rinse is adequate to provide selective plating (Fig.5). Although acidic rinsing will help in removing excess activator solution, it may also cause aluminum to further etch and undercut the palladium on its surface. This will then cause the partial plating similar to that shown by Figure 2.

Ultrasonic soldering techniques have been applied in the electronic industry for many years. It has also been successfully applied to the solder bump formation for silicon wafers [6]. Ultrasonic soldering is a process where a molten solder alloy is ultrasonically agitated to enhance metallurgical bonding of the substrate and the solder. This ultrasonic agitation can be achieved either by vibrating the entire solder pot or by submerging ultrasonic probe-type transducers in the molten solder. The major purposes of this ultrasonic agitation are to provide mechanical scrubbing action to remove the dirt particles and surface oxides so that the solder can directly contact and wet the base metal. In our approach, a thin layer of gold was used to prevent oxidation subsequent to nickel bump formation. When the sample is dipped in the solder pot, this thin layer of gold will dissolve and provide a oxide-free metal surface onto which the solder will immediately wet to.

During the process development, it was found that one of the problems was oxidation of the molten solder. Oxidized solder tends to form a crust or

dross which floats on the surface of the molten solder. As the die sample is drawn out of the solder pot, the dross tends to adhere to the passivation film and cause solder blanketing. Further treatment such as reflow may provide selectivity but this will then cause bump height irregularities. In order to prevent this, nitrogen inerting equipment was applied to the solder pot. It is constructed of stainless steel and the nitrogen injection scheme is designed to maintain a good inert atmosphere without excessive gas consumption. This inerting atmosphere can prevent molten solder from oxidizing during solder dipping and therefore provide a oxide-free surface of the molten solder. This arrangement will provide an excellent control of the solder coating (Fig.6 -Fig. 10).

Conclusion

A process was developed that selectively activates and deposits electroless nickel on aluminum pads. This process is extendable to the bumping of single devices and would be a significant advantage for user companies which are not also IC manufacturers. The process, because of its selective nature, can be used to produce bumps of very tight pitches. In the bumping process described, aluminum surface pretreatment appears to be critical to the degree of coverage of the electroless metal on the aluminum pads. Selectivity is determined by the activation chemistry used. We have also demonstrated that the use of a thin gold overcoat on the nickel bumps can effectively maintain an oxide-free surface which can subsequently be wetted by solder without the assistance of flux or mechanical scrubbing. Acceptable solder bump height uniformity was observed to be easily achieved by controlling the molten solder temperature and by the use of an inert atmosphere.

REFERENCES

(1) P. Hoffman, Solid State Technology, June, **85** (1988)
(2) J. Walker, Surface Mount Technology, January, **45** (1990)
(3) R.C. Hooper, A.J. Harrover, M.J. VanHoy and C.E. Terry, U.S. Patent 4,182,781
(4) E.K. Yung and I.Turlik, IEEE Transactions on CHMT, 14, No.3, **549** (1991)
(5) E.A. Guditz and R.L. Burke, U.S. Patent 4,372,996
(6) K. Wong, K. Chi and A. Rangappan, Plat. and Surf. Fin. July, **70** (1988)
(7) J. Simon and H. Reichl, Proceedings, ITAB '90, **49** (1990)
(8) K. Yamakawa, M. Inaba and N. Iwase, Proceedings, ISHM '89, **620** (1989)

FIG.1. Extraneous plating caused by improper activation process.

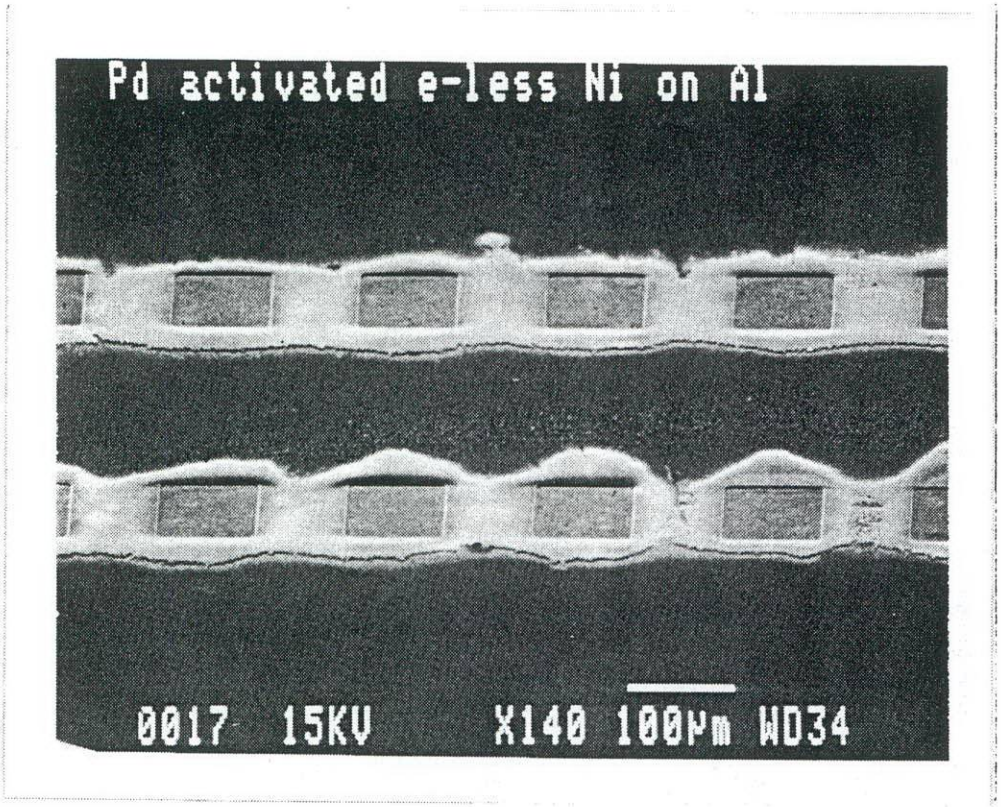

FIG.2. Electroless partial plating caused by aluminum overetching.

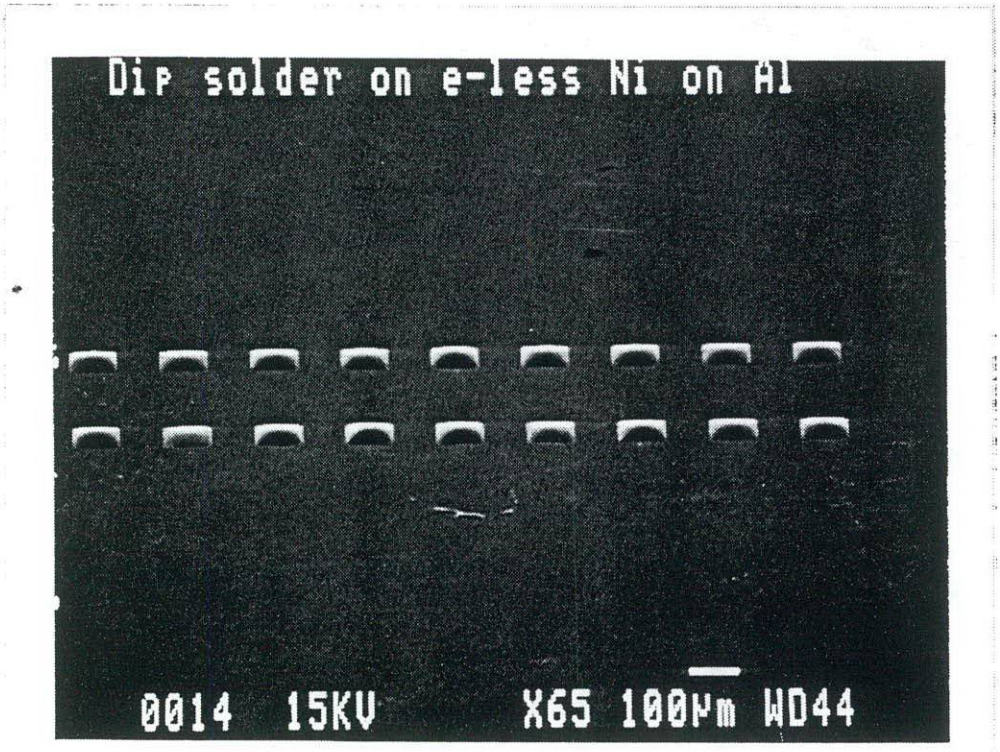

FIG.3. Incomplete nickel coverage caused by inadequate oxide removal.

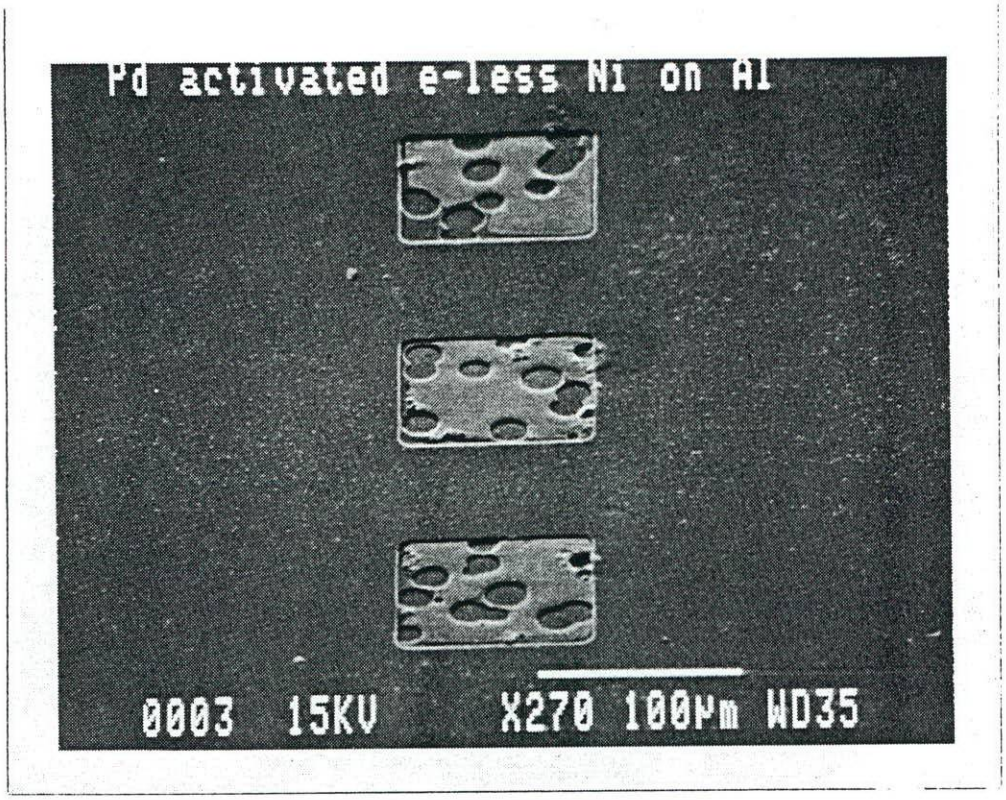

FIG.4. Partial electroless plating caused by poor activation process.

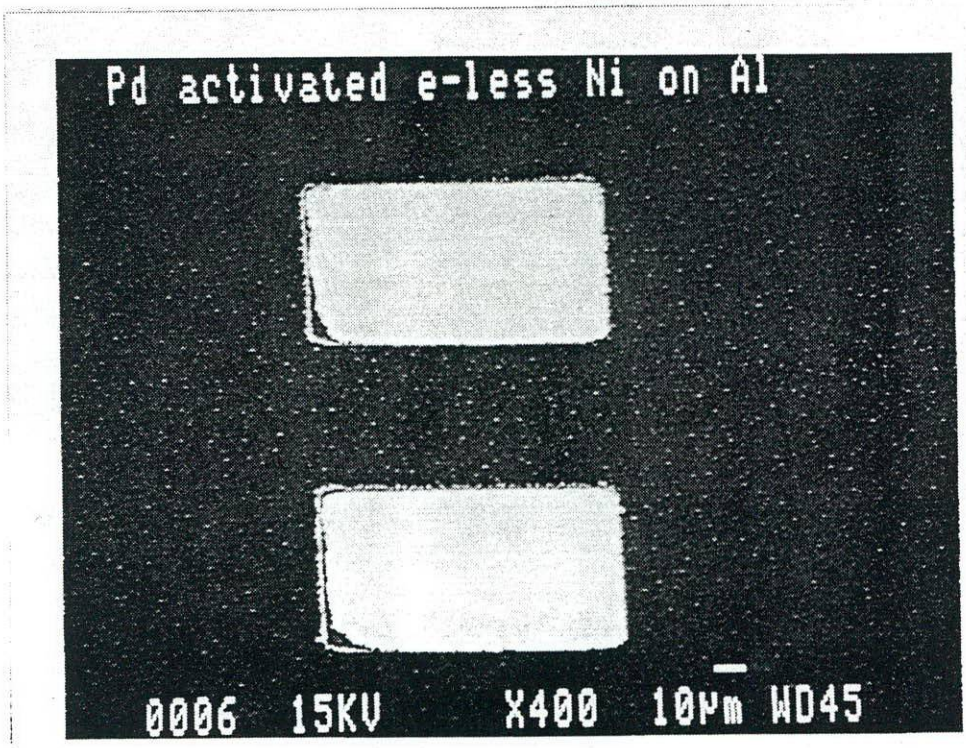

FIG.5. Uniform gold coated nickel bump on Al bond pad.



FIG.6. Poor solder coating with incomplete nickel bump.

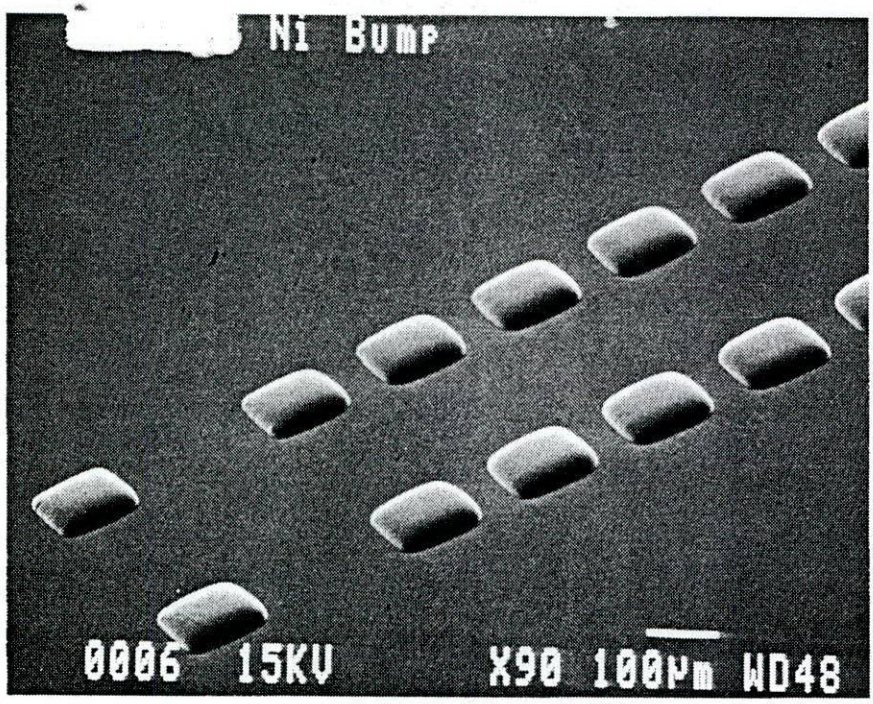

FIG.7. Poor solder coating with incomplete nickel plating.

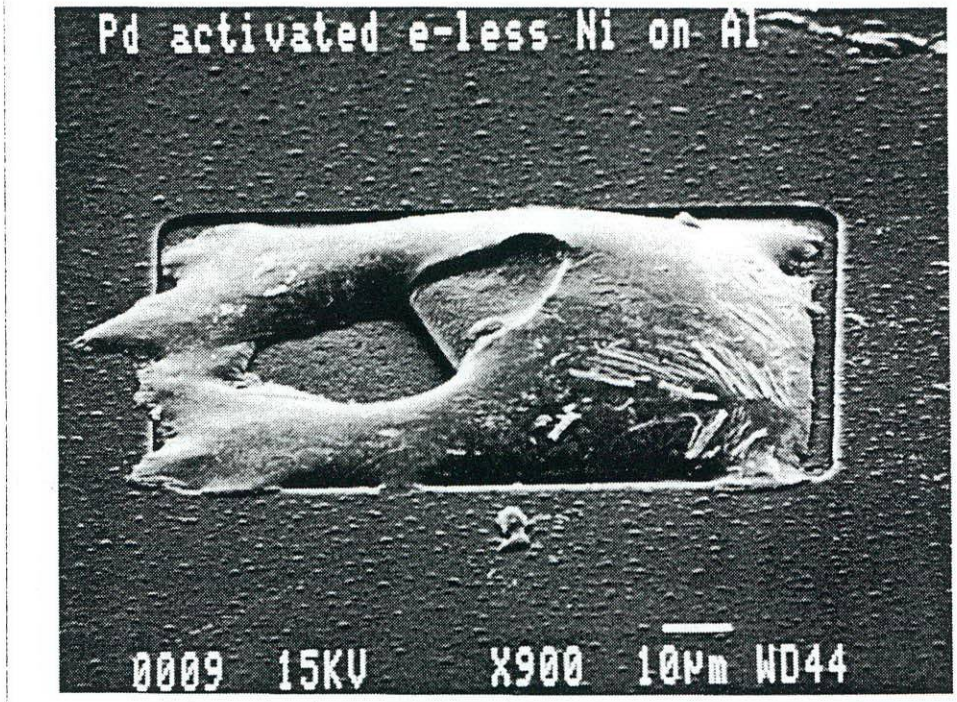

FIG.8. Solder coated nickel bump on Al bond pad.

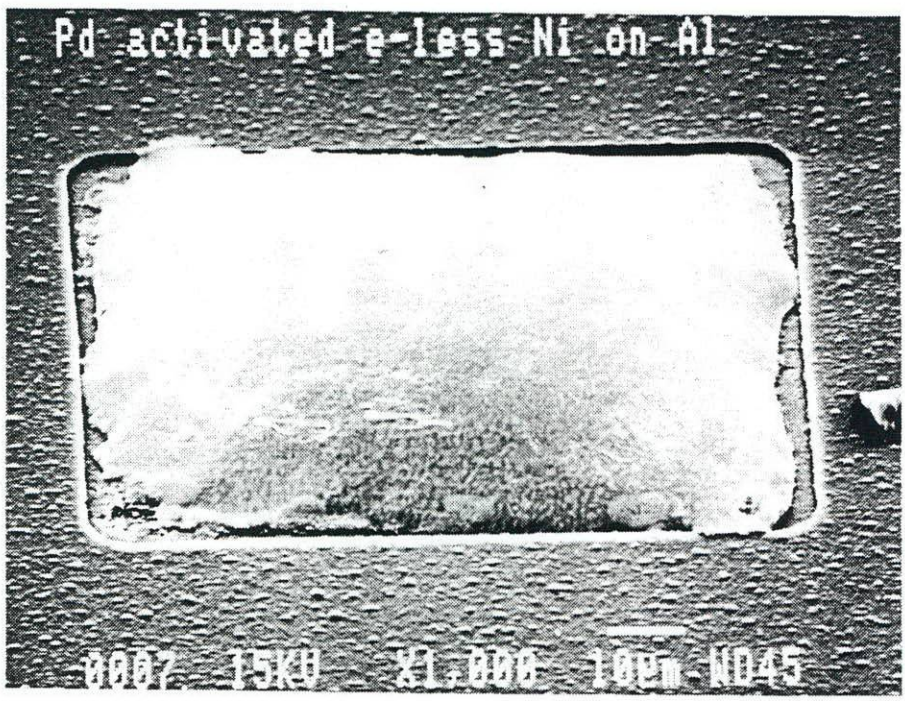

FIG.9. Uniform solder coated nickel bumps on Al bond pad.

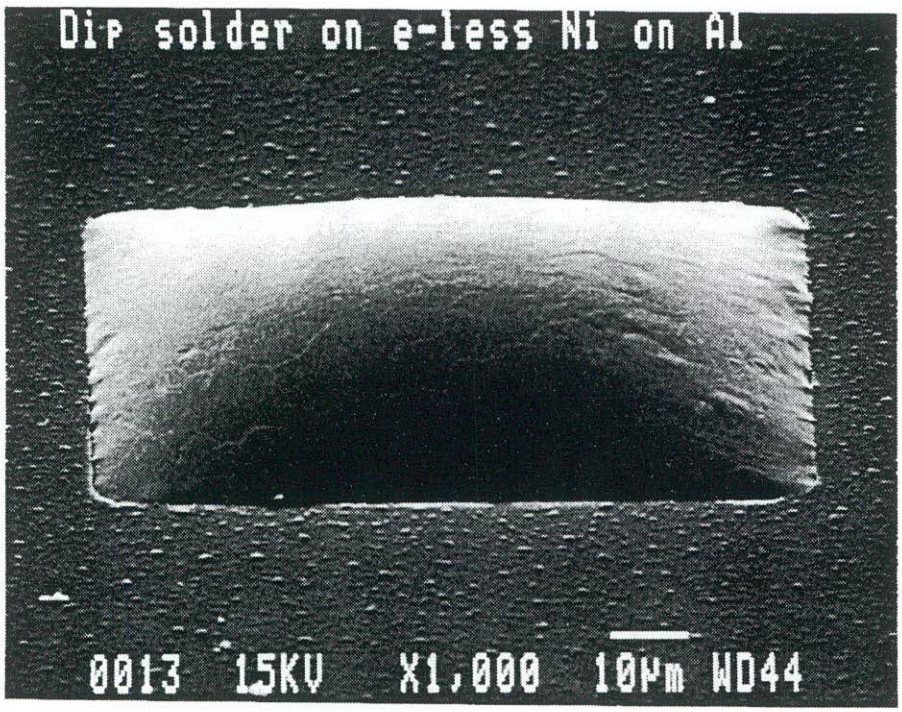

FIG.10. Uniform solder coated nickel bumps on Al bond pad.

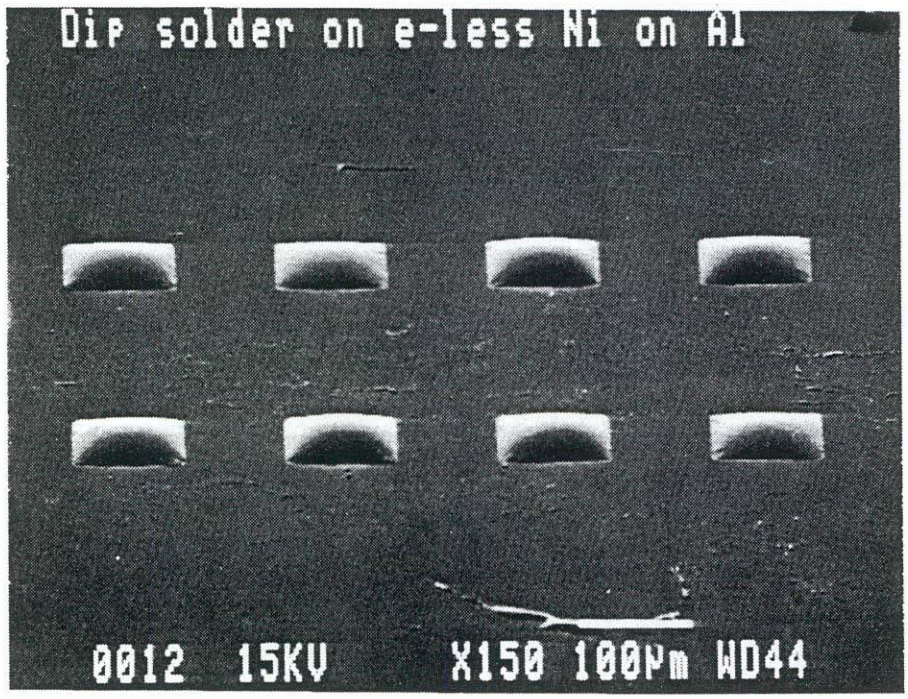

Laser-induced Gold Deposit on InP Substrate

Wang Xuhong Yu Zuzhan

Chemistry Department of Fudan University

Zhao Guoqing

Nuclear Science Department of Fudan University

Shanghai, 200433, P.R. China

Abstract

Laser-induced and laser-enhanced plating will be widely applied in the electronics industry due to its high speed and highly spatial resolution. A thin gold deposit on InP substrate was obtained in an aqueous solution of aurichlorohydric acid by using a He-Ne laser beam. This spotwise deposit with a diameter 0.5 mm was studied by RBS and SEM. The circle deposit with thickness 0.05 μm was identified to be gold and the gold atoms have diffused into the substrate. A photoelectrochemical mechanism bringing about this process is discussed. The laser irradiation gives rise to the potential difference between the laser irradiation zone and non-illuminated zone, which accelerates the anodic dissolving reaction, coupled with the reduction of metal ion from the plating solution.

Introduction

In recent years, laser-induced metal depositions on semiconductor surfaces have been receiving more and more attention for possible use in microelectronic device fabrication and repair. The new techniques offer many advantages over conventional electroless plating: first, the speed of metal deposition can be greatly increased because of the local high temperature induced by laser irradiation: second, metals can be only deposited at the irradiated zone, so a highly selective deposition picture can be produced by using a computer to control the laser beam without the complex technology which makes use of several stages of photolithography; third, due to the high local temperature induced by laser irradiation, metal deposition and alloying of the metal/semiconductor interface may take place simultaneously leading to good ohmic contact between metal and substrate (1)~(5). In this work, direct laser-induced deposition of gold on InP was studied, with the deposit formed by He-Ne laser irradiation of the substrate immersed in the plating solution.

Experimental

The experimental setup (Fig. 1) consisted of a small plating bath on a x-y table. The substrate was mounted in a specimen holder which served also as the bottom of the bath. A He-Ne laser with a wavelength 632.8 nm, output power 8.5 mw and a beam diameter Ø.5 mm was used in the experiments. The plating medium was an aqueous solution of acid gold tetrachloride ($HAuCI_4$), and absorption of the laser radiation, by the solution, was measured and found negligible. The substrate was n- type InP oriented in <1ØØ> direction, doped with Te -1E18 atoms/cm^3 and polished with bromine-methanol. Before being immersed into the solution, the substrate was cleaned in de-ionized water by ultrasonic wave. The laser output was directed to irradiate the semiconductor surface at normal incident, obtaining a metal deposit. The deposit composition and the deposit thickness are analyzed by Rutherford backscattering (RBS) (6). The deposit structure is studied by scanning electron microscopy (SEM), and the type of electrical contact between substrate and deposit is characterized by electronic means.

Results and Discussion

Laser-induced deposition on InP was obtained at laser output power 5.5 mw with a Ø.5 mm spot size. It was studied by RBS and SEM. The deposit appearance is shown in Fig. 2.

A. RBS Results

The RBS spectrum of the deposit demonstrated in Fig. 3 shows that the peak of the deposit is at Channel Number 96Ø. According to RBS theory (7) and the RBS spectrum obtained in the experiment, the deposit is identified to be gold. We also calculated the thickness of the gold deposit as Ø.Ø5 μm. The lower energy portion of the gold peak in the RBS spectrum interlapped with the substrate peak and demonstrated that gold atoms diffused into the substrate during the depositing process.

B. SEM Results

Fig. 4 (a-c) shows the SEM micrographs of the gold deposit. The spotwise deposit has an interesting cyclic band structure. Fig. 4a is a SEM micrograph of the first cyclic band at the edge of the deposit. It reveals sparse distribution of gold in this region. Fig. 4b is a SEM micrograph of the second cyclic band where there is a fine and dense deposit. Fig. 4c shows a SEM micrograph of the third cyclic band (in the center of the deposit), the deposit is sparse and has bigger crystalic grains.

C. Discussion

The The initial stage of laser-induced deposition of gold on InP appears o occur via a photoelectrochemical process. Other mechanisms, such as hotolytic solute decomposition or photothermal chemical reactions are nlikely. In the former mechanism, laser photolysis of solute molecules annot occur because the metal salt solutions are transparent at the rradiation wavelength, used in our experiment; while the latter mechanism is nlikey because the laser irradiation with lower power density of 40 mW/cm^2 ould not cause so high a temperature leading to decomposition of the solute old chloride and phosphorus loss from InP.

In fact, the forbidden band gap of Inp is 1.28 eV (300K), the photon energy f He-Ne laser with wavelength 632.8 nm used in this experiment is 3.1 eV, hich is higher than the former. So, the laser irradiation may induce the lectron in the semiconductor to leap directly from lower energy level to igher, and electron-void pairs are generated, leading to photoelectric otential difference between the irradiated zone which for n-type emiconductor is in the anode region and the dark zone, which is in cathode egion, the reaction as follows occurs:

$InP \text{ ----} In^{3+} + P + 3e$ anode reaction

$HAuCI_4 + 3e \text{ ----} Au + H+ + 4CI$ cathode reaction

he anode dissolvation generates numerous defects at the irradiated zone hich may be nucleation sites, while gold atoms and phosphorous atoms "melt" o form "alloy" under the high temperature because of the laser irradiation ith 2.8 W/cm^2. Gold deposit is obtained.

We can use this mechanism to explain the SEM results of the deposit. So the nergy distribution of He-Ne laser obeys Gauss distribution law, so the nergy in the outer region was lower, the reaction rate was slower, sparse eposit was observed; in the inner region, the laser energy was higher, the eaction rate was faster, therefore a fine and dense deposit was produced. n the center, the laser energy was the highest, anode dissolving reaction is ery intense,inducing too much damage on the surface of the substrate ampering the deposit formation in this region, therefore the deposit was ery sparse. In fact, when the laser power density is higher (4.1 W/cm^2), he anode dissolvation is so strong it causes a deep crater, but deposit was roduced, shown in fig.5.

The RBS spectrum of the deposit reveals that the gold atoms diffuse into he substrate when "melting" at the interface, and there is good ohmic ontact between metal and substrate. This also demonstrates the "melting" rocess during the formation of deposit.

Conclusion

It has been demonstrated that gold can be deposited on InP via He-Ne laser rradiation on polished InP substrates immersed in an aqueous solution of $AuCI_4$. This process can be explained by a photoelectrochemical mechanism roposed in this report. An advantage of this approach is that maskless etal deposition, alloying of the metal and the semiconductor surface occur imultaneously,and may present a useful approach to the fabrication of ohmic ontacts on a semiconductor.

Because this is essentially a lower temperature alloying process, it may offer some advantages over conventional alloying in circumstances where high temperatures degrade the device.

Reference

<1> S.Tamir and J.Zahavi, J.Vac.Sci.Technnol.A 3(6), 1985 p2312
<2> F.W.Oseermayer and P.A.Kohl, Appl.Phys.Lett.39, 76 (1981)
<3> J.Zahavi et al. Plating and Surface Finishing 1986(2), p57
<4> R.F.Karlicck and V.M.Donnelly, J.Appl.Phys. 53(2), Feb.1982
<5> T.J.Hirsch et al.,Appl.Phys.Lett. 57(13), 24 Sept, 1990,p1357
<6> G.Q.Zhao et al.,Nucl. Instr.Meth. B 48 (1990) 513
<7> W.K.hu et al. Backscattering Spectrometry,Academic press New York, 1978

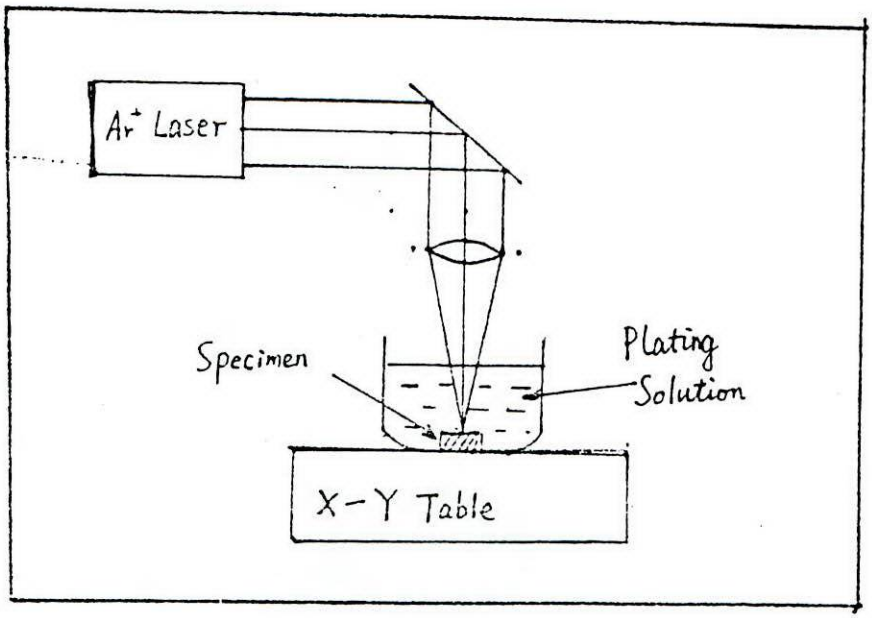

Fig. 1 Schematic illustration of experimental setup.

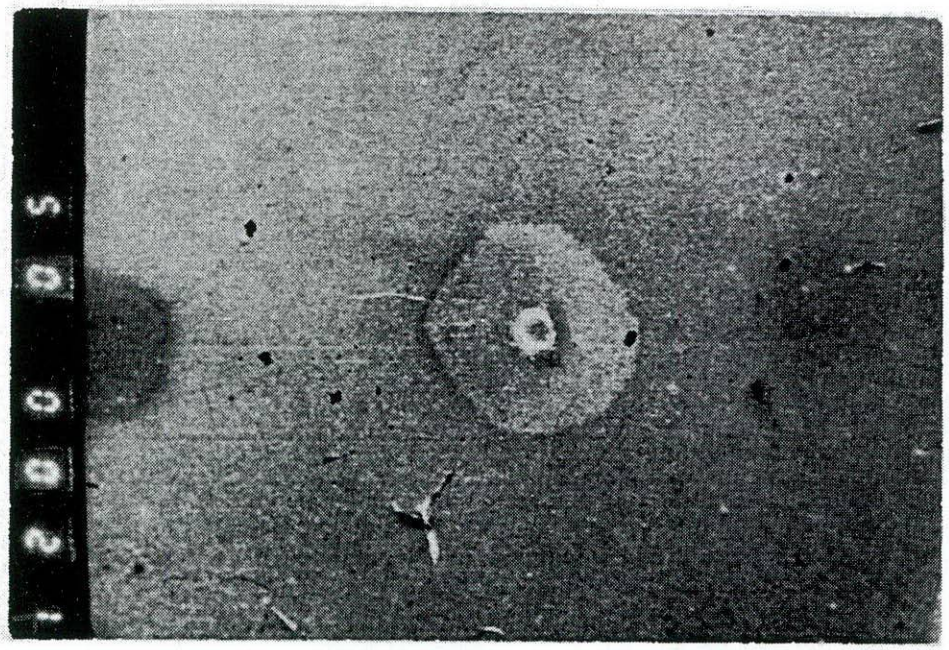

Fig. 2 SEM micrograph of gold deposit obtained in the experiment (X50).

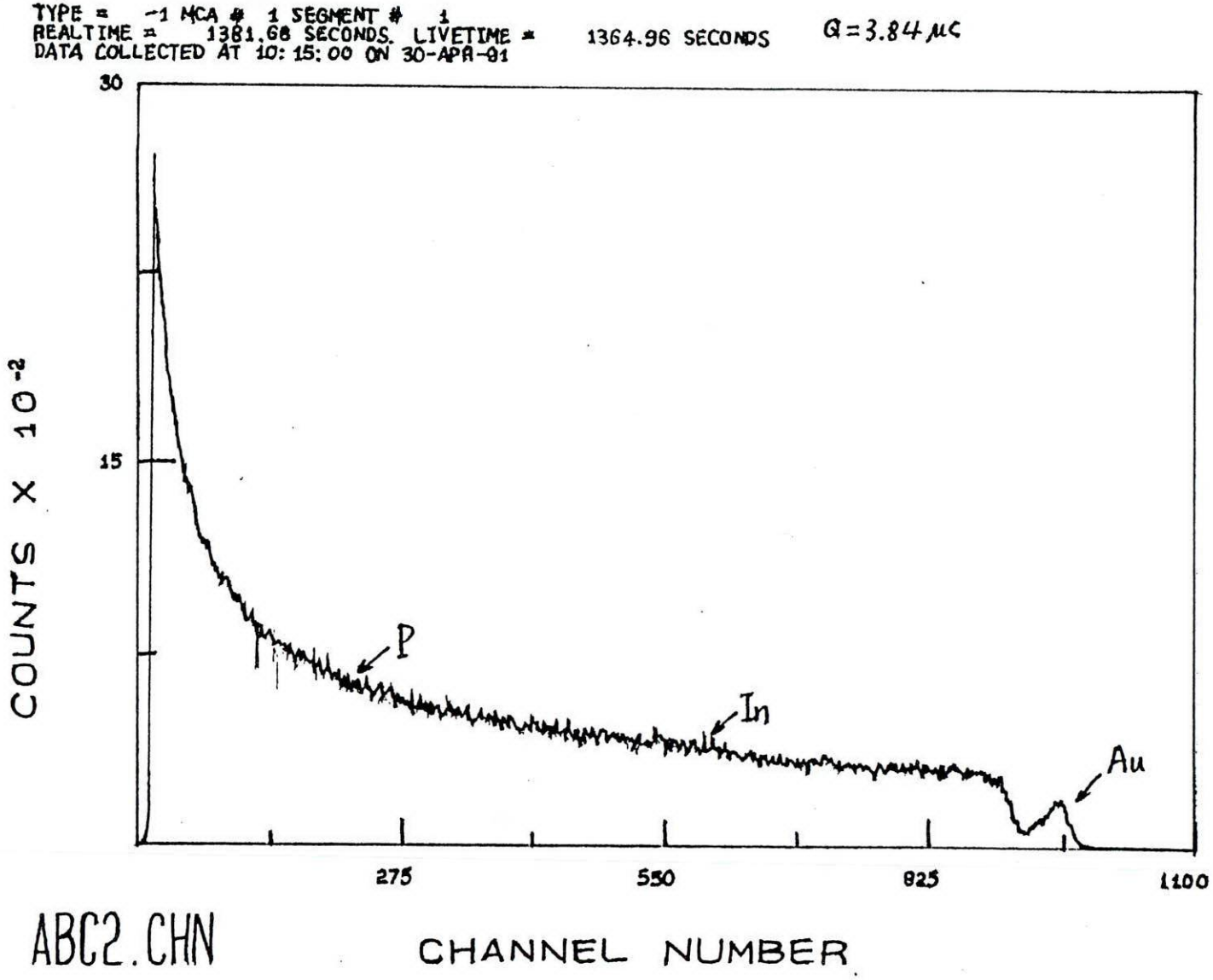

Fig. 3 RBS spectrum of gold deposit on InP.

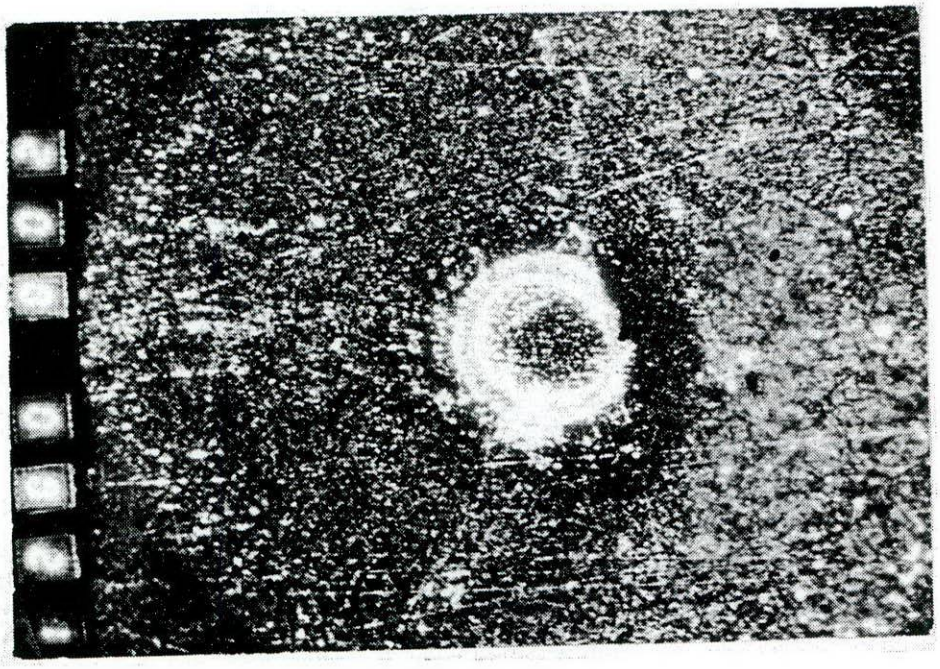

a. The outer region of gold deposit (X200)

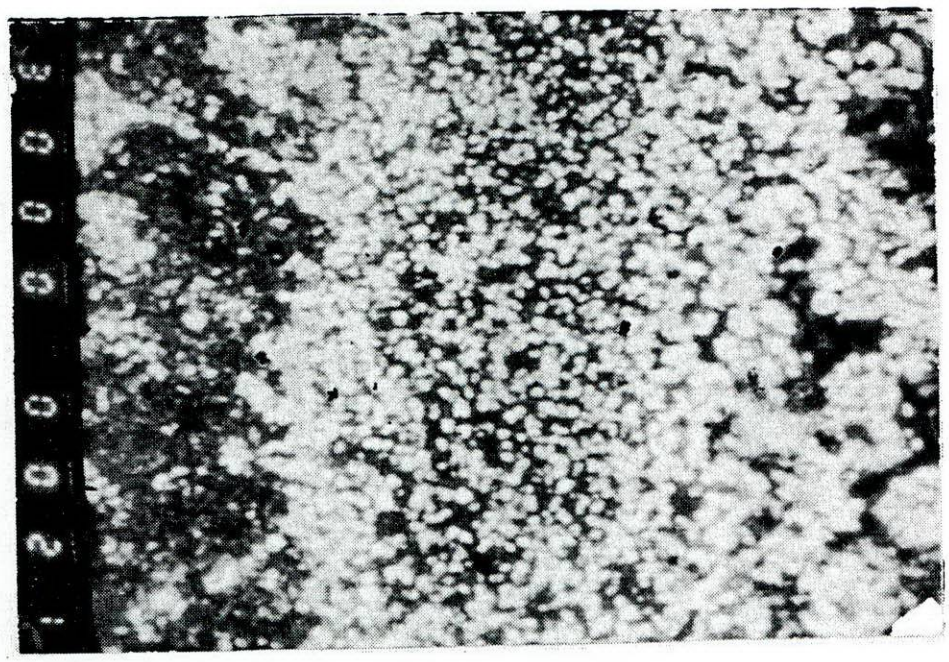

b. The inner region of gold deposit (X3000)

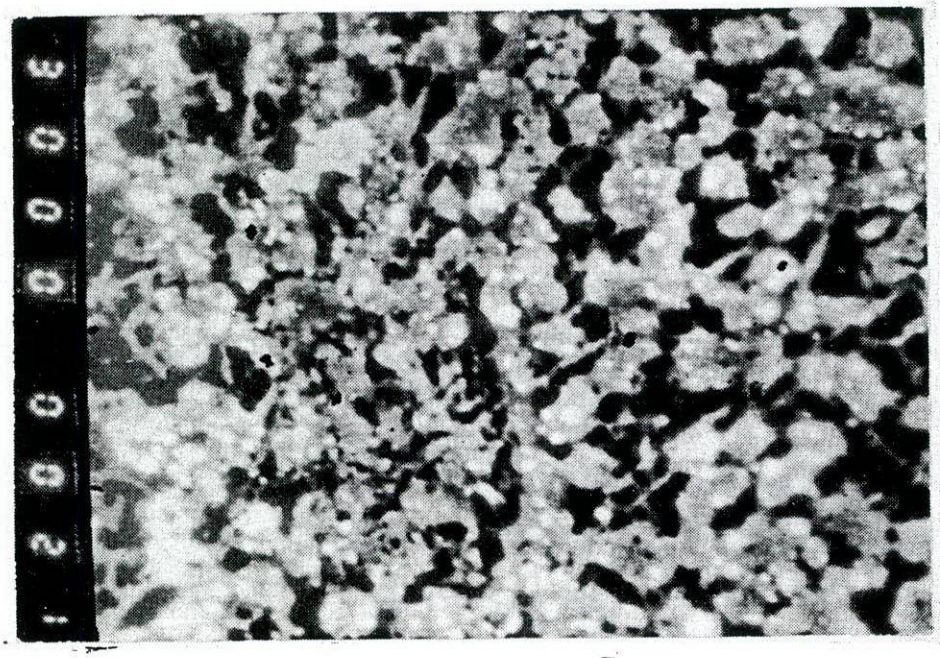

c. The central region of gold deposit (X3000)

Fig. 4 SEM micrograph showing cyclic band structure of laser-induced gold deposit.

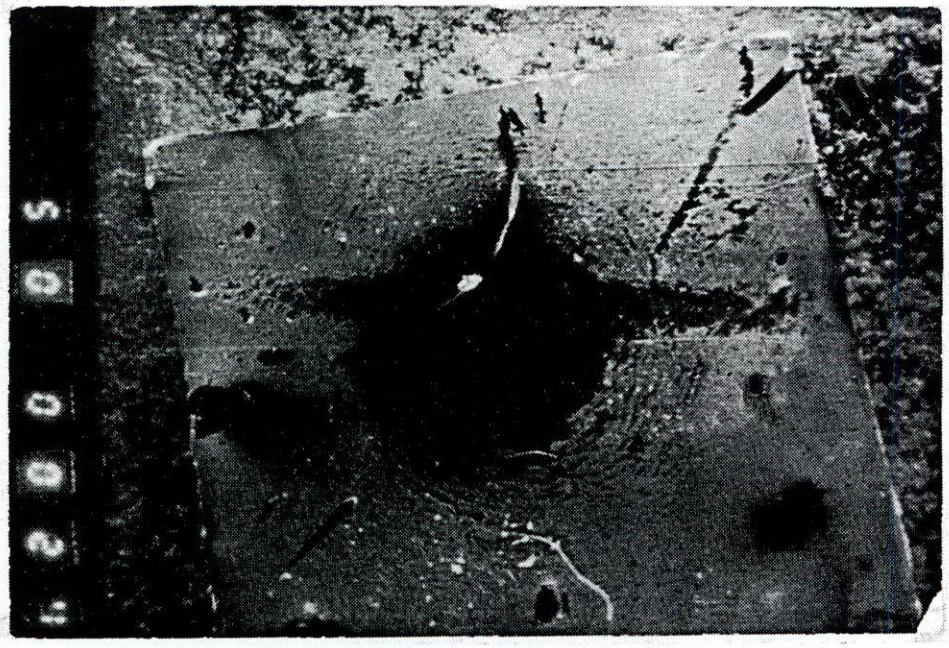

Fig.5 SEM micrograph of the crater obtained under higher laser power irradiation

HIGH PERFORMANCE GOLD PLATING FOR MICRODEVICES

A. Gemmler, W. Keller

Fraunhofer Institute of Manufacturing and Automation (IPA), Eierstr. 46, D-7000 Stuttgart 1, Germany

H. Richter, K. Ruess

Alcatel - SEL Research Center, Lorenzstr. 10, D-7000 Stuttgart 1, Germany

Abstract

Tremendous improvements in the performance of microelectronic devices have been creating increased demands on fabrication processes such as gold plating. By means of continuous bath control and consequent application of a synergistic operational model, high quality gold layers have been deposited from a sulfitic gold electrolyte.

Periodic recording both of existing process data and resulting layer properties yielded a synergistic model to control the plating process. Sources of voids by nodules or pits were characterized using SEM and acoustomicroscopy. Further factors that influence quality of gold deposits (hardness, roughness, uniformity) could be optimized by flexible process control.

Introduction

VLSI - techniques (very large scale integration) have been key components for developing future products in micro-electronics, -mechanics and -optics.

The increase in performance of semiconductor circuits demands adapted miniaturized fine pitch packages with high interconnection densities. Several techniques have been developed to diminish the electronic gap between the wiring densities of chip and board: MCMs (multi-chip-modules) are an attractive packaging solution, if interchip delays are critical to the system performance. TAB (tape automated bonding) and FC (flip chip) techniques for the mounting of bare dice are promising assembly alternatives to wire bonding /1-5/. TAB requires the bonding of tape leads to gold bumps on the semiconductor (Figure 1a). The gold bumps serve the immediate purpose of elevating the height of the semiconductor bond pad in order to avoid shorting. Alignment accuracy, bonding speed and process control are crucial criteria for reliable TAB applications.

Another fast-growing microtechnological area represents the fabrication of small three-dimensional microstructures by application of the LIGA process /6-10/. Main advantages of this technology are the very high aspect ratio as well as its wide material selection. Microstructures of copper or gold are preferably produced to meet demands on conductivity, such as nickel (Figure 1b) Nickel cobalt alloys are used to obtain good mechanical strengths. The large potential of LIGA-applications could be significantly extended through techniques with sacrificial layers as intermediates. As a latest novelty, an electrostatic micromotor has been introduced /11/.

Electroforming of microstructures

Both the bumping and the LIGA process start by sputtering a Ti/W diffusion barrier on a silicon substrate and a gold strike layer as a plating base. Microstructural patterning is achieved by photolithographic processes. During the subsequent plating operations within the resist windows the metal is deposited up to a nominal height of typically 25 µm for bumps or 100 - 300 µm for LIGA-products (Figure 2). Finally, the photoresist and the conductive layer are removed.

Successful processing depends on several conditions: While resist layers of insufficient thickness result in mushroom shaped structures, excessively thick resist deposits may lead to an uncontrolled amount of residues after developing /12/. However, the most important step for high-accuracy electroforming is due to the knowledge to manage a flexible control of the plating process. Analogous methods have been recently described for electroless nickel /13/. In this paper, the aspects of high performance gold plating will be demonstrated and discussed exemplarily for the bump plating process.

Gold Plating

Gold has fought off many challenges in the last forty years to remain the first choice in two major areas of electronics /14/: Surface finishing and interconnection technologies. Gold is preferred to cheaper alternatives such as solder when high performance and reliability is

Pure gold deposits have usually been obtained from potassium cyanide gold plating baths at neutral pH ranges. Due to the poor resist compatibility of such electrolytes, resists are partially underplated at their bases and, as a result, the formation of a bump foot is a common feature /15/. Non-cyanide pure gold electrolytes are available based on the sulfitic gold complex $[Au(SO_3)_2^{3-}]$. In contrast to cyanide baths, they have a better compatibility towards comparable resists. Furthermore, they have an increased throwing power and yield deposits which exhibit more

uniformity in thickness. Along with the improved grain refinement and smoother topography of the deposited gold bumps (Figure 3), all these advantages have led to the almost exclusive utilization of sulfite gold baths for high performance plating processes like wafer bumping.

The plating process

The gold (I) sulfite complex dissociates according to the following equation into free aurous and sulfite ions:

$$Au(SO_3)_2^{3-} \rightleftharpoons Au^+ + 2\ SO_3^{2-}$$

$$K = \frac{[Au^+][SO_3^{2-}]^2}{[Au(SO_3)_2^{3-}]} = 10^{-10}$$

The gold (I) sulfite complex is about 10^{28} times weaker than the gold (I) cyanide complex ($K = 10^{-38}$). Although its stability is improved through a high free sulfite concentration in the electrolyte, a gradual precipitation of gold can happen. Cathodic reduction of sulfite to dithionite and its subsequent reaction with free aurous ions must additionally be taken into account /16-18/.

Considering the sensitivity of gold plating and its application in microforming, sophisticated process engineering must be realized to optimize the plating process to allow us to predict failures before they occur. This method involves using a model of the process in order to calculate the output or hard-to-measure variables from other, easy to measure input variables. Mathematically, the set of existing process parameters x_m have to be mapped on the set of the deposit properties y_n (Figure 4). To create the graph of corresponding relation, all measurable plating parameters and selected deposit characteristics are monitored in the course of processing one hundred wafers. These process parameters and their values are shown in the upper part of Figure 5, whereas in the lower part some objective deposit characteristics are listed.

In Figure 6 a, the concentrations of gold and leveller/grain refiner are documented as "input variables"' hardness and roughness of the gold deposits as "output variables".

Gold has been monitored by two different analyzing methods: Atomic absorption spectroscopy (AAS) and gravimetry (GM). Figure 6 clearly suggests, that AAS-values are dependent on the metal turnovers of the bath. Therefore, a more reliable analytical procedure is represented by gravimetry. Trivalent arsenic ions act as levelling and grain refining agents. They operate at extremely low concentrations of only a few ppm (Figure 6 b). Arsenite was obtained from modified bath samples by differential pulse polarography (DPP) as the only reliable method.

Gold bumps for TAB interconnections must meet a rigid set of criteria including excellent height uniformity, good coplanarity and adhesion to the bump base, and no type of deposit defects. Furthermore, they should be sufficiently ductile and of hardness low enough to prevent cracking of the passsivation and cratering which is a common ILB (inner lead bounding) failure mechanism /19/.

By nature of the plating process utilized to grow gold bumps, tensile and compressive stresses are encountered and must be annealed out. Figure 6 c demonstrates an increasing hardness (Vickers, load 25 g) of the deposit as plated versus number of processed wafers. This corresponds very significantly with arsenite concentrations in the range of about 60 to 70 processed wafers where lower arsenite concentrations produce lower hardness. As described by Wilkinson /18/, the hardness is not due to arsenic in the deposit, but to grain refining. This is in accordance with an almost constant level of hardness after annealing.

The surface roughness of the deposit as plated and after quick etch - to remove the conducting strike layer - has a slight tendency to increase, depending on the number of processed wafers (Figure 6 d). In general for pure gold deposits, the roughness obtained from sulfitic solutions is 10 to 20 times lower than that from cyanide electrolytes (see Figure 3). Concentrations of essential bath components at the start and after processing of 100 wafers including replenishments are shown in Figure 7. It indicates that the total amount of salts in the bath has considerably increased: however, the deposit characteristics cannot be derived directly thereof.

Process modelling

Due to complex cross-linking between process variables and resulting deposit characteristics an operational model of sulfitic gold plating was developed. This synergistic model is identical with the graph of the relation between the set of the existing process parameters (x_m) and the set of the deposit properties (y_n) which was mentioned above. The qualitative chemical part of the operational model is presented in Figure 8.

The quality of the gold deposit is influenced by the process parameters, pictured at the top and bottom lines of Figure 8.

Thus, causes of occurring effects are classified to distinguish primary and secondary origins. Primary causes can be derived from plating variables like current density, pH, sulfite or arsenite concentrations; secondary causes stem from external process parameters e.g. resist impurities or uncarefully prepared $Au(SO_3)_2^{3-}$ solutions.

As shown in Figure 9 the concentration of different trivalent arsenic species substantially depends on pH. The sulfitic gold electrolyte is maintained at a pH of 9.0. Arsenic additives of pH 14 contain as main component $H_2AsO_3^-$. Practically, $H_2AsO_3^-$ is protonated in the bath to give corresponding amounts of polyarsenite $[As(OH)_3]_x$. The part of polyarsenite which preliminarily remains soluble acts as levelling and grain refining agent
(polyarsenite $_{active}$). Aged polyarsenite precipitates (see in Figure 8: polyarsenite $_{particles}$) and is incorporated into the deposit. The effect of polyarsenite $_{active}$ is influenced among others by salt enrichment and filtration. Due to the mass transport control in the cathodic diffusion layer, salt enrichment implies a lower amount of the active species at the cathodic surface. As a result, the deposit roughness is slightly increased. Salt enrichment can be traced to higher concentrations of sulfate, sulfite and chloride (see Figure 7). Conditionally, fine filtration can diminish polyarsenite $_{active}$.

Deposit defects

Periodically, a characteristic deposit defect can be observed during bump plating: Nodules may vary in size and height (Figure 10 a). Their presence leads to increased stresses at ILB-processes and finally to a less reliable TAB assembly. Lateral bump nodules can cause short circuits between adjacent bumps after quick etching. Subsurface imaging was achieved by scanning acoustic microscopy (SAM). In the SAM-photograph, Figure 10 b, the penetration depth of ultrasonic was calculated to be about 9-15 µm. The two centered discs illustrate the growing of two gold particles which were trapped during plating and adhered on the intermediate layer surface. A comparison between the cross section and a computer simulation (Figure 10 c,d) demonstrates the effect of nodular bump growth by incorporating very small metallic particles.

According to the operational model in Figure 8, gold particles can either be produced by reactions in the electrolyte (primary causes) or are dragged in with uncarefully prepared gold sulfite complex (secondary causes). Both the filtration of the particle containing solution and/or dummy plating are methods to remove such gold particles.

The following primary causes originate from the bath:

- Precipitation of gold results when the concentration of uncomplexed Au (I) -ions in the gold sulfite solution is locally exaggerated e.g. by anodic oxidation of sulfite to sulfate or by its oxidation at the phase boundary liquid/air. Controlling anode potential and minimizing the extension of the phase boundary liquid/air will hinder gold precipitation.

- Dithionite which is formed from sulfite at the cathode and subsequently transported to the bulk electrolyte reduces aurous ions to gold. By using a stabilizer, the formation of dithionite is restrained.

Another typical defect which affects gold plating is the appearance of pits (Figure 11 a). Pits can be traced to secondary causes. Scanning acoustic microscopy indicates a characteristic irregular shape of gold growth (Figure 11 b). The process model (see Figure 8) and supplemental investigations give evidence of two possible failure mechanisms:

- residues in the resist openings (Figure 11 c),

- incorporation of dragged-in resist or other non-conductive particles (Figure 10 d)

Like nodules, pits give rise to less reliable TAB-assemblies by weakening the bumping strength between bumps and inner leads of the TAB-frame. They can be avoided by careful control of the lithographic process and proper operating conditions.

The results of interactions between particles and cathodes are supported by recent calculations of J.P. Celis, et.al., which describe the primary current distributions at cathodes, with both adjacent conductive and nonconductive particles /20/. The modification of the current field around absorbed particles is characteristically evident. In compliance with the current distributions, pit formation in the presence of non-conductive species, like resist residues (upper part of Figure 12) and nodules growing from conductive gold particles (lower part of Figure 12), can be easily understood.

Summarized, the presented investigations yield a synergistic operational model by periodic recording of existing process data and the resulting layer properties. The functionality of the deposit is provided by the concurrence of the plating parameters and deposit characteristics. Consequent application of the model allows installation and effective control of high performance.

gold plating. Figure 13 shows series of bumps after optimizing the plating process.

Conclusions

Semiconductor complexity has been advanced to VLSI-techniques with 100,000 or more components per chip. Interconnection and packaging densities are to follow. A similar trend towards continuously decreasing pattern sizes is expected for devices in micromechanics, microsensoring and micro-optics.

High per4formance electroforming will participate with a higher standard of process engineering. High performance plating exhibits improved understanding, improved controlling and improved precision.

Acknowledgments

The authors would like to thank M. Worbs, W.Jörg and H. Hanisch for the experimental work, L. Brummer, B. Frey and W. Leonhard for analytical assistance. The cooperation and support of H. Reichl, O. Ehrmann, G. Englemann and J. Simon, Technical University of Berlin, is gratefully acknowledged.

References

/1/ T.S. Liu, W.R. Rodrigues de Miranda and P.R. Zipperlin, "A Review of Wafer Bumping for Tape Automated Bonding", Solid State Techn. **23**, 71-75 (March 1980)

/2/ H. Reichl, "Tape Automated Bonding", DVS-Berichte Bd. **129**, 10-15

/3/ S. Khadpe, "Developments in Tape Automated Bonding", Electronic Packaging and Production Nov. 1991, pp 42-45

/4/ P.W. Rima, "TAB Gains", Connection Technology August 1987, pp 28-32

/5/ J. Simon, E. Zakel and H. Reichl, "Electroless Deposition of Bumps for TAB Technology", Metal Finishing Oct. 1990, pp 23-26

/6/ E.W. Becker, W. Ehrfeld, P. Hagmann, A. Maner, D. Münchmeyer, "Fabrication of Microstructures with High Aspect Ratios and Great Structural Heights by Synchrotron Radiation Lithography, Electroforming and Plastic Moulding (LIGA Process)", Microelectronic Engineering **4**, 35-56 (1986)

/7/ A. Maner, S. Harsch, W. Ehrfeld, "Mass Production of Microdevices with Extreme Aspect Ratios by Electroforming", Plating **75**, 60-65 (1988)

/8/ H. Guckel, T.R. Christenson, K.J. Skrobis, D.D. Denton, B. Choi, E.G. Lovell, J.W. Lee, S.S. Bajikar, T. W. Chapman, "Deep X-Ray and UV Lithographies for Micromechanics", 1990 IEEE Solid State Sensor and Actuator Workshop, pp 118-122

/9/ W. Menz, W. Bacher, M. Harmening, A. Michel, "The LIGA-Technique - A Novel Concept for Microstructures and the Combination with Si-Technologies by Injection Molding", Micro Electro Mechanical Systems, Nara, Japan, 30.1.-2.2.1991 Proc. IEEE, pp 69-73 (1991)

/10/ S. Harsch, D. Münchmeyer, H. Reinecke, "A New Process for Electroforming Movable Microdivices", SUR/FIN '91, Toronto, Canada, Proceedings, pp 449-461 (1991)

/11/ "LIGA - Movable Microsructures" Kernforschungszentrum Karlsruhe 1992

/12/ I. Milosevic, J. Jasper, "Straight Wall Bumps for High Lead Count Devices - Photolithography and Physical Properties", Mat. Res. Soc. Symp. Proc. Vol. **154**, pp 425-430

/13/ A. Gemmler, T. Bolch, H. Gut, W. Keller, "Mechanism of Electroless Nickel Deposition and its Utilization in Expert Systems", SUR/FIN '90, Boston, U.S.A., Proceedings

/14/ J. Lovie, "Nickel and Gold Plating in Electronic Packaging", Electronic Packaging and Production March 1991, pp 56-60

/15/ J. Traut, J. Wright, J. Williams, "Gold Plating Optimization for Tape Automated Bonding", Plating **77**, pp 49-53 (1990)

/16/ P. Wilkinson, "Theoretical Considerations of Acid Gold Plating", Trans. Inst. Metal Finish. **59**, 149-153 (1981)

/17/ Arakawa Kako KK, Jpn. Pat. Application 57203788 (1981)

/18/ P. Wilkinson, "Understanding Gold Plating", Gold Bull. **19**, 75-81 (1986)

/19/ D. Tovar, "Optimization of a Gold Bump Process for TAB by Statistically Designed Experimentation", ITAB `91 Proceed.

/20/ J.P. Celis, J.R. Roos, C. Buelens, J. Fransaer, "Mechanism of Electrolytic Composite Plating: Survey and Trends", Trans. Inst. Metal Finish. **69**, 133-139 (1991)

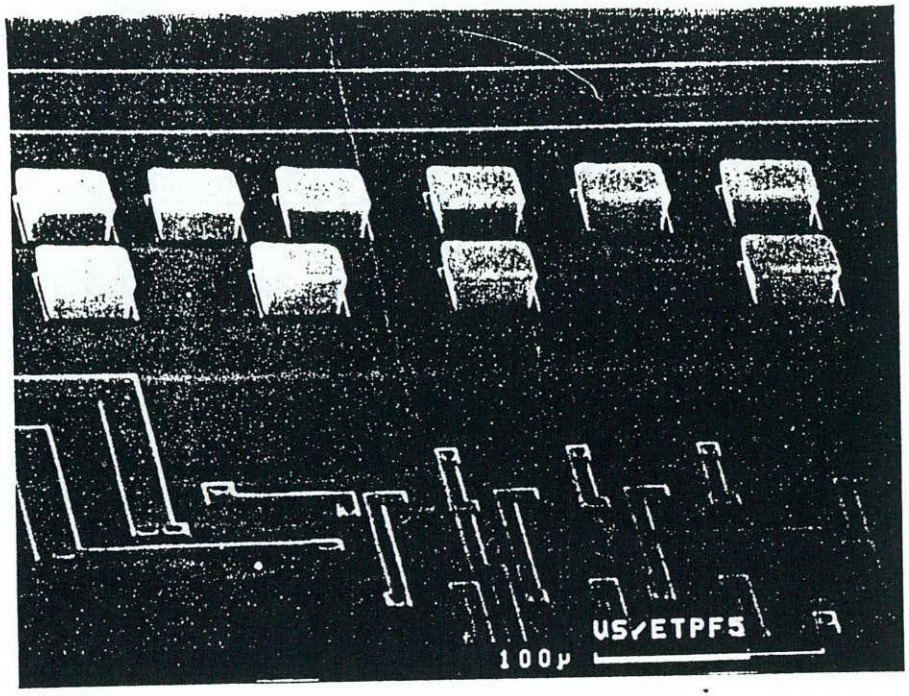

a) Bumps on a test-IC

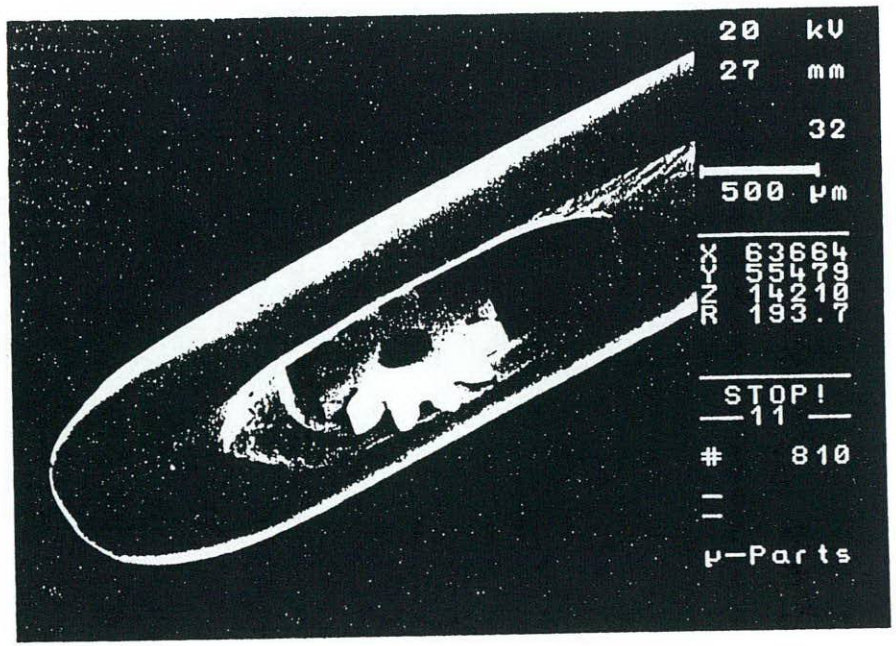

b) LIGA-fabricated micro-gear inside of a needle eye (by courtesy of MicroParts GmbH, Karlsruhe, /8/)

Figure 1. Representative microdevices

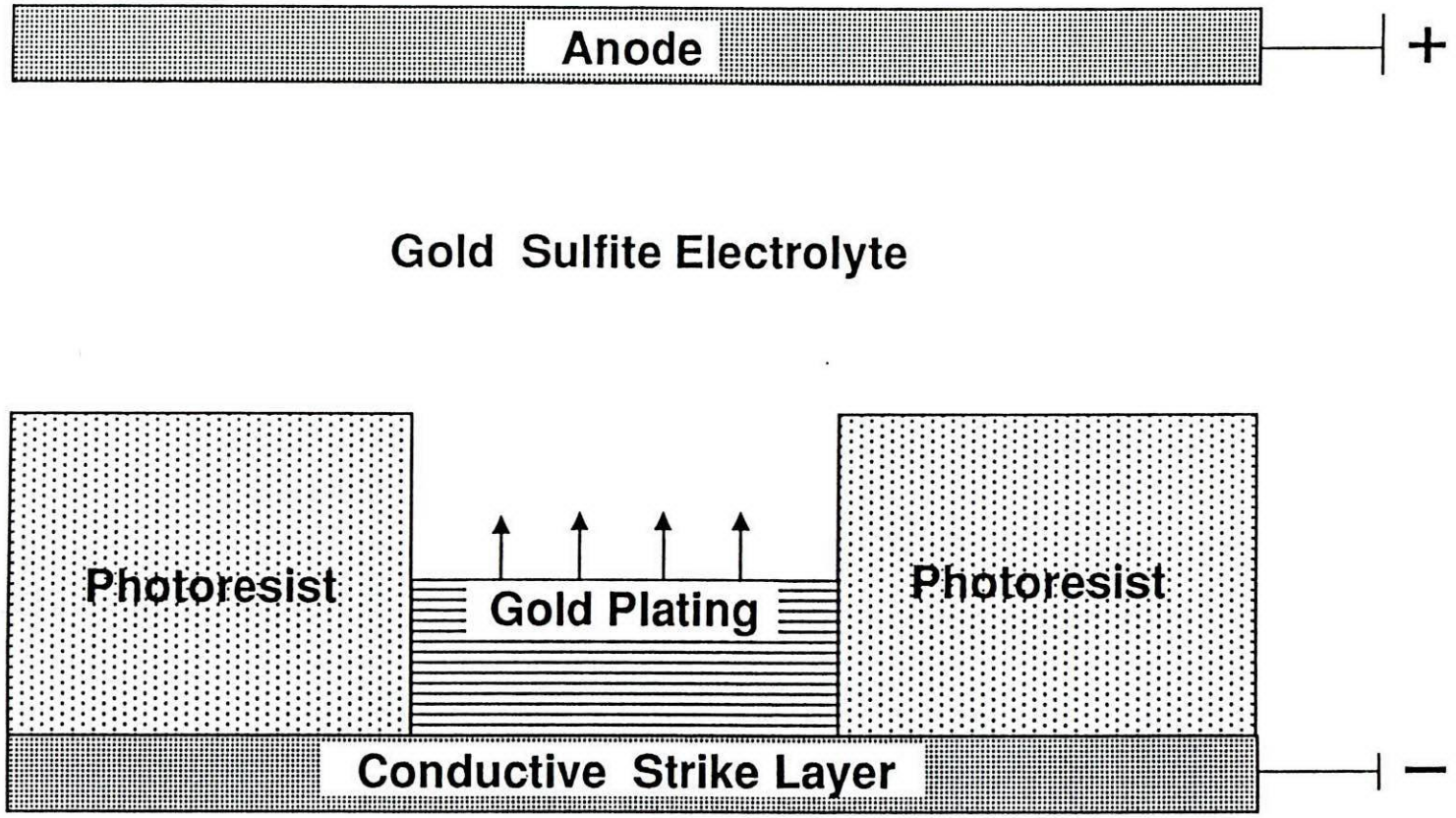

Figure 2. Plating of gold microstructures

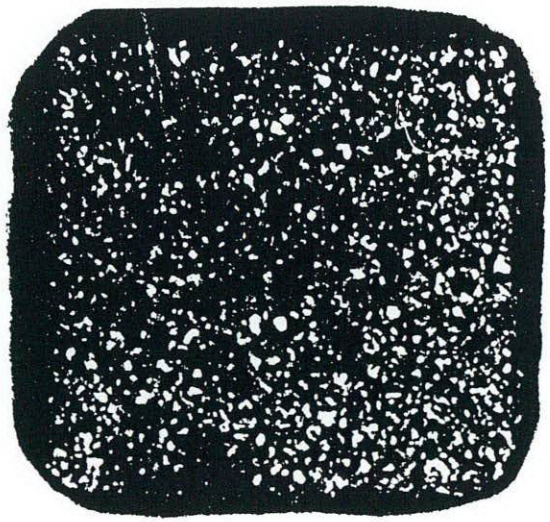

from a cyanide gold bath

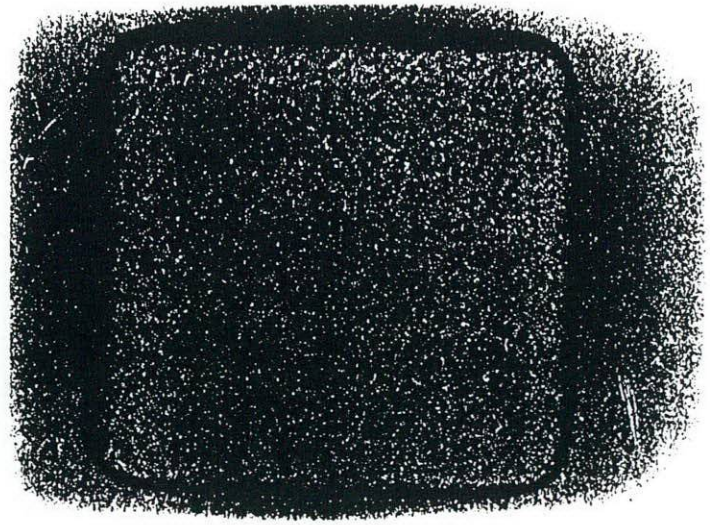

from a sulfitic gold bath

Figure 3. Surface topographies of gold bumps

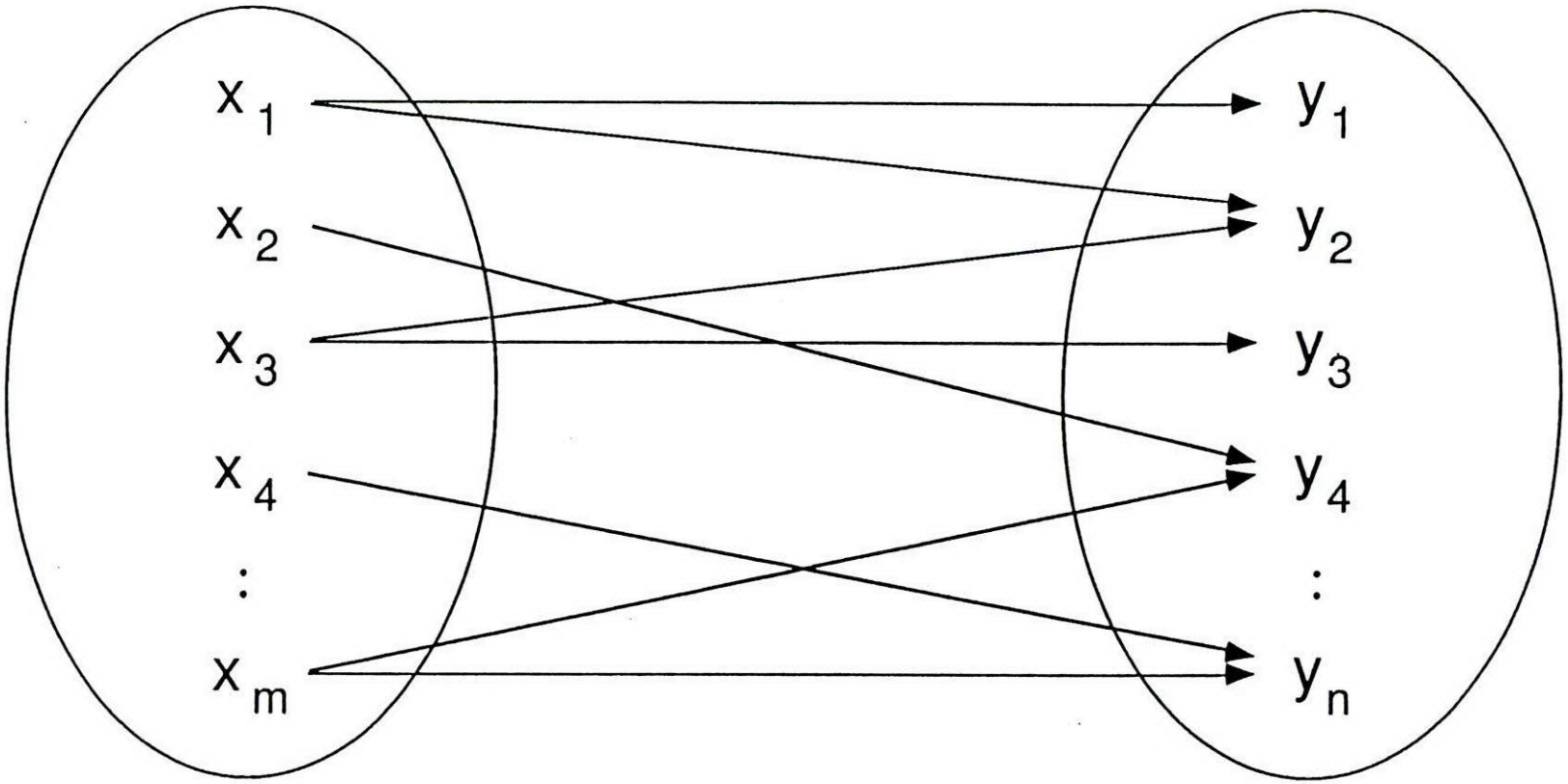

Figure 4. Process modelling and engineering: Mapping of process parameters x_m on deposit properties y_n

Process parameters x_m	
Temperature	47 ± 1°C
pH	9.0 ±0.2
Current density	0.25 - 0.3 A/dm^2
Anode material	Platinated Titanium
Plating rate	0.16 - 0.18 µm/h (at 0.3 A/dm^2)
Agitation mode	Mechanical stirring
Gold(I)	10 ± 1 g/l
Leveller / Grain refiner	1.5 - 3.5 mg/l *
Sulfite	26 g/l **
Sulfate	21 g/l **
Chloride	1.7 g/l **
EDTA	15 g/l **

* adapted to process continuance ** starting conditions

Deposit characteristics y_n	
Hardness *	100 < ±10 MHV (30 min 340°C)
Roughness**	R_z < 0.1 µm, R_a < 0.02 µm
Bump height	25 µm (typical)
Height uniformity	< ± 0.5 µm per chip, < ± 2 µm per 4" wafer
Bump shape	Straight wall, high coplanarity to bump base
Molding accuracy	High
Voids	None (no nodules, pits etc)

* measurement accuracy ± 5 MHV ** as plated

Figure 5. Selected sulfitic gold process parameters x_m and objective deposit characteristics y_n

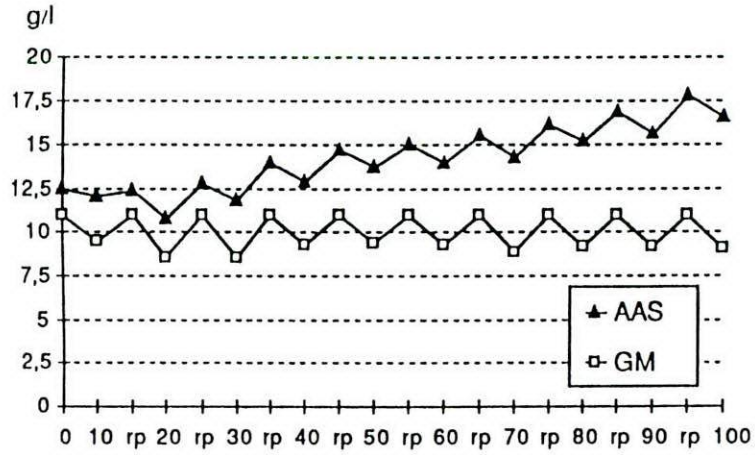

a) **Gold Concentration** vs. number of processed wafers (rp= replenish)
Analyzing mehod: AAS= atomic absorption sectroscopy, GM = gravimetry

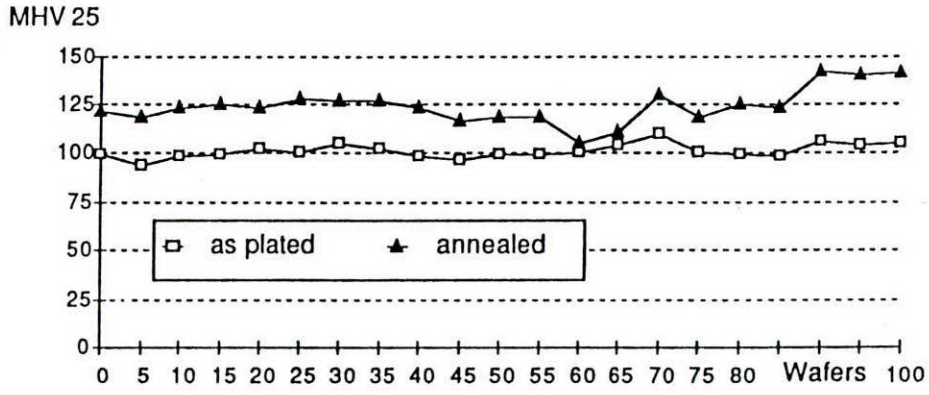

c) **Hardness** vs. number of processed wafers

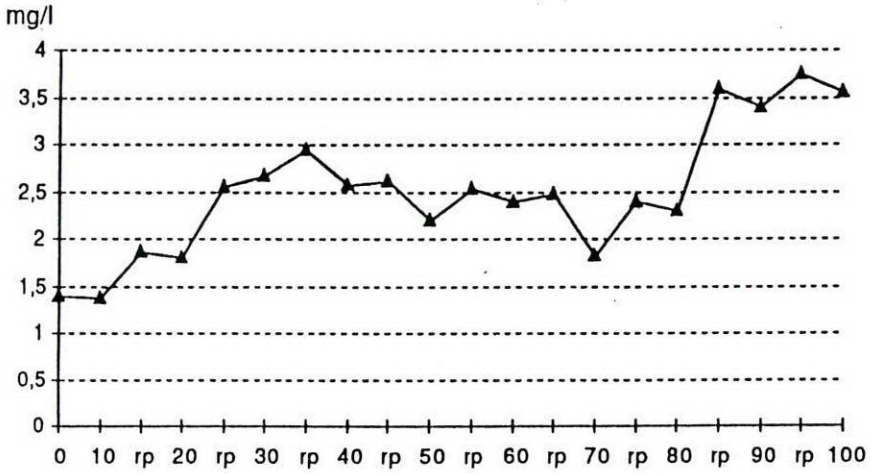

b) **Arsenite-concentration** vs. number of processed wafers (rp= replenish)
Analyzing method: DPP= differential pulse polarography

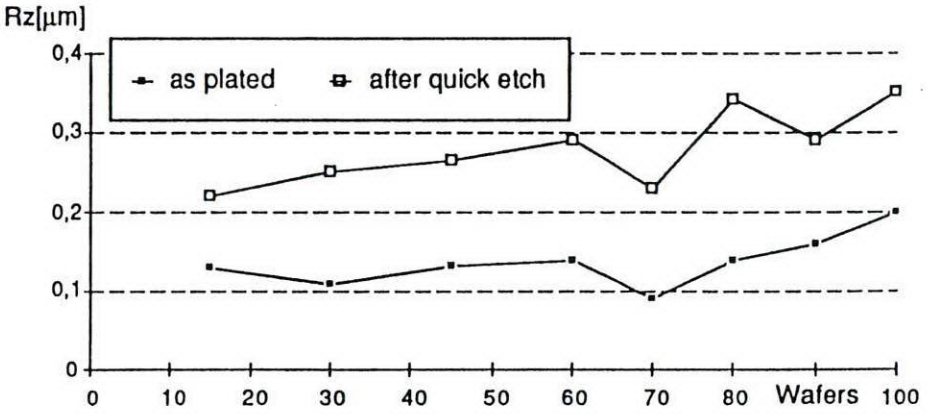

d) **Roughness** vs. number of processed wafers

Figure 6. Monitoring of process (x_m) and deposit variables (y_m)

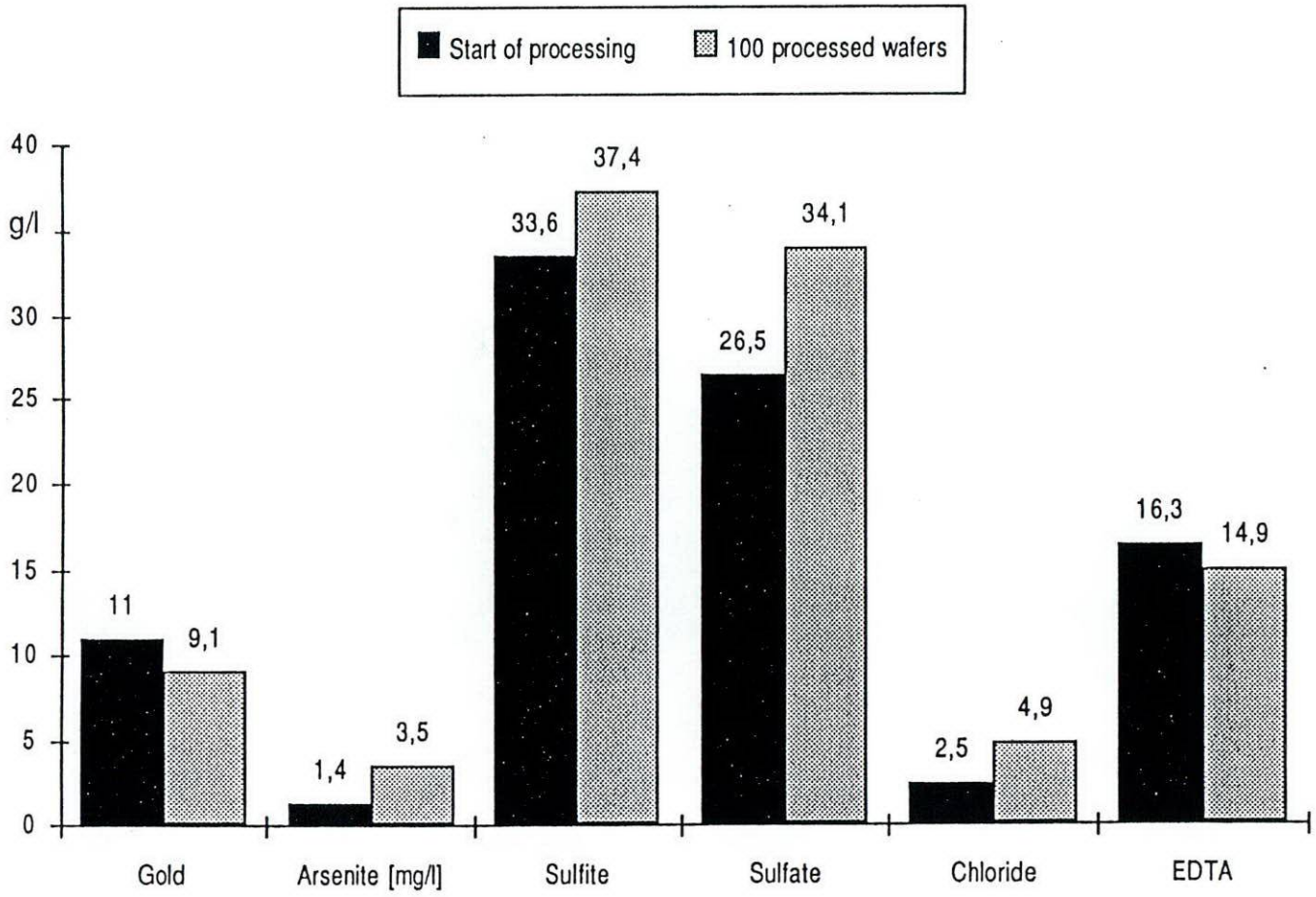

Figure 7. Concentrations of essential bath components at the start and after processing of 100 wafers incl. replenishments

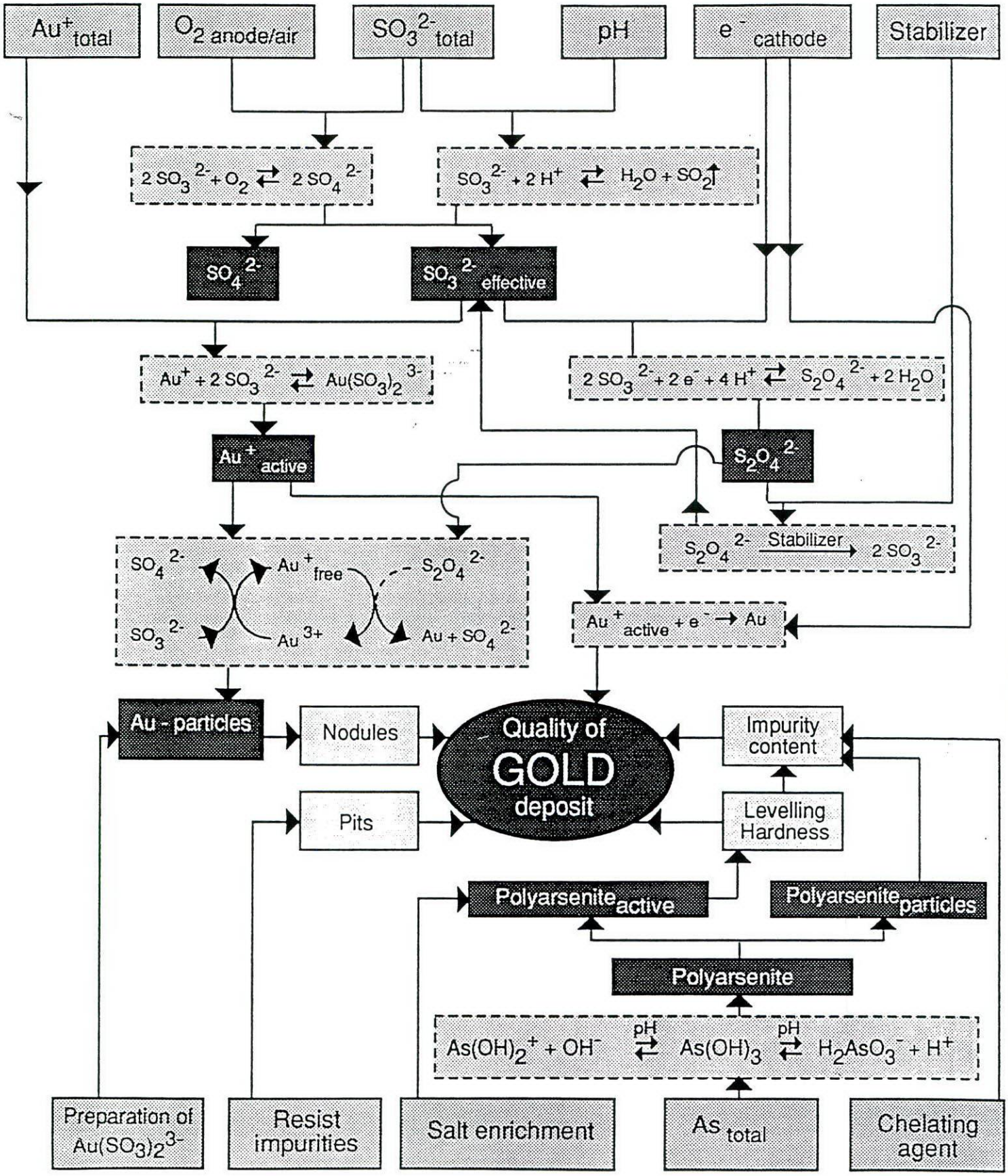

Figure 8. Basic operational model of sulfitic gold plating

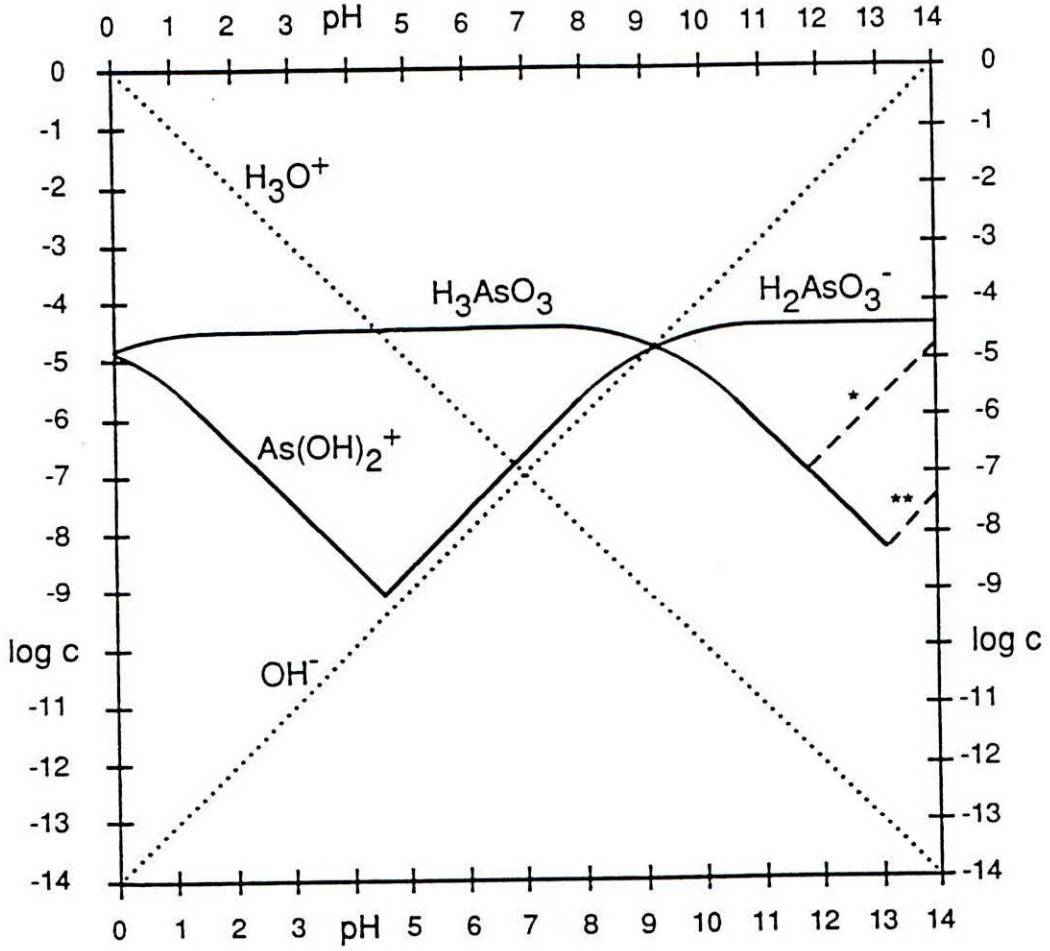

* Assumptive line for $HAsO_3^{2-}$

** Assumptive line for AsO_3^{3-}

Figure 9. pH - depending ratios of concentration for trivalent arsenic species

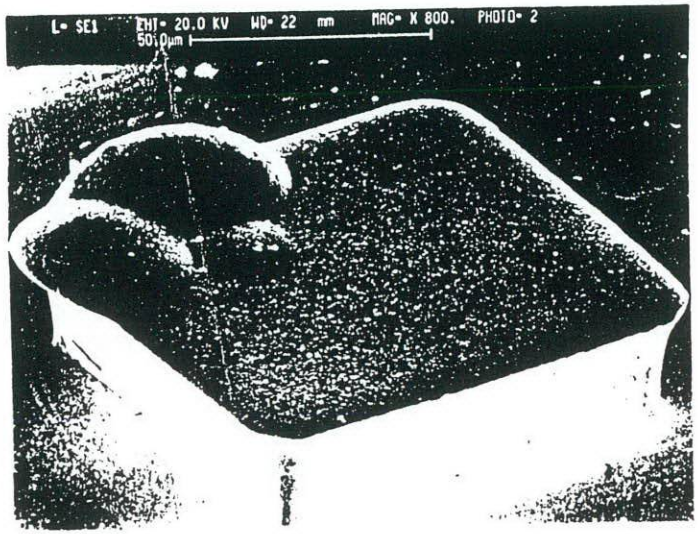

a) SEM - photograph (800 : 1)

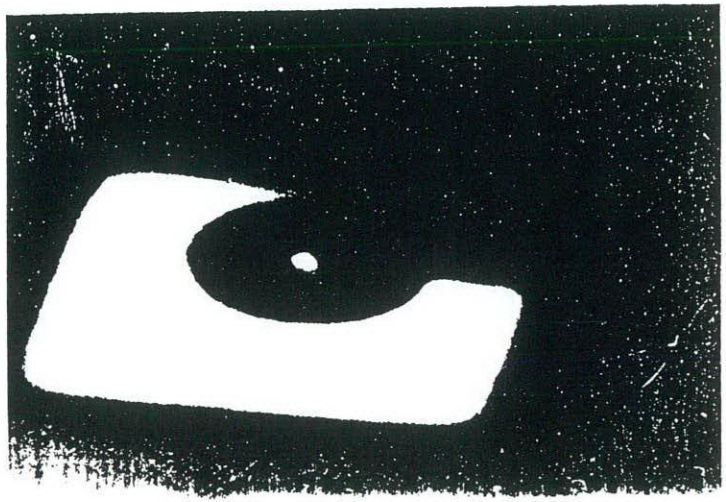

b) Acoustomicroscopic photograph (600 : 1, 200 MHz, Z = 9 - 15 µm)

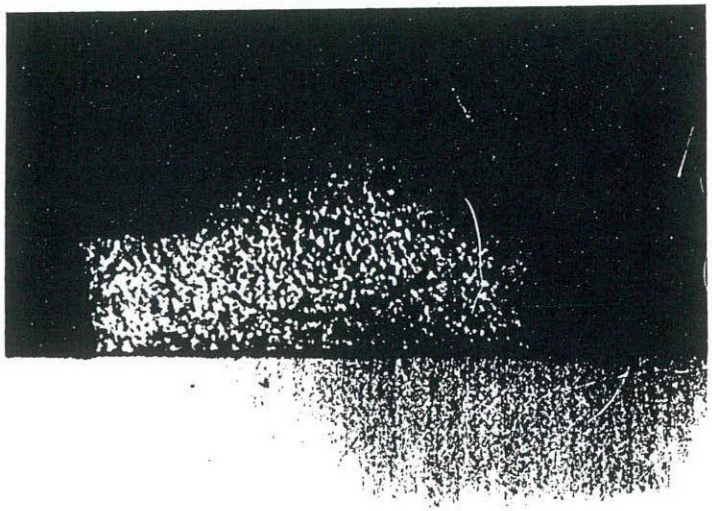

c) Etched cross-section (600 : 1)

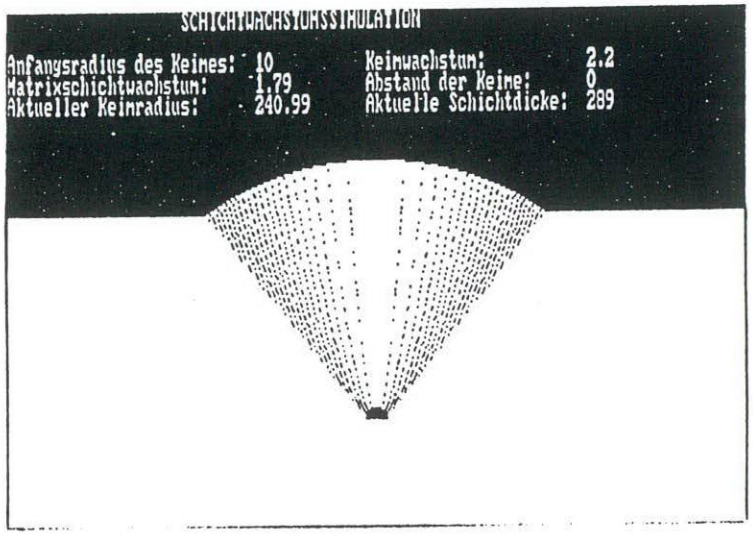

d) Computer simulation

Figure 10. Gold deposit defect: Nodule

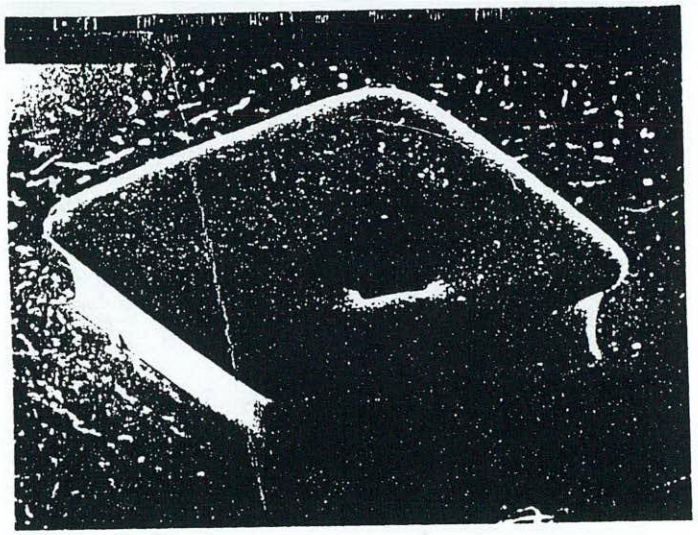

a) SEM - photograph (700 : 1)

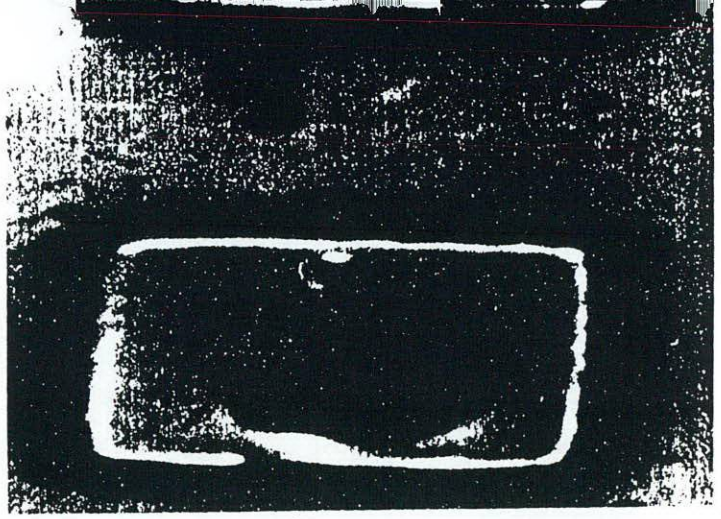

b) Acoustomicroscopic photograph (600 : 1, 400 MHz, Z = 3 - 5 µm)

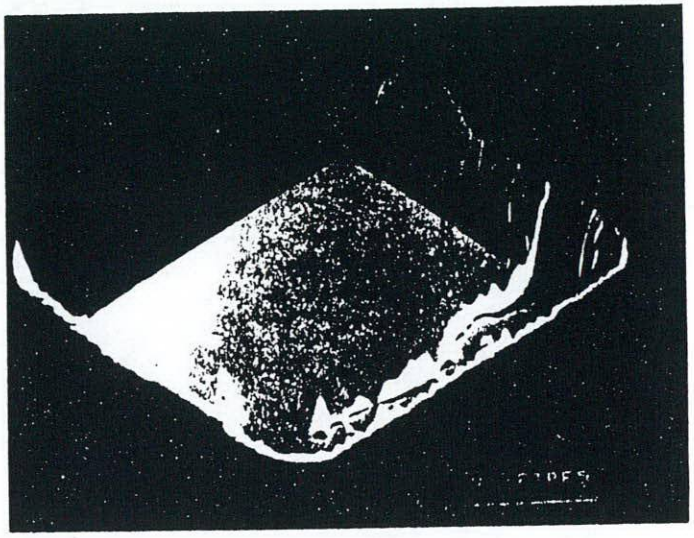

c) SEM - photograph (700 : 1) of an incompletely developed resist window

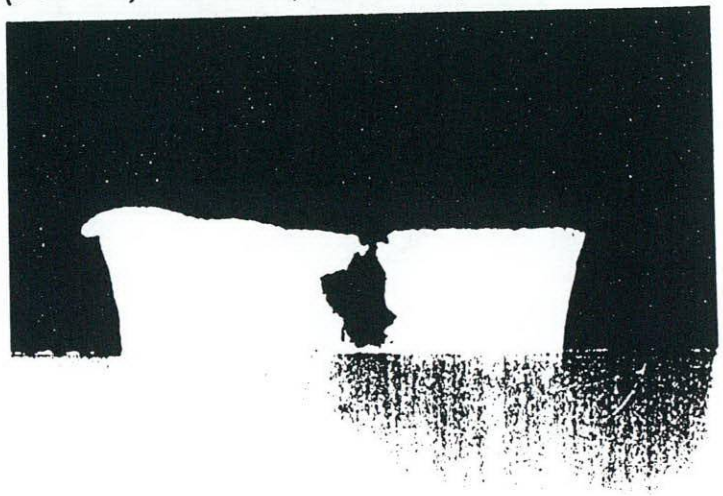

d) Cross-section (600 : 1) showing an incorporated non-conductive particle

Figure 11. Gold deposit defect: Pit

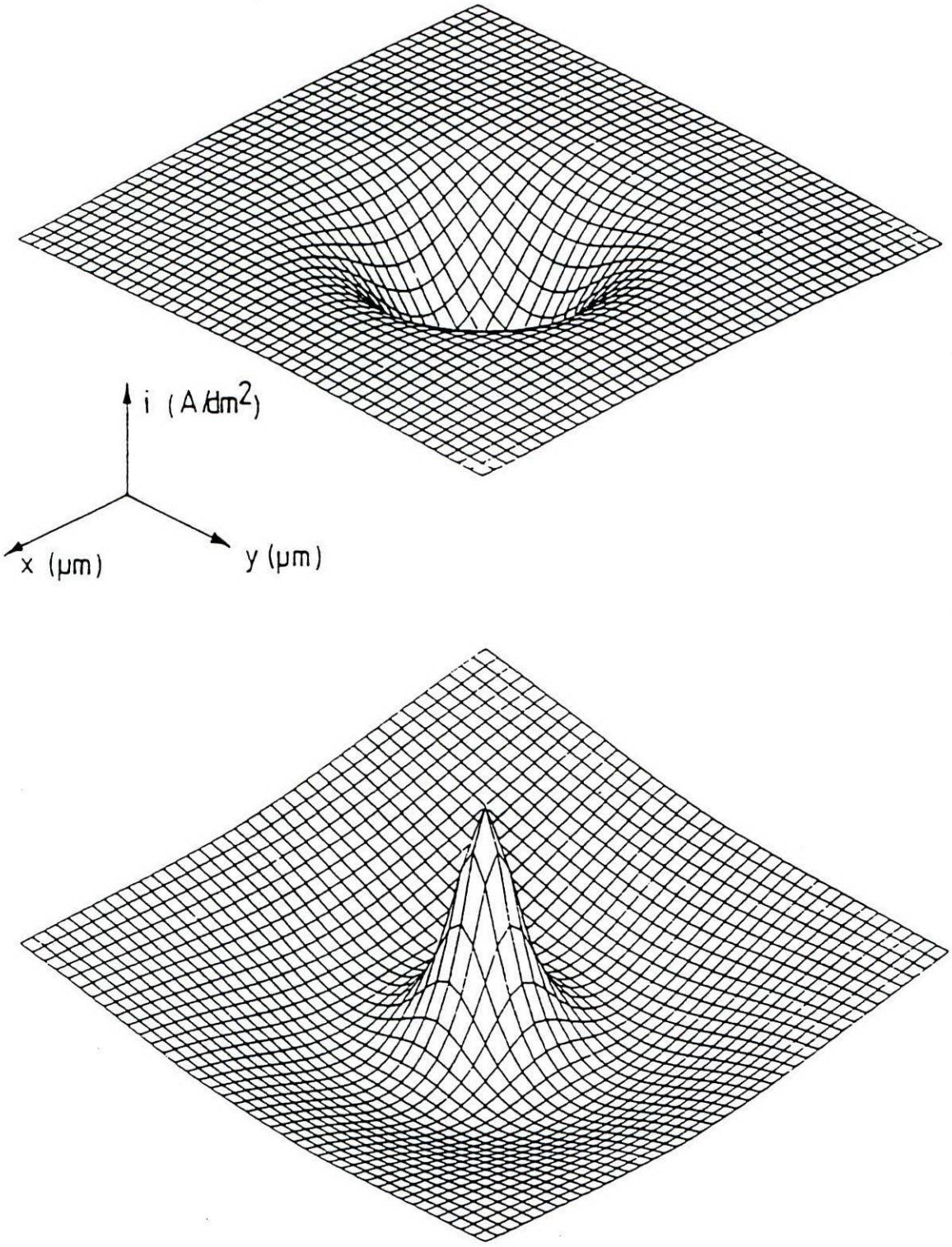

Figure 12. Primary current distribution at a cathode in presence of a non-conductive particle (top) and a conductive gold particle (bottom) /20/

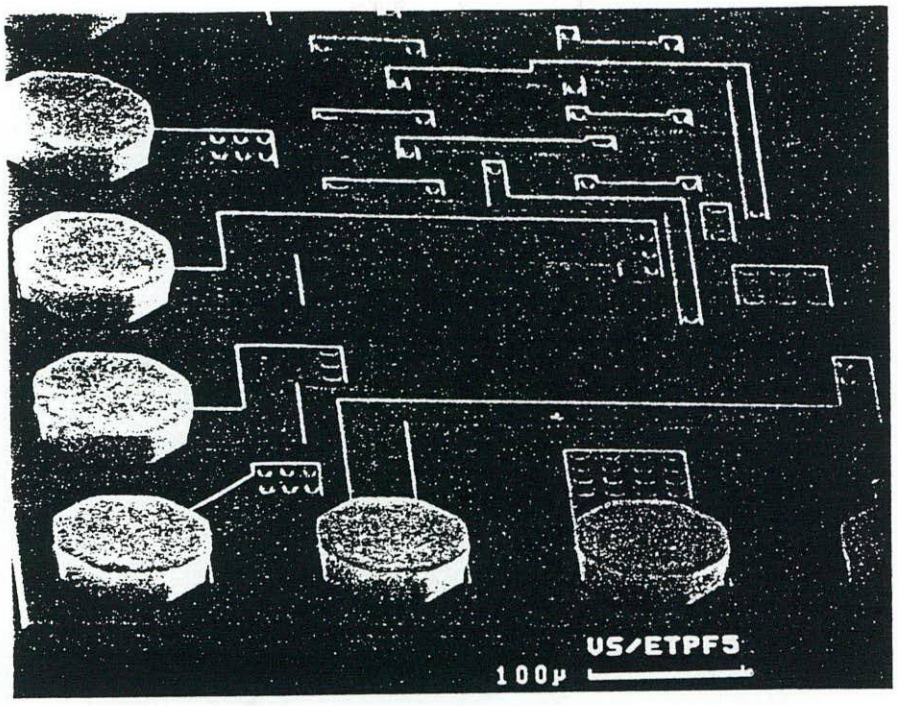

Figure 13. Series of gold bumps on a processed wafer

ELECTROCHEMICAL DEPOSITION OF TIN-ZINC ALLOYS.

Chemist, Grad. scient. Jean Rasmussen[1]
Centre of Advanced Electroplating
The Technical University of Denmark.

Electrodeposition of a tin-zinc alloy is optimized using Taguchi statistics. Interactions between process parameters are investigated. Furthermore the diffusion of hydrogen into the steel substrate during plating, giving rise to hydrogen embrittlement is measured using a sealed Devanathan cell. The type and magnitude of internal stress under various plating conditions is examined by dilatometry. Control of the plating bath is made using Differential Pulse Polarography and Hull cell panels. Results from corrosion tests - field and accelerated - will be presented at the conference. Comparisons will be made with other coatings.

1 INTRODUCTION.

Both tin and zinc are widely used for the protection of steel against corrosion. Each has a different sphere of application and each protects steel by a different mechanism. Tin is more noble than steel and, under ordinary atmospheric exposure, protects steel by forming a corrosion resistant envelope around it. However, rusting takes place in pinholes or imperfections in the tin coating, and is accelerated galvanically by the difference in potential between steel and tin. Zinc is less noble than steel and protects by a sacrificial action. Even when steel is exposed through faults in the coating, it is protected galvanically by the zinc.

The protective properties of the two metals are nicely balanced in a tin-zinc alloy containing about 80 percent of tin. The coating protects steel by a sacrificial action similar to that of zinc. Consequently, steel does not rust through pinholes and yet the coating does not form as voluminous white corrosion products as with zinc coatings. The alloy has a solderability which is better than that of cadmium.

A tin-zinc alloy containing about 80 perccent tin has been used because of the superior corrosion protection it affords steel. However, alloys over the complete range of compositions can be deposited if bath parameters are adjusted accordingly.

Until recently, plating was mainly done in cyanide-stannate baths. New non-cyanide processes are now available and offer (compared to the cyanide bath), several advantages, such as better bath stability, less parameters to control, and less after treatment of effluents. Furthermore, the alloy is deposited as a bright coating and the composition, contrary to cynide-stannate baths, is less sensitive to current density.

2 FUNDAMENTALS.

The standard electrode potentials of tin and zinc are more than 0.6 volt apart. Consequently, the alloys cannot be deposited readily from acid solutions (1). The deposition potentials of the two metals are much closer in alkaline solutions. Moreover, the presence of a complexing agent is necessary for the deposition of usable tin-zinc alloys.

In a weak acid solution, the complexant is a carboxylic acid (2). Oxidation of tin(II) to tin(IV) by dissolved oxygen is prevented by the addition of an antioxidant. A metallic lustre is obtained by the addition of a brightner.

Compared to normal one-metal processes, several parameters are involved in the deposition of tin-zinc alloys. However, a simultaneous deposition of both metals is relatively unsensitive to the concentration of one of the metals. Use of metals

[1] *Danfoss A/S, Corporate Production, L3-V127, DK-6430 Nordborg, Denmark.*
Direct dialing + 45 74 88 44 32, telefax + 45 74 45 48 18.

during plating is compensated by an almost balanced dissolution of tin-zinc anodes. Drag out is the main reason for the losses.

3 EXPERIMENTS.

The investigations were based on Taguchi statistic experimental planning (3). It is used to rank the importance of the different parameters and interactions involved in deposition of both zinc and tin in a slightly acidic bath. The composition of the bath was kept inside the tolerance limits listed in table 1.

The first series of experiments was based on a Taguchi L_{18} orthogonal array, which allows variations of 8 parameters - one at two levels and the rest at three. The main reason for using this balanced table is that the number of experiments compared to a total factor investigation is reduced from 729 experiments to 18. Variations associated with uncontrolled conditions is also incorporated in the orthogonal array. The experimental conditions are shown in table 2.

The composition of tin-zinc alloys plated on Hull cell panels, as well as thickness distribution, is determined by X-ray analysis.

Based on the results from the first series of experiments, a Taguchi L_8 orthogonal array is used to examine possible interactions. In this balanced table (see figure 1), interactions between the first two parameters will show up in column III. The fourth column is reserved for the third parameter, and interactions with the first parameter, respectively the second, will show up in column V and VI. The seventh column is reserved for the pH, which does not interact at all with the other parameters. The experimental conditions are shown in table 3. Compared to a total factor investigation,

Tin [g/l]	20	± 5
Zinc [g/l]	8	± 5
Complexant [g/l]	120	± 10
Antioxidant [g/l]	60	± 10
Brightner [ml/l]	8	± 1
Current density [A/dm^2]	2	0.5 - 5
Temperature [°C]	25	± 5

Table 1. Dipsol SZ-240®: Concentration of the process parameters and operational conditions for deposition of tin-zinc alloys of 80 wgt-% tin.

Parameter

Experiment no.	L_8	I	II	III	IV	V	VI	VII
	1	1	1	1	1	1	1	1
	2	1	1	1	2	2	2	2
	3	1	2	2	1	1	2	2
	4	1	2	2	2	2	1	1
	5	2	1	2	1	2	1	2
	6	2	2	2	2	1	2	1
	7	2	1	1	1	2	2	1
	8	2	2	1	2	1	1	2

Liniar graph

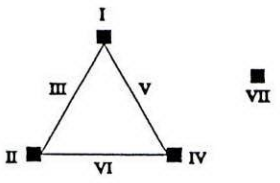

Figure 1.The L_8 orthogonal array and the corresponding liniar graph showing interactions. 7 parameters are investigated at 2 adjustments in 8 experiments (1-8).

the number of experiments are reduced by 50 percent.

Hydrogen embrittlement is investigated using a Dry Hydrogen Contact Cell - HCC 11 (4). This is a contact cell for monitoring hydrogen permeation through a steel substrate. The HCC 11 is a sealed Devanathan cell with a paladium window capable of transmitting hydrogen.Through oxidation, the cell converts the flux of hydrogen into an electrical current, which is registered on a X-Y plotter.

When hydrogen emanates from the steel, the cell will receive a part of this flux giving rise to a current from the cell. This current is measured as a voltage drop across a resistance, and can be expressed as a hydrogen flux instead of a current.

Care must be taken to ensure that the surface conditions of the steel are the same from one plating to another. It is possible to achieve reproducible results within a relative uncertantity of 5-8% by grinding the cell with emery paper before each plating.

Internal stress in the deposits is investigated by a dilatometric method (5), where the length changes of thin straight strips plated on both sides is mea-

BATH PARAMETERS								
Level	Day	Additive ml/l	Tin g/l	Zinc g/l	Complexant g/l	Antioxidant g/l	pH	N/S
1	Mon	7	15	3	110	40	5	none
2	Thu	8	20	8	120	60	6	none
3	none	9	25	12	130	80	7	none

Table 2. Parameters and levels of adjustments in the Taguchi experiment based on a L_{18} orthogonal array.

sured. Specimens used in the experiments were thin copper strips, 10 ± 0,1 mm wide and 0.055 mm thick. The specimen length is about 210 mm.

From the measured dimensional changes it is possible (in every stage of the plating process) to calculate the value of the average internal stress in the deposit.

The largest single contribution to errors of measurements is the dilatometer reading itself, but this error diminishes rapidly with increasing time and deposit thickness. Above a thickness of 2 µm the errors of measurement are small compared to the measured internal stress. The reproducibility of the method is better than 95%.

4 RESULTS.

In the L_{18} experiment, an analysis of the variance (ANOVA) showed that non-controlled factors did not have an effect upon the results. On the other hand, the only parameters of significant importance are the concentration of zinc, and the noise signal ratio (N/S in table 2). The latter indicates the existence of important interactions between some of the parameters.

A multi regression analysis (assuming liniarity) showed that the following interactions were of importance: the ratio between the concentrations of tin and zinc, tin and complexant and zinc and complexant.

PARAMETER		LEVEL	
I	Tin [g/l]	15	20
II	Zinc [g/l]	3	8
IV	Complexant [g/l]	120	130
VII	pH	6	7

Table 3. Process parameters in the Taguchi experiment based on a L_8 orthogonal array and the level of adjustments. See also figure 1.

There is only a perfect fit to the observed compositions of the tin-zinc alloy, for the highest current density investigated (7.6 A/dm^2). With a confidence limit of 95%, 16 out of the 18 observations can significantly be described by the following formula (concentrations in g/l):

Zinc content [wgt-% at 7.6 A/dm^2] =
- 209.85 + 1.13pH - 14.65Sn
+ 11.77Zn + 1.87Complexant
- 1.63Sn/Zn - 1218.05Sn/complexant
+ 1721.38Zn/complexant

Some of the results from the L_{18} experiment are shown in figure 2. Even though the parameters were kept inside the limits of tolerance (see table 1), the composition along the Hull cell panels varied significantly. Three examples are given in curves a-c. The pH of the bath is an important parameter. A low value causes a pronounced reduction of the zinc-content (curve d) as current density is lowered. A pure tin coating can be deposited at pH = 5 when the zinc concentration in the bath is 3 g/l. At pH values between 6 and 7 the alloy composition is relatively stable over a broad range of current densities. A pH in the higher end of this interval seems to reduce the difference in composition when going from high to low current density (curve e and f).

A high tin content in relation to zinc, causes a displacement of the alloy composition towards higher tin-content. This displacement is almost the same over the total range of current densities (curve g-i).

Interactions between the concentrations of the two metals and the complexing agent are shown in curves j-k. Increasing the concentration of tin relative to the complexant, displaces the alloy

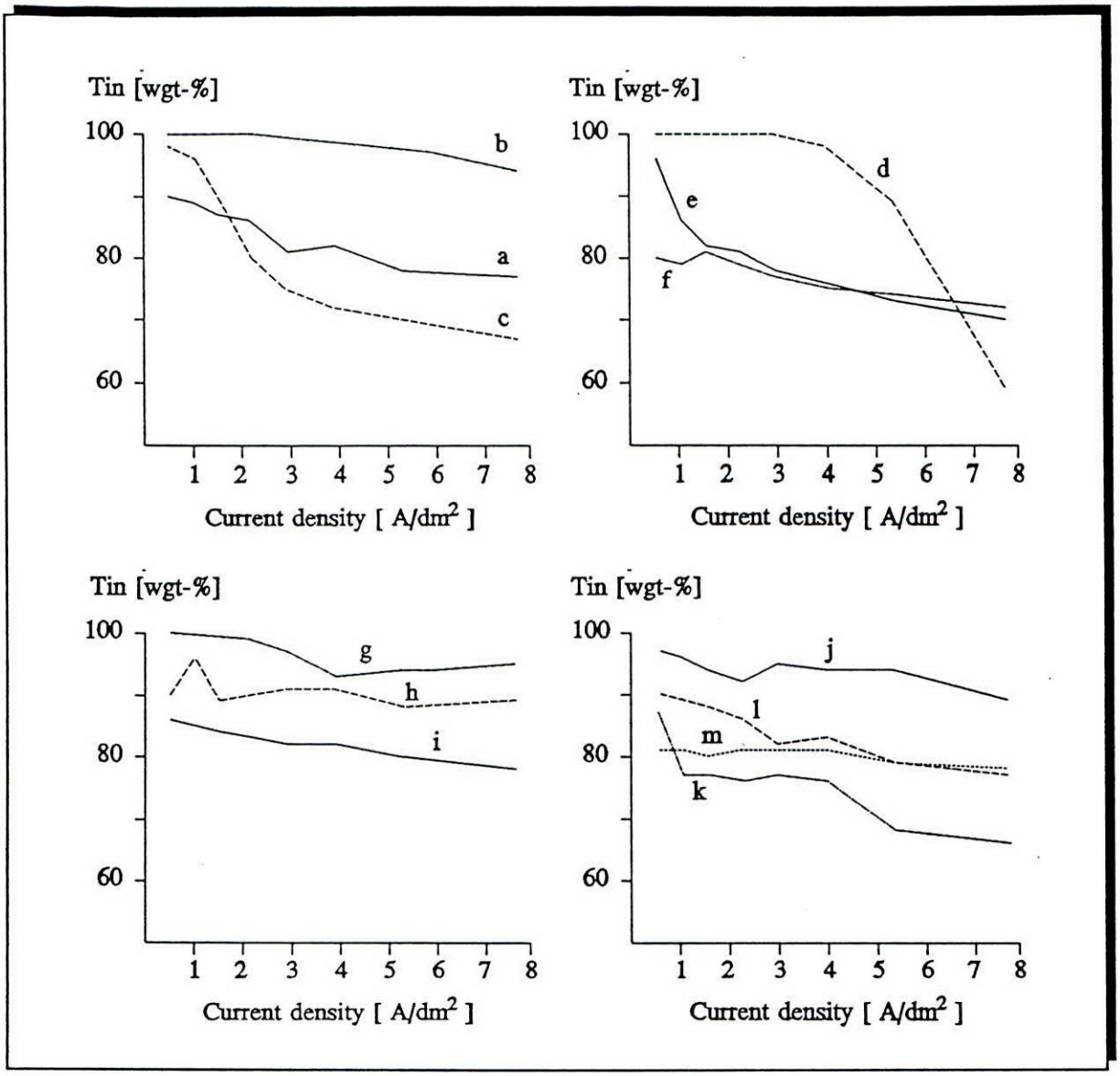

Figure 2. The composition of alloys plated on the Hull-cell panels versus current density and experimental conditions in the L_{18} experiments. ***Curves a-c:*** *illustration of variation with the parameters kept inside the limits of tolerance,* ***curves d-f:*** *pH = 5.0 (d), 6.0 (e) and 7.0(f),* ***curves g-i:*** *interaction between tin and zinc, tin/zinc = 6.7 (g), 6.0 (h) and 2.1 (i),* ***curves j-k:*** *interaction between tin and complexant, tin/complexant = 0,13 (j) and 0,18 (k),* ***curves l-m:*** *interaction between zinc and complexant, zinc/complexant = 0,07 (l) and 0,11 (m).*

composition towards lower tin content. Once more the magnitude of the shift is more or less the same over the whole range of current densities (curve j and k). The interaction between zinc and complexant does not have great influence on the alloy composition. The difference in the lower range of current densities is likely to be a result of more important interactions. Comparison of the curves in figure 2 is based on experiments where other interactions are of approximately the same magnitude.

The results from a multi regression analysis (assuming liniarity) on the measured differences in the composition at high and low current density (7.6 and 0.15 A/dm^2) are shown in figure 3. At a confidence limit of 95%, 14 out of the 18 Hull cell panels can significantly be descriebed by the following equation (concentrations in g/l):

Variation of tin content [wgt-%] =
- 448.2 - 21.0Sn + 3.8Complexant
+ 35.6Zn/Sn + 2467.9Sn/Complexant

The interactions found are further investigated in an L_8 experiment (see table 3 and figure 1). An analysis of the variance showed that the importance of the parameters and the interaction between

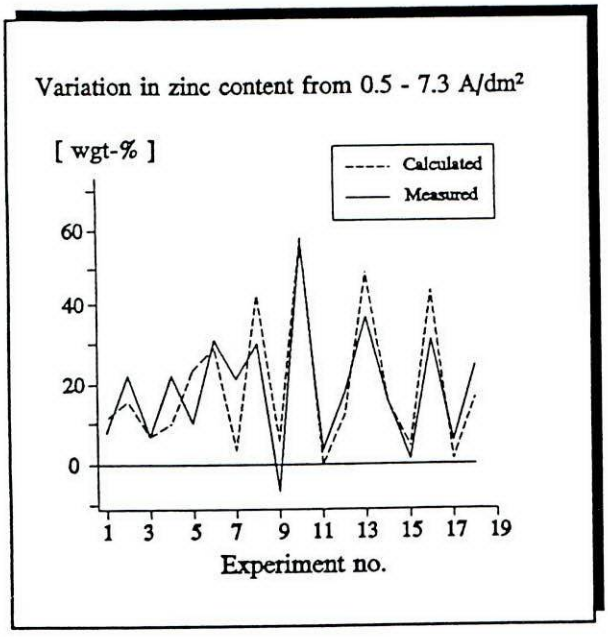

Figure 3. Measured and calculated variation in the alloy composition from high to low current density (A/dm²). The calculations are based on multi regression analysis (assuming linearity) on the Hull cell panels (from the L_{18} experiments).

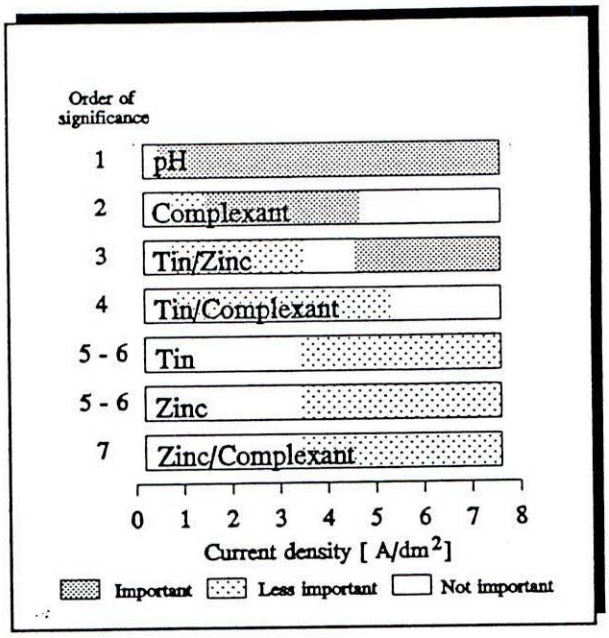

Figure 4. Ranked importance of process parameters and interactions, based on analysis of variance of Hull cells from the L_8 experiment. See text for further information.

them depends on the current density. An attempt to rank them is shown in figure 4. The most important parameter is the pH value of the bath, which is important for the whole range of current densities investigated. The concentration of the complexant is the second most important parameter, especially in the middle and the higher current density range. The two most important interactions are between tin-zinc and tin-complexant.

The relative importance of the bath parameters and the interactions between them (calculated on the basis of a ranking procedure similar to a non parametric Mann-Whitney U-test (6)), is shown in table 4 for the whole range of current densities investigated, and for the range likely to be used in practice.

5 BATH CONTROL.

Measurements of the concentration of tin and zinc are easily performed using Differential Pulse Polarography (7). Both metals are electroactive in an ammoniumacetate buffer adjusted to pH=4.5, and simultaneous determination is possible. Concentrations are found using the principles of standard addition. The reduction of tin(II) takes place in the above mentioned supporting electrolyte at -600 mV vs. a saturated calomel electrode. Zinc is reduced at -1000 mV. A total analysis for both metals is performed in approximately 10 minutes (excluding time for deaeration).

The metal concentrations are determined using standard addition and linear regression. The numerical value of the intercept with the x-axis indicates the concentration sought after. An example of metal analysis is shown in figure 5.

Tin(IV) is not electroactive in the above mentioned electrolyte. An analysis of unwanted tin(IV) can be made using a supporting electrolyte of HCl and Na-citrate. The reduction of tin(IV) takes

Parameter/ interaction	Current density [A/dm²]	
	0.15 - 7.6	1.0 - 4.0
pH	100	100
Complexant	32	44
Tin/zink	29	23
Tin/Complexant	27	31
Tin	23	18
Zinc	23	21
Zinc/Complexant	21	16

Table 4. Relative importance of process parameters and interactions in relation to the operative range of current density. See text for further information.

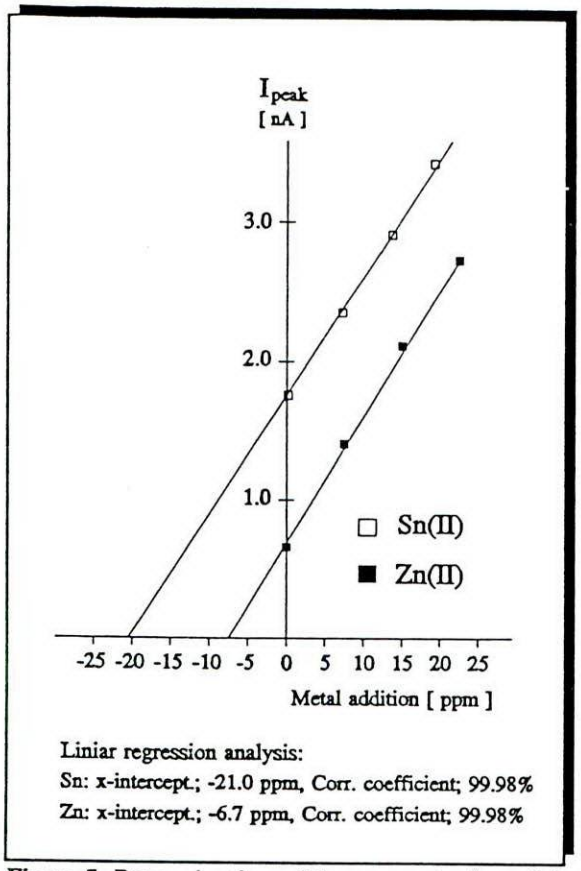

Figure 5. Determination of the concentration of tin and zinc is based upon Differential Pulse Polarography and standard addition.

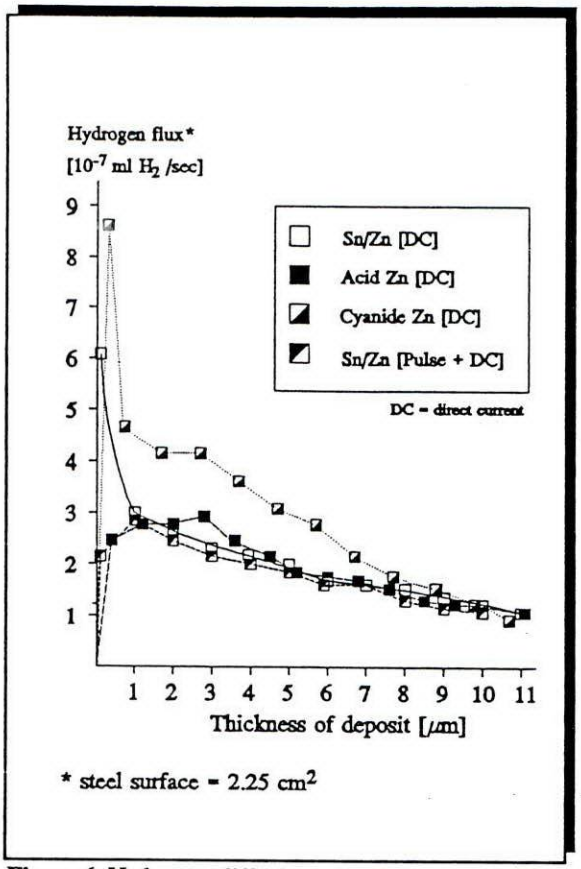

Figure 6. Hydrogen diffusion into steel during plating with cyanide zinc, acid zinc and tin-zinc. Measured with a Devanathan cell.

place at -800 mV.

The pH of the bath is adjusted by the addition of ammonium hydroxide for acidity, and sulfuric acid for alkalinity.

The amount of complexant can be followed using Hull cell panels. Too low a concentration will show up as "burnings" at high current density and loss of brightness at low current density. Pitting at high current density is observed if the concentration is too high.

6 TIN-ZINC PROPERTIES.

Diffusion of hydrogen into steel during plating can lead to hydrogen embrittlement. In the tin-zinc process the hydrogen diffusion is lower than cyanide zinc and comparable to acid zinc. Experiments with pulse plating have shown, that high frequency pulse/reverse causes depositions of tin only. It has been shown that the diffusion of hydrogen into steel in the first minute of plating can be lowered if such a pulse pattern is used at the beginning of plating. Increasing the current density causes a shift of the curves shown towards higher hydrogen flux.

The mean internal stress in electroplated tin-zinc alloys is low and the current density does not have any influence (figure 7). In comparison, measurements of zinc coatings from a cyanide process have a higher internal stress, and the magnitude depends strongly upon the current density. For a 4 μm zinc coating plated at 2 A/dm^2, the internal stress is 2.7 kp/mm^2 and for 10 μm zinc plated at 4 A/dm^2 it is 10.9 kp/mm^2.

The superior protection against corrosion achieved when steel is plated with tin-zinc, depends strongly on the composition of the alloy. The best protection against corrosion is achieved when the composition is 80% tin and 20% zinc. In neutral salt spray tests - ASTM B117 - an unpassivatet coating performs much better than a chromated zinc coating (1,2).

An even better result can be obtained if the tin/zinc coating is chromated (2). Dissolution of zinc leads to changes in the composition of the alloy when chromate treatment takes places in the chromic acid. This should be kept in mind, when the corrosion protective properties are compared to other coatings.

Field tests and accelerated tests (Prohesion (8) and Humidity) are expected to be completed by

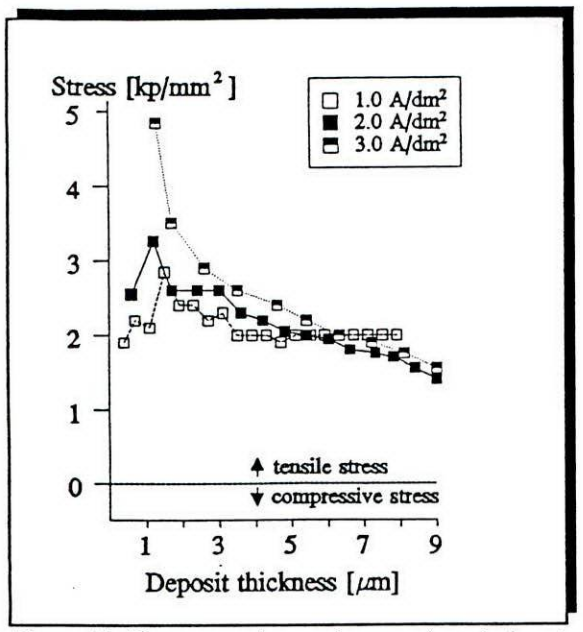

Figure 7. The mean internal stress in relation to thickness and current density, as measured by a dilatometric method.

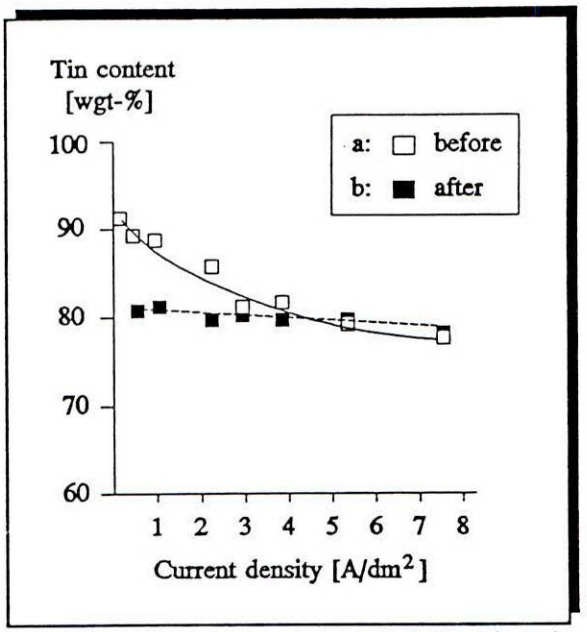

Figure 8. The composition of electrodeposited tin-zinc alloys i relation to current density. Curve a: recommended composition, curve b: after optimization using Taguchi statistics.

Spring 1992. The tests involve galvanic and crevice corrosion. Unpassivated and passivated coatings (with chromate and with a new non-chromate process) will be tested and comparisons will be made to acid and cyanide zinc. The results will be presented in the oral presentation of this paper.

7 CONCLUSION.

The experiments show that Taguchi statistics is a very powerful and useful method for optimizing plating conditions and investigating interactions between bath parameters.

The electrochemical deposition of tin-zinc alloys in a slightly acid bath was improved. With an optimized composition of the bath it is possible - over a broad range of current densities - to deposit an alloy with uniform composition. Figure 8 shows the alloy composition in relation to current density before and after the conditions have been optimized using Taguchi statistics.

Bath parameters of main importance are the acidity, the concentration of complexant and the ratio between tin-zinc and tin-complexant. The concentration of the two metals and the ratio between zinc and the amount of complexant is less important.

The composition of the bath does not have a marked influence on the rate of deposition.

Bath control is easily done using Differential Pulse Polarography and Hull cell panels. The need for analysis of the constituents of the bath is reduced when tin-zinc anodes are used. The consumption is almost balanced. Drag out is the main reason for loss.

The general conclusion concerning bath parameters is that the pH should be kept at 7 and that the concentrations of tin, zinc and complexant should be 20, 12 and 110 g/l, respectively.

Changes in the composition of the deposited alloy can take place if the components of the bath are altered. In the lower end of the current density (0.5 - 4 A/dm^2) a reduction of the ratio between tin and zinc will result in a low content of tin in the plated alloy. Lowering the ratio between tin and complexant will have the opposite effect. At high current densities (> 4 A/dm^2) the reduction of the ratio, will result in a deposit low in tin.

The diffusion of hydrogen into the steel during plating is comparable to the acid zinc process. The use of high frequency pulse/reverse plating at the start of a deposition, will reduce the risk of hydrogen embrittlement. The internal stress is of tensile character and is lower than zinc coatings from cyanide-processes. The internal stress is unsensitive towards changes in current density.

8 ACKNOWLEDGEMENTS.
The author is indebted to Dr. Dan Ulrich, NKT Wire Work, Denmark for help and support in the multi regression analysis and interpretation of the results from the Taguchi experiments.

9 NOTES.
Conversion of a hydrogen flux to a current is done using the equation

$$V_H = \frac{4.251 \cdot 10^{-10} \cdot (T + 273) \cdot E}{R}$$

where V_H is the volume of hydrogen, given in ml H_2/sec. T is the temperature measured in centigrade, E is the measured voltage drop (in mV), and R is the shunt resistance (in kΩ). Alternatively, E/R can be replaced by the current I (measured in μA). A current of 1 μA corresponds to a flux of $1.27 \cdot 10^{-7}$ ml H_2/sec at 25 °C.

Calculation of the mean internal stress is done using the equation

$$\Sigma = \frac{E \cdot d \cdot \delta l}{2 \cdot l \cdot t}$$

where Σ is the internal stress (kp/mm^2), E the modulus of elasticity (1.2033×10^4 kp/mm^2 for copper), d the thickness and l the plated length of the specimen (mm), t is the thickness of the deposit (mm) and δl the dimensional changes of the specimen (mm).

10 LIST OF REFERENCES.
1. *H. W. Dettner & J. Elze: "Handbuch der Galvanotechnik - band II". Carl Hanser Verlag, München 1966, pp. 498-523.*
2. *Dipsol Chemicals Co. Ltd: "Dipsol SZ-240 & SZ-242, Tin-Zinc Alloy Plating Processes".*
3. *G. Taguchi and S. Konishi: "Taguchi methods, Orthogonal arrays and linear graphs". American supplier Institute 1987.*
4. *"The Dry Hydrogen Contact Cell - HCC 11". Paper from FORCE Institutes, Corrosion Dept. Denmark, 1991.*
5. *A. Dvorak and L. Vrobel: "A new method for the measurement of internal stress in electrodeposits". Transactions of the Institute of Metal Finishing, 1971, Vol 49.*
6. *J. M. Elliott: "Some methods for the statistical analysis of samples of benthic invertebrates". Freshwater Biological Association, 1977.*
7. *J. Burmicz, P. Rach & C. Grether: "Polarography and Voltammetry". Methrohm 1983.*
8. *B. S. Skerry, C. H. Simpson and G. R. Wilson: "Combined corrosion/weathering testing of coated steel products for automotive applications". Paper no. 912280, p. 143. Proceedings of the fifth automotive corrosion and prevention conference, 1991.*

ELECTRODEPOSITION OF Ni-Fe ALLOYS FROM SULFATE, SULFATE-CHLORIDE AND CHLORIDE BATHS

N.Furukawa, M. Hanabusa and T. Hayashi*
(Dept. of Applied Chem., Univ. of Osaka Prefecture, Sakai-shi, Osaka 591, Japan)

Abstract

In an attempt to control the film composition, factors affecting the composition of Ni-Fe alloy deposits and their crystal structure have been analyzed as a function of bath composition, cathode current density, bath pH, temperature and an addition of citric acid.

Measurement of the pH of the cathode surface by using an antimony electrode revealed that the deposition potential of Fe coincides with the potential where the abrupt increase of pH was observed. Ni-Fe alloy deposits have the layer structure and the thickness of each layer increased with an increase of the Fe content of the alloy deposits.

Introduction

Nickel-iron alloy coatings have many potential applications in industry as a functional coating because the alloy deposits have unique properties such as high hardness and strength, good ductility, brightness, sound corrosion resistance, etc[1-5].

These physical and chemical properties of the Ni-Fe alloy coating are dependent on the composition and also on the structure of the deposits[6-8].

However, the deposition process of the Ni-Fe alloy is rather complex because of the anomalous codeposition of alloys. It is necessary, therefore, to obtain more electrochemical insight into the formation of Ni-Fe alloy films.

In the present study, an attempt was made to elucidate the mechanism of the anomalous codeposition of Ni-Fe alloys from the mixed type sulfate-chloride bath as well as from the simple sulfate and chloride baths. The effect of plating variables on the codeposition of Ni-Fe alloys was also investigated.

Experimental

The composition of the bath used in this study is shown in Table 1. The cathode used for the polarization measurement was a platinum disc (0.75-4 cm^2) plated with thin Ni-Fe alloy deposit. Cathode current efficiency was calculated from the total weight of the Ni-Fe alloy deposits and the quantity of the electricity passed during electrolysis. Measurement of the cathodic polarization curves was carried out by the potentiostatic and also galvanostatic methods by using a saturated calomel electrode (SCE) as a reference electrode. Partial

current for the electrodeposition of each metal in the alloy plating baths was evaluated by using the cathode current efficency data. The atomic absorption spectrometer was used to analyze the solutions for the Ni and Fe content in the alloy deposits.

The pH of the electrolyte films in the vicinity of the growing cathode surface was measured by an antimony microelectrode, which was fixed at the electrode surface through a hole behind the test electrode.

The X-ray diffraction patterns of the Ni-Fe alloy deposits were obtained with Fe-Kα radiation. A manganese filter was used to absorb Kα radiation. Ni-Fe alloy deposits of 50 μm in thickness were plated on copper substrate.

The Ni-Fe alloy plating bath was operated at pH 2 to 4. The bath temperature was varied from 30 to 60°C.

Results and Discussion

The effect of bath composition on the Fe content of the alloy deposits is shown in Fig. 1 as a function of current density. The Fe content of the alloy deposits increased with an increase of the conentration of ferrous ions in the plating bath in the current density range of 1 to 10 A/dm^2. The Fe content of the Ni-Fe alloy deposits obtained from the bath containing various amounts of Fe^{2+}, was always in the upper part of the concentration reference line (C.R.L.). These results imply that the preferential deposition of Fe occurs in the Ni-Fe bath and these phenomena were much more pronounced in the lower current density region.

The cathode polarization curves for the electrodeposition of Ni-Fe alloys are shown in Fig. 2 as a function of bath pH. The partial current-potential curves for the deposition of Fe were found to shift to more noble potentials with an increase of pH of the bath from 2 to 4. Under these conditions, Fe deposition was limited in the less noble potentials than -1.1 - -1.15 V vs. SCE, while Ni deposition was found to increase with an increase of the total current over the entire potential region. These results were well accord with the phenomena in which the Fe content of Ni-Fe alloy gave the maximum value in the potential region of -1.0 to -1.1 V as shown in Fig. 3.

Figure 4 shows the partial currents and pH change near the cathode surface in the electrodeposition of Ni-Fe alloys from the sulface-chloride bath. As the deposition rate of Ni(i_{Ni}) becomes significant, the rise in pH on the electrode surface was clearly detected by the antimony electrode during the electrodeposition of Ni-Fe alloys. The pH change was found to be more significant in the less noble potential regions. An increase in pH near the electrode surface seemed to enhance the deposition of Fe leading to the anomalous codeposition of Ni-Fe alloys.

According to the microscopic analysis, all the Ni-Fe alloy depsoits containing 9-77 wt.% Fe obtained from the sulfate-

chloride bath have the banded microstructure. The X-ray diffraction patterns of the Ni-Fe alloy deposits obtained in this study are shown in Figs. 5 and 6. The X-ray diffraction lines corresponding to Fe(100) facets was observed in Fe rich alloy coatings (Fe content, 79.5 wt%). With an increase in the Fe content of the alloy deposits, the diffraction lines shifted toward a lower angle and was broadened and the lattice spacing increased. The Ni rich alloy deposits obtained at the less noble potentials gave the diffraction lines corresponding to Ni_3Fe phase as well as Ni(111) and Ni(200) facets.

Conclusions

Polarization curves for Ni-Fe alloy deposition shifted toward a less noble value with an increase in the ferrous sulfate concentration. The Fe content of the Ni-Fe alloy deposits obtained from the baths containing various amounts of ferrous iron was always in the upper part of the CRL and the preferential deposition of Fe was confirmed to occur in the electrodeposition of Ni-Fe alloys. Nickel-iron alloy deposits containing 9-77 wt% Fe had the banded microstructure and the X-ray diffraction lines corresponding to the Fe(110) facets was found in Fe rich alloy deposits.

References

1) R.J. Clauss, R.A.Tremmel, Plating, 60, 803 (1973)
2) H.Chessin, E.J.Seyb, P.D.Walker, Plating and Surface Finishing, 63(12), 32 (1976)
3) K. Nakamura, T. Hayashi, KINZOKU HYOMEN GIJYUTSU, 34, 165 (1983)
4) S. Biallozor, M. Lieder, Surface Technology, 21, 1 (1984); 26, 23 (1986)
5) M. Chomakova, S. Vitkova, J. Appl. Electrochem., 16, 669 (1980)
6) H. Dahms, J.M. Croll, J. Electrochem. Soc., 112, 771 (1965)
7) J. Horkans, J. Electrochem. Soc., 126, 1861 (1979); 128, 45 (1981)
8) H. Deligiammi, L.T. Romankiv, in Magnetic Materials Processes, and Devices, Proc. Vol. 90-8, Electrochem. Soc., Pennington, NJ, 423 (1990)

Table 1 Bath composition and operating conditions

Sulfate-chloride bath				
$NiSO_4 \cdot 6H_2O$	0	-	0.4	M
$NiCl_2 \cdot 6H_2O$			0.1	M
$FeSO_4 \cdot 7H_2O$	0	-	0.4	M
H_3BO_3			30	g/L
Saccharin			3	g/L
Citric acid	0	-	30	g/L
pH	2.0	-	4.0	
Temp.	30	-	60	°C
Sulfate bath				
$NiSO_4 \cdot 6H_2O$	0.4	-	0.45	M
$FeSO_4 \cdot 7H_2O$	0.05	-	0.1	M
H_3BO_3			30	g/L
Saccharin			3	g/L
Citric acid	0	-	30	g/L
pH			3.0	
Temp.			40	°C
Chloride bath				
$NiCl_2 \cdot 6H_2O$	0.4	-	0.45	M
$FeCl_2 \cdot nH_2O$ (n=4)	0.05	-	0.1	M
H_3BO_3			30	g/L
Saccharin			3	g/L
Citric acid	0	-	30	g/L
pH			3.0	
Temp.			40	°C

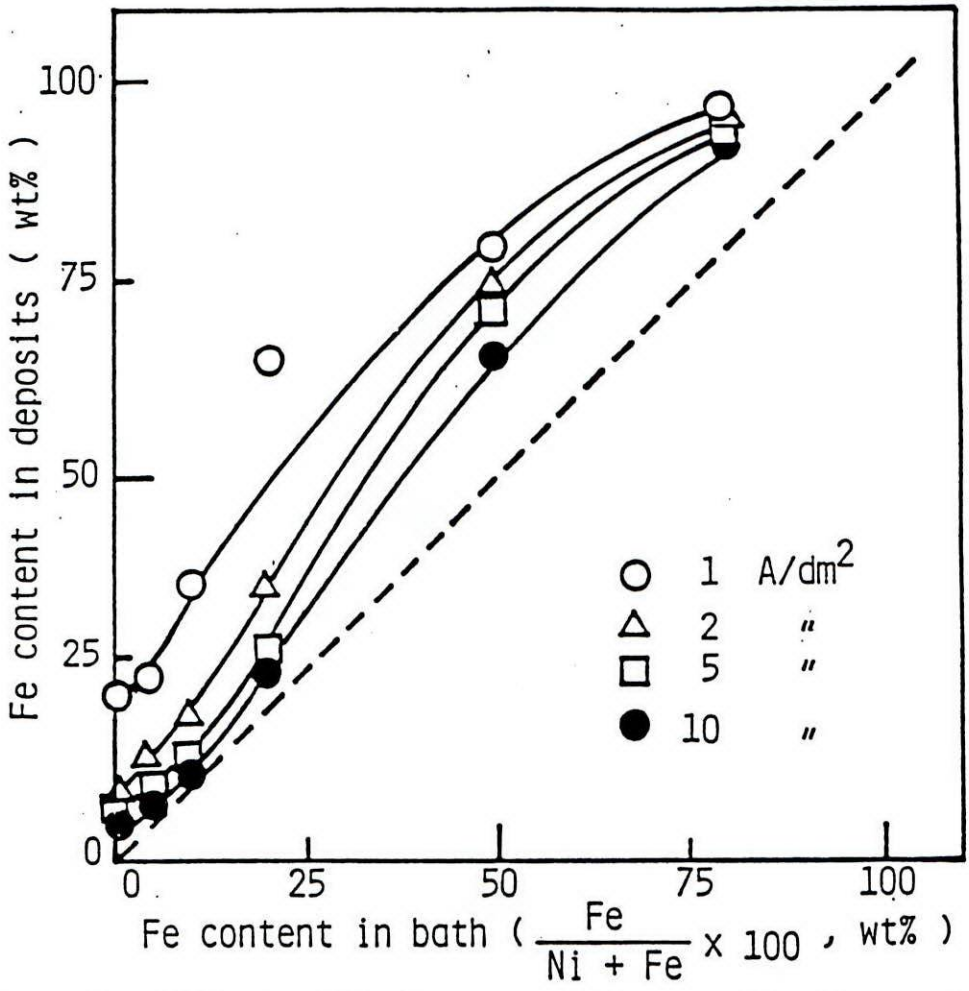

Fig. 1 Effect of bath composition on the Fe content of Ni-Fe alloy deposits
(Citric acid; 30 g/L, Temp.; 40 °C, pH 3.0
Sulfate-chloride bath)

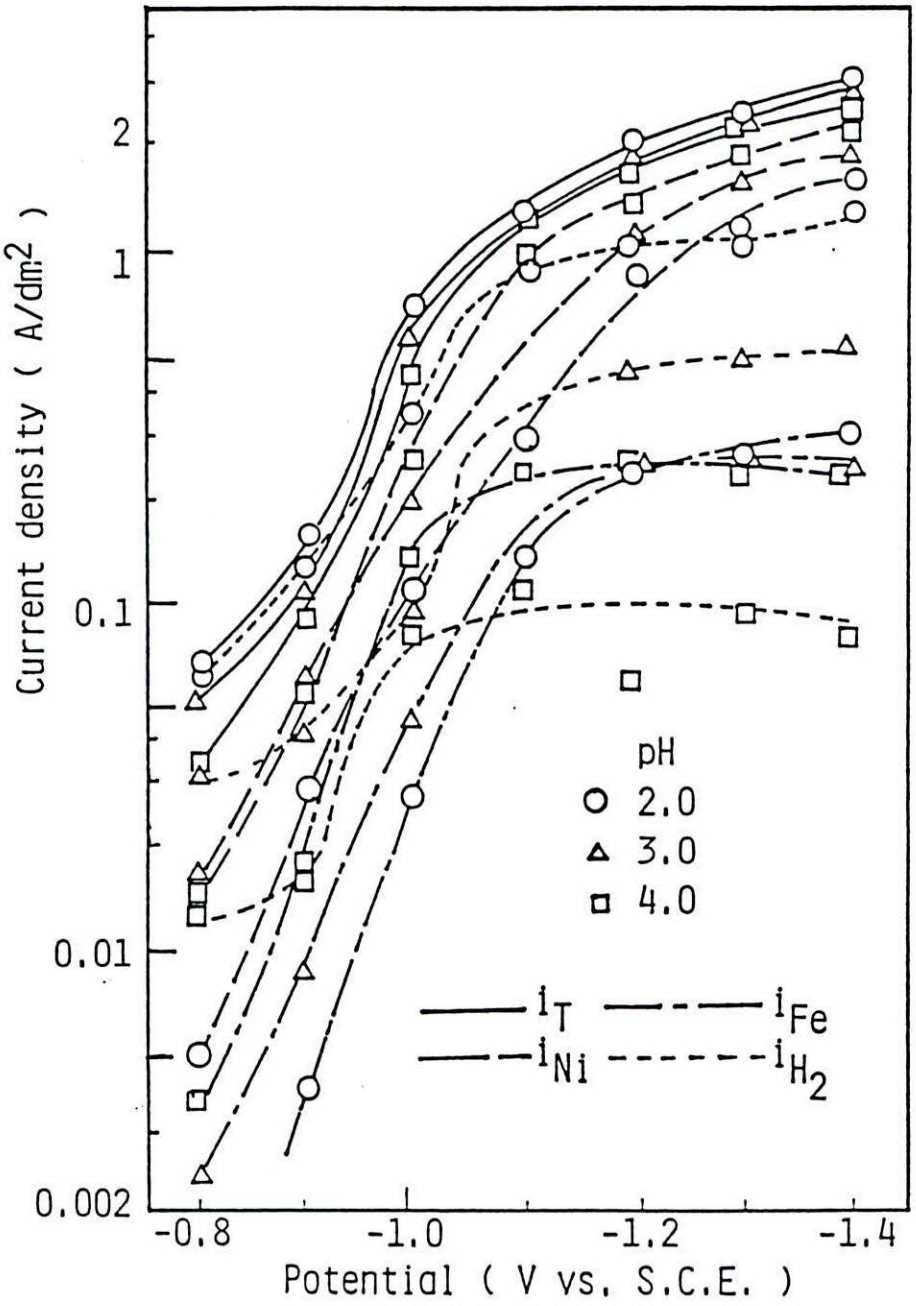

Fig. 2 Cathodic polarization curves for the electrodeposition of Ni-Fe alloys

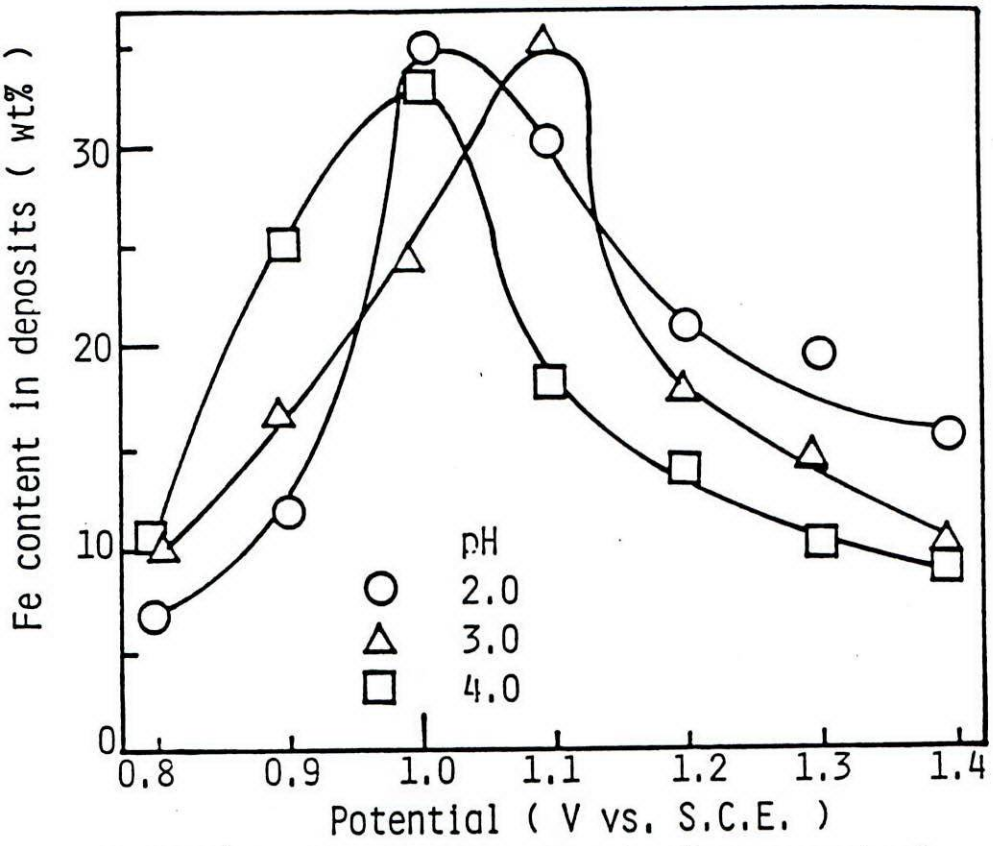

Fig. 3 Effect of potential on the Fe content of Ni-Fe alloy deposits
(Fe/Ni; 1/19, Citric acid; 30 g/L, Temp.; 40°C
Sulfate-chloride bath)

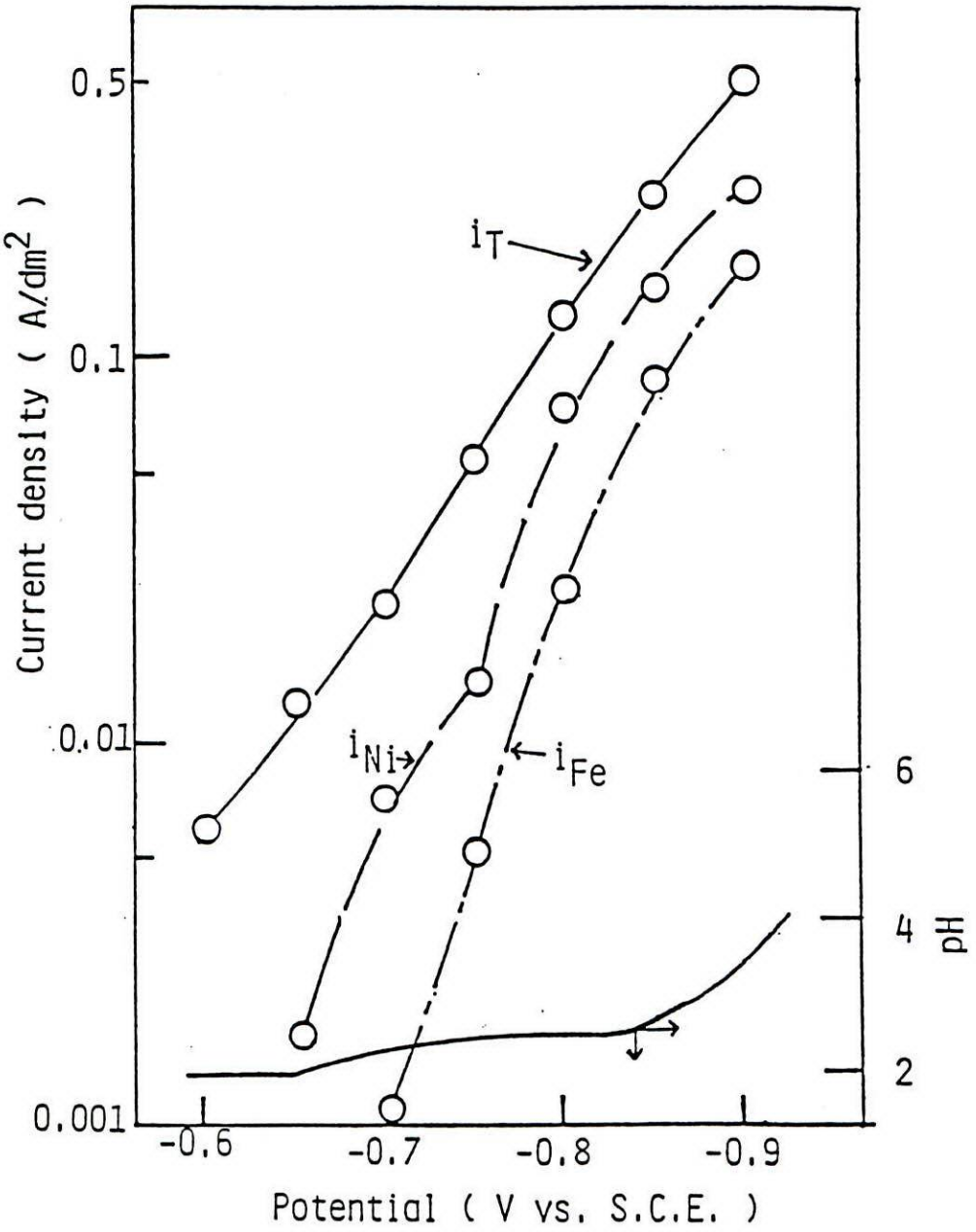

Fig. 4 Cathodic polarization curves for the Ni-Fe alloy deposition

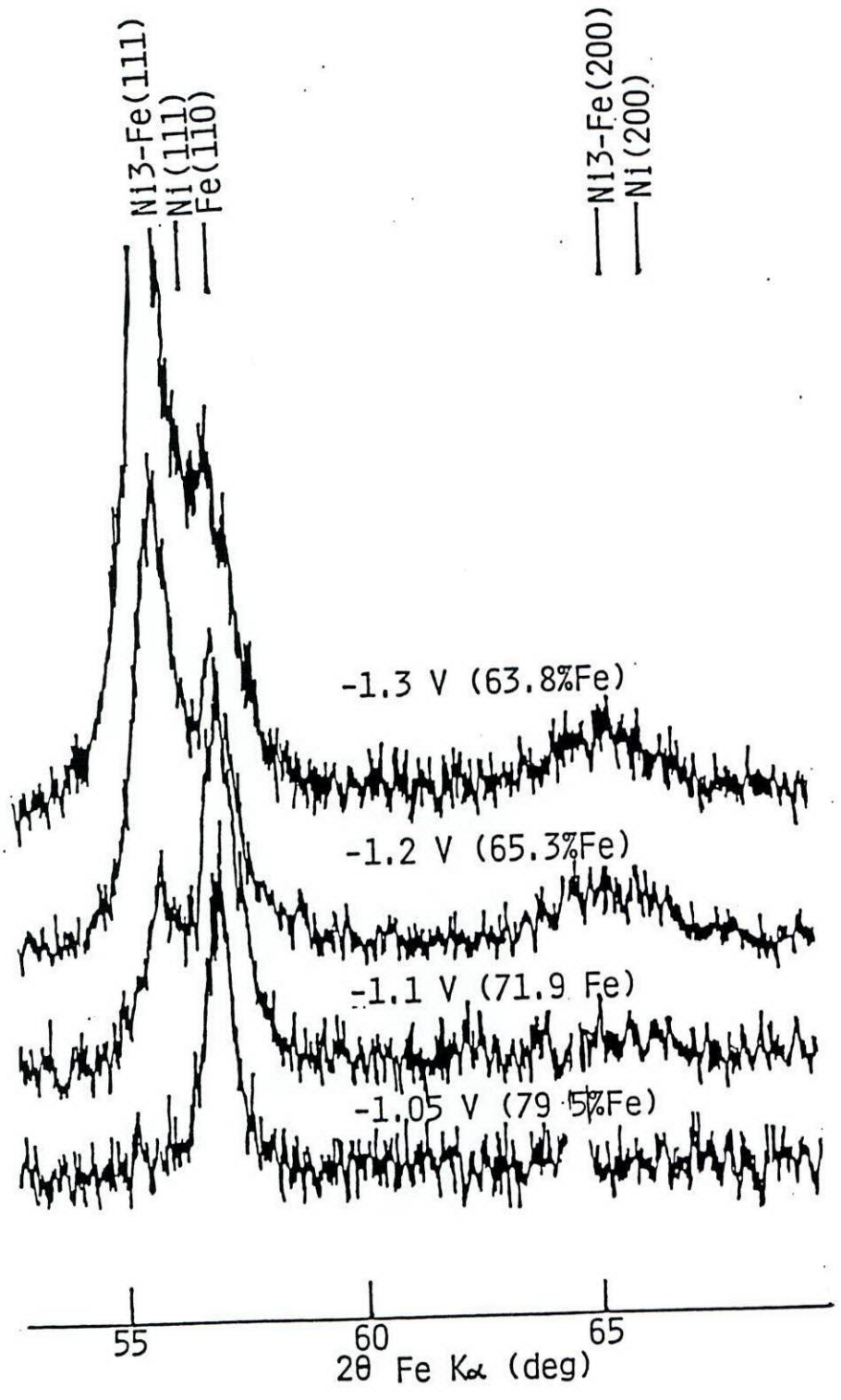

Fig. 5 X-ray diffraction profiles of the Ni-Fe alloy deposits
(Fe/Ni; 1/1, Citric acid; 15 g/L pH 2.0)

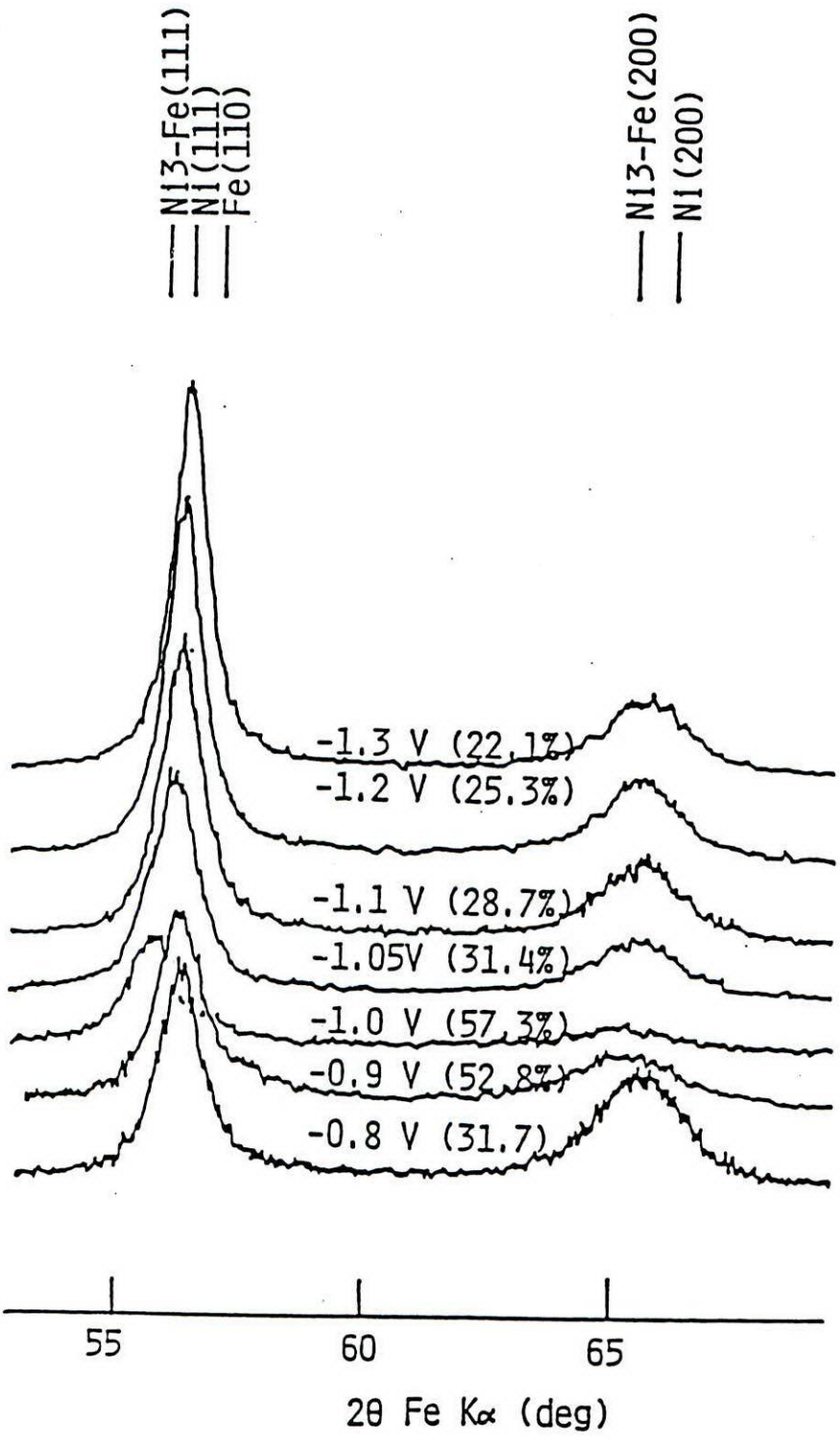

Fig. 6 X-ray diffraction profiles of the Ni-Fe alloy deposits
(Fe/Ni; 1/4, Citric acid; 15 g/L pH 2.0)

*** PAPER NOT AVAILABLE IN TIME FOR PUBLICATION ***

Optimization of the Alkaline Zinc-Iron Alloy Plating Bath Composition for Optimum Corrosion Results Using Taguchi D.O.E. Methodology

B. Dafonte, Jr. and Naomi Holmes, Quin-Tec, Inc., Warren, MI
and Sally Escota, Rampart Industries, Detroit, MI

The application of Taguchi D.O.E. methodology will be discussed for optimizing the alkaline zinc-iron bath composition to give improved corrosion resistant deposits. The influence of each parameter, such as iron content, stabilizer content, plating current density, bath temperature, post-bake, type of passivate, etc., will be discussed as it relates to the corrosion resistance of the deposit.

*** For copies of this paper please contact the author directly:**

Mr. B. Dafonte, Jr.
Technical Director
Quin-Tec, Inc.
14057 Stephens
Warren, MI 48089
313/774-8010

ELECTROCHEMICAL DEPOSITION OF ZINC-NICKEL ALLOYS IN THE PRESENCE OF ORGANIC ADDITIVES

B. N. Popov, Ken-Ming Yin, O. Velev and R. E. White

Center for Electrochemical Engineering

Department of Chemical Engineering, Texas A&M University, College Station, TX 77843–3122

ABSTRACT

Linear sweep voltammetry has been used as an "in situ" technique to characterize thin layers of ZnNi alloys. The zinc dissolution peak potentials from ZnNi deposits were found to be more noble [E_{1pa}= -0.7V (SCE) and E_{2pa}= -0.575 V (SCE)] than those of the pure metal ions [-0.83 V (SCE)] due to a formation of two ZnNi intermediate phases γ and δ respectively. The effect of d c and pulse parameters on deposition of ZnNi alloys from sulfate electrolytes in the presence and absence of organic compounds have been studied in unagitated solutions and with a rotating disc electrode The additive had a major effect on crystal size and the brightness of the deposits. At overpotentials of –0.75 V (SCE) and current density of 2 A/dm^2 or less, Ni deposition and hydrogen evolution occurs and on the stripping voltammograms only the anodic nickel peak is observed. At sufficient high cathodic overpotentials Zn deposition reaction is mass-transport control. Ni deposition reaction is inhibited when Zn is codeposited. The mechanism of ZnNi codeposition is discussed.

INTRODUCTION

Anomalous codeposition has been recognized in connection with several alloy deposition systems such as NiFe, NiCo and NiZn (1–11). In the case of ZnNi, zinc deposits at a faster rate which leads to a higher concentration of the alloy composition in Zn, different than one would expect based on the composition of the plating solution, where the concentration of Ni(II) ions are higher than those of Zn(II). Kurachi et al (12–18) have deposited successfully NiZn layers using only low current densities up to 5 A/dm^2. They found that the cathode deposits have a complex structure corresponding to γ phase which behaves like a monometallic electrode and has a higher overpotential than pure zinc. Several authors (19–22) considered this alloy to be a possible substitute to cadmium. According to Noumi et al (23), ZnNi alloys may be prepared at high current densities from sulphate solutions and pH in range of 1.5 to 2.5. More recently, the same alloy was prepared using chloride electrolytes (24–25). According to these authors NiZn alloy with γ phase is obtained which shows the best corrosion resistance at 12–13 % nickel content. The alloy was found to have excellent coating adhesion and weldability but poor phosphatability and paintability (26). The effects of pulse plating on Ni-Zn alloy structure in unagitated solutions were studied by Nishimura et al. (27). They found that the pulse period has a major effect on crystal size. Off time also affected the Ni content and the structure of the ZnNi electrodeposits.

Existing limitations to deposit ZnNi layers on the pH and the concentration of Zn(II) ions in the electrolyte indicate that both hydrogen evolution and Zn deposition are mass-transport controlled. Accordingly, the agitation and the presence of organic additives which may suppress the hydrogen evolution (28–33) should play a significant role in the Ni-Zn deposition system. Systematic studies of these effects have not been reported in the literature. This paper examines the d c plating and pulse plating (PP) of Ni-Zn alloys on stationary and rotating disc electrode from different electrolytes and in

the absence and presence of organic compounds.

EXPERIMENTAL

The electrochemical cell employed was a conventional three-compartment design with contact between the working electrode compartment and the reference electrode compartment via a Luggin probe. Measurements were carried out with a platinum rotating disc electrode with geometric area of 1 cm^2 and with a rotating copper disc electrode with a geometric area of 0.8 cm^2. All potentials are referred to saturated calomel electrode, where a platinum gauze was used as a counter electrode. All electrochemical measurements were carried out using a corrosion system with a potentiostat and a scanning potentiostat with a x-y recorder. Analytical grade $NiSO_4$, Na_2SO_4, $ZnSO_4$, $ZnCl_2$, organic additive (NPO) and high purity water were used to prepare the solution. The pH of the solution was adjusted with addition of NH_4OH or 20% H_2SO_4. Atomic absorption spectrophotometry and EDS were used to determine the Zn content in deposits.

RESULTS AND DISCUSSION

Linear Sweep Voltammetry (LSV). LSV was used as an "in situ" technique to characterize the electrochemically formed thin layers of Zn, Ni and ZnNi alloys. The studies were carried out using a fixed and rotating disc electrode.

By comparing LSV voltammograms of pure metal deposition with those when both metals are present in solution, one can obtain information for any interaction present between the deposition process and deposited metals.

In order to determine the nature of the zinc electrodeposition, linear sweep voltametric curves were recorded from two types of electrolytes: 1. 7.2 $x10^{-1}$M $ZnCl_2$ + 1.8 M NH_4Cl, pH=4.5 and 2. 0.2 M $ZnSO_4$+0.5 M Na_2SO_4 at pH=2.5 in the presence and absence of organic additives. In the chloride electrolyte, the organic compound (NPO) was added in increasing amounts to the solution in the cathode compartment during the course of the run. Figure (1) shows cyclic voltammograms taken at 0.05 V/s in the absence of organic additive (curve 1) and for different concentrations of the organic additive. According to Figure (1), the electrochemical deposition of zinc in the absence of the organic additive occurs at –1,15 V vs SCE, and at –0.83 V (SCE), the dissolution of the electrodeposited zinc is observed. In Figure (2), zinc peak current was found to be a linear function of the square root of the sweep rate, suggesting a diffusion controlled process for zinc electrodeposition. An average value of $(0.69 \pm 0.19)x10^{-5}cm^2/s$ was obtained for the diffusion coefficient. The peak potential in Figure (1), shifts appreciably to more cathodic value as the concentration of the additive is increased. It was also found that the peak current of zinc deposition process decreases in the presence of the organic compound. The cathodic charges were calculated by integrating the surface under the peaks. The charge under the peak in Figure (1) decreases from Q= 3.2 C/cm^2 in the absence of the organic additive to 1.1 C/cm^2 in the presence of the additive. Figure (3) shows the dependence of the thickness of the coating as a function of the cathodic current density applied for different concentrations of the organic additive in the electrolyte. The experiments were carried out at constant current density of 10 mA/cm^2 and at room temperature. Possible explanations for the peak potential shift and the cathodic charge decrease in the presence of the organic additive are:

– increase in ohmic resistance of the cathode film, caused by the presence of the organic additive (NPO).

– changes in concentration of zinc ions in the cathode film due to possible complexing.

– changes in pH in the cathode film induced by the additive.

–adsorption of the organic compound with resultant changes in the rate with which the zinc reduction process occurs.

According to Figure (4), the peak potential shift was too great to account for the pH change on the metal surface. A decrease of the concentration of zinc ions as a result of complexation would increase the cathode potential (34). From the zinc peak currents in the presence and absence of the additives (assuming the same diffusion coefficient), the concentration of the electroactive zinc species that are not complexed can be calculated. An average decrease of Zn ions of 3.07×10^{-4} was calculated, which is too small to account for the peak potential shift observed.

Adsorption of the additive on the electrode surface will decrease the surface concentration of the Zn electroactive species. As it is observed in Figure (3) the decrease of the Zn electroactive species on the surface shifts the zinc peak potential in cathodic direction. As shown in Figure (4), the thickness of the deposited zinc decreases as the concentration of the additive in the electrolyte increases.

The cathodic peak due to zinc deposition from sulfate electrolytes containing: 0.2 M $ZnSO_4$ + 0.5 M Na_2SO_4 at pH=2.5 is covered by the hydrogen evolution reaction peak and at higher overpotentials by water reduction. Thus, in order to study the electrodeposition of zinc in sulfate solutions, the anodic zinc peak was investigated as function of different scan rates and electrode rotation speeds. Potentiodynamic stripping voltammograms of Zn film electrodeposited on Cu disc electrode are shown in Figure (5) and Figure (6). A well defined anodic peak is observed at –0.8 V vs SCE. The zinc anodic peak current decreases with the decrease in scan rate. From the data obtained it was not possible to make any conclusion concerning the nature of the rate determining step which controls the electrodeposition.

Potentiodynamic stripping voltammograms of a Zn film electrodeposited for different electrode rotation speeds are shown in Figure (7) for w=0 rpm; w=100 rpm; w=500 rpm; w=1000; w=2000 rpm and w=3000 rpm. According to Levich equation if the electrodeposition of zinc is a mass transfer controlled reaction, for a constant sweep rate, more zinc will be deposited and subsequently stripped at higher rotation speeds. An increase of the anodic peak area is observed in Figure (7) as the rotation rate of the copper disc electrode is increased, indicating that the zinc electrodeposition from sulfate electrolytes, (as it was previously shown for chloride electrolytes), is controlled by the diffusion of the zinc electroactive species.

Potentiodynamic stripping curves recorded in solutions containing 0.5 M $NiSO_4$ + 0.5 M Na_2SO_4, pH=2.5 are shown in Figure (8) and Figure (9). Ni film was electrodeposited using copper rotating disc electrode at v=30 mV/s and at different rotation rates. The nickel anodic peak increases under agitation conditions. A peak current of $2mA/cm^2$ was obtained for w=0 compared with a value of 7.2 mA/cm^2 for w=50 rpm. However, the amount of the stripped nickel doesn't increase with increasing the rotation speed. In contrary as the electrode rotation rate increases from w=50 rpm to w=1000 rpm, as it is shown in Figure (8) and Figure (9), the area of the anodic peak decreases, indicating that nickel deposition from sulfate electrolytes is not mass transfer controlled.

Linear sweep voltammograms recorded on fixed copper disc electrodes from electrolytes containing both metals: 0.5 M $NiSO_4$ + 0.2 M $ZnSO_4$ + 0.5 M Na_2SO_4 and for different sweep rates are shown in Figure (10) and Figure (11). As it is seen in Figure (10), the LSVs are different when both metals are present in the solution compared to those which would be obtained by superposition of the LSVs from the electrolytes containing pure zinc and nickel ions. This indicates that the interaction between the two deposition processes and deposited metals does exist.

The curve recorded in Figure (10) for sweep rate of 100 mV/s shows on the anodic branch two well defined current peaks. A broad peak at E_{1pa}=– 0.7 V vs SCE and the second peak at E_{2a}=–0.24 V vs SCE are observed. The peak at – 0.7 V vs SCE is more noble than zinc dissolution peak as shown in Figure (6) and Figure (7). The anodic peak at –0.24 V vs SCE corresponds to the Ni dissolution peak. The reversible potential and the free energy of each component in the ZnNi alloy should be the same as the reversible potential of the pure components.

The dissolution peak potential being more noble than that of the pure metal ions may result from: a significant free energy change in mixing of ZnNi in the solid phase or formation of intermediate phases in the case of ZnNi alloys. The LSVs of dissolution of zinc-nickel alloys for sweep rates in the range from v= 250 mV/s to 2000 mV are shown in Figure (11). As it is seen in this figure, the broad peak observed at –0.7 V (SCE) in Figure (10) splits in two distinct peaks. A sharp peak occurs at E_{1pa}= –0.7 V (SCE) and the other at – 0.575 V (SCE) followed by the third peak pertaining to dissolution of nickel. The shape of the voltammograms depends upon the amount of the deposited nickel. At overpotentials of –0.75 V (SCE) and current density of 2 A/dm^2 or less, nickel deposition and hydrogen evolution occurs on the rotating disc electrode and only the anodic nickel peak is observed.

At higher overpotentials and current densities above 2 A/dm^2 ZnNi alloy anomalous codeposition begins. The zinc content in deposited ZnNi alloys at various electrodeposition conditions contained from 84% to 91% Zn is shown in Figure 12. According to the ZnNi phase diagram, shown in Figure (12), alloy with a zinc content between 84% and 92% should be characterized at low temperatures with two intermediate phases γ and δ respectively. The LSV's of dissolution of that alloy possess two peaks which could be ascribed to dissolution of zinc from the two intermediate phases. The first dissolution is at E_{1a}=– 0.7V (SCE), where Zn dissolves from reach in Zn, δ phase (90% Zn). The second peak at – 0.575 (SCE) corresponds to dissolution of Zn from γ phase (84 to 88% Zn). The third peak observed in Figure (12) is dissolution of nickel. The small difference in the chemical potential of zinc in the two phases is due to the small difference in the nickel content in the alloy.

Figure (13A) shows the composition of the alloy determined by EDS. The alloy was deposited potentiostatically with a current of 15 A/dm^2 and with the same I-t transient as in Figure (12). According to the alloy composition shown in EDS spectrum, both intermediate phases are present in the alloy in agreement with the Zn dissolution shape observed in Figure (12). SEM of the alloy which EDS spectrum is given in Figure (13A) is presented in Figure (13B).

Figure (14) shows the zinc polarization curves for several rotation speeds. In this figure the logarithm of zinc deposition partial current density, I_{Zn} in mA/cm^2 is plotted against the plating potential. The solution composition was the same as in Figure (10), pH=2.5, and T= 50°C. In the potential interval between –0.85 V and –0.95 V, the agitation of the electrolyte does not have any influence on the slope of log I_{Zn} vs E. At higher cathodic overpotentials, the Zn partial current depends on the rotation speeds which imply mass-transport for the Zn(II) ion. For Ni, the relationship between log I_{Ni} vs E was linear and even at –1.0 V vs SCE the nickel electrode process was kinetically controlled.

Since the electrodeposition of zinc is a mass transfer controlled reaction, one can expect that at constant sweep rate, an alloy reach in zinc will be electrodeposited and subsequently stripped at higher rotation rates. Indeed this phenomena was observed in Figure (12). In this Figure, potentiodynamic stripping voltammograms of ZnNi alloys are electrodeposited on the copper rotating disc electrode at a constant sweep rate of 20 mV/s and for different rotation speeds: w= 100 rpm; w=500 rpm; w= 1000 rpm; w= 2000 rpm and w= 3000 rpm. In Figure (12) an alloy with the intermediate phase reach in zinc (δ) is deposited and subsequently stripped as the rotation speed of the copper disc electrode is increased.

Effect of Agitation on D C and Pulse Plating of ZnNi Alloys. Figure (15) is a shematic representation of the current waveform for pulse plating. The average current density is I_px(duty cycle), where duty cycle is defined as $t_{on}/t_{on}+ t_{off}$. The alloy deposition was carried out from a sulfate based plating solution containing: 0.5 M $NiSO_4$ + 0.2 M $ZnSO_4$ + 0.5 M Na_2SO_4 in the presence of 4 g/l of the organic additive (NPO), pH=2.5 and T=50°C.

Figure (16) shows the zinc content of the deposits obtained using d c deposition. The zinc content in the deposit was studied for different rotation rates of the copper disc electrode as a function of the applied cathodic current density. By proper choice of the current density and the agitation conditions, alloy compositions with a Zn content between 82% and 93% were obtained. A maximum in zinc content in the alloy occurs for all rotation speeds, which shifts in the direction of higher current densities as the rotation speed of the copper disc electrode increases, indicating that Zn is deposited under mass-transport controlled conditions. Similar behavior was observed by Andricacos et al (3) for deposition of Fe-Ni alloys. Figure (16) also shows that the mass-transfer effects of Zn deposition reaction are becoming more important as the current density increases.

The effects of pulse parameters on the electrodeposition of ZnNi alloys were investigated using fixed and rotating disc electrodes. Curve (1) in Figure (17) was obtained from sulfate electrolyte in the absence of the organic additive, using a peak cathodic current density of I_p= 60 A/dm^2 and frequency of 50 Hz. For average current densities between 5 and 25 A/dm^2, pulse plating resulted in similar deposit composition as it has been obtained for d c plating in Figure (16). Increasing the current density, the zinc content reaches a maximum at about 10 A/dm^2 and then decreases. Curve 2 in Figure (19) was recorded from the same electrolyte used to obtain curve 1 but in the presence of 4 g/l organic additive (PVO). It is seen from this curve that for all average current densities used, the zinc content in the alloy is lower than in the absence of the organic additive. The absorption of the organic additive decreases the electrode surface concentration of the zinc electroactive species with resultant change of the rate of zinc deposition.

Figure (18) shows the composition of ZnNi film plated on the rotating disc electrode as a function of the average current densities and for different electrode rotation speeds. The deposition was carried out using pulse plating with a duty cycle of 0.3 and frequency of 80 Hz at T= 50°C. The composition of the electrolyte was the same as in Figure (16). The zinc content in Figure (18) reaches a maximum and then decreases with increasing current density. At lower current densities, below 10 A/dm^2, the Zn limiting current is not attained and the zinc content in the deposit increases as the current increases. Because of the proportionality which exists between the zinc limiting current and the rotation rate of the electrode, one can expect the position of the maximum observed in Figure (16) and in Figure (18) to be a function of the rotation rate and to shift to higher current densities as the rotation speed is increased. In other words, at higher rotation speeds, the limiting current is attained at higher current densities. The zinc content increases in the deposits when the rate of the electrode rotation increases indicating again the significance of the mass transport processes in ZnNi codeposition. Figure (18) also shows that for average current densities used above 10 A/dm^2, and for all rotation rates studied, the deposits precipitated using pulse plating have the zinc content similar to those obtained from d c plating in Figure (16).

The quantities of electricity for deposition of nickel, zinc and their sum until the end of the pulse, and the current efficiency η_{Ni}, η_{Zn} and η_{Ni+Zn} as a function of the pulse length are shown in Figure (19). It was found that the current deposition efficiency is not a function of the investigated range of the pulse lengths.

The dependence of the partial current efficiency upon the average current density used to deposit the alloy is shown in Figure (20). The partial current efficiency for Zn sharply increases with increasing current density and then levels off at 59–64%, depending on the electrode rotation rate. Increasing the current density, zinc partial current efficiency for all rotation rates studied gradually decreases in agreement with the previous results obtained in this study.

One should expect that the zinc partial current efficiency decreases with increasing agitation, due to the hydrogen evolution under mass-transport control. This behavior was observed by Andricacos et al (3) and Grimmett et al (4) in the studies of the deposition of Iron-Nickel alloys. In Figure (20) a small decrease of the current efficiency is observed as the agitation increases from w=0 to 2000 rpm.

Ni partial current efficiency increases gradually as the average current density increases and is independent of the agitation. This is in agreement with the previous results, which indicated that Ni deposition is a kinetically controlled reaction in the case of ZnNi codeposition.

Morphology and Structure of the Coatings. In order to study the influence of the organic additive on the morphology of the electrodeposited zinc, metallographic investigations were carried out using incident light microscopy and incident interference microscopy. The results of these investigations are summarized in Figure (21). Like many other metals, zinc shows dendritic crystal growth when electrodeposited from baths without organic additives, shown by Figure (21A). Addition of a specific organic compound even in small amount remarkably changes the morphology of the deposit, as shown in Figure (21B). The surface becomes brighter and the marks of the dendritic growth disappear. The concentration of the organic additive is not the only factor which influences the deposition process, because many other, like bath temperature and current density also have great influence on the morphology of the deposited zinc. This is illustrated in Figure (21C) which shows the same place of the surface as in Figure (21B) but in this case as an interference metallographic picture. The interference lines are not completely straight, showing that bright and smooth deposits are not formed over the whole surface. When optimal current density is applied and the electrodeposition is carried out using 4 g/l NPO as the organic additive, a mirror bright deposit is obtained over the whole surface, Figure (21D).

The electrodeposition of ZnNi alloys was carried out in the presence and absence of organic additives. ZnNi alloy was deposited using sulfate electrolytes containing: 0.5 M $NiSO_4$ + 0.2 M $ZnSO_4$ + 0.5 M Na_2SO_4 + 4 g/l organic additive, pH = 2.5 and T= 50°C. The current densities were in the range between 10 A/dm^2 and 80 A/dm^2. Best alloy appearance was observed when the electrodeposition was carried out in the presence of organic additives, at lower current densities and for longer deposition time, shown by Figure (22C). The alloy deposited at high current densities and in the absence of an organic compound shows evidence of cracks, shown in Figure (22B). For comparison, SEM of pure deposited zinc is shown in Figure (22A). The EDS soectrum of the alloy deposited in the presence of the additive is given in Figure(23).

The XRD pattern of ZnNi alloy deposited in the absence of organic additive and at 30A/dm^2 is shown in Figure 24. All peaks can be attributed to γ ZnNi intermediate phase

CONCLUSION

By comparing LSV voltammograms of pure metal deposition with those when both metals are present in solution, one can obtain information for any interactions present between the deposition process and the deposited metals. In the absence of interaction, the reversible potential and the free energy of each component in the ZnNi alloy should be the same as the reversible potential of the pure components. The zinc dissolution peak potentials from ZnNi deposits were found to be more noble

[E_{1pa}=– 0.7 V (SCE) and E_{2pa}=– 0.575 V (SCE)] than those of the pure metal ions [– 0.83 V (SCE)], due to a formation of two intermediate phases named γ and δ phase. The small difference in the chemical potential of zinc in the two phase was found to be due to the small difference in the nickel content in the intermediate phases of the deposited alloy. The shape of the ZnNi potentiodynamic stripping voltammograms was found to depend upon the amount of the codeposited nickel. At overpotentials of – 0.75 V (SCE) and current density of 2A/dm^2 or less, nickel deposition and hydrogen evolution occur. On the stripping voltammograms only the anodic nickel peak is observed. At higher overpotentials above 2.5A/dm^2, ZnNi alloy anomalous codeposition begins. The Zn partial current was found to depend upon the rotation speeds which implies mass-transport control for the Zn(II) ion in the ZnNi codeposition process. For Ni, the relationship between the partial current density and E was linear and independent on the electrode rotation speeds and even at 1.0 V (SCE) was kinetically controlled. By proper choice of the current density and the agitation conditions, alloy compositions with a Zn content between 83.5 % and 93% were obtained. For average current densities between 5 and 25 A/dm^2, pulse plating resulted in similar deposit composition as it has been obtained for d c plating. The zinc content deposited from unagitated solutions reaches a maximum at about 10 A/dm^2 and then decreases as the average current density increases. In the presence of the organic additives and for the same average current densities, the zinc content in the alloy was found to be lower than the zinc content found on the absence of the additive. Agitation has a strong effect on alloy composition over a wide range of plating current densities. At lower current densities, below 10 A/dm^2, the Zn limiting current in ZnNi codeposition is not attained and the zinc content in the deposit increases as the current increases. At higher electrode rotation speeds, the zinc limiting current is attained at higher current density causing the maximum observed in ZnNi codeposition vs average current plot to shift in the direction of higher current densities. The partial current efficiency for Zn sharply increases with increasing current density and then levels off at 59–64% depending on the electrode rotation rate. A small decrease of the current efficiency was observed as the agitation increases due to the hydrogen evolution under mass-transport control.

According to the results obtained in this study the process of codeposition of ZnNi alloys might be explained in the following way. Bressan and Wiart (35) show that for zinc deposition from acidic solutions, the following reactions may take place at the interface:

$$H^+ + e^- \overset{K_1}{\rightarrowtail} H_{ads} \tag{1}$$

$$H^+ + H_{ads} + e^- \overset{K_2}{\rightarrowtail} H_2 \tag{2}$$

$$Zn(II) + Zn(I)_{ads} + e^- \underset{K_{-3}}{\overset{K_3}{\rightleftarrows}} 2Zn(I)_{ads} \tag{3}$$

$$Zn(II) + H_{ads} + e^- \overset{K_4}{\rightleftarrows} Zn(I)_{ads} + H_{ads} \tag{4}$$

$$Zn(I)_{ads} + H_{ads} \overset{K_5}{\rightleftarrows} Zn + H^+ \tag{5}$$

$$Zn(I)_{ads} + e^- \overset{K_5}{\rightleftarrows} Zn \tag{6}$$

Batrakov et al. (36) and Baugh et al (37) found that the reactions which lead to corrosion and to anodic dissolution of zinc can involve the adsorption of anions such as OH^-:

$$Zn + OH^- \underset{K_{-7}}{\overset{K_7}{\rightleftarrows}} ZnOH_{ads} + e^- \tag{7}$$

In the presence of Ni(II) ions one can expect at the interface also $Ni(OH)^+_{ads}$ to be present, according to the following chemical and electrochemical reactions (38):

$$Ni(II) + H_2O \rightarrowtail (NiOH)^+ + H^+ \tag{8}$$

$$(NiOH)^+ + e^- \underset{K_{-8}}{\overset{K_8}{\rightleftarrows}} (NiOH)_{ads} \tag{9}$$

$(NiOH)_{ads}$ is an intermediate consumed at the electrode :

$$(NiOH)_{ads} + e^- \underset{K_{-9}}{\overset{K_9}{\rightleftarrows}} Ni + OH^- \tag{10}$$

Either complexed or solvated zinc ion is absorbed on the surface of the electrode through the autocatalytic reaction (3) and also through reaction (4) which is catalyzed by H_{ads} (35). According to reactions (1) to (10), the following species $Zn(I)_{ads}$, H_{ads}, $ZnOH_{ads}$, $Ni(OH)_{ads}$ exist at the interface. Reaction (9), assuming it is irreversible, also takes place on a fraction of the cathodic surface.

According to the results obtained in this study, the first cathodic process on a copper disc electrode is an electrochemical reaction (9) followed by discharge of $(NiOH)_{ads}$ which deposits a thin film of nickel. From the shape of the cathodic branch of the voltammetric curves in Figures (6) and (10) one can conclude that the character of zinc nucleation is not changed in the presence of nickel. It was also observed that as a result of codeposition with zinc and deposition upon the uncovered copper electrode, the overall current of the system is higher at constant potential due to the catalytically activated hydrogen reaction by deposited nickel. Since both the electrochemical discharge reactions of zinc and nickel are cases of irreversible processes with $I_{Zn}^{\circ} = 10^{-5}$ A/cm^2 and $I_{Ni}^{\circ} = 10^{-8}$ A/cm^2, one can expect the I-E relationships recorded at different scanning rates (v) as it is observed in Figures (5) and (6) and in Figures (10) and (11) to be affected by (v).

At lower overpotentials [– 0.75 V (SCE)] and low current density, the reverse reactions (1) through (6) take place and only nickel deposition and hydrogen evolution occur. Thus, on the potentiodynamic stripping voltammogram only the nickel anodic peak is observed.

The coverage fraction and accordingly the surface concentration of all electroactive species which participate in ZnNi electrodeposition process will depend on the applied current (overpotential) and pH of the solution. At overpotentials where codeposition begins, more sites of the cathode will be occupied by H_{ads} increasing the surface concentration of Zn^+_{ads} according to reactions (4). The surface concentration of Zn^+_{ads} electroactive species as the current increases will also increase on the surface through the autocatalytic step (3), inhibiting the nickel discharge reaction by decreasing the fraction of the available cathode surface for reaction (9). In such a case, less electroactive $NiOH_{ads}$ will be produced on the surface decreasing the nickel discharge rate. In other words as the current increases

and reaches the codeposition potential, the adsorbed H_{ads} and $(NiOH)_{ads}$ are progressively replaced by $Zn(I)_{ads}$ species. One can also expect that the anion coverage $ZnOH_{ads}$ will decrease with increasing current. From $Z(I)_{ads}$ intermediate, reduction to metal occurs through chemical reaction (5) and through electrochemical reaction (6).

Adsorption of the additive on the electrode surface will decrease the surface concentration of $Zn(I)_{ads}$ causing the zinc peak potential to shift in cathodic direction in Figure (3), and the thickness and the zinc content in the alloy to decrease as observed in Figure (4) and Figure (17).

Acknowledgments.

This work was supported by the Macedonian Science Foundation..

REFERENCES

1. H. Dahms, ***J. Electroanal. Chem. 8,*** 5, (1964).
2. A. Dahms and I. M. Croll, ***J. Electrochem. Soc. 112,*** 771, (1965).
3. P. Andricacos, C. Arana, J. Tabib, J. Dukovic and L.T. Romankiw, ***J. Electrochem. Soc. 136,*** 1336, (1989).
4. D. L. Grimmett, M. Schwartz and K. Nobe, ***J. Electrochem. Soc. 137,*** 11, 3414, (1990).
5. M. Lieder and S. Biallozor, ***Surf. Technol. 26*** 23, (1985).
6. S. Biallozor and M. Lieder, ***Surf. Technol. 21,*** (1) (1984).
7. M. Maksimovic and S. Djokic, ***Surf. Techmol. 31,*** 325 (1987).
8. T. Fedoseva and A. Vagramyan, ***Sov. Electrochim. 8,*** 825, (1972).
9. A. Brenner, ***Electrodeposition of Alloys, 1***, pp. 77, Academic Press, New York, (1963).
10. A. Vagramyan and T. Fatuyeva, ***J. Electrochem. Soc. 110,*** 1030 (1963).
11. S. H. Hessami and C. W. Tobias, ***J. Electrochem. Soc. 136,*** 3611 (1989).
12. M. Kurachi, K. Fujiwara and T. Tanaka, ***Proceedings of the 8th Congress of the International Union for Electrodeposition and Surface Finishing***, p 152–157, (1973).
13. M. Kurachi and K. Fujiwara, ***Trans. J.I.M. 11,*** 311–317, (1970).
14. Y. Imai, Sh. Ohsumi and M. Kurachi, ***Denki Kagaku, 46,*** , 264–269, (1978).
15. Y. Imai and M. Kurachi, ***Denki Kagaku, 47,*** 89–94, (1979).
16. Y. Imai and M. Kurachi, ***Denki kagaku, 45,*** 728–733, (1977).
17. Y. Imai, T. Watanabe, and M. Kurachi, ***Denki Kagaku 46,*** 202–207, (1978).
18. M. Kurachi and K. Fujiwara, ***Denki Kagaku 38,*** 600–608 (1970).
19. J. Dini and H. Johnson, ***Metal Finishing, 77,*** 8, 31–35, (1979).
20. J. Dini and H. Johnson, ***Metal Finishing, 77,*** 9, 53–57, (1979).
21. G. Hsu, ***Plating and Surface Finishing, 72,*** 3, 54–57, (1985).
22. R. Baker and C. Holden, ***Plating and Surface Finishing, 72,*** 3, 54–57, (1985).
23. R. Noumi, H. Nagasaki, Y. Foboh and A. Shibya, ***SAE Technical Paper Series 820332–Detroit-Michigan,*** Feb, 22–26, (1982).
24. A. Matsuda, T. Yoshihara, K. Miyachi, A. Komoda and S. Kikuchi, ***ISIJ, 24,*** p B267, (1984).
25. A. Shibuya, T. Kurimoto, Y. Hoboh and N. Usuki, ***ISIJ, 23,*** 923–929, (1983).
26. T. Watanabe, M. Ohmura, M. Sagiyama, T. Honma, ***SAE, 90,*** 3, 30–32, (1982).
27. K. Nishimura, I. Kikuchi and H. Odashima, ***J. Surf. Technol. 42,*** 6, 627, (1991).
28. B. N. Popov, D. Slavkov, T. Grcev, Lj. Arsov and S. Karaivanov, ***Kem. Ind. 35,*** ,1, 1–7, (1986).

29. B. N. Popov, ***Kem. Ind. 31,*** 9, 455–461, (1982).
30. B. N. Popov, R. E. White, ***Plating and Surface Finishing,*** , 61–65, December, (1991).
31. B. N. Popov and R. E. White, ***J. Electrochem. Soc. 139,*** 1, 91, (1992).
32. R. Bindlosh, B. N. Popov and R. E. White, ***Plating and Surface Finishing*** accepted for publication.
33. W. Li, B. N. Popov and R. E. White, ***Plating and Surface Finishing*** submitted for publication (1991).
34. P. Delahay, ***New Instrumental Methods in Electrochemistry,*** Interscience Publ., p. 124–125, (1966).
35. J. Bressan and R. Wiart, ***J. Appl. Electrochem. 9,*** 43–45 (1979).
36. V. Batrakiv and A. Sidnin, ***Elektrokhimiya, 8,*** 122, (1972).
37. L. M. Baugh and J. A. Lee, ***J. Electroanal. Chem, 48,*** 55, (1973).
38. I. Epelboin and R. Wiart, ***J. Electrochem. Soc. 118,*** 10, 1577, (1971).

604

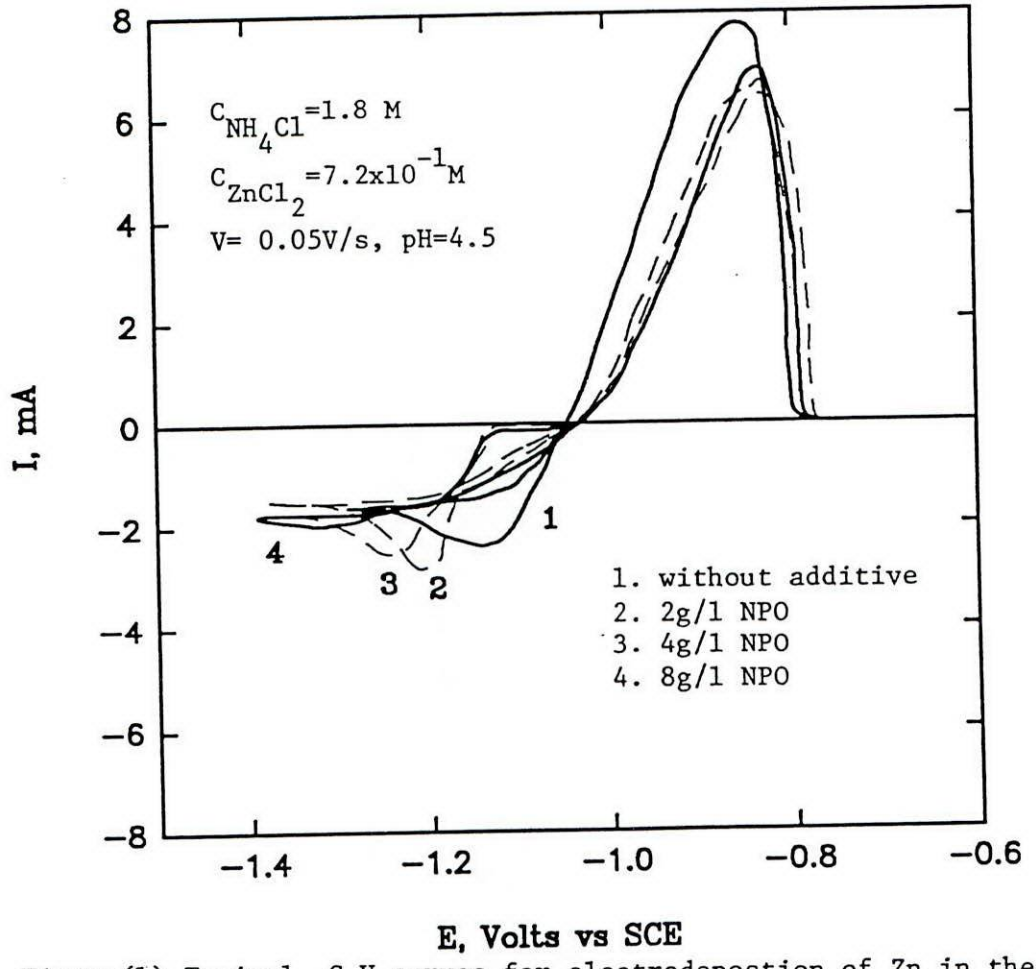

Figure(1).Typical C V curves for electrodepostion of Zn in the presence of organic additive (NPO)

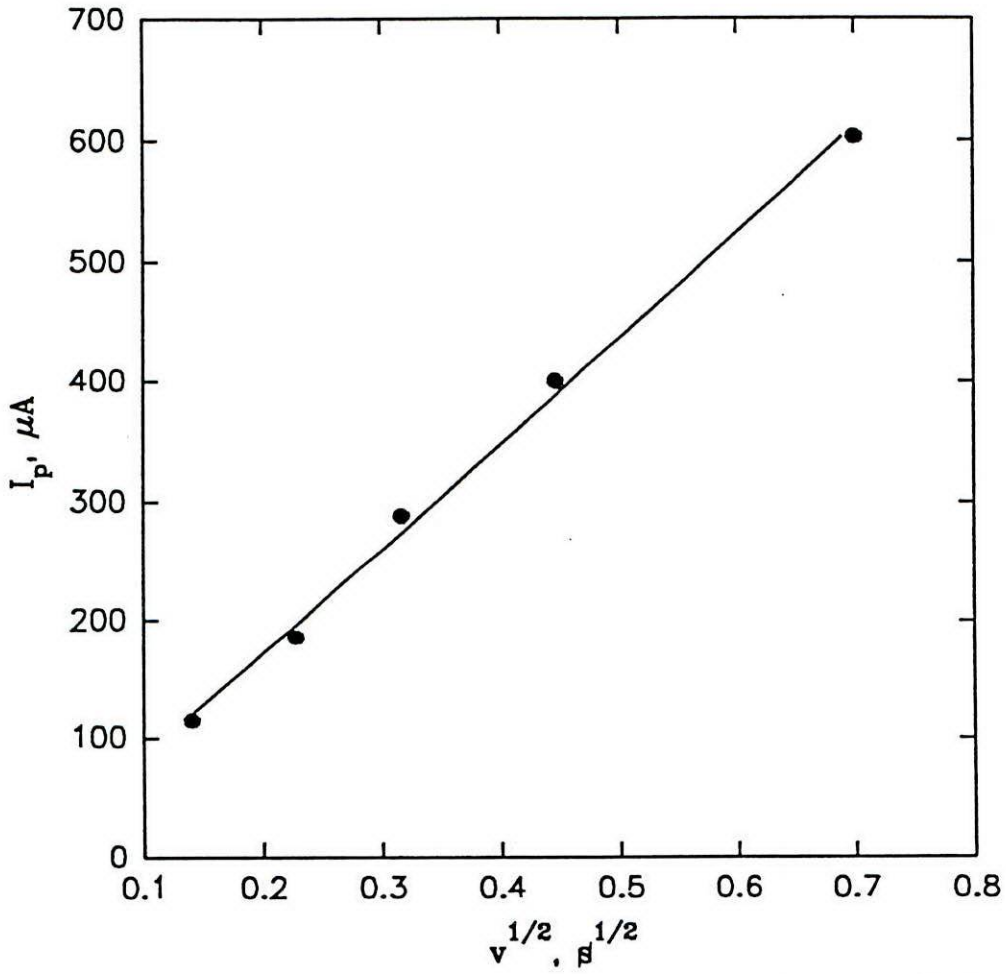

Figure (2) Cathodic peak current as a function of the sweep rate. Same solution as in Figure (1).

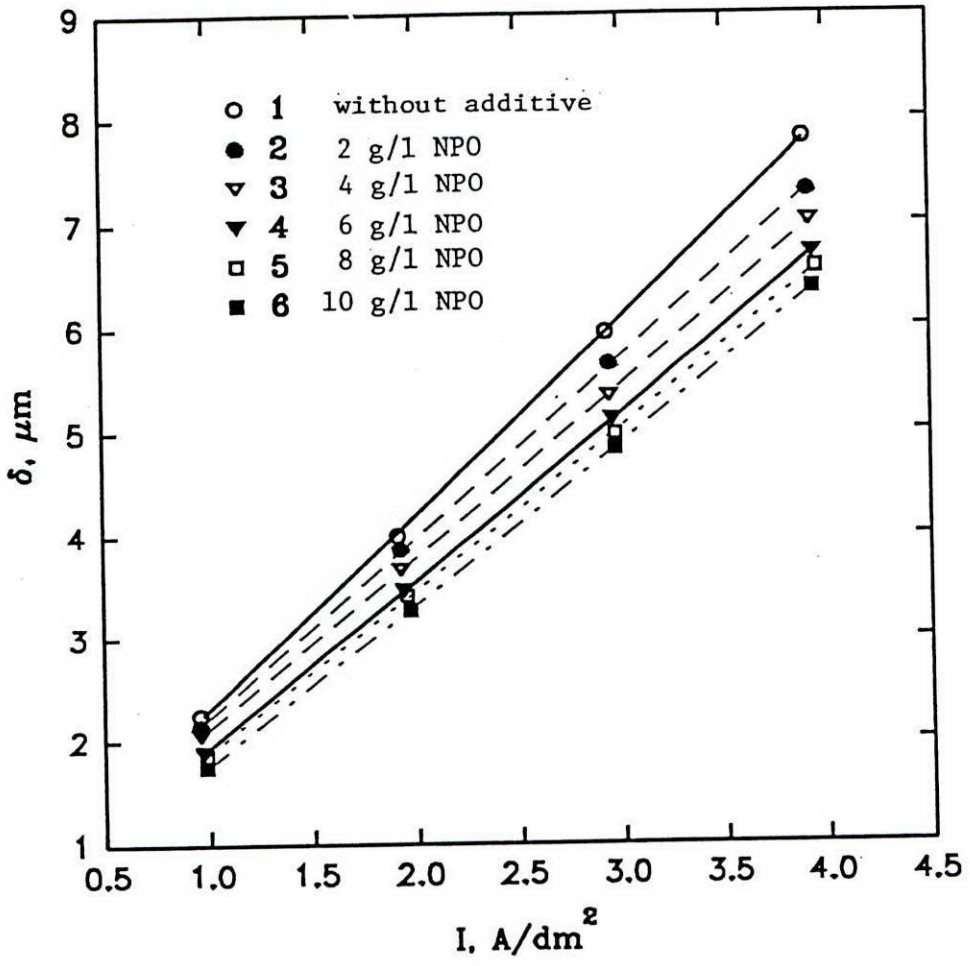

Figure (3) Dependence of the thickness of the coating on the applied current density for different concentration of the organic additive in the electrolyte. Same solution as in Figure (1).

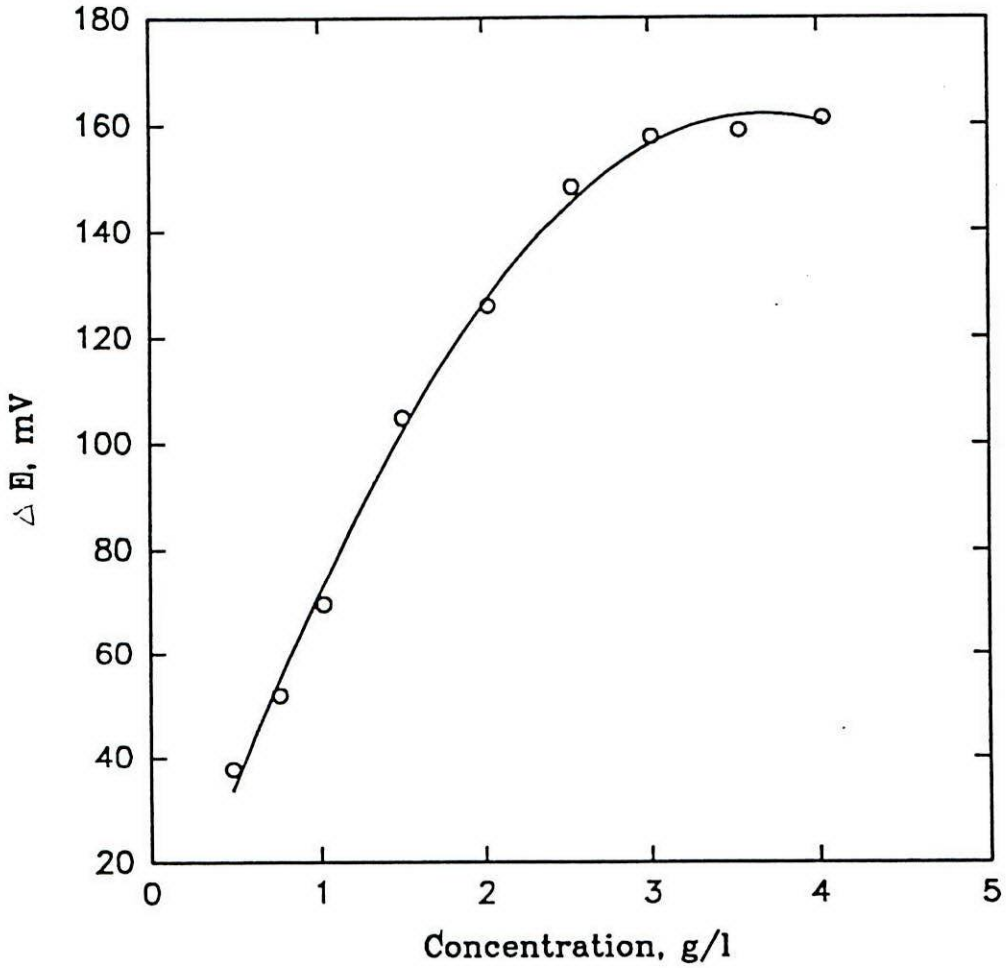

Figure (4) Dependence of the cathodic potential shift upon the concentration of the additive.

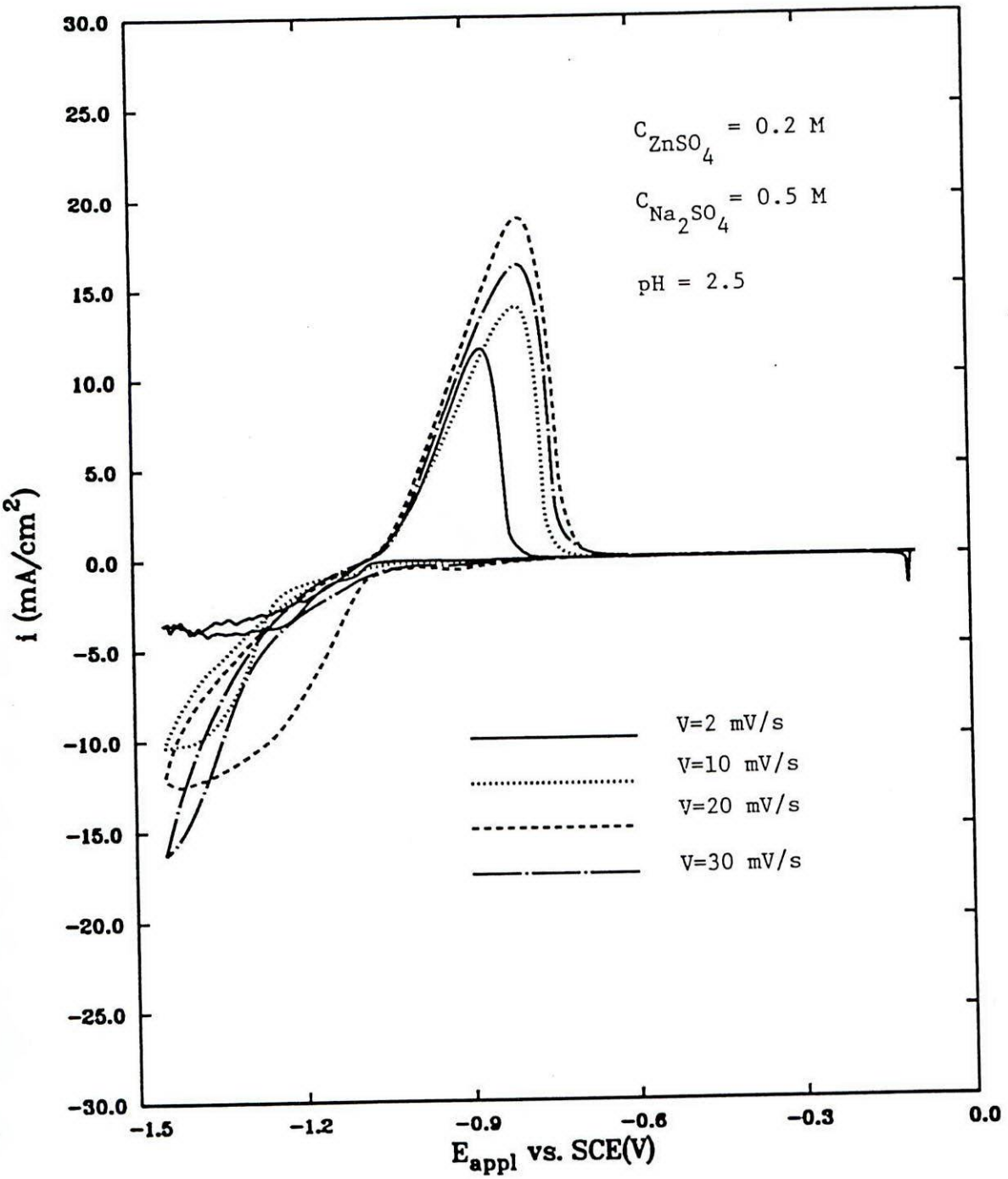

Figure (5) Stripping voltammograms of Zn film recorded on fixed copper disc electrode for different sweep rates.

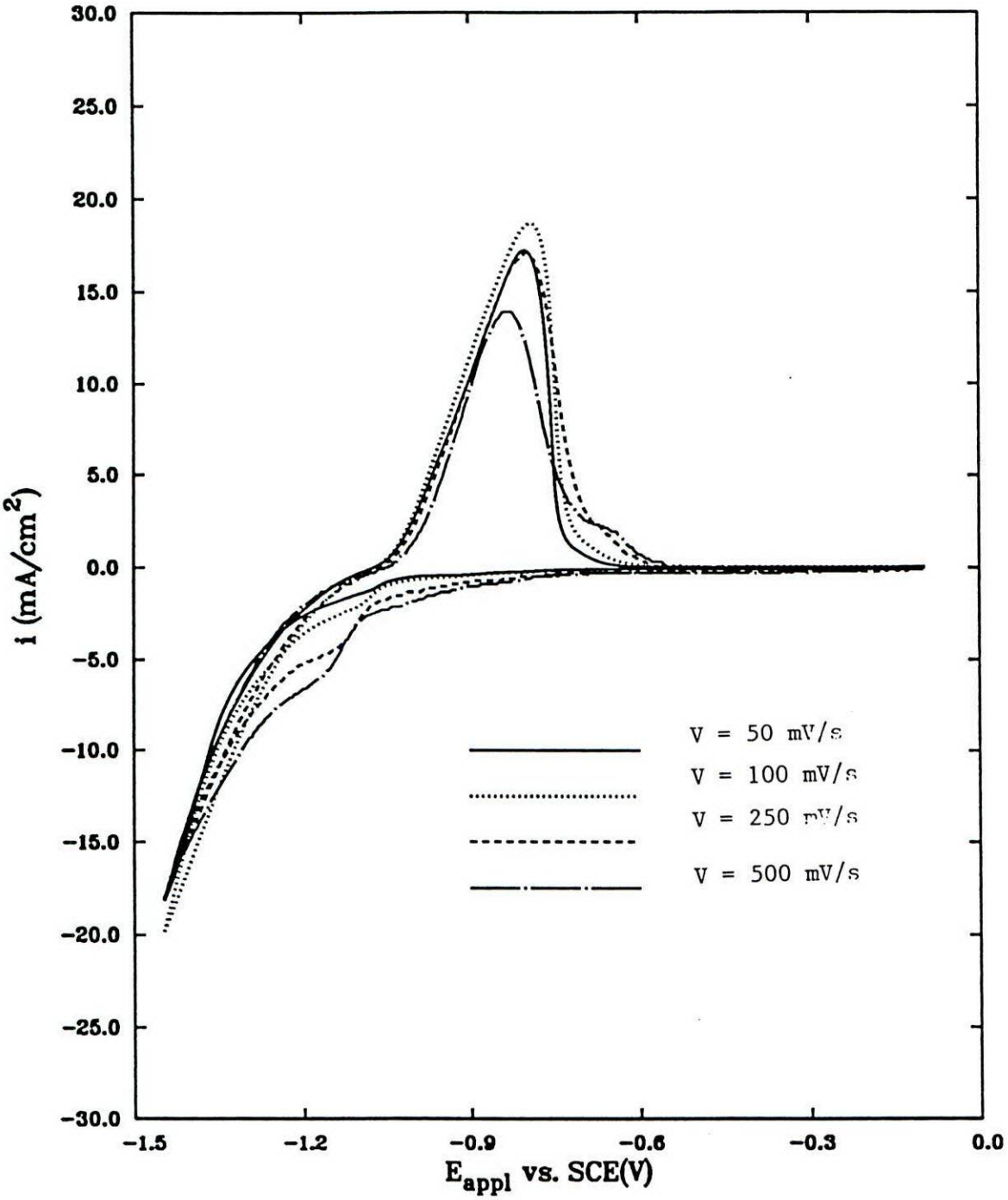

Figure (6) Stripping voltammograms of Zn film recorded on fixed copper disc electrodes for different sweep rates in the same electrolyte as in Figure (5).

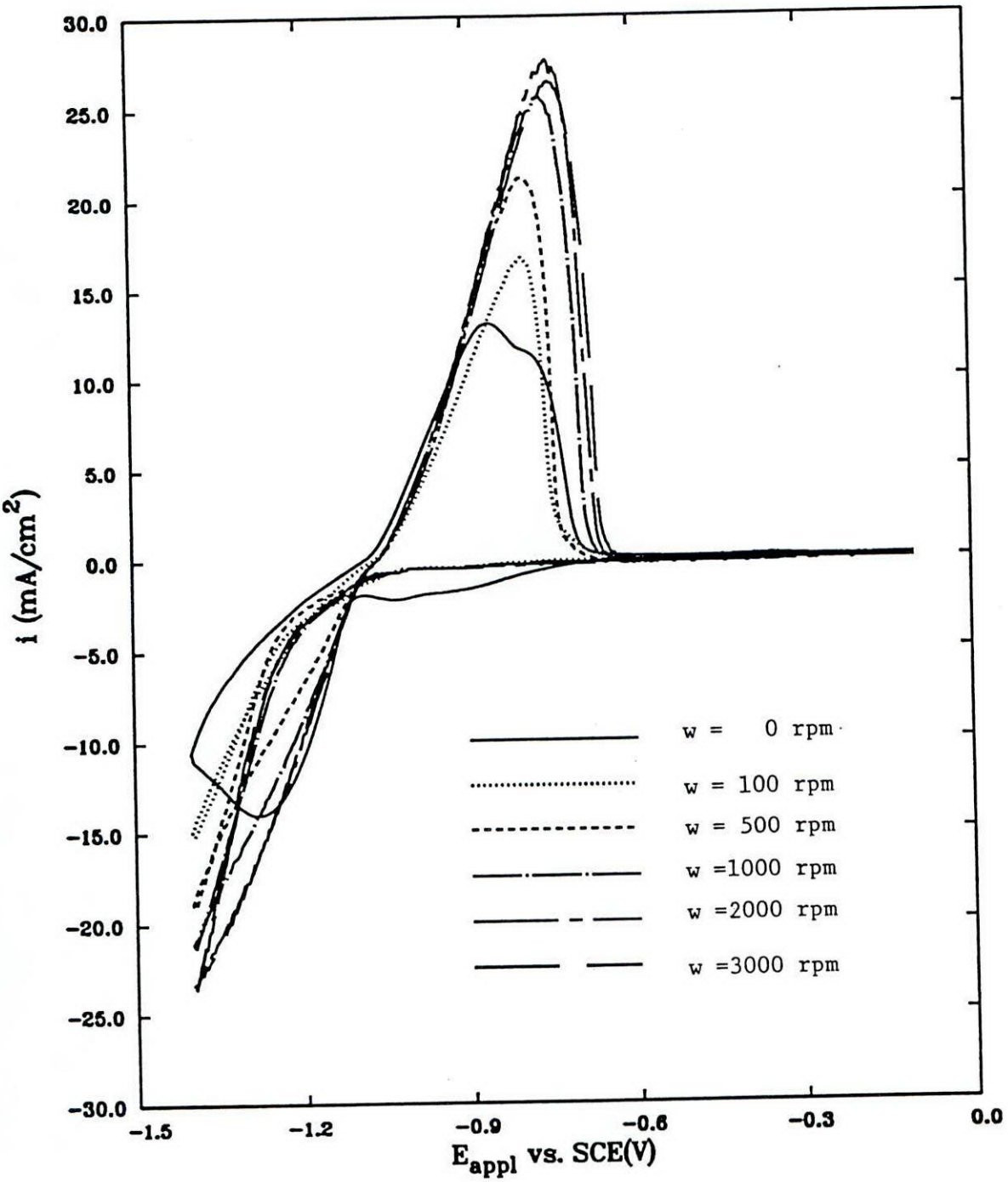

Fig. c

Figure (7) Potentiodynamic stripping voltammograms of a Zn film electrodeposited from the same electrolyte as in Figure(5) for different electrode rotation speeds. V = 30 mV/s.

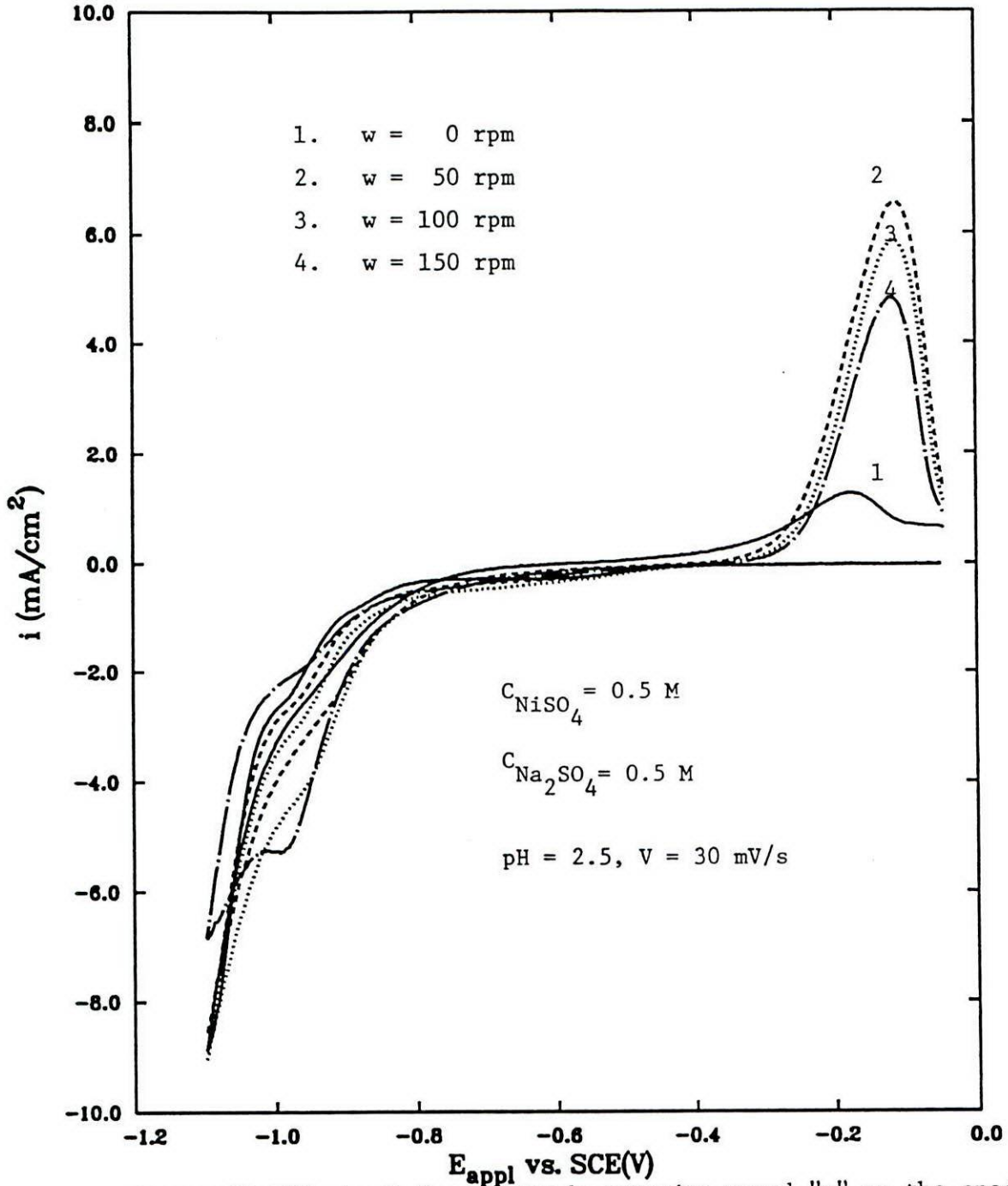

Figure 8) Effect of the electrode rotation speed "w" on the anodic nickel peak.

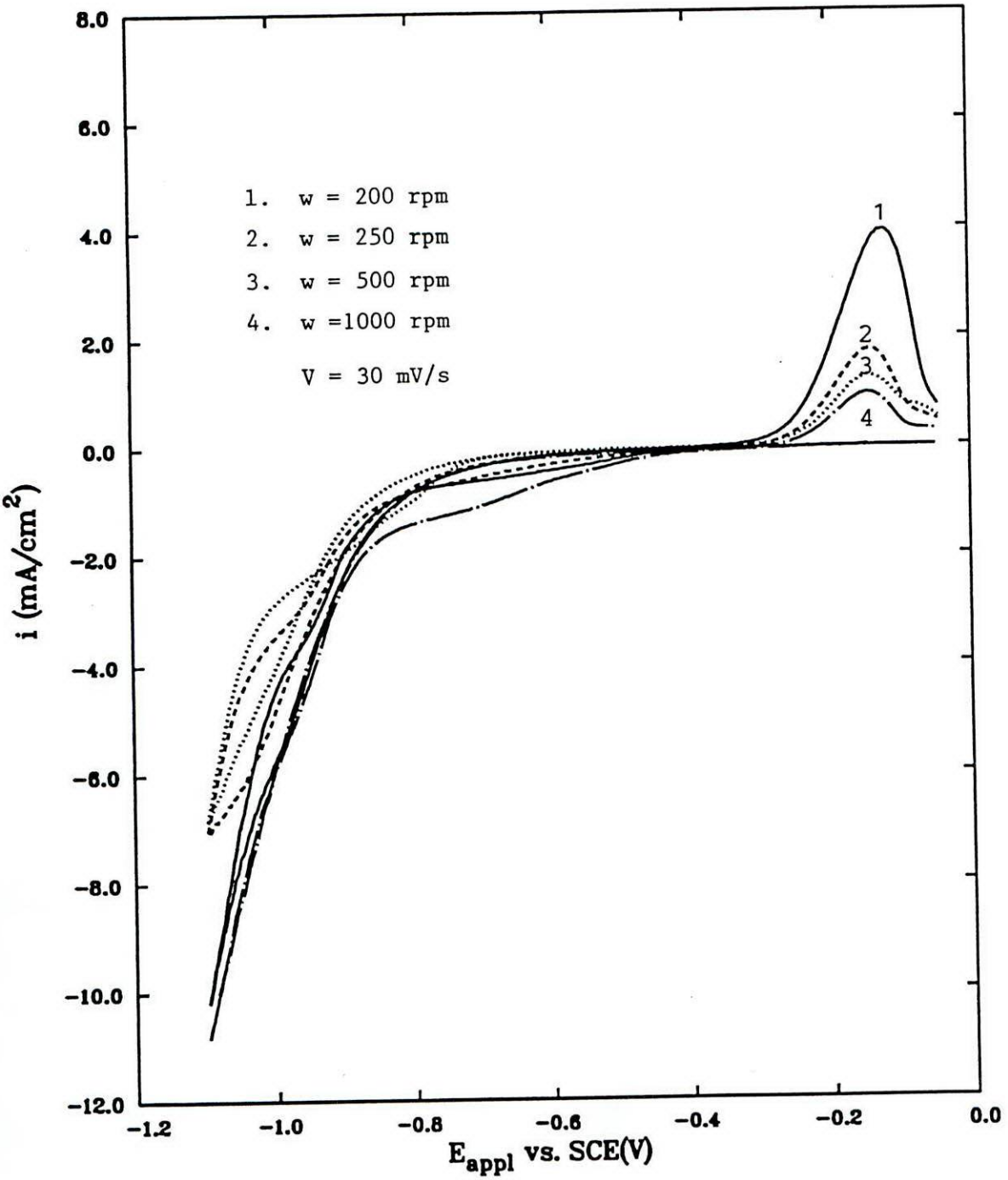

Figure (9) Effect of the electrode rotation speed "w" on the anodic nickel peak. The same conditions as in Figure (8), but at different rotation speeds.

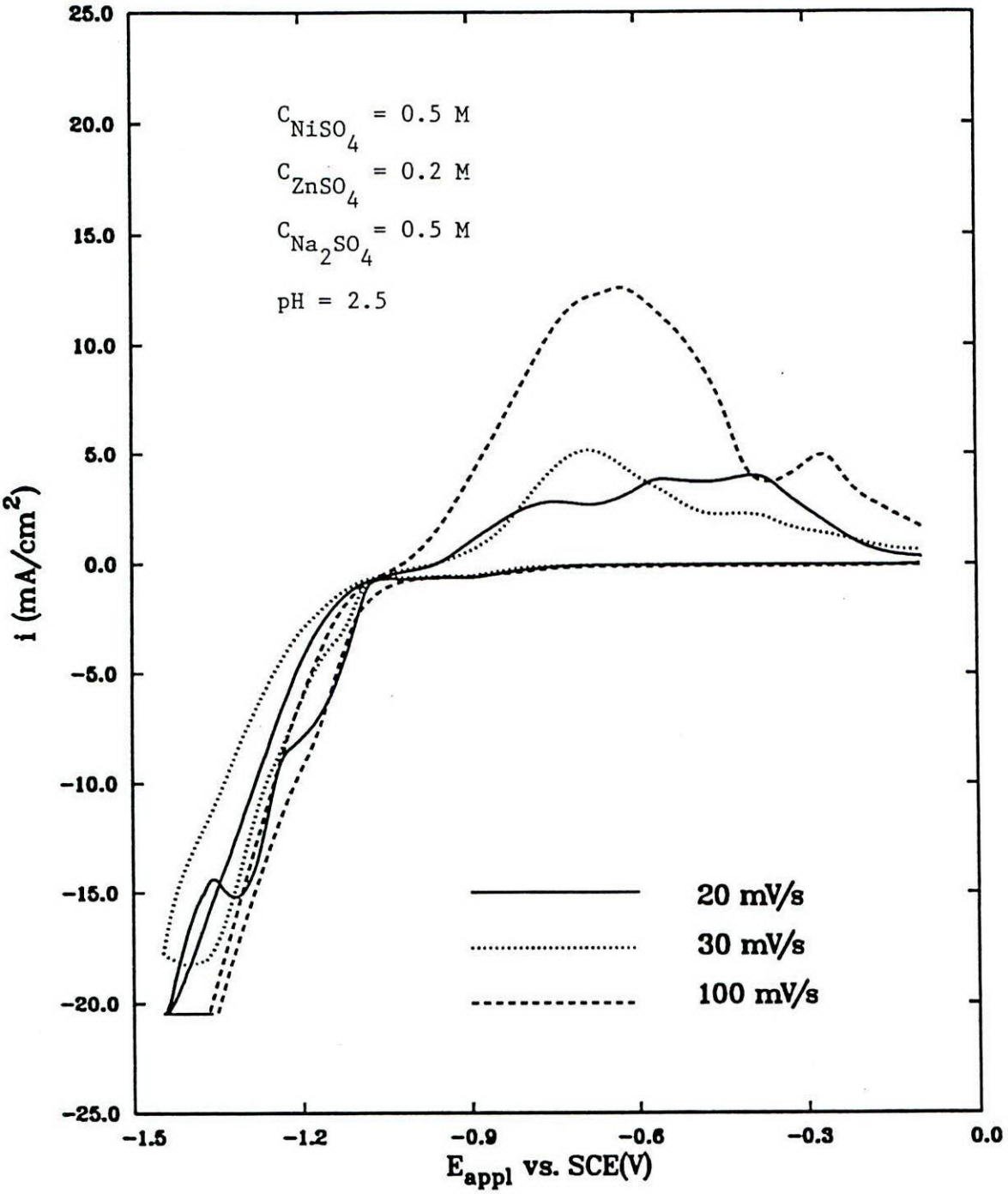

Figure (10) Linear sweep voltammograms recorded on a fixed copper disc electrode for different sweep rates

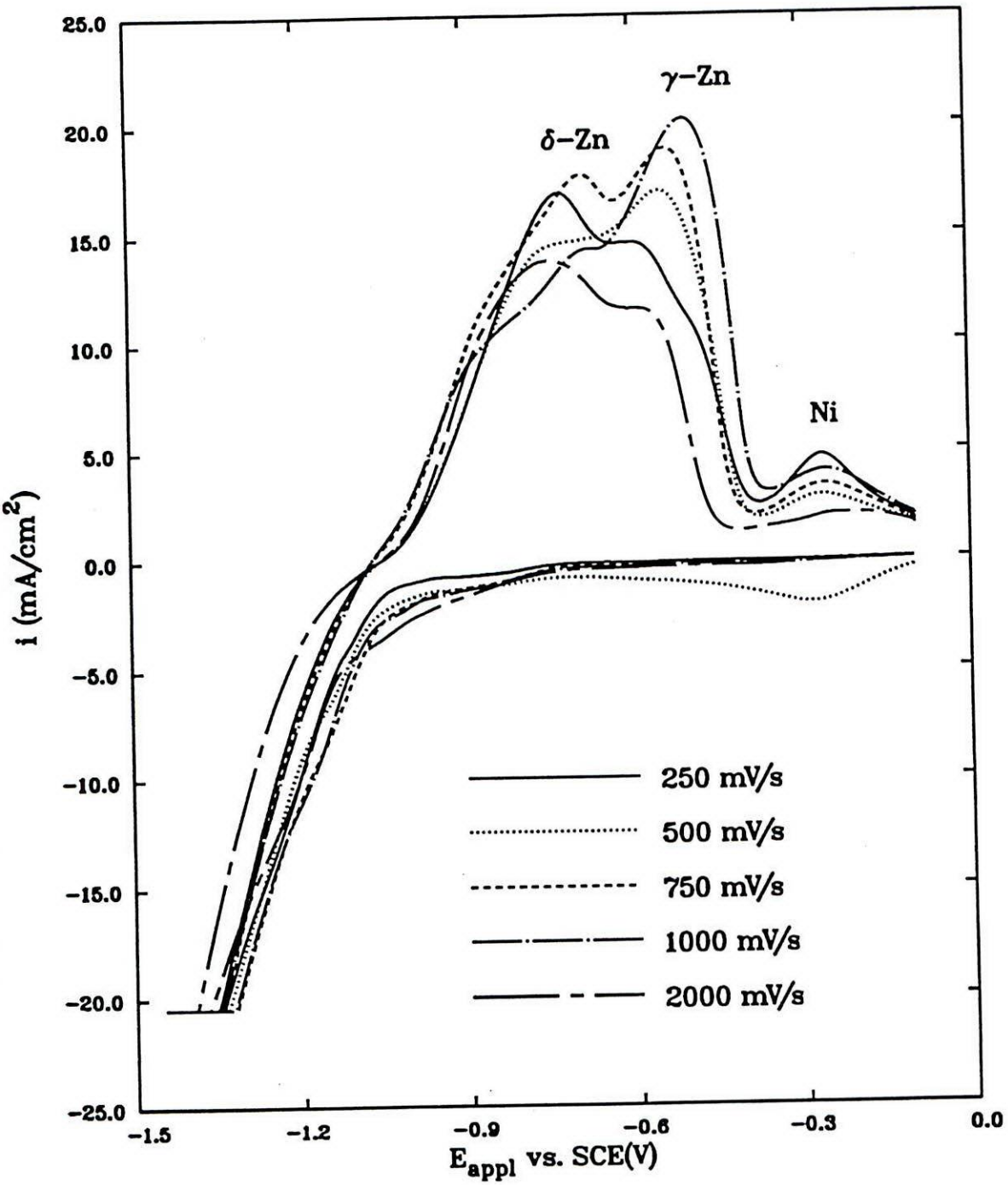

Figure (11) Linear sweep voltammograms recorded on fixed copper disc electrode from the same electrolyte as in Figure(10) for different sweep rates.

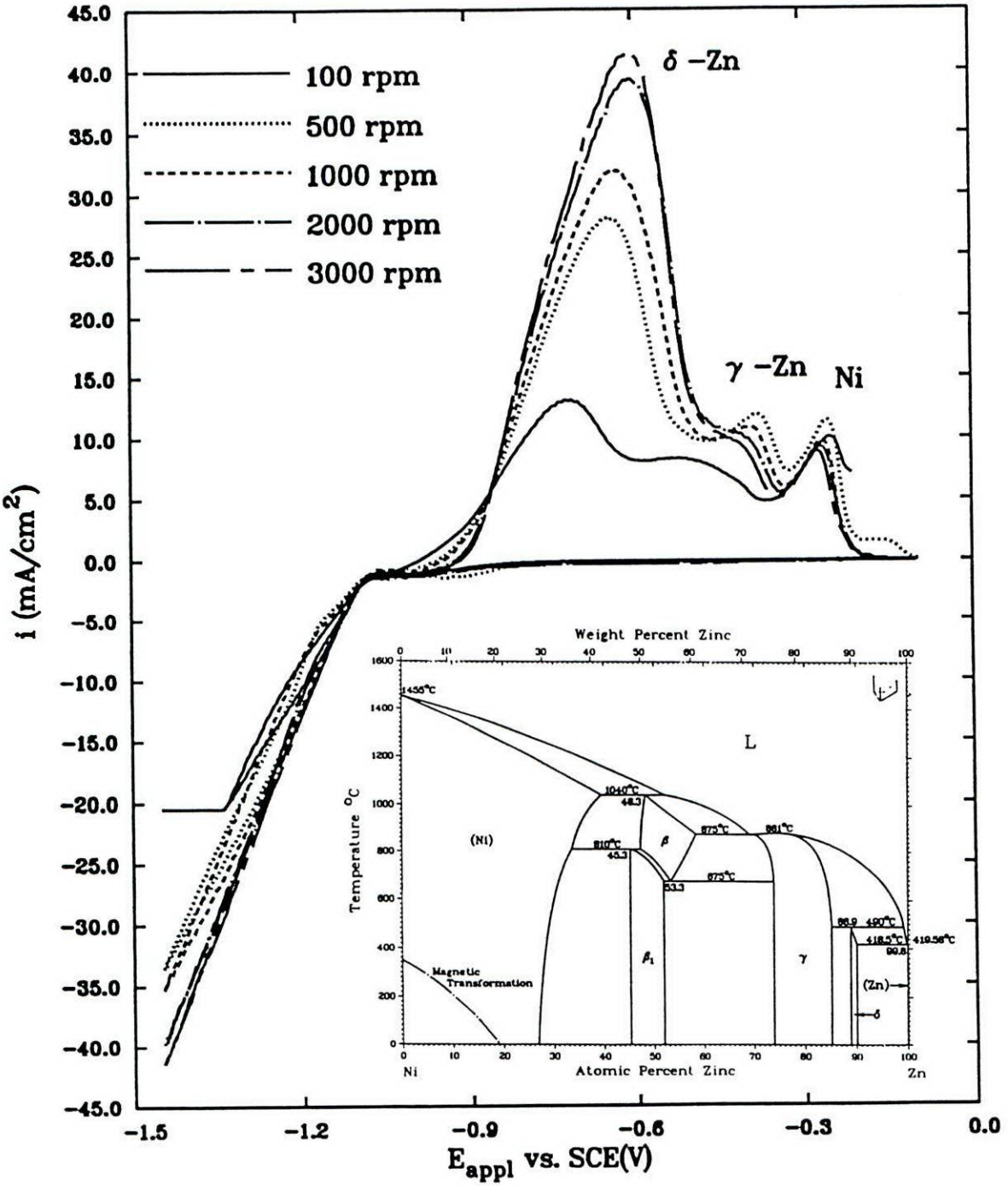

Figure (12) Phase diagram of Zn-Ni alloy and linear sweep voltamograms obtained using a rotating copper disc electrode in the same solution as in Figure (10) for different rotation speeds. Sweep rate, V = 20 mV/s

616

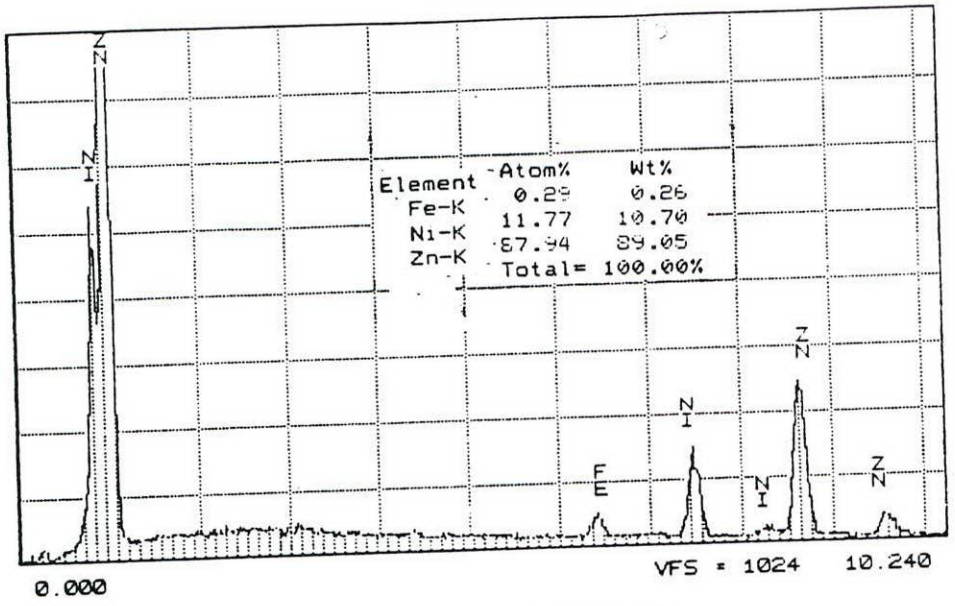

Figure(13A) EDS Spectum of ZnNi Alloy.

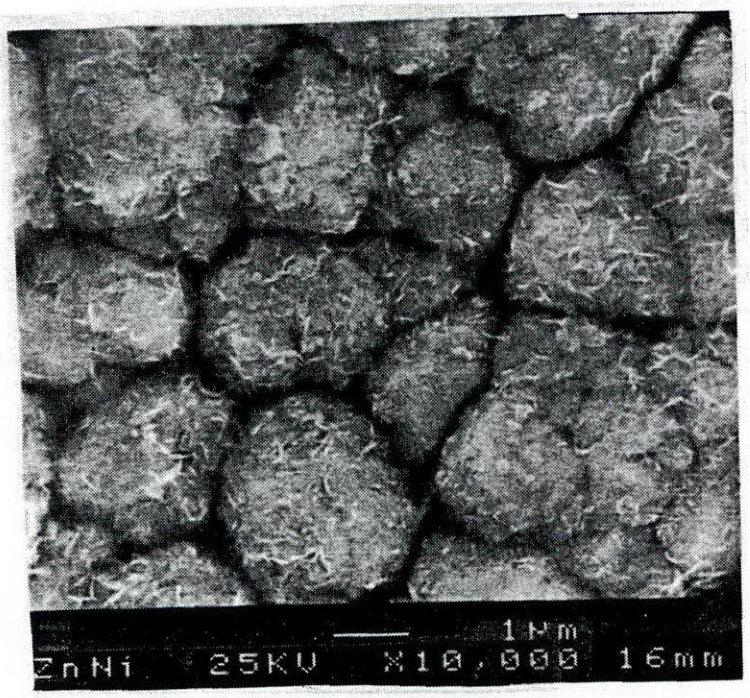

Figure(13B) SEM of the alloy which EDS spectrum is given in Figure (13A)

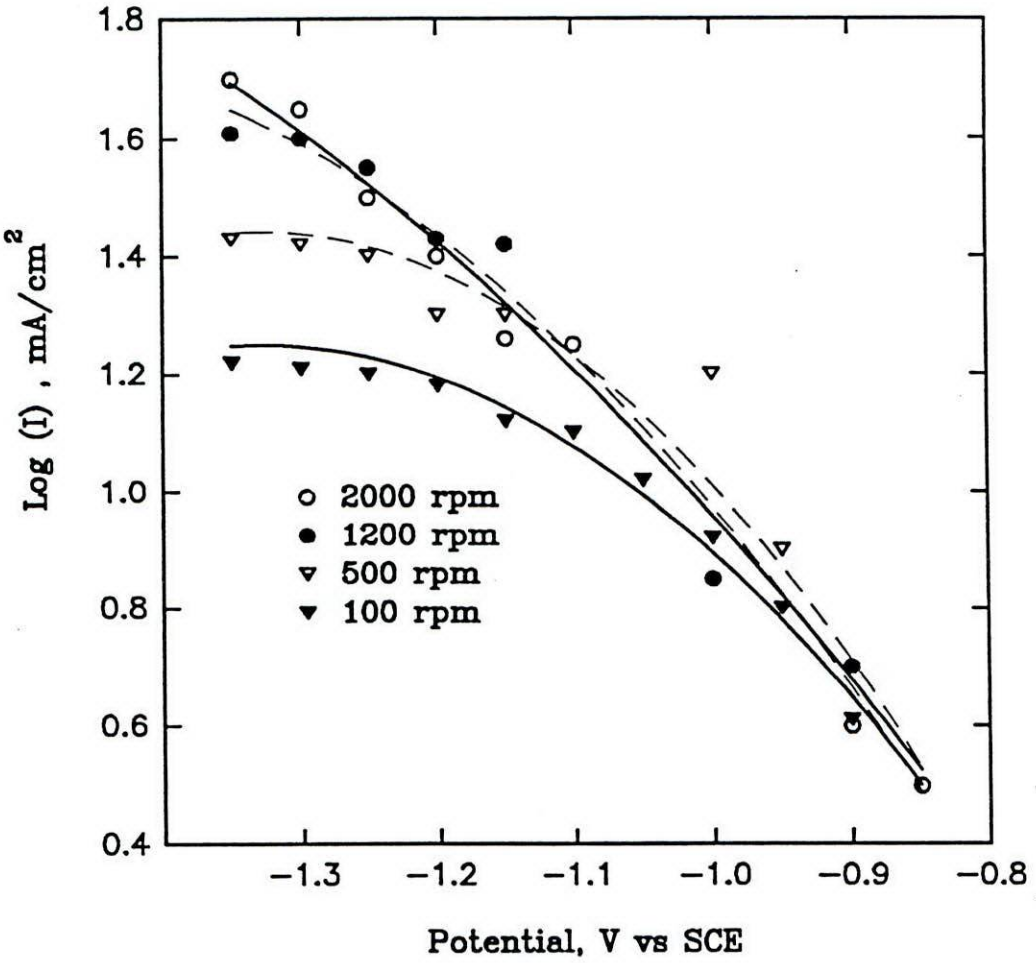

Figure (14) Dependence of the zinc deposition partial current density on electrode potential for several rotation speeds. Solution composition as in Figure (10). pH = 2.5, T=50°C.

618

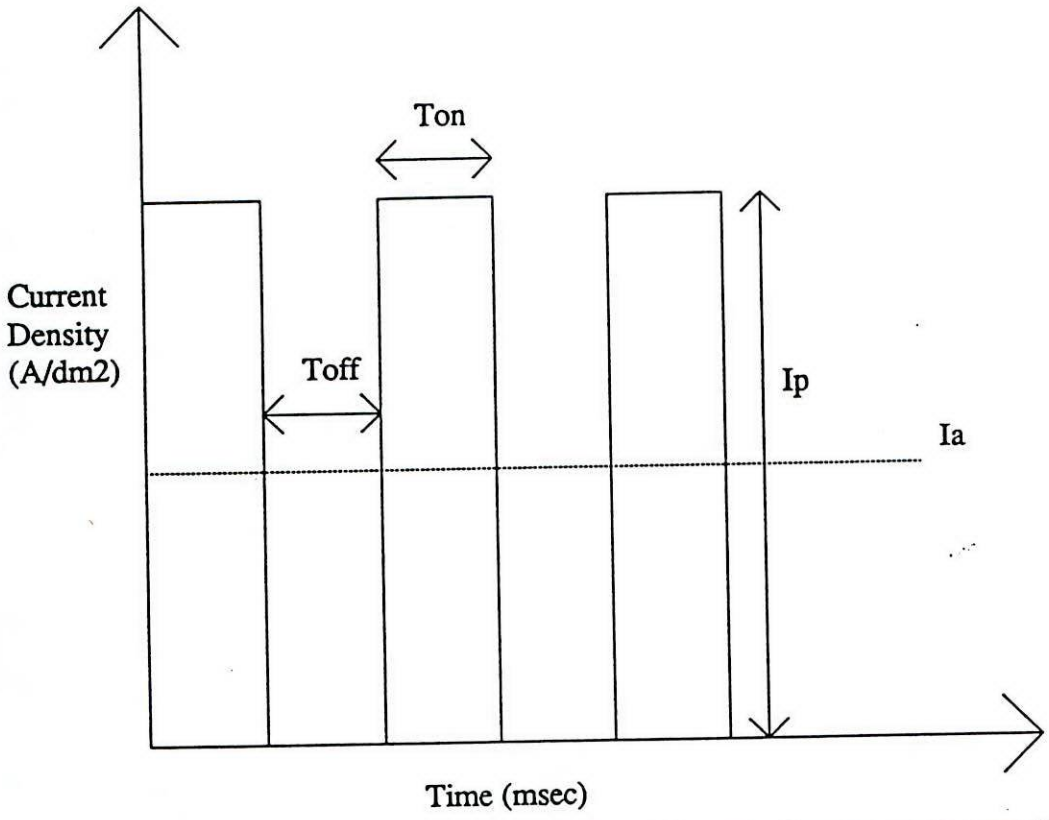

Figure (15) Shematic representation of the current waveform used for pulse plating.

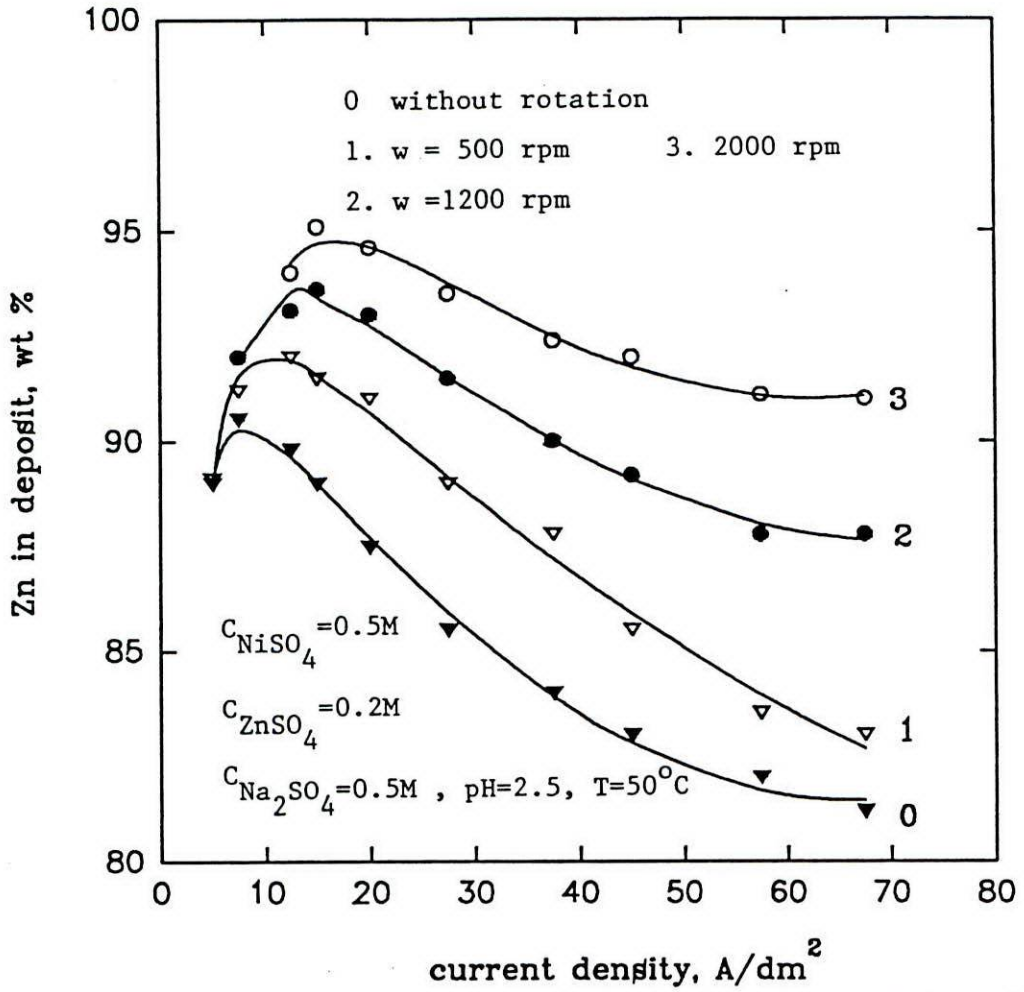

Figure (16) Composition of the Zn-Ni film plated on the RDE as a function of the total applied current density for several rotation speeds.

620

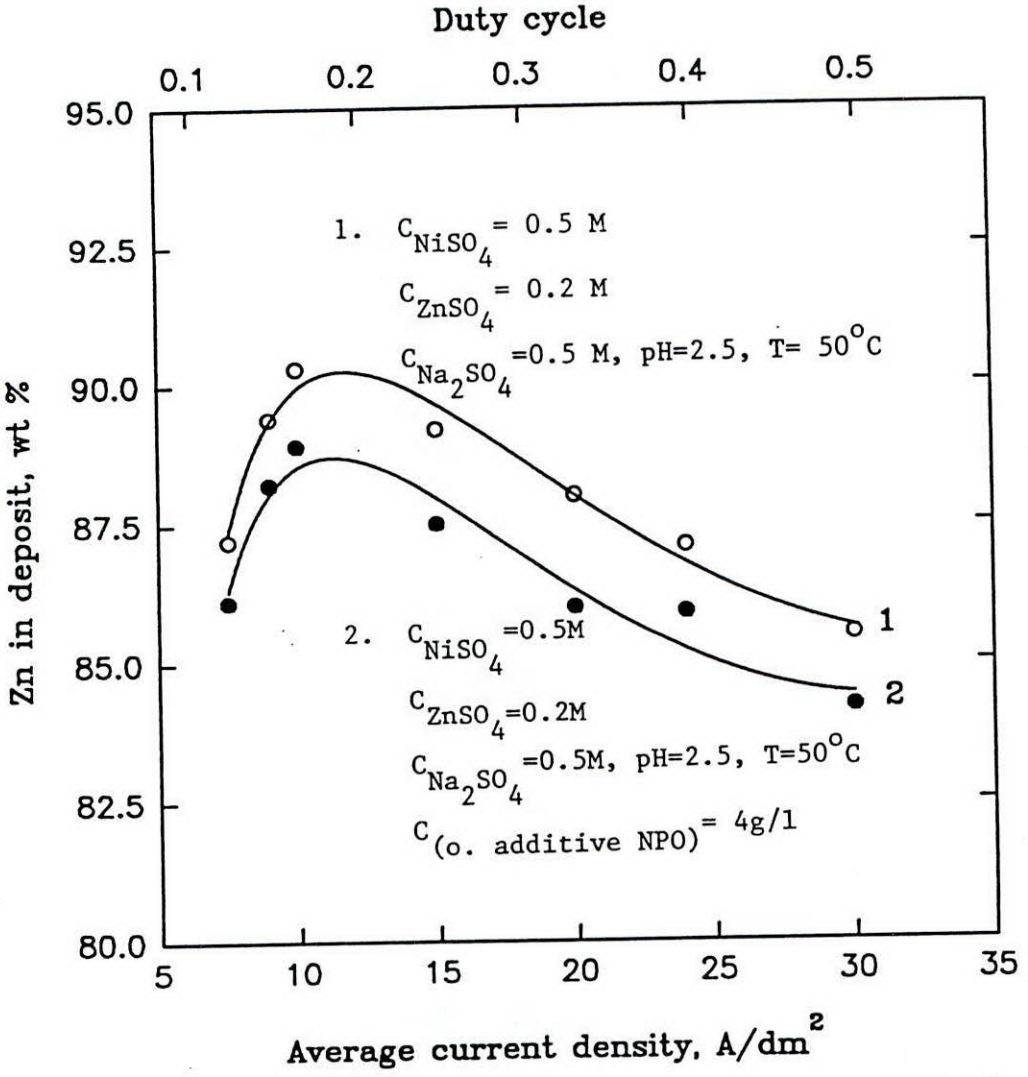

Figure (17) Deposit Composition vs average current density for pulse plating, 50 Hz, I_p=60 A/dm^2, T= 10 ms.

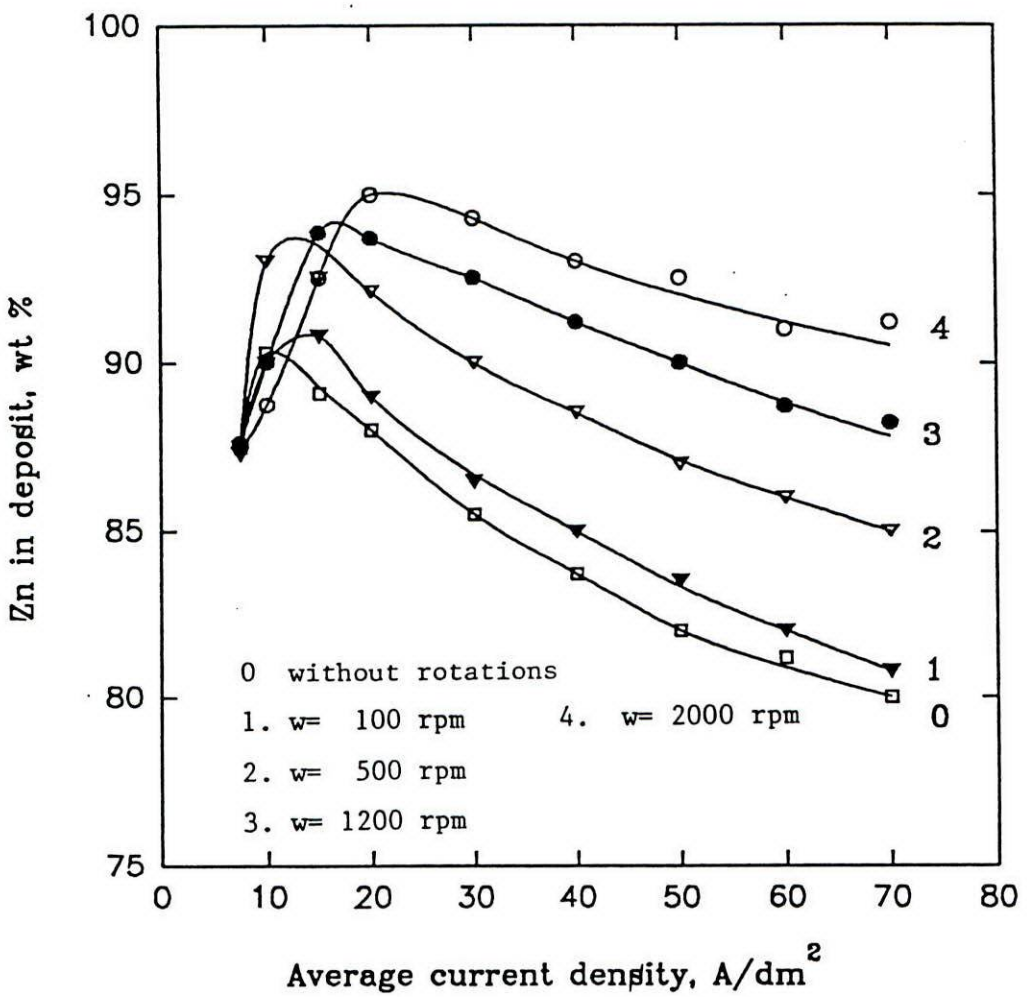

Figure (18) Composition of Zn-Ni film plated on RDE at various rotation speeds. Pulse plating was carried out with duty cycle = 0.3, f=80 Hz. Composition of the electrolyte as in Figure (16).

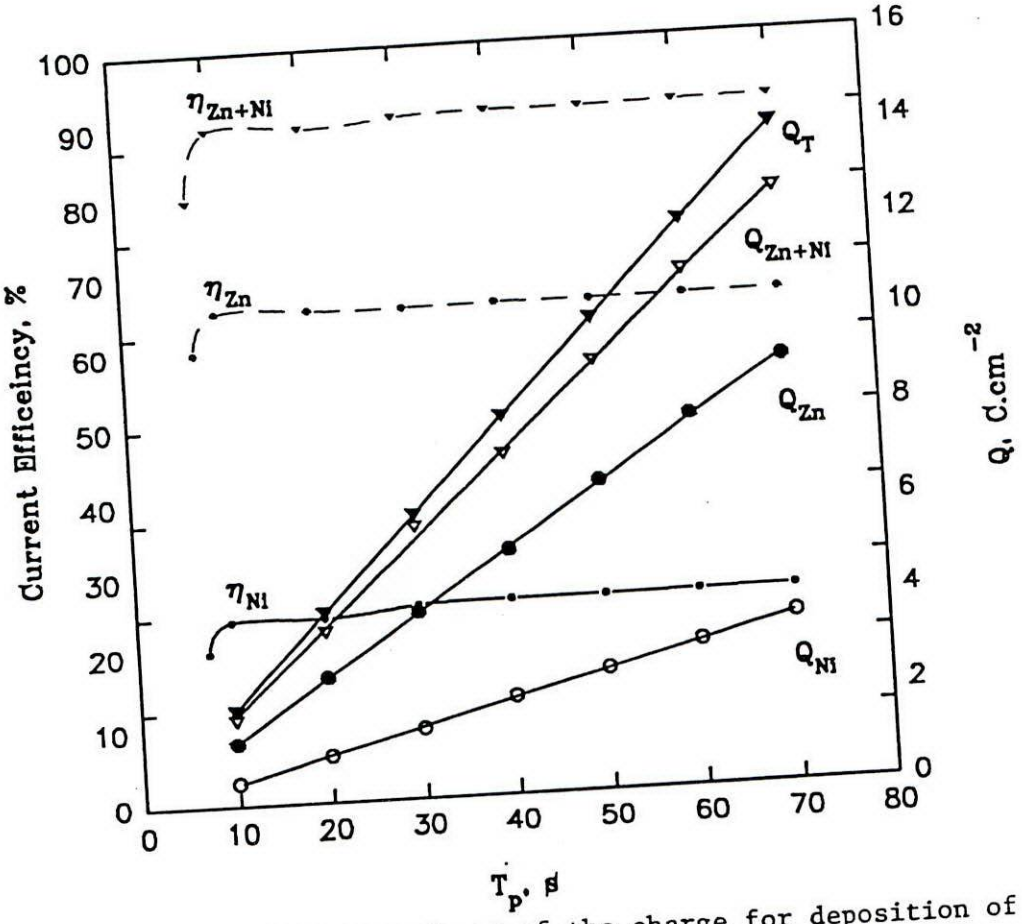

Figure (19) Dependence of the charge for deposition of Ni, Zn and Ni+Zn and the current efficiency on the pulse length. I_p = 200 mA/cm^2, pH=2.5, T=50°C. Solution composition as in Figure (16).

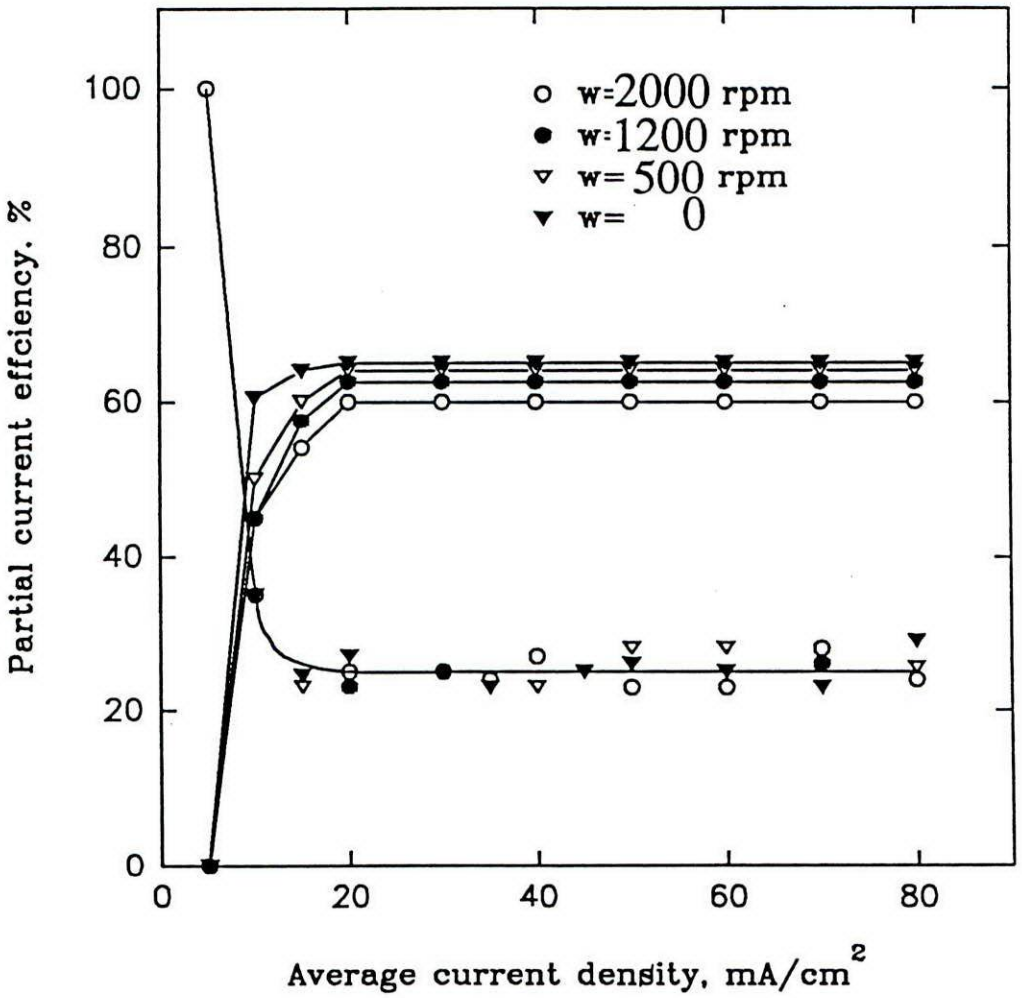

Figure (20) Current efficiency vs average current density for several rotation speeds. Solution composition as in Figure (16), pH= 2.5, I_p= 10 A/dm^2, T= 50°C

624



Figure(21A)

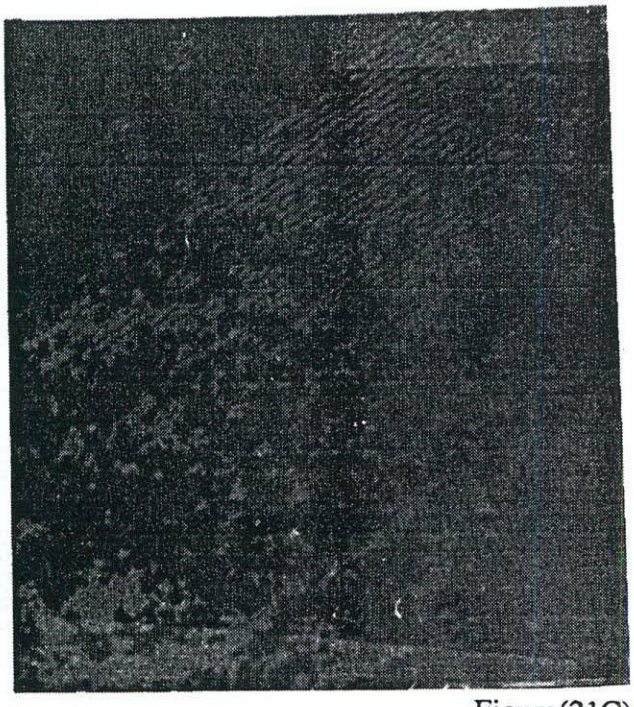

Figure(21C)

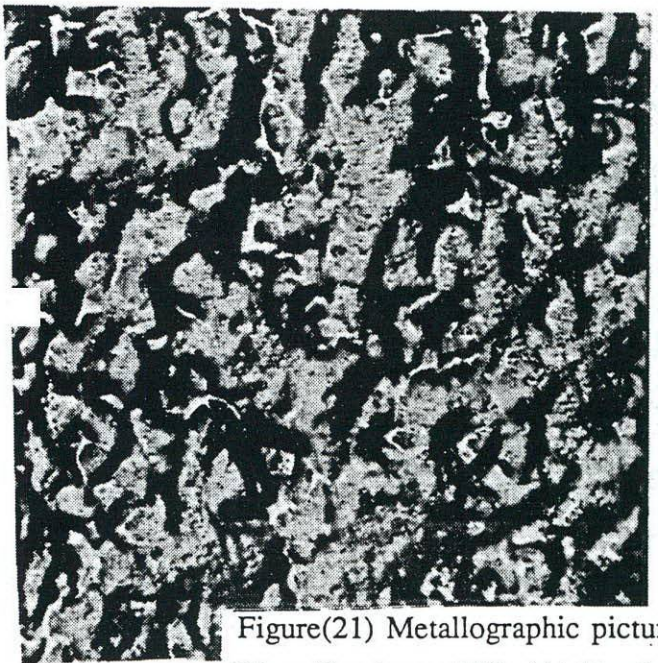

Figure(21B)

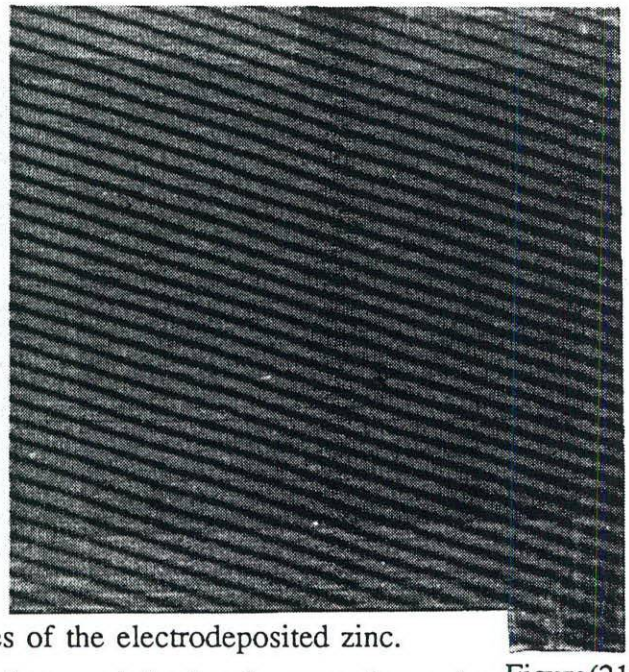

Figure(21D)

Figure(21) Metallographic pictures of the electrodeposited zinc. Magnification x 100. (A) Dendrytic growth in the absence of organic additives, I=3A/dm^2. (B) Morphology of the deposited zinc in the presence of 1g/l additive., I= 3A/dm^2, (C) Interference Metallographic picture of the same place as in Figure(21B). (D) Interference Metallographic picture obtained at optimal plating conditions using current density of 10 A/dm^2 and optimal concentration of the additive.

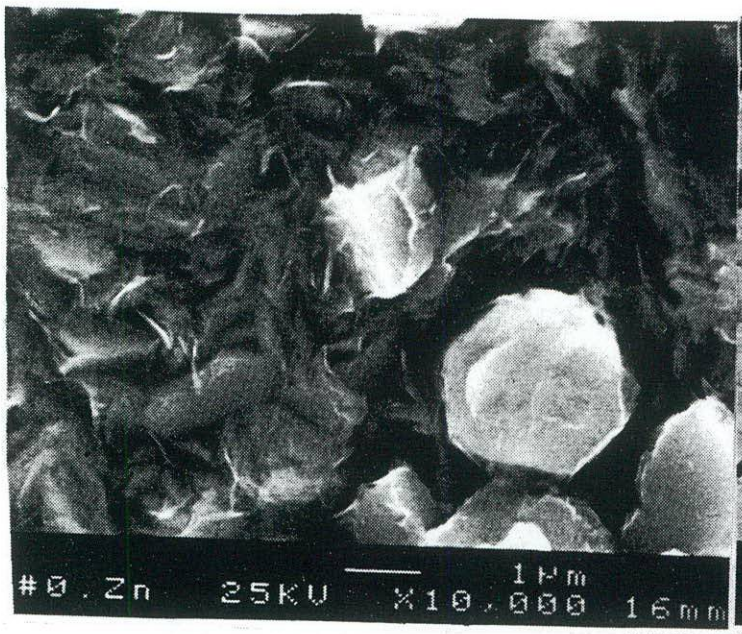

Figure(22A)

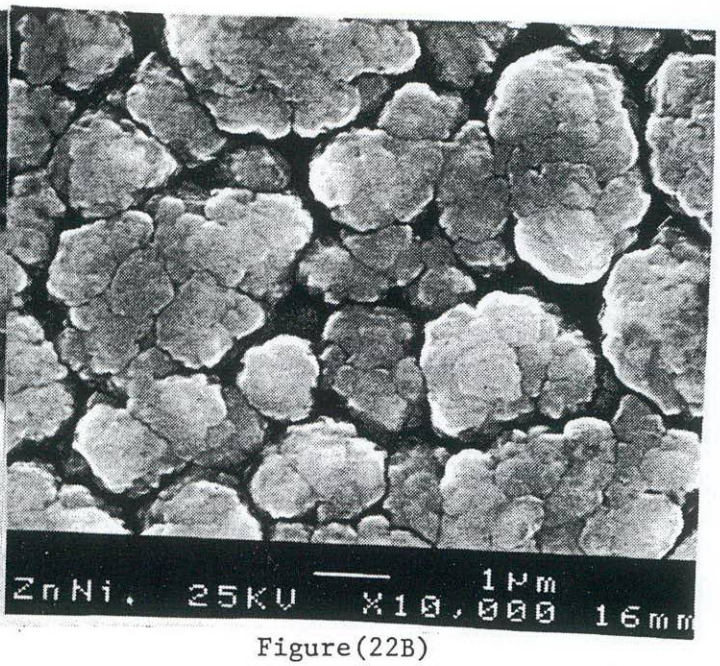

Figure(22B)

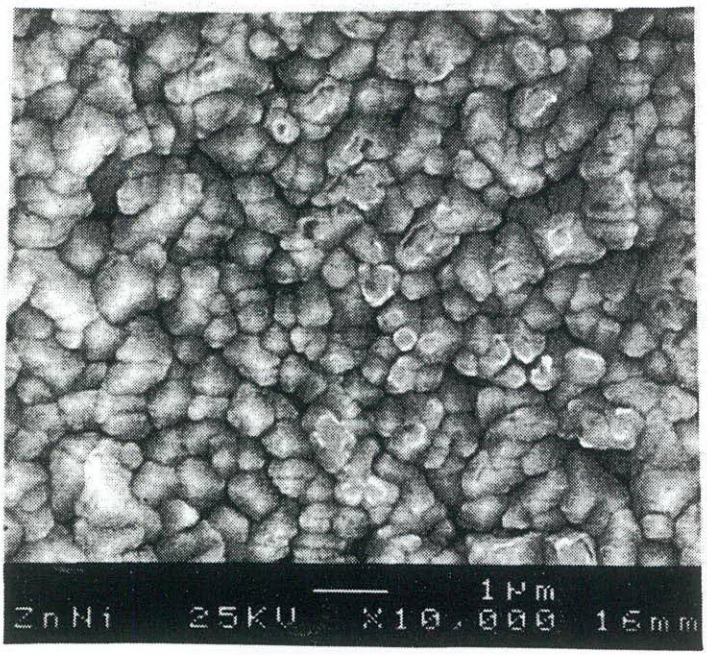

Figure(22C)

Figure(22) SEMs of Zn-Ni alloy. (A) Pure zinc, According to EDS Zn wt% =99.1, Fe wt% = 0.7%. (B) Zn-Ni alloy deposited at 30 A/dm^2 from the same solution as in Figure(18) in the absence of the organic additive. (C) Zn-Ni alloy deposited from the same solution as in Figure(22B), but in the presence of 8 g/l organic additive.

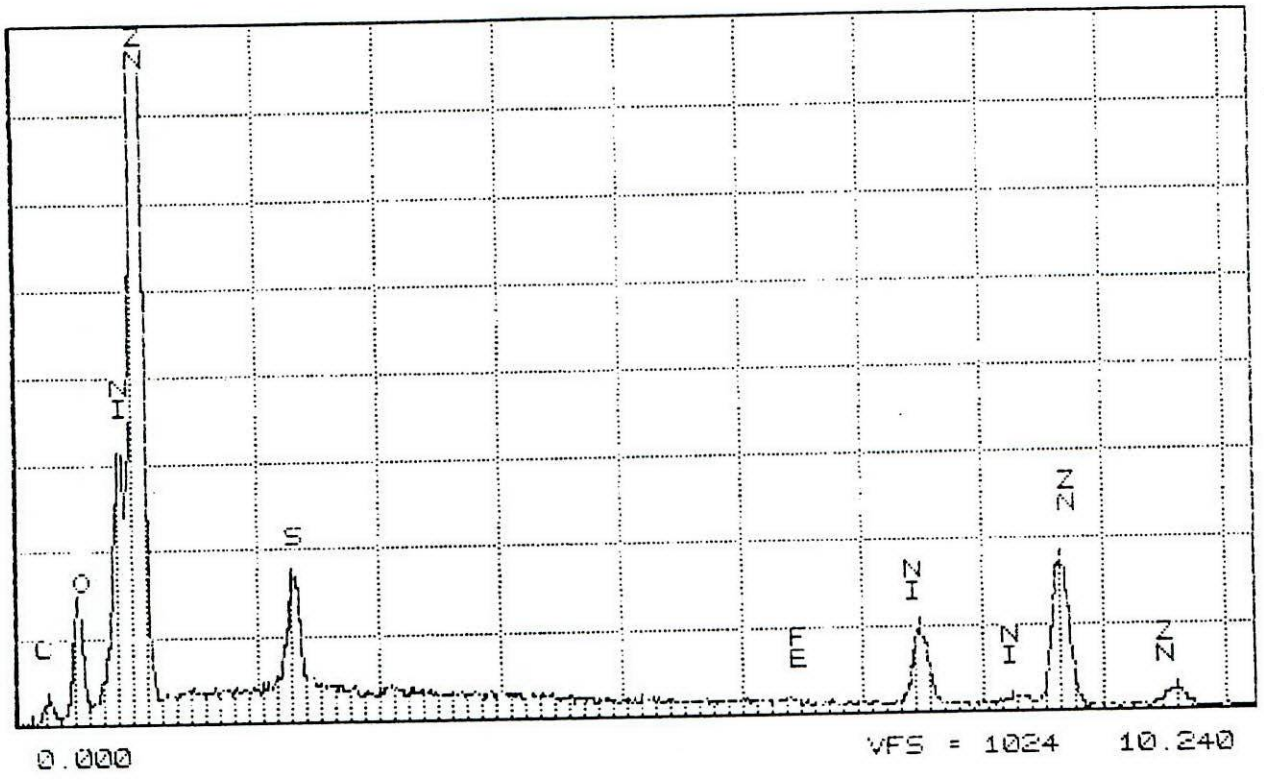

Figure (23) EDSspectrum of Zn-Ni alloy obtained from the same place of the surface as it is in Figure(22C). Zn wt%=86.06, Ni wt %=12.01.

Figure (24). XRD pattern of ZnNi alloy. According to EDS Zn wt%=84.7% Ni wt%=15.2%. I_{app}=30 A/dm^2. Solutions is the same as in Figure (18), but without additives.

INTERNAL STRESS CONTROL OF ELECTROFORMED NICKEL-IRON ALLOYS

H.M. Wu and H.J. Shy
Materials R&D Center
Chung Shan Institute of Science and Technology
Taoyuan, Taiwan, R.O. China

C.H. Huang
Chemistry Department
Soochow University
Shihlin, Taipei, Taiwan, R.O. China

Abstract

Optical mirrors were prepared by electroformed nickel-iron alloys. The influence of organic additives on the internal stress of nickel-iron alloy electroforming in a sulfamate bath was controlled by a strain gauge. By varying the amount of organic additives, additional controls on the composition, corrosive-protection, and hardness were also studied in this paper.

Introduction

With its unique capability of duplicating exact definition of an original design, electroforming is being used in the optical field. In addition, with the benefits of low thermal-expansion and high brightness or leveling characteristics,(1) electroformed nickel-iron was used to prepare spheric optical mirrors in this work.

Low internal stress of deposits was necessary for exact duplication of the optical mirror. Any stress distortion in the alloy deposits would lose the surface accuracy of optical mirrors. Therefore, optical mirrors were prepared from a low-stress sulfamate solution containing saccharin as a stress-releasing agent to avoid the disadvantage of stress.

Due to the electrochemically more negative metal-iron, the corrosive-protection of electroformed nickel-iron alloy would be expected to be inferior to that of electroformed nickel.(2) By varying the amount of added saccharin and operating parameters, high corrosion-protective alloy deposits were developed. With these results, optical mirrors with low stress and high corrosive-protection were prepared in this work.

Experimental Procedure

After preliminary experiments in a 267-mL Hull cell, the electroforming baths in Table 1 were prepared. Since the ferrous ion is more stable in acdic solution, the pH of the studied baths were in the range of 1.5 to 2.0. The anodes were electrolyzed

nickel pieces. The solution was agitated with mandrel rotation at a rate of 100 rpm and continuously filtered. The mandrels of optical mirrors were prepared of 304 stainless steel. Optical mirrors of 2 to 7 cm diameters were prepared in a 15 L bath at 30°C.

The internal stress of the nickel-iron alloy deposits was determined by using a spiral contractometer(3). During electroforming, a strain gauge was used to indicate the stress change of alloy deposits.

The corrosion rate of alloy deposits in 1 percent acetic acid and 5 percent NaCl solution at 60°C for 30 days was ascertained by measuring weight loss. After weight loss test, the surface pits of these tested deposits were examined by using a scanning electron microscopy (SEM). Tarnishing(4) was evaluated by examining the appearance of the alloy deposits on Hull cell cathode panels. Hardness of deposits was measured on a microhardness tested with a 200 g load. The accuracy of the electroformed optical mirror surfaces was examined by their corresponding interference lines.

Each of the nickel and iron concentration in the electroforming baths was determined photometrically and volumetrically. The saccharin concentration was determined by cyclic voltammetric stripping analysis (CVS)(5). Atomic absorption spectrophotometry was used to determine the iron content in the alloy deposits.

Results and Discussion

1. Nickel-iron Bath Compositions

Although more than 0.3 g/L of saccharin (SAC), 5-sulfoisophthalic acid dimethylester sodium salt (SADS), or bis(benzenesulfonyl)imide (BBI) added in Bath A or B showed low internal stress of nickel-iron deposits by the thin-strip method(6) of Hull cell test, the alloy deposits of Bath B containing organic additives showed better throwing power than that of Bath A. Therefore, Bath B, which is used to produce deposits with low stress , was selected for our study.

The tarnish observations indicated that the nickel-iron deposits prepared by Bath B contained SADS or BBI. Black surface appeared after two months exposure, whereas even after one year, no tarnish phenomenon was observed for the alloy deposits prepared by Bath B contained SAC. Besides, the thin-strip method it was also shown that the nickel-iron deposits prepared by Bath B containing SAC at 50°C had higher internal stress than that of 30°C. Consequently, the optical mirrors were prepared by Bath B containing SAC at 30°C.

2. Internal Stress of Deposits

Stress control is very important in this work to prevent

deformation of the electroformed optical mirrors. Stress was investigated by varying the current density from 1.0 to 7.0 A/dm^2 and the SAC concentrations from 0 to 3.0 g/L. Figure 1 shown that stress increased with an increasing current density, especially for the SAC-free baths. Therefore, electroforming at lower current density is better for this work.

Measuring by using a spiral contractometer, the stress values of Fig. 1 were only the final stress of deposits. In order to have a deposit with even lower stress, a strain gauge was used to measure the strains of x and y axis directions of deposits. Therefore, the stress of deposits could be continuously controlled, resulting in a high surface quality of optical mirrors could be prepared. For comparision with Fig. 1, some typical strain signals of deposits prepared by using Bath B containing 1.0 g/L SAC were shown in Figure 2, the strain signals also showed that stress increased with an increasing current density.

3. Corrosive-protection of Deposits

Besides the tarnish tests, the corrosion rate of deposits were also conduted by measuring weight loss in acidic salt solutions. In comparision with electroformed nickel-iron, Bath C with almost same metal content as Bath B was conduted to prepare electroformed nickel. As shown in Fig. 3, alloy deposits prepared using Bath B containing 1.0 g/L SAC not only has a lower corrosion rate than that of Bath B containing 3.0 g/L SAC but appears to have better corrosive-protection than that of Bath C.

After the weight loss tests, the extent of surface pits on these tested deposits were examined by using a SEM. Alloy deposits prepared using Bath B, containing 3.0 g/L SAC, not only had higher corrosion rate but also had many pits after only 7 days in weight loss testing solution (a typical SEM photograph was shown in Fig. 4a). After a 30 days weight loss test, no pit was observed for both deposits prepared by using Bath B containing 1.0 g/L SAC and Bath C. Figure 4b is a typical SEM photograph of corrosive deposit prepared by using Bath B containing 1.0 g/L SAC, in which some brightness still existed after 30 days in weight loss testing solution.

Consequently, lower current densities of Bath B containing 1.0 g/L SAC were adopted to prepare the corrosive-protection optical mirrors.

4. Other Results of Alloy Deposits

The nickel-iron alloy system is classified as anomalous codeposition(7) because the less noble metal (iron) deposits preferentially. Figure 5 details data on the iron content of the deposit as a function of current density. Both the current density and the SAC concentration in solution affected the iron

content of the alloy deposits, which increased with a decreasing current density or an increasing SAC concentration.

As shown in Fig. 6, the harder deposits were obtained at higher current densities in the Bath B containing 1.0 g/L SAC.

5. Control of Bath Compositions

Changes of the concentrations of nickel, iron and SAC during experiments were examined in 0.5 and 3 L solutions in order to develop information on bath control. Variations in nickel concentrations were small in both baths. For example, the change in nickel concentration after 30,000 coulombs electroforming were less than 1 percent in a 3 L bath. For the control of SAC, as shown in Fig. 7, CVS was developed to analyze the consumption rate of SAC. In both baths, no more than 5 percent change of SAC concentrations was observed for 5,000 coulombs electroforming.

The iron decreased to a greater degree in both baths. As shown in Fig. 8, due to a higher amount of iron deposits, the consumption rates of iron were higher at lower current densities. The change of iron concentrations decreased in the 3.0 L bath than that of 0.5 L bath. Therefore, it was judged that large baths could be operated in a preduction mode with only a smaller change in the composition of the alloy deposits.

6. Practical Operations

Spheric shaped optical mirrors (as shown in Fig. 9) were prepared at 1~2 A/dm^2 by using Bath B containing 1.0 g/L SAC at $30^{\circ}C$ to take the advantages of the low internal stress and better corrosive-protection. During alloy electroforming, the stress of alloy deposits was observed continuously by a strain gauge, therefore, high quality optical mirrirs were obtained by appropriate control of bath compositions. After electroforming, alloy deposits was removed carefully from the edges of the mandrel, these electroformed optical mirrors have surface accuracy better than 0.3 μm.

Conclusions

The results of this work indicated that optical mirrors of nickel-iron alloy with low internal stress and high corrosive-protection can be obtained by using electroforming process.

References

1. R.A. Tremmel, Plat. and Surf. Fin., **68**, 22 (Jan. 1981).
2. M. Kouncheva, et al., Surface and Coatings Technology, **31**, 137 (1987).
3. C.H. Huang, et al., Plat. and Surf. Fin., **77**, 56 (April 1990).
4. C.H. Huang, ibid., **73**, 96 (June 1986).

5. H.M. Wu, et al., Chemistry (The Chinese Chem. Soc., Taiwan, China), **48(3)**, 227 (Sep. 1990).

6. C.H. Huang, Plat. and Surf. Fin., **71**, 104 (May 1984).

7. C.H. Huang, ibid., **76**, 64 (Dec. 1989).

Table 1

Nickel-iron Bath Compositions

Bath	$NiSO_4 \cdot 6H_2O$ (g/L)	$FeSO_4 \cdot 7H_2O$ (g/L)	$Ni(NH_2SO_3)_2$ $4H_2O$, (g/L)	$Fe(NH_2SO_3)_2$ $7H_2O$, (g/L)	H_3BO_3 (g/L)	NH_2SO_3H (g/L)
A	200	11	-	-	30	10
B	-	-	240	15	30	10
C	-	-	250	0	30	10

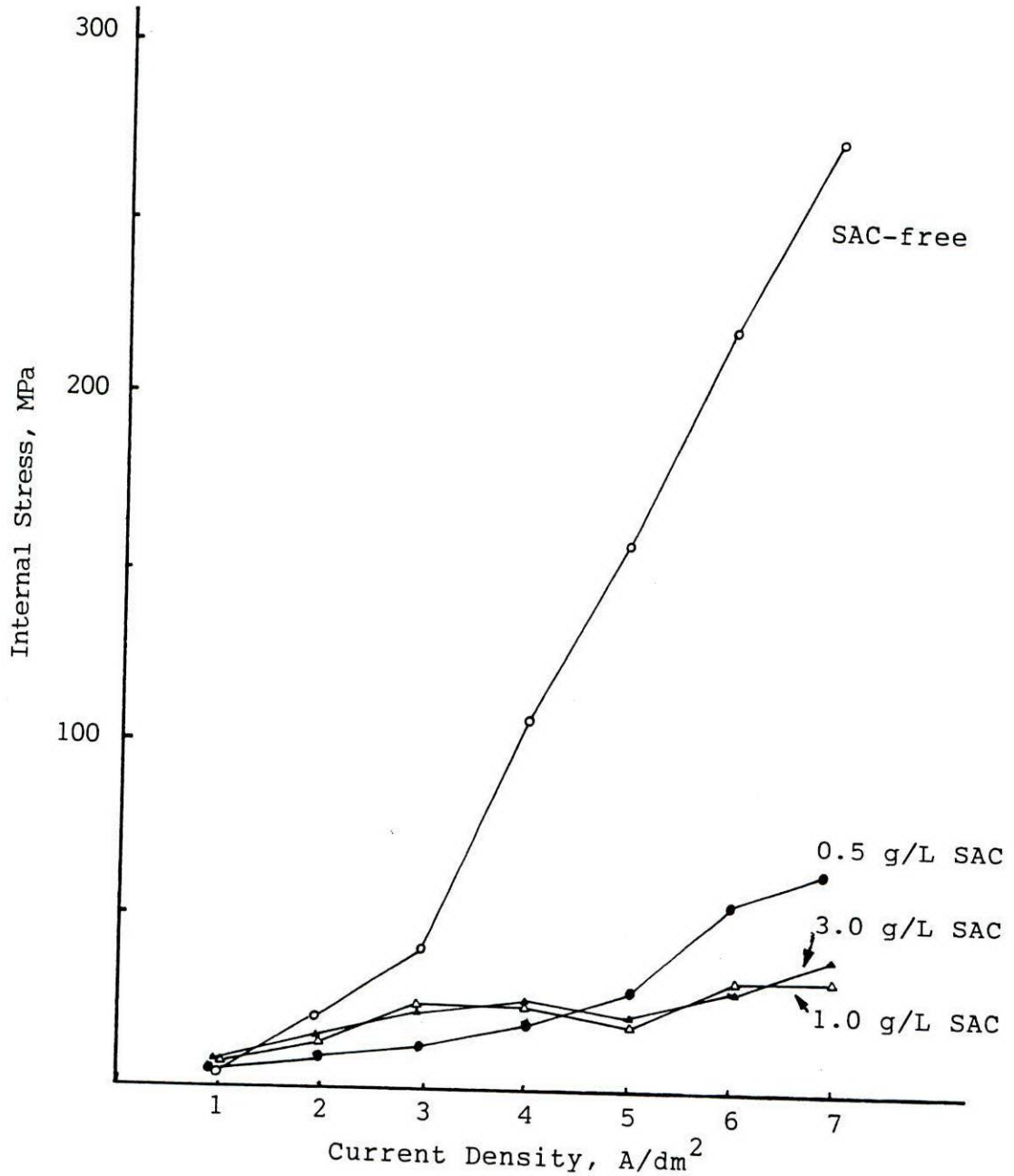

Fig. 1 - Internal stress of electroformed Ni-Fe alloy as a function of current density at 30°C.

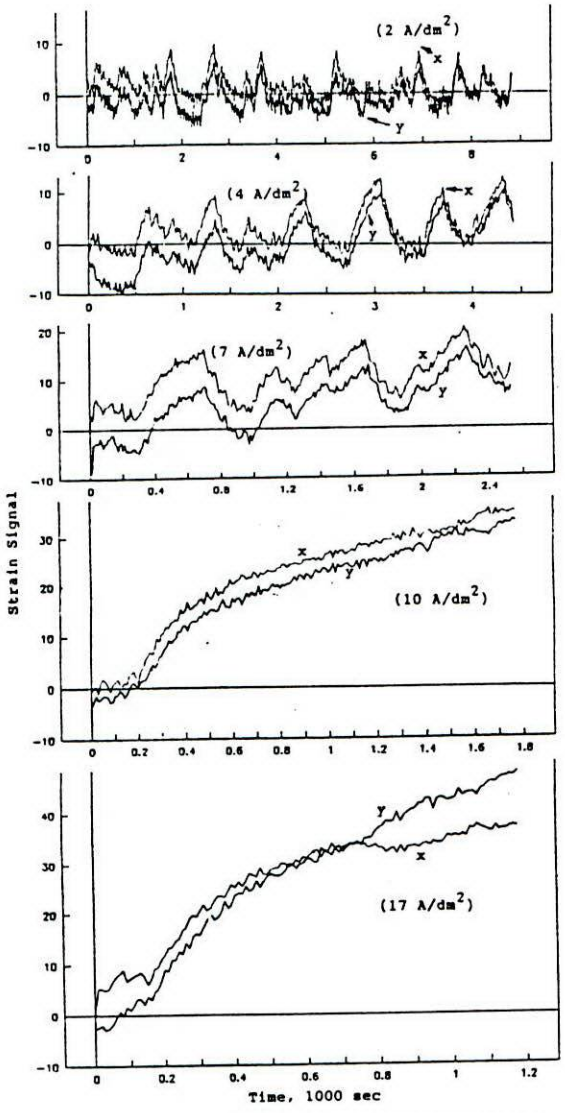

Fig. 2 - Strain signals of Ni-Fe alloy electroforming as a function of time. (Bath B contzining 1.0 g/L SAC at 30°C)

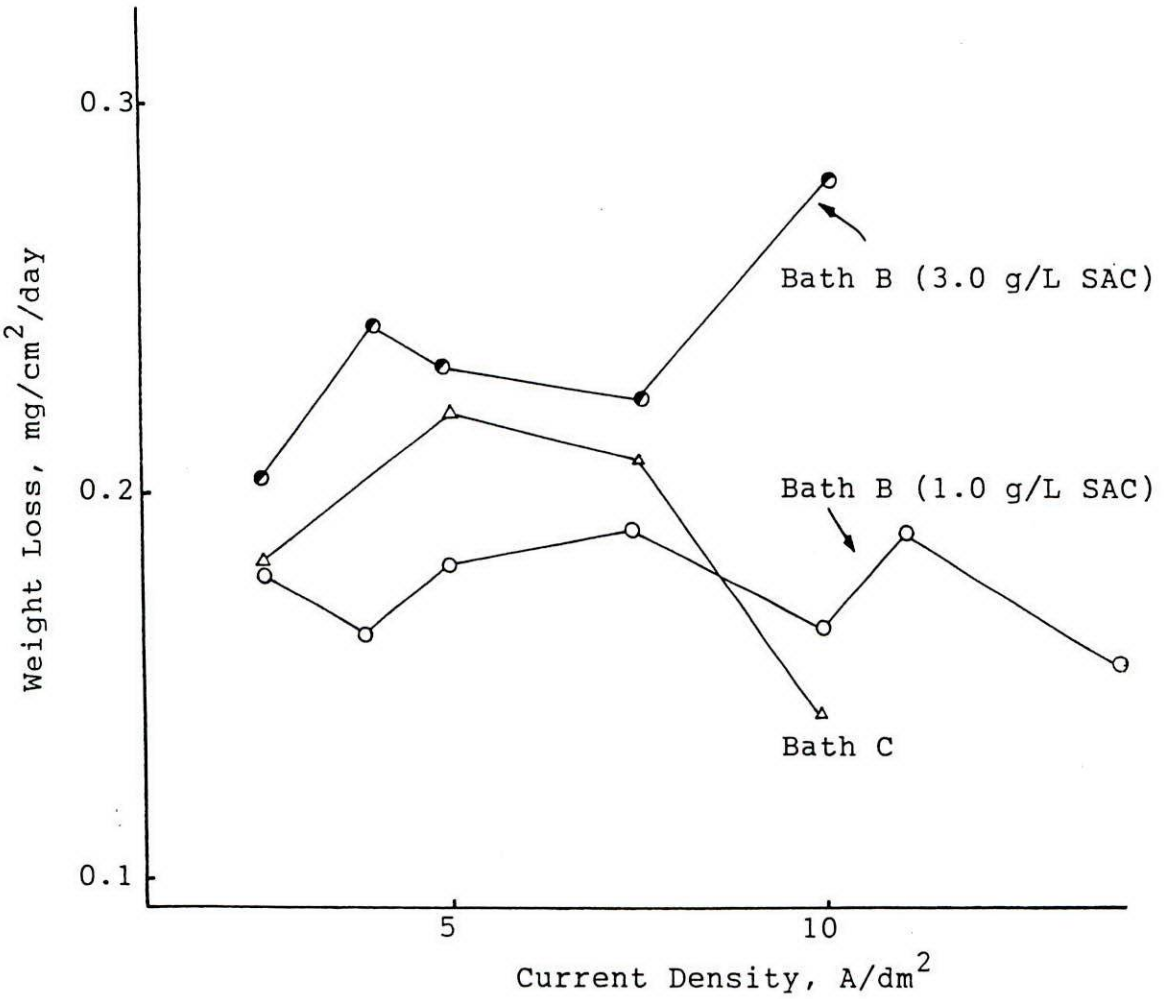

Fig. 3 - Corrosion rate of electroformed deposits immersed in acidic NaCl solution at 60°C for 30 days.

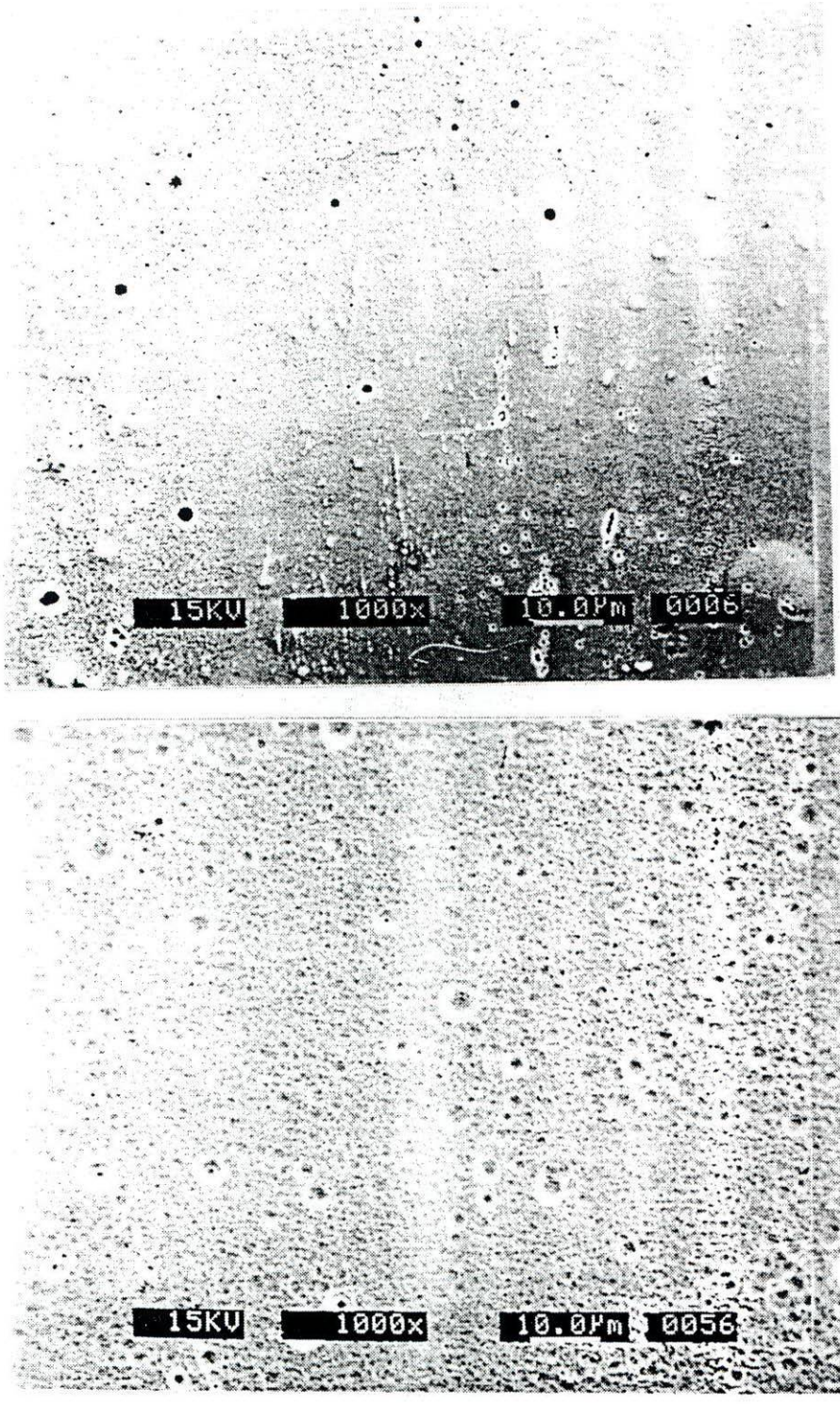

(a)

(b)

Fig. 4 - SEM photograph of surfaces of Ni-Fe alloy deposit prepared by using Bath B at 10 A/dm^2 and 30°C. The deposit immersed in acidic NaCl solution: (a) for 7 days and Bath B containing 3.0 g/L SAC, (b) for 30 days and Bath B containing 1.0 g/L SAC.

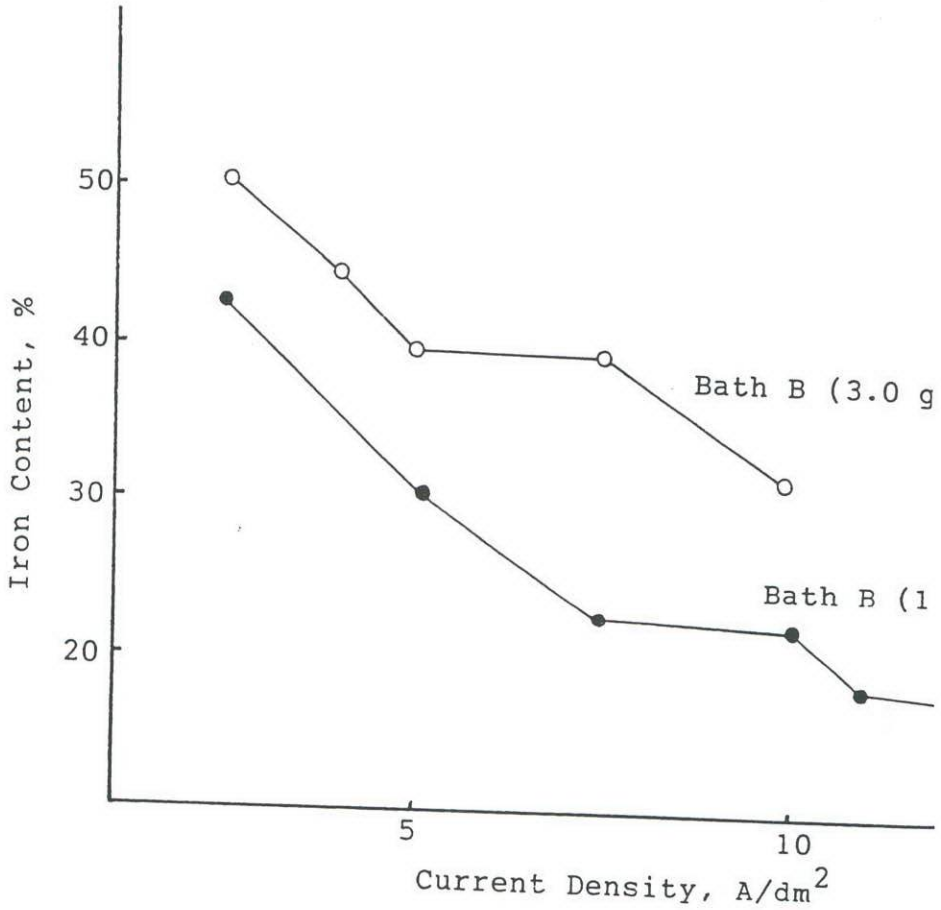

Fig. 5 - Iron content of electroformed Ni-Fe alloy function of current density.

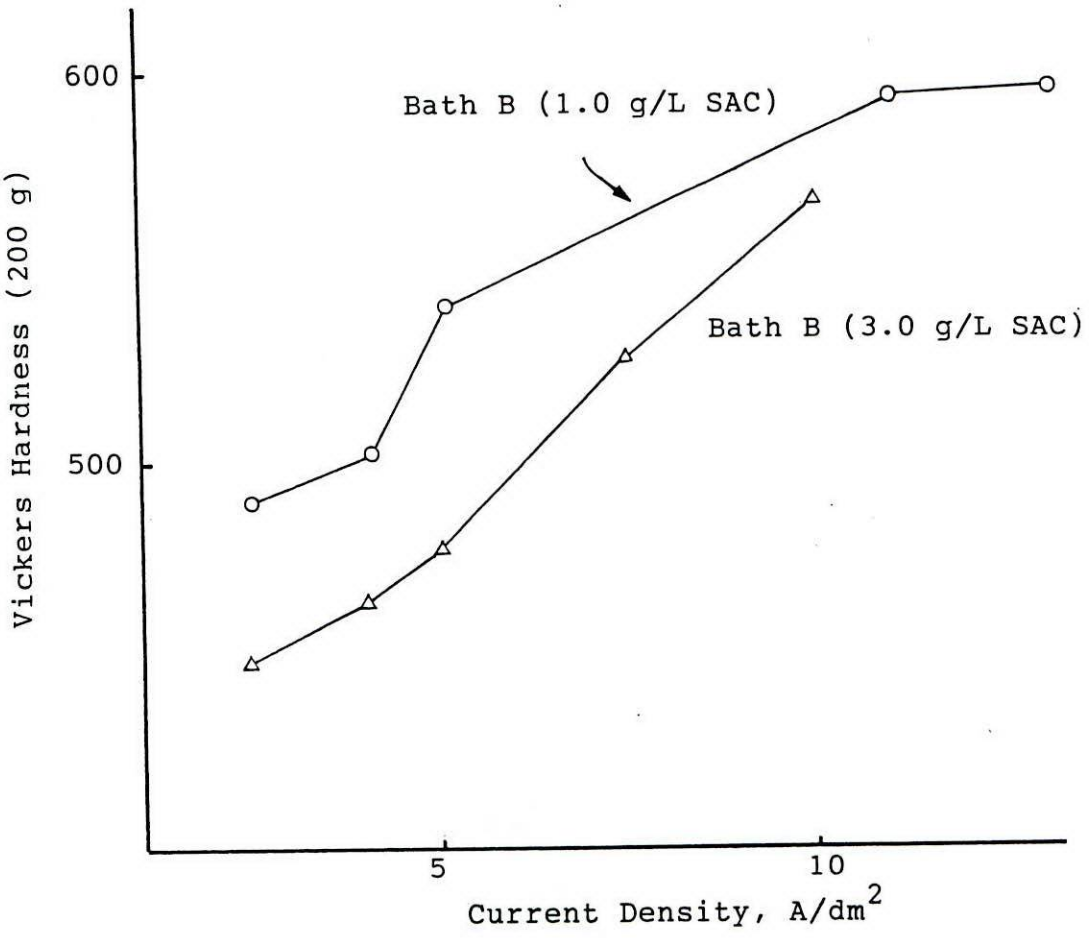

Fig. 6 - Variation of Ni-Fe deposit hardness as a function of current density.

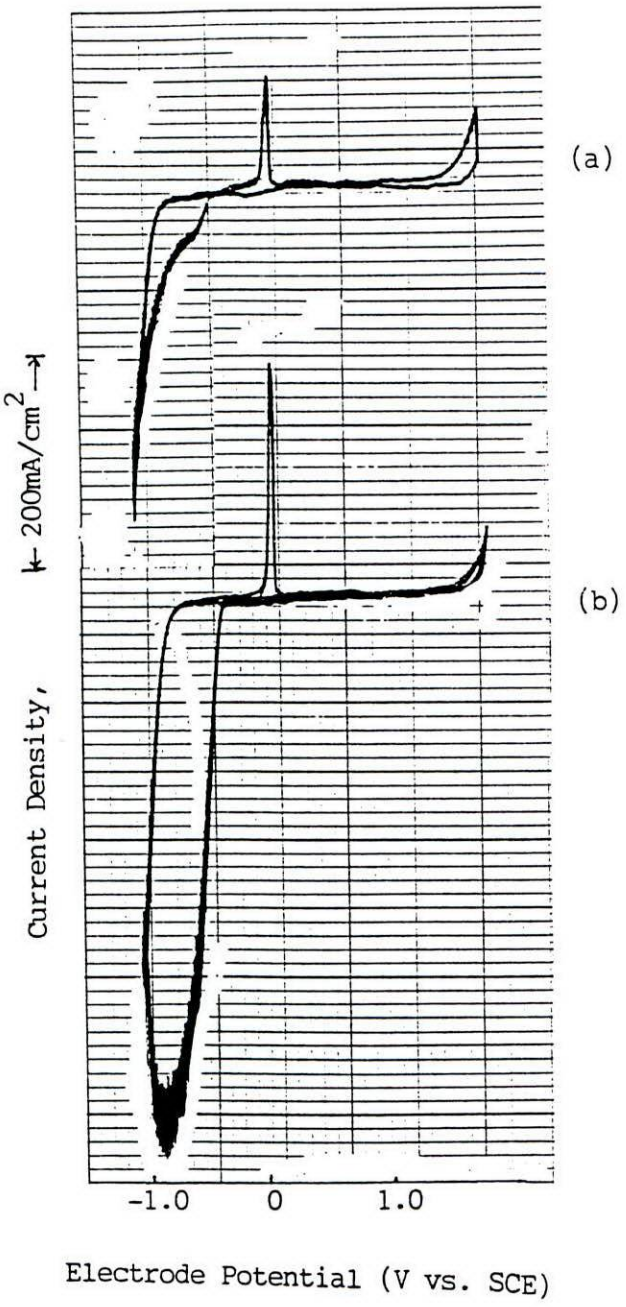

Fig. 7 - Cyclic voltammograms at 10 mV/sec for a Pt electrode rotating at 2500 rpm in Bath B containing: (a) 1.5 g/L SAC, (b) 3.0 g/L SAC.

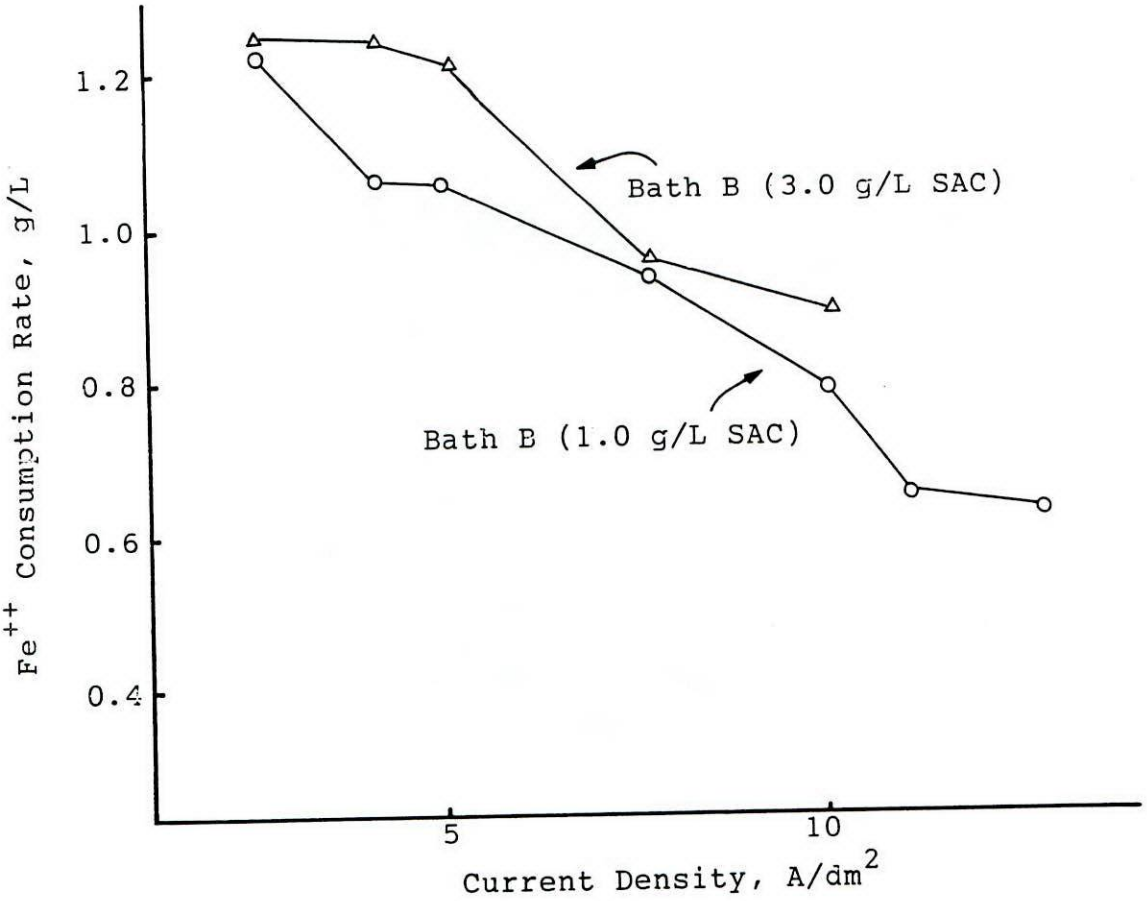

Fig. 8 - Changes in the concentrations of iron during 5000 coulombs of operation of 0.5 L electroforming baths.

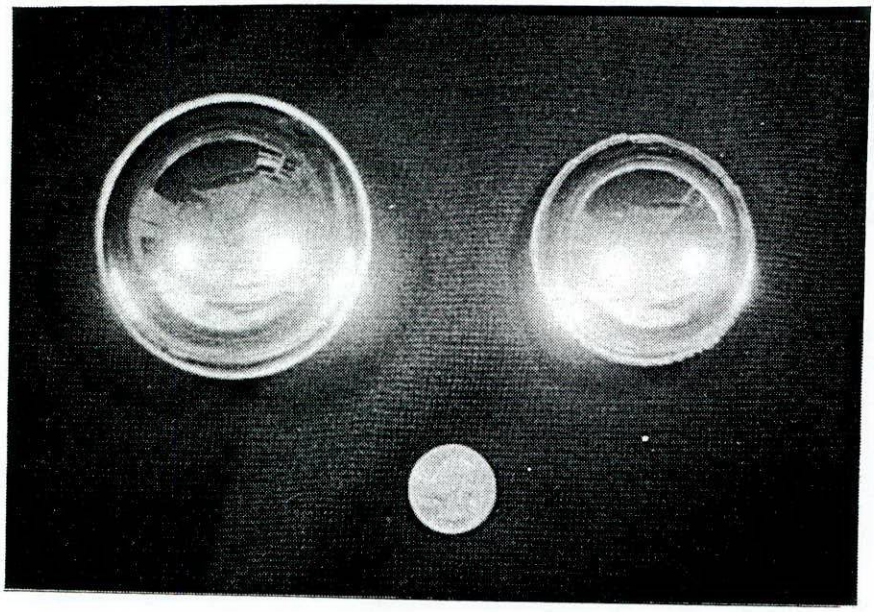

Fig. 9 - Spheric optical mirrors prepared by using Ni-Fe electroforming.

DEVELOPMENT OF THE HIGH SPEED BLACK ELECTROPLATING PROCESS

Katsushi Saito
Nippon Steel Corp., Kimitsu R & D Laboratory
Chiba Kimitsu city , Japan

ABSTRACT

High speed black electroplating process have been developed . The black coatings are deposited on cathode surface by electrolysis in acid solution containing Zn^{2+},Ni^{2+},Cr^{3+} and NO_3^- . Quantities of electricity to obtain the black surface are only 2 X 10^3 to 3 X 10^3 coulomb/m^2.

The black coatings are mainly composed of hydrated oxides , metallic Zn and Zn-Ni alloy.The blacked Zn-Ni alloy plated steel sheet with chromate and resin-silica coat has exellent properties ,for examplescratch resistance ,corrosion reistance , adhesion and weldability .

1 . Introduction

Many processes[1)2)] related to the black electroplating are disclosed , however the high speed electrodeposition process applicable for the continuous electrogalvanizing lines has not been established.

The fig.1 is the illustration of the new black electroplating steel sheet and a conventional prepaint steel sheet.

The left figure is a schematic cross section view of the new black electro-plating steel sheet (Inorganic type).

The inorganic type is composed of 3 micrometers in thickness of Zn-Ni alloy plating , about 0.3 micrometers in thickness black electroplating ,very thin chromating and 1 micrometer in thickness of the resin-silica coating .

The right one is a cross section view of a prepaint steel sheet (Prepaint type).

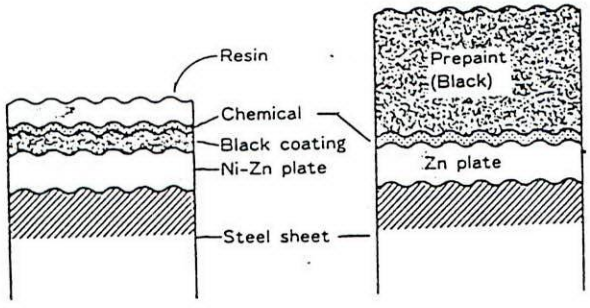

Fig.1 Schematic diagram of black coated steel sheet.

Table 1 shows the comparison of the each black coated electrogalvanized steel sheet. The prepaint type has exellent appearance ,pressformability and corrosion resistance, but poor finger print proof,scratch resistance and spot weldability.

On the other hand, the inorganic type shows opposite performance to prepaint type . The performance difference between two types depend on coating structure.

Table.1 Comparison of the black coated steel sheets

	Appearance	Press-formability	Corrosion resistance	Finger print proof	Scratch resistance	Weldability
Prepainted black type	VG	VG	VG	NG	NG	NG
Inorganic black type	G	G	G	VG	VG	VG

Very good > Good > No-good

2 . Experimental method

A sheet of steel is electroplated in Zn-Ni sulphate solution and water rinsed then black electroplated ,chromated ,finaly acrylic resin-silica coated and baked at 120℃.

The black coatings are electrodeposited in sulphate solution by a vertical type plating cell with Pb-Sn anode as shown in Fig.2 .Lightness value of the coatings are measured by the color difference meter as Lab. The black coatings are investigated by SEM , X-ray (on steel) and others .

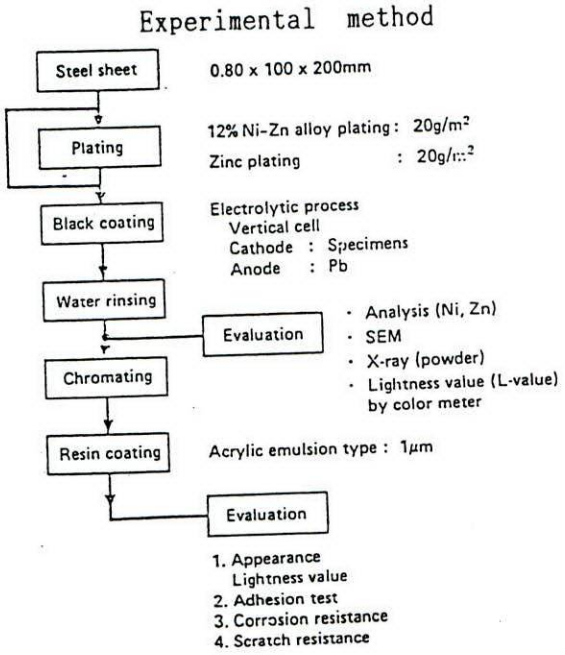

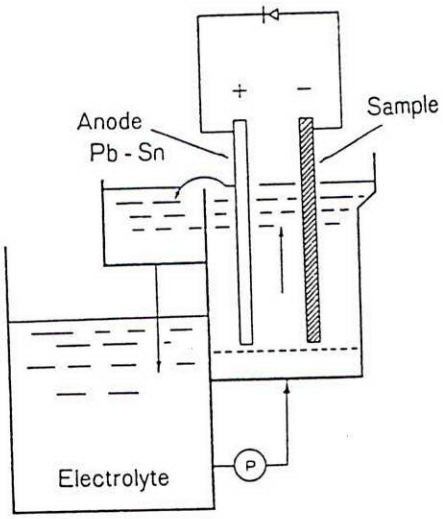

Fig.2 The experimental vertical

3 . Result

3.1 Black plating solution

Nickel oxides [NiO and Ni_2O_3] are black compounds . We undertook studies of deposition methods of these compounds electrolytically on steel.

We found that oxidizing ion and zinc ion with nickel ion are very effective to deposit the black coatings. This is a characteristic point of this process.

$NaNO_3$ is an exellent compound for use as an oxidizing agent in this process.

The relation between lightness value of the coatings and $NaNO_3$ concentration are shown in Figure 3 . The valuable black appearance needs lightness value below 20 .

$NaNO_3$ reduce lightness value of the coating and its concentration should be maintained at more than 4 grams per liter .

Higher current density is effective to reduce lightness value. Coating with a acrylic resin-silica significantly reduces lightness value.

Fig.4 shows zinc ion effect on lightness value of the coatings.

Because of a great deal of hydrogen gas generated at cathode in the solution without zinc ion ,low lightness value coating could not be deposited in a short time .

Zinc ion more than 70 g/ℓ as $ZnSO_4 \cdot 7H_2O$ is neccessary in this process.

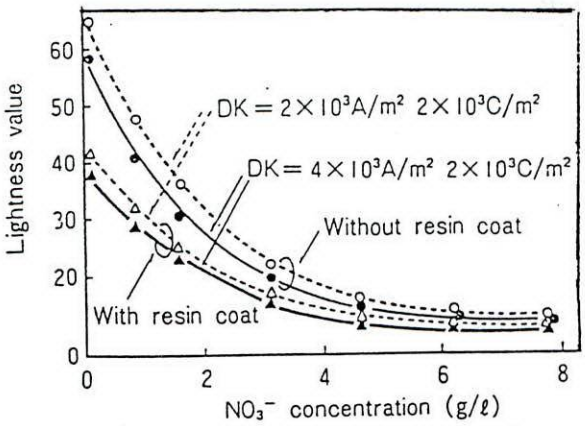

Fig.3 The effect of NO_3^- on L-value

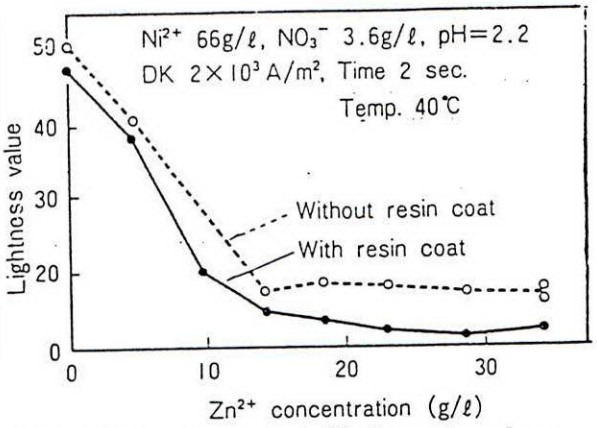

Fig.4 The effect of NO_3^- on L-value

3.2 Electrolytic condition

Relation between electrolytic conditions and lightness value without resin coatings are shown in fig.5 as solid line with open marks .It needs only 30 coulomb/dm² to deposit black coating below lightness value 20. Preferable current density ranges are within 20 to 40 A/dm². Therefore neccessary time is only 1 second . Solid line with solid marks in fig.5 shows the black coating weight deposited. The coating weight of the black coating is about 1 g/m² .

The effects of current density on lightness value are shown in fig. 6 . In this experiment we used solutions composed of different concentrations of zinc ,nickel and chromium ion. Lightness value of the coatings electrodeposited under low current density are high and unstable. Whereas lightness value of the coatings electrodeposited under high current density is low and stable .

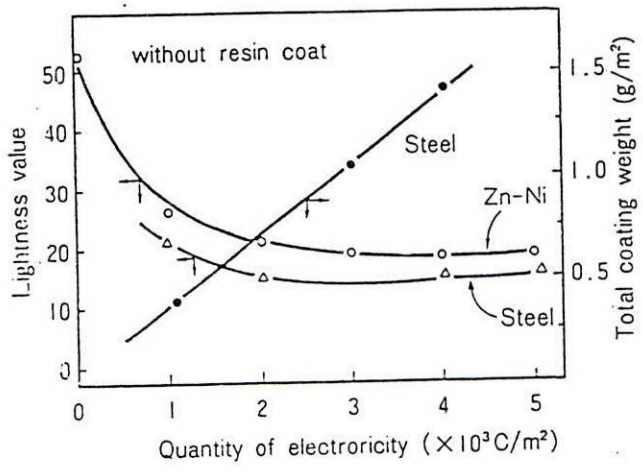

Fig.5 Relation between coulomb and L-value of the coating

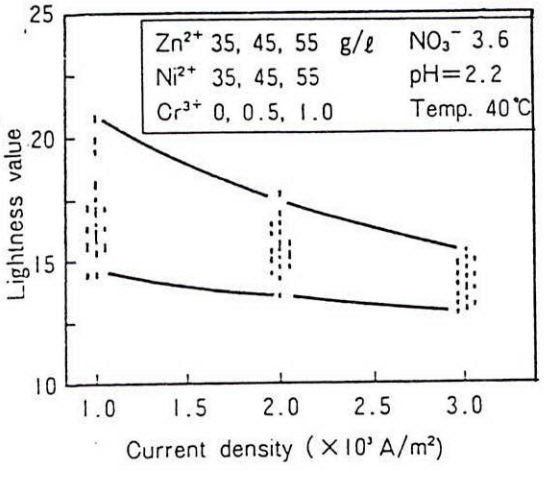

Fig.6 The effect of current density on the black coatings

3.3 Improvement

The above method did not substantially improve performance of black electroplated steel sheet especially corrosion resistance and adhesion. However, we found that the addition of small amounts of trivalent chromium ion improved adhesion and corrosion resistance of the black electroplating steel sheet.

Fig.7 shows the effect of added trivalent chromium ion on corrosion resistance evaluated by salt spray fog test. Chromium hydroxides such as $Cr(OH)_3$ codeposited in the coating did improve the performance.

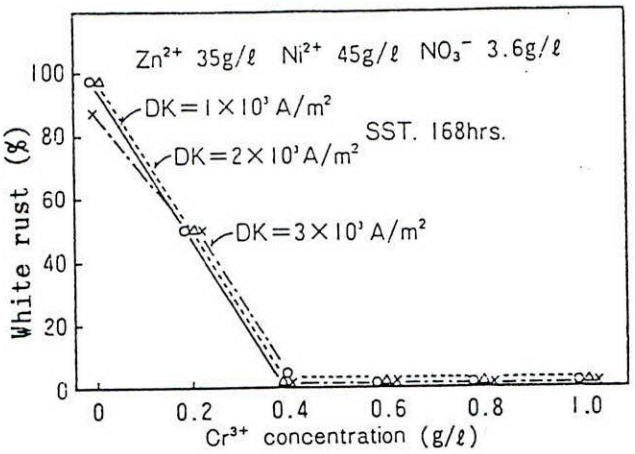

Fig. 7 Effect of Cr^{3+} on corrosion resistance

3.4 Typical Performance

(1) Adhesion

We evaluated by cellophane taping after erichsen 8mm forming and 1mm cross cutting. Adhesion of the black Zn-Ni electroplating steel sheet was excellent.

(2) Scratch resistance

Scratch resistance is evaluated by commercial scratch resistance machine which evaluated minimum weight injury by a sapphire tip 0.1 mm in dia.

It depends on base metal hardness(fig.8). The hard Zn-Ni plating is exellent .

(3) Weldability

The black electroplating steel sheet is weldable .Fig.9 shows suitable current range under spot welding.

Zn-Ni plated steel sheet has wide current range(6.5-12.0 KA). Current ranges of the black coated Zn-Ni plated steel sheet depending on pH in the solution.

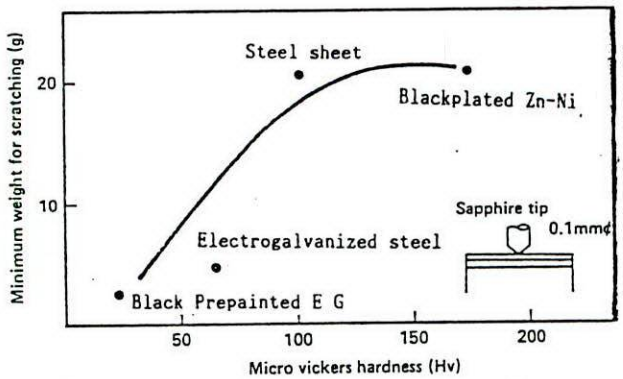

Fig.8 Relation between scratch resistance and base metal hardness

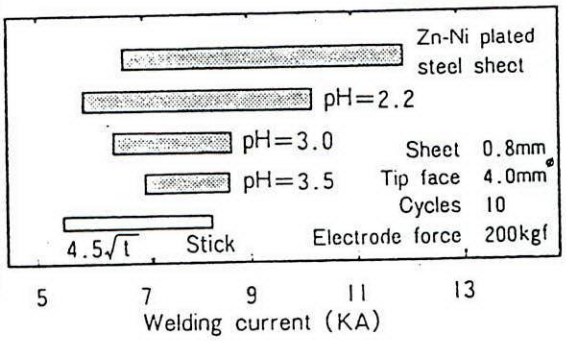

Fig.9 Weldable current ranges of the black plated steel sheet

3.5 Structure of the coatings

Structure of the black coatings deposited are investigated .

Fig.10 is the X-ray analysis of the powder removed and the coatings deposited on steel sheet .

The coatings are composed of metal and hydrated oxides. The coatings deposited under higher current density and lower pH solution include higher metal content than the coatings under lower current density and higher pH solution .

This is also observed by glow discharge spectroscopy analysis(GDS).

Fig.11 shows intensity ratio Oxgen/Zinc of the deposited coating in depth.

The coatings deposited under high current density have the lower O/Zn ratio . Surface of the black electroplated coatings are shown in photo.1 observed by a field emission scanning electron microscope (FE-SEM). The black coating is fine and has needle-like crystals .

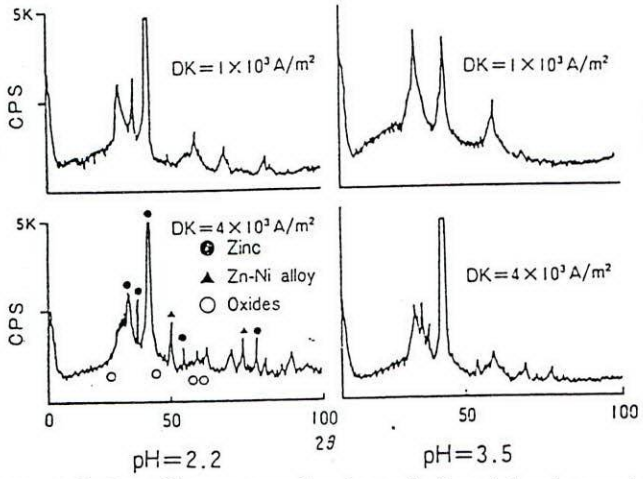

Fig.10 The X-ray analysis of the black coatings on steel

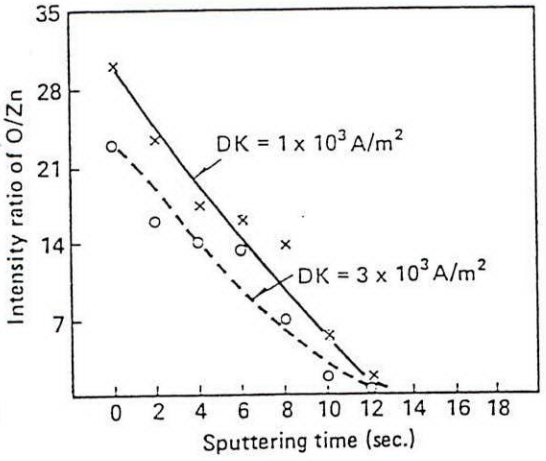

Fig.11 GDS analysis of the black coatings in depth

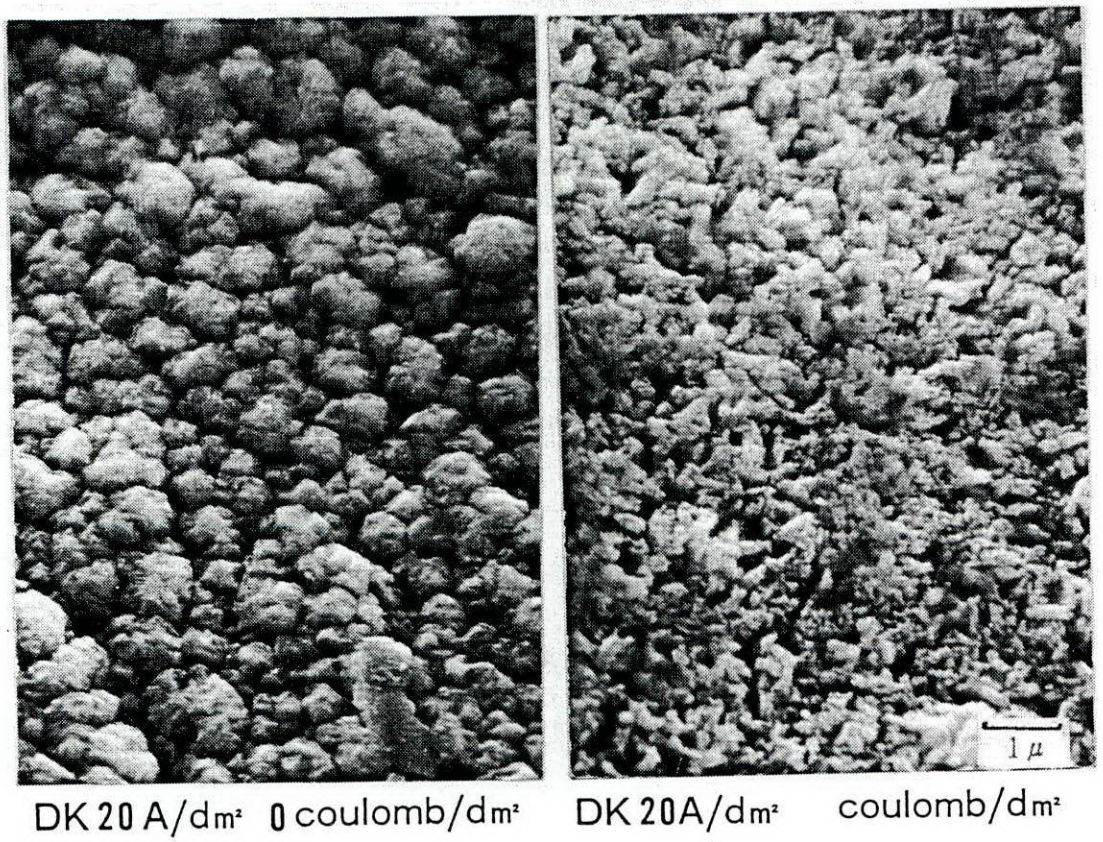

Photo 1. FE-SEM observation of the black coatings on Zn-Ni plated steel sheet

4.Discussion

1) Black appearance

The black coatings are composite plating including oxides and metals and the degree of blackness is proportional to Ni content in the coating .

It is well known some nickel oxides are black . This is one reason why coatings are black . Another reason is relation to surface morphology . The coatings such as needle-like is easy to absorb light.

2)Deposition of the composite plating

The NO_3^- is reduced with Zn^{2+} and Ni^{2+} and solution pH is also increased at cathode surface . Therefore deposition of insoluble hydroxides are possible with metal platings .

However the consumption of NO_3^- is a little and NO_2^- is little in the solution .

It is considered that NO_3^- is regenerated by oxidizing at anode.

5. Conclusion

(1)The black coatings are deposited on cathode surface by electrolysis in acid solution containing Zn^{2+},Ni^{2+},Cr^{3+} and NO_3^- .Quantities of electricity to obtain the black surface are only 2×10^3 to 3×10^3 coulomb/m^2.

(2)The black coatings are mainly composed of hydrated oxides , metallic Zn and Zn-Ni alloy.

(3)The blacked Zn-Ni alloy plated steel sheet with chromate and resin-silica coat has exellent properties,for example scratch resistance ,corrosion resistance adhesion and weldability .

The black electroplating steel strips have been produced in a continuous electrogalvanizing line with some improvements.

Fig.12 is a schematic diagram of the electrolytic cell for black plating in the continuous electro-galvanizing line.

Electrolyzing is only executed in the up pass section in order to obtain high current density electrolyzing .

The predipping in the down pass section improve uniformity of the black coatings.

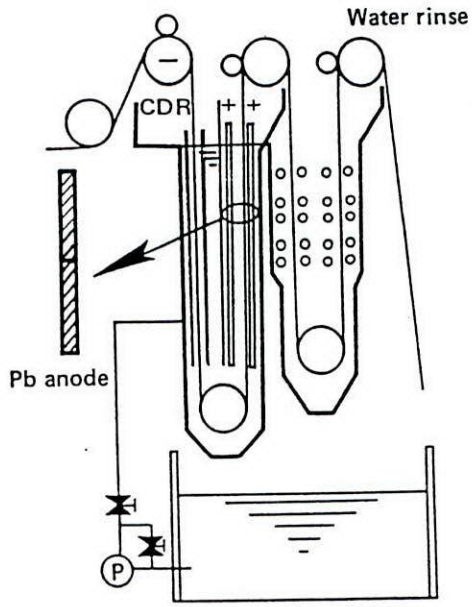

Fig.12 A electoplating cell for the black electroplating in the continuous E.G.L.

6. Refference

1) E.Barth, R.Kammel , U. Landau , J. Osterwald and M. Mayer ; Inter Finish '84 (1984) , p85

2) M.S.E.Abdo and T. Sahhf ; Plating and Surface Finishing , 75 ,(1986) 6 ,p108